frontiers | Research Topics

Cancer immunotherapy – diagnostic and therapeutic strategies to enhance antitumoral efficacies whilst minimizing toxicity

Edited by
Roza Nurieva, Sang T. Kim and Yeonseok Chung

Published in
Frontiers in Immunology
Frontiers in Oncology

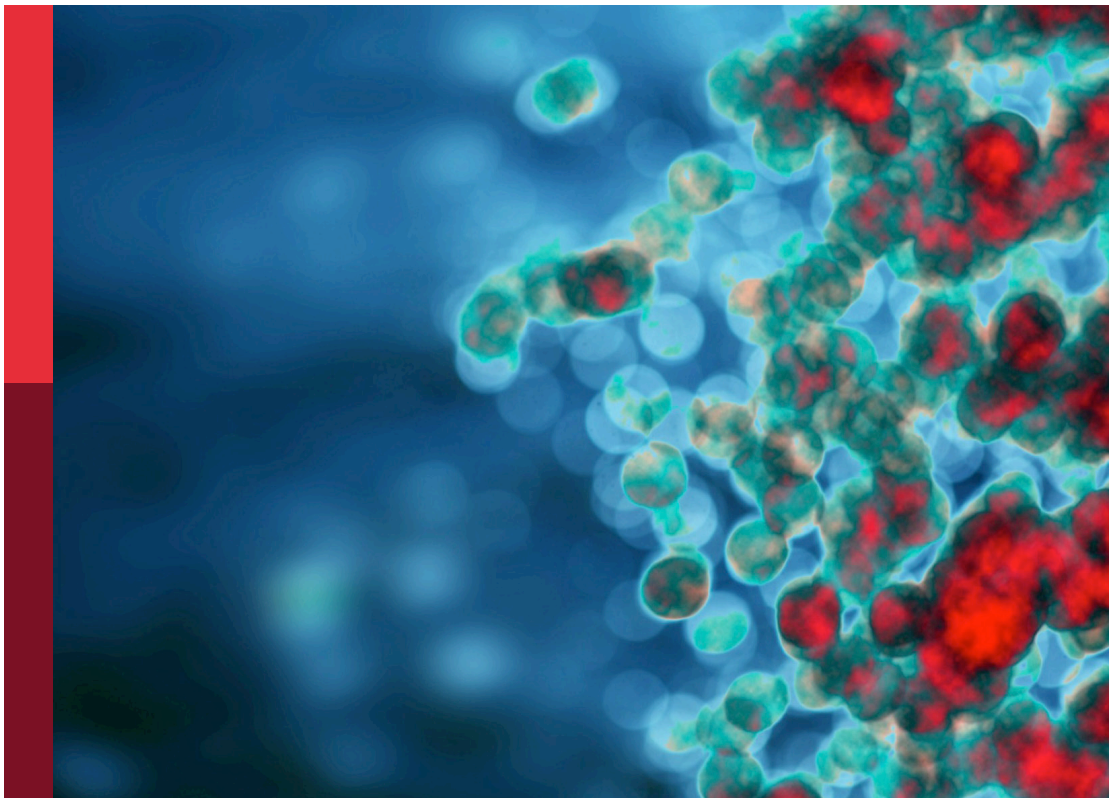

ISSN 1664-8714
ISBN 978-2-8325-5581-1
DOI 10.3389/978-2-8325-5581-1

About Frontiers

Frontiers is more than just an open access publisher of scholarly articles: it is a pioneering approach to the world of academia, radically improving the way scholarly research is managed. The grand vision of Frontiers is a world where all people have an equal opportunity to seek, share and generate knowledge. Frontiers provides immediate and permanent online open access to all its publications, but this alone is not enough to realize our grand goals.

Frontiers journal series

The Frontiers journal series is a multi-tier and interdisciplinary set of open-access, online journals, promising a paradigm shift from the current review, selection and dissemination processes in academic publishing. All Frontiers journals are driven by researchers for researchers; therefore, they constitute a service to the scholarly community. At the same time, the *Frontiers journal series* operates on a revolutionary invention, the tiered publishing system, initially addressing specific communities of scholars, and gradually climbing up to broader public understanding, thus serving the interests of the lay society, too.

Dedication to quality

Each Frontiers article is a landmark of the highest quality, thanks to genuinely collaborative interactions between authors and review editors, who include some of the world's best academicians. Research must be certified by peers before entering a stream of knowledge that may eventually reach the public - and shape society; therefore, Frontiers only applies the most rigorous and unbiased reviews. Frontiers revolutionizes research publishing by freely delivering the most outstanding research, evaluated with no bias from both the academic and social point of view. By applying the most advanced information technologies, Frontiers is catapulting scholarly publishing into a new generation.

What are Frontiers Research Topics?

Frontiers Research Topics are very popular trademarks of the *Frontiers journals series*: they are collections of at least ten articles, all centered on a particular subject. With their unique mix of varied contributions from Original Research to Review Articles, Frontiers Research Topics unify the most influential researchers, the latest key findings and historical advances in a hot research area.

Find out more on how to host your own Frontiers Research Topic or contribute to one as an author by contacting the Frontiers editorial office: frontiersin.org/about/contact

Cancer immunotherapy – diagnostic and therapeutic strategies to enhance antitumoral efficacies whilst minimizing toxicity

Topic editors

Roza Nurieva — University of Texas MD Anderson Cancer Center, United States
Sang T. Kim — Yale University, United States
Yeonseok Chung — Seoul National University, Republic of Korea

Citation

Nurieva, R., Kim, S. T., Chung, Y., eds. (2024). *Cancer immunotherapy – diagnostic and therapeutic strategies to enhance antitumoral efficacies whilst minimizing toxicity*. Lausanne: Frontiers Media SA. doi: 10.3389/978-2-8325-5581-1

Table of contents

frontiers | Frontiers in Immunology

TYPE Review
PUBLISHED 22 February 2023
DOI 10.3389/fimmu.2023.1139821

OPEN ACCESS

EDITED BY
Yeonseok Chung,
Seoul National University, Republic of Korea

REVIEWED BY
Hun Sik Kim,
University of Ulsan, Republic of Korea
Youngjun Park,
Jeju National University, Republic of Korea

*CORRESPONDENCE
Mingzhi Zhang
mingzhi_zhang1@163.com
Zhaoming Li
fcclizm@zzu.edu.cn

SPECIALTY SECTION
This article was submitted to Cancer Immunity and Immunotherapy, a section of the journal Frontiers in Immunology

RECEIVED 07 January 2023
ACCEPTED 13 February 2023
PUBLISHED 22 February 2023

CITATION
Shi Z, Li H, Song W, Zhou Z, Li Z and Zhang M (2023) Emerging roles of the gut microbiota in cancer immunotherapy. *Front. Immunol.* 14:1139821. doi: 10.3389/fimmu.2023.1139821

Emerging roles of the gut microbiota in cancer immunotherapy

Zhuangzhuang Shi[1,2,3], Hongwen Li[1,2], Wenting Song[1,2,3], Zhiyuan Zhou[1,2], Zhaoming Li[1,2,4]* and Mingzhi Zhang[1,2,4]*

[1]Department of Oncology, The First Affiliated Hospital of Zhengzhou University, Zhengzhou, China, [2]Lymphoma Diagnosis and Treatment Centre of Henan Province, Zhengzhou, China, [3]Academy of Medical Sciences of Zhengzhou University, Zhengzhou, Henan, China, [4]State Key Laboratory of Esophageal Cancer Prevention and Treatment and Henan Key Laboratory for Esophageal Cancer Research, The First Affiliated Hospital of Zhengzhou University, Zhengzhou, Henan, China

Gut microbiota represents a hidden treasure vault encompassing trillions of microorganisms that inhabit the intestinal epithelial barrier of the host. In the past decade, numerous *in-vitro*, animal and clinical studies have revealed the profound roles of gut microbiota in maintaining the homeostasis of various physiological functions, especially immune modulation, and remarkable differences in the configuration of microbial communities between cancers and healthy individuals. In addition, although considerable efforts have been devoted to cancer treatments, there remain many patients succumb to their disease with the incremental cancer burden worldwide. Nevertheless, compared with the stability of human genome, the plasticity of gut microbiota renders it a promising opportunity for individualized treatment. Meanwhile, burgeoning findings indicate that gut microbiota is involved in close interactions with the outcomes of diverse cancer immunotherapy protocols, including immune checkpoint blockade therapy, allogeneic hematopoietic stem cell transplantation, and chimeric antigen receptor T cell therapy. Here, we reviewed the evidence for the capacity of gut microflora to modulate cancer immunotherapies, and highlighted the opportunities of microbiota-based prognostic prediction, as well as microbiotherapy by targeting the microflora to potentiate anticancer efficacy while attenuating toxicity, which will be pivotal to the development of personalized cancer treatment strategies.

KEYWORDS

Gut microbiota, immunotherapy, immune checkpoint blockade, allogeneic hematopoietic stem cell transplantation, chimeric antigen receptor T cell therapy

Abbreviations: ICB, immune checkpoint blockade; allo-HSCT, allogeneic hematopoietic stem cell transplantation; CAR-T, chimeric antigen receptor T; PD-1/PD-L1, programmed cell death protein 1/programmed cell death ligand 1; CTLA-4, cytotoxic T lymphocyte-associated antigen-4; TME, tumor microenvironment; NSCLC, non-small cell lung cancer; irAEs, immune-related adverse events; OS, overall survival; FMT, fecal microbiota transplantation; SCFAs, short–chain fatty acids; CRC, colorectal cancer; GVHD, graft-versus-host disease; HR, hazard ratio; CI, confidence interval; IECs, intestinal epithelial cells; LBP, *Lactobacillus plantarum*.

Introduction

The human gut microbiota refers to the vast collection of various microbes living on the epithelial barrier surfaces of the gastrointestinal tract, including bacteria, fungi, viruses, archaea, and protozoa (1). With the advances of molecular tools and technologies such as 16S ribosomal RNA sequencing, metagenomic, metabolomic, and metatranscriptomic, as well as the use of gnotobiotic animal models, the intricate host-microbiota interactions are progressively being deciphered (2). For one thing, substantial researches have featured the key roles of gut microbiota in human pathophysiological processes (3–5), including immunity, metabolism, and inflammatory response. For another, albeit multiple factors are proposed to propel cancer progression, the deviation of gut microbiota, known as dysbiosis, is entertained as a harbinger, promoter or even cause of a variety of malignant conditions (6). Thereinto, a panel of potential pro-tumorigenesis or anti-tumorigenesis microbial species have been identified too (7), which lays the groundwork for the regulation of gut microbiota in cancer therapy.

Meanwhile, with the incremental cancer burden worldwide, it places greater demands on personalized cancer treatments with powerful efficacy (8), although substantial advancements have been made, especially cancer immunotherapy. Most notably, the limited efficacy and undesired toxicities still remain the major hurdles of current cancer therapies, which has been found to be heavily influenced by distinct gut microflora patterns (9). Of them, immunotherapy has been considered as a major revolution, which provides exciting hopes for patients in the fight against cancer, and the effects of certain gut species on immunotherapy have now become a topic of great scientificity (10, 11). In the light of these findings, there is emerging interest in microbiotherapy by the modulation of intestinal flora as one of the antitumor strategies in recent years.

In this review, we mainly discussed the interactions between gut microbiota and cancer immunotherapies, including immune checkpoint blockade (ICB) therapy, allogeneic hematopoietic stem cell transplantation (allo-HSCT), and chimeric antigen receptor T (CAR-T) cell therapy, and the opportunities of microbiota-based patient stratification strategies such as the prediction of response and the early recognition of toxic events, as well as the evidence for the ability of microbiotherapy in the management of cancer immunotherapy, including enhancing anticancer efficacy and alleviating toxicity, thus, to decipher the roadmap of gut microbiota in the exploitation of custom-fit therapeutic strategies for cancer care. A diagrammatic representation of the interactions between gut microbiota and cancer immunotherapy is described in Figure 1.

Immune checkpoint blockade therapy

Currently, one hotspot of cancer immunotherapy is the ICB therapy that inhibits programmed cell death protein 1/programmed

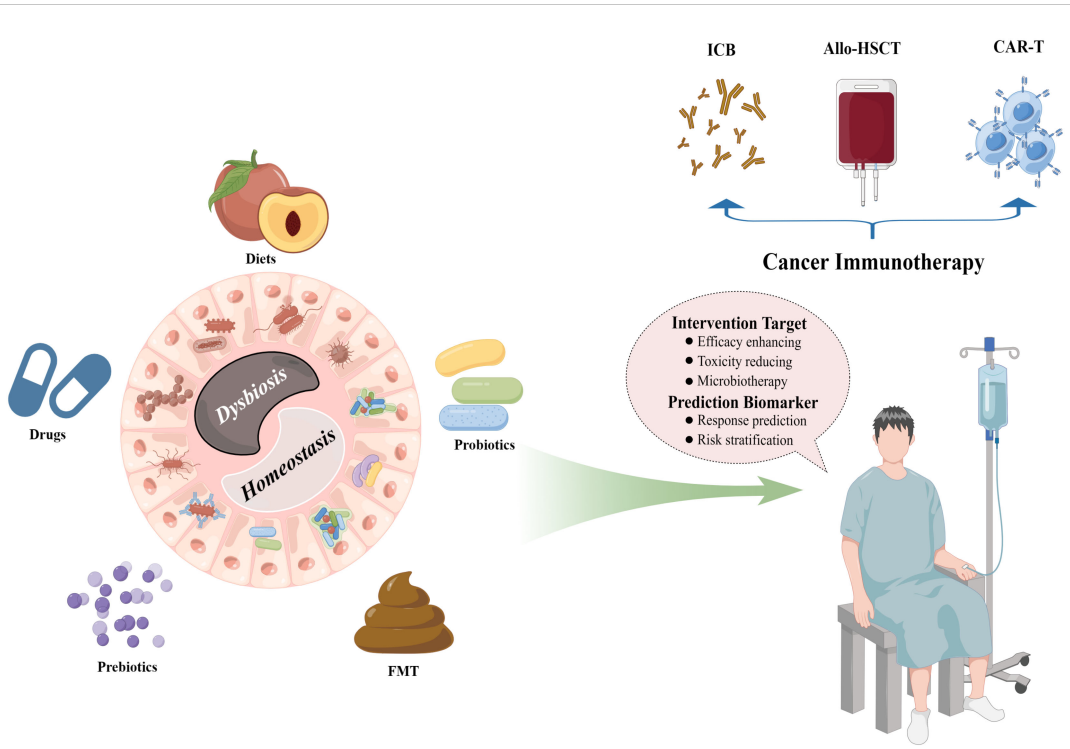

FIGURE 1
Interactions between the gut microbiota and cancer immunotherapy. The intestinal microbial ecosystem can be well modified by multiple patterns, including diets, drugs, prebiotics, probiotics, and FMT, which provide fascinating opportunities for the clinical managements of diverse cancer immunotherapy protocols such as ICB therapy, allo-HSCT, and CAR-T cell therapy. FMT, fecal microbiota transplantation; ICB, immune checkpoint blockade; allo-HSCT, allogeneic hematopoietic stem cell transplantation; CAR-T, chimeric antigen receptor T. (By Figdraw).

cell death ligand 1 (PD-1/PD-L1) and cytotoxic T lymphocyte-associated antigen-4 (CTLA-4) signaling to reinvigorate CD8+ T cells in the tumor microenvironment (TME) to potentiate killing of tumor cells (12). Despite the remarkable effectiveness of ICB therapy in a subset of patients of several cancer types, including metastatic melanoma (13), classical Hodgkin lymphoma (14), non-small cell lung cancer (NSCLC) (15), and colon cancers (16), most patients were observed with primary or acquired resistance. Furthermore, a number of challenges such as the immune-related adverse events (irAEs) and biomarkers to predict response remain to be determined (17). However, accumulating data have pinpointed the indispensable roles of intestinal microbiota in ICB therapy.

The effects of antibiotics on the response of ICB therapy

Antibiotics-associated gut dysbiosis frequently confers deleterious effects on cancer patients treated with ICB (18). Derosa and colleagues (19) reported that antibiotics administration within 30 days of beginning ICB therapy was closely related to the inferior prognosis, including shorter progression free survival and overall survival (OS), in both advanced renal cell carcinoma and NSCLC patients. Similarly, the negative influences of antibiotics on the clinical outcomes of ICB have also be indicated in patients with melanoma (20), urothelial carcinoma (21), and bladder cancer (22). Nevertheless, Cheung et al. (23) and Fessas et al. (24) inversely revealed the detrimental and protective effects of antibiotics use on the survival of ICB treated hepatocellular carcinoma patients, respectively, which might be attributable to the difference of the antibiotic types, therapeutic regimens, baseline clinical characteristics and gut microbial features of patients. In addition, one caveat here is the antibiotics application might simply constitute a surrogate indicator of unsuited or immunodeficient cancer patients who were non-responsive for ICB therapy, which deserves further evaluation.

Influence of gut microbiota on the effectiveness of ICB therapy

The significance of commensal intestinal bacteria on the efficacy of ICB therapy has been well established in both pre-clinical models and patients. A plethora of microbial taxa, including *Akkermansia muciniphila*, *Faecalibacterium* spp., *Bifidobacterium* spp., and *Bacteroides fragilis* (25), have been reported to potentiate the antitumor efficacy of ICB therapy in both animal models and cancer patients. Of specific note, it has been well demonstrated that gut commensal bacteria such as *Bifidobacterium* and *Bacteroidales* could significantly improve tumor control of melanoma treated by anti-PD-L1 or anti-CTLA-4 *via* enhancing antitumor immunity response in mice models (26, 27). Further, this favorable role of commensal microbiome in ICB therapy was elucidated in melanoma patients (28, 29). Additionally, a higher diversity of gut microbiota at the starting point exhibited intimate relationships with the favorable responses to anti-PD-1 immunotherapy in patients with hepatocellular carcinoma and advanced NSCLC (30, 31), which might be involved in the enhanced memory T cell and natural killer cell signatures in the periphery in response to anti-PD-1 therapy. Interestingly, *Helicobacter pylori* seropositivity has been reported to be linked with an inferior NSCLC patient survival on anti-PD-1 therapy (32), and further be confirmed in *in vitro* co-culture assay and in *H. pylori*-infected mice with reduced number and activation status of tumor-specific CD8+ T cells in the tumors. Strikingly, apart from the linkages between individual bacterial taxa and ICB therapy outcome, the association of enteric microbiotypes (including diverse discrete ecologically balanced communities) with the response to melanoma patients treated by anti-PD-1 has also been proposed in a recent combination analysis (33). That is, four superclusters of a panel of microbial species, including two enriched in favorable taxa (Favorable 1: *Bifidobacteriaceae*, *Eggerthelacea*, *Coriobacteriales*, *Akkermansia muciniphila*, *Fusobacteriaceae*, *Erysipelotrichaceae*, *Lachnospiraceae*, *Streptococcaceae*, *Lactobacillaceae*, and *Porphyromonadaceae*; Favorable 2: *Oscillospiraceae*; by linear discriminant analyses) and two enriched in unfavorable taxa (Unfavorable 1: *Prevotellaceae* and *Bacteroidales*; Unfavorable 2: *Rikenellaceae*; by linear discriminant analyses), were defined, which comprised distinct microbiotypes with similar relationship between microbial composition and clinical outcome.

Various publications have now demonstrated a role for gut microbes in regulating responses to ICB therapy across several cancer types (Table 1). In a phase I clinical trial including ten patients with anti-PD-1-refractory metastatic melanoma (52), the researchers found that re-induction of anti-PD-1 combination with fecal microbiota transplantation (FMT) from complete response donors exhibited inspiring outcomes with clinical remission in three patients. Of them, FMT could remarkably increase the intra-tumoral immune activity, which supports the concept of overcoming resistance to immunotherapy through manipulating the intestinal microflora. Another multicenter retrospective study from Japan (53) revealed that probiotics administration was relevant to the survival and disease control in advanced or recurrent NSCLC patients that undergone anti-PD-1 monotherapy. Despite this, more thoughtful evaluations of the effects of current commercially available probiotic formulations on anticancer immunotherapy should be made, as they might be harmful in the setting of ICB therapy by impairing intra-tumoral IFN-γ T cell responses (40).

Interactions of gut microbiota with the toxicities related to ICB therapy

Evidence is accumulating that certain fecal microbiota composition is related to the development of several toxicities following ICB therapy such as irAEs, which result from off-tumor immune activation. McCulloch et al. (33) indicated that two microbial signatures, enriched for *Streptococcaceae* spp. and *Lachnospiraceae* spp., were involved in distinct irAEs, and

TABLE 1 Representative researches on the interactions between gut microbiota and the outcomes of ICB therapy across cancers in recent three years.

Patients	Studies	ICB agents	Main findings
NSCLC	Grenda et al. (34)	Pembrolizumab, n = 12, 25%; nivolumab or atezolizumab, n = 35, 75%	Favorable survival: a high abundance of *Bacteroidaaceae*, *Barnesiellaceae*, and *Tannerellaceae*; Inferior survival: a high content of *Ruminococcaceae* family while a low abundance of *Clostridia UCG-014*.
	Shoji et al. (35)	Nivolumab, pembrolizumab, atezolizumab, or durvalumab, n = 24, 85.7%; pembrolizumab combined with platinum-doublet chemotherapy, n = 4, 14.3%	Responders: higher gut alpha diversity; enrichment of *g_Blautia*; Non-responders: enrichment of *o_RF32* order.
	Newsome et al. (36)	Anti-PD-1, n = 44, 67.7%; anti-PD-L1, n = 19, 29.2%; combination of anti-PD-L1/CTLA-4, n = 2, 3.1%	Responders: enrichment of the genera *Ruminococcus*, *Akkermansia*, and *Faecalibacterium*.
	Zhang et al. (37)	A total of 69 patients receiving ICB monotherapy, including nivolumab, pembrolizumab, or atezolizumab	Prolonged survival: enrichment of *Phascolarctobacterium*; Reduced survival: overrepresentation of *Dialister*.
	Zhang et al. (38)	Nivolumab, n = 36, 48.0%; pembrolumab, n = 39, 52.0%	Responders: higher gut microbiota alpha diversity; enrichment of *Desulfovibrio*, *Actinomycetales*, *Bifidobacterium*, *Odoribacteraceae*, *Anaerostipes*, *Rikenellaceae*, *Faecalibacterium*, and *Alistipes*; Non-responders: overrepresentation of *Fusobacterales*, *Fusobacteriia*, *Fusobacterium*, *Fusobacteria*, and *Fusobacteriaceae*.
	Botticelli et al. (39)	Nivolumab, n =12, 100%	Clinical benefits: short chain fatty acids (i.e., propionate, butyrate), lysine and nicotinic acid were significantly associated with long-term beneficial effects; Disease progression: 2-Pentanone (ketone) and tridecane (alkane) were significantly associated with early progression.
Melanoma	McCulloch et al. (33)	A total of 94 patients receiving single-agent anti-PD-1 immunotherapy, including nivolumab, pembrolizumab or investigational anti-PD-1, or pembrolizumab in combination with pegylated interferon	Non-progressors: enrichment of *Ruminococcus* (*Mediterraneibacter*) *torques*, *Blautia producta*, *Blautia wexlerae*, *Blautia hansenii*, *Eubacterium rectale*, *Ruminococcus* (*Mediterraneibacter*) *gnavus* and *Anaerostipes hadrus*; Progressors: increased abundance of *Prevotella* spp., *Oscillibacter* spp., *Alistipes* spp. and *Sutterellaceae* spp.
	Spencer et al. (40)	Anti-PD-1, n = 132, 100%	Responders: higher abundance of *Ruminococcaceae* family and *Faecalibacterium* genus than non-responders.
	Andrews et al. (41)	A total of 77 patients receiving ipilimumab (anti-CTLA-4) in combination with PD-1 checkpoint blockade agent (either nivolumab or pembrolizumab)	Responders: enrichment of *Bacteroides stercoris*, *Parabacteroides distasonis* and *Fournierella massiliensis*; Non-responders: overrepresentation of *Klebsiella aerogenes* and *Lactobacillus rogosae*.
HCC	Lee et al. (42)	Nivolumab, n = 24, 58.5%; pembrolizumab, n = 17, 41.5%	Responders: enrichment of *Lachnoclostridium*, *Lachnospiraceae*, and *Veillonella*; Disease progression: overrepresentation of *Prevotella 9*.
	Wu et al. (43)	A total of 61 patients receiving intravenously anti-PD-1 based systemic therapy	Responders: enrichment of *Faecalibacterium*, *Blautia*, *Lachnospiracea incertae* Sedis, *Megamonas*, *Ruminococcus*, *Coprococcus*, *Dorea* and *Haemophilus*; Non-responders: overrepresentation of *Atopobium*, *Leptotrichia*, *Campylobacter*, *Allisonella*, *Methanobrevibacter*, *Parabacteroides*, *Bifidobacterium* and *Lactobacillus*.
	Ponziani et al. (44)	A total of 11 patients received tremelimumab, an anti-CTLA-4 monoclonal antibody, and/or Durvalumab, an anti-PD-L1 monoclonal antibody	Responders: enrichment of *Akkermansia* whereas depletion of *Enterobacteriaceae* in disease control group versus non-responders.
HBC	Mao et al. (45)	Thirty patients with HCC and 35 patients with biliary tract cancer who were treated with anti-PD-1 based systemic therapy	Favorable survival: enrichment of *Lachnospiraceae bacterium-GAM79*, *Alistipes sp Marseille-P5997*, *Ruminococcus calidus*, and *Erysipelotichaceae bacterium-GAM147*; Worse survival: higher abundance of *Veillonellaceae*.
CRC	Wang et al. (46)	Phase Ib/II study of regorafenib plus toripalimab enrolled forty-two subjects	Non-responders: increased relative abundance and positive detection rate of *Fusobacterium* than responders.
GC	Che et al. (47)	Nivolumab, n = 43, 55.8%; pembrolizumab, n = 29, 37.7%; camrelizumab/toripalimab/ tislelizumab, n = 5, 6.5%	*Helicobacter pylori*-negative group: a longer overall survival (OS) and progression-free survival (PFS) than those in the positive group, with an estimated median OS of 17.5 months vs. 6.2 months (HR = 2.85, 95% CI: 1.70-4.78; P = 0.021) and a median PFS of 8.4 months vs. 2.7 months (HR = 3.11, 95% CI: 1.96-5.07, P = 0.008); *H. pylori*-positive group: a higher risk of nonclinical response to anti-PD-1 antibody, with an OR of 2.91 (95% CI: 1.13-7.50).

(Continued)

TABLE 1 Continued

Patients	Studies	ICB agents	Main findings
GI cancer	Peng et al. (48)	Anti-PD-1, n = 48, 64.9%; anti-PD-L1, n = 12, 16.2%; anti-PD-1 + anti-CTLA-4, n = 14, 18.9%	Responders: an elevation of the *Prevotella*/*Bacteroides* ratio; moreover, gut bacteria with the ability of SCFA production, including *Eubacterium*, *Lactobacillus*, and *Streptococcus*, were positively associated with anti-PD-1/PD-L1 response across different GI cancer types (colorectal cancer, n = 19; esophageal cancer, n = 14; gastric cancer, n = 23; Others, n = 18).
RCC	Salgia et al. (49)	Nivolumab, n = 24, 77.4%; nivolumab plus ipilimumab, n = 7, 22.6%	Clinical benefits: a higher gut microbial alpha diversity according to the Shannon index; enrichment of *Bifidobacterium adolescentis*, *Barnesiella intestinihominis*, *Odoribacter splanchnicus*, and *Bacteroides eggerthii*.
Thoracic carcinoma※	Yin et al. (50)	A total of 42 patients receiving nivolumab or other anti-PD-1 inhibitors	Responders: enrichment of the *Akkermansiaceae*, *Enterococcaceae*, *Enterobacteriaceae*, *Carnobacteriaceae* and *Clostridiales Family XI* bacterial families.
Solid cancer tumors#	Cheng et al. (51)	A total of 72 patients receiving nivolumab, pembrolizumab, sintilimab, camrelizumab, and toripalimab	Responders: enrichment of *Archaea*, *Lentisphaerae*, *Victivallaceae*, *Victivallales*, *Lentisphaeria*, *Methanobacteriaceae*, *Methanobacteria*, *Euryarchaeota*, *Methanobrevibacter*, and *Methanobacteriales* before immunotherapy; Non-responders: increased in the abundance of *Clostridiaceae* before immunotherapy.

ICB, immune checkpoint blockade; NSCLC, non-small cell lung cancer; HCC, hepatocellular carcinoma; HBC, hepatobiliary cancer; CRC, colorectal cancer; GC, gastric cancer; GI, gastrointestinal; RCC, renal cell carcinoma; PD-1, programmed cell death protein 1; PD-L1, programmed cell death ligand 1; CTLA-4, cytotoxic T lymphocyte-associated antigen-4; OS, overall survival; PFS, progression-free survival. ※: included 23 lung squamous carcinomas, 15 lung adenocarcinomas, 1 SCLC, 1 NSCLC, 1 thymic squamous carcinoma, and 1 large cell neuroendocrine carcinoma; #: included 18 non-squamous NSCLC, 14 lung squamous cell carcinoma, 7 HCC, 5 GC, 5 CRC, 5 melanoma, 4 nasopharyngeal carcinoma, 3 cervical cancer, 2 small-cell lung cancer, and other cancers (1 case of laryngeal cancer, 1 case of osteosarcoma, 1 case of renal pelvic carcinoma, 1 case of bladder cancer, 1 case of pancreatic cancer, 1 case of esophageal cancer, 1 case of ureteral cancer, 1 case of mediastinal carcinoma, and 1 case of cholangiocarcinoma).

melanoma patients with high *Streptococcus* spp. abundance in pretreatment microbiome samples tended to develop irAEs. Although higher rates of irAEs than anti-PD-1 or anti-CTLA-4 monotherapy, responders to combined ICB therapy targeting both CTLA-4 and PD-1 and responders to monotherapy exhibited similar compositional characteristics of gut microbiota with an enrichment of *Ruminococcus*/*Ruminococcaceae* consistently observed across diverse melanoma cohorts (41). Moreover, the researchers found a significantly higher abundance of *Bacteroides intestinalis* in patients developed ≥grade 3 irAEs versus those who did not, with upregulation of mucosal IL-1β in patient samples of colitis and in pre-clinical models.

Disturbances of intestinal homeostasis play a key role in driving ICB-associated toxicity. $Stat3^{+/+}$ melanoma-bearing mice with acquired gastrointestinal impairment by *Citrobacter rodentium* infection and dextran sodium sulfate treatment displayed a predilection for anti-CTLA-4-mediated irAEs, with accumulation of neutrophils, cytotoxic and IFN-γ+ CD8+ and CD4+ T cells, and inflammatory cytokines such as IFN-γ and IL-6 in the colon (54). Furthermore, the pre-inflammation fecal microbiota of melanoma patients that presented a paucity of genetic pathways related to polyamine transport and B vitamin biosynthesis was linked with an increased risk of colitis (55). Remarkably, modulation of the gut microbiota can mitigate irAEs in cancers (56). Of them, ICB-related colitis could be successfully treated by FMT, with reconstitution of the intestinal microflora and increase in the proportion of regulatory T cells within the colonic mucosa (57). Additionally, microbial metabolites working at the interface between microorganisms and host immune system might abrogate ICB-induced colitis too. Renga et al. demonstrated that indole-3-carboxaldehyde, a microbial tryptophan catabolite, protected ICB-induced colitis mice from intestinal injury through a dual action on both the host and the microbes (58), which provides a new avenue in optimizing ICB therapy based on bacterial metabolome.

Prognostic utility of the gut microbiota-derived models for the outcome of ICB therapy

Gut microflora has emerged as a tumor-extrinsic predictive biomarker to the response of ICB therapy, and the machine learning models trained by microbial features provide a hopeful opportunity for outcome prediction. Recently, despite the heterogeneity across five melanoma cohorts, three modified leave-one-out cross-validation methods, including generalized linear model, random forest, and polynomial support-vector machine, based on batch-corrected intestinal microbiome data consistently predicted the outcomes to anti-PD-1 therapy in all cohorts (33). Of them, the *Clostridium* phylum was identified as a predictor of favorable outcome for a subset of cohorts, while the *Bacteroidetes* phylum was entertained as an unfavorable predictive indicator for the response of most melanoma cohorts. In addition, based on the bacterial signatures of five cancer cohorts, including melanoma, NSCLC, and renal cell carcinoma, treated with ICB, Shaikh et al. (59) constructed a non-responder "Integrated Microbiome Prediction Index" (calculated by assigning a weighted coefficient for the microbial species enriched in non-responders, including *Bacteroides coprocola*, *Bacteroides fragilis*, *Bacteroides thetaiotaomicron*, *Bacteroides uniformis*, *Clostridium hathewayi*, *Clostridium hylemonae*, *Clostridium methylpentosum*, *Megasphaera micronuciformis*, *Oribacterium sinus*, *Parasutterella excrementihominis*, *Scardovia wiggsiae*, and *Veillonella parvula*), rather than responder, that displayed the strongest and most

consistent signal using a random effects model, which highlighted a novel avenue to recognize specific patients that probably benefit from microbiota-derived interventions to improve the outcomes of ICB therapy.

Gut microbiota-derived metabolites mediate the responses of ICB therapy

The gut microbial metabolites, a vast array of small molecules produced or transformed by intestinal microorganisms, represent one of the primary patterns by which the gut microbiota regulate antitumor immunity response, which are capable of conferring both local and systemic effects by spreading from their original location in the gastrointestinal tract to circulatory system (10, 60). Accordingly, it is necessary to dissect the underlying mechanistic pathways through which the specific bacterial metabolites impact on antitumor immunity and immunotherapeutic responses (Figure 2). Most notably, short–chain fatty acids (SCFAs, mainly including acetate, propionate, and butyrate), synthetized by the bacterial fermentation of dietary fiber, play a central role in the complicated gut microbial immune and metabolic networks (61). Of them, the gut microbial metabolite butyrate has been reported to engage in the enhanced anti-PD-1 therapeutic efficacy through increasing the CD4+ and CD8+ T cell infiltration in the TME in the tumor-bearing mice humanized with the intestinal microbes from colorectal cancer (CRC) patients (62). Moreover, replenishing butyrate prior to anti-PD-1 treatment was sufficient to recover the therapeutic efficacy in the non-responders. Similarly, He and colleagues indicated that the SCFAs butyrate could directly potentiate the antitumor CD8+ T cell response *via* ID2-dependent IL-12 signaling (63), suggesting the potential beneficial roles of butyrate supplementation in anticancer immunity therapy. However, the roles of SCFAs in ICB therapy might be ambiguous. In a study conducted by Coutzac and colleagues in both mice and melanoma patients treated with anti-CTLA-4 monoclonal antibody, the authors found that SCFAs limited the efficacy of anti-CTLA-4 treatment. Namely, high levels of blood butyrate and propionate were involved in the resistance to CTLA-4 blockade and higher frequency of Treg cells, and butyrate could impede the accumulation of tumor-specific T cells and memory T cells (64). Therefore, further evaluations are warranted to reveal a more nuanced illustration for the effects of SCFAs on antitumor immune and the responses to ICB therapy.

In addition to SCFAs, other gut microbial metabolites also exhibit profound effects on the treatment of ICB. Strikingly, the bacterial metabolite inosine has been demonstrated to modulate enhanced ICB therapy response in mouse models of intestinal and

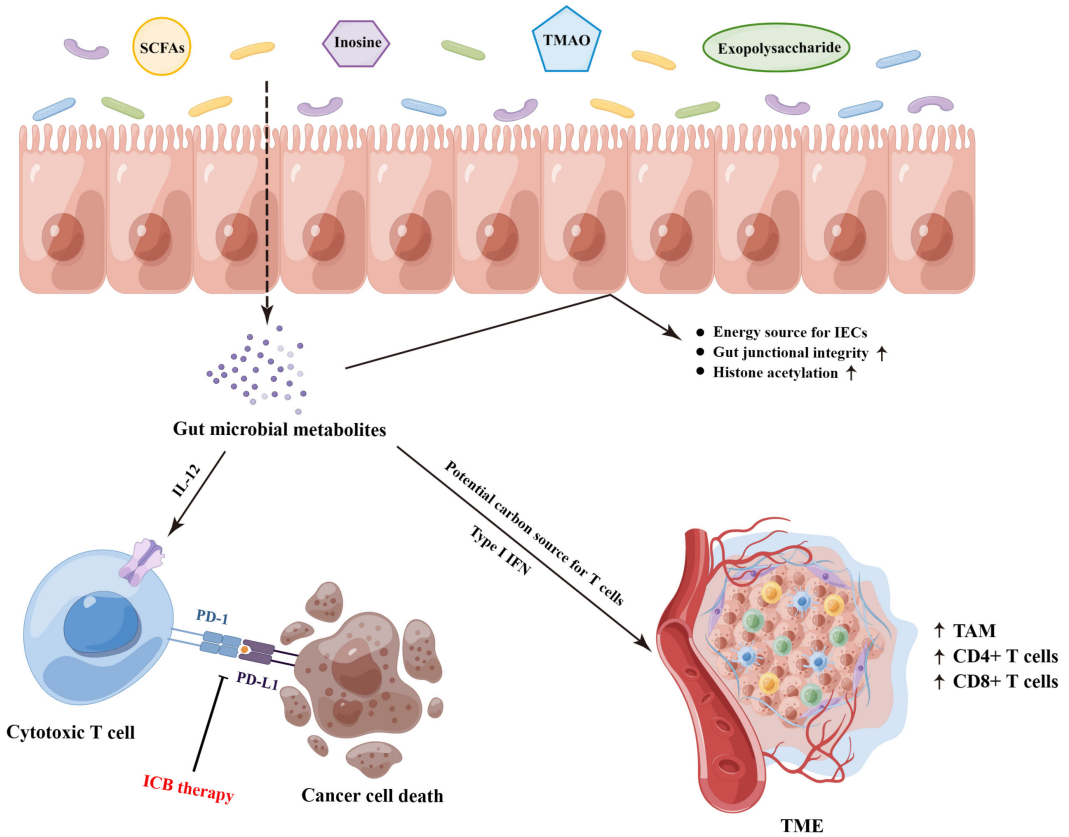

FIGURE 2
The underlying molecular mechanisms on the gut microbiota-derived metabolites that mediated the responses of ICB therapy. SCFAs, short–chain fatty acids; TMAO, trimethylamine N-oxide; IECs, intestinal epithelial cells; ICB, immune checkpoint blockade; TAM, tumor-associated macrophage; TME, tumor microenvironment. (By Figdraw).

epithelial tumors, which was dependent on T cell expression of the adenosine A_{2A} receptor to promote Th1 cell activation (65). Furthermore, as a substitute carbon source for the metabolism of T lymphocyte in glucose-restricted environments such as TME, inosine can assist T cell proliferation and differentiation while fueling sensitivity to ICB therapy (66). Another gut microbiota-derived metabolite trimethylamine N-oxide, identified as a driver of antitumor immunity, exhibited the ability to boost the response to ICB therapy in pancreatic cancer-bearing mouse model (67). Of them, the administration of trimethylamine N-oxide was related to an immunostimulatory tumor-associated macrophage phenotype, and activated effector T cell response in the TME in a type I IFN-dependent manner. Interestingly, Kawanabe-Matsuda et al. (68) illustrated that oral consumption of *Lactobacillus*-derived exopolysaccharide could bolster the efficacy of ICB therapy against CCL20-expressing tumors *via* inducing CCR6+ CD8+ T cells in Peyer's patches and improving the TME in experimental mouse tumor models, which provided compelling evidence on the dietary ingestion of exopolysaccharide for further clinical trials. Altogether, these studies lay the groundwork for the potential cancer immunotherapeutic strategies by targeting gut microbiota-derived metabolites.

Allogeneic hematopoietic stem cell transplantation

Allo-HSCT remains a curative approach for a range of hematological malignancies and might be recognized as one of the earliest effective modalities for cancer immunotherapy, but it is still hindered by high mortality rates, mainly because of graft-versus-host disease (GVHD) (69). Notably, at present the interactions between the intestinal microbiota and patient outcome after allo-HSCT have been well established (70). Particularly, ample evidence indicates an effect of gut microbial dysbiosis on GVHD. Furthermore, gut microbiota modulation through FMT also exhibits a promising revolution in the managements of allo-HSCT recipients, including ameliorating treatment-associated complications and improving patient outcomes.

Relationships between gut microbiota and allo-HSCT

Holler et al. (71) conducted a prospective research to collect stool specimens from 31 patients receiving allo-HSCT, and revealed that the loss of bacterial diversity and predominance of *enterococci* induced by systemic antibiotics might involve in the pronounced gastrointestinal GVHD for the first time. The patterns of microbial dysregulation during allo-HSCT were similar across diverse transplantation centers and geographic locations, and the depletion of gut diversity during allo-HSCT (accompanied by the domination of single taxa such as the genera *enterococcus* and *streptococcus*) has been observed to be linked with higher risks of transplantation-associated death in a large multi-center study (72). Recently, Andrlová and colleagues (73) indicated that a diverse gut microbiota early after allo-HSCT could produce more activating ligands for innate-like mucosal-associated invariant T cells and Vδ2 cells to maintain the immunological link between these populations, which contributed to improved OS and less acute GVHD. Furthermore, *Enterococcal* expansion after allo-HSCT as a remarkable risk factor for the occurrence of acute GVHD and reduced OS has been observed again in another multi-center study including 1325 recipients, and further be demonstrated in mouse models (74). Moreover, the researchers also found that posttransplant *enterococcal* enrichment was accompanied by the depletion of *clostridia*, with a significant reduction in fecal butyrate in both pre-clinical models and patients with GVHD. This result was consistent with a recent prospective single-center study that included 201 patients undergoing allo-HSCT and 28 healthy donors (75), indicating that butyrate-producing *Clostridiales* diminished early in the course of allo-HSCT, which was involved in the increased acute GVHD severity and transplantation associated mortality. In addition, it has also been illustrated that patients suffering chronic GVHD exhibited lower circulating concentrations of the butyrate and propionate in day 100 plasma samples (76). Most recently, Hino and colleagues (77) analyzed the gut microbial signatures of 59 long-term survivors (1-21.7 years; median, 6.4 years) after allo-HSCT, and found that intestinal dysbiosis with decreased abundance of the butyrate-producing bacteria was present over a 10-year lifetime after discharge following allo-HSCT. Of them, only limited chronic GVHD patients displayed no depletion of butyrate-producing *Faecalibacterium*. Similarly, a study including 541 patients admitted for allo-HSCT conducted by Peled et al. (78) indicated that patients with the dominance of another butyrate-producing *Eubacterium limosum* also displayed a close association with the reduced risk of relapse or progression of disease (hazard ratio [HR], 0.82 per 10-fold increase in abundance; 95% confidence interval (CI), 0.71 to 0.95; $P = .009$). Of note, as a major energy source for intestinal epithelial cells (IECs), evidence indicated that butyrate could improve IECs junctional integrity, decrease apoptosis and mitigate GVHD in mice, and the loss of butyrate led to reduced degree of histone acetylation in IECs (79).

Apart from the associations with GVHD, gut microbiota also has potential implications for a variety of other toxic effects, including *γ-proteobacteria* domination predicting pulmonary complications after engraftment (80), and gram-negative intestinal domination predicting subsequent bloodstream infection (81), while a more stable gut microbial configuration protecting febrile neutropenia (82), and three distinct bacterial taxa (*Bacteroidetes*, *Lachnospiraceae*, and *Ruminococcaceae*) protecting post-engraftment *Clostridium difficile* infection (83). In addition, it has to be noted the critical roles of intestinal microorganisms beyond bacteria played in allo-HSCT. Of them, Legoff and colleagues (84), characterizing the dynamic evolution of gut virome in 44 recipients during allo-HSCT by metagenomics, found that the overall proportion of vertebrate viral sequences in the guts of all recipients increased progressively during the weeks following transplantation, and the RNA viral reads from picobirnaviruses were predictive of later occurrence of severe enteric GVHD of stage 2 or higher (HR = 2.66; 95% CI = 1.46-

4.86; P = 0.001) through a time-dependent Cox proportional-hazards model. In addition, Rolling et al. (85) reported the fungal dysbiosis in a cohort of 156 patients during allo-HSCT by both longitudinal amplicon-based and culture-dependent analyses in 1279 fecal samples. Notably, *Candida parapsilosis* complex species, including *C. parapsilosis*, *C. orthopsilosis*, and *C. metapsilosis*, were the most common cultured fungi. Compared with those without pre-engraftment domination by *C. parapsilosis* complex species, patients with *C. parapsilosis* complex domination pre-engraftment exhibited a higher transplant-related mortality and worse OS.

Effects of the gut microbial modulation on allo-HSCT recipients

On the basis of these findings, there has been tremendous interests in gut microbial modulation with the aim to improve the outcome of patients undergoing allo-HSCT (86–88), including antibiotics, diets, prebiotics, probiotics, and FMT.

Antibiotics

Recently, Severyn and colleagues (89) found that gut decontamination, by oral vancomycin-polymyxin B in patients undergoing allo-HSCT, might protect recipients against gut-derived bloodstream infection by reducing the prevalence of gut pathogens. Additionally, previous research has suggested that occurrence of GVHD after allo-HSCT in obesity mice could be mitigated by prophylactic antibiotic treatment (90). Despite this, great caution should be exercised when delineating the effects of antibiotics on allo-HSCT as increasing evidence has illustrated the detrimental roles of antibiotic administration in recipients. A retrospective research examined 857 allo-HSCT recipients from Shono and colleagues (91) reported that the use of antibiotics such as imipenem-cilastatin and piperacillin-tazobactam were linked with elevated GVHD-related mortality at 5 years. Through GVHD mice model, the authors further illustrated that imipenem-cilastatin treatment led to the loss of the protective mucus lining of the colon and intestinal barrier impairment, which might be explained by the enrichment of mucus-degrading *Akkermansia muciniphila*. Furthermore, an increased risk of patients occurring acute and intestinal GVHD by gut decontamination and prophylaxis has also been revealed in a meta-analysis of 18 references (92). Of note, the conflicting clinical results regarding the influence of antibiotics on the outcome of allo-HSCT might be explained by the different types of antibiotics and timing of treatment (87).

Diets, prebiotics, and probiotics

Dietary elements and nutritional strategies have been increasingly evaluated regarding the impact on allo-HSCT outcomes through modulating intestinal microorganisms (93). It has been revealed that mice with diet-induced obesity exhibited reduced survival associated with acute and severe gut GVHD, which was consistent with the inferior survival of allo-HSCT recipients with a high body mass index (BMI, >30) that presented decreased gut diversity and *Clostridiaceae* abundance (90). In addition, Li and colleagues (94) demonstrated the roles of tyrosine in acute GVHD murine models. Specifically, additional tyrosine supplementation could significantly prolong OS, alleviate symptoms at the early stage of acute GVHD by regulating the microbial composition and fecal metabolic phenotype. Likewise, prebiotic intake has also been observed to be an effective strategy for preventing acute GVHD in allo-HSCT in a prospective study (95). Namely, from pre-transplantation conditioning to day 28 after allo-HSCT, the combined administration of resistant starch and a commercially available prebiotics mixture (including glutamine, fiber, and oligosaccharide) decreased the incidence of all acute GVHD grades combined and of acute GVHD grades 2 to 4, and maintained the intestinal diversity and butyrate-producing bacterial population.

Compared with prebiotics, probiotics are viable microorganisms for healthy gut restoration. Importantly, the protective roles of the butyrate-producing *Clostridia* have been well demonstrated in preclinical allo-HSCT models (79, 96). Of them, Mathewson and colleagues (79) indicated that altering the indigenous microbiota, using the cocktail of 17 rationally selected *Clostridial* strains with the ability to produce high amounts of butyrate, could remarkably attenuate GVHD severity and improve survival. Furthermore, the safety and feasibility of another probiotic: *Lactobacillus plantarum* (LBP), have been also evaluated in children and adolescents undergoing allo-HSCT (97), and with no cases of LBP-bacteremia or LBP-associated severe adverse events recorded. Nevertheless, the safety and efficacy of probiotics in HSCT therapy remain elusive. For example, *Lactobacillus acidophilus* sepsis secondary to the excessive consumption of probiotic-enriched yogurt has been reported in a case with mantle cell lymphoma receiving HSCT (98).

Fecal microbiota transplantation

FMT refers to the transfer of fecal microbial content from a healthy donor to the intestine of a recipient (99), and represents a promising approach for the management of allo-HSCT patients (88), including alleviating infection of multidrug-resistant bacteria and GVHD, as well as promoting gut microbiota reconstitution. Bluestone and colleagues (100) reported that FMT displayed better safety and tolerance in three children developing recurrent *Clostridium difficile* infection after allo-HSCT, and one case did obtain successful clearance of *C. difficile* at follow-up 1 year 10 months after the FMT. Moreover, the safety and efficacy of FMT in the decolonization of multidrug-resistant bacteria, including vancomycin-resistant *enterococci* (n=2) or carbapenemase-producing bacteria (n=8), have also been presented in ten allo-HSCT patients with hematologic malignancies (101). Of them, seven of ten patients achieved decolonization and almost all patients without severe infectious events occurred during the first three months after FMT.

In a prospective, single-center, single-arm study enrolling 15 patients with steroid-refractory or steroid-dependent, acute or late-onset acute intestinal GVHD suffering allo-HSCT, van Lier et al. (102) found that ten of 15 subjects obtained a complete clinical

response within 1 month after FMT, with a partial engraftment of donor microbial species, increased gut microbial α-diversity, and enrichment of butyrate-producing *Clostridiales* and *Blautia* species. As mentioned above, loss of intestinal diversity involves unfavorable allo-HSCT outcomes. Interestingly, FMT after allo-HSCT tends to be related to the improvement of recipients' gut diversity that could be attributable to expansion of stool-donor taxa (103). In addition, it has been reported that autologous FMT (feces were provided by participants before the initiation of allo-HSCT), after microbiota-depleting antibiotic treatment, had the ability to boost microbial diversity and reestablished the commensal bacterial populations at the critical early immune reconstitution stage after allo-HSCT (104). Taken together, although FMT seemed safe and well-tolerated, further larger prospective studies are urgently required to deal with several safety concerns such as potential risks of infection upon FMT in these immunocompromised patients.

Chimeric antigen receptor T cell therapy

CAR-T cell therapy stands at the novel forefront of current cancer therapy, which has demonstrated unprecedented responses in patients with high-risk hematologic malignancies, including lymphoma, leukemia, and multiple myeloma (105–108). CAR-T cell therapy involves genetically modified T cells that express specific CAR, followed by *in vitro* cell amplification and reinfusion back into the patient to eradicate tumors (109). Given the intimate interactions of gut microflora with human T cell function and anti-tumor immunity (110, 111), it is not unexpected that the interactions and potential mechanisms of gut microbiota with CAR-T cell therapy have begun to be investigated in recent years (112, 113). Of them, Uribe-Herranz et al. (114) illustrated that gut microflora could modulate the anti-tumor efficacy of adoptive T cell therapy, mediated by $CD8\alpha^+$ dendritic cells and IL-12, in the tumor-bearing mice model.

Although the success of CAR-T cell therapy, several obstacles, including CAR-mediated toxicities, CAR-T cell dysfunction, antigen loss, tumor heterogeneity, and disease relapse, have impeded the utility of CAR-T cell therapy. Therefore, biomarkers for the favorable prognostic identification of patients receiving CAR-T cells are urgently needed. Inspiringly, in a multi-center retrospective study including patients with B-cell lymphoma and leukemia, Smith et al. (115) found that exposure to antibiotics prior to CD19 CAR-T cell infusion was involved in significantly inferior survival and increased immune effector cell-associated neurotoxicity syndrome. Moreover, enrichment of certain members within the class *Clostridia*, including *Faecalibacterium*, *Ruminococcus*, and *Bacteroides*, were linked with day 100 complete response to CAR-T cell therapy. Similarly, Hu and colleagues (116) also revealed the significant differences in the abundance of *Bifidobacterium*, *Prevotella*, *Sutterella*, and *Collinsella* between multiple myeloma patients in complete remission and those in partial remission, and observed a higher abundance of *Bifidobacterium*, *Leuconostoc*, *Stenotrophomonas*, and *Staphylococcus* in patients with severe cytokine release syndrome. Altogether, despite the research on the role of intestinal microbiota in CAR-T cell therapy is still at the very earliest stages, these findings suggest the tremendous potential of gut microbiota as a non-invasive prognostic marker for CAR-T cell therapy, and provide a novel reference to alleviate CAR-T cell therapy-induced toxic effects and to improve therapeutic outcome by modulating the gut microbiota.

Future perspectives and current challenges

Although major strides have been made toward the treatment of cancers, there remain many patients succumb to their disease (117). However, different from the stability of human genome, the modifiable nature of gut microbiota renders it a promising opportunity for cancer therapy (118). And meanwhile, there are emerging lines of evidence suggest the therapeutic potential of microbiotherapy by targeting the microbial flora. Among these, FMT appears central in the intervention options to restore microbial richness, as well as amend microbial dysbiosis and altered host-microbiota symbiosis related to cancer genesis and treatment (70). Moreover, utilizing bacteria strains or its proteins and peptides substances, including bacteriocins and toxins, as the anticancer agents on various cancers, termed bacteriotherapy, has also attracted salient attention, which can be employed alone or in conjunction with traditional therapies as an enhancer (119). Of interest, Montalban-Arques et al. (120) reported that oral supplementations of a mix of four *Clostridiales* species, namely *Roseburia intestinalis*, *Eubacterium hallii*, *Faecalibacterium prausnitzii*, and *Anaerostipes caccae*, outperformed anti-PD-1 therapy in mouse models of CRC and melanoma, which provided a strong preclinical foundation for exploring gut flora as novel stand-alone therapy against solid tumors. Additionally, despite the safety of probiotics in the management of cancer patients remains largely undefined, several gut next-generation probiotics such as *Faecalibacterium prausnitzii*, *Akkermansia muciniphila*, and *Bacteroides fragilis* exhibit their beneficial roles in supporting cancer therapy (121).

Most importantly, with mounting evidence of microorganisms colonizing tumors, synthetic biology approaches are being leveraged to improve the effectiveness of bacteriotherapy agents by repurposing bacteria. As an intelligent medicine, engineering bacteria are able to demonstrate autonomous control, sensing and responding to the internalization process, and subsequently releasing cargo (122). Furthermore, combinations of engineering bacteria with drug-loaded nanoparticles, monoclonal antibodies, oncolytic virus, and even CAR-T cells will also open charming options in oncology (123, 124).

Following the tremendous advances of cultivation-independent technologies and microbial analysis tools, the profiles of gut microbiota have been extensively revealed. While much attention has been given to gut bacteria, the contributions of other intestinal microorganisms such as viruses and fungi to cancer genesis and

treatment also deserve further scrutiny. Furthermore, given the overlapped alterations of gut species across cancers (125, 126), future work is warranted to clarify the roles of gut microbiota-derived strategies, using machine learning algorithms, in precise risk stratification, prognostication, and therapeutic decision-making of cancer patients.

Although we believe that modulation of gut microflora will probably be the next vanguard in the management of cancer patients, however, several potential challenges should be mentioned. First, the exact mechanisms of action between gut dysbiosis and cancer genesis and therapy remain poorly characterized, and proofs of causation between them are still lacking. Therefore, continual efforts should be made to rationally select intestinal probiotics. On top of that, as a living body, the complexity of bacteria determines the hardships and risks such as biocontainment and safety concerns of transforming them into weapons to fight against cancers. Finally, considering the complex physiological conditions such as gastric acid and diverse enzymes that might digest or deactivate bacteriotherapy agents before they reach the action site, appropriate delivery route and dose of administration are also need to be investigated during clinical translations.

Conclusion

In recent years, overwhelming pre-clinical and patient-oriented evidence supports a critical role of gut microbiota in cancer immunotherapies such as improving efficacy and mitigating toxicity, and the manipulation of gut microbiota confers a promising therapeutic strategy for the clinical management of malignancies as well. Currently, microbiotherapy for cancers is still in its infancy. With the formidable challenges notwithstanding, it deserves further mechanistic dissection by cellular and animal studies as well as validation with larger longitudinal clinical cohorts.

Author contributions

MZ, ZL, and ZS conceived the study. ZS, HL, WS, and ZZ collected the related references and participated in the discussion. ZS and ZL drafted the manuscript and prepared the figures. MZ and ZS revised the manuscript. All authors contributed to the article and approved the submitted version.

Funding

This work was supported by the Funds for Creative Research Groups of the First Affiliated Hospital of Zhengzhou university (QNCXTD2023012) and the National Natural Science Foundation of China (81970184; 82170183; U1904139; 82070209).

Conflict of interest

The authors declare that the research was conducted in the absence of any commercial or financial relationships that could be construed as a potential conflict of interest.

Publisher's note

References

1. Aggarwal N, Kitano S, Puah GRY, Kittelmann S, Hwang IY, Chang MW. Microbiome and human health: Current understanding, engineering, and enabling technologies. *Chem Rev* (2023) 123(1):31–72. doi: 10.1021/acs.chemrev.2c00431

2. de Vos WM, Tilg H, Van Hul M, Cani PD. Gut microbiome and health: mechanistic insights. *Gut* (2022) 71(5):1020–32. doi: 10.1136/gutjnl-2021-326789

3. Scott AJ, Alexander JL, Merrifield CA, Cunningham D, Jobin C, Brown R, et al. International cancer microbiome consortium consensus statement on the role of the human microbiome in carcinogenesis. *Gut* (2019) 68(9):1624–32. doi: 10.1136/gutjnl-2019-318556

4. Fan Y, Pedersen O. Gut microbiota in human metabolic health and disease. *Nat Rev Microbiol* (2021) 19(1):55–71. doi: 10.1038/s41579-020-0433-9

5. Shi Z, Zhang M. Emerging roles for the gut microbiome in lymphoid neoplasms. *Clin Med Insights Oncol* (2021) 15:11795549211024197. doi: 10.1177/11795549211024197

6. Cullin N, Azevedo Antunes C, Straussman R, Stein-Thoeringer CK, Elinav E. Microbiome and cancer. *Cancer Cell* (2021) 39(10):1317–41. doi: 10.1016/j.ccell.2021.08.006

7. Bhatt AP, Redinbo MR, Bultman SJ. The role of the microbiome in cancer development and therapy. *CA Cancer J Clin* (2017) 67(4):326–44. doi: 10.3322/caac.21398

8. Kocarnik JM, Compton K, Dean FE, Fu W, Gaw BL, Harvey JD, et al. Cancer incidence, mortality, years of life lost, years lived with disability, and disability-adjusted life years for 29 cancer groups from 2010 to 2019: A systematic analysis for the global burden of disease study 2019. *JAMA Oncol* (2022) 8(3):420–44. doi: 10.1001/jamaoncol.2021.6987

9. Liu L, Shah K. The potential of the gut microbiome to reshape the cancer therapy paradigm: A review. *JAMA Oncol* (2022) 8(7):1059–67. doi: 10.1001/jamaoncol.2022.0494

10. Wang Y, Zhang H, Liu C, Wang Z, Wu W, Zhang N, et al. Immune checkpoint modulators in cancer immunotherapy: Recent advances and emerging concepts. *J Hematol Oncol* (2022) 15(1):111. doi: 10.1186/s13045-022-01225-3

11. Gopalakrishnan V, Helmink BA, Spencer CN, Reuben A, Wargo JA. The influence of the gut microbiome on cancer, immunity, and cancer immunotherapy. *Cancer Cell* (2018) 33(4):570–80. doi: 10.1016/j.ccell.2018.03.015

12. Ribas A, Wolchok JD. Cancer immunotherapy using checkpoint blockade. *Science* (2018) 359(6382):1350–5. doi: 10.1126/science.aar4060

13. Robert C, Thomas L, Bondarenko I, O'Day S, Weber J, Garbe C, et al. Ipilimumab plus dacarbazine for previously untreated metastatic melanoma. *New Engl J Med* (2011) 364(26):2517–26. doi: 10.1056/NEJMoa1104621

14. Ansell SM, Lesokhin AM, Borrello I, Halwani A, Scott EC, Gutierrez M, et al. PD-1 blockade with nivolumab in relapsed or refractory hodgkin's lymphoma. *New Engl J Med* (2015) 372(4):311–9. doi: 10.1056/NEJMoa1411087

15. Reck M, Rodríguez-Abreu D, Robinson AG, Hui R, Csőszi T, Fülöp A, et al. Pembrolizumab versus chemotherapy for PD-L1-Positive non-Small-Cell lung cancer. *New Engl J Med* (2016) 375(19):1823–33. doi: 10.1056/NEJMoa1606774

16. Le DT, Uram JN, Wang H, Bartlett BR, Kemberling H, Eyring AD, et al. PD-1 blockade in tumors with mismatch-repair deficiency. *New Engl J Med* (2015) 372(26):2509–20. doi: 10.1056/NEJMoa1500596

17. Morad G, Helmink BA, Sharma P, Wargo JA. Hallmarks of response, resistance, and toxicity to immune checkpoint blockade. *Cell* (2021) 184(21):5309–37. doi: 10.1016/j.cell.2021.09.020

18. Elkrief A, Derosa L, Kroemer G, Zitvogel L, Routy B. The negative impact of antibiotics on outcomes in cancer patients treated with immunotherapy: a new independent prognostic factor? *Ann Oncol* (2019) 30(10):1572–9. doi: 10.1093/annonc/mdz206

19. Derosa L, Hellmann MD, Spaziano M, Halpenny D, Fidelle M, Rizvi H, et al. Negative association of antibiotics on clinical activity of immune checkpoint inhibitors in patients with advanced renal cell and non-small-cell lung cancer. *Ann Oncol* (2018) 29(6):1437–44. doi: 10.1093/annonc/mdy103

20. Mohiuddin JJ, Chu B, Facciabene A, Poirier K, Wang X, Doucette A, et al. Association of antibiotic exposure with survival and toxicity in patients with melanoma receiving immunotherapy. *J Natl Cancer Inst* (2021) 113(2):162–70. doi: 10.1093/jnci/djaa057

21. Hopkins AM, Kichenadasse G, Karapetis CS, Rowland A, Sorich MJ. Concomitant antibiotic use and survival in urothelial carcinoma treated with atezolizumab. *Eur Urol* (2020) 78(4):540–3. doi: 10.1016/j.eururo.2020.06.061

22. Pederzoli F, Bandini M, Raggi D, Marandino L, Basile G, Alfano M, et al. Is there a detrimental effect of antibiotic therapy in patients with muscle-invasive bladder cancer treated with neoadjuvant pembrolizumab? *Eur Urol* (2021) 80(3):319–22. doi: 10.1016/j.eururo.2021.05.018

23. Cheung KS, Lam LK, Seto WK, Leung WK. Use of antibiotics during immune checkpoint inhibitor treatment is associated with lower survival in hepatocellular carcinoma. *Liver Cancer* (2021) 10(6):606–14. doi: 10.1159/000518090

24. Fessas P, Naeem M, Pinter M, Marron TU, Szafron D, Balcar L, et al. Early antibiotic exposure is not detrimental to therapeutic effect from immunotherapy in hepatocellular carcinoma. *Liver Cancer* (2021) 10(6):583–92. doi: 10.1159/000519108

25. Routy B, Gopalakrishnan V, Daillere R, Zitvogel L, Wargo JA, Kroemer G. The gut microbiota influences anticancer immunosurveillance and general health. *Nat Rev Clin Oncol* (2018) 15(6):382–96. doi: 10.1038/s41571-018-0006-2

26. Sivan A, Corrales L, Hubert N, Williams JB, Aquino-Michaels K, Earley ZM, et al. Commensal bifidobacterium promotes antitumor immunity and facilitates anti-PD-L1 efficacy. *Science* (2015) 350(6264):1084–9. doi: 10.1126/science.aac4255

27. Vétizou M, Pitt JM, Daillère R, Lepage P, Waldschmitt N, Flament C, et al. Anticancer immunotherapy by CTLA-4 blockade relies on the gut microbiota. *Science* (2015) 350(6264):1079–84. doi: 10.1126/science.aad1329

28. Matson V, Fessler J, Bao R, Chongsuwat T, Zha Y, Alegre ML, et al. The commensal microbiome is associated with anti-PD-1 efficacy in metastatic melanoma patients. *Science* (2018) 359(6371):104–8. doi: 10.1126/science.aao3290

29. Gopalakrishnan V, Spencer CN, Nezi L, Reuben A, Andrews MC, Karpinets TV, et al. Gut microbiome modulates response to anti-PD-1 immunotherapy in melanoma patients. *Science* (2018) 359(6371):97–103. doi: 10.1126/science.aan4236

30. Zheng Y, Wang T, Tu X, Huang Y, Zhang H, Tan D, et al. Gut microbiome affects the response to anti-PD-1 immunotherapy in patients with hepatocellular carcinoma. *J Immunother Cancer* (2019) 7(1):193. doi: 10.1186/s40425-019-0650-9

31. Jin Y, Dong H, Xia L, Yang Y, Zhu Y, Shen Y, et al. The diversity of gut microbiome is associated with favorable responses to anti-programmed death 1 immunotherapy in Chinese patients with NSCLC. *J Thorac Oncol* (2019) 14(8):1378–89. doi: 10.1016/j.jtho.2019.04.007

32. Oster P, Vaillant L, Riva E, McMillan B, Begka C, Truntzer C, et al. Helicobacter pylori infection has a detrimental impact on the efficacy of cancer immunotherapies. *Gut* (2022) 71(3):457–66. doi: 10.1136/gutjnl-2020-323392

33. McCulloch JA, Davar D, Rodrigues RR, Badger JH, Fang JR, Cole AM, et al. Intestinal microbiota signatures of clinical response and immune-related adverse events in melanoma patients treated with anti-PD-1. *Nat Med* (2022) 28(3):545–56. doi: 10.1038/s41591-022-01698-2

34. Grenda A, Iwan E, Krawczyk P, Frąk M, Chmielewska I, Bomba A, et al. Attempting to identify bacterial allies in immunotherapy of NSCLC patients. *Cancers (Basel)* (2022) 14(24):6250. doi: 10.3390/cancers14246250

35. Shoji F, Yamaguchi M, Okamoto M, Takamori S, Yamazaki K, Okamoto T, et al. Gut microbiota diversity and specific composition during immunotherapy in responders with non-small cell lung cancer. *Front Mol Biosci* (2022) 9:1040424. doi: 10.3389/fmolb.2022.1040424

36. Newsome RC, Gharaibeh RZ, Pierce CM, da Silva WV, Paul S, Hogue SR, et al. Interaction of bacterial genera associated with therapeutic response to immune checkpoint PD-1 blockade in a united states cohort. *Genome Med* (2022) 14(1):35. doi: 10.1186/s13073-022-01037-7

37. Zhang F, Ferrero M, Dong N, D'Auria G, Reyes-Prieto M, Herreros-Pomares A, et al. Analysis of the gut microbiota: An emerging source of biomarkers for immune checkpoint blockade therapy in non-small cell lung cancer. *Cancers (Basel)* (2021) 13(11):2514. doi: 10.3390/cancers13112514

38. Zhang C, Wang J, Sun Z, Cao Y, Mu Z, Ji X. Commensal microbiota contributes to predicting the response to immune checkpoint inhibitors in non-small-cell lung cancer patients. *Cancer Sci* (2021) 112(8):3005–17. doi: 10.1111/cas.14979

39. Botticelli A, Vernocchi P, Marini F, Quagliariello A, Cerbelli B, Reddel S, et al. Gut metabolomics profiling of non-small cell lung cancer (NSCLC) patients under immunotherapy treatment. *J Trans Med* (2020) 18(1):49. doi: 10.1186/s12967-020-02231-0

40. Spencer CN, McQuade JL, Gopalakrishnan V, McCulloch JA, Vetizou M, Cogdill AP, et al. Dietary fiber and probiotics influence the gut microbiome and melanoma immunotherapy response. *Science* (2021) 374(6575):1632–40. doi: 10.1126/science.aaz7015

41. Andrews MC, Duong CPM, Gopalakrishnan V, Iebba V, Chen WS, Derosa L, et al. Gut microbiota signatures are associated with toxicity to combined CTLA-4 and PD-1 blockade. *Nat Med* (2021) 27(8):1432–41. doi: 10.1038/s41591-021-01406-6

42. Lee PC, Wu CJ, Hung YW, Lee CJ, Chi CT, Lee IC, et al. Gut microbiota and metabolites associate with outcomes of immune checkpoint inhibitor-treated unresectable hepatocellular carcinoma. *J Immunother Cancer* (2022) 10(6):e004779. doi: 10.1136/jitc-2022-004779

43. Wu H, Zheng X, Pan T, Yang X, Chen X, Zhang B, et al. Dynamic microbiome and metabolome analyses reveal the interaction between gut microbiota and anti-PD-1 based immunotherapy in hepatocellular carcinoma. *Int J Cancer* (2022) 151(8):1321–34. doi: 10.1002/ijc.34118

44. Ponziani FR, De Luca A, Picca A, Marzetti E, Petito V, Del Chierico F, et al. Gut dysbiosis and fecal calprotectin predict response to immune checkpoint inhibitors in patients with hepatocellular carcinoma. *Hepatol Commun* (2022) 6(6):1492–501. doi: 10.1002/hep4.1905

45. Mao J, Wang D, Long J, Yang X, Lin J, Song Y, et al. Gut microbiome is associated with the clinical response to anti-PD-1 based immunotherapy in hepatobiliary cancers. *J Immunother Cancer* (2021) 9(12):e003334. doi: 10.1136/jitc-2021-003334

46. Wang F, He MM, Yao YC, Zhao X, Wang ZQ, Jin Y, et al. Regorafenib plus toripalimab in patients with metastatic colorectal cancer: a phase Ib/II clinical trial and gut microbiome analysis. *Cell Rep Med* (2021) 2(9):100383. doi: 10.1016/j.xcrm.2021.100383

47. Che H, Xiong Q, Ma J, Chen S, Wu H, Xu H, et al. Association of helicobacter pylori infection with survival outcomes in advanced gastric cancer patients treated with immune checkpoint inhibitors. *BMC Cancer* (2022) 22(1):904. doi: 10.1186/s12885-022-10004-9

48. Peng Z, Cheng S, Kou Y, Wang Z, Jin R, Hu H, et al. The gut microbiome is associated with clinical response to anti-PD-1/PD-L1 immunotherapy in gastrointestinal cancer. *Cancer Immunol Res* (2020) 8(10):1251–61. doi: 10.1158/2326-6066.CIR-19-1014

49. Salgia NJ, Bergerot PG, Maia MC, Dizman N, Hsu J, Gillece JD, et al. Stool microbiome profiling of patients with metastatic renal cell carcinoma receiving anti-PD-1 immune checkpoint inhibitors. *Eur Urol* (2020) 78(4):498–502. doi: 10.1016/j.eururo.2020.07.011

50. Yin H, Yang L, Peng G, Yang K, Mi Y, Hu X, et al. The commensal consortium of the gut microbiome is associated with favorable responses to anti-programmed death protein 1 (PD-1) therapy in thoracic neoplasms. *Cancer Biol Med* (2021) 18(4):1040–52. doi: 10.20892/j.issn.2095-3941.2020.0450

51. Cheng X, Wang J, Gong L, Dong Y, Shou J, Pan H, et al. Composition of the gut microbiota associated with the response to immunotherapy in advanced cancer patients: A Chinese real-world pilot study. *J Clin Med* (2022) 11(18):5479. doi: 10.3390/jcm11185479

52. Baruch EN, Youngster I, Ben-Betzalel G, Ortenberg R, Lahat A, Katz L, et al. Fecal microbiota transplant promotes response in immunotherapy-refractory melanoma patients. *Science* (2021) 371(6529):602–9. doi: 10.1126/science.abb5920

53. Takada K, Shimokawa M, Takamori S, Shimamatsu S, Hirai F, Tagawa T, et al. Clinical impact of probiotics on the efficacy of anti-PD-1 monotherapy in patients with nonsmall cell lung cancer: A multicenter retrospective survival analysis study with inverse probability of treatment weighting. *Int J Cancer* (2021) 149(2):473–82. doi: 10.1002/ijc.33557

54. Zhou Y, Medik YB, Patel B, Zamler DB, Chen S, Chapman T, et al. Intestinal toxicity to CTLA-4 blockade driven by IL-6 and myeloid infiltration. *J Exp Med* (2023) 220(2):e20221333. doi: 10.1084/jem.20221333

55. Dubin K, Callahan MK, Ren B, Khanin R, Viale A, Ling L, et al. Intestinal microbiome analyses identify melanoma patients at risk for checkpoint-blockade-induced colitis. *Nat Commun* (2016) 7:10391. doi: 10.1038/ncomms10391

56. Chang AE, Golob JL, Schmidt TM, Peltier DC, Lao CD, Tewari M. Targeting the gut microbiome to mitigate immunotherapy-induced colitis in cancer. *Trends Cancer* (2021) 7(7):583–93. doi: 10.1016/j.trecan.2021.02.005

57. Wang Y, Wiesnoski DH, Helmink BA, Gopalakrishnan V, Choi K, DuPont HL, et al. Fecal microbiota transplantation for refractory immune checkpoint inhibitor-associated colitis. *Nat Med* (2018) 24(12):1804–8. doi: 10.1038/s41591-018-0238-9

58. Renga G, Nunzi E, Pariano M, Puccetti M, Bellet MM, Pieraccini G, et al. Optimizing therapeutic outcomes of immune checkpoint blockade by a microbial tryptophan metabolite. *J Immunother Cancer* (2022) 10(3):e003725. doi: 10.1136/jitc-2021-003725

59. Shaikh FY, White JR, Gills JJ, Hakozaki T, Richard C, Routy B, et al. A uniform computational approach improved on existing pipelines to reveal microbiome biomarkers of nonresponse to immune checkpoint inhibitors. *Clin Cancer Res* (2021) 27(9):2571–83. doi: 10.1158/1078-0432.CCR-20-4834

60. Krautkramer KA, Fan J, Backhed F. Gut microbial metabolites as multi-kingdom intermediates. *Nat Rev Microbiol* (2021) 19(2):77–94. doi: 10.1038/s41579-020-0438-4

61. Deleu S, Machiels K, Raes J, Verbeke K, Vermeire S. Short chain fatty acids and its producing organisms: An overlooked therapy for IBD? *EBioMedicine* (2021) 66:103293. doi: 10.1016/j.ebiom.2021.103293

62. Zhang SL, Mao YQ, Zhang ZY, Li ZM, Kong CY, Chen HL, et al. Pectin supplement significantly enhanced the anti-PD-1 efficacy in tumor-bearing mice humanized with gut microbiota from patients with colorectal cancer. *Theranostics* (2021) 11(9):4155–70. doi: 10.7150/thno.54476

63. He Y, Fu L, Li Y, Wang W, Gong M, Zhang J, et al. Gut microbial metabolites facilitate anticancer therapy efficacy by modulating cytotoxic CD8(+) T cell immunity. *Cell Metab* (2021) 33(5):988–1000 e7. doi: 10.1016/j.cmet.2021.03.002

64. Coutzac C, Jouniaux JM, Paci A, Schmidt J, Mallardo D, Seck A, et al. Systemic short chain fatty acids limit antitumor effect of CTLA-4 blockade in hosts with cancer. *Nat Commun* (2020) 11(1):2168. doi: 10.1038/s41467-020-16079-x

65. Mager LF, Burkhard R, Pett N, Cooke NCA, Brown K, Ramay H, et al. Microbiome-derived inosine modulates response to checkpoint inhibitor immunotherapy. *Science* (2020) 369(6510):1481–9. doi: 10.1126/science.abc3421

66. Samami E, Aleebrahim-Dehkordi E, Mohebalizadeh M, Yaribash S, Saghazadeh A, Rezaei N. Inosine, gut microbiota, and cancer immunometabolism. *Am J Physiol Endocrinol Metab* (2023) 324(1):E1–e8. doi: 10.1152/ajpendo.00207.2022

67. Mirji G, Worth A, Bhat SA, El Sayed M, Kannan T, Goldman AR, et al. The microbiome-derived metabolite TMAO drives immune activation and boosts responses to immune checkpoint blockade in pancreatic cancer. *Sci Immunol* (2022) 7(75): eabn0704. doi: 10.1126/sciimmunol.abn0704

68. Kawanabe-Matsuda H, Takeda K, Nakamura M, Makino S, Karasaki T, Kakimi K, et al. Dietary lactobacillus-derived exopolysaccharide enhances immune-checkpoint blockade therapy. *Cancer Discovery* (2022) 12(5):1336–55. doi: 10.1158/2159-8290.CD-21-0929

69. Chang YJ, Pei XY, Huang XJ. Haematopoietic stem-cell transplantation in China in the era of targeted therapies: current advances, challenges, and future directions. *Lancet Haematol* (2022) 9(12):e919–e29. doi: 10.1016/S2352-3026(22)00293-9

70. Malard F, Gaugler B, Mohty M. Faecal microbiota transplantation in patients with haematological malignancies undergoing cellular therapies: From translational research to routine clinical practice. *Lancet Haematol* (2022) 9(10):e776–e85. doi: 10.1016/S2352-3026(22)00223-X

71. Holler E, Butzhammer P, Schmid K, Hundsrucker C, Koestler J, Peter K, et al. Metagenomic analysis of the stool microbiome in patients receiving allogeneic stem cell transplantation: loss of diversity is associated with use of systemic antibiotics and more pronounced in gastrointestinal graft-versus-host disease. *Biol Blood Marrow Transplant* (2014) 20(5):640–5. doi: 10.1016/j.bbmt.2014.01.030

72. Peled JU, Gomes ALC, Devlin SM, Littmann ER, Taur Y, Sung AD, et al. Microbiota as predictor of mortality in allogeneic hematopoietic-cell transplantation. *New Engl J Med* (2020) 382(9):822–34. doi: 10.1056/NEJMoa1900623

73. Andrlová H, Miltiadous O, Kousa AI, Dai A, DeWolf S, Violante S, et al. MAIT and Vδ2 unconventional T cells are supported by a diverse intestinal microbiome and correlate with favorable patient outcome after allogeneic HCT. *Sci Trans Med* (2022) 14 (646):eabj2829. doi: 10.1126/scitranslmed.abj2829

74. Stein-Thoeringer CK, Nichols KB, Lazrak A, Docampo MD, Slingerland AE, Slingerland JB, et al. Lactose drives enterococcus expansion to promote graft-versus-host disease. *Science* (2019) 366(6469):1143–9. doi: 10.1126/science.aax3760

75. Meedt E, Hiergeist A, Gessner A, Dettmer K, Liebisch G, Ghimire S, et al. Prolonged suppression of butyrate-producing bacteria is associated with acute gastrointestinal graft-vs-Host disease and transplantation-related mortality after allogeneic stem cell transplantation. *Clin Infect Dis* (2022) 74(4):614–21. doi: 10.1093/cid/ciab500

76. Markey KA, Schluter J, Gomes ALC, Littmann ER, Pickard AJ, Taylor BP, et al. The microbe-derived short-chain fatty acids butyrate and propionate are associated with protection from chronic GVHD. *Blood* (2020) 136(1):130–6. doi: 10.1182/blood.2019003369

77. Wang Y, Zhang Z, Liu B, Zhang C, Zhao J, Li X, et al. A study on the method and effect of the construction of a humanized mouse model of fecal microbiota transplantation. *Front Microbiol* (2022) 13:1031758. doi: 10.3389/fmicb.2022.1031758

78. Peled JU, Devlin SM, Staffas A, Lumish M, Khanin R, Littmann ER, et al. Intestinal microbiota and relapse after hematopoietic-cell transplantation. *J Clin Oncol* (2017) 35(15):1650–9. doi: 10.1200/JCO.2016.70.3348

79. Mathewson ND, Jenq R, Mathew AV, Koenigsknecht M, Hanash A, Toubai T, et al. Gut microbiome-derived metabolites modulate intestinal epithelial cell damage and mitigate graft-versus-host disease. *Nat Immunol* (2016) 17(5):505–13. doi: 10.1038/ni.3400

80. Harris B, Morjaria SM, Littmann ER, Geyer AI, Stover DE, Barker JN, et al. Gut microbiota predict pulmonary infiltrates after allogeneic hematopoietic cell transplantation. *Am J Respir Crit Care Med* (2016) 194(4):450–63. doi: 10.1164/rccm.201507-1491OC

81. Stoma I, Littmann ER, Peled JU, Giralt S, van den Brink MRM, Pamer EG, et al. Compositional flux within the intestinal microbiota and risk for bloodstream infection with gram-negative bacteria. *Clin Infect Dis* (2021) 73(11):e4627–e35. doi: 10.1093/cid/ciaa068

82. Masetti R, D'Amico F, Zama D, Leardini D, Muratore E, Ussowicz M, et al. Febrile neutropenia duration is associated with the severity of gut microbiota dysbiosis in pediatric allogeneic hematopoietic stem cell transplantation recipients. *Cancers (Basel)* (2022) 14(8):1932. doi: 10.3390/cancers14081932

83. Lee YJ, Arguello ES, Jenq RR, Littmann E, Kim GJ, Miller LC, et al. Protective factors in the intestinal microbiome against clostridium difficile infection in recipients of allogeneic hematopoietic stem cell transplantation. *J Infect Dis* (2017) 215(7):1117–23. doi: 10.1093/infdis/jix011

84. Legoff J, Resche-Rigon M, Bouquet J, Robin M, Naccache SN, Mercier-Delarue S, et al. The eukaryotic gut virome in hematopoietic stem cell transplantation: new clues in enteric graft-versus-host disease. *Nat Med* (2017) 23(9):1080–5. doi: 10.1038/nm.4380

85. Rolling T, Zhai B, Gjonbalaj M, Tosini N, Yasuma-Mitobe K, Fontana E, et al. Haematopoietic cell transplantation outcomes are linked to intestinal mycobiota dynamics and an expansion of candida parapsilosis complex species. *Nat Microbiol* (2021) 6(12):1505–15. doi: 10.1038/s41564-021-00989-7

86. Ciernikova S, Kasperova B, Drgona L, Smolkova B, Stevurkova V, Mego M. Targeting the gut microbiome: An emerging trend in hematopoietic stem cell transplantation. *Blood Rev* (2021) 48:100790. doi: 10.1016/j.blre.2020.100790

87. Khuat LT, Dave M, Murphy WJ. The emerging roles of the gut microbiome in allogeneic hematopoietic stem cell transplantation. *Gut Microbes* (2021) 13(1):1966262. doi: 10.1080/19490976.2021.1966262

88. Henig I, Yehudai-Ofir D, Zuckerman T. The clinical role of the gut microbiome and fecal microbiota transplantation in allogeneic stem cell transplantation. *Haematologica* (2021) 106(4):933–46. doi: 10.3324/haematol.2020.247395

89. Severyn CJ, Siranosian BA, Kong ST, Moreno A, Li MM, Chen N, et al. Microbiota dynamics in a randomized trial of gut decontamination during allogeneic hematopoietic cell transplantation. *JCI Insight* (2022) 7(7):e154344. doi: 10.1172/jci.insight.154344

90. Khuat LT, Le CT, Pai CS, Shields-Cutler RR, Holtan SG, Rashidi A, et al. Obesity induces gut microbiota alterations and augments acute graft-versus-host disease after allogeneic stem cell transplantation. *Sci Trans Med* (2020) 12(571):eaay7713. doi: 10.1126/scitranslmed.aay7713

91. Shono Y, Docampo MD, Peled JU, Perobelli SM, Velardi E, Tsai JJ, et al. Increased GVHD-related mortality with broad-spectrum antibiotic use after allogeneic hematopoietic stem cell transplantation in human patients and mice. *Sci Trans Med* (2016) 8(339):339ra71. doi: 10.1126/scitranslmed.aaf2311

92. Gavriilaki M, Sakellari I, Anagnostopoulos A, Gavriilaki E. The impact of antibiotic-mediated modification of the intestinal microbiome on outcomes of allogeneic hematopoietic cell transplantation: Systematic review and meta-analysis. *Biol Blood Marrow Transplant* (2020) 26(9):1738–46. doi: 10.1016/j.bbmt.2020.05.011

93. Muratore E, Leardini D, Baccelli F, Venturelli F, Prete A, Masetti R. Nutritional modulation of the gut microbiome in allogeneic hematopoietic stem cell transplantation recipients. *Front Nutr* (2022) 9:993668. doi: 10.3389/fnut.2022.993668

94. Li X, Lin Y, Li X, Xu X, Zhao Y, Xu L, et al. Tyrosine supplement ameliorates murine aGVHD by modulation of gut microbiome and metabolome. *EBioMedicine* (2020) 61:103048. doi: 10.1016/j.ebiom.2020.103048

95. Yoshifuji K, Inamoto K, Kiridoshi Y, Takeshita K, Sasajima S, Shiraishi Y, et al. Prebiotics protect against acute graft-versus-host disease and preserve the gut microbiota in stem cell transplantation. *Blood Adv* (2020) 4(19):4607–17. doi: 10.1182/bloodadvances.2020002604

96. Simms-Waldrip TR, Sunkersett G, Coughlin LA, Savani MR, Arana C, Kim J, et al. Antibiotic-induced depletion of anti-inflammatory clostridia is associated with the development of graft-versus-Host disease in pediatric stem cell transplantation patients. *Biol Blood Marrow Transplant* (2017) 23(5):820–9. doi: 10.1016/j.bbmt.2017.02.004

97. Ladas EJ, Bhatia M, Chen L, Sandler E, Petrovic A, Berman DM, et al. The safety and feasibility of probiotics in children and adolescents undergoing hematopoietic cell transplantation. *Bone Marrow Transplant* (2016) 51(2):262–6. doi: 10.1038/bmt.2015.275

98. Mehta A, Rangarajan S, Borate U. A cautionary tale for probiotic use in hematopoietic SCT patients-lactobacillus acidophilus sepsis in a patient with mantle cell lymphoma undergoing hematopoietic SCT. *Bone Marrow Transplant* (2013) 48 (3):461–2. doi: 10.1038/bmt.2012.153

99. Keller JJ, Ooijevaar RE, Hvas CL, Terveer EM, Lieberknecht SC, Högenauer C, et al. A standardised model for stool banking for faecal microbiota transplantation: a consensus report from a multidisciplinary UEG working group. *United Eur Gastroenterol J* (2021) 9(2):229–47. doi: 10.1177/2050640620967898

100. Bluestone H, Kronman MP, Suskind DL. Fecal microbiota transplantation for recurrent clostridium difficile infections in pediatric hematopoietic stem cell transplant recipients. *J Pediatr Infect Dis Soc* (2018) 7(1):e6–8. doi: 10.1093/jpids/pix076

101. Battipaglia G, Malard F, Rubio MT, Ruggeri A, Mamez AC, Brissot E, et al. Fecal microbiota transplantation before or after allogeneic hematopoietic transplantation in patients with hematologic malignancies carrying multidrug-resistance bacteria. *Haematologica* (2019) 104(8):1682–8. doi: 10.3324/haematol.2018.198549

102. van Lier YF, Davids M, Haverkate NJE, de Groot PF, Donker ML, Meijer E, et al. Donor fecal microbiota transplantation ameliorates intestinal graft-versus-host disease in allogeneic hematopoietic cell transplant recipients. *Sci Trans Med* (2020) 12 (556):eaaz8926. doi: 10.1126/scitranslmed.aaz8926

103. DeFilipp Z, Peled JU, Li S, Mahabamunuge J, Dagher Z, Slingerland AE, et al. Third-party fecal microbiota transplantation following allo-HCT reconstitutes microbiome diversity. *Blood Adv* (2018) 2(7):745–53. doi: 10.1182/bloodadvances.2018017731

104. Taur Y, Coyte K, Schluter J, Robilotti E, Figueroa C, Gjonbalaj M, et al. Reconstitution of the gut microbiota of antibiotic-treated patients by autologous fecal microbiota transplant. *Sci Trans Med* (2018) 10(460):eaap9489. doi: 10.1126/scitranslmed.aap9489

105. Raje N, Berdeja J, Lin Y, Siegel D, Jagannath S, Madduri D, et al. Anti-BCMA CAR T-cell therapy bb2121 in relapsed or refractory multiple myeloma. *New Engl J Med* (2019) 380(18):1726–37. doi: 10.1056/NEJMoa1817226

106. Jacobson CA, Chavez JC, Sehgal AR, William BM, Munoz J, Salles G, et al. Axicabtagene ciloleucel in relapsed or refractory indolent non-Hodgkin lymphoma (ZUMA-5): a single-arm, multicentre, phase 2 trial. *Lancet Oncol* (2022) 23(1):91–103. doi: 10.1016/S1470-2045(21)00591-X

107. Locke FL, Miklos DB, Jacobson CA, Perales MA, Kersten MJ, Oluwole OO, et al. Axicabtagene ciloleucel as second-line therapy for Large b-cell lymphoma. *New Engl J Med* (2022) 386(7):640–54. doi: 10.1056/NEJMoa2116133

108. Brentjens RJ, Rivière I, Park JH, Davila ML, Wang X, Stefanski J, et al. Safety and persistence of adoptively transferred autologous CD19-targeted T cells in patients with relapsed or chemotherapy refractory b-cell leukemias. *Blood* (2011) 118(18):4817–28. doi: 10.1182/blood-2011-04-348540

109. Lu J, Jiang G. The journey of CAR-T therapy in hematological malignancies. *Mol Cancer* (2022) 21(1):194. doi: 10.1186/s12943-022-01663-0

110. Tanoue T, Morita S, Plichta DR, Skelly AN, Suda W, Sugiura Y, et al. A defined commensal consortium elicits CD8 T cells and anti-cancer immunity. *Nature* (2019) 565(7741):600–5. doi: 10.1038/s41586-019-0878-z

111. Rangan P, Mondino A. Microbial short-chain fatty acids: a strategy to tune adoptive T cell therapy. *J Immunother Cancer* (2022) 10(7):e004147. doi: 10.1136/jitc-2021-004147c

112. Abid MB, Shah NN, Maatman TC, Hari PN. Gut microbiome and CAR-T therapy. *Exp Hematol Oncol* (2019) 8:31. doi: 10.1186/s40164-019-0155-8

113. Schubert ML, Rohrbach R, Schmitt M, Stein-Thoeringer CK. The potential role of the intestinal micromilieu and individual microbes in the immunobiology of chimeric antigen receptor T-cell therapy. *Front Immunol* (2021) 12:670286. doi: 10.3389/fimmu.2021.670286

114. Uribe-Herranz M, Bittinger K, Rafail S, Guedan S, Pierini S, Tanes C, et al. Gut microbiota modulates adoptive cell therapy *via* CD8α dendritic cells and IL-12. *JCI Insight* (2018) 3(4):e94952. doi: 10.1172/jci.insight.94952

115. Smith M, Dai A, Ghilardi G, Amelsberg KV, Devlin SM, Pajarillo R, et al. Gut microbiome correlates of response and toxicity following anti-CD19 CAR T cell therapy. *Nat Med* (2022) 28(4):713–23. doi: 10.1038/s41591-022-01702-9

116. Hu Y, Li J, Ni F, Yang Z, Gui X, Bao Z, et al. CAR-T cell therapy-related cytokine release syndrome and therapeutic response is modulated by the gut microbiome in hematologic malignancies. *Nat Commun* (2022) 13(1):5313. doi: 10.1038/s41467-022-32960-3

117. Siegel RL, Miller KD, Fuchs HE, Jemal A. Cancer statistics, 2022. *CA Cancer J Clin* (2022) 72(1):7–33. doi: 10.3322/caac.21708

118. Schupack DA, Mars RAT, Voelker DH, Abeykoon JP, Kashyap PC. The promise of the gut microbiome as part of individualized treatment strategies. *Nat Rev Gastroenterol Hepatol* (2022) 19(1):7–25. doi: 10.1038/s41575-021-00499-1

119. Soleimanpour S, Hasanian SM, Avan A, Yaghoubi A, Khazaei M. Bacteriotherapy in gastrointestinal cancer. *Life Sci* (2020) 254:117754. doi: 10.1016/j.lfs.2020.117754

120. Montalban-Arques A, Katkeviciute E, Busenhart P, Bircher A, Wirbel J, Zeller G, et al. Commensal clostridiales strains mediate effective anti-cancer immune response against solid tumors. *Cell Host Microbe* (2021) 29(10):1573–88 e7. doi: 10.1016/j.chom.2021.08.001

121. Kaźmierczak-Siedlecka K, Skonieczna-Żydecka K, Hupp T, Duchnowska R, Marek-Trzonkowska N, Połom K. Next-generation probiotics - do they open new therapeutic strategies for cancer patients? *Gut Microbes* (2022) 14(1):2035659. doi: 10.1080/19490976.2022.2035659

122. Gurbatri CR, Arpaia N, Danino T. Engineering bacteria as interactive cancer therapies. *Science* (2022) 378(6622):858–64. doi: 10.1126/science.add9667

123. Huang X, Pan J, Xu F, Shao B, Wang Y, Guo X, et al. Bacteria-based cancer immunotherapy. *Adv Sci (Weinh)* (2021) 8(7):2003572. doi: 10.1002/advs.202003572

124. Vincent RL, Gurbatri CR, Redenti A, Coker C, Arpaia N, Danino T. Probiotic-guided CAR-T cells for universal solid tumor targeting. *bioRxiv* (2021) 2021:10. doi: 10.1101/2021.10.10.463366

125. Su Q, Liu Q, Lau RI, Zhang J, Xu Z, Yeoh YK, et al. Faecal microbiome-based machine learning for multi-class disease diagnosis. *Nat Commun* (2022) 13(1):6818. doi: 10.1038/s41467-022-34405-3

126. Shi Z, Hu G, Li MW, Zhang L, Li X, Li L, et al. Gut microbiota as non-invasive diagnostic and prognostic biomarkers for natural killer/T-cell lymphoma. *Gut* (2022). doi: 10.1136/gutjnl-2022-328256

frontiers | Frontiers in Immunology

TYPE Review
PUBLISHED 23 February 2023
DOI 10.3389/fimmu.2023.1133207

OPEN ACCESS

EDITED BY
Yeonseok Chung,
Seoul National University, Republic of Korea

REVIEWED BY
Todd Bartkowiak,
Vanderbilt University, United States
Bixia Tang,
Beijing Cancer Hospital, China

*CORRESPONDENCE
Rafael Duran
rafael.duran@chuv.ch

SPECIALTY SECTION
This article was submitted to Cancer Immunity and Immunotherapy, a section of the journal Frontiers in Immunology

RECEIVED 28 December 2022
ACCEPTED 10 February 2023
PUBLISHED 23 February 2023

CITATION
Berz AM, Boughdad S, Vietti-Violi N, Digklia A, Dromain C, Dunet V and Duran R (2023) Imaging assessment of toxicity related to immune checkpoint inhibitors. *Front. Immunol.* 14:1133207. doi: 10.3389/fimmu.2023.1133207

Imaging assessment of toxicity related to immune checkpoint inhibitors

Antonia M. Berz[1,2], Sarah Boughdad[3], Naïk Vietti-Violi[1], Antonia Digklia[4], Clarisse Dromain[1], Vincent Dunet[1] and Rafael Duran[1]*

[1]Department of Diagnostic and Interventional Radiology, Lausanne University Hospital and University of Lausanne, Lausanne, Switzerland, [2]Department of Radiology, Charité – Universitätsmedizin Berlin, Corporate Member of Freie Universität Berlin and Humboldt- Universität zu Berlin, Berlin, Germany, [3]Department of Nuclear Medicine and Molecular Imaging, Lausanne University Hospital and University of Lausanne, Lausanne, Switzerland, [4]Department of Oncology, Lausanne University Hospital and University of Lausanne, Lausanne, Switzerland

In recent years, a wide range of cancer immunotherapies have been developed and have become increasingly important in cancer treatment across multiple oncologic diseases. In particular, immune checkpoint inhibitors (ICIs) offer promising options to improve patient outcomes. However, a major limitation of these treatments consists in the development of immune-related adverse events (irAEs) occurring in potentially any organ system and affecting up to 76% of the patients. The most frequent toxicities involve the skin, gastrointestinal tract, and endocrine system. Although mostly manageable, potentially life-threatening events, particularly due to neuro-, cardiac, and pulmonary toxicity, occur in up to 30% and 55% of the patients treated with ICI-monotherapy or -combination therapy, respectively. Imaging, in particular computed tomography (CT), magnetic resonance imaging (MRI), and 2-deoxy-2-[^{18}F]fluoro-D-glucose positron emission tomography/computed tomography (^{18}F-FDG-PET/CT), plays an important role in the detection and characterization of these irAEs. In some patients, irAEs can even be detected on imaging before the onset of clinical symptoms. In this context, it is particularly important to distinguish irAEs from true disease progression and specific immunotherapy related response patterns, such as pseudoprogression. In addition, there are irAEs which might be easily confused with other pathologies such as infection or metastasis. However, many imaging findings, such as in immune-related pneumonitis, are nonspecific. Thus, accurate diagnosis may be delayed underling the importance for adequate imaging features characterization in the appropriate clinical setting in order to provide timely and efficient patient management. ^{18}F-FDG-PET/CT and radiomics have demonstrated to reliably detect these toxicities and potentially have predictive value for identifying patients at risk of developing irAEs. The purpose of this article is to provide a review of the main immunotherapy-related toxicities and discuss their characteristics on imaging.

KEYWORDS

immunotherapy, immune checkpoint inhibitor, checkpoint inhibition, toxicity, immune-related adverse event, imaging assessment

Introduction

Immunotherapies, in particular immune checkpoint inhibitors (ICIs), have led to a paradigm shift in cancer treatment in only a few decades and provide promising therapy options across many oncologic diseases (1). The market release of monoclonal antibodies (mABs) targeting the T-lymphocyte-associated protein-4 (anti-CTLA-4) as the first US Food and Drug Administration approved ICI for advanced-stage melanoma in 2011 was followed by the approval of mAbs targeting other ICIs such as programmed cell death protein-1 (anti-PD-1) and PD-1 ligand (anti-PD-L1) (2, 3). Importantly, the sites of action of anti-CTLA-4 and anti-PD-1/PD-L1 antibodies are different. Thus, anti-CTLA-4 acts at the lymph node level at the time of priming, while anti-PD-1/PD-L1 becomes active later in the activation cascade and directly at the tumor site. Their complementary mechanisms of action allow the combined use of these two types of treatment for certain indications (4). Being extensively studied, these novel therapies have demonstrated unprecedented prolongation of patient survival compared with non-ICI treatment (5). This is the case for cancers such as metastatic melanoma, non-small cell lung cancer, renal cell carcinoma, bladder cancer, and refractory Hodgkin's lymphoma for which only limited treatments options were available before the advent of immune checkpoint blockade (6). Based upon the success gathered by ICIs, many novel molecules are currently being investigated.

However, the unique mechanism of action of ICIs, eliciting a T-cell mediated immune response, has led to two major problems. First, ICI therapy causes specific tumor response patterns, including imaging progression prior to response (pseudoprogression), the paradoxical acceleration of tumor growth kinetics after initiation of immunotherapy (hyperprogression), and the coexistence of responding and non-responding lesions within the same patient (dissociated responses), which are less commonly observed following cytotoxic chemotherapy and targeted therapies (7, 8). These response characteristics lead to a complete revision of the traditionally used Response Evaluation Criteria in Solid Tumors version 1.1 (RECIST 1.1) to accurately assess the tumor response after immunotherapy; the immune-related response criteria (irRC) and subsequently the immune-related RECIST criteria (irRECIST) were introduced (9–11). Second, ICIs can lead to immune-related adverse events (irAEs), which may occur in the majority of patients (up to 76%) with off-target effects potentially affecting any organ system or tissue due to an over activated immune system (12). Several irAE mechanisms have been described, including increasing T-cell activity against antigens present in healthy tissue, upregulation of pre-existing autoantibodies and inflammatory cytokines, as well as enhanced complement-mediated inflammation by direct binding of anti-CTLA-4 antibody's to CTLA-4 expressed in normal tissue (13). Many of these events are mild and manageable. However, life threatening events, requiring ICI therapy discontinuation, occur in 3%-30% of patients treated with ICI-monotherapy and in up to 55% of patients receiving ICI-combination therapy (12, 14, 15). In clinical practice, it remains a major challenge to detect and adequately address these toxicities. Many hospitals have implemented clinical units specialized in irAEs to ensure optimal patient management. Imaging has also proven to be valuable in this setting as 70% of irAEs can be diagnosed already on ultrasound (US), 79% on computed tomography (CT), 83% on magnetic resonance imaging (MRI) and up to 74% on 2-deoxy-2-[18F] fluoro-D-glucose positron emission tomography/CT (^{18}F-FDG-PET/CT) (16). This is all the more interesting as for some patients, irAEs can be detected on imaging even prior to the onset of clinical symptoms (8, 17, 18). This underscores the importance for radiologists and nuclear medicine physicians to become familiar with irAEs and recognize their imaging features, especially as there is some overlap between these toxicities and immunotherapy-related response patterns.

The purpose of this article was to provide a detailed review of main immunotherapy-related toxicities and to discuss their characteristics on imaging.

Clinical relevance of immune-related adverse events

Immunotherapies, although generally considered to be safer than standard chemotherapies, have a different spectrum of toxicities, most of which are due to excessive immune reactions that can potentially affect any organ system and tissue (13, 19–21). In general, the onset of irAEs is less predictable than for cytotoxic chemotherapy-related side effects which usually appear shortly after treatment initiation. By contrast, the median time from ICI therapy initiation and appearance of irAEs ranges from 2 to 16 weeks but can occur any time during or after the treatment (22, 23). Nonetheless, the risk of irAEs is 3 times higher in the first 4 weeks of treatment, consisting mainly of dermatologic disorders (24, 25). However, delayed irAEs manifesting ≥90 days after discontinuation of immunotherapy may occur in 5.7% of the patients (26, 27).

In general, most frequent irAEs include dermatologic, gastrointestinal, and endocrine toxicities (15, 27, 28). Conversely, neurological, cardiological and pulmonary toxicities have been described as most lethal (15, 29). The occurrence of a certain type of irAEs is highly dependent on a particular drug. A recent meta-analysis, which included 36 head-to-head phase II and III randomized trials, showed that the most common drug-dependent toxicities are hypothyroidism, nausea, and vomiting for atezolizumab (anti-PD-L1 mAb), endocrine toxicities for nivolumab, arthralgia, pneumonitis and hepatic toxicities for pembrolizumab (anti-PD1 mAb), and dermatologic, gastrointestinal and renal toxicities for ipilimumab (anti-CTLA-4 mAb) (12). In addition, the severity of these toxicities also highly depends on the drug target, with atezolizumab (probability 76%, pooled incidence of grade 1-5 adverse events 66.4%) having the best safety profile, followed by nivolumab (56%, 71.8%), pembrolizumab (55%, 75.1%), and ipilimumab (55%, 86.8%) (12). Lethal irAEs occur in 0.37% of anti-PD1, in 0.38% of anti-PD-L1, in 1.08% of anti-CTLA-4, and in 1.23% of patients receiving anti-CTL-4/anti-PD1/PD-L1 combination immunotherapy (15). Risk factors for the development of irAEs are genetics, environmental factors, previous toxicities with immunotherapies, the patient's own microbiome,

and recent severe or chronic viral infections (28). Besides, a systematic review showed that antitumor immune responses and possible toxicity can vary among patients treated with the same ICI depending on the oncologic diseases. Melanoma patients have a significantly higher prevalence of gastrointestinal and skin irAEs, whereas they are less likely to have pneumonitis compared with patients with non-small cell lung cancer. Arthritis and myalgias occur more frequently in melanoma patients than in renal cell cancer, where pneumonitis and dyspnea are more common (30).

Moreover, the combination of different immunotherapies increases the risk, frequency, and severity of side effects significantly (21). These severe irAEs often lead to ICI treatment discontinuation and initiation of immunosuppressive therapy, e.g. with corticosteroids.

In order to compare treatment-related complications in a reproducible manner, the U.S. National Cancer Institute has classified the severity of adverse events in the Common Terminology Criteria for Adverse Events (CTCAE) version 6.0 (Table 1) (31). CTCAE facilitates a consistent and reproducible comparison of toxicities across clinical trials and can also be applied in the assessment of irAEs in patients treated with immunotherapy (31). Nevertheless, several studies have reported that the presence and severity of irAEs in patients treated with ICI is associated with treatment response suggesting a good prognostic value (32, 33).

Table 2 summarizes recommended imaging to be prescribed in the presence of suspected irAEs. In this context, it should be noted that many irAEs can be diagnosed clinically (and/or based on blood testing) without necessarily the need to perform imaging. Moreover, the choice of an imaging modality may vary based on all clinical parameters and patient's condition, and based on available imaging equipment. Table 3 summarizes the visibility of irAEs on imaging.

Imaging of immune-related adverse events

Abdominal toxicities

Diarrhea is one of the most common irAEs, affecting approximately 44% (vs. 10% for grade 3-4) of patients treated with a combination of CTLA-4 and PD-(L)1 inhibitors, 36% (vs. 8% for grade 3-4) of patients treated with anti-CTLA-4, and 11% (vs. 1% for grade 3-4) of patients treated with anti-PD-(L)1 (34). This symptom is often associated with colitis, another common irAE, as it is reported in 16% (vs. 11% for grade 3-4) (combination of CTLA-4 and PD-(L)1 inhibitors), 8% (vs. 5% for grade 3-4) (anti-CTLA-4), and 1% (vs. 1% for grade 3-4) (anti-PD-(L)1) of ICI-treated patients (34). With a median time to full onset of 5 to 10 weeks, colitis can lead to various complications, including intestinal perforation, ischemia, necrosis, hemorrhage, and toxic megacolon (35, 36). Therefore, the typical diagnostic workup in these cases includes contrast-enhanced CT, in which ICI-induced colitis appears as diffuse inflammation with bowel wall thickening (>4mm), mucosal hyperenhancement, mesenteric hyperemia, mesenteric vessel congestion, and air-fluid levels (8, 37). In addition, cases of segmental colitis in association with diverticulosis and isolated rectosigmoid colitis without diverticulosis have been described (38, 39). A recent study including patients with various types of cancer showed CT findings suggestive of colitis in 20 of 34 patients with symptoms of colitis and in 5 of 19 patients even without clinical presentation of colitis (40). ^{18}F-FDG PET/CT may reveal increased partial or diffuse tracer uptake in colitis or throughout the entire bowel in patients with extensive inflammation (41, 42) (Figure 1). Moreover, it has been reported that it might be more sensitive than CT for the early detection of colitis in patients undergoing ICI treatment (43). However, its lack of specificity for instance due to physiological muscular activity or in patients treated with metformin hinders its value in routine practice (41, 43).

In the context of ICI therapy, hepatitis, characterized by elevation of serum alanine transaminase and/or aspartate transaminase, is often initially clinically asymptomatic but can potentially lead to transient life-threatening liver dysfunction (35). It occurs in 19% (vs. 9% for grade 3-4) of patients treated with ICI-combination therapy, in 5% (vs. 2% for grade 3-4) of patients receiving anti-CTLA-4 and in 19% (vs. 9% for grade 3-4) of patients receiving anti-PD-(L)1 treatment (34). Although hepatic toxicity can occur with a delay of months to years, it typically manifests between 1 and 15 weeks after treatment (36). Recently, in a large population of melanoma patients treated with ipilimumab and/or nivolumab, especially in ICI-combination treatment caused higher rates of grade 3-4 liver toxicity with aminotransferase levels of 6.1% (for aspartate aminotransferase) and 8.3% (for alanine aminotransferase), and have been shown to lead frequently to ICI treatment discontinuation (44). Evidence for hepatitis can be found on US as a diffusely hypoechogenic liver parenchyma with periportal thickening and hyperechogenic dots, known as "starry sky pattern" sign (Supplementary Figure 1), as well as gallbladder wall thickening (45). CT and MRI findings are often nonspecific and comparable to those of other causes of acute liver dysfunction, ranging from the absence of detectable abnormalities to hepatomegaly, heterogeneous parenchymal enhancement with areas of low attenuation, periportal/gallbladder edema (diffuse parenchymal hypoattenuation on CT or T2-weighted hyperintensity on MRI), and perihepatic ascites (36, 37, 42, 45). Interestingly, while other causes of diffuse liver disease might not be

TABLE 1 Common Terminology Criteria for Adverse Events (CTCAE) version 6.0 to classify immune irAEs (31).

Grade	Severity and clinical description
1	Mild: asymptomatic or mild symptoms; clinical or diagnostic observations only; intervention not indicated.
2	Moderate: minimal, local or noninvasive intervention indicated; limiting age-appropriate instrumental ADL.
3	Severe or medically significant but not immediately life-threatening: hospitalization or prolongation of hospitalization indicated; disabling; limiting self-care ADL.
4	Life-threatening consequences: urgent intervention indicated.
5	Death related to the adverse event.

ADL, activity of daily living.

TABLE 2 Recommended imaging to be prescribed in the presence of suspected immune-related adverse events (irAEs).

irAEs	US	CT	MRI	^{18}F-FDG PET/CT
Enteritis	–	√	(√)	–
Colitis	–	√	(√)	–
Hepatitis	√	(√)	(√)	–
Cholecystitis and cholangitis	√	(√)	√	–
Pancreatitis	√	√	(√)	–
Acute kidney injury	√	–	(√)	–
Pneumonitis	–	√	–	–
Sarcoid-like reactions	–	√	–	(√)
Myocarditis	√	–	√	(√ *)
Pericarditis	√	–	√	–
Myositis	–	–	√	(√ *)
Encephalitis	–	–	√	(√)
Aseptic meningitis	–	–	√	–
Central nervous system vasculitis	–	(√)	√	(√)
Hypophysitis	–	–	√	√
Thyroid dysfunction	√	–	–	–
Primary adrenal insufficiency or adrenalitis	–	(√)	(√)	–

US, ultrasound; CT, computed tomography; MRI, magnet resonance imaging; ^{18}F-FDG PET/CT, 2-deo-y-2-[18F]fluoro-D-glucose positron emission tomography.
√, 1st choice modality; (√), optional imaging; -, usually not prescribed or not applicable; * ^{68}Ga-DOTATOC PET/CT as additional option.

visualized on PET/CT, increased liver ^{18}F-FDG avidity in the setting of ICI-induced hepatitis is often reported (46). However, its visualization using ^{18}F-FDG PET/CT might be limited by physiological uptake or a reversal in liver-to-spleen ratio due to higher spleen uptake resulting from ICI-induced T-cell activation especially at an early stage (47). Some authors have suggested the use of a liver-to-blood pool standard uptake value (SUV) mean ratio to detect pathologic hepatic uptake and thus possible hepatitis compared to SUVmean alone because various parameters can influence SUV measurements (48, 49).

Cholecystitis and cholangitis are forms of hepatobiliary toxicity that are rarely associated with ICI therapy, and because of the small reported number of cases, it is difficult to estimate the actual incidence and causal relationship, if any, with immunotherapy (35, 50, 51). Despite its low incidence characteristic imaging features on US and CT for cholecystitis such as gallbladder distension and wall thickening, as well as inflammation of the pericholecystic tissue with increased ^{18}F-FDG uptake on PET/CT, have been suggested (52). On MRI and MR cholangiopancreatography (MRCP), as the imaging modalities of choice in clinical practice, cholangitis is characterized by localized dilatation and diffuse non-obstructive hypertrophy and hyperenhancement of the extrahepatic bile duct wall with portions of biliary dilatation and narrowing (Figure 2) (51, 52).

The diagnosis of pancreatitis requires the presence of at least two of the following three features: abdominal pain suggestive of pancreatitis, elevated amylase or lipase to more than three times of the upper normal limit, and characteristic imaging features (53) because ICI-related acute pancreatitis is relatively rare and patients with elevated amylase and lipase are often initially asymptomatic, only few cases have been reported (54). Radiologic findings on CT and MRI are similar to pancreatitis from other origin and include in the acute phase focal or diffuse pancreatic enlargement with decreased enhancement and peripancreatic fat stranding associated with edema and fluid collections without a focal lesion suspicious for metastasis (37, 42, 55). On ^{18}F-FDG-PET/CT diffuse tracer uptake might be seen (56). After resolution of the clinical presentation, imaging might be characterized by parenchymal atrophy and loss of normal lobulations (55).

Acute kidney injury (AKI) is the most common renal toxicity in patients receiving ICI therapy (57). However, it is generally not a direct consequence of ICI's toxicity, as it can be caused by various etiologies. Therefore, it is important to distinguish between AKI as an irAE and AKI induced by e.g. hypovolemia or acute tubular necrosis (57). Notwithstanding, the incidence of AKI after ICI treatment is reported to be 2.2% overall and 0.6% in severe cases requiring renal transplantation (58). AKI occurs more frequently in patients treated with ICI-combination therapy (4.9%) than with anti-CTLA-4 (2%) or anti-PD-(L)1 (1.4%-1.9%) monotherapy (58). The interval between ICI treatment initiation to AKI ranges from 21 to 245 days, and from 7 to 63 days between the last ICI treatment

TABLE 3 Visibility of immune-related adverse events (irAEs) on imaging.

		Visibility of irAEs on imaging			
irAEs	Best imaging for visualization	US	CT	MRI	^{18}F-FDG PET/CT
Enteritis	CT	–	√	(√)	(√)
Colitis	CT	–	√	(√)	(√) *
Hepatitis	US	(√)	(√)	(√)	(√) *
Cholecystitis and cholangitis	US	√	(√)	√	(√)
Pancreatitis	CT	(√)	√	√	√
Acute kidney injury	US	(√)	(√)	(√)	(√) *
Pneumonitis	CT	–	√	–	√
Sarcoid-like reactions	PET/CT	–	√	(√)	√
Myocarditis	MRI - PET/CT	(√)	(√)	√	√ **
Pericarditis	MRI	(√)	(√)	√	√
Myositis	MRI	(√)	(√)	√	√ **
Encephalitis	MRI	–	–	√	√ *
Aseptic meningitis	MRI	–	–	√	–
Central nervous system vasculitis	MRI	–	(√)	√	(√)
Hypophysitis	MRI	–	(√)	√	√
Thyroid dysfunction	US	√	√	√	√
Primary adrenal insufficiency or adrenalitis	MRI	–	√	√	√

US, ultrasound; CT, computed tomography; MRI, magnet resonance imaging; ^{18}F-FDG PET/CT, 2-deo-y-2-[18F]fluoro-D-glucose positron emission tomography.
√, good visibility; (√), moderate visibility; -, poor visibility or not applicable; * Decreased visibility due to physiological ^{18}F-FDG uptake; ** ^{68}Ga-DOTATOC PET/CT as an additional option.

dose and onset of AKI (58) A ccase of ipilimumab-induced immune-related kidney failure was reported with bilateral renal enlargement visualized on CT and rapid resolution after steroid therapy (59). In addition, PET/CT shows increased ^{18}F-FDG uptake in the renal cortex (60, 61). Moreover, diffuse or even segmental uptake in the renal parenchyma can be seen on ^{18}F-FDG PET/CT especially in delayed imaging. However, the very high pelvicalyceal activity and low spatial resolution in older generation PET/CT scanners are clear limiting factors for accurate assessment of the kidneys in patients undergoing ICI treatments (42). Therefore, for patients with clinical suspicion of AKI and contraindication for biopsies, ^{18}F-FDG PET/CT might provide some diagnostic clues (60). However, the specific imaging characteristics have not been defined yet and distinguishing between immune-related and non-immune-related AKI remains challenging.

Thoracic toxicities

Pneumonitis is a relatively common irAE that manifests with clinical symptoms ranging from mild dyspnea to potential lethal respiratory failure and is associated with lower patient survival (62). Pneumonitis occurs in approximately 1% of patients receiving anti-CTLA-4 therapy and in 4% of patients receiving anti-PD-(L)1 treatment, with around 1% of the cases being severe (34). In patients receiving ICI-combination treatment (nivolumab + ipilimumab or peptide vaccines), the incidence is significantly higher at 6.6% and 1.5% for severe cases, respectively (63). The median time to onset of clinical symptoms is 4.6 months in patients receiving ICI-monotherapy versus 2.7 months in patients receiving ICI-combination therapy (64, 65). Radiologic findings of ICI-related pneumonitis range from mild interstitial abnormalities to acute interstitial pneumonia and acute respiratory distress syndrome (66). The best imaging modality in this setting is CT. Based on the CT findings, irAE-related pneumonitides can be divided into five distinct phenotypes (37, 65):

1. cryptogenic organizing pneumonia-like pneumonitis with patchy or confluent consolidation with or without air bronchograms and predominantly peripheral or subpleural distribution (Figure 3),
2. ground glass opacities with variable expression and location,
3. increased interstitial markings, interlobular septal thickening with peribronchovascular infiltration,
4. hypersensitivity with centrilobular nodules, bronchiolitis-like appearance, and tree-in-bud micronodularity, and
5. lesions which cannot be further classified.

Ground glass opacities (55%) and consolidations (32%) non-segmentally distributed in the dominant lung or bilaterally opposite

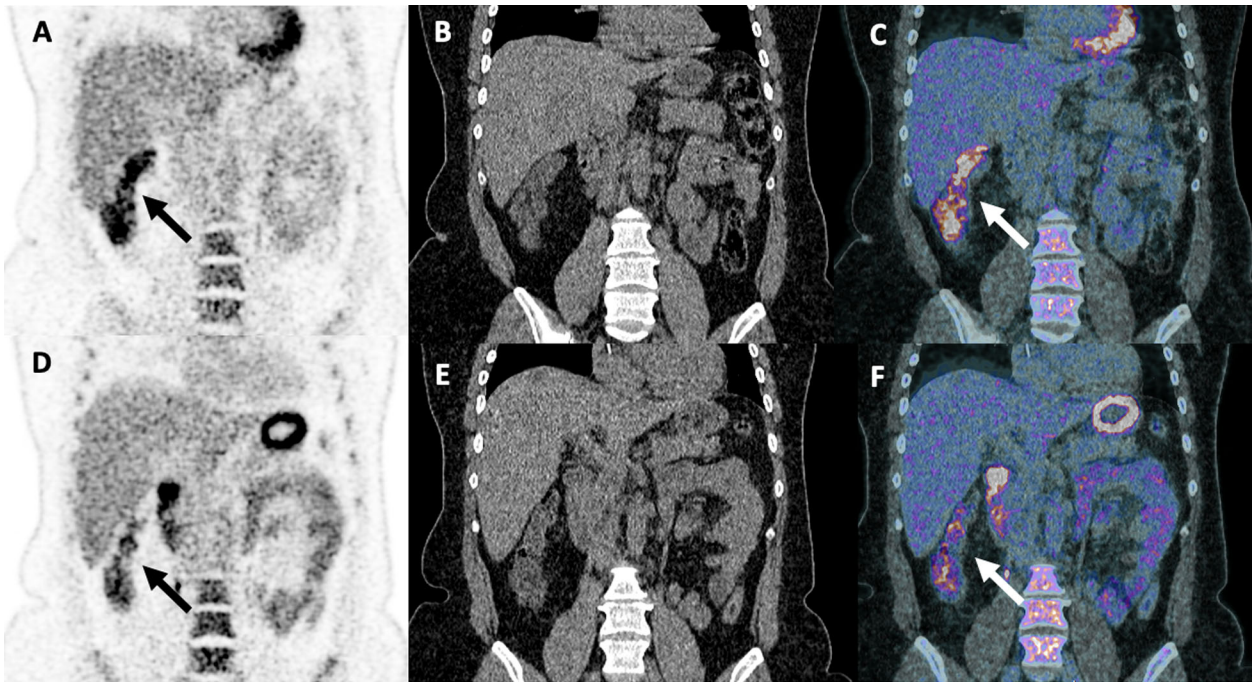

FIGURE 1
Partial pathological uptake of the right colon suspecting early signs of colitis in a 48-year-old woman with stage IV melanoma treated with two cycles of ipilimumab (anti-CTLA-4) and nivolumab (anti-PD-1). Treatment was discontinued due to grade II colitis diagnosed 3 weeks after the first ^{18}F-FDG PET/CT scan [arrows; coronal PET **(A)**, CT **(B)** and merged PET/CT **(C)** images], which required high-dose steroid treatment for 3 months. A decreased right colon uptake was observed on follow-up ^{18}F-FDG PET/CT examination performed 4 weeks after the introduction of steroid treatment [arrows; coronal PET **(D)**, CT **(E)** and fused PET/CT images **(F)**].

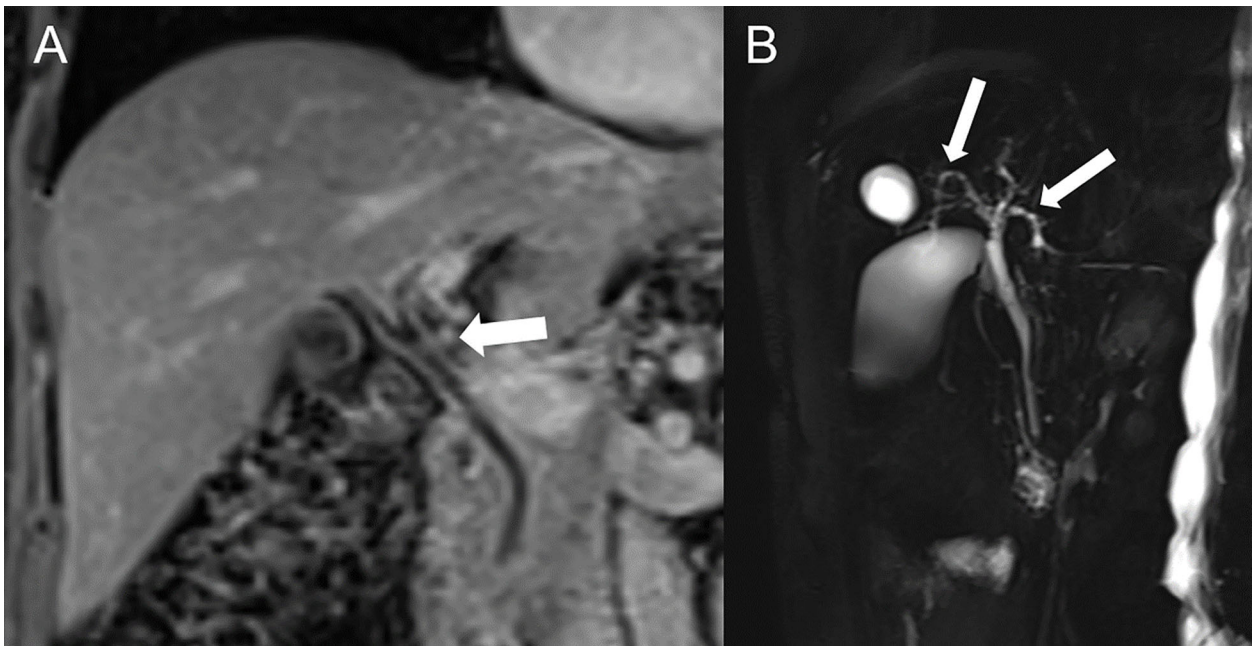

FIGURE 2
Immune-related hepatitis and cholangitis in a 73-year-old female with metastatic melanoma of the tibia on nivolumab (anti-PD-1) and ipilimumab (anti-CTLA-4) who developed grade 3 hepatitis. **(A)** Contrast-enhanced MRI in coronal view show hyperhemic and slightly thickened bile duct walls (arrow) and **(B)** MR cholangiopancreatography demonstrate bile ducts irregularities (arrows) compatible with immune-mediated cholangitis.

the tumor have been shown the most frequently in ICI-treated non-small cell lung cancer patients according to a systematic review by Zhang et al. (67).

A case of progressive pleural effusion as rare irAE has been reported for instance in a non-small cell lung cancer patient treated with cisplatin, pemetrexed, and pembrolizumab (68) and as late toxicity in a primary lung adenocarcinoma patient following 94 cycles of nivolumab (69). Importantly, CT scans are also of interest for ruling out differential diagnoses such as pulmonary embolism.

On PET/CT an interstitial pneumonia type pattern characterized by non-specific moderate to intense ^{18}F-FDG uptake might be seen (70). However, one major diagnostic challenge is to distinguish infectious diseases from tumor lesions, e.g., nodular aspects that mimic tumor recurrence, whereas an underlying disease, such as chronic obstructive pulmonary disease, may further complicate the final diagnosis (71).

In terms of clinical management, corticosteroids are recommended as primary therapy approach based on severeness of the case and clinical expertise (67). In addition, for patients with grade 3-4 ICI-induced pneumonitis, ICI-treatment should be discontinued immediately and permanently. Clinical improvement, especially in low-grade disease is usually observed within 48-72 hours of corticosteroid use. Patients with grade 2 pneumonitis, who resolved symptoms show the highest overall survival (86%) compared with grade 3 or 4 pneumonitis (36% or 43%, respectively) (67).

Immunotherapy-related sarcoid-like reactions are often asymptomatic and appear in 5–7% of patients (37, 72). They might be related to the involvement of primary and secondary systemic lymphoid organs in the systemic antitumor response required for effective ICI treatment (37, 72, 73). In general, the formation of sarcoid-like granulomas occurs most frequently in lymph nodes (71%), lungs (60%), and skin (55%) and can be easily confused with disease progression or tumor recurrence (7, 74). The median time between initiation of ICI treatment and the development of sarcoid-like reactions is 14 weeks (37, 75). During the course of ICI therapy, metabolic changes in lymphoid organs could be monitored using ^{18}F-FDG-PET/CT. Indeed, an increase in immune cells populations and their higher growth rate leads to higher energetic requirements often translating in high avidity for ^{18}F-FDG (76, 77). Imaging findings include a new bilateral symmetric mediastinal and hilar lymphadenopathy resembling sarcoidosis in up to 10% of the patients (78), often high ^{18}F-FDG avidity on PET/CT, and an association with (subpleural) perilymphatic distribution of micronodules without suspicion of intercurrent infection or new metastasis (Figure 4) (37, 79). It is critical to recognize these sarcoid-like irAEs as a classic response pattern to immunotherapy (initial increase of the tumor burden unconfirmed at the next imaging follow-up) in order to distinguish it from true progression or pseudoprogression (80). In cases where the diagnosis on imaging is unclear, an assessment of angiotensin converting enzyme serum levels can be performed, as elevated levels have been associated with ICI-induced sarcoidosis-like reactions (75). If true tumor progression is still suspected after this, a targeted biopsy should be strongly considered for definitive diagnosis (75).

Cardiac toxicities associated with ICI treatment are relatively rare. Myocarditis, as the most common one, occurs in 0.1% to 1% of patients with symptoms such as dyspnea (49%), weakness (25%), chest pain (17%), syncope (9%), fever (6%), and cough (4%) (20, 21, 81). In most of these cases, the onset is shortly after initiation of the ICI therapy, and because of the high mortality rate of 50%, it is of the utmost importance to make the diagnosis and start the appropriate treatment as early as possible (20, 21, 82). Besides clinical features, laboratory markers and electrocardiogram changes, non-invasive imaging modalities, especially cardiac MRI (CMRI) has become more and more important in the diagnostic workup, to reduce the necessity of invasive biopsies as the current diagnostic gold standard (83, 84). In clinical practice, transthoracic echocardiography (TTE) is the first imaging modality that should be performed if acute myocarditis is suspected. Suggestive TTE findings include abnormalities of the segmental wall motion, increased thickness of the left ventricular wall, global hypokinesia (fulminant myocarditis), and pericardial effusion (84). However, a recent review of 88 ICI-induced myocarditis cases showed normal morphological TEE findings in 23% and normal left ventricular ejection fraction in 32.5% (81). Regarding CMRI, at least one criterion on T2-based (regional or global increase in myocardial relaxation time or increased signal intensity) with at least one criterion on T1-weighted imaging (increase in myocardial T1, extracellular volume, late gadolinium enhancement) should be analyzed for sufficient diagnostic accuracy according to the recently updated Lake Louise criteria (85). In 48% of cases late gadolinium enhancement (LGE)

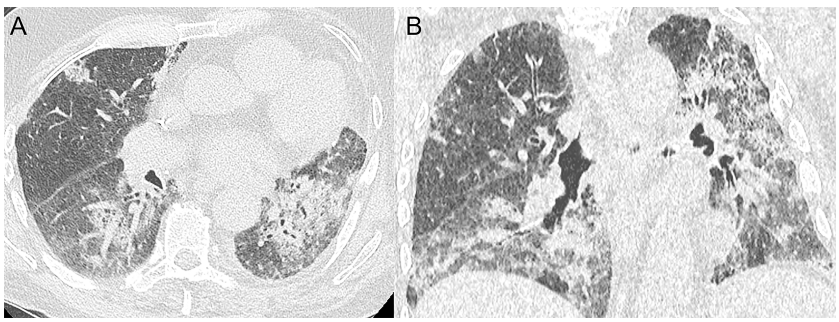

FIGURE 3
Immune-related pneumonitis in a 79-year-old male with stage IV non-small cell lung cancer in the left lower lobe. After second line treatment with nivolumab (anti-PD-1) (5 cycles), the patient developed progressive dyspnea and dry cough. Axial **(A)** and coronal **(B)** CT images demonstrate multifocal alveolar consolidations in a predominantly peribronchovascular and subpleural location compatible with a drug-induced pneumonitis.

predominantly distributed in the anteroseptal, inferoseptal, inferior, and inferolateral segments (atypical localizations possible), and in 28% of the cases myocardial oedema in T2-weighted short-tau inversion recovery (STIR) is described (83, 86). However, these characteristics are limited due to their low specificity. In a study of an international registry of patients with ICI-associated myocarditis (n=103), only 48% of patients with ICI-induced myocarditis had LGE when compared to 90% of patients with other causes of myocarditis (83). Herby it is important to note that CMRI assessment >4 days after admission showed significantly more positive LGE findings than if CMRI was performed earlier (72.0% vs 21.6%, p<0.001) (83). Moreover, LGE was not associated with clinical symptoms, patient outcomes, ECG or echocardiographic findings. Finally, nuclear medicine findings might provide important clues for the diagnostic of immune-related acute myocarditis (Figure 5). Interestingly, ^{18}F-FDG-PET/CT has a very limited role in this setting as demonstrated in a recent study of 61 patients with suspicion of ICI-related myocarditis where its sensitivity was below 30% (87). However, other PET tracers have been proven useful in this context, such as ^{68}Ga-DOTATOC which showed high sensitivity for the early detection of pathological myocardial uptake in a small population of patients (n=9) with clinical suspicion of ICI-related myocarditis (88). A pathological diffuse tracer uptake in the myocardium was the most frequent pattern detected. Interestingly, ^{68}Ga-DOTATOC PET/CT showed a good correlation with elevated serum cardiac troponin I and immune correlates such as inflammatory cytokines (IL-6) and chemokines (CXCL9, CXCL10 and CXCL13) by contrast evocative lesions for myocarditis were only seen in 3 out of the 8 patients that had a CMRI (88).

Pericarditis is reported to be the second most common immune-related cardiotoxicity, although data is lacking regarding its exact incidence (82). The median onset of pericardial disease is estimated to be 30 days (82). Symptoms include shortness of breath, pericardial pain without pericardial effusion or jugular vein congestion, and cardiogenic shock with cardiac tamponade due to pericardial effusion, resulting in a high mortality rate of 21% (82, 89). Moreover, pericardial toxicity can occur alone or in combination with ICI-associated myocarditis (myopericarditis) (89). The diagnostic work-up includes detailed physical examination, electrocardiogram, echocardiogram, CMRI and cardiac PET/CT (89, 90). On CMRI, ICI-related pericardial disease demonstrates focal myocardial LGE in the mid-lateral wall and mild LGE of the pericardium along the lateral wall in cases suggestive of myopericarditis (90).

Neuromuscular toxicity

Regarding peripheral neuromuscular toxicities, myositis is the most common syndrome. While being the most prevalent in anti-PD(L)-1 therapy, it occurs in approximately 0.4-3% of ICI-treated patients (Figure 6) (91–93). The median time of ICI-administration to myositis symptom development ranges from 5 to 87 days (94).

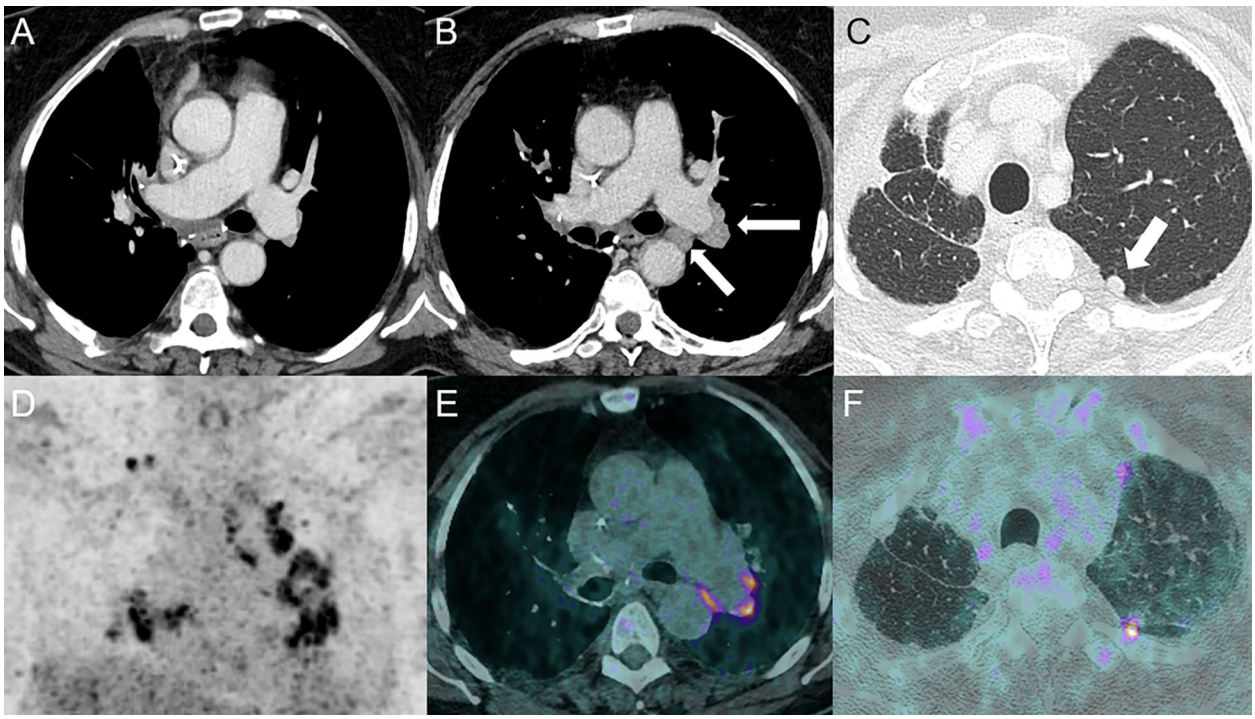

FIGURE 4
Sarcoidosis-like reaction in a 69-year-old female with stage IIIa lung adenocarcinoma in the right upper lobe treated by neoadjuvant cisplatin-docetaxel followed by durvalumab (anti-PD-L1) with subsequent right upper lobe lobectomy and lymphadenectomy. The patient received adjuvant durvalumab 1 month post-surgery. Baseline CT following surgery is shown in **(A)**. Follow-up CT at 5 months showed the development of bilateral hilar and mediastinal lymphadenopathies [arrows, **(B)**] and an increasing nodule in the left upper lobe (arrow) **(C)**. ^{18}F-FDG PET-CT confirmed high uptake of mediastinal and hilar lymph nodes [PET **(D)** and fused PET/CT **(E)** images] and the upper left lobe nodule [fused PET/CT images **(F)**]. A wedge resection confirmed the sarcoidosis-like nature of the nodule.

Interestingly, the clinical manifestation from immunotherapy-related myositis differs markedly from that of idiopathic and paraneoplastic inflammatory myopathies such as dermatomyositis and polymyositis. Progressive symptom development, as well as oculomotor and axial muscle involvement are uncommon, but have been reported. Bulbar symptoms, such as dyspnea, dysarthria, and dysphonia have been described (95, 96). However, sudden onset of stable myalgia with or without elevated creatine kinase is the most common symptom of immune-related myositis (96). The differential diagnosis to myastenia gravis is sometimes challenging, since on one side, myastenia gravis is often associated with optical myositis and on the other side, acetylcholine receptor binding antibodies can occasionally be detected in optical myositis in the absence of myasthenia gravis (97, 98). On brain MRI, immunotherapy-related myositis is characterized by fat-suppressed T1/T2-weighted intramuscular hyperintensity with or without gadolinium enhancement (96, 99). The ocular phenotype presents contrast-enhanced orbital edema as well as abnormal enhancement and enlargement of the extraocular muscles (Figure 7). Moreover, PET/CT with increased muscular ^{18}F-FDG uptake can support the diagnosis and help to estimate the severity by assessing how many muscle groups are affected (96, 99). Pathological muscle uptake suggestive of myositis could also be detected using ^{68}Ga-DOTATOC PET/CT as shown in 5 out of the 6 patients that presented with myositis concomitant to an ICI-related myocarditis (88). In addition, rheumatological disorders are also frequent irAEs during the course of ICI treatment and ^{18}F-FDG-PET/CT could be useful for the detecting and assessing the severity of the inflammation associated with those events in particular for arthritis affecting several articulations but also tenosynovitis or polymyalgia rheumatica (41).

Central neurologic toxicity

In contrast to peripheral nervous toxicities, irAE of the central nervous system such as encephalitis, aseptic meningitis, vasculitis, cranial neuropathies, and myelitis are uncommon (100).

Although in recent years an increasing number of immune-related encephalitis have been described and may occur with each treatment cycle, it remains a rare immune-related toxicity with an incidence of 0.1–0.2% (94, 100). These cases present a wide range of potential life-threatening symptoms, including confusion, agitation, fever, headache, fatigue, short-term memory impairment, neck stiffness, behavioral changes, and psychiatric symptoms (101, 102). The diagnostic workup usually includes brain MRI, lumbar puncture, paraneoplastic autoantibodies, electroencephalography, and laboratories, notably to rule out infectious agents related diseases. MRI, particularly T2-weighted and/or fluid-attenuated inversion recovery (FLAIR), reveals encephalitis features such as

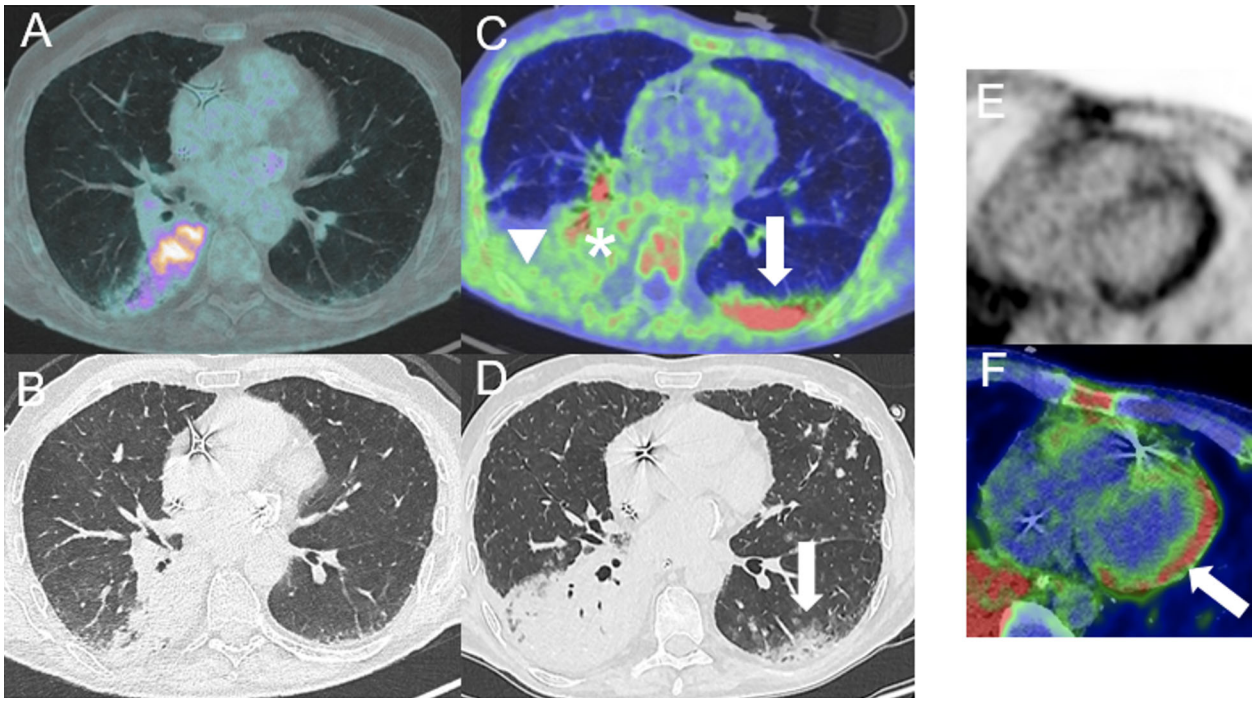

FIGURE 5
Immune-related myocarditis in a 61-year-old male with mucinous lung adenocarcinoma in right lower lobe [cT4 (>7cm) cN0 cM0] initially treated with carboplatin, vinorelbine and radiation therapy followed by consolidation treatment with durvalumab (anti-PD-L1). Baseline (before ICI) fused axial ^{18}FDG PET/CT image **(A)** and corresponding axial CT image **(B)**. After 2 cycles of durvalumab, the patient experienced severe dyspnea, atrial fibrillation leading to cardiogenic shock with clinical suspicion of ICI-related myocarditis. ^{68}Ga-DOTATOC-PET/CT showed necrotic areas in the lung cancer [asterisk, **(C)**] with presence of peripheral inflammatory/infectious uptake [arrowhead, **(C)**] and newly appeared subpleural alveolar consolidations in the left lower lobe compatible with an organizing pneumonia [arrow, **(C, D)**]. ^{68}Ga-DOTATOC-PET/CT showed diffuse myocardial uptake in the left ventricle (LV) [**(E, F)**], with an increased uptake ratio of 2.6 (SUVpeak $LV_{myocardium}$/SUVmean LV_{cavity}) suggestive of myocarditis [arrow, fused axial PET/CT image **(F)**].

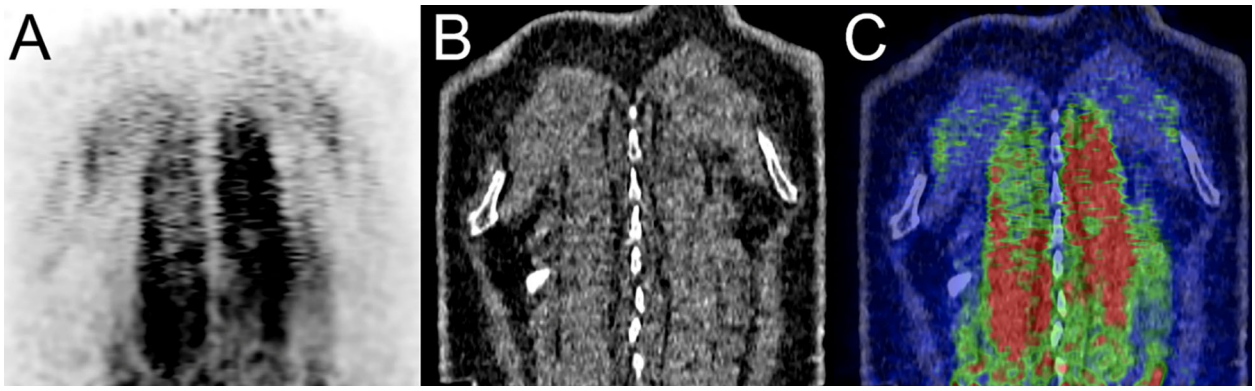

FIGURE 6
Immune-related myositis in a 61-year-old male patient with small cell neuroendocrine carcinoma of the right lung hilum (cT4 cN2 cM0, stage IIIB) initially treated with chemo-radiation therapy who developed diffuse metastatic disease. A treatment with ipilimumab (anti-CTLA-4) and nivolumab (anti-PD-1) was administered. At 1-month post-immunotherapy, a ^{68}Ga-DOTATOC-PET/CT showed diffuse myositis of paraspinal muscles coronal PET, CT and fused PET/CT images **(A–C)** respectively showing spinalis, longissimus thoracis and iliocostalis thoracis muscles.

ill-defined uni- or bilateral hyperintense signals in the limbic cortex, the cerebellum, basal ganglia or scattered in the gray or white matter, with or without enhancement corresponding to zones of inflammatory infiltrates and epileptogenic activity (93, 103, 104), some being associated with auto-antibodies (105). Multifocal lesions involving the white matter, optical nerve, and spinal cord, which mimic demyelinating diseases, have also been described (106, 107). The physiological high ^{18}F-FDG uptake of the brain limits somehow the irAEs assessment using ^{18}F-FDG-PET/CT (41). However, there is evidence of the utility of ^{18}F-FDG-PET/CT, showing increased or decreased metabolic activity, to detect ICI-induced encephalitis earlier than standard diagnostic approaches (108). A recent study in patients with autoimmune encephalitis, which shares many similarities with ICI-related encephalitis, described 6 cases with metabolic abnormalities on ^{18}F-FDG-PET/CT with normal MRI (n=2), lumbar puncture (n=3), and electroencephalography (n=2) findings (109). Finally, cases of posterior reversible encephalopathy syndrome have been occasionally reported following ICI administration alone or in combination with chemotherapy (110–112).

Aseptic meningitis is present in <0.1% of ICI-treated patients overall (93). This condition is more commonly associated with anti-CTLA-4 and ICI-combination treatments (93, 100). Moreover, the time to clinical disease onset is short, with a delay of 9 days from the first dose of immunotherapy (100). Aseptic meningitis is characterized by the subacute onset of nonspecific symptoms such as headache, neck stiffness, photophobia, low-grade fever, and nausea, and must be distinguished from infectious or carcinomatous causes of meningitis (93). In 42% of the patients, brain MRI shows diffuse leptomeningeal enhancement with or without parenchymal abnormalities as a nonspecific sign of inflammation and is consistent with the presence of lymphocytic or neutrophil pleocytosis, while overlapping with findings of immune-induced meningoencephalitis (113, 114) (Figure 8). However, 46% of brain MRI findings are normal in ICI-induced aseptic meningitis (113). However, this even underlines the importance of imaging to rule out differential diagnosis such as (ischemic) stroke, infection, and brain metastasis.

In recent years, there is increasing evidence for ICI-associated central nervous system vasculitis. However, the exact frequency (currently estimated to be <0.01%), timing and association with a specific type of immunotherapy is still unclear (93). Commonly reported types of vasculitis are large vessel vasculitis (giant cell arteritis and isolated aortitis) and vasculitis of the nervous system (primary angiitis of the central nervous system, PANCS, and isolated vasculitis of the peripheral nervous system) (93, 115). With a median time of 3 months from the initiation of ICI treatment to their development, symptoms are often unspecific and include headaches (60%), altered cognitive status (50%), and focal neurologic deficits. Most commonly, they are mild, and no fatalities related to vasculitis have been observed (93, 115). Although considered to be the gold standard for diagnosis, biopsy of the brain and/or spinal cord showing segmental inflammatory infiltration leading to blood vessel walls thickening and stenosis, resulting in decreased blood flow or even secondary to hemorrhagic vessel rupture, has only a sensitivity of 53% (116). However, this sensitivity can be increased to more than 80% by identifying focal lesions previously on neurologic imaging techniques (117). Brain MRI is altered in more than 90% of patients with PANCS, showing (nonspecific) signs of microangiopathy, hemorrhage, or ischemic infarction, as well as multifocal bilateral T2- weighted, FLAIR and diffusion-weighted sequence abnormalities in the cortical-subcortical area (118). However, the occasional presence of solid lesions and gadolinium enhancement of leptomeninges complicate the distinction to tumors and abscesses and requires additional imaging modalities such as CT angiography, high-resolution contrast-enhanced MRI, or ^{18}F-FDG-PET/CT to detect vascular inflammatory activity (119).

Endocrine toxicities

Endocrinopathies are observed in up to 10% of patients treated with anti-CTLA-4 and in 4-14% of patients treated with anti-PD-1 therapy (120, 121).

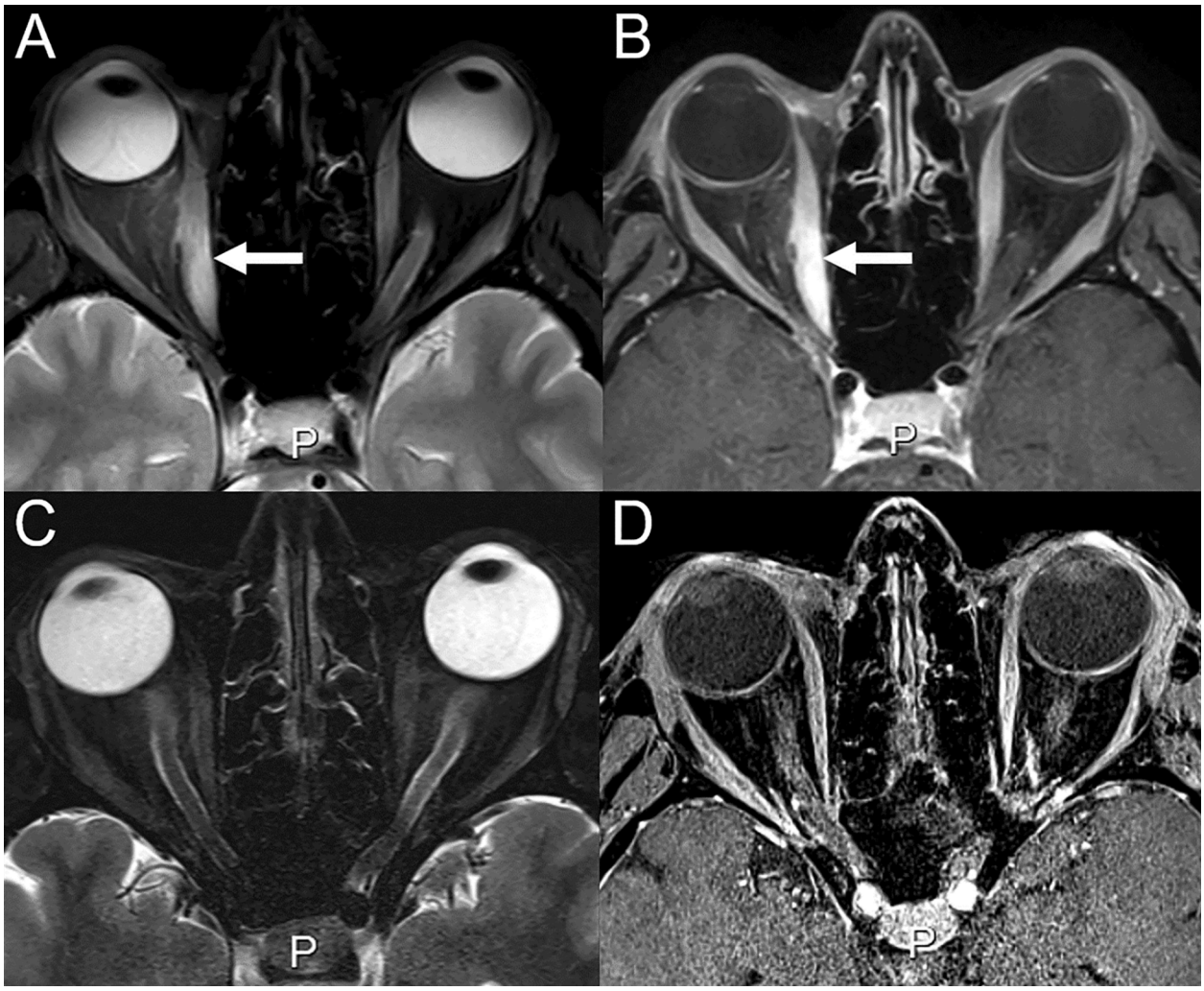

FIGURE 7
Immune-related orbital myositis in a 43-year-old female with cutaneous melanoma treated with ipilimumab (anti-CTLA-4) and nivolumab (anti-PD-1). After 3 cycles of ipilimumab and nivolumab, the patient reported diplopia. **(A)** On T2-weighted and **(B)** contrast-enhanced images, orbital edema, abnormal enhancement and thickening of the right medial occulomotor muscle can be seen, consistent with orbital myositis (arrows). **(C, D)** MRI at 1 month from treatment discontinuation with disappearance of signs of inflammation.

Hypophysitis occurs in 4.5% (0.8% severe cases) of the patients treated with anti-CTLA-4, whereas it is reported in less than 1% (0.1%) of patients with anti-PD-(L)1 treatment (122). The clinical features of pituitary dysfunction can be nonspecific and include fatigue, headache, or weakness with additional symptoms related to hypopituitarism (122, 123). The median time to symptom onset ranges between 11 weeks (ipilimumab), 17 weeks (combination of impilimumab and nivolumab), 22 weeks (nivolumab), and 26 weeks (pembrolizumab) (124). Since pituitary inflammation can be caused by ICI therapy as well as by pituitary metastasis and adenomas, MRI and ^{18}F-FDG-PET/CT are playing a crucial role in distinguishing these diseases as they often show imaging findings of immune-related hypophysitis before the appearance of symptoms (18, 42, 45). Contrast-enhanced MRI of immune-related hypophysitis shows enhancement of the posterior portion of the pituitary gland in 89% of the patients, whereas the enhancement is homogeneous in 63.3% (vs. heterogeneous enhancement, 36.7%) (16, 125) (Figure 9). This pattern is important for distinguishing this toxicity from pituitary metastasis, as differential diagnosis, which show heterogeneous enhancement in the vast majority of cases (82.6%) (16). Moreover, thickening of the pituitary stalk has been identified in 29/49 (59.2%) cases of hypophysitis and only in 16/58 (27.6%) cases with pituitary metastasis (16). On PET/CT, immune-related hypophysitis shows ^{18}F-FDG-avid pituitary gland often enlarged but without mass effect on the optic chiasm and with thickening of the infundibulum (125, 126). A recent study in 162 advanced melanoma patients who received ipilimumab/nivolumab combination therapy showed that ^{18}F-FDG-PET/CT was able to predict the appearance of hypophysitis with high positive (86%) and negative (87%) predictive values (127).

ICI-induced thyroid dysfunction is often clinically asymptomatic and transient, and identified by blood tests as mild hypo- or hyperthyroidism associated with elevated anti-thyroid peroxidase and/or anti-thyroglobulin antibodies (128). In terms of frequency, hypothyroidism is more common, affecting 15% of patients receiving ICI-combination therapy, 3% of patients

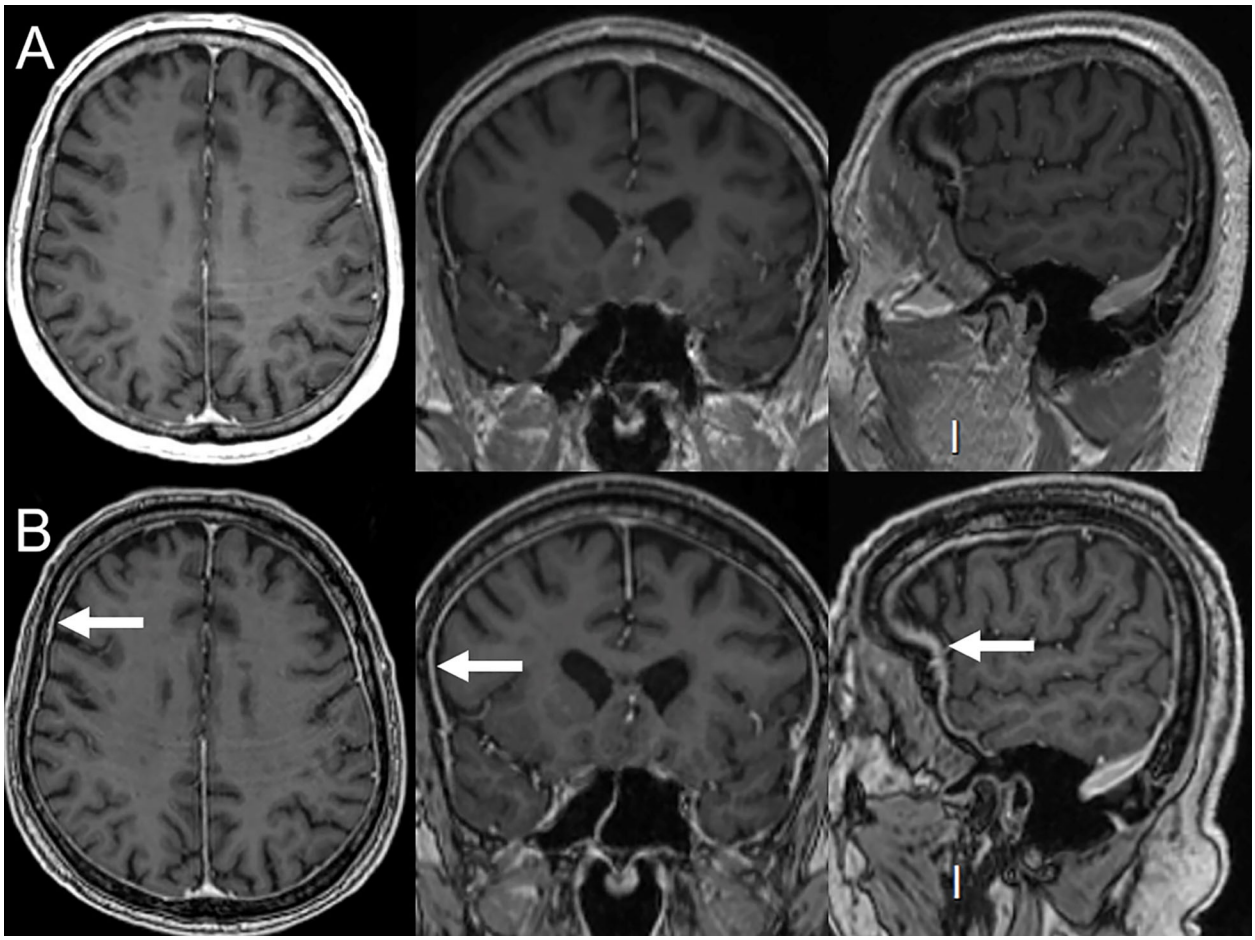

FIGURE 8
Immune-related aseptic meningitis in a 78-year-old female with NSCLC treated with ipilimumab (anti-CTLA-4) and nivolumab (anti-PD-1). **(A)** Normal brain MRI (axial, coronal and sagittal plans) performed 6 months prior to immunotherapy. After 3 cycles of ipilimumab and nivolumab, the patient developed headaches. **(B)** MRI performed 2 months after the beginning of immunotherapy showed smooth diffuse dura mater thickening (arrows) compatible with aseptical meningitis. Patient's symptoms and signs of inflammation on MRI disappeared upon immunotherapy discontinuation.

receiving anti-CTLA-4, and 8% of patients receiving anti-PD-(L)1 therapy (34). Hyperthyroidism is observed in only 4% of patients treated with anti-CTLA-4 and 5% of patients treated with anti-PD-(L)1 molecules (34). In few cases, ICI therapy did lead to Graves' disease (129). Immune-related thyroiditis, which usually occurs within 5 to 10 weeks following treatment, is mostly mild and CTCAE grade ≥3 is rarely observed (34, 130). US is the imaging modality of choice and new enlargement of the thyroid gland with heterogeneous hypoechoic parenchyma, (pseudo)nodular pattern, and increased vascularity on color Doppler is commonly observed (37, 42). CT findings are unspecific as they present a new enlargement of the thyroid gland associated with a heterogeneous parenchymal enhancement (37, 42). Still, thyroiditis remains frequently an incidental finding on ^{18}F-FDG-PET/CT with a diffuse increased uptake of the thyroid gland (Figure 10) (37, 42).

Compared with the more common secondary adrenal insufficiency caused by pituitary dysfunction, primary adrenal insufficiency, in which the adrenal glands are directly damaged due to ICI therapy, has been rarely described (131). Adrenal insufficiency is estimated to occur in 5% of patients treated with ICI-combination therapy and in 1% of patients treated with anti-CTLA-4 or anti-PD-(L)1 mAbs, whereas CTCAE grade ≥3 is rarely reported (34, 132). Disease onset after initiation of ICI treatment is in between 9 weeks (ipilimumab), 3.3 month (pembrolizumab) and 5 months (nivolumab) (121, 133). Symptoms are characterized by electrolyte abnormalities, dehydration and altered mental status. Life-threatening adrenal crisis with vasodilatator shock and hypotension, requiring permanent steroid replacement therapy, was reported following nivolumab therapy (134). Therefore, rapid diagnosis and close monitoring are required. On CT and MRI, adrenal glands show bilateral, symmetrical, and smooth enlargement, while uniform mild hypermetabolism is seen on ^{18}F-FDG PET/CT (42, 135).

Current challenges and future directions

The increasing use of immunotherapies in clinical practice has led to the challenge of individually managing their treatment-

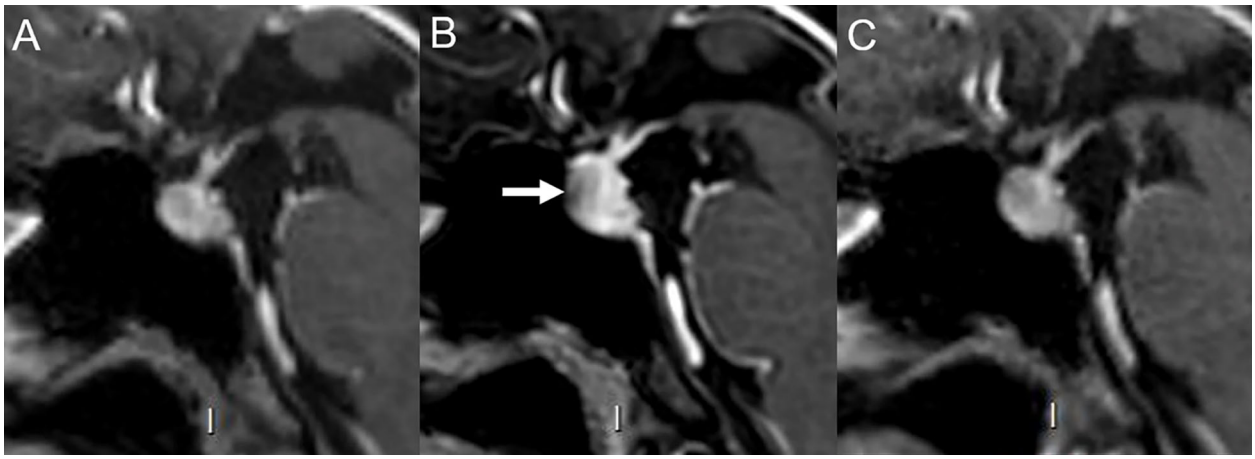

FIGURE 9
Immune-related hypophysitis in a 43-year-old female with cutaneous melanoma treated with ipilimumab and nivolumab. **(A)** Normal hypophyseal MRI performed 4 months prior to immunotherapy. After 3 cycles of ipilimumab (anti-CTLA-4) and nivolumab (anti-PD-1), the patient developed headaches. **(B)** MRI revealed increased hypophyseal height with mild pituitary stalk thickening and reduced opto-chiasmatic cistern size compatible with hypophysitis (arrow). Ipilimumab was discontinued and 2 more cycles of nivolumab alone were administered. Eventually, nivolumab was discontinued due to a grade 3 toxidermia. **(C)** Hypophyseal MRI performed 3 months after the last immunotherapy cycle was normal with disappearance of signs of inflammation.

related toxicities. It is particularly important to distinguish patients who benefit from therapy from those who are at risk of experiencing drug-related toxicities. Imaging plays a central role in the detection and characterization of these irAEs as well as in the differentiation of immunotherapy-associated response patterns such as pseudoprogression . In severe cases, appropriate treatment of these ICI-induced toxicities must be initiated as early as possible, and it may even be necessary to discontinue ICI treatment. However, it is important to note that many ICI-induced toxicities are mild and manageable. Since the increased use of imaging may lead to important financial costs and resources associated with e.g. monitoring of these irAEs with imaging, it is crucial to define parameters, to distinguish patients who benefit from imaging follow-up from patients for whom blood-based monitoring or simply clinical monitoring is sufficient. Moreover, the role of imaging still needs to be defined in other ICI-related phenomena, such as the presumably rare and previously poorly described but possibly fatal cytokine release syndrome which occurs usually within 4 weeks of ICI-treatment initiation (136, 137).

Interestingly, the occurrence of (low-grade) irAEs has been correlated with treatment efficacy and improved clinical outcomes as measured by overall response rate, progression-free survival and overall survival (6, 17). Furthermore early-onset immune-related hepatitis as irAEs was used to detect pseudoprogression and to distinguish this response pattern from true progression in a case of metastatic ovarian cancer treated with nivolumab (138).

A current research topic is the use of radiomics and deep learning techniques to evaluate and even predict cancer therapy success. Radiomics has already been proven to predict toxicity in the assessment of chemotherapy (139). Liver toxicity could be identified using liver texture analysis on the first follow-up CT before any increase in liver function tests could be detected in a proof-of-concept study of colorectal cancer patients treated with 5-fluorouracil (139). It is conceivable that similar approaches can be used to identify patients who benefit most from immunotherapies, as opposed to patients at higher risk for developing irAEs (140, 141). Preliminary studies in non-small cell lung cancer patients showed promising results. Radiomics could potentially predict the development of ICI-induced pneumonitis based on baseline CT characteristics with 100% accuracy (p = 0.0033) and a strong predictive power (area under the curve 1.0, p = 0.0033) (142). Despite the limited size of the training sample (2 patients who developed pneumonitis and 30 patients who did not), these results may help to stratify patients at risk for developing pulmonary toxicities and therefore allowing for pre-treatment modifications and changes of the therapy. Moreover, radiomic signatures on baseline CT have been shown to be more sensitive than clinical findings in identifying patients at risk for developing ICI-induced pneumonitis (143). Furthermore, radiomic features extracted from ^{18}F-FDG PET/CT might provide important clues for the prediction of irAEs. A retrospective study of 146 patients with advanced non-small cell lung cancer was used to develop a multi-factorial radiomic model based on a radiomic score, generated using features extracted from PET, CT and PET/CT fusion images of baseline ^{18}F-FDG-PET/CT (117). The combination of high radiomics score values with the type and dose of immunotherapy have been shown to be associated with the development of severe irAE (144). These findings underscore the value of a comprehensive baseline imaging analysis in patients treated with ICIs, as it could help predicting and preventing even life-threatening irAEs that may not be detected during baseline clinical or biological assessments.

Recently, several studies have demonstrated an association between irAEs detected on ^{18}F-FDG PET/CT and favorable clinical outcomes, suggesting the value of ^{18}F-FDG PET/CT in predicting responses to immunotherapy (32, 78, 145, 146). In 10% of patients with unresectable metastatic melanoma treated with

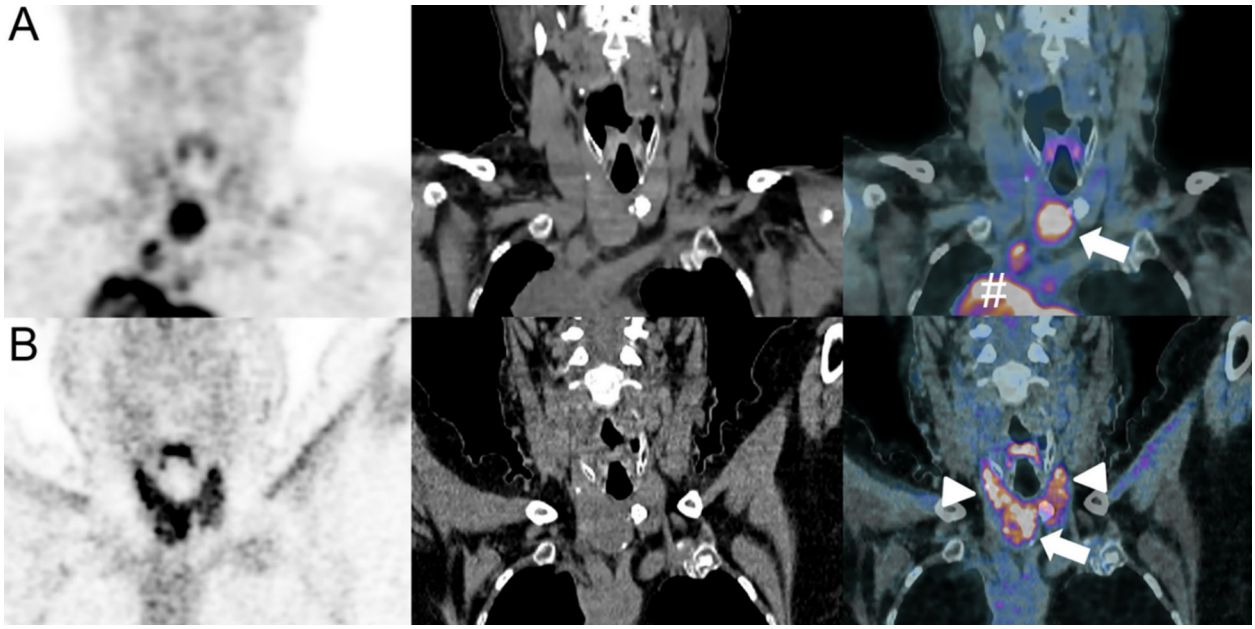

FIGURE 10
Immune-related thyroiditis in a 50-year-old female with lower leg Meckel-cell carcinoma who developed mediastinal metastatic spread as shown on baseline ^{18}F-FDG-PET/CT [coronal PET, CT and merged PET/CT images, # **(A)**]. A thyroid nodule was also present [arrow, fused PET/CT image **(A)**]. Pembrolizumab (anti-PD-1) was administered. Follow-up 18F-FDG-PET/CT at 6 months showed disappearance of mediastinal disease and decrease in metabolic activity of the thyroid nodule [arrow, fused PET/CT image **(B)**]. However, a marked increase in thyroid activity was also evident, consistent with a thyroiditis [arrowheads, fused PET/CT image **(B)**].

ipilimumab who underwent interim or late ^{18}F-FDG-PET/CT sarcoid-like mediastinal-hilar lymphadenopathy was reported and all these patients showed disease control (78). This pattern was not seen in patients with progressive disease, suggesting an association of sarcoid-like reactions with clinical benefits of anti-CTLA-4 therapy. Similarly, a small study of 16 patients with BRAF-mutated metastatic melanoma treated with vemurafenib/ipilimumab combination therapy who underwent ^{18}F-FDG-PET/CT detected 7 patients developing at least one irAE (most frequently colitis and arthritis) (146). All these patients had a significantly longer progression-free survival than those without irAEs ($p = 0.036$) (146). Similary, in ICI-treated patients with either renal cell carcinoma, malignant melanoma, or lymphoma who underwent early time-point ^{18}F-FDG-PET/CT, an association was found between thyroiditis and improvement of clinical symptoms at the 12-month follow-up (32). This finding was confirmed in another study which examined 91 patients treated with anti-PD-L1 therapy, suggesting that immune-related thyroiditis could be a potential predictor of response to ICI treatment (147). Overall, although imaging such as ^{18}F-FDG PET/CT can contribute to the (early) detection of irAEs and irAE detected on this imaging modality might contribute to predict patient's prognosis, these findings must always be considered in the context of patient's symptoms (if any), comorbidities, and other findings (e.g., laboratory values) in order to decide whether or not ICI treatment should be continued.

The recent development of immune-PET tracers may improve ICI response monitoring and diagnosis of irAEs by increasing the specificity of pathological uptake seen on molecular imaging compared with ^{18}F-FDG-PET/CT which, although widely used, has poor cell specificity (76, 148). This could be particularly useful when findings on ^{18}F-FDG-PET/CT are inconclusive and cannot distinguish between irAEs and true or pseudo-progression. In this setting, ^{89}Zr and ^{64}Cu-Keytruda could be useful as anti-PD-1 human antibody immuo-PET tracers as they represent a specific imaging modality for PD-1-expressing tumor-infiltrating lymphocytes (149). Similarly, ^{89}Zr-Nivolumab uptake on PET/CT correlates with PD-1-expressing lymphocytes and offers the possibility of a real-time imaging of tumor infiltrating T-cells (150). Granzyme B-targeted PET tracer (GZP) as another novel PET tracer for detection of irAEs, has also shown promising results in a murine model (151). This recent study showed an increased uptake of GZP in organs affected by irAEs and a decreased uptake after anti-inflammatory treatment, with a good correlation with immune infiltration on histology (151). This is all the more interesting since granzyme B was also found in colon and kidney samples of patients with irAEs, suggesting its potential utility in routine practice for patients treated with ICI (151, 152). However, even though novel immune-PET tracers seem to be useful and to provide important clues mainly in nonspecific cases, most findings are based on small (preclinical) studies.

In addition to ICI therapy, there are many other types of immunotherapies that may be associated with different spectra of irAEs (Figure 11). Chimeric antigen receptor (CAR) T-cell therapy has been shown to induce rapid and durable responses in many types of cancers (153). However, treatment associated toxicities can be severe and even fatal, such as most commonly the cytokine-release syndrome which has a comparable clinical presentation to hemophagocytic lymphohistiocytosis or macrophage-activation

syndrome and is characterized by hepatosplenomegaly, hepatic dysfunction, hyperferritinemia, hypofibrinogenemia, and coagulopathy (153, 154). In addition, irAEs associated with CAR T-cell therapy include the immune effector cell-associated neurotoxicity syndrome, characterized by initial global aphasia (153, 154). During the course of disease, patients usually experience subclinical or clinical seizures and rarely diffuse cerebral edema within 28 days (153). The diagnostic workup includes clinical and neurological examination, an electroencephalogram, and a brain MRI (153). A single-center study investigated 133 patients with relapsed and/or refractory $CD19^+$ B-cell acute lymphatic leucemia, non-Hodgkin lymphoma, and chronic lymphoid lymphoma who received CD19-CAR-T cell therapy (155). Acute abnormalities in brain MRI examinations were noted in 30% which were associated with poor outcome, especially in severe cases (155). Changes in T2-weighted/FLAIR brain MRI indicative of vasogenic edema, leptomeningeal enhancement, and/or multifocal microhemorrhages could be found in most of the patients with clinically severe neurotoxicity and abnormal MRI scans (155). In addition, contrast enhancement suggestive of blood-brain barrier breakdown has been noted in some patients (155). One patient showed extensive cortical diffusion restriction indicative of cytotoxic edema and several others showed vasogenic edema that developed into cortical laminar necrosis (155). However, larger, high-quality multicenter studies are needed to more thoroughly investigate the toxicities associated with CAR-T cells and, in particular, regarding their potentially specific imaging properties.

Interestingly, peptide-based vaccines show a better tolerance and safety compared with conventional chemotherapy and ICI, and serious irAEs, such as pulmonary embolism, are rarely described (156). A meta-analysis that included 500 patients demonstrated that only 1.2% of vaccinated patients suffered from serious adverse events related to the vaccine (157). The vaccine-related irAEs include most commonly erythema and induration related to the injection side (156). Moreover, nonspecific symptoms such as nausea, diarrhea, myalgia, fatigue, increased aspartate aminotransaminase and alkaline phosphatase, and rarely hematological toxicities as well as autoimmunity have been described (156).

Finally, adverse events associated with oncolytic virus therapy are also mostly mild and usually include flulike symptoms and local reactions at the injection sites (158). However, more severe toxicities such as anemia, leukopenia, lymphopenia, neutropenia, thrombocytopenia, liver dysfunction, and hematological abnormalities, pleural effusion, herpes virus infection, and central nervous system symptoms have been described (158).

Overall, no specific imaging features of irAEs have been described yet. As the clinical use of these novel treatments increases, problems

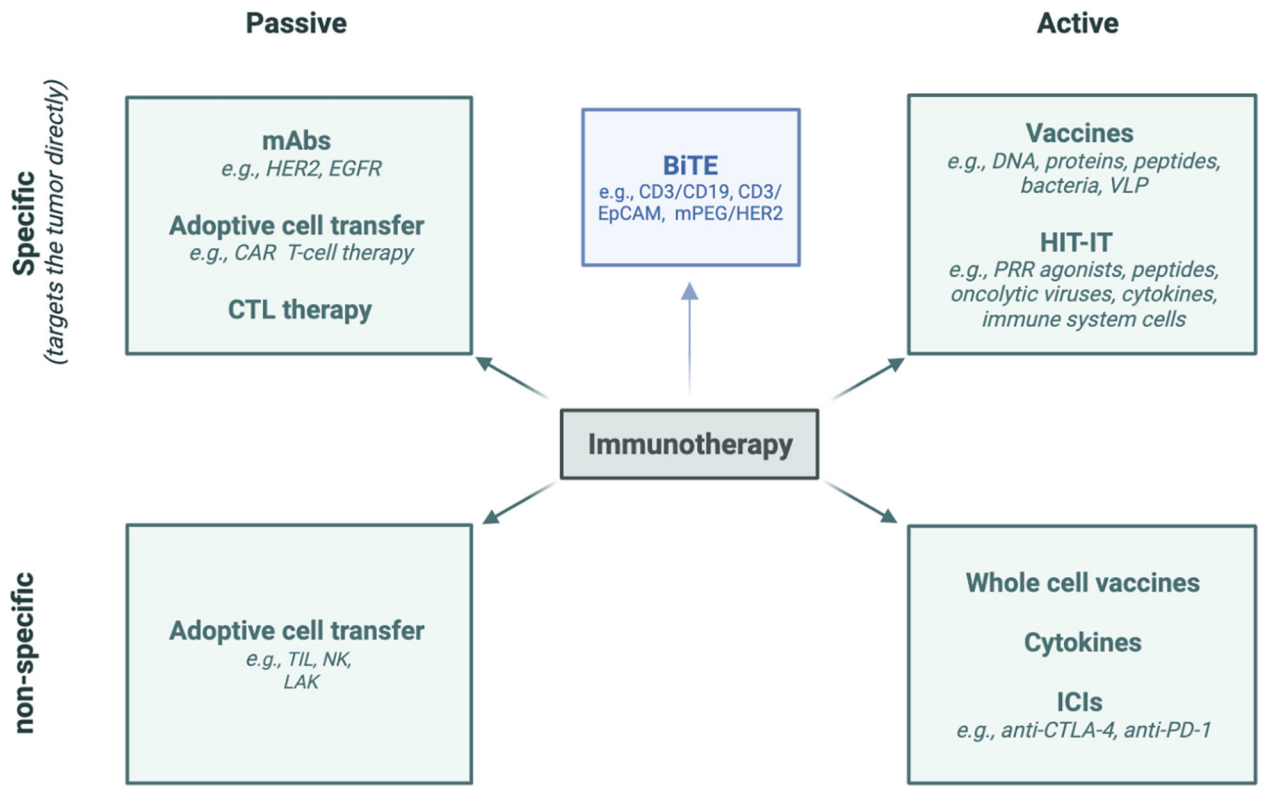

FIGURE 11
Diverse methods of immunotherapy. HER2, human epidermal growth factor receptor 2; EGFR, Epidermal Growth Factor Receptor; CAR, chimeric antigen receptor; CTL, cytotoxic T-lymphocyte; TIL, tumor-infiltrating lymphocyte; NK cell, natural killer cell; LAK cell, lymphokine-activated killer cell; BiTE, Bi-specific T-cell engagers; EpCAM, epithelial cell adhesion molecule; DNA, deoxyribonucleic acid; VLP, virus-like particle; HIT-IT, human intratumoral immunotherapy; PRR: pattern-recognition receptor; ICI, immune checkpoint inhibitor; CTLA-4, cytotoxic T-lymphocyte-associated protein-4; PD-1, programmed cell death protein-1; PD-L1, programmed death-ligand 1.

in the toxicity screening will, therefore, arise. However, over time, more information on non-ICI immunotherapies will be collected that will shed light on their specific toxicity profile and help to define their imaging characteristics.

To conclude, imaging can contribute to the detection and characterization of ICI-related toxicities, while radiomics can even help to predict these toxicities. However, reliable toxicity screening of irAEs remains challenging for rarer irAEs and non-ICI immunotherapeutics. Therefore, there is a need for large-scale clinical trials across various oncologic diseases and immunotherapeutic agents to better assess the characteristics of both ICIs and non-ICI-immunotherapies in order to establish evidence-based guidelines as support for imaging assessment and clinical decision-making.

Author contributions

All authors contributed to manuscript drafting, revision and approved the submitted version.

Funding

Open access funding provided by University of Lausanne.

Acknowledgments

All figures included in the manuscript contain imaging performed at the Department of Diagnostic and Interventional Radiology at Lausanne University Hospital and have not been published in any previous publication.

Conflict of interest

The authors declare that the research was conducted in the absence of any commercial or financial relationships that could be construed as a potential conflict of interest.

Publisher's note

Supplementary material

The Supplementary Material for this article can be found online at: https://www.frontiersin.org/articles/10.3389/fimmu.2023.1133207/full#supplementary-material

SUPPLEMENTARY FIGURE 1
"Starry sky" appearance. Small echogenic foci representing portal triads and portal venous walls (stars; arrows) can be seen throughout a diffusely hypoechogenic liver parenchyma (sky). This pattern, although non-specific, can be seen with hepatitis.

References

1. Bagchi S, Yuan R, Engleman EG. Immune checkpoint inhibitors for the treatment of cancer: Clinical impact and mechanisms of response and resistance. *Annu Rev Pathol* (2021) 16:223–49. doi: 10.1146/annurev-pathol-042020-042741

2. McDermott D, Haanen J, Chen T-T, Lorigan P, O'day S. Efficacy and safety of ipilimumab in metastatic melanoma patients surviving more than 2 years following treatment in a phase III trial (MDX010-20). *Ann Oncol* (2013) 24:2694–8. doi: 10.1093/annonc/mdt291

3. Vaddepally RK, Kharel P, Pandey R, Garje R, Chandra AB. Review of indications of FDA-approved immune checkpoint inhibitors per NCCN guidelines with the level of evidence. *Cancers (Basel)* (2020) 12(3):738. doi: 10.3390/cancers12030738

4. Wojtukiewicz MZ, Rek MM, Karpowicz K, Górska M, Polityńska B, Wojtukiewicz AM, et al. Inhibitors of immune checkpoints-PD-1, PD-L1, CTLA-4-new opportunities for cancer patients and a new challenge for internists and general practitioners. *Cancer Metastasis Rev* (2021) 40(3):949–82. doi: 10.1007/s10555-021-09976-0

5. Soerensen AV, Ellebaek E, Bastholt L, Schmidt H, Donia M, Svane IM. Improved progression-free long-term survival of a nation-wide patient population with metastatic melanoma. *Cancers (Basel)* (2020) 12(9):2591. doi: 10.3390/cancers12092591

6. Das S, Johnson DB. Immune-related adverse events and anti-tumor efficacy of immune checkpoint inhibitors. *J Immunother Cancer* (2019) 7(1):306. doi: 10.1186/s40425-019-0805-8

7. Berz AM, Dromain C, Vietti-Violi N, Boughdad S, Duran R. Tumor response assessment on imaging following immunotherapy. *Front Oncol* (2022). doi: 10.3389/fonc.2022.982983

8. Dromain C, Beigelman C, Pozzessere C, Duran R, Digklia A. Imaging of tumour response to immunotherapy. *Eur Radiol Exp* (2020) 4(1):2. doi: 10.1186/s41747-019-0134-1

9. Schwartz LH, Litière S, de Vries E, Ford R, Gwyther S, Mandrekar S, et al. RECIST 1.1-update and clarification: From the RECIST committee. *Eur J Cancer* (2016) 62:132–7. doi: 10.1016/j.ejca.2016.03.081

10. Wolchok JD, Hoos A, O'Day S, Weber JS, Hamid O, Lebbé C, et al. Guidelines for the evaluation of immune therapy activity in solid tumors: immune-related response criteria. *Clin Cancer Res* (2009) 5(23):7412–20. doi: 10.1158/1078-0432.CCR-09

11. Nishino M, Giobbie-Hurder A, Gargano M, Suda M, Ramaiya NH, Hodi FS, et al. Developing a common language for tumor response to immunotherapy: immune-related response criteria using unidimensional measurements. *Clin Cancer Res* (2013) 19(14):3936–43. doi: 10.1158/1078-0432.CCR-13-0895

12. Xu C, Chen YP, Du XJ, Liu JQ, Huang CH, Chen L, et al. Comparative safety of immune checkpoint inhibitors in cancer: systematic review and network meta-analysis. *BMJ* (2018) 363:k4226. doi: 10.1136/bmj.k4226

13. Postow MA, Sidlow R, Hellmann MD. Immune-related adverse events associated with immune checkpoint blockade. *N Engl J Med* (2018) 378(2):158–68. doi: 10.1056/NEJMra1703481

14. Wolchok JD, Chiarion-Sileni V, Gonzalez R, Rutkowski P, Grob JJ, Cowey CL, et al. Overall survival with combined nivolumab and ipilimumab in advanced melanoma. *N Engl J Med* (2017) 377(14):1345–56. doi: 10.1056/NEJMoa1709684

15. Wang DY, Salem JE, Cohen JV, Chandra S, Menzer C, Ye F, et al. Fatal toxic effects associated with immune checkpoint inhibitors: A systematic review and meta-analysis. *JAMA Oncol* (2018) 4(12):1721–8. doi: 10.1001/jamaoncol.2018.3923

16. Mekki A, Dercle L, Lichtenstein P, Nasser G, Marabelle A, Champiat S. Machine learning defined diagnostic criteria for differentiating pituitary metastasis from autoimmune hypophysitis in patients undergoing immune checkpoint blockade blockade therapy. *Eur J Cancer* (2019) 119:44–56. doi: 10.1016/j.ejca.2019.06.020

17. Bronstein Y, Ng CS, Hwu P, Hwu WJ. Radiologic manifestations of immune-related adverse events in patients with metastatic melanoma undergoing anti-CTLA-4 antibody therapy. *AJR Am J Roentgenol* (2011) 197(6):W992–W1000. doi: 10.2214/AJR.10.6198

18. Kwak JJ, Tirumani SH, Van den Abbeele AD, Koo PJ, Jacene HA. Cancer immunotherapy: imaging assessment of novel treatment response patterns and immune-related adverse events. *Radiographics* (2015) 35(2):424–37. doi: 10.1148/rg.352140121

19. Bai R, Chen N, Li L, Du N, Bai L, Lv Z, et al. Mechanisms of cancer resistance to immunotherapy. *Front Oncol* (2020) 10:1290. doi: 10.3389/fonc.2020.01290

20. Haanen JBAG, Carbonnel F, Robert C, Kerr KM, Peters S, Larkin J, et al. Management of toxicities from immunotherapy: ESMO clinical practice guidelines for diagnosis, treatment and follow-up. *Ann Oncol* (2018) 29(Suppl 4):iv264–6. doi: 10.1093/annonc/mdy162

21. Martins F, Sofiya L, Sykiotis GP, Lamine F, Maillard M, Fraga M, et al. Adverse effects of immune-checkpoint inhibitors: epidemiology, management and surveillance. *Nat Rev Clin Oncol* (2019) 16(9):563–80. doi: 10.1038/s41571-019-0218-0

22. Weber JS, D'Angelo SP, Minor D, Hodi FS, Gutzmer R, Neyns B, et al. Nivolumab versus chemotherapy in patients with advanced melanoma who progressed after anti-CTLA-4 treatment (CheckMate 037): a randomised., controlled, open-label, phase 3 trial. *Lancet Oncol* (2015) 16(4):375–84. doi: 10.1016/S1470-2045(15)70076-8

23. Ramos-Casals M, Brahmer JR, Callahan MK. Immune-related adverse events of checkpoint inhibitors. *Nat Rev Dis Primers* (2020) 6(1):38. doi: 10.1038/s41572-020-0160-6

24. Sandigursky A, Mor A. Immune-related adverse events in cancer patients treated with immune checkpoint inhibitors. *Curr Rheumatol Rep* (2018) 20(10):65. doi: 10.1007/s11926-018-0770-0

25. Kanjanapan Y, Day D, Butler MO, Wang L, Joshua AM, Hogg D, et al. Delayed immune-related adverse events in assessment for dose-limiting toxicity in early phase immunotherapy trials. *Eur J Cancer* (2018) 107:1–7. doi: 10.1016/j.ejca.2018.10.017

26. Couey MA, Bell RB, Patel AA, Romba MC, Crittenden MR, Curti BD, et al. Delayed immune-related events (DIRE) after discontinuation of immunotherapy: diagnostic hazard of autoimmunity at a distance. *J Immunother Cancer* (2019) 7(1):165. doi: 10.1186/s40425-019-0645-6

27. Kanjanapan Y, Day D, Butler MO, Wang L, Joshua AM, Hogg D, et al. Delayed immune-related adverse events in assessment for dose-limiting toxicity in early phase immunotherapy trials. *Eur J Cancer* (2019) 107:1–7. doi: 10.1016/j.ejca.2018.10.017

28. Dougan M, Luoma AM, Dougan SK, Wucherpfennigm KW. Understanding and treating the inflammatory adverse events of cancer immunotherapy. *Cell* (2021) 184(6):1575–88. doi: 10.1016/j.cell.2021.02.011

29. Choi J, Lee SY. Clinical characteristics and treatment of immune-related adverse events of immune checkpoint inhibitors. *Immune Netw* (2020) 20(1):e9. doi: 10.4110/in.2020.20.e9

30. Khoja L, Day D, Wei-Wu Chen T, Siu LL, Hansen AR. Tumour- and class-specific patterns of immune-related adverse events of immune checkpoint inhibitors: a systematic review. *Ann Oncol* (2017) 28(10):2377–85. doi: 10.1093/annonc/mdx286

31. National Cancer Institute. *Common terminology criteria for adverse events (CTCAE)* (2022). Available at: https://ctep.cancer.gov/protocolDevelopment/electronic_applications/ctc.htm#ctc_60 (Accessed 25, 2022).

32. Nobashi T, Baratto L, Reddy SA, Srinivas S, Toriihara A, Hatami N, et al. Predicting response to immunotherapy by evaluating tumors, lymphoid cell-rich organs, and immune-related adverse events using FDG-PET/CT. *Clin Nucl Med* (2019) 44(4):e272–9. doi: 10.1097/RLU.0000000000002453

33. Hussaini S, Chehade R, Boldt RG, Raphael J, Blanchette P, Maleki Vareki S, et al. Association between immune-related side effects and efficacy and benefit of immune checkpoint inhibitors - a systematic review and meta-analysis. *Cancer Treat Rev* (2021) 92:102134. doi: 10.1016/j.ctrv.2020.102134

34. Arnaud-Coffin P, Maillet D, Gan HK, Stelmes JJ, You B, Dalle S, et al. A systematic review of adverse events in randomized trials assessing immune checkpoint inhibitors. *Int J Cancer* (2019) 145(3):639–48. doi: 10.1002/ijc.32132

35. Brahmer JR, Abu-Sbeih H, Ascierto PA, Brufsky J, Cappelli LC, Cortazar FB, et al. Society for immunotherapy of cancer (SITC) clinical practice guideline on immune checkpoint inhibitor-related adverse events. *J Immunother Cancer* (2021) 9(6):e002435. doi: 10.1136/jitc-2021-002435

36. Kumar V, Chaudhary N, Garg M, Floudas CS, Soni P, Chandra AB. Current diagnosis and management of immune related adverse events (irAEs) induced by immune checkpoint inhibitor therapy. *Front Pharmacol* (2017) 8:49. doi: 10.3389/fphar.2017.00049

37. Tirumani SH, Ramaiya NH, Keraliya A, Bailey ND, Ott PA, Hodi FS, et al. Radiographic profiling of immune-related adverse events in advanced melanoma patients treated with ipilimumab. *Cancer Immunol Res* (2015) 3(10):1185–92. doi: 10.1158/2326-6066.CIR-15-0102

38. Kim KW, Ramaiya NH, Krajewski KM, Shinagare AB, Howard SA, Jagannathan JP, et al. Ipilimumab-associated colitis: CT findings. *AJR Am J Roentgenol* (2013) 200:W468–74. doi: 10.2214/AJR.12.9751

39. Barina AR, Bashir MR, Howard BA, Hanks BA, Salama AK, Jaffe TA. Isolated rectosigmoid colitis: a new imaging pattern of ipilimumab-associated colitis. *Abdom Radiol* (2016) 41:207–14. doi: 10.1007/s00261-015-0560-3

40. Rovira JI, Thirumurthi S, Taggart M, Yilmaz B, Lin H, Zhong LL, et al. Role of abdominal and pelvic CT scans in diagnosis of patients with immunotherapy-induced colitis. *J Immunother Precis Oncol* (2022) 5(2):32–6. doi: 10.36401/JIPO-21-21

41. Schierz JH, Sarikaya I, Wollina U, Unger L, Sarikaya A. Immune checkpoint inhibitor-related adverse effects and 18 f-FDG PET/CT findings. *J Nucl Med Technol* (2021) 49(4):324–9. doi: 10.2967/jnmt.121.262151

42. Alessandrino F, Sahu S, Nishino M, Adeni AE, Tirumani SH, Shinagare AB, et al. Frequency and imaging features of abdominal immune-related adverse events in metastatic lung cancer patients treated with PD-1 inhibitor. *Abdom Radiol (NY)* (2019) 44(5):1917–27. doi: 10.1007/s00261-019-01935-2

43. Lang N, Dick J, Slynko A, Schulz C, Dimitrakopoulou-Strauss A, Sachpekidis C, et al. Clinical significance of signs of autoimmune colitis in 18 f-fluorodeoxyglucose positron emission tomography-computed tomography of 100 stage-IV melanoma patients. *Immunotherapy* (2019) 11(8):667–76. doi: 10.2217/imt-2018-0146

44. Larkin J, Chiarion-Sileni V, Gonzalez R, Grob JJ, Cowey CL, Lao CD, et al. Combined nivolumab and ipilimumab or monotherapy in untreated melanoma. *N Engl J Med* (2015) 373:23–34. doi: 10.1056/NEJMoa1504030

45. Kim KW, Ramaiya NH, Krajewski KM, Jagannathan JP, Tirumani SH, Srivastava A, et al. Ipilimumab associated hepatitis: imaging and clinicopathologic findings. *Invest New Drugs* (2013) 31:1071–7. doi: 10.1007/s10637-013-9939-6

46. Raad RA, Pavlick A, Kannan R, Friedman KP. Ipilimumab-induced hepatitis on 18F-FDG PET/CT in a patient with malignant melanoma. *Clin Nucl Med* (2015) 40(3):258–9. doi: 10.1097/RLU.0000000000000606

47. Prigent K, Aide N. 18 f-fludeoxyglucose PET/Computed tomography for assessing tumor response to immunotherapy and detecting immune-related side effects: A checklist for the PET reader. *PET Clin* (2020) 15(1):1–10. doi: 10.1016/j.cpet.2019.08.006

48. Boktor RR, Walker G, Stacey R, Gledhill S, Pitman AG. Reference range for intrapatient variability in blood-pool and liver SUV for 18F-FDG PET. *J Nucl Med* (2013) 54(5):677–82. doi: 10.2967/jnumed.112.108530

49. Sarikaya I, Albatineh AN, Sarikaya A. Revisiting weight-normalized SUV and lean-Body-Mass-Normalized SUV in PET studies. *J Nucl Med Technol* (2020) 48(2):163–7. doi: 10.2967/jnmt.119.233353

50. Abu-Sbeih H, Tran CN, Ge PS. Case series of cancer patients who developed cholecystitis related to immune checkpoint inhibitor treatment. *J Immunother Cancer* (2019) 7(1):118. doi: 10.1186/s40425-019-0604-2

51. Kawakami H, Tanizaki J, Tanaka K, Haratani K, Hayashi H, Takeda M, et al. Imaging and clinicopathological features of nivolumab-related cholangitis in patients with non-small cell lung cancer. *Invest New Drugs* (2017) 35(4):529–36. doi: 10.1007/s10637-017-0453-0

52. Pourvaziri A, Parakh A, Biondetti P, Sahani D, Kambadakone A. Abdominal CT manifestations of adverse events to immunotherapy: a primer for radiologists. *Abdom Radiol* (2020) 45:2624–36. doi: 10.1007/s00261-020-02531-5

53. Banks PA, Bollen TL, Dervenis C, Gooszen HG, Johnson CD, Sarr MG, et al. Classification of acute pancreatitis - 2012: revision of the Atlanta classification and definitions by international consensus. *Gut* (2013) 62(1):102–11. doi: 10.1136/gutjnl-2012-302779

54. Friedman CF, Clark V, Raikhel AV, Barz T, Shoushtari AN, Momtaz P, et al. Thinking critically about classifying adverse events: Incidence of pancreatitis in patients treated with nivolumab + ipilimumab. *J Natl Cancer Inst* (2016) 109(4):djw260. doi: 10.1093/jnci/djw260

55. Hoadley A, Sandanayake N, Long GV. Atrophic exocrine pancreatic insufficiency associated with anti-PD1 therapy. *Ann Oncol* (2017) 28:434–5. doi: 10.1093/annonc/mdw626

56. Wachsmann JW, Ganti R, Peng F. Immune-mediated disease in ipilimumab immunotherapy of melanoma with FDG PET-CT. *Acad Radiol* (2017) 24:111–5. doi: 10.1016/j.acra.2016.08.005

57. Seethapathy H, Zhao S, Chute DF, Zubiri L, Oppong Y, Strohbehn I, et al. The incidence, causes, and risk factors of acute kidney injury in patients receiving immune checkpoint inhibitors. *Clin J Am Soc Nephrol* (2019) 14(12):1692–700. doi: 10.2215/CJN.00990119

58. Cortazar FB, Marrone KA, Troxell ML, Ralto KM, Hoenig MP, Brahmer JR, et al. Clinicopathological features of acute kidney injury associated with immune checkpoint inhibitors. *Kidney Int* (2016) 90(3):638–47. doi: 10.1016/j.kint.2016.04.008

59. Forde PM, Rock K, Wilson G, O'Byrne KJ. Ipilimumab-induced immune-related renal failure–a case report. *Anticancer Res* (2012) 32(10):4607–8.

60. Qualls D, Seethapathy H, Bates H, Tajmir S, Heidari P, Endres P, et al. Positron emission tomography as an adjuvant diagnostic test in the evaluation of checkpoint inhibitor- associated acute interstitial nephritis. *J Immunother Cancer* (2019) 7(1):356. doi: 10.1186/s40425-019-0820-9

61. Seethapathy H, Herrmann SM, Sise ME. Immune checkpoint inhibitors and kidney toxicity: Advances in diagnosis and management. *Kidney Med* (2021) 3(6):1074–81. doi: 10.1016/j.xkme.2021.08.008

62. Chuzi S, Tavora F, Cruz M, Costa R, Chae YK, Carneiro BA, et al. Clinical features, diagnostic challenges, and management strategies in checkpoint inhibitor-related pneumonitis. *Cancer Manag Res* (2017) 9:207–13. doi: 10.2147/CMAR.S136818

63. Nishino M, Giobbie-Hurder A, Hatabu H, Ramaiya NH, Hodi FS. Incidence of programmed cell death 1 inhibitor-related pneumonitis in patients with advanced cancer: A systematic review and meta-analysis. *JAMA Oncol* (2016) 2(12):1607–16. doi: 10.1001/jamaoncol.2016.2453

64. Rizvi NA, Mazières J, Planchard D, Stinchcombe TE, Dy GK, Antonia SJ, et al. Activity and safety of nivolumab, an anti-PD-1 immune checkpoint inhibitor, for patients with advanced, refractory squamous non-small-cell lung cancer (CheckMate 063): a phase 2, single-arm trial. *Lancet Oncol* (2015) 16(3):257–65. doi: 10.1016/S1470-2045(15)70054-9

65. Naidoo J, Wang X, Woo KM, Lyriboz T, Halpenny D, Cunningham J, et al. Pneumonitis in patients treated with anti-programmed death-1/Programmed death ligand 1 therapy. *J Clin Oncol* (2017) 35(7):709–17. doi: 10.1200/JCO.2016.68.2005

66. Nishino M, Ramaiya NH, Awad MM, Sholl LM, Maattala JA, Taibi M, et al. PD-1 inhibitor-related pneumonitis in advanced cancer patients: Radiographic patterns and clinical course. *Clin Cancer Res* (2016) 22(24):6051–60. doi: 10.1158/1078-0432.CCR-16-1320

67. Zhang Q, Tang L, Zhou Y, He W, Li W. Immune checkpoint inhibitor-associated pneumonitis in non-small cell lung cancer: Current understanding in characteristics, diagnosis, and management. *Front Immunol* (2021) 12:663986 : s.n. doi: 10.3389/fimmu.2021.663986

68. Shen CI, Yeh YC, Chiu CH. Progressive pleural effusion as an immune-related adverse event in NSCLC: A case report. *JTO Clin Res Rep* (2021) 2(5):100156. doi: 10.1016/j.jtocrr.2021.100156

69. Sawada R, Matsui Y, Uchino J, Okura N, Morimoto Y, Iwasaku M, et al. Late-onset pleural and pericardial effusion as immune-related adverse events after 94 cycles of nivolumab. *Intern Med* (2021) 60(22):3585–8. doi: 10.2169/internalmedicine.7219-21

70. Gandy N, Arshad MA, Wallitt KL, Dubash S, Khan S, Barwick TD. Immunotherapy-related adverse effects on 18 f-FDG PET/CT imaging. *Br J Radiol* (2020) 93(1111):20190832. doi: 10.1259/bjr.20190832

71. Carter BW, Halpenny DF, Ginsberg MS, Papadimitrakopoulou VA, de Groot PM. Immunotherapy in non-small cell lung cancer treatment: Current status and the role of imaging. *J Thorac Imaging* (2017) 32(5):300–12. doi: 10.1097/RTI.0000000000000291

72. Nishino M, Hatabu H, Hodi FS. Imaging of cancer immunotherapy: Current approaches and future directions. *Radiology* (2019) 290(1):9–22. doi: 10.1148/radiol.2018181349

73. Spitzer MH, Carmi Y, Reticker-Flynn NE, Kwek SS, Madhireddy D, Martins MM, et al. Systemic immunity is required for effective cancer immunotherapy. *Cell* (2017) 168(3):487–502.e15. doi: 10.1016/j.cell.2016.12.022

74. Rambhia PH, Reichert B, Scott KF, Feneran AN, Kazakov JA, Honda K, et al. Immune checkpoint inhibitor-induced sarcoidosis-like granulomas. *Int J Clin Oncol* (2019) 24(10):1171–81. doi: 10.1007/s10147-019-01490-2

75. Gkiozos I, Kopitopoulou A, Kalkanis A, Vamvakaris IN, Judson MA, Syrigos KN. Sarcoidosis-like reactions induced by checkpoint inhibitors. *J Thorac Oncol* (2018) 13(8):1076–82. doi: 10.1016/j.jtho.2018.04.031

76. Vander Heiden MG, Cantley LC, Thompson CB. Understanding the warburg effect: the metabolic requirements of cell proliferation. *Science* (2009) 324(5930):1029–33. doi: 10.1126/science.1160809

77. Zhang G, Li J, Wang X, Ma Y, Yin X, Wang F, et al. The reverse warburg effect and 18F-FDG uptake in non-small cell lung cancer A549 in mice: a pilot study. *J Nucl Med* (2015) 56(4):607–12. doi: 10.2967/jnumed.114.148254

78. Sachpekidis C, Larribère L, Kopp-Schneider A, Hassel JC, Dimitrakopoulou-Strauss A. Can benign lymphoid tissue changes in 18 f-FDG PET/CT predict response to immunotherapy in metastatic melanoma? *Cancer Immunol Immunother* (2019) 68 (2):297–303. doi: 10.1007/s00262-018-2279-9

79. Montaudié H, Pradelli J, Passeron T, Lacour JP, S Leroy S. Pulmonary sarcoid-like granulomatosis induced by nivolumab. *Br J Dermatol* (2017) 176(4):1060–3. doi: 10.1111/bjd.14808

80. Borcoman E, Nandikolla A, Long G, Goel S, Le Tourneau C. Patterns of response and progression to immunotherapy. *Am Soc Clin Oncol Educ Book.* (2018) 38:169–78. doi: 10.1200/EDBK_200643

81. Pradhan R, Nautiyal A, Singh S. Diagnosis of immune checkpoint inhibitor-associated myocarditis: A systematic review. *Int J Cardiol* (2019) 296:113–21. doi: 10.1016/j.ijcard.2019.07.025

82. Salem JE, Manouchehri A, Moey M, Lebrun-Vignes B, Bastarache L, Pariente A. Cardiovascular toxicities associated with immune checkpoint inhibitors: an observational, retrospective, pharmacovigilance study. *Lancet Oncol* (2018) 19 (12):1579–89. doi: 10.1016/S1470-2045(18)30608-9

83. Zhang L, Awadalla M, Mahmood SS, Nohria A, Hassan MZO, Thuny F, et al. Cardiovascular magnetic resonance in immune checkpoint inhibitor-associated myocarditis. *Eur Heart J* (2020) 41(18):1733–43. doi: 10.1093/eurheartj/ehaa051

84. Ederhy S, Salem JE, Dercle L, Hasan AS, Chauvet-Droit M, Nhan P, et al. Role of cardiac imaging in the diagnosis of immune checkpoints inhibitors related myocarditis. *Front Oncol* (2021) 13;11:640985. doi: 10.3389/fonc.2021.640985

85. Friedrich MG, Sechtem U, Schulz-Menger J, Holmvang G, Alakija P, Cooper LT, et al. Cardiovascular magnetic resonance in myocarditis: A JACC white paper. *J Am Coll Cardiol* (2009) 53(17):1475–87. doi: 10.1016/j.jacc.2009.02.007

86. Löffler AI, Salerno M. Cardiac MRI for the evaluation of oncologic cardiotoxicity. *J Nucl Cardiol* (2018) 25(6):2148–58. doi: 10.1007/s12350-018-1293-9

87. Ederhy S, Devos P, Pinna B, Funck-Brentano E, Abbar B, Fenioux C, et al. 18 f-fluorodeoxyglucose positron emission tomography/computed tomography imaging for the diagnosis of immune checkpoint inhibitor-associated myocarditis. *Arch Cardiovasc Dis* (2022) 115(2):114–6. doi: 10.1016/j.acvd.2021.12.001

88. Boughdad S, Latifyan S, Fenwick C, Bouchaab H, Suffiotti M, Moslehi JJ. 68 Ga-DOTATOC PET/CT to detect immune checkpoint inhibitor-related myocarditis. *J Immunother Cancer* (2021) 9(10):e003594. doi: 10.1136/jitc-2021-003594

89. Patel RP, Parikh R, Gunturu KS, Tariq RZ, Dani SD, Ganatra S, et al. Cardiotoxicity of immune checkpoint inhibitors. *Curr Oncol Rep* (2021) 23(7):79. doi: 10.1007/s11912-021-01070-6

90. Hu JR, Florido R, Lipson EJ, Naidoo J, Ardehali R, Tocchetti CG, et al. Cardiovascular toxicities associated with immune checkpoint inhibitors. *Cardiovasc Res* (2019) 115(5):854–68. doi: 10.1093/cvr/cvz026

91. Hamada N, Maeda A, Takase-Minegishi K, Kirino Y, Sugiyama Y, Namkoong H, et al. Incidence and distinct features of immune checkpoint inhibitor-related. myositis from idiopathic inflammatory myositis: A single-center experience with system. *Front Immunol* (2021) 12:803410. doi: 10.3389/fimmu.2021.803410

92. Cappelli LC, Gutierrez AK, Bingham CO3rd, Shah AA. Rheumatic and musculoskeletal immune-related adverse events due to immune checkpoint inhibitors: A systematic review of the literature. *Arthritis Care Res (Hoboken)* (2017) 69(11):1751–63. doi: 10.1002/acr.23177

93. Albarrán V, Chamorro J, Rosero DI, Saavedra C, Soria A, Carrato A, et al. Neurologic toxicity of immune checkpoint inhibitors: A review of literature. *Front Pharmacol* (2022) 13:774170. doi: 10.3389/fphar.2022.774170

94. Touat M, Talmasov D, Ricard D, Psimaras D. Neurological toxicities associated with immune-checkpoint inhibitors. *Curr Opin Neurol* (2017) 30(6):659–68. doi: 10.1097/WCO.0000000000000503

95. Kao JC, Liao B, Markovic SN, Klein CJ, Naddaf E, Staff NP, et al. Neurological complications associated with anti-programmed death 1 (PD-1) antibodies. *JAMA Neurol* (2017) 74(10):1216–22. doi: 10.1001/jamaneurol.2017.1912

96. Moreira A, Loquai C, Pföhler C, Kähler KC, Knauss S, Heppt MV, et al. Myositis and neuromuscular side-effects induced by immune checkpoint inhibitors. *Eur J Cancer* (2019) 106:12–23. doi: 10.1016/j.ejca.2018.09.033

97. Bitton K, Michot JM, Barreau E, Lambotte O, Haigh O, Marabelle A, et al. Prevalence and clinical patterns of ocular complications associated with anti-PD-1/PD-L1 anticancer immunotherapy. *Am J Ophthalmol* (2019) 202:109–17. doi: 10.1016/j.ajo.2019.02.012

98. Maddison P, Sadalage G, Ambrose PA, Jacob S, Vincent A. False-positive acetylcholine receptor antibody results in patients without myasthenia gravis. *J Neuroimmunol* (2019) 332:69–72. doi: 10.1016/j.jneuroim.2019.04.001

99. Shelly S, Triplett JD, Pinto MV, Milone M, Diehn FE, Zekeridou A, et al. Immune checkpoint inhibitor-associated myopathy: a clinicoseropathologically distinct myopathy. *Brain Commun* (2020) 2(2):fcaa181. doi: 10.1093/braincomms/fcaa181

100. Johnson DB, Manouchehri A, Haugh AM, Quach HT, Balko JM, Lebrun-Vignes B, et al. Neurologic toxicity associated with immune checkpoint inhibitors: a pharmacovigilance study. *J Immunother Cancer* (2019) 7(1):134. doi: 10.1186/s40425-019-0617-x

101. Hottinger AF. Neurologic complications of immune checkpoint inhibitors. *Curr Opin Neurol* (2016) 29(6):806–12. doi: 10.1097/WCO.0000000000000391

102. Freitas C, Sampaio L, Fernandes G. Fatal encephalopathy after pembrolizumab treatment for advanced non-small cell lung carcinoma. *J Neurooncol* (2019) 145 (2):399–402. doi: 10.1007/s11060-019-03289-7

103. Cheng K, Wang Y, Zhou Y, Xia R, Tang L, Liu J. Neurological adverse events induced by immune checkpoint inhibitors in non-small cell lung cancer: Current perspectives and new development. *Clin Med Insights Oncol* (2021) 15:11795549211056261. doi: 10.1177/11795549211056261

104. Stuby J, Herren T, Schwegler Naumburger G, Papet C, Rudiger A. Immune checkpoint inhibitor therapy-associated encephalitis: a case series and review of the literature. *Swiss Med Wkly* (2020) 150:w20377. doi: 10.4414/smw.2020.20377

105. Graus F, Dalmau J. Paraneoplastic neurological syndromes in the era of immune-checkpoint inhibitors. *Nat Rev Clin Oncol* (2019) 16(9):535–48. doi: 10.1038/s41571-019-0194-4

106. Pillonel V, Dunet V, Hottinger AF, Berthod G, Schiappacasse L, Peters S, et al. Multiple nivolumab-induced CNS demyelination with spontaneous resolution in an asymptomatic metastatic melanoma patient. *J Immunother Cancer* (2019) 7(1):336. doi: 10.1186/s40425-019-0818-3

107. Oliveira MCB, de Brito MH, Simabukur MM. Central nervous system demyelination associated with immune checkpoint inhibitors: Review of the literature. *Front Neurol* (2020) 11:538695. doi: 10.3389/fneur.2020.538695

108. Abboud H, Probasco JC, Irani S, Ances B, Benavides DR, Bradshaw M. Autoimmune encephalitis: proposed best practice recommendations for diagnosis

and acute management. *J Neurol Neurosurg Psychiatry* (2021) 92(7):757–68. doi: 10.1136/jnnp-2020-325300

109. Moreno-Ajona D, Prieto E, Grisanti F, Esparragosa I, Sánchez Orduz L, Pérez-Larraya JG. ^{18}F-FDG-PET imaging patterns in autoimmune encephalitis: Impact of image analysis on the results. *Diagnostics (Basel).* (2020) 10(6):356. doi: 10.3390/diagnostics10060356

110. Evin C, Lassau N, Balleyguier C, Assi T, Ammari S. Posterior reversible encephalopathy syndrome following chemotherapy and immune checkpoint inhibitor combination in a patient with small-cell lung cancer. *Diagnostics (Basel)* (2022) 12(6):1369. doi: 10.3390/diagnostics12061369.:s.n

111. Kim D. Posterior reversible encephalopathy syndrome induced by nivolumab immunotherapy for non-small-cell lung cancer. *Clin Case Rep* (2019) 1;7(5):935–8. doi: 10.1002/ccr3.2122

112. Maur M, Tomasello C, Frassoldati A, Dieci MV, Barbieri E, Conte P. Posterior reversible encephalopathy syndrome during ipilimumab therapy for malignant melanoma. *J Clin Oncol* (2012) 30(6):e76–8. doi: 10.1200/JCO.2011.38.7886.:s.n

113. Nannini S, Koshenkova L, Baloglu S, Chaussemy D, Noël G, Schott R. Immune-related aseptic meningitis and strategies to manage immune checkpoint inhibitor therapy: a systematic review. *J Neurooncol* (2022) 157(3):533–50. doi: 10.1007/s11060-022-03997-7

114. Shields LBE, Alsorogi MS, Mar N, Kalebasty AR. Immune-related meningoencephalitis following nivolumab in metastatic renal cell carcinoma. *Case Rep Oncol* (2021) 14(2):1051–8. doi: 10.1159/000513001

115. Daxini A, Cronin K, Sreih AG. Vasculitis associated with immune checkpoint inhibitors-a systematic review. *Clin Rheumatol* (2018) 37(9):2579–84. doi: 10.1007/s10067-018-4177-0

116. Giannini C, Salvarani C, Hunder G, Brown RD. Primary central nervous system vasculitis: pathology and mechanisms. *Acta Neuropathol* (2012) 123(6):759–72. doi: 10.1007/s00401-012-0973-9

117. Calabrese LH, Furlan AJ, Gragg LA, Ropos TJ. Primary angiitis of the central nervous system: diagnostic criteria and clinical approach. *Cleve Clin J Med* (1992) 59 (3):293–306. doi: 10.3949/ccjm.59.3.293

118. Hajj-Ali RA, Singhal AB, Benseler S, Molloy E, Calabrese LH. Primary angiitis of the CNS. *Lancet Neurol* (2011) 10(6):561–72. doi: 10.1016/S1474-4422(11)70081-3

119. Salvarani C, Brown RD, Calamia KT, Christianson TJH, Huston J3rd, Meschia JF, et al. Primary central nervous system vasculitis with prominent leptomeningeal enhancement: a subset with a benign outcome. *Arthritis Rheumatol* (2018) 58(2):595–603. doi: 10.1002/art.23300

120. Corsello SA, Barnabei A, Marchetti P, De Vecchis L, Salvatori R, Torino F. Endocrine side effects induced by immune checkpoint inhibitors. *J Clin Endocrinol Metab* (2013) 98(4):1361–75. doi: 10.1210/jc.2012-4075

121. Sznol M, Postow MA, Davies MJ, Pavlick AC, Plimack ER, Shaheen M, et al. Endocrine-related adverse events associated with immune checkpoint blockade and expert insights on their management. *Cancer Treat Rev* (2017) 58:70–6. doi: 10.1016/j.ctrv.2017.06.002

122. Lu J, Li L, Lan Y, Liang Y, Meng H. Immune checkpoint inhibitor-associated pituitary-adrenal dysfunction: A systematic review and meta-analysis. *Cancer Med* (2019) 8(18):7503–15. doi: 10.1002/cam4.2661

123. Dillard T, Yedinak CG, Alumkal J, Fleseriu M. Anti-CTLA-4 antibody therapy associated autoimmune hypophysitis: serious immune related adverse events across a spectrum of cancer subtypes. *Pituitary* (2010) 13(1):29–38. doi: 10.1007/s11102-009-0193-z

124. Garon-Czmil J, Petitpain N, Rouby F, Sassier M, Babai S, Yéléhé-Okouma M, et al. Immune check point inhibitors-induced hypophysitis: a retrospective analysis of the French pharmacovigilance database. *Sci Rep* (2019) 9(1):19419. doi: 10.1038/s41598-019-56026-5

125. Solinas C, Porcu M, De Silva P, Musi M, Aspeslagh S, Scartozzi M, et al. Cancer immunotherapy-associated hypophysitis. *Semin Oncol* (2018) 45(3):181–6. doi: 10.1053/j.seminoncol.2018.09.002

126. Kurokawa R, Ota Y, Gonoi W, Hagiwara A, Kurokawa M, Mori H, et al. MRI Findings of immune checkpoint inhibitor-induced hypophysitis: Possible association with fibrosis. *AJNR Am J Neuroradiol* (2020) 41(9):1683–9. doi: 10.3174/ajnr.A6692

127. Iravani A, Galligan A, Lasocki A, Wallace R, Weppler A, Yeung GA. FDG PET in the evaluation of immune-related hypophysitis and thyroiditis following combination ipilimumab and nivolumab in advanced melanoma. *J Nucl Med* (2020) 47(12):2776–86. doi: 10.1007/s00259-020-04815-w

128. Lee H, Hodi FS, Giobbie-Hurder A, Ott PA, Buchbinder EI, Haq R, et al. Characterization of thyroid disorders in patients receiving immune checkpoint inhibition therapy. *Cancer Immunol Res* (2017) 5(12):1133–40. doi: 10.1158/2326-6066.CIR-17-0208

129. Brancatella A, Viola N, Brogioni S, Brogioni S, Montanelli L, Sardella C, et al. Graves' disease induced by immune checkpoint inhibitors: A case report and review of the literature. *Eur Thyroid J* (2019) 8(4):192–5. doi: 10.1159/000501824

130. Lyer PC, Cabanillas ME, Waguespack SG, Hu MI, Thosani S, Lavis VR, et al. Immune-related thyroiditis with immune checkpoint inhibitors. *Thyroid* (2018) 28 (10):1243–51. doi: 10.1089/thy.2018.0116

131. Tan MH, Iyengar R, Mizokami-Stout K, Yentz S, MacEachern MP, Shen LY, et al. Spectrum of immune checkpoint inhibitors-induced endocrinopathies in cancer patients: a scoping review of case reports. *Clin Diabetes Endocrinol* (2019) 5:1. doi: 10.1186/s40842-018-0073-4

132. De Filette J, Andreescu CE, Cools F, Bravenboer B, Velkeniers B. A systematic review and meta-analysis of endocrine-related adverse events associated with immune checkpoint inhibitors. *Horm Metab Res* (2019) 51(3):145–56. doi: 10.1055/a-0843-3366

133. Min L, Hodi FS, Giobbie-Hurder A, Ott PA, Luke JJ, Donahue H, et al. Systemic high-dose corticosteroid treatment does not improve the outcome of ipilimumab-related hypophysitis: a retrospective cohort study. *Clin Cancer Res* (2015) 21(4):749–55. doi: 10.1158/1078-0432.CCR-14-2353

134. Akarca FK, Can O, Yalcinli S, Altunci YA. Nivolumab, a new immunomodulatory drug, a new adverse effect; adrenal crisis. *Turk J Emerg Med* (2017) 17(4):157–9. doi: 10.1016/j.tjem.2017.05.007

135. Bacanovic S, Burger IA, Stolzmann P, Hafner J, Huellner MW. Ipilimumab-induced adrenalitis: A possible pitfall in 18F-FDG-PET/CT. *Clin Nucl Med* (2015) 40 (11):e518–9. doi: 10.1097/RLU.0000000000000887

136. Ceschi A, Noseda R, Palin K, Verhamme K. Immune checkpoint inhibitor-related cytokine release syndrome: Analysis of WHO global pharmacovigilance database. *Front Pharmacol* (2020) 11:557. doi: 10.3389/fphar.2020.00557

137. Tay SH, Toh MMX, Thian YL, Vellayappan BA, Fairhurst AM, Chan YH, et al. Cytokine release syndrome in cancer patients receiving immune checkpoint inhibitors: A case series of 25 patients and review of the literature. *Front Immunol* (2022) 13:807050. doi: 10.3389/fimmu.2022.807050

138. Li H, Zhou X, Zhang D, Wang G, Cheng X, Xu C, et al. Early onset immune-related adverse event to identify pseudo-progression in a patient with ovarian cancer treated with nivolumab: A case report and review of the literature. *Front Med (Lausanne)* (2020) 7:366. doi: 10.3389/fmed.2020.00366

139. Alessandrino F, Qin L, Cruz G, Sahu S, Rosenthal MH, Meyerhardt JA, et al. 5-fluorouracil induced liver toxicity in patients with colorectal cancer: role of computed tomography texture analysis as a potential biomarker. *Abdom Radiol (NY)* (2019) 44 (9):3099–106. doi: 10.1007/s00261-019-02110-3

140. Yousefi B, Katz SI, Roshkovan L. Radiomics: A path forward to predict immunotherapy response in non-small cell lung cancer. *Radiol Artif Intell* (2020) 2 (5):e200075. doi: 10.1148/ryai.2020200075

141. Kang CY, Duarte SE, Kim HS, Kim E, Park J, Lee AD. Artificial intelligence-based radiomics in the era of immuno-oncology. *Oncologist* (2022) 27(6):e471–83. doi: 10.1093/oncolo/oyac036

142. Colen RR, Fujii T, Bilen MA, Kotrotsou A, Abrol S, Hess KR, et al. Radiomics to predict immunotherapy-induced pneumonitis: proof of concept. *Invest New Drugs* (2018) 36(4):601–7. doi: 10.1007/s10637-017-0524-2

143. Spieler B, Azzam G, Kwon D, Saravia D, Lopes G, Dal Pra A, et al. Checkpoint inhibitor pneumonitis in patients with advanced NSCLC on nivolumab monotherapy is underreported and associated with prior radiotherapy history. *Int J Radiat Oncol Biol physics* (2020) 108(3):e89–90. doi: 10.1016/j.ijrobp.2020.07.1188

144. Mu W, Tunali I, Qi J, Schabath MB, Gillies RJ. Radiomics of 18 f fluorodeoxyglucose PET/CT images predicts severe immune-related adverse events in patients with NSCLC. *Radiol Artif Intell* (2020) 2(1):e190063. doi: 10.1148/ryai.2019190063

145. Decazes P, Bohn P. Immunotherapy by immune checkpoint inhibitors and nuclear medicine imaging: Current and future applications. *Cancers (Basel)* (2020) 12 (2):371. doi: 10.3390/cancers12020371

146. Sachpekidis C, Kopp-Schneider A, Hakim-Meibodi L, Dimitrakopoulou-Strauss A, Hassel JC. 18F-FDG PET/CT longitudinal studies in patients with advanced metastatic melanoma for response evaluation of combination treatment with vemurafenib and ipilimumab. *Melanoma Res* (2019) 29:178–86. doi: 10.1007/s00262-018-2279-9

147. Kotwal A, Kottschade L, Ryder M. PD-L1 inhibitor-induced thyroiditis is associated with better overall survival in cancer patients. *Thyroid* (2020) 30(2):177–84. doi: 10.1089/thy.2019.0250

148. Jin P, Li J, Meng Y, Wu L, Bai M, Yu J, et al. PET/CT metabolic patterns in systemic immune activation: A new perspective on the assessment of immunotherapy response and efficacy. *Cancer Lett* (2021) 520:91–9. doi: 10.1016/j.canlet.2021.06.028

149. Natarajan A, Mayer AT, Reeves RE, Nagamine CM, Gambhir SS. Development of novel ImmunoPET tracers to image human PD-1 checkpoint expression on tumor-infiltrating lymphocytes in a humanized mouse model. *Mol Imaging Biol* (2017) 19 (6):903–14. doi: 10.1007/s11307-017-1060-3

150. England CG, Jiang D, Ehlerding EB, Rekoske BT, Ellison PA, Hernandez R, et al. 89 zr-labeled nivolumab for imaging of T-cell infiltration in a humanized murine model of lung cancer. *Eur J Nucl Med Mol Imaging* (2018) 45(1):110–20. doi: 10.1007/s00259-017-3803-4

151. Ferreira CA, Heidari P, Ataeinia B, Sinevici N, Sise ME, Colvin PB, et al. Non-invasive detection of immunotherapy-induced adverse events. *Clin Cancer Res* (2021) 27(19):5353–64. doi: 10.1158/1078-0432.CCR-20-4641

152. Larimer BM, Wehrenberg-Klee E, Dubois F, Mehta A, Kalomeris T, Flaherty K, et al. Granzyme b PET imaging as a predictive biomarker of immunotherapy response. *Cancer Res* (2017) 77(9):2318–27. doi: 10.1158/0008-5472.CAN-16-3346

153. Kennedy LB, Salama AKS. A review of cancer immunotherapy toxicity. *CA Cancer J Clin* (2020) 70(2):86–104. doi: 10.3322/caac.21596

154. Neelapu SS, Tummala S, Kebriaei P, Wierda W, Gutierrez C, Locke FL, et al. Chimeric antigen receptor T-cell therapy - assessment and management of toxicities. *Nat Rev Clin Oncol* (2018) 15(1):47–62. doi: 10.1038/nrclinonc.2017.148

155. Gust J, Hay KA, Hanafi LA, Li D, Myerson D, Gonzalez-Cuyar LF, et al. Endothelial activation and blood-brain barrier disruption in neurotoxicity after adoptive immunotherapy with CD19 CAR-T cells. *Cancer Discovery* (2017) 7 (12):1404–19. doi: 10.1158/2159-8290.CD-17-0698.

156. Liu W, Tang H, Li L, Wang X, Yu Z, Li J, et al. Peptide-based therapeutic cancer vaccine: Current trends in clinical application. *Cell Prolif* (2021) 54(5):e13025. doi: 10.1111/cpr.13025

157. Yoshida K, Noguchi M, Mine T, Komatsu N, Yutani S, Ueno T, et al. Characteristics of severe adverse events after peptide vaccination for advanced cancer patients: Analysis of 500 cases. *Oncol Rep* (2011) 25(1):57–62.

158. Li L, Liu S, Han D, Tang B, Ma J. Delivery and biosafety of oncolytic virotherapy. *Front Oncol* (2020) 10:475. doi: 10.3389/fonc.2020.00475

Glossary

AKI	acute kidney injury
CAR	chimeric antigen receptor
CMRI	cardiac magnetic resonance imaging
CT	computer tomography
CTCAE	Common Terminology Criteria for Adverse Events
CTLA-4	cytotoxic T-lymphocyte-associated protein-4
FLAIR	fluid-attenuated inversion recovery
GZP	granzyme B-targeted PET tracer
ICI	immune checkpoint inhibitor
irAE	immunotherapy-related adverse events
irRC	immune-related response criteria
irRECIST	immune-related RECIST
LGE	late gadolinium enhancement
mAb	monoclonal antibody
MRCP	magnetic resonance cholangiopancreatography
MRI	magnet resonance imaging
PANCS	primary angiitis of the central nervous system
PD-1	programmed cell death protein-1
PD-L1	PD-1 ligands
PET	positron emission tomography
RECIST 1.1	Response Evaluation Criteria in Solid Tumors version 1.1
STIR	short-tau inversion recovery
SUV	standard uptake value
TTE	transthoracic echocardiography
US	ultrasound
^{18}F-FDG	2-deoxy-2-[18F]fluoro-D-glucose

frontiers | Frontiers in Immunology

TYPE Review
PUBLISHED 23 February 2023
DOI 10.3389/fimmu.2023.1130438

OPEN ACCESS

EDITED BY
Yeonseok Chung,
Seoul National University, Republic of Korea

REVIEWED BY
Jessica Crystal,
University of Miami, United States
Guoqiang Gu,
Second Hospital of Hebei Medical University, China

*CORRESPONDENCE
Runxiang Yang
yrx_research@163.com

SPECIALTY SECTION
This article was submitted to Cancer Immunity and Immunotherapy, a section of the journal Frontiers in Immunology

RECEIVED 23 December 2022
ACCEPTED 13 February 2023
PUBLISHED 23 February 2023

CITATION
Li X, Peng W, Wu J, Yeung S-CJ and Yang R (2023) Advances in immune checkpoint inhibitors induced-cardiotoxicity.
Front. Immunol. 14:1130438.
doi: 10.3389/fimmu.2023.1130438

Advances in immune checkpoint inhibitors induced-cardiotoxicity

Xiang Li[1], Wenying Peng[1], Jiao Wu[1], Sai-Ching Jim Yeung[2] and Runxiang Yang[1]*

[1]Department of the Second Medical Oncology, The Third Affiliated Hospital of Kunming Medical University, Kunming, Yunnan, China, [2]Department of Emergency Medicine, The University of Texas MD Anderson Cancer Center, Houston, Texas, TX, United States

Immune checkpoint inhibitors (ICIs) are approved as the first-line drug for treating many cancers and has shown significant survival benefits; however, it also causes immune-related adverse events (irAEs) while activating the immune system, involving multiple organs. Among them, cardiovascular immune-related adverse events (CV-irAE) are rare, but common causes of death in ICIs treated cancer patients, which manifest as myocardial, pericardial, vascular and other cardiovascular toxicities. Therefore, it is important that irAEs, especially CV-irAE should be carefully recognized and monitored during the whole ICIs treatment because early detection and treatment of CV-irAE can significantly reduce the mortality of such patients. Consequently, it is urgent to fully understand the mechanism and management strategies of CV-irAE. The effects of ICIs are multifaceted and the exact mechanism of CV-irAE is still elusive. Generally, T cells identify tumor cell antigens as well as antigen in cardiomyocytes that are the same as or homologous to those on tumor cells, thus causing myocardial damage. In addition, ICIs promote formation of cardiac troponin I (cTnI) that induces cardiac dysfunction and myocardial dilatation; moreover, ICIs also increase the production of cytokines, which promote infiltration of inflammation-linked molecules into off-target tissues. Currently, the management and treatment of cardiovascular toxicity are largely dependent on glucocorticoids, more strategies for prevention and treatment of CV-irAE, such as predictive markers are being explored. This review discusses risk factors, potential pathophysiological mechanisms, clinical manifestations, and management and treatment of CV-irAE, guiding the development of more effective prevention, treatment and management strategies in the future.

KEYWORDS

cardiotoxicity, immune checkpoint inhibitors, immune-related adverse events, Myocarditis, Pericarditis, Vasculitis

1 Introduction

During tumorigenesis, tumor cells inhibit the activation and effector process of T cells by hijacking immune checkpoints molecules, then evade the surveillance and attack of the immune system. Thus, immune checkpoint related to the regulation of T-cell activity is an important target for anti-tumor therapy (1). Tumor microenvironmental factors also

modify the anti-tumor immune response, such as T-cell infiltration and expression of immune checkpoint proteins (2). Currently, the main immune checkpoints include cytotoxic T-lymphocyte antigen 4 (CTLA-4), programmed cell death receptor 1 (PD-1), programmed cell death ligand 1 (PD-L1) and lymphocyte activation gene 3 protein (LAG3). Immune checkpoint inhibitors (ICIs) are now approved for treating many malignancies and significantly prolonged the survival of cancer patients (3–6). At the beginning of ICIs application, reports of immune-related adverse events (irAEs) were rare and did not attract broad attention. However, with the rapidly increased use of ICIs and the improvement of patients' survival, the importance of cardiovascular immune-related adverse events (CV-irAE) therapy has come to the forefront. Despite its low incidence, immune-related adverse events (CV-irAEs) require high attention from clinicians (7). Therefore, through exploring the underlying mechanisms of CV-irAE, we developed more effective prevention, treatment, and management strategies, thus improving the quality of life and patients' survival. Herein, we review the pharmacological mechanisms of ICIs, current research progression in CV-irAEs epidemiology, risk factors, potential pathophysiological mechanisms as well as clinical manifestation, the management and treatment of CV-irAEs mentioned in guidelines and literatures. The above statements are gross generalizations based on our synthesis of the current litereature.Some statements are not accepted by all, but most of them are based on guidelines published by prestigious professional organizations.

2 Epidemiology

Current reports about epidemiology of CV-irAE are limited because of its low incidence (8). CV-irAEs occur as early as a few days after ICIs initiation, but may also present late until one year after ICIs treatment, the median onset time of CV-irAE was 34 days after starting ICIs (9, 10). In a Danish national study, patients with lung cancer and malignant melanoma had a higher risk rate of CV-irAE in patients treated with ICIs than those who did not receive ICIs therapy (11). Wang et al. (12) performed a retrospective analysis of published irAEs queried in the pharmacovigilance database (Vigilyze) and found that myocarditis had the highest fatality rate among all CV-irAEs (39.7%). Rubio et al. analyzed 1265 papers published before August 31, 2020 and found the total incidence of CV-irAE was about 1.3%, among them myocarditis was the most common irAE, accounting for 50.8%. Notably, a high mortality rate of 24.6% of patients died due to CV-irAE (13). In this study, ICIs included ipilimumab, tremelimumab, nivolumab, pembrolizumab, atezolizumab, durvalumab and avelumab. In addition to these ICIs, there are emerging ICIs, which may also occur CV-irAEs such as relatlimab, a emerging monoclonal antibody that targets LAG-3, relatlimab had a higher incidence in myocarditis (14, 15). Since relatlimab has been approved soon, relatlimab related cardiotoxicity needs to be further explored. The incidence of CV-irAE appears to increase in recent years, probably due to the increased scope and frequency of use of ICIs and the heightened awareness of cardiotoxicity (16–18). However, the real-world prevalence of CV-irAE may be higher than expected, and we currently lack the support of large-sample clinical studies that could offer further in-depth investigation (9, 17).

3 Risk factors for CV-irAE

The risk factors of CV-irAE need further investigation, dual ICIs combination therapy is the greatest risk factor for CV-irAE over other risk factors such as autoimmune diseases (19). Several investigations have also confirmed that dual ICI leads to a higher incidence of CV-irAE than monotherapy or ICI plus chemotherapy (19, 20). A meta-analysis of CV-irAE concluded that the incidence was 3.1% for ICI monotherapy, 2.5% for ICI plus chemotherapy and 5.8% for dual ICIs treatment (anti-PD-1 plus anti-CTLA-4/anti-PD-1 plus anti-PD-L1) (13). The emerging bispecific antibody also causes CV-irAE. The incidence of CV-irAE is 0.9% in 458 patients treated with Cadonilimab (anti-PD-1/CTLA-4) (21). Cardiotoxicity of AK112 (NCT04047290)—anti-PD-1/VEGF and IBI318 (NCT03875157)—anti-PD-1/PD-L1 has not been reported.

It was demonstrated that the PD-1 modulates radiation-induced cardiotoxicity in an animal model, acute toxicity was increased with anti-PD-1 treatment in mice with radiotherapy, but further research is needed to get a deep insight (22). Osaka Medical School in Japan established a mouse model of experimental autoimmune myocarditis (EAM) by administration of PD-1 antibodies in mice (23). The study indicated that ICIs-induced autoimmune myocarditis may be related to autoimmunity prior to ICIs administration (23). CV-irAE is more frequently reported in patients diagnosed with autoimmune diseases (24). In a retrospective case-match control study comparing 251 ICI-treated patients who had autoimmune diseases with 251 ICI-treated patients who did not have autoimmune diseases, the risk of CV-irAEs was higher in patients with autoimmune diseases than those without (hazard ratio:1.77) (25).

In addition, the observation of sporadic ICIs-associated myocarditis cases revealed that patients with diabetes were more common in these cases (9, 26). In addition, the patients' pre-existing cardiovascular risk factors (age ≥80 years, hypertension, diabetes mellitus and chronic kidney disease) and the presence of cardiovascular toxicity caused by previous anti-neoplastic drugs should also be brought to our attention (27). Comparing 35 patients who had ICIs-related myocarditis with 105 ICIs-treated patients who did not have ICIs-related myocarditis, 34% of patients with ICIs-related myocarditis had pre-existing diabetes but only 13% of ICIs-treated patients without myocarditis had diabetes (28).

4 Mechanism of CV-irAE

4.1 Pharmacological mechanism of ICIs

The immune system plays an important role in the surveillance and wiping malignant cells. T cells undergo positive and negative selection in thymic to ensure self-tolerance and specific recognition of abnormal cells (including cancer cells) (29). Tumor cells

presenting or releasing tumor antigens are engulfed by antigen presenting cells (APCs), which process tumor antigens and present MHC-I and MHC-II molecular complexes to CD8+ T-cell and CD4 + T-cell receptors then accurately identify cancer cells. A combination of B7, on the surface of APCs, and CD28, on the surface of T cells, constitute synergistic signals in T cells activation, the combination of CD28-B7 lead to cytoskeleton remodelling, cytokines secretion and T cells differentiation. Activated CD4+ T cells secrete cytokines to stimulate CD8+ T cells proliferation in lymph nodes. Activated CD8+ T cells can reach the tumor through circulation, recognize the MHC-I molecular complex on the tumor cells, and kill tumor cells (30–33). Activated CTLA-4, PD-1 and LAG-3 to protect the host from self-attack by abnormally activated T cells (6, 34, 35). CTLA-4, a CD28 homolog, has stronger affinity than CD28, and can induce trans-endocytosis of B7 ligands to reduce the co-stimulatory signal (36–38). PD-1, combined with PD-L1, negatively mediates T cell proliferation and activation (39, 40). CTLA-4 not only competes with CD28 for B7 but also induces regulatory T cells (Treg, inhibitory immune cells) to death, leading to unbalance between Treg and cytotoxic T cells (41, 42). CTLA-4 monoclonal antibody clears Treg in tumor effectively through FcR mediated ADCC (antibody-dependent cell-mediated cytotoxicity), thus relieving immunosuppressive of Treg to achieve anti-tumor (42–44). However, Treg cells are important in peripheral tolerance (45). Reducing peripheral Treg cells lead to the immune system attacking organism, resulting in serious side effects (45, 46). PD-1 plays an important role in T-cell homeostasis and inflammatory inhibition in peripheral tissues (34, 47). Lymphocyte activation gene 3 protein (LAG3) is a negative immunomodulator that regulates the function of T cells and dendritic cells (DC) by binding with MHC-II (6). LAG-3 has an intracellular short tail domain that inhibits the function of LAG-3 in effector CD4+ T cells and an extracellular domain similar to CD4 but possess higher affinity to combine with MHC-II than CD4 (6, 48). FGL1, the ligand of LAG-3, expressed on the surface of cancer cells. When FGL1 combines with LAG-3 on the surface of T cells, immune system mistake cancer cells as normal, contributing to immune-escape of tumor cells (49). After immunoediting (50–52), tumor cells would also express immune checkpoint, so ICIs are designed to reactivate anti-tumor immune response by targeting specific immune checkpoint (Figure 1). Therefore, CTLA-4, PD-1, PD-L1and LAG3 inhibitors have been approved for clinical treatment in several cancer types by Food and Drug Administration (FDA) (1, 53). In addition, new-type ICIs through targeting inhibitory receptors [e.g,. T cell immunoglobulin domain and mucin domain-3 (TIM-3), T cell Ig and ITIM domain (TIGIT) and BTLA (CD272)] and ligand of the B7 family [e.g., V-domain Ig suppressor of T cell activation (VISTA), B7-H3] are being actively investigating and developed for clinical trials in increasing numbers (54–57).

4.2 Potential pathophysiological mechanisms of CV-irAEs

The mechanism of CV-irAE might be ICIs disrupt the autoimmune tolerance of myocardial cell (58). irAEs are reversible in most cases treated appropriately; however, heart is a vital organ so CV-irAE can be fatal (20, 59). Though the effects of ICIs are multifaceted, the exact mechanisms of CV-irAE are still elusive (52) (Figure 2).

4.2.1 The common antigens in tumor cells and cardiomyocytes leading to cross-reaction

T cells identify tumor cell antigens as well as antigen in cardiomyocytes same with or homologous to those on tumor cells simultaneously. In two cases of fulminant myocarditis caused by ICIs, postmortem found that T cell marker (CD3) was positive in myocardial and skeletal muscle infiltrating cells. T cells receptor sequence revealed that patients had high frequency of shared T cell receptor sequences in cardiac and skeletal muscle and tumor infiltrating cells (20). Taken together, these suggest that activated T cells not only attacked tumor cells but also caused cross-reaction with common antigens on skeletal and cardiac muscles, but the specific antigen was not identified in the study. T cells-mediated immune responses in the heart may cause abnormal heart electrical rhythm and irreparable damage to myocardium (58).

4.2.2 Increase of autoantibody

ICIs promote the formation of autoantibodies. Lack of PD-1 caused autoimmune dilated cardiomyopathy in mouse model with *Pdcd1* gene knockout, and high titers of circulating immunoglobulins (IgGs) deposited on surface of mouse cardiomyocytes (60). Subsequent experiments showed that the autoantibodies are against cTnI. cTnI induced cardiac dysfunction and myocardial dilatation by means of chronically stimulating influx of calcium ions in cardiomyocytes (61).

4.2.3 Cardiac myosin drive cell-mediated cytotoxicity

Won et al. (62) used anti-PD-1 monoclonal antibodies to induce the development of myocarditis in mice and they found that myosin-specific T cells were increased in such mice. *Axelrod et al.* (63) has established P*dcd1*$^{-/-}$/*Ctla4*$^{+/-}$ mouse model to characterize ICIs-related myocarditis. Single-cell RNA and T cell receptor (TCR) sequencing were arranged and found increasing CD8+T cells in ICIs-related myocarditis. They subsequently found that specific TCRs recognize α-myosin, suggesting α-myosin may drive cytotoxic T-cell-mediated killing.

4.2.4 High level of cytokines

Cytokines that recruit immune cells to tumor microenvironment are significant modulators for immune response (58). ICIs lead to increased pro-inflammatory cytokines, which activate T-cells proliferation and result in anti-tumor immune response (64–66). *Tarhini* et al. (64) found that restraining immune checkpoints result in higher circulating pro-inflammatory cytokines [interferon (IFN)-γ, tumor necrosis factor (TNF)-α, interleukin (IL), and granulocyte macrophage colony-stimulating factor (GM-CSF)]. Those cytokines contribute to ICIs penetration into non-target organs (including cardiovascular cells) (64, 65, 67, 68).

10.3389/fimmu.2023.1130438

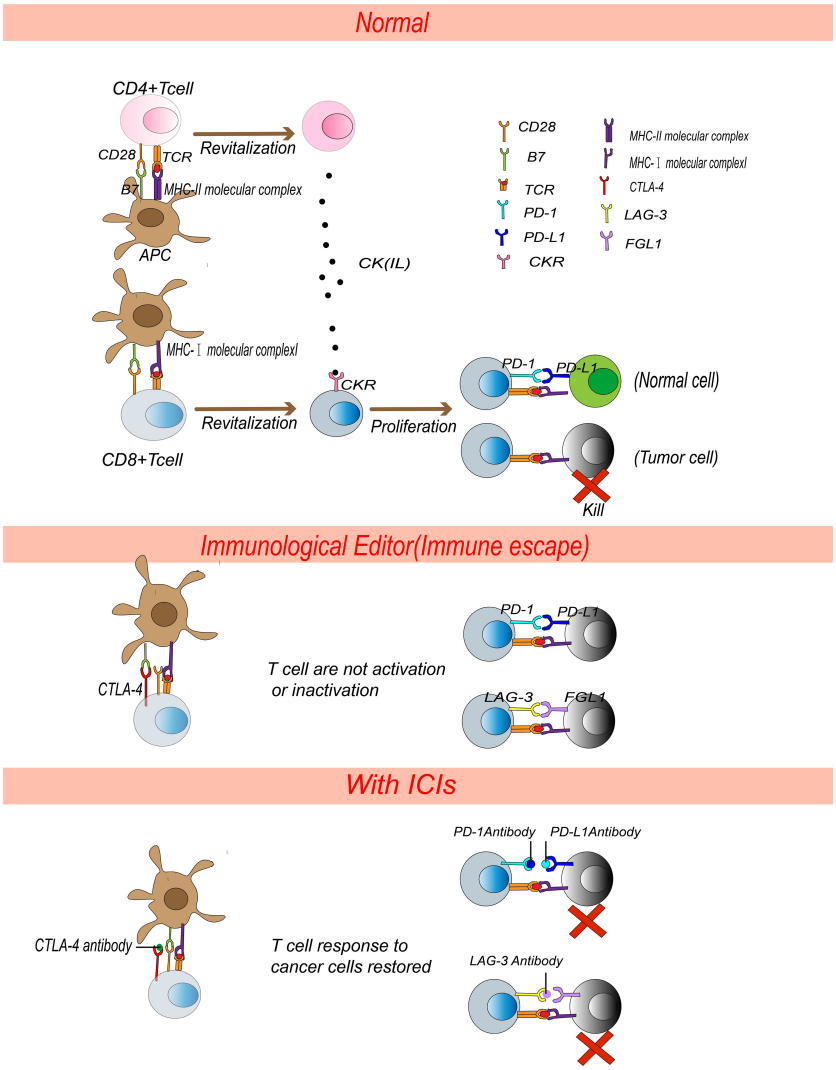

FIGURE 1
Pharmacological mechanism of ICIs. APCs present MHC molecular complexes to TCR on T cells and activate T cells. CD4+ T cells secrete cytokines and stimulate CD8+ T cells proliferation. Activated CD8+ T cells kill tumor cells precisely. Normally, PD-L1 binds to PD-1, FGL-1 binds to LAG-3, inactivating CD8+ T cells and leading to autoimmune tolerance. After immunoediting, tumor cells express PD-L1 and FGL-1 and T cells express CTLA-4 and LAG-3, receptors on T cells bound with ligands on tumor cells or APCs, which will inactivate T cells. ICIs devitalized the PD-1/PD-L1, LAG-3/FGL-1 and CTLA-4/B7 signals and reactivated T cells to kill tumor cells.

4.2.5 Immune tolerance

Immune checkpoints inhibit T cells activation is called immune tolerance. For example, the PD-1/PD-L1 pathway prevents T cells overactivation to maintain immune balance. Blocking PD1/PD-L1will not only promote anti-tumor immunity but also inhibit Treg cells and Forkhead Box P3 (FOXP3) expression, leading to loss of self-tolerance (69). Treg cells have an effective role in keeping peripheral tolerance. Systemic application of ICIs may disrupt immune homeostasis between cytotoxic T cells and Treg cells in normal myocardial tissue, causing the development of cardiotoxicity (70, 71).

4.2.6 Atherosclerosis

Atherosclerosis is the inflammation of large arteries (72). PD-1 and CTLA-4 restrain formation of atherosclerosis. PD-1 deficient bone marrow progenitor cells up-regulate genes involved in cholesterol synthesis and ingestion, leading to elevated cholesterol (73). Blockading CTLA-4 increases T cells abundance in plaques and exacerbates atherosclerosis in mouse model (74). *Banerjee et al.* (75) found that senescence-associated secretory phenotype (SASP) are intersections of cancer and cardiovascular events, and SASP can aggravate atherosclerosis. More importantly, ICIs can lead to therapy-induced SASP and accelerate atherosclerosis, so atherosclerosis should be monitored while using ICIs ((75, 76). A matched cohort study (77) showed that patients treated with ICIs have a 3-fold increase risk for cardiovascular events (77). Autopsies were performed on tumor decedents who received ICIs and those who did not, and the result showed that the ratio of CD3/CD68 was significantly elevated in atherosclerotic plaques among patients undergoing ICIs (78). After treated with ICIs, inflammation in atherosclerotic plaques was dominated by lymphocytes rather than

10.3389/fimmu.2023.1130438

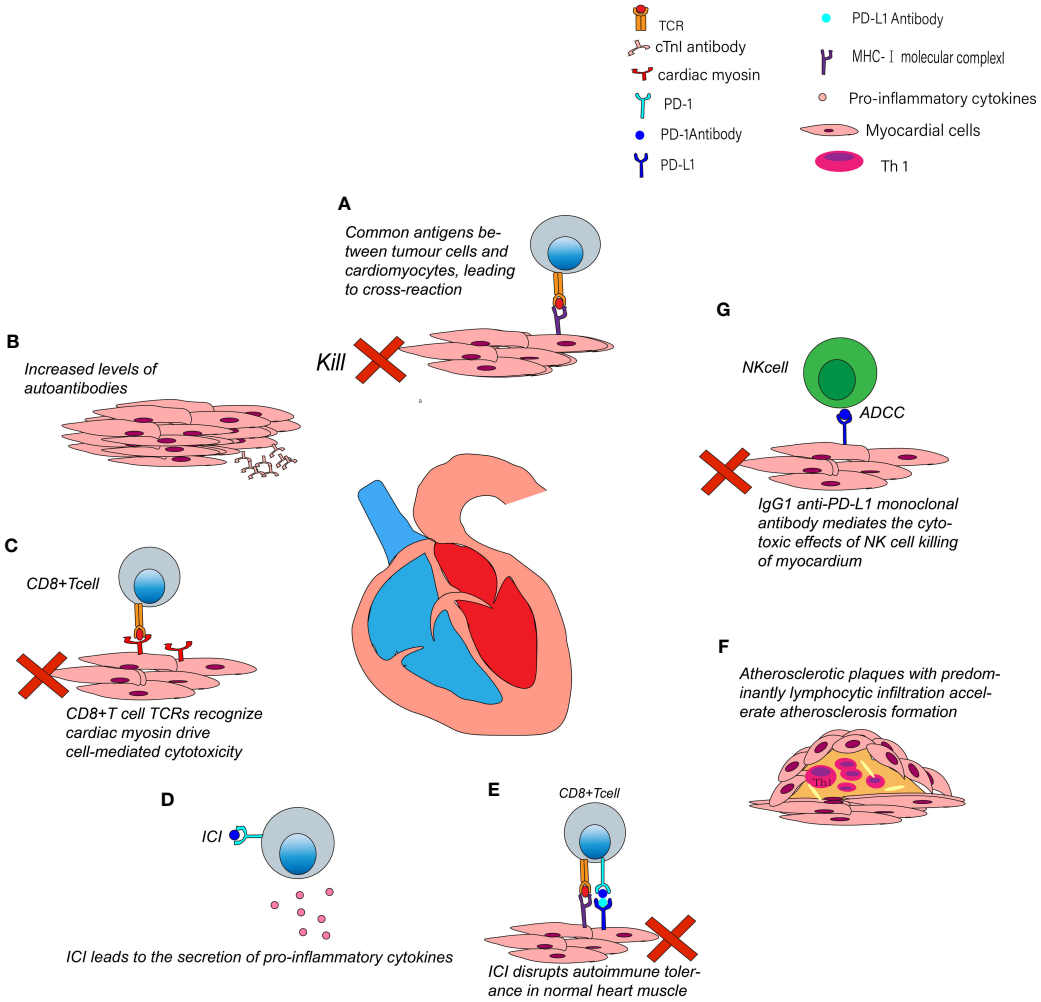

FIGURE 2
Possible mechanisms of CV-irAE. **(A)** Activated T cells not only attack tumor cells but also cross-reactivate with cardiac muscle. **(B)** Cardiac myocytes secrete cTnI antibodies after using ICIs. **(C)** Myosin-specific T cells TCRs can recognize myosin and drive cytotoxic T-cell-mediated killing. **(D)** ICIs can lead to increased levels of pro-inflammatory cytokines. **(E)** Systemic application of ICI may disrupt immune homeostasis between cytotoxic T cells and Tregs. **(F)** ICIs may contribute to plaques progression and coronary events. **(G)** Anti-PD-L1 monoclonal antibodies may mediate NK cells killing cardiomyocytes through the ADCC pathway.

macrophages, which is usually primary cell of atherosclerosis (78). Lymphocytes have a significant effect on the development of atherosclerosis, and in mouse model Th1 cells promote the development of atherosclerosis by secreting IFN-γ (79–81). In summary, this evidence suggests that ICIs may contribute to plaques and coronary events by altering the type of inflammation in atherosclerotic plaques (78).

4.2.7 ADCC(antibody-dependent cell-mediated cytotoxicity)

ICIs interact with proteins expressed on myocardial tissue, such as CTLA-4, FGL1, LAG-3, PD-1 and PD-L1, resulting in complement-mediated tissue injury. The Fc region of human IgG1 monoclonal antibodies binds to receptors on natural killer (NK) cells mediating ADCC. Therefore, most immune checkpoint monoclonal antibodies are IgG4 that do not mediate ADCC; however, avelumab is a human IgG1 anti-PD-L1 monoclonal antibody. Theoretically, the antibodies, bind to PD-L1 on surface of cardiomyocytes, and may mediate killing of cardiomyocytes by NK cells through ADCC (82–84).

5 Clinical manifestations of CV-irAE

CV-irAE may appear as symptoms from the myocardial, pericardial and vascular system of the body (71, 85).

5.1 Myocardial disease

5.1.1 Myocarditis

Myocarditis appears as early as 2 weeks after ICIs, and the median time is 65 days (86, 87). Myocarditis is the most frequent CV-irAE, possibly shown as asymptomatic myocarditis with an increase of cardiac biomarkers, or could be severe cardiac damage, even break out fulminant or life-threatening manifestations such as

cardiogenic shock, heart failure, arrhythmias, advanced atrioventricular block or ventricular tachycardia (9, 20, 86, 88). Progression of ICIs-associated myocarditis is fulminant but can also be doubted by clinical symptoms, electrocardiography and biomarkers [troponin, brain natriuretic peptide (BNP)] and imaging (17). Myocardial biopsy is the definitive standard to identify myocarditis. The typical myocarditis clinical symptoms include palpitations, chest pain, heart failure and a range of other manifestations (89).

5.1.2 Takotsubo syndrome

Takotsubo syndrome usually appears between 15 weeks to 8 months after ICIs; however, due to its low incidence, epidemiological data are lacking and the literatures are still limited to only case reports (87). Takotsubo syndrome is an acute and transient syndrome of regional left ventricular insufficiency (90). It was first identified in Japan and characterized by myocardium dilating like a balloon and may lead to several dangerous symptoms. It was usually caused by severe stress. For clinical examination, echocardiograph shows apical or mid-left ventricular dyskinesia and troponin and NT-proBNP will elevate (91–93). A melanoma patient present takotsubo syndrome after ICIs combination therapy, and echocardiograph showed apical motion with ballooning, electrocardiogram showed V2-V6 ST elevation 1-2 mm. Cardiac MRI showed that left ventricular ejection fraction (LVEF) and systolic function returned to normal after corticosteroid treatment (94).

5.1.3 Dilated cardiomyopathy

Activated T cells result in an immune response in vessels and myocardium lead to development of dilated cardiomyopathy (95). Similarly, epidemiological data on ICIs-induced dilated cardiomyopathy is insufficient due to its low incidence. Nishimura et al. (60) found that PD-1 knockout mice developed severe dilated cardiomyopathy. Subsequently, they found that cTnI can induce cardiac dysfunction and myocardial dilatation in cardiomyocytes. Although the clinical manifestation of Takotsubo syndrome and dilated cardiomyopathy is similar, the echocardiogram of dilated cardiomyopathy does not have apical ballooning syndrome (96). There is a dilated cardiomyopathy patient after Nivolumab treatment. Echocardiography shows diffuse hypokinesis and 20% Left Ventricular Ejection Fractions (LVEF), and myocardial biopsy found inflammatory cells and interstitial fibrosis, which did not consistent with myocarditis (96).

5.2 Pericardium

ICIs related pericardium include pericarditis and pericardial effusion (97, 98). In a retrospective study, the median onset time was 40 days for pericardial effusion in 6.7% of patients treated with ICIs (99). However, it can also occur very late after the start of ICIs. In a case of advanced non-small cell lung cancer, after Nivolumab the patient developed pericardial thickening and effusion after 18 months (100). Pericarditis and pericardial effusion may be asymptomatic or mild and life-threatening symptoms may also occur when hemodynamic is unstable (101). Breathlessness is the predominant symptom and is followed by tachycardia and chest pain (102). At the time of diagnosis, the effusion should be distinguished between tumor progression related pericarditis and CV-irAE by TTF-1 immunohistochemical staining (101).

5.3 Vascular diseases

5.3.1 Vasculitis

Vasculitis caused by self-immune disorder can occur in vessels of all sizes (103). The incidence of ICIs-associated vasculitis is lower than 1%, and there was no clear epidemiological data on the median time (104). In a retrospective analysis of 1215 patients treated with ICIs, cardiovascular events occurred in approximately 1% of patients, and the median time to event was 97 days after ICIs (105, 106). Currently, irAE about vasculitis are reported mainly about large vessel and neurological vasculitis (107). ICIs lead to the activation of T cells and NK cells and the secretion of pro-inflammatory cytokines, resulting in inflammation of the vessel wall, revascularization and even vascular occlusion (108, 109). CT or MR can diagnose vasculitis that is characterized by diffuse peripheral thickening of the vessel wall, enhanced wall thickness, or thrombosis (104). Daxini et al. (107) reviewed 20 case reports that met the criteria by searching multiple medical databases, and the results showed that the most common types of ICIs-related vasculitis were macrovasculitis, such as giant cell arteritis (GCA). GCA is an inflammation of blood vessels that occurs in people older than 50 years and primarily affects the great and middle arteries, especially the extracranial branches of the aorta and external carotid arteries (108). The manifestations of GCA are various based on the vessels, leading to blindness, stroke and aneurysms (110). GCA can develop into vascular occlusion, leading to tissue ischemia and should be considered in patients with lately reported headache, visual impairment, claudication of the jaw and polymyositis rheumatica (PMR) symptoms (110). Atherosclerosis is an inflammation of the large arteries, and the primary outcome of accelerated atherosclerosis after ICIs was the occurrence of cardiovascular events (defined as a combination of myocardial infarction, coronary revascularization, and ischemic stroke) (77). A previous study found that atherosclerotic plaque can be ameliorated by the concomitant use of corticosteroids and statins (77).

6 Management and treatment of CV-irAE

6.1 Screening of baseline cardiovascular disease and risk factor

Prior to ICIs, physicians need to assess the potential cardiotoxicity of ICIs and educate patients to report suspicious symptoms to medical personnel in time (27). According to the

European Society of Cardiology recommendations, risk factors of baseline include pre-existing cardiovascular disease, elevated cardiac biomarkers, and previous cardiotoxic antineoplastic drugs history (27). Baseline assessment includes physical examination and auxiliary examination, such as an electrocardiogram (ECG), echocardiogram and cardiac troponin and natriuretic peptide etc. Individualized baseline monitoring improves the survival of patients. Patients with abnormal baseline examination results (ECG, cardiac biomarkers) require therapy under the guidance of an integrated oncology and cardiology team (111, 112).

6.2 Monitoring of toxicity

Toxicity monitoring is performed through the process of ICIs, especially in patients with prior cardiac injury. Physicians should assess the possibility of CV-irAE at each follow-up visit. Monitoring of toxicity includes electrocardiogram, echocardiograms, myocardial markers, troponin and NT-proBNP: (1) electrocardiogram is routinely performed before each cycle of treatment, (2) patients are advised to follow-up regularly for echocardiograms and myocardial markers every 2-4 cycles and 6/12 months after ending using ICIs (86, 111, 113), (3) As recommended by 2021 American Society of Clinical Oncology (ASCO) guideline, there is no clear recommendation on the frequency of troponin and NT-proBNP (114). But a literature recommended testing troponin and NT-proBNP at baseline and 2-4 cycles (28).Toxicity monitoring may detect abnormal biomarkers prior to symptoms of CV-irAE. When troponin is elevated, physicians should look out for potential triad myositis-myositis, muscle weakness, and myocarditis. For patients suspicious of myositis, not only creatine kinase (CK) but also lactate dehydrogenase (LDH) should be tested because cardiotoxicity, myositis and myalgia may happen in the same patient. Once the patient appears suspicious clinical symptoms, a cardiology specialist should immediately be consulted (16, 17, 108, 111).

6.3 Diagnosis of CV-irAE

Diagnosis of CV-irAE is a challenge because there are many manifestations of CV-irAEs (115). The clinical presentation is similar to viral myocarditis which may confuse the diagnosis. The evaluation should include telemetry monitoring, serum marker (e.g., cardiac markers, CK, LDH), electrocardiogram and cardiac magnetic resonance (CMR) (116). Myocardial and vascular biopsies are the standard for diagnosing CV-irAE. Finally, diagnosis of CV-irAE should be integrated by a multidisciplinary cardio-oncology team (117).

6.4 Management and treatment of CV-irAE

6.4.1 Grade and management

Management and treatment of CV-irAE mainly depend on toxicity grading, based on the dose and dosage of given immunosuppressants. ASCO, National Comprehensive Cancer Network (NCCN) and Chinese Society of Clinical Oncology (CSCO) have classified CV-irAE in detail (Table 1).

6.4.2 Similarities and differences between guidelines

Although the incidence of CV-irAE is low, ESMO/ASCO/NCCN/CSCO guidelines all consider CV-irAE as a disease characterized by diverse manifestations, rapid progression and high mortality. However, different recommended doses for glucocorticoid were given. ASCO guidelines recommended methylprednisolone 1-2 mg/kg•d, NCCN guidelines recommended pulsed methylprednisolone 1 g/d, and ESMO/CSCO guidelines recommend 500 to 1000mg/d (114, 116, 118) (Table 2).

6.4.3 Steroid refractory CV-irAE

Other immunosuppressive agents (e.g., gammaglobulin, anti-thymocyte globulin, infliximab and morte-macrolimus)

TABLE 1 Grading, manifestation, and management of CV-irAE.

Grade	Manifestation	Management
G1	No cardiovascular symptoms, cardiac biomarkers (creatine kinase, troponin) or electrocardiogram abnormalities	(1) If cardiac markers are mildly abnormal and remain stable, continue ICIs (2) Otherwise, ICIs should be discontinued until the markers recover to normal.
G2	Mild or moderate symptoms of activity or fatigue, abnormalities in cardiac biomarkers and electrocardiograms	(1) Discontinue ICIs (2) Be hospitalized (3) Cardiology consultation (4) High-dose steroids such as methylprednisolone pulse dosing 1 g/d IV for 3-5 days (5) ICIs should be used cautiously even if relevant indicators recover to normal.
G3	Cardiovascular symptoms at rest or after mild activity, ULN<cardiac biomarkers ≤ 3ULN, significant changes of echocardiographic, but no hypotension.	(1) Terminate using ICIs (2) High-dose steroids such as methylprednisolone pulse dosing 1 g/d IV for 3-5 days (3) MDT (4) Advanced Life Support in ICU
G4	Moderate to severe decompensation, hemodynamic instability (hypotension), and cardiac biomarkers >3ULN.	

ULN, upper limit of normal; ICU, intensive Care unit; MDT, Multi-Disciplinary Treatment.

TABLE 2 Recommended doses of glucocorticoids in different guidelines.

Guideline	Grade	Dose of steroids
2022ESMO		Methylprednisolone 500-1000 mg/d, 3 days or until clinically stable
2021ASCO	G2-G4	Methylprednisolone 1-2 mg/kg•d, oral or IV depending on the symptoms
2022NCCN	G1-G4	Methylprednisolone 1g/d IV, 3–5 days
2021CSCO	G2	Methylprednisolone 1-2 mg/kg•d, 3–5 days
	G3-G4	Methylprednisolone 500-1000mg/d, 3–5 days

can be added if glucocorticoid mono-treatment fails after 24 hours. However, it should be noted that high-dose infliximab is forbidden if the patients have moderate to serious heart failure. Pacemakers can be installed in patients with arrhythmias if necessary, and mechanical hemodynamic support should be given promptly in critical patients (111, 118–120). All guidelines' recommendations are based on high levels of evidence and recommended high doses of glucocorticoids. The different doses of glucocorticoid in guidelines maybe due to differences in panel references and reference areas. NCCN/ASCO have published many clinical practice guidelines with high level of evidence which have been recognized and followed by clinicians worldwide. The CSCO guidelines include a large number of toxicity data from China, and is more suitable for Chinese.

6.4.4 Re-challenge of ICIs

ASCO guidelines recommended to terminate the use of ICIs in all patients with CV-irAE, while NCCN/CSCO guidelines recommend patients with grade 1-2 cardiotoxicity restart ICIs after symptom remission.

7 Emerging predictive markers

When patients show symptoms of CV-irAE, myocardial damage already exists. In addition to conventional markers, more sensitive predictive markers are needed to prevent myocardial damage in advance. Few studies of toxicity prediction of myocarditis have been reported, but a promising toxicity prediction marker of CV-irAE need to be further explored. Drobni et al. (121) conducted a case-control study in patients with ICIs myocarditis or without CV-irAE after ICIs treatment, showing that significantly higher neutrophil/lymphocyte ratio (NLR) was found in patients with ICI related myocarditis (121). Another study compared echocardiographic global longitudinal strain (GLS) in patients with ICIs myocarditis or without CV-irAE after ICIs treatment. They found that GLS is lower in patients with ICI related myocarditis and suggested a poor prognosis (122). In summary, NLR and GLS are potential makers of immune-mediated myocarditis.

8 Discussion

CV-irAE is lethal, so we expect to detect abnormalities before irreversible myocardial damage happens; therefore, more sensitive and reliable makers are urgently needed (123–125). Although ICIs have been widely used in treating cancer and achieved good results, a series of adverse events may happen after the application of ICIs. Cardiovascular toxicities are rare but usually fatal when it occurs. Therefore, we should continually explore the mechanism of CV-irAE, summarizing the cases that have occurred, strengthening awareness of prevention and improving the management of CV-irAE, and introducing of a new surveillance strategy.

Author contributions

RY conceived the idea, XL wrote the manuscript, WP and JW revised the content and grammar of the manuscript. RY and S-CY reviewed the structure and content of the manuscript in the revision. All authors provided critical feedback and analysis and manuscript, and contributed to the final manuscript.

Funding

This work was supported by the National Natural Science Foundation of China [82072622 and 81860488 to RY; 82202888 to JW]. The work was funded by "Xing Dian Ying Cai given to RY" and Mong-Hong Lee expert workstation [202205AF150027].

Conflict of interest

The authors declare that the research was conducted in the absence of any commercial or financial relationships that could be construed as a potential conflict of interest.

Publisher's note

References

1. Vaddepally RK, Kharel P, Pandey R, Garje R, Chandra AB. Review of indications of FDA-approved immune checkpoint inhibitors per NCCN guidelines with the level of evidence. *Cancers (Basel)* (2020) 12(3):738. doi: 10.3390/cancers12030738

2. Han X, Wei Q, Lv Y, Weng L, Huang H, Wei Q, et al. Ginseng-derived nanoparticles potentiate immune checkpoint antibody efficacy by reprogramming the cold tumor microenvironment. *Mol Ther* (2022) 30(1):327–40. doi: 10.1016/j.ymthe.2021.08.028

3. Weber JS, Yang JC, Atkins MB, Disis ML. Toxicities of immunotherapy for the practitioner. *J Clin Oncol* (2015) 33(18):2092–9. doi: 10.1200/JCO.2014.60.0379

4. Thompson JA. New NCCN guidelines: Recognition and management of immunotherapy-related toxicity. *J Natl Compr Canc Netw* (2018) 16(5S):594–6. doi: 10.6004/jnccn.2018.0047

5. Haslam A, Prasad V. Estimation of the percentage of US patients with cancer who are eligible for and respond to checkpoint inhibitor immunotherapy drugs. *JAMA Netw Open* (2019) 2(5):e192535. doi: 10.1001/jamanetworkopen.2019.2535

6. Solinas C, Migliori E, De Silva P, Willard-Gallo K. LAG3: The biological processes that motivate targeting this immune checkpoint molecule in human cancer. *Cancers (Basel)* (2019) 11(8):1213. doi: 10.3390/cancers11081213

7. Sun JY, Qu Q, Lou YX, Hua Y, Sun GZ, Sun W, et al. Cardiotoxicity in cancer immune-checkpoint therapy: Mechanisms, clinical evidence, and management strategies. *Int J Cardiol* (2021) 344:170–8. doi: 10.1016/j.ijcard.2021.09.041

8. Agostinetto E, Ceppi M, Bruzzone M, Lambertini M, de Azambuja E. Response to letter entitled: Re: Cardiotoxicity of immune checkpoint inhibitors: A systematic review and meta-analysis of randomised clinical trials. *Eur J Cancer* (2021) 155:303–6. doi: 10.1016/j.ejca.2021.06.042

9. Mahmood SS, Fradley MG, Cohen JV, Nohria A, Reynolds KL, Heinzerling LM, et al. Myocarditis in patients treated with immune checkpoint inhibitors. *J Am Coll Cardiol* (2018) 71(16):1755–64. doi: 10.1016/j.jacc.2018.02.037

10. Matsuo K, Ishiguro T, Najama T, Shimizu Y, Kobayashi Y, Mutou M. Nivolumab-induced myocarditis successfully treated with corticosteroid therapy: A case report and review of the literature. *Intern Med* (2019) 58(16):2367–72. doi: 10.2169/internalmedicine.2596-18

11. Souza M, Nielsen D, Svane IM, Iversen K, Rasmussen PV, Madelaire C, et al. The risk of cardiac events in patients receiving immune checkpoint inhibitors: a nationwide Danish study. *Eur Heart J* (2021) 42(16):1621–31. doi: 10.1093/eurheartj/ehaa884

12. Wang DY, Salem JE, Cohen JV, Chandra S, Menzer C, Ye F, et al. Fatal toxic effects associated with immune checkpoint inhibitors: A systematic review and meta-analysis. *JAMA Oncol* (2018) 4(12):1721–8. doi: 10.1001/jamaoncol.2018.3923

13. Rubio-Infante N, Ramírez-Flores YA, Castillo EC, Lozano O, García-Rivas G, Torre-Amione G. Cardiotoxicity associated with immune checkpoint inhibitor therapy: a meta-analysis. *Eur J Heart Fail* (2021) 23(10):1739–47. doi: 10.1002/ejhf.2289

14. Larkin J, Chiarion-Sileni V, Gonzalez R, Grob JJ, Cowey CL, Lao CD, et al. Combined nivolumab and ipilimumab or monotherapy in untreated melanoma. *N Engl J Med* (2015) 373(1):23–34. doi: 10.1056/NEJMoa1504030

15. Tawbi HA, Schadendorf D, Lipson EJ, Ascierto PA, Matamala L, Castillo Gutiérrez E, et al. Relatlimab and nivolumab versus nivolumab in untreated advanced melanoma. *N Engl J Med* (2022) 386(1):24–34. doi: 10.1056/NEJMoa2109970

16. Moslehi JJ, Salem JE, Sosman JA, Lebrun-Vignes B, Johnson DB. Increased reporting of fatal immune checkpoint inhibitor-associated myocarditis. *Lancet* (2018) 391(10124):933. doi: 10.1016/S0140-6736(18)30533-6

17. Salem JE, Manouchehri A, Moey M, Lebrun-Vignes B, Bastarache L, Pariente A, et al. Cardiovascular toxicities associated with immune checkpoint inhibitors: an observational, retrospective, pharmacovigilance study. *Lancet Oncol* (2018) 19(12):1579–89. doi: 10.1016/S1470-2045(18)30608-9

18. Zamami Y, Niimura T, Okada N, Koyama T, Fukushima K, Izawa-Ishizawa Y, et al. Factors associated with immune checkpoint inhibitor-related myocarditis. *JAMA Oncol* (2019) 5(11):1635–7. doi: 10.1001/jamaoncol.2019.3113

19. Pirozzi F, Poto R, Aran L, Cuomo A, Galdiero MR, Spadaro G, et al. Cardiovascular toxicity of immune checkpoint inhibitors: Clinical risk factors. *Curr Oncol Rep* (2021) 23(2):13. doi: 10.1007/s11912-020-01002-w

20. Johnson DB, Balko JM, Compton ML, Chalkias S, Gorham J, Xu Y, et al. Fulminant myocarditis with combination immune checkpoint blockade. *N Engl J Med* (2016) 375(18):1749–55. doi: 10.1056/NEJMoa1609214

21. Keam SJ. Cadonilimab: First approval. *Drugs* (2022) 82(12):1333–9. doi: 10.1007/s40265-022-01761-9

22. Du S, Zhou L, Alexander GS, Park K, Yang L, Wang N, et al. PD-1 modulates radiation-induced cardiac toxicity through cytotoxic T lymphocytes. *J Thorac Oncol* (2018) 13(4):510–20. doi: 10.1016/j.jtho.2017.12.002

23. Tsuruoka K, Wakabayashi S, Morihara H, Matsunaga N, Fujisaka Y, Goto I, et al. Exacerbation of autoimmune myocarditis by an immune checkpoint inhibitor is dependent on its time of administration in mice. *Int J Cardiol* (2020) 313:67–75. doi: 10.1016/j.ijcard.2020.04.033

24. Xie W, Huang H, Xiao S, Fan Y, Deng X, Zhang Z. Immune checkpoint inhibitors therapies in patients with cancer and preexisting autoimmune diseases: A meta-analysis of observational studies. *Autoimmun Rev* (2020) 19(12):102687. doi: 10.1016/j.autrev.2020.102687

25. Lee C, Drobni ZD, Zafar A, Gongora CA, Zlotoff DA, Alvi RM, et al. Pre-existing autoimmune disease increases the risk of cardiovascular and noncardiovascular events after immunotherapy. *JACC Cardio Oncol* (2022) 4(5):660–9. doi: 10.1016/j.jaccao.2022.11.008

26. Tocchetti CG, Galdiero MR, Varricchi G. Cardiac toxicity in patients treated with immune checkpoint inhibitors: It is now time for cardio-Immuno-Oncology. *J Am Coll Cardiol* (2018) 71(16):1765–7. doi: 10.1016/j.jacc.2018.02.038

27. Lyon AR, Dent S, Stanway S, Earl H, Brezden-Masley C, Cohen-Solal A, et al. Baseline cardiovascular risk assessment in cancer patients scheduled to receive cardiotoxic cancer therapies: a position statement and new risk assessment tools from the cardio-oncology study group of the heart failure association of the European society of cardiology in collaboration with the international cardio-oncology society. *Eur J Heart Fail* (2020) 22(11):1945–60. doi: 10.1002/ejhf.1920

28. Lyon AR, Yousaf N, Battisti N, Moslehi J, Larkin J. Immune checkpoint inhibitors and cardiovascular toxicity. *Lancet Oncol* (2018) 19(9):e447–447e458. doi: 10.1016/S1470-2045(18)30457-1

29. Waliany S, Lee D, Witteles RM, Neal JW, Nguyen P, Davis MM, et al. Immune checkpoint inhibitor cardiotoxicity: Understanding basic mechanisms and clinical characteristics and finding a cure. *Annu Rev Pharmacol Toxicol* (2021) 61:113–34. doi: 10.1146/annurev-pharmtox-010919-023451

30. Chen DS, Irving BA, Hodi FS. Molecular pathways: next-generation immunotherapy–inhibiting programmed death-ligand 1 and programmed death-1. *Clin Cancer Res* (2012) 18(24):6580–7. doi: 10.1158/1078-0432.CCR-12-1362

31. Sharma P, Allison JP. The future of immune checkpoint therapy. *Science* (2015) 348(6230):56–61. doi: 10.1126/science.aaa8172

32. Wei SC, Duffy CR, Allison JP. Fundamental mechanisms of immune checkpoint blockade therapy. *Cancer Discovery* (2018) 8(9):1069–86. doi: 10.1158/2159-8290.CD-18-0367

33. Chen DS, Mellman I. Elements of cancer immunity and the cancer-immune set point. *Nature* (2017) 541(7637):321–30. doi: 10.1038/nature21349

34. Schildberg FA, Klein SR, Freeman GJ, Sharpe AH. Coinhibitory pathways in the B7-CD28 ligand-receptor family. *Immunity* (2016) 44(5):955–72. doi: 10.1016/j.immuni.2016.05.002

35. Krummel MF, Allison JP. CTLA-4 engagement inhibits IL-2 accumulation and cell cycle progression upon activation of resting T cells. *J Exp Med* (1996) 183(6):2533–40. doi: 10.1084/jem.183.6.2533

36. Qureshi OS, Zheng Y, Nakamura K, Attridge K, Manzotti C, Schmidt EM, et al. Trans-endocytosis of CD80 and CD86: a molecular basis for the cell-extrinsic function of CTLA-4. *Science* (2011) 332(6029):600–3. doi: 10.1126/science.1202947

37. Walunas TL, Bakker CY, Bluestone JA. CTLA-4 ligation blocks CD28-dependent T cell activation. *J Exp Med* (1996) 183(6):2541–50. doi: 10.1084/jem.183.6.2541

38. Bluestone JA, Anderson M. Tolerance in the age of immunotherapy. *N Engl J Med* (2020) 383(12):1156–66. doi: 10.1056/NEJMra1911109

39. Freeman GJ, Long AJ, Iwai Y, Bourque K, Chernova T, Nishimura H, et al. Engagement of the PD-1 immunoinhibitory receptor by a novel B7 family member leads to negative regulation of lymphocyte activation. *J Exp Med* (2000) 192(7):1027–34. doi: 10.1084/jem.192.7.1027

40. Keir ME, Butte MJ, Freeman GJ, Sharpe AH. PD-1 and its ligands in tolerance and immunity. *Annu Rev Immunol* (2008) 26:677–704. doi: 10.1146/annurev.immunol.26.021607.090331

41. Curiel TJ, Coukos G, Zou L, Alvarez X, Cheng P, Mottram P, et al. Specific recruitment of regulatory T cells in ovarian carcinoma fosters immune privilege and predicts reduced survival. *Nat Med* (2004) 10(9):942–9. doi: 10.1038/nm1093

42. Liu Y, Zheng P. How does an anti-CTLA-4 antibody promote cancer immunity. *Trends Immunol* (2018) 39(12):953–6. doi: 10.1016/j.it.2018.10.009

43. Du X, Tang F, Liu M, Su J, Zhang Y, Wu W, et al. A reappraisal of CTLA-4 checkpoint blockade in cancer immunotherapy. *Cell Res* (2018) 28(4):416–32. doi: 10.1038/s41422-018-0011-0

44. Waight JD, Chand D, Dietrich S, Gombos R, Horn T, Gonzalez AM, et al. Selective FcγR Co-engagement on APCs modulates the activity of therapeutic antibodies targeting T cell antigens. *Cancer Cell* (2018) 33(6):1033–47.e5. doi: 10.1016/j.ccell.2018.05.005

45. Ferrara AL, Liotti A, Pezone A, De Rosa V. Therapeutic opportunities to modulate immune tolerance through the metabolism-chromatin axis. *Trends Endocrinol Metab* (2022) 33(7):507–21. doi: 10.1016/j.tem.2022.04.002

46. Ferreira L, Muller YD, Bluestone JA, Tang Q. Next-generation regulatory T cell therapy. *Nat Rev Drug Discovery* (2019) 18(10):749–69. doi: 10.1038/s41573-019-0041-4

47. Agata Y, Kawasaki A, Nishimura H, Ishida Y, Tsubata T, Yagita H, et al. Expression of the PD-1 antigen on the surface of stimulated mouse T and b lymphocytes. *Int Immunol* (1996) 8(5):765–72. doi: 10.1093/intimm/8.5.765

48. Anderson AC, Joller N, Kuchroo VK. Lag-3, Tim-3, and TIGIT: Co-inhibitory receptors with specialized functions in immune regulation. *Immunity* (2016) 44 (5):989–1004. doi: 10.1016/j.immuni.2016.05.001

49. Maruhashi T, Okazaki IM, Sugiura D, Takahashi S, Maeda TK, Shimizu K, et al. LAG-3 inhibits the activation of CD4(+) T cells that recognize stable pMHCII through its conformation-dependent recognition of pMHCII. *Nat Immunol* (2018) 19 (12):1415–26. doi: 10.1038/s41590-018-0217-9

50. Bhatia A, Kumar Y. Cellular and molecular mechanisms in cancer immune escape: a comprehensive review. *Expert Rev Clin Immunol* (2014) 10(1):41–62. doi: 10.1586/1744666X.2014.865519

51. Tumeh PC, Harview CL, Yearley JH, Shintaku IP, Taylor EJ, Robert L, et al. PD-1 blockade induces responses by inhibiting adaptive immune resistance. *Nature* (2014) 515(7528):568–71. doi: 10.1038/nature13954

52. Zhang JC, Chen WD, Alvarez JB, Jia K, Shi L, Wang Q, et al. Cancer immune checkpoint blockade therapy and its associated autoimmune cardiotoxicity. *Acta Pharmacol Sin* (2018) 39(11):1693–8. doi: 10.1038/s41401-018-0062-2

53. Chocarro L, Bocanegra A, Blanco E, Fernández-Rubio L, Arasanz H, Echaide M, et al. Cutting-edge: Preclinical and clinical development of the first approved lag-3 inhibitor. *Cells* (2022) 11(15):2351. doi: 10.3390/cells11152351

54. Curigliano G, Gelderblom H, Mach N, Doi T, Tai D, Forde PM, et al. Phase I/Ib clinical trial of sabatolimab, an anti-TIM-3 antibody, alone and in combination with spartalizumab, an anti-PD-1 antibody, in advanced solid tumors. *Clin Cancer Res* (2021) 27(13):3620–9. doi: 10.1158/1078-0432.CCR-20-4746

55. Niu J, Maurice-Dror C, Lee DH, Kim DW, Nagrial A, Voskoboynik M, et al. First-in-human phase 1 study of the anti-TIGIT antibody vibostolimab as monotherapy or with pembrolizumab for advanced solid tumors, including non-small-cell lung cancer. *Ann Oncol* (2022) 33(2):169–80. doi: 10.1016/j.annonc.2021.11.002

56. Yarchoan M, Cope L, Ruggieri AN, Anders RA, Noonan AM, Goff LW, et al. Multicenter randomized phase II trial of atezolizumab with or without cobimetinib in biliary tract cancers. *J Clin Invest* (2021) 131(24):e152670. doi: 10.1172/JCI152670

57. Aggarwal C, Prawira A, Antonia S, Rahma O, Tolcher A, Cohen RB, et al. Dual checkpoint targeting of B7-H3 and PD-1 with enoblituzumab and pembrolizumab in advanced solid tumors: interim results from a multicenter phase I/II trial. *J Immunother Cancer* (2022) 10(4):e004424. doi: 10.1136/jitc-2021-004424

58. Grabie N, Lichtman AH, Padera R. T Cell checkpoint regulators in the heart. *Cardiovasc Res* (2019) 115(5):869–77. doi: 10.1093/cvr/cvz025

59. Hodi FS, O'Day SJ, McDermott DF, Weber RW, Sosman JA, Haanen JB, et al. Improved survival with ipilimumab in patients with metastatic melanoma. *N Engl J Med* (2010) 363(8):711–23. doi: 10.1056/NEJMoa1003466

60. Nishimura H, Okazaki T, Tanaka Y, Nakatani K, Hara M, Matsumori A, et al. Autoimmune dilated cardiomyopathy in PD-1 receptor-deficient mice. *Science* (2001) 291(5502):319–22. doi: 10.1126/science.291.5502.319

61. Okazaki T, Tanaka Y, Nishio R, Mitsuiye T, Mizoguchi A, Wang J, et al. Autoantibodies against cardiac troponin I are responsible for dilated cardiomyopathy in PD-1-deficient mice. *Nat Med* (2003) 9(12):1477–83. doi: 10.1038/nm955

62. Won T, Kalinoski HM, Wood MK, Hughes DM, Jaime CM, Delgado P, et al. Cardiac myosin-specific autoimmune T cells contribute to immune-checkpoint-inhibitor-associated myocarditis. *Cell Rep* (2022) 41(6):111611. doi: 10.1016/j.celrep.2022.111611

63. Axelrod ML, Meijers WC, Screever EM, Qin J, Carroll MG, Sun X, et al. T Cells specific for α-myosin drive immunotherapy-related myocarditis. *Nature* (2022) 611 (7937):818–26. doi: 10.1038/s41586-022-05432-3

64. Tarhini AA, Zahoor H, Lin Y, Malhotra U, Sander C, Butterfield LH, et al. Baseline circulating IL-17 predicts toxicity while TGF-β1 and IL-10 are prognostic of relapse in ipilimumab neoadjuvant therapy of melanoma. *J Immunother Cancer* (2015) 3:39. doi: 10.1186/s40425-015-0081-1

65. Lim SY, Lee JH, Gide TN, Menzies AM, Guminski A, Carlino MS, et al. Circulating cytokines predict immune-related toxicity in melanoma patients receiving anti-PD-1-Based immunotherapy. *Clin Cancer Res* (2019) 25(5):1557–63. doi: 10.1158/1078-0432.CCR-18-2795

66. Baik AH, Oluwole OO, Johnson DB, Shah N, Salem JE, Tsai KK, et al. Mechanisms of cardiovascular toxicities associated with immunotherapies. *Circ Res* (2021) 128(11):1780–801. doi: 10.1161/CIRCRESAHA.120.315894

67. Varricchi G, Galdiero MR, Tocchetti CG. Cardiac toxicity of immune checkpoint inhibitors: Cardio-oncology meets immunology. *Circulation* (2017) 136 (21):1989–92. doi: 10.1161/CIRCULATIONAHA.117.029626

68. Tsuruda T, Yoshikawa N, Kai M, Yamaguchi M, Toida R, Kodama T, et al. The cytokine expression in patients with cardiac complication after immune checkpoint inhibitor therapy. *Intern Med* (2021) 60(3):423–9. doi: 10.2169/internalmedicine.5317-20

69. Kumar P, Bhattacharya P, Prabhakar BS. A comprehensive review on the role of co-signaling receptors and treg homeostasis in autoimmunity and tumor immunity. *J Autoimmun* (2018) 95:77–99. doi: 10.1016/j.jaut.2018.08.007

70. Alissafi T, Hatzioannou A, Legaki AI, Varveri A, Verginis P. Balancing cancer immunotherapy and immune-related adverse events: The emerging role of regulatory T cells. *J Autoimmun* (2019) 104:102310. doi: 10.1016/j.jaut.2019.102310

71. Kumar P, Saini S, Prabhakar BS. Cancer immunotherapy with check point inhibitor can cause autoimmune adverse events due to loss of treg homeostasis. *Semin Cancer Biol* (2020) 64:29–35. doi: 10.1016/j.semcancer.2019.01.006

72. Lutgens E, Seijkens T. Cancer patients receiving immune checkpoint inhibitor therapy are at an increased risk for atherosclerotic cardiovascular disease. *J Immunother Cancer* (2020) 8(1):e000300. doi: 10.1136/jitc-2019-000300

73. Strauss L, Mahmoud M, Weaver JD, Tijaro-Ovalle NM, Christofides A, Wang Q, et al. Targeted deletion of PD-1 in myeloid cells induces antitumor immunity. *Sci Immunol* (2020) 5(43):eaay1863. doi: 10.1126/sciimmunol.aay1863

74. Seijkens T, van Tiel CM, Kusters P, Atzler D, Soehnlein O, Zarzycka B, et al. Targeting CD40-induced TRAF6 signaling in macrophages reduces atherosclerosis. *J Am Coll Cardiol* (2018) 71(5):527–42. doi: 10.1016/j.jacc.2017.11.055

75. Dominic A, Banerjee P, Hamilton DJ, Le NT, Abe JI. Time-dependent replicative senescence vs. disturbed flow-induced pre-mature aging in atherosclerosis. *Redox Biol* (2020) 37:101614. doi: 10.1016/j.redox.2020.101614

76. Banerjee P, Kotla S, Reddy Velatooru L, Abe RJ, Davis EA, Cooke JP, et al. Senescence-associated secretory phenotype as a hinge between cardiovascular diseases and cancer. *Front Cardiovasc Med* (2021) 8:763930. doi: 10.3389/fcvm.2021.763930

77. Drobni ZD, Alvi RM, Taron J, Zafar A, Murphy SP, Rambarat PK, et al. Association between immune checkpoint inhibitors with cardiovascular events and atherosclerotic plaque. *Circulation* (2020) 142(24):2299–311. doi: 10.1161/CIRCULATIONAHA.120.049981

78. Newman JL, Stone JR. Immune checkpoint inhibition alters the inflammatory cell composition of human coronary artery atherosclerosis. *Cardiovasc Pathol* (2019) 43:107148. doi: 10.1016/j.carpath.2019.107148

79. Gupta S, Pablo AM, Xc J, Wang N, Tall AR, Schindler C. IFN-gamma potentiates atherosclerosis in ApoE knock-out mice. *J Clin Invest* (1997) 99 (11):2752–61. doi: 10.1172/JCI119465

80. Zhou X, Robertson AK, Rudling M, Parini P, Hansson GK. Lesion development and response to immunization reveal a complex role for CD4 in atherosclerosis. *Circ Res* (2005) 96(4):427–34. doi: 10.1161/01.RES.0000156889.22364.f1

81. Zhou X, Robertson AK, Hjerpe C, Hansson GK. Adoptive transfer of CD4+ T cells reactive to modified low-density lipoprotein aggravates atherosclerosis. *Arterioscler Thromb Vasc Biol* (2006) 26(4):864–70. doi: 10.1161/01.ATV.0000206122.61591.ff

82. Boyerinas B, Jochems C, Fantini M, Heery CR, Gulley JL, Tsang KY, et al. Antibody-dependent cellular cytotoxicity activity of a novel anti-PD-L1 antibody avelumab (MSB0010718C) on human tumor cells. *Cancer Immunol Res* (2015) 3 (10):1148–57. doi: 10.1158/2326-6066.CIR-15-0059

83. Fujii R, Friedman ER, Richards J, Tsang KY, Heery CR, Schlom J, et al. Enhanced killing of chordoma cells by antibody-dependent cell-mediated cytotoxicity employing the novel anti-PD-L1 antibody avelumab. *Oncotarget* (2016) 7(23):33498–511. doi: 10.18632/oncotarget.9256

84. Khanna S, Thomas A, Abate-Daga D, Zhang J, Morrow B, Steinberg SM, et al. Malignant mesothelioma effusions are infiltrated by CD3(+) T cells highly expressing PD-L1 and the PD-L1(+) tumor cells within these effusions are susceptible to ADCC by the anti-PD-L1 antibody avelumab. *J Thorac Oncol* (2016) 11(11):1993–2005. doi: 10.1016/j.jtho.2016.07.033

85. Hu JR, Florido R, Lipson EJ, Naidoo J, Ardehali R, Tocchetti CG, et al. Cardiovascular toxicities associated with immune checkpoint inhibitors. *Cardiovasc Res* (2019) 115(5):854–68. doi: 10.1093/cvr/cvz026

86. Escudier M, Cautela J, Malissen N, Ancedy Y, Orabona M, Pinto J, et al. Clinical features, management, and outcomes of immune checkpoint inhibitor-related cardiotoxicity. *Circulation* (2017) 136(21):2085–7. doi: 10.1161/CIRCULATIONAHA.117.030571

87. Chen DY, Huang WK, Chien-Chia Wu V, Chang WC, Chen JS, Chuang CK, et al. Cardiovascular toxicity of immune checkpoint inhibitors in cancer patients: A review when cardiology meets immuno-oncology. *J Formos Med Assoc* (2020) 119 (10):1461–75. doi: 10.1016/j.jfma.2019.07.025

88. Palaskas N, Lopez-Mattei J, Durand JB, Iliescu C, Deswal A. Immune checkpoint inhibitor myocarditis: Pathophysiological characteristics, diagnosis, and treatment. *J Am Heart Assoc* (2020) 9(2):e013757. doi: 10.1161/JAHA.119.013757

89. Bonaca MP, Olenchock BA, Salem JE, Wiviott SD, Ederhy S, Cohen A, et al. Myocarditis in the setting of cancer therapeutics: Proposed case definitions for emerging clinical syndromes in cardio-oncology. *Circulation* (2019) 140(2):80–91. doi: 10.1161/CIRCULATIONAHA.118.034497

90. Serzan M, Rapisuwon S, Krishnan J, Chang IC, Barac A. Takotsubo cardiomyopathy associated with checkpoint inhibitor therapy: Endomyocardial biopsy provides pathological insights to dual diseases. *JACC Cardio Oncol* (2021) 3 (2):330–4. doi: 10.1016/j.jaccao.2021.02.005

91. Tsuchihashi K, Ueshima K, Uchida T, Oh-mura N, Kimura K, Owa M, et al. Transient left ventricular apical ballooning without coronary artery stenosis: a novel heart syndrome mimicking acute myocardial infarction. *Angina Pectoris-Myocardial Infarction Investigations Japan J Am Coll Cardiol* (2001) 38(1):11–8. doi: 10.1016/s0735-1097(01)01316-x

92. El-Hussein MT, Kilfoil L. The story of a broken heart: Takotsubo cardiomyopathy. *J Emerg Nurs* (2021) 47(4):635–42. doi: 10.1016/j.jen.2020.12.014

93. Heinzerling L, Ott PA, Hodi FS, Husain AN, Tajmir-Riahi A, Tawbi H, et al. Cardiotoxicity associated with CTLA4 and PD1 blocking immunotherapy. *J Immunother Cancer* (2016) 4:50. doi: 10.1186/s40425-016-0152-y

94. Oldfield K, Jayasinghe R, Niranjan S, Chadha S. Immune checkpoint inhibitor-induced takotsubo syndrome and diabetic ketoacidosis: rare reactions. *BMJ Case Rep* (2021) 14(2):e237217. doi: 10.1136/bcr-2020-237217

95. Herzum M, Maisch B. Humoral and cellular immune response in human myocarditis and dilated cardiomyopathy. *Pathol Immunopathol Res* (1988) 7(4):240–50. doi: 10.1159/000157120

96. Samejima Y, Iuchi A, Kanai T, Noda Y, Nasu S, Tanaka A, et al. Development of severe heart failure in a patient with squamous non-small-cell lung cancer during nivolumab treatment. *Intern Med* (2020) 59(16):2003–8. doi: 10.2169/internalmedicine.4550-20

97. Amiri-Kordestani L, Moslehi J, Cheng J, Tang S, Schroeder R, Sridhara R, et al. Cardiovascular adverse events in immune checkpoint inhibitor clinical trials: A US food and drug administration pooled analysis. *J Clin Oncol* (2018) 36(15_suppl):3009–9. doi: 10.1200/JCO.2018.36.15_suppl.3009

98. Zhu H, Ivanovic M, Nguyen A, Nguyen PK, Wu SM. Immune checkpoint inhibitor cardiotoxicity: Breaking barriers in the cardiovascular immune landscape. *J Mol Cell Cardiol* (2021) 160:121–7. doi: 10.1016/j.yjmcc.2021.07.006

99. Canale ML, Camerini A, Casolo G, Lilli A, Bisceglia I, Parrini I, et al. Incidence of pericardial effusion in patients with advanced non-small cell lung cancer receiving immunotherapy. *Adv Ther* (2020) 37(7):3178–84. doi: 10.1007/s12325-020-01386-y

100. Moriyama S, Fukata M, Tatsumoto R, Kono M. Refractory constrictive pericarditis caused by an immune checkpoint inhibitor properly managed with infliximab: a case report. *Eur Heart J Case Rep* (2021) 5(1):ytab002. doi: 10.1093/ehjcr/ytab002

101. Saade A, Mansuet-Lupo A, Arrondeau J, Thibault C, Mirabel M, Goldwasser F, et al. Pericardial effusion under nivolumab: case-reports and review of the literature. *J Immunother Cancer* (2019) 7(1):266. doi: 10.1186/s40425-019-0760-4

102. Zarogoulidis P, Chinelis P, Athanasiadou A, Tsiouda T, Trakada G, Kallianos A, et al. Possible adverse effects of immunotherapy in non-small cell lung cancer; treatment and follow-up of three cases. *Respir Med Case Rep* (2017) 22:101–5. doi: 10.1016/j.rmcr.2017.07.004

103. Lindner AK, Gruenbacher G, Schachtner G, Thurnher M, Pichler R. Rare, but severe: Vasculitis and checkpoint inhibitors. *Eur Urol Focus* (2020) 6(3):609–12. doi: 10.1016/j.euf.2019.04.014

104. Gosangi B, McIntosh L, Keraliya A, Irugu D, Baheti A, Khandelwal A, et al. Imaging features of toxicities associated with immune checkpoint inhibitors. *Eur J Radiol Open* (2022) 9:100434. doi: 10.1016/j.ejro.2022.100434

105. Bar J, Markel G, Gottfried T, Percik R, Leibowitz-Amit R, Berger R, et al. Acute vascular events as a possibly related adverse event of immunotherapy: a single-institute retrospective study. *Eur J Cancer* (2019) 120:122–31. doi: 10.1016/j.ejca.2019.06.021

106. Schiffer WB, Deych E, Lenihan DJ, Zhang KW. Coronary and aortic calcification are associated with cardiovascular events on immune checkpoint inhibitor therapy. *Int J Cardiol* (2021) 322:177–82. doi: 10.1016/j.ijcard.2020.08.024

107. Daxini A, Cronin K, Sreih AG. Vasculitis associated with immune checkpoint inhibitors-a systematic review. *Clin Rheumatol* (2018) 37(9):2579–84. doi: 10.1007/s10067-018-4177-0

108. Samson M, Corbera-Bellalta M, Audia S, Planas-Rigol E, Martin L, Cid MC, et al. Recent advances in our understanding of giant cell arteritis pathogenesis. *Autoimmun Rev* (2017) 16(8):833–44. doi: 10.1016/j.autrev.2017.05.014

109. Hid Cadena R, Abdulahad WH, Hospers G, Wind TT, Boots A, Heeringa P, et al. Checks and balances in autoimmune vasculitis. *Front Immunol* (2018) 9:315. doi: 10.3389/fimmu.2018.00315

110. Schmidt J, Warrington KJ. Polymyalgia rheumatica and giant cell arteritis in older patients: diagnosis and pharmacological management. *Drugs Aging* (2011) 28(8):651–66. doi: 10.2165/11592500-000000000-00000

111. Brahmer JR, Lacchetti C, Schneider BJ, Atkins MB, Brassil KJ, Caterino JM, et al. Management of immune-related adverse events in patients treated with immune checkpoint inhibitor therapy: American society of clinical oncology clinical practice guideline. *J Clin Oncol* (2018) 36(17):1714–68. doi: 10.1200/JCO.2017.77.6385

112. Thompson JA, Schneider BJ, Brahmer J, Andrews S, Armand P, Bhatia S, et al. NCCN guidelines insights: Management of immunotherapy-related toxicities, version 1.2020. *J Natl Compr Canc Netw* (2020) 18(3):230–41. doi: 10.6004/jnccn.2020.0012

113. Puzanov I, Diab A, Abdallah K, Bingham CO3rd, Brogdon C, Dadu R, et al. Managing toxicities associated with immune checkpoint inhibitors: consensus recommendations from the society for immunotherapy of cancer (SITC) toxicity management working group. *J Immunother Cancer* (2017) 5(1):95. doi: 10.1186/s40425-017-0300-z

114. Schneider BJ, Naidoo J, Santomasso BD, Lacchetti C, Adkins S, Anadkat M, et al. Management of immune-related adverse events in patients treated with immune checkpoint inhibitor therapy: ASCO guideline update. *J Clin Oncol* (2021) 39(36):4073–126. doi: 10.1200/JCO.21.01440

115. Arangalage D, Degrauwe N, Michielin O, Monney P, Özdemir BC. Pathophysiology, diagnosis and management of cardiac toxicity induced by immune checkpoint inhibitors and BRAF and MEK inhibitors. *Cancer Treat Rev* (2021) 100:102282. doi: 10.1016/j.ctrv.2021.102282

116. Thompson JA, Schneider BJ, Brahmer J, Achufusi A, Armand P, Berkenstock MK, et al. Management of immunotherapy-related toxicities, version 1.2022, NCCN clinical practice guidelines in oncology. *J Natl Compr Canc Netw* (2022) 20(4):387–405. doi: 10.6004/jnccn.2022.0020

117. Ammirati E, Cipriani M, Moro C, Raineri C, Pini D, Sormani P, et al. Clinical presentation and outcome in a contemporary cohort of patients with acute myocarditis: Multicenter Lombardy registry. *Circulation* (2018) 138(11):1088–99. doi: 10.1161/CIRCULATIONAHA.118.035319

118. Haanen J, Carbonnel F, Robert C, Kerr KM, Peters S, Larkin J, et al. Management of toxicities from immunotherapy: ESMO clinical practice guidelines for diagnosis, treatment and follow-up. *Ann Oncol* (2017) 28(suppl_4):iv119–119iv142. doi: 10.1093/annonc/mdx225

119. Kwon HJ, Coté TR, Cuffe MS, Kramer JM, Braun MM. Case reports of heart failure after therapy with a tumor necrosis factor antagonist. *Ann Intern Med* (2003) 138(10):807–11. doi: 10.7326/0003-4819-138-10-200305200-00008

120. Dueck AC, Mendoza TR, Mitchell SA, Reeve BB, Castro KM, Rogak LJ, et al. Validity and reliability of the US national cancer Institutes patient-reported outcomes version of the common terminology criteria for adverse events (PRO-CTCAE). *JAMA Oncol* (2015) 1(8):1051–9. doi: 10.1001/jamaoncol.2015.2639

121. Drobni ZD, Zafar A, Zubiri L, Zlotoff DA, Alvi RM, Lee C, et al. Decreased absolute lymphocyte count and increased Neutrophil/Lymphocyte ratio with immune checkpoint inhibitor-associated myocarditis. *J Am Heart Assoc* (2020) 9(23):e018306. doi: 10.1161/JAHA.120.018306

122. Awadalla M, Mahmood SS, Groarke JD, Hassan M, Nohria A, Rokicki A, et al. Global longitudinal strain and cardiac events in patients with immune checkpoint inhibitor-related myocarditis. *J Am Coll Cardiol* (2020) 75(5):467–78. doi: 10.1016/j.jacc.2019.11.049

123. Li Y, Ju L, Hou Z, Deng H, Zhang Z, Wang L, et al. Screening, verification, and optimization of biomarkers for early prediction of cardiotoxicity based on metabolomics. *J Proteome Res* (2015) 14(6):2437–45. doi: 10.1021/pr501116c

124. Hopkins AM, Rowland A, Kichenadasse G, Wiese MD, Gurney H, McKinnon RA, et al. Predicting response and toxicity to immune checkpoint inhibitors using routinely available blood and clinical markers. *Br J Cancer* (2017) 117(7):913–20. doi: 10.1038/bjc.2017.274

125. Varricchi G, Marone G, Mercurio V, Galdiero MR, Bonaduce D, Tocchetti CG. Immune checkpoint inhibitors and cardiac toxicity: An emerging issue. *Curr Med Chem* (2018) 25(11):1327–39. doi: 10.2174/0929867324666170407125017

frontiers | Frontiers in Immunology

TYPE Original Research
PUBLISHED 07 March 2023
DOI 10.3389/fimmu.2023.1127623

OPEN ACCESS

EDITED BY
Sang T. Kim,
University of Texas MD Anderson Cancer Center, United States

REVIEWED BY
Jean-Marc Barret,
GamaMabs Pharma, France
Nahum Puebla-Osorio,
University of Texas MD Anderson Cancer Center, United States

*CORRESPONDENCE
Domenico Grieco
domenico.grieco@unina.it

SPECIALTY SECTION
This article was submitted to Cancer Immunity and Immunotherapy, a section of the journal Frontiers in Immunology

RECEIVED 19 December 2022
ACCEPTED 23 February 2023
PUBLISHED 07 March 2023

CITATION
Serpico AF, Pisauro C and Grieco D (2023) cGAS-dependent proinflammatory and immune homeostatic effects of the microtubule-targeting agent paclitaxel. *Front. Immunol.* 14:1127623. doi: 10.3389/fimmu.2023.1127623

cGAS-dependent proinflammatory and immune homeostatic effects of the microtubule-targeting agent paclitaxel

Angela Flavia Serpico[1,2], Caterina Pisauro[1] and Domenico Grieco[1,2]*

[1]CEINGE Biotecnologie Avanzate Franco Salvatore, Naples, Italy, [2]Dipartimento di Medicina Molecolare e Biotecnologie Mediche (DMMBM), University of Naples "Federico II", Naples, Italy

Taxanes are Microtubule-Targeting Agents (MTAs) that exert potent anticancer activity by directly killing cancer cells. However, recent evidence suggests that they may also stimulate inflammation and anticancer adaptive immunity and that these actions strongly contribute to their therapeutic efficacy. Details on how Taxanes may modulate inflammation and anticancer immunity are, nevertheless, still missing. We show here that at very low doses the Taxane Paclitaxel (Pxl) indeed induces a potent proinflammatory response in various cancer cell types in a cyclic GMP-AMP (cGAMP) synthase (cGAS)- and Stimulator of Interferon Genes (STING)-dependent manner, leading to interferon (IFN) signaling. However, we find that Pxl treatment also strongly upregulates the expression of the immune checkpoint protein Programmed Death-Ligand 1 (PD-L1) in cancer cells, therefore, inducing an inhibitory response to adaptive immunity potentially attenuating anticancer immunity and therapeutic success. These observations provide a mechanistic explanation of why clinical benefit may derive from the combination of Pxl with Immune Checkpoint Inhibitors (ICIs) and suggest that more accurately tailoring dosage and schedule of this combination therapy may provide benefit in the management of a larger number of cancer types and stages.

KEYWORDS

microtubule-targeting agents, Paclitaxel, cGAS, STING, IFN, PD-L1, immune checkpoint inhibitors

Introduction

Microtubule-Targeting Agents (MTAs) are very widely used and effective anticancer drugs. In particular, the microtubule stabilizer MTA Paclitaxel (Pxl) is used for the therapy of a variety of different cancers. By perturbing microtubule dynamics, Pxl affects mitotic progression by activating the spindle assembly checkpoint (SAC), a safeguard mechanism

that delays mitosis exit when spindle assembly is incomplete or abnormal (1–3). Prolongation of mitosis may result in activation of apoptotic pathways and efficient cancer cell killing, however, cancer cells can adapt to the SAC and slip through an abnormal mitosis and this may result in cancer resistance to Pxl treatment (4). Cancer cell response to Pxl appears, therefore, somewhat variable and evidence also suggests that the therapeutic efficacy of Pxl correlates with induction of chromosome segregation defects rather than with delayed mitosis (5).

Chromosome segregation errors are often accompanied by the formation of micronuclei (1). Indeed, chromosomes that are segregated asynchronously relatively to the majority will be enveloped in a nuclear membrane separated from that of the main nucleus, forming micronuclei (1). In addition, micronuclear membrane can be different from the membrane of the main nucleus and micronuclear DNA can undergo damage, fragmentation and rearrangements, a phenomenon called chromothripsis (6). While chromothripsis may be a mechanism that increases genome instability and fuels carcinogenesis, endogenous damaged DNA, altered micronuclear membrane as well as DNA bridges resulting from abnormal chromosome segregation induced by Taxanes also promote activation of the cytosolic DNA sensor cyclic GMP-AMP (cGAMP) synthase (cGAS) (1, 7, 8). The cGAS enzyme was originally identified as an important regulator of the innate immunity in response to infection because of its ability to recognize pathogen DNA in the cytoplasm of an infected cell (9). More recently, cGAS has been shown to be activated also by binding to endogenous cytosolic DNA fragments, as in senescent or damaged cells, or to endogenous DNA within micronuclei that form in cells following chromosome segregation errors (8–11). Indeed, the membrane of micronuclei is often prone to breakage, due to alterations in assembly of the micronuclear lamina, and broken micronuclear membrane causes cytosolic exposure of micronuclear DNA that can consequently interact with cGAS and activate it (7–11).

Active cGAS generates the cyclic dinucleotide cGAMP that, acting as a second messenger, binds the adaptor protein Stimulator of Interferon Genes (STING), resident in the endoplasmic reticulum (9, 11, 12). cGAMP binding to STING promotes conformational changes in STING that allows its interaction with TANK-binding kinase 1 (TBK1), resulting in TBK1 activation (9). Active TBK1 phosphorylates and activates the Interferon Regulatory Factor 3 (IRF3) leading to upregulation of expression of interferons (IFNs) and promoting the inflammatory response (9, 11–13). The inflammatory response and IFN-pathway activation may further call in the intervention of the adaptive immune system (13). These observations have led to the hypothesis that Taxane-based cancer therapy may also work because it promotes inflammation, rendering “hot” the tumor microenvironment, and favoring the intervention of the adaptive immune system to kill cancer cells (1, 14, 15).

Here, by analyzing the effect of low doses of Pxl in various cancer cell lines, we show that Pxl treatment indeed results in a cGAS-dependent activation of a proinflammatory cascade. However, we also find that Pxl stimulates, in a cGAS-dependent fashion, upregulation of the expression of the immune checkpoint protein PD-L1 in cancer cells that, on the other hand, may favor cancer cell evasion form immunosurveillance. On the basis of these findings, we propose that Plx treatment may prime cancer cells to susceptibility to therapy with Immune Checkpoint Inhibitors (ICIs) and that the timing and dosage of the combination therapy of Pxl, and possibly other Taxanes, with ICIs may strongly affect treatment efficacy.

Materials and methods

Cell lines and cell culture

A549, HeLa, MCF7, MDA-MB231cells were form CEINGE Cell Culture Facility. A549 cells were grown in Roswell Park Memorial Institute Medium - 2% L-glutamine (RPMI-1640; Cat# R8758; Sigma-Aldrich, St. Louis, MO, USA), HeLa cells were grown in Dulbecco’s Modified Eagle Medium - high glucose (DMEM; Cat# D6429; Sigma-Aldrich), MCF7 cells were grown in Minimum Essential Medium - 2% L-glutamine (MEM; Cat# M4655; Sigma-Aldrich), MDA-MB231 cells were grown in Dulbecco’s Modified Eagle Medium – low glucose (DMEM; Cat# D6046; Sigma-Aldrich), all supplemented with 10% fetal bovine serum (FBS; Cat# CHA30160L; GE Healthcare Life Sciences, Pittsburgh, PA, USA), 1% penicillin/streptomycin (Cat# ECB3001D; Euroclone, Pero, MI, Italy), and incubated in a humidified incubator at 37° C with 5% CO_2.

Cell treatments and chemicals

For biochemical and immunofluorescence studies, cells were seeded at a cell density of 7000/cm^2 either into 10 cm dishes or onto glass coverslips and treated with vehicle, dimethylsulfoxide (DMSO), as control or Paclitaxel (Plx; Cat# T1912; Calbiochem, Merck Millipore, Billerica, MA, USA) at the indicated doses, after 24 hours from seeding. Cell samples were taken at the indicated time points, washed once in PBS (Cat# ECB4004LX; 10Euroclone) and lysed with 5 volumes of lysis buffer (LB; 0.2% Igepal; 80 mM b-glycerophosphate, 10 mM $MgCl_2$, 20 mM EGTA, 250 mM NaCl; Sigma-Aldrich) or fixed as described in Immunofluorescence fixation and staining section. Lysates were incubated 30 min on ice and then spun for 20 min at 13.200 rpm in a refrigerated microcentrifuge (4°C; Eppendorf centrifuge 5424R). For cell counting and viability assays, cells were seeded at 7000 cells/cm2 density. After 24 hours of incubation, one cell sample per cell type was trypsinized, collected and resuspended in PBS and loaded into a Bürker counting chamber, cells were counted manually under a microscope for the Time 0 cell count. Other cell samples were treated with either vehicle (DMSO) as control or with 2, 4 and 8 nM Plx and incubated for 48 hours, then cells were trypsinized and resuspended in PBS, mixed to an equal volume of Trypan Blue and counted (Trypan Blue solution 0.4%; Cat# 15250061; Gibco - Thermo Fisher Scientific, Waltham, MA, USA). Cell counting was conducted manually under a microscope and cell viability was determined by Trypan Blue exclusion.

RNA interference

RNA interference *via* siRNAs was performed using DharmaFECT 1 siRNA Transfection Reagent (Cat# T200103; Dharmacon). For efficient knock-down cells were plated 24 hours prior to treatment and transfected with 25 nM of non-targeting or targeting siRNAs duplex using DharmaFECT 1, according to the manufacturer's protocol. DharmaFECT 1 and siRNAs were mixed in RPMI-1640 medium and incubated at room temperature (rt) for 20 min, then, the mixture was added to the cells and incubated for 24 hours before Paclitaxel addition. Non-targeting or human cGAS-targeting siRNAs (Non-Targeting SMARTpool Cat# L-009326-00-0020; MB21D1-Targeting SMARTpool Cat# L-015607-02-0020) were purchased from Dharmacon.

Immunoblotting

Immunoblotting was performed as described (16). Briefly, samples were prepared by adding SDS loading buffer (Laemmli sample buffer; Cat# 1610747; BioRad, MI, Italy) to lysates. Samples were boiled for 10 min at 99°C before being separated on SDS-PAGE (poly-acrylamide percentage spanning from 10 to 12%). Proteins were blotted onto nitrocellulose membrane (Cat# GEH10600002; GE Healthcare) using a wet-transfer system (Cat# EI0001; ThermoFisher). Membranes were incubated with 5% not fat dry milk (NFDM; Cat# A0830; AppliChem GmbH, DA, Germany) or 3% bovine serum albumin (BSA; Cat# A7030; Sigma-Aldrich) in PBS or TBS (tris buffered saline; Cat# T5912; Sigma-Aldrich) supplemented with 0.01% Tween20 (Cat# P9416; Sigma-Aldrich; TPBS or TTBS, respectively) for 1 hour at rt. Then, membranes were incubated with primary antibodies, diluted in TPBS or TTBS, at 4°C overnight. After washing twice with TPBS or TTBS, filters were incubated with secondary peroxidase-conjugated antibodies, diluted in TPBS or TTBS, for 1 hour at rt. Detection was performed using an Enhanced ChemiLuminescence (ECL) kit (Cat# GEHRPN2106; GE Healthcare). Blots were acquired using Canon CanoScan LiDE 300 scanner (Canon) and scanned at 300 dpi. Primary and secondary antibodies used for immunoblotting are listed in Table 1.

Immunofluorescence

Cells were plated onto glass coverslips 24 hours prior to Paclitaxel addition. After 48 hours Plx treatment, coverslips were briefly washed in PBS and cells fixed with 4% paraformaldehyde (Cat# P6148; Sigma-Aldrich) in PBS (Euroclone) for 10 min at rt. Cells were washed twice with PBS and permeabilized with 0.25% Triton X- 100 (Cat# T9284; Sigma-Aldrich) in PBS for 15 min. The permeabilization step was omitted for PD-L1 immunofluorescence. Then, cells were washed once with PBS and incubated with 3% bovine serum albumin (BSA; Sigma-Aldrich) in PBS for 1 hour at rt. Coverslips were transferred into a humidity chamber and incubated with primary antibodies in 1.5% (w/v) BSA-PBS solution for 2 hours at rt, except for PD- L1 immunofluorescence for which incubation with primary antibody was performed overnight at 4°C. After incubation, cells were washed three times with PBS and incubated with fluorescently labelled secondary antibodies, diluted in 1.5% BSA-PBS solution, for 1 hour at rt. DNA was stained with Hoechst 33258 (1 mg/mL; Cat# 94403; Invitrogen, Waltham, MA, USA) by incubation for 10 min. Finally, cells were washed four times with PBS and slides mounted with Mowiol 40-88 (Cat# 81381; Sigma-Aldrich). Primary and secondary antibodies used for immunofluorescence are listed in Table 1.

Microscopy

Fixed cells were photographed using an inverted confocal fluorescence microscope LSM 980 (Zeiss) equipped with a 63X/1.4 oil objective (Zeiss). Representative images were obtained collecting 5 Z-stack series. The acquisitions were deconvoluted and projected into one plane using the ZEN3.1 software.

TABLE 1 Antibodies used in this study.

Antibodies	Source	Catalog number
Primary		
rabbit anti-cGAS	Cell Signaling Technology, Danvers, MA, USA	15102S
mouse anti-α-tubulin	Sigma-Aldrich, St. Louis, MO, USA	T9026
rabbit anti-phospho-serine-366-STING (p-S366-STING)	Cell Signaling Technology	50907S
rabbit anti-STING	Cell Signaling Technology	13647S
rabbit anti-phospho-serine-386-IRF3 (p-S386-IRF3)	Thermo Fisher Scientific, Waltham, MA, USA	PA5-99387
rabbit anti-IRF3	Cell Signaling Technology	4302S
rabbit anti-phospho-tyrosine-701-STAT1 (p-Y701-STAT1)	Cell Signaling Technology	9167S
rabbit anti-STAT1	Cell Signaling Technology	14994S
mouse anti-γ-tubulin	Sigma-Aldrich	T5326; Clone GTU-88
rabbit anti-PD-L1	Cell Signaling Technology	15165S 86744S
Secondary		
sheep anti-mouse IgG HRP linked	GE Healthcare Life Sciences, Pittsburgh, PA, USA	NA931
donkey anti-rabbit IgG HRP linked	GE Healthcare	NA934
goat anti-mouse IgG Alexa Fluor 488	Thermo Fisher Scientific	A11029
donkey anti-rabbit IgG Alexa Fluor 594	Thermo Fisher Scientific	A21207

Results

Pxl treatment induces formation of cGAS-positive micronuclei

It has been proposed that chromosome segregation defects in chromosomally unstable cancer cells or upon treatment of cancer cells with Taxanes can cause formation of cGAS-positive micronuclei and activation of proinflammatory pathways (1, 15, 17). To investigate potential immunomodulatory effects of the Taxane Pxl, we started asking whether treatment with low doses of Pxl promoted formation of cGAS-positive micronuclei in various cancer cell lines: lung adenocarcinoma A549 cells, triple negative breast cancer (TNBC) MDA-MB231 cells, hormone-responsive breast cancer MCF7 cells and cervical cancer HeLa cells. We chose a low Pxl concentration range, between 2 and 8 nM, because it is known that Pxl concentrates within cells about 50 to 1000 folds, depending on the cell type, so that after a 20-hour treatment with Pxl concentrations in the low nM range in the cell culture medium, Pxl can reach intracellular concentrations similar to those reached, *in vivo*, in tumor cells of patients treated with Pxl infusions (5). In addition, since Pxl-induced micronucleation requires passage through mitosis, we chose a treatment time of 48 hours since, under our experimental conditions, the cell doubling time was approximately 22 hours for A549, 24 hours for HeLa, 27 hours for MCF7 and 29 hours for MDA-MB231 in control cells (treated just with dimethylsulfoxide, DMSO, vehicle; Supplementary Figure 1), so that by 48 hours all cell types had undergone mitosis at least once (1, 5). Moreover, a 48-hour Pxl treatment had mostly a cytostatic effect at the doses used in all cell lines tested, while cytotoxicity was relatively modest since the highest drop of cell viability (measured by trypan blue exclusion) was around 20% in MDA-MB231 cells treated with 8 nM Pxl (Supplementary Figure 1).

Thus, to determine whether Pxl treatment promoted formation of cGAS-positive micronuclei, the four cell lines were treated with vehicle, as control, or with 4 nM Pxl for 48 hours and the presence of cGAS-positive micronuclei assessed by immunofluorescence (IF; Figure 1). In all cell lines tested, including MDA-MB231 that are very genetically unstable and show a higher basal level of cGAS-positive micronuclei, Pxl treatment strongly increased the number of cells with cGAS-positive micronuclei (Figure 1).

Chromatin bridges that form during altered mitosis exit induced by Pxl have also been shown to recruit cGAS and activate the cGAS-STING pathway involved in activation of cGAS (17). We also found evidence of Pxl-induced cGAS-positive chromatin bridges under our experimental conditions (an example is shown in Supplementary Figure 2).

Pxl induces a proinflammatory cascade in cancer cells

Next, we analyzed whether Pxl treatment led to activation of a proinflammatory cascade in cancer cells. To this end we analyzed

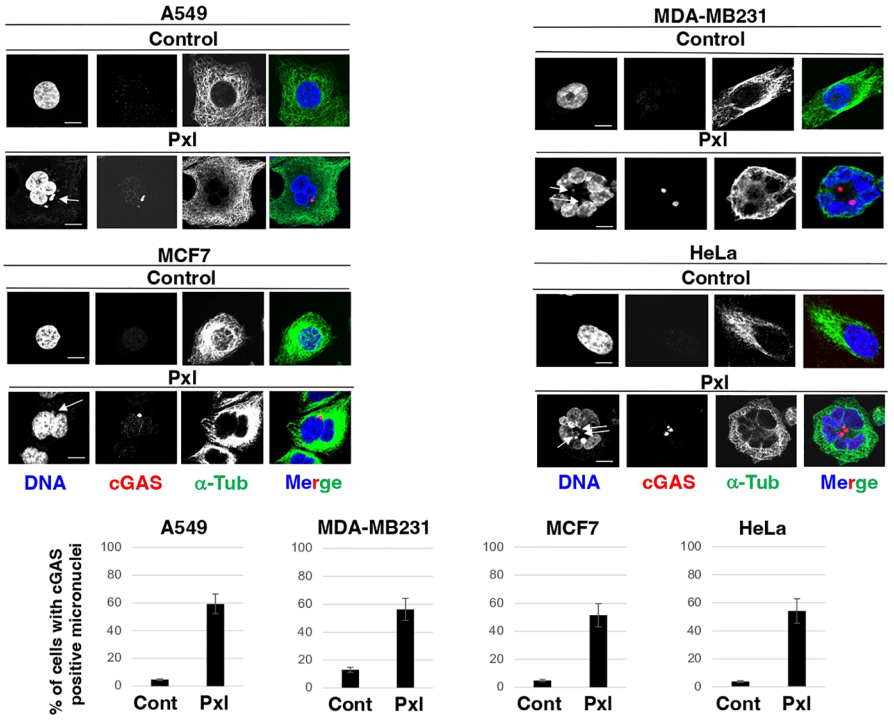

FIGURE 1
Pxl increases cGAS-positive micronuclei formation. A549, MDA-MB231, MCF7 and HeLa cells were treated for 48 hours with either vehicle (DMSO) as control or Pxl (4 nM), fixed and processed for indirect immunofluorescence (IF) staining for the indicated antigens. Representative IF images are shown. Scale bar: 5 µm. Lower graphs show a quantitation of cGAS-positive micronuclei (error bars refer to variability within three independent experiments; around 200 cells were scored for control and Pxl treatment per experiment).

the phosphorylation status of STING at serine 366 (S366), a site known to be phosphorylated by TBK1 and required for further activation of IRF3, and the STING-TBK1-dependent, activating, phosphorylation of IRF3 at serine 386 (S386) upon treatment of A549, MDA-MB231, MCF7 and HeLa cells with increasing doses of Pxl in the low nanomolar range (2, 4 and 8 nM; Figure 2) (18, 19). Indeed, the Pxl treatment induced S366-STING and S386-IRF3 phosphorylations in all cell lines (Figure 2). The phosphorylated forms of STING and IRF3 tended to decline at 8 nM relatively to 4 nM Pxl treatment (Figure 2; see quantitative graphs of the phosphorylated forms). We do not have an exact explanation for this phenomenon, but we believe that it may possibly indicate that negative feedbacks, that attenuate excess proinflammatory signals, are initiated at the highest Pxl concentration (20).

Pxl upregulates STAT1 phosphorylation as well as cGAS and PD-L1 protein levels in cancer cells

Following IRF3 activation, IFN type 1 genes are potently transcribed and IFN proteins produced and secreted (21). IFNs activate the JAK/STAT signaling cascade and phosphorylation of STAT1 at tyrosine 701 (Y701) is a hallmark of IFN pathway activation (22). Moreover, IFN and cGAS have been shown to be linked by positive feedback loops in which cGAS-dependent IFN induction further stimulates cGAS expression (23). In addition to the innate immunity-promoting action of cGAS, also recruitment of cytolytic CD8 T cells in the tumor microenvironment has been shown to be very dependent on cGAS activity (24). Considering that Pxl has also been shown to upregulate MHC class I, these effects of Pxl treatment may, indeed, strongly favor antitumor adaptive immunity (14).

Nevertheless, several lines of evidence also link the cGAS-STING pathway, STAT1 activation and IFN signaling to the upregulation of the expression of the immune checkpoint protein PD-L1 in cancer cells as well in cells of the immune system (25, 26). Thus, if the Pxl-activated cGAS/STING pathway would increase PD-L1 expression in cancer cells, this might promote, on the other hand, cancer cell escape from surveillance by the adaptive immune system (25, 26).

We thus asked whether Pxl treatment led to Y701-STAT1 phosphorylation and upregulated cGAS and PD-L1 protein levels. To this end, A549, MDA-MB231, MCF7 and HeLa cells were treated for 48 hours with low doses of Pxl and the levels of phosphorylated Y701-STAT1 (p-Y701-STAT1) and of cGAS and PD-L1 protein analyzed (Figure 3A). Indeed, in all cell lines tested Pxl induced Y701-STAT1 phosphorylation, marker of IFN pathway activation, and significantly upregulated cGAS and PD-L1 expression (Figure 3A). In addition, Pxl treatment induced a

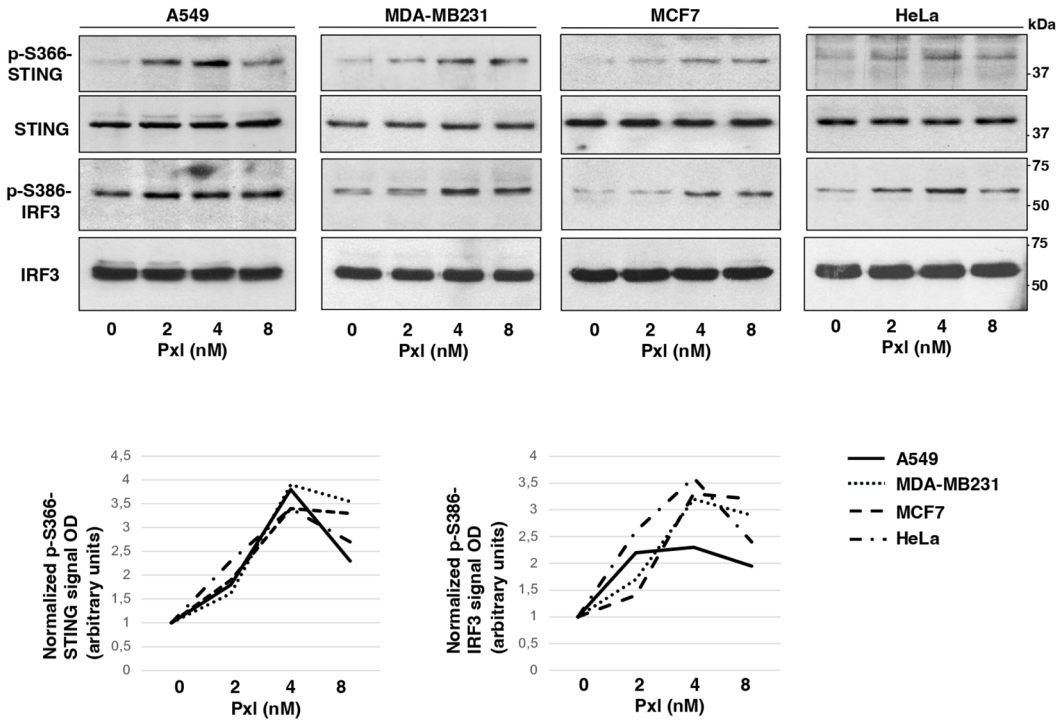

FIGURE 2
Pxl induces activating phosphorylations of STING and IRF3. A549, MDA-MB231, MCF7 and HeLa cells were treated for 48 hours with either vehicle (DMSO; 0 nM Pxl) or the indicated doses of Pxl (2, 4, 8 nM), lysed and proteins probed for the indicated antigens (the blots shown are representative of three independent experiments giving similar results). Lower graphs show a quantitation of optical density values of the phosphorylated STING and IRF3 signals normalized to the optical density values of the relative total protein signal.

substantial increase of PD-L1 at the cell surface in all cell types, as shown by PD-L1 immunofluorescence of non-permeabilized cells (Figure 3B).

Pxl-induced upregulation of STAT1 phosphorylation and PD-L1 protein levels is cGAS-dependent

We asked whether Pxl-induced upregulation of STAT1 phosphorylation and of PD-L1 expression were mediated by the cGAS/STING pathway. To this end, MDA-MB231 cells were treated with non-targeting (NT-siRNAs) or cGAS-targeting small interfering RNAs (cGAS-siRNAs) 24 hours before Pxl (4 nM) or vehicle (Pxl 0 nM; as control) addition, then, cells were taken after further 48 hours incubation (Figures 4A, B). The siRNAs treatment resulted in more than 90% downregulation of the cGAS protein expression in cGAS-siRNA-treated cells compared with NT-siRNAs-treated cells (Figure 4A). Moreover, induction of Y701-STAT1 phosphorylation as well as the increase of PD-L1 protein expression induced by Pxl in control (NT-siRNA-treated) cells were completely blunted in the cGAS-downregulated (cGAS-siRNA-treated) cells, while the levels of total STAT1 protein were not affected by cGAS downregulation (Figure 4B). Similar results were obtained by downregulating cGAS expression in A459 cells under similar treatment conditions as described for MDA-MB231 cells

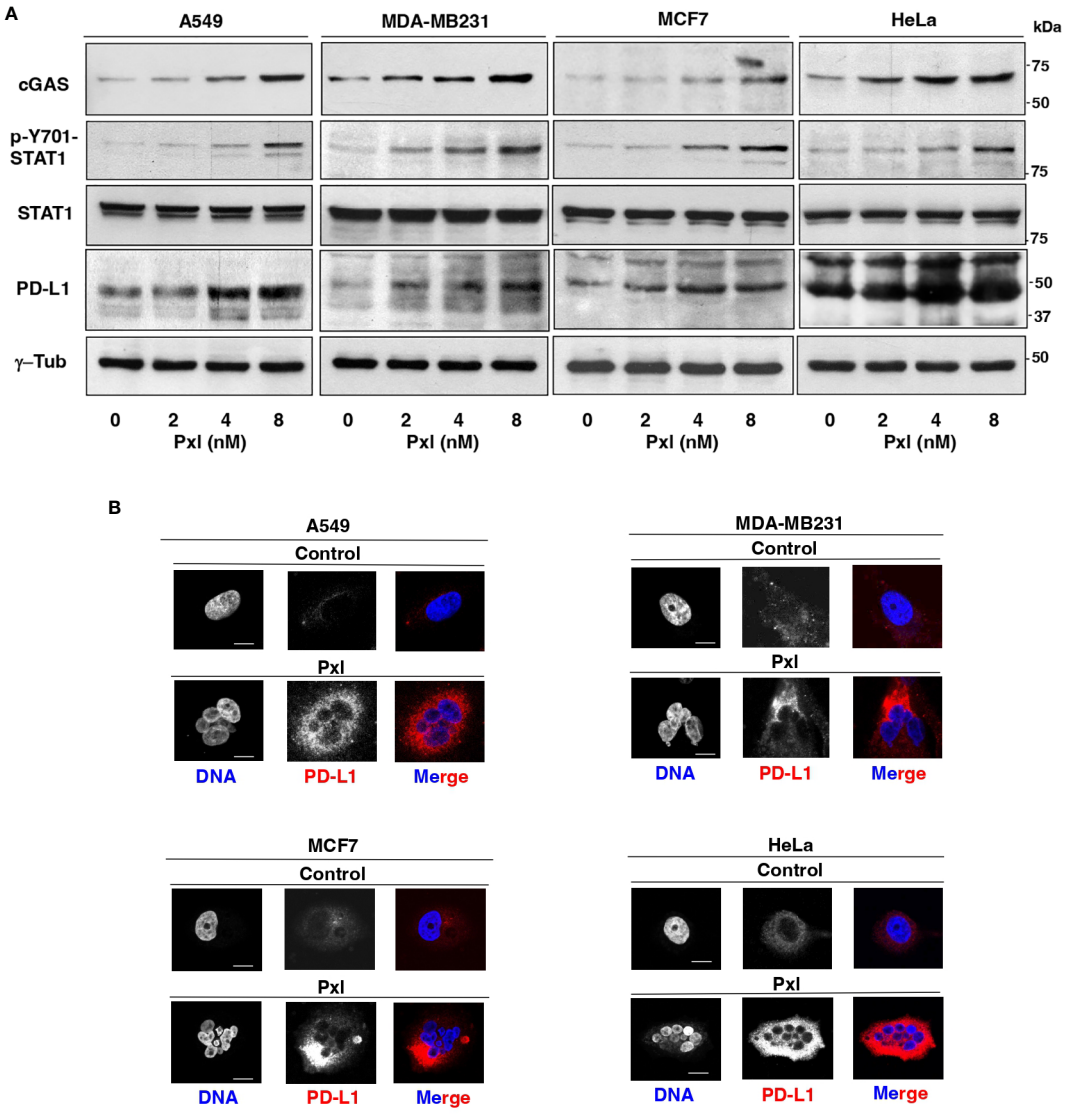

FIGURE 3
Pxl upregulates STAT1 phosphorylation and cGAS and PD-L1 protein levels in cancer cells. **(A)** A549, MDA-MB231, MCF7 and HeLa cells were treated for 48 hours with either vehicle (DMSO; 0 nM Pxl) or the indicated doses of Pxl (2, 4, 8 nM), lysed and proteins probed for the indicated antigens (the blots shown are representative of three independent experiments giving similar results). **(B)** A549, MDA-MB231, MCF7 and HeLa cells were treated for 48 hours with DMSO (Control) or 8 nM Pxl (Pxl). Cells were fixed and processed for indirect PD-L1 immunofluorescence and DNA staining. Scale bar: 5 μm.

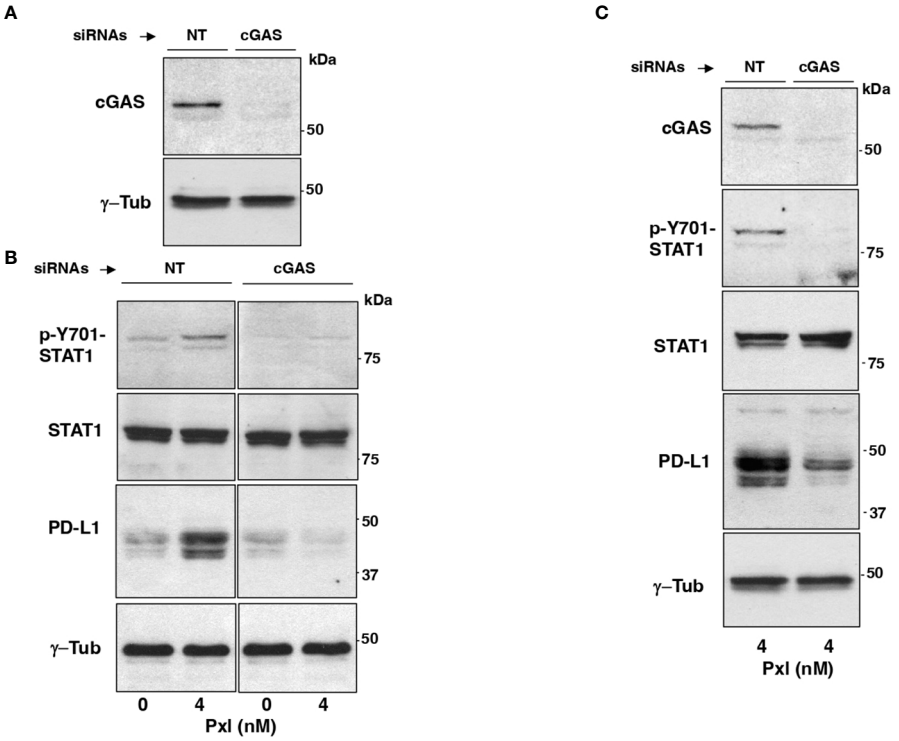

FIGURE 4
Pxl induction of STAT1 phosphorylation and PD-L1 upregulation require cGAS. **(A, B)** MDA-MB231 cells were treated with non-targeting (NT-siRNAs) or cGAS-targeting small interfering RNAs (cGAS-siRNAs) 24 hours before vehicle (DMSO; 0 nM Pxl) or Pxl (4 nM) addition, then, cells were taken after further 48 hours incubation. **(A)** The siRNAs treatment resulted in more than 90% downregulation of the cGAS protein expression in cGAS-siRNA-treated cells compared with NT-siRNAs-treated cells. **(B)** Lysates of NT-siRNA- or cGAS-siRNA-treated cells treated with vehicle (DMSO; 0 nM Pxl) or Pxl (4 nM) were probed for the indicated antigens. **(C)** A549 cells were treated with non-targeting (NT-siRNAs) or cGAS-targeting small interfering RNAs (cGAS-siRNAs) 24 hours before Pxl (4 nM) addition. Cells were further incubated for 48 hours, then, lysed and proteins probed for the indicated antigens. The blots shown are representative of three independent experiments giving similar results.

(Figure 4C). These data indicate that IFN pathway activation and upregulation of PD-L1 protein in cancer cells treated with Pxl are indeed cGAS-dependent.

Discussion

Recent evidence suggests that MTAs like Taxanes are efficient anticancer drugs because, in addition to directly kill cancer cells, they induce a proinflammatory response that may strongly contribute to their therapeutic effects (1, 14, 17, 27). By upsetting chromosome segregation and producing micronuclei or DNA bridges, Taxanes ultimately activate the cGAS/STING pathway that helps killing cancer cells through several inflammation-dependent mechanisms, including induction of higher sensitivity to apoptosis and increased recruitment of anticancer adaptive immunity (17, 25, 28). Indeed, the proinflammatory effects of Taxanes have stimulated the idea that their combination with ICIs could improve the therapeutic outcome. In fact, several clinical trials have shown some benefit from this therapeutic combination (27, 29, 30).

Our data from cancer cell cultures confirm, indeed, that Pxl promotes a cGAS-STING pathway-dependent proinflammatory cascade, but they also show that Pxl treatment induces a strong upregulation of the PD-L1 protein in cancer cells in a cGAS-STING pathway-dependent manner (see Figures 3, 4). These observations are consistent with the view that negative feedbacks regulate the inflammatory response and with notion that the inflammatory response may have opposite effects on cancer development (20, 31). Indeed, the upregulation of PD-L1 expression by cancer cell is believed to substantially contribute to cancer cell resistance to immunosurveillance and to promote cancer cell growth and migration in an auto/paracrine manner as well (32). In addition, our data indicate that micronucleation, activation of a proinflammatory cascade and PD-L1 upregulation are induced by very low doses of Pxl (see Figures 1–3).

On the basis of these findings, we believe that combination therapy of Pxl, and possibly its derivatives, with ICIs should be tailored in way that takes into account that low doses of Pxl are indeed sufficient to induce a proinflammatory cascade, so that even poorly inflamed, “cold”, tumors can be turned into “hot” tumors increasing the recruitment of immune cells in the tumor microenvironment, but at the same time low Pxl doses are as well able to upregulate immune checkpoint proteins like PD-L1 that would, on the contrary, block adaptive immunosurveillance (33–

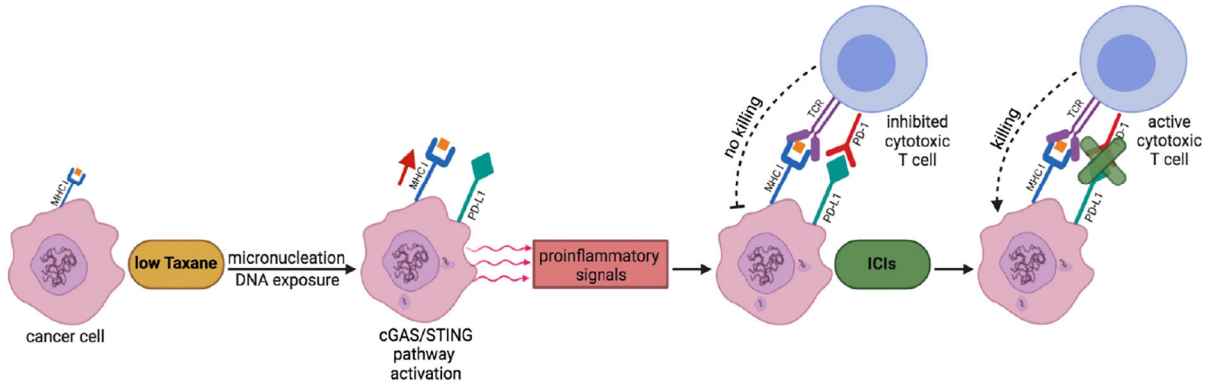

FIGURE 5
A scheme to potentiate Pxl + ICI combination therapy. Low Taxane dose induces micronucleation and cytosolic exposure of DNA. The following cGAS-STING pathway activation leads to release by cancer cells of proinflammatory signals that render "hot" the tumor microenvironment and help recruitment of cytotoxic T cells. At the same time, however, the cGAS-STING pathway leads to the upregulation of PD-L1 expression in cancer cells that inhibits T cell activation. The sequential treatment with ICIs unlocks the cancer cell killing potential of T cells.

35). In addition, although Taxanes have been shown to upregulate MHC molecules and reduce immunosuppressive T regulatory cells, thus favoring anticancer adaptive immunity, like other chemotherapeutic drugs, they are strongly myelosuppressive and may cause overall lymphopenia (36).

Indeed, the Taxane/ICI combination therapy has been already tested in clinic and appears to result in beneficial effects (29, 30, 37, 38). Nevertheless, based on our findings, we would like to propose that the combination therapy may require further testing in terms of Taxane dosing and scheduling relatively to the ICI treatment in clinical trials to further improve clinical benefit (33–35, 39). In particular, we would like to propose that combination therapies with Pxl, and possibly its derivatives, and ICIs, especially anti PD-L1/PD targets, should be approached first by a low dosage, rather than near to maximum tolerated, Pxl regimen in order to render "hot" the tumor microenvironment and to "prime" cancer cells for a sequential, rather than concurrent, treatment with ICIs (see Figure 5) (14, 15, 27, 35, 39). In addition, our data further support the evaluation of cGAS levels as a biomarker, that could be more technically reliable than evaluation of PD-L1 itself, to predict beneficial effects of an ICI adjuvant treatment when Pxl and derivatives are used in neodjuvant setting (40).

Data availability statement

The original contributions presented in the study are included in the article/Supplementary Material. Further inquiries can be directed to the corresponding author.

Author contributions

Conceptualization, AS and DG. Methodology, experimental work, AS and CP. Writing, original draft preparation, DG. Writing, review and editing, AS, CP and DG. Supervision, DG. All authors contributed to the article and approved the submitted version.

Funding

This work was supported by AIRC, Associazione Italiana per la Ricerca sul Cancro: IG grant 2017; Id. 19851 to DG.

Conflict of interest

The authors declare that the research was conducted in the absence of any commercial or financial relationships that could be construed as a potential conflict of interest.

Publisher's note

Supplementary material

The Supplementary Material for this article can be found online at: https://www.frontiersin.org/articles/10.3389/fimmu.2023.1127623/full#supplementary-material

References

1. Mitchison TJ, Pineda J, Shi J, Florian S. Is inflammatory micronucleation the key to a successful anti-mitotic cancer drug? *Open Biol* (2017) 7(11):170182. doi: 10.1098/rsob.170182

2. Serpico AF, Grieco D. Recent advances in understanding the role of Cdk1 in the spindle assembly checkpoint. *F1000Res* (2020) 9:F1000 Faculty Rev–57. doi: 10.12688/f1000research.21185.1

3. Wang TH, Wang HS, Soong YK. Paclitaxel-induced cell death: where the cell cycle and apoptosis come together. *Cancer* (2000) 88(11):2619–28. doi: 10.1002/1097-0142(20000601)88:11<2619::aid-cncr26>3.0.co;2-j

4. Topham CH, Taylor SS. Mitosis and apoptosis: how is the balance set? *Curr Opin Cell Biol* (2013) 25(6):780–5. doi: 10.1016/j.ceb.2013.07.003

5. Weaver BA. How taxol/paclitaxel kills cancer cells. *Mol Biol Cell* (2014) 25 (18):2677–81. doi: 10.1091/mbc.E14-04-0916

6. Crasta K, Ganem NJ, Dagher R, Lantermann AB, Ivanova EV, Pan Y, et al. DNA Breaks and chromosome pulverization from errors in mitosis. *Nature* (2012) 482 (7383):53–8. doi: 10.1038/nature10802

7. Liu S, Kwon M, Mannino M, Yang N, Renda F, Khodjakov A, et al. Nuclear envelope assembly defects link mitotic errors to chromothripsis. *Nature* (2018) 561 (7724):551–5. doi: 10.1038/s41586-018-0534-z

8. Harding SM, Benci JL, Irianto J, Discher DE, Minn AJ, Greenberg RA. Mitotic progression following DNA damage enables pattern recognition within micronuclei. *Nature* (2017) 548(7668):466–70. doi: 10.1038/nature23470

9. Yum S, Li M, Frankel AE, Chen ZJ. Role for the cGAS-STING pathway in cancer immunosurveillance and immunotherapy. *Annu Rev Cancer Biol* (2019) 3:323–44. doi: 10.1146/annurev-cancerbio-030518-055636

10. Hatch EM, Fischer AH, Deerinck TJ, Hetzer MW. Catastrophic nuclear envelope collapse in cancer cell micronuclei. *Cell* (2013) 47. 154(1):47–60. doi: 10.1016/j.cell.2013.06.007

11. Mackenzie KJ, Carroll P, Martin CA, Murina O, Fluteau A, Simpson DJ, et al. cGAS surveillance of micronuclei links genome instability to innate immunity. *Nature* (2017) 548(7668):461–5. doi: 10.1038/nature23449

12. Sun L, Wu J, Du F, Wu J, Sun L, Chen X, et al. Cyclic GMP-AMP synthase is a cytosolic DNA sensor that activates the type I interferon pathway. *Science* (2013) 339 (6121):786–91. doi: 10.1126/science.1232458

13. Zitvogel L, Galluzzi L, Kepp O, Smyth MJ, Kroemer G. Type I interferons in anticancer immunity. *Nat Rev Immunol* (2015) 15(7):405–14. doi: 10.1038/nri3845

14. Fong A, Durkin A, Lee H. The potential of combining tubulin-targeting anticancer therapeutics and immune therapy. *Int J Mol Sci* (2019) 20(3):586. doi: 10.3390/ijms20030586

15. Serpico AF, Visconti R, Grieco D. Exploiting immune-dependent effects of microtubule-targeting agents to improve efficacy and tolerability of cancer treatment. *Cell Death Dis* (2020) 11(5):361. doi: 10.1038/s41419-020-2567-0

16. Serpico AF, D'Alterio G, Vetrei C, Della Monica R, Nardella L, Visconti R, et al. Wee1 rather than Plk1 is inhibited by AZD1775 at therapeutically relevant concentrations. *Cancers* (2019) 11(6):819. doi: 10.3390/cancers11060819

17. Flynn PJ, Koch PD, Mitchison TJ. Chromatin bridges, not micronuclei, activate cGAS after drug-induced mitotic errors in human cells. *Proc Natl Acad Sci USA* (2021) 118(48):e2103585118. doi: 10.1073/pnas.2103585118

18. Tanaka Y, Chen ZJ. STING specifies IRF3 phosphorylation by TBK1 in the cytosolic DNA signaling pathway. *Sci Signal* (2012) 5(214):ra20. doi: 10.1126/scisignal.2002521

19. Mori M, Yoneyama M, Ito T, Takahashi K, Inagaki F, Fujita T. Identification of ser-386 of interferon regulatory factor 3 as critical target for inducible phosphorylation that determines activation. *J Biol Chem* (2004) 279(11):9698–702. doi: 10.1074/jbc.M310616200

20. Ge Z, Ding S. Regulation of cGAS/STING signaling and corresponding immune escape strategies of viruses. *Front Cell Infect Microbiol* (2022) 12:954581. doi: 10.3389/fcimb.2022.954581

21. Dhanwani R, Takahashi M, Sharma S. Cytosolic sensing of immuno-stimulatory DNA, the enemy within. *Curr Opin Immunol* (2018) 50:82–7. doi: 10.1016/j.coi.2017.11.004

22. Sadzak I, Schiff M, Gattermeier I, Glinitzer R, Sauer I, Saalmüller A, et al. Recruitment of Stat1 to chromatin is required for interferon-induced serine phosphorylation of Stat1 transactivation domain. *Proc Natl Acad Sci USA* (2008) 105 (26):8944–9. doi: 10.1073/pnas.0801794105

23. Ma F, Li B, Liu SY, Iyer SS, Yu Y, Wu A, et al. Positive feedback regulation of type I IFN production by the IFN-inducible DNA sensor cGAS. *J Immunol* (2015) 194 (4):1545–54. doi: 10.4049/jimmunol.1402066

24. Wang H, Hu S, Chen X, Shi H, Chen C, Sun L, et al. cGAS is essential for the antitumor effect of immune checkpoint blockade. *Proc Natl Acad Sci USA* (2017) 114 (7):1637–42. doi: 10.1073/pnas.1621363114

25. Garcia-Diaz A, Shin DS, Moreno BH, Saco J, Escuin-Ordinas H, Rodriguez GA, et al. Interferon receptor signaling pathways regulating PD-L1 and PD-L2 expression. *Cell Rep* (2017) 19(6):1189–201. doi: 10.1016/j.celrep.2017.04.031

26. Benci JL, Xu B, Qiu Y, Wu TJ, Dada H, Twyman-Saint Victor C, et al. Tumor interferon signaling regulates a multigenic resistance program to immune checkpoint blockade. *Cell* (2016) 167(6):1540–1554.e12. doi: 10.1016/j.cell.2016.11.022

27. Soliman HH. *nab*-paclitaxel as a potential partner with checkpoint inhibitors in solid tumors. *Onco Targets Ther* (2016) 10:101–12. doi: 10.2147/OTT.S122974

28. Iwasaki A, Medzhitov R. Control of adaptive immunity by the innate immune system. *Nat Immunol* (2015) 16(4):343–53. doi: 10.1038/ni.3123

29. Emens LA, Adams S, Barrios CH, Diéras V, Iwata H, Loi S, et al. First-line atezolizumab plus nab-paclitaxel for unresectable, locally advanced, or metastatic triple-negative breast cancer: IMpassion130 final overall survival analysis. *Ann Oncol* (2021) 32(8):983–93. doi: 10.1016/j.annonc.2021.05.355

30. Ghebeh H, Al-Sayed A, Eiada R, Cabangon L, Ajarim D, Suleman K, et al. Weekly paclitaxel given concurrently with durvalumab has a favorable safety profile in triple-negative metastatic breast cancer. *Sci Rep* (2021) 11(1):19154. doi: 10.1038/s41598-021-98113-6

31. Shalapour S, Karin M. Immunity, inflammation, and cancer: an eternal fight between good and evil. *J Clin Invest* (2015) 125(9):3347–55. doi: 10.1172/JCI80007

32. Tang Q, Chen Y, Li X, Long S, Shi Y, Yu Y, et al. The role of PD-1/PD-L1 and application of immune-checkpoint inhibitors in human cancers. *Front Immunol* (2022) 13:964442. doi: 10.3389/fimmu.2022.964442

33. Wu M, Huang Q, Xie Y, Wu X, Ma H, Zhang Y, et al. Improvement of the anticancer efficacy of PD-1/PD-L1 blockade *via* combination therapy and PD-L1 regulation. *J Hematol Oncol* (2022) 15(1):24. doi: 10.1186/s13045-022-01242-2

34. Mpekris F, Voutouri C, Panagi M, Baish JW, Jain RK, Stylianopoulos T. Normalizing tumor microenvironment with nanomedicine and metronomic therapy to improve immunotherapy. *J Control Release* (2022) 345:190–9. doi: 10.1016/j.jconrel.2022.03.008

35. Kwon M, Jung H, Nam GH, Kim IS. The right timing, right combination, right sequence, and right delivery for cancer immunotherapy. *J Control Release* (2021) 331:321–34. doi: 10.1016/j.jconrel.2021.01.009

36. Jun J, Li R, Yang Y, Dong W, Wang Y, Wang H, et al. Comparative colloidal stability, antitumor efficacy, and immunosuppressive effect of commercial paclitaxel nanoformulations. *J Nanobiotechnol* (2021) 19(1):199. doi: 10.1186/s12951-021-00946-w

37. Sasaki A, Kawazoe A, Eto T, Okunaka M, Mishima S, Sawada K, et al. Improved efficacy of taxanes and ramucirumab combination chemotherapy after exposure to anti-PD-1 therapy in advanced gastric cancer. *ESMO Open* (2020) 4(Suppl 2):e000775. doi: 10.1136/esmoopen-2020-000775

38. Bilger G, Toffart AC, Darrason M, Duruisseaux M, Ulmer L, Wang P, et al. Paclitaxel-bevacizumab combination in advanced non-squamous non-small-cell lung cancer (NSCLC): AVATAX, a retrospective multicentric study. *Ther Adv Med Oncol* (2022) 14:17588359221099399. doi: 10.1177/17588359221099399

39. Hwang M, Seiwert TY. Are taxanes the future for head and neck cancer? pragmatism in the immunotherapy era. *Lancet Oncol* (2021) 22(4):413–5. doi: 10.1016/S1470-2045(21)00121-2

40. Zhao X, Bao Y, Meng B, Xu Z, Li S, Wang X, et al. From rough to precise: PD-L1 evaluation for predicting the efficacy of PD-1/PD-L1 blockades. *Front Immunol* (2022) 13:920021. doi: 10.3389/fimmu.2022.920021

frontiers | Frontiers in Oncology

TYPE Review
PUBLISHED 24 April 2023
DOI 10.3389/fonc.2023.1167105

OPEN ACCESS

EDITED BY
Yeonseok Chung,
Seoul National University, Republic of Korea

REVIEWED BY
Xianwen Wang,
Anhui Medical University, China
Chuanhui Song,
Nanjing Drum Tower Hospital, China

*CORRESPONDENCE
Meng Du
dumeng_work@126.com
Zhiyi Chen
zhiyi_chen@usc.edu.cn

SPECIALTY SECTION
This article was submitted to Cancer Immunity and Immunotherapy, a section of the journal Frontiers in Oncology

RECEIVED 16 February 2023
ACCEPTED 11 April 2023
PUBLISHED 24 April 2023

CITATION
Wang T, Peng W, Du M and Chen Z (2023) Immunogenic sonodynamic therapy for inducing immunogenic cell death and activating antitumor immunity.
Front. Oncol. 13:1167105.
doi: 10.3389/fonc.2023.1167105

Immunogenic sonodynamic therapy for inducing immunogenic cell death and activating antitumor immunity

Ting Wang[1,2], Wangrui Peng[2,3], Meng Du[1,2*] and Zhiyi Chen[1,2,3*]

[1]The First Affiliated Hospital, Medical Imaging Centre, Hengyang Medical School, University of South China, Hengyang, Hunan, China, [2]Institute of Medical Imaging, Hengyang Medical School, University of South China, Hengyang, China, [3]The Seventh Affiliated Hospital, Hunan Veterans Administration Hospital, Hengyang Medical School, University of South China, Changsha, Hunan, China

Immunotherapy is widely regarded as a promising treatment for cancer. However, the immune effector phase suppression of tumor microenvironment (TME) and the generation of immune-related adverse events limit its application. Research indicates that sonodynamic therapy (SDT) can effectively activate antitumor immunity while killing tumor cells. SDT produces cytotoxic substances of tumors, and then cell apoptosis and immunogenic death occur by selectively activating the sonosensitizer under ultrasound. In recent years, various SDT alone as well as SDT in combination with other therapies have been developed to induce immunogenic cell death (ICD) and enhance immunotherapy. This paper overviews the research progress of SDT and nanotechnology in recent years, including the strategies involving SDT alone, SDT-based synergistic induction of antitumor immunity, and immunotherapy based on SDT for multimodal immunotherapy. Finally, the prospects and challenges of these SDT-based therapies in cancer immunotherapy are discussed.

KEYWORDS

sonodynamic therapy (SDT), immunogenic cell death, cancer immunotherapy, nanoplatforms, tumor therapy

Abbreviations: TME, Tumor microenvironment; irAEs, Immune-related adverse events; SDT, Sonodynamic therapy; PDT, Photodynamic therapy; CDT, Chemodynamic therapy; ICD, Immunogenic cell death; CTL, Cytotoxic lymphocyte; TAAs, Tumor-associated antigens; ROS, Reactive oxygen species; CRT, Calreticulin; ATP, Adenosine triphosphate; DAMPs, Damage-associated molecular patterns.

1 Introduction

In recent years, immunotherapy, as a new generation of anticancer therapy, has developed rapidly in clinical application, especially checkpoint blockade immunotherapy and chimeric antigen receptor T-cell immunotherapy, which has led to the significant development of clinical research direction (1, 2). Unlike traditional treatment methods, immunotherapy adjusts and strengthens the antitumor effect and produces a therapeutic effect to mobilize the body's immune function. Under physiological conditions, the immune system can recognize tumor antigens and attack tumor cells with the help of immune adjuvants. However, with the tumor progressed and an immunosuppressive tumor microenvironment (TME) established, immunotherapy failed to drive an efficient immune response (3). As a result, only a few patients have proven to respond to immunotherapy, and adverse immune-related adverse events are often triggered during treatment. Therefore, enhancing the immune reactivity of tumor sites is of great significance for enhancing antitumor immunity.

Induction of local immunogenic cell death (ICD) in tumor areas can transform low immunogenicity into high immunogenicity, which is an effective strategy to potentiate antitumor immunity. After some physical or chemical stimulation, tumor cells can transform low immunogenicity into high immunogenicity, which is an effective strategy to potentiate antitumor immunity (4–6). The host immune response can be reactivated by stimulating the antitumor immune effect, resulting in a better therapeutic effect and prognosis, which is of great significance to improving the prognosis and prolonging the survival of patients.

At present, more and more research has proven that antitumor immunity can be triggered under multiple treatments, such as chemotherapy, radiotherapy, photodynamic therapy (PDT), and sonodynamic therapy (SDT) (7–10). However, chemotherapy and radiotherapy inevitably cause damage to normal tissues, and the phototoxicity and low penetrability of PDT limit its further application. SDT is an emerging cancer treatment based on PDT (11). Similar to PDT, SDT can also be used as an effective cancer vaccine for antitumor therapy (12–14). SDT is a safe and noninvasive local treatment that can selectively kill tumor cells under ultrasound irradiation and cause minor damage to adjacent normal tissues (15–17). The penetration depth in soft tissues can reach tens of centimeters (18, 19), and has excellent potential for inducing immunogenicity and activating antitumor immunity in deep tumor therapy (20, 21).

SDT effectively induces and releases the tumor-associated antigens (TAAs) and damage-associated molecular patterns (DAMPs), thereby activating inflammatory responses in TME and draining lymph nodes (dLNs), inducing systemic antitumor immunity and immune memory, and inhibiting tumor growth and recurrence (Figure 1) (22, 23). However, cancer immunotherapy based on SDT is insufficient to achieve satisfactory therapeutic effects. Therefore, designing an effective combined treatment strategy for SDT-driven immunotherapy is necessary.

SDT is considered a promising strategy for immune cancer treatment. Combining SDT or SDT-based multimodal therapy with immunotherapy plays an essential role in antitumor immunotherapy (24). In this review, we will discuss the mechanisms of SDT-driven immunotherapy, and then provide an overview of the strategies involving SDT and SDT in combination with other therapies for immune therapy (Figure 2). Finally, we conclude with a brief overview of the limitations and future of SDT.

2 Main mechanism of SDT induction ICD

SDT has a direct killing effect on tumor cells. To date, the potential mechanisms of SDT have not been fully elucidated.

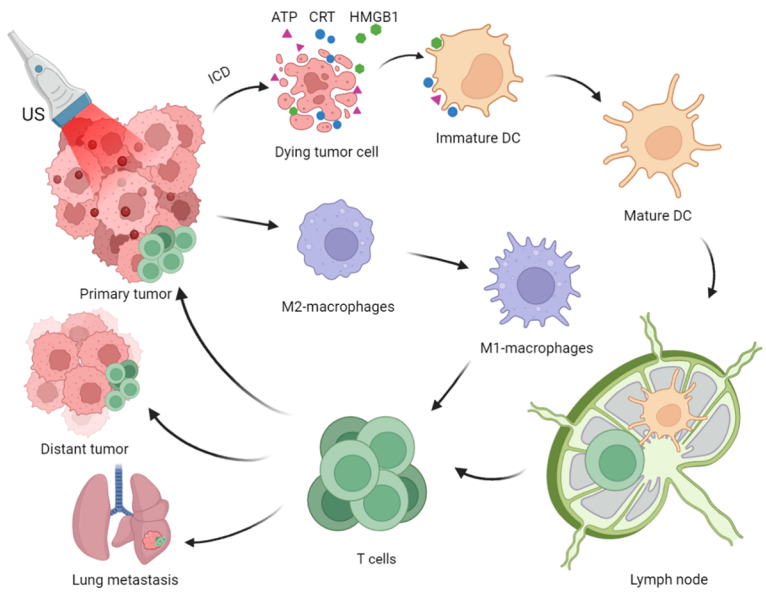

FIGURE 1
Process of Immunogenic Sonodynamic Therapy in tumor immunotherapy (Created with BioRender.com).

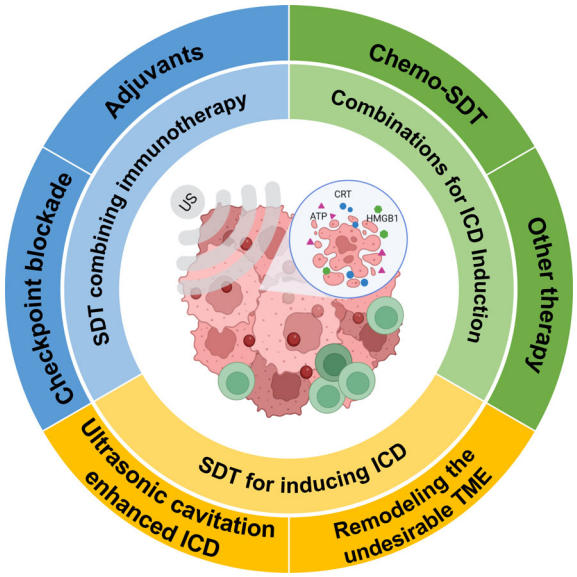

FIGURE 2
Schematic representation of SDT for inducing immunogenic cell death and potentiating cancer immunotherapy (Created with BioRender.com).

Conventional mechanisms have been accredited that reactive oxygen species produced by sonosensitizers and the cavitation effect induced by ultrasound irradiation act mainly during SDT (25). Activate the enriched sonosensitizer in the local disease site under ultrasound, thereby generating reactive oxygen species (ROS). Extreme oxidative properties stimulate biochemical reactions, including reduced intracellular mitochondrial membrane potential, DNA fracture, cytoskeletal contraction, and chromatin condensation, which causes irreversible damage to tumor cells (26). At the same time, the ultrasound-mediated cavitation effect causes the bubbles in the fluid to contract and expand periodically with ultrasound, which can enhance the permeability of the adjacent cell membrane. The generation of sharp shock when the bubbles undergo rupture can cause mechanical damage to the cells (27).

SDT induces tumor cell death, such as apoptosis and necrosis, and promotes the exposure and release of TAAs, enhancing tumor cells' antigenicity. At the same time, SDT also generates a series of adjuvant-like signaling molecules, namely DAMPs, including calreticulin (CRT) exposed on the cell surface, high mobility group protein 1 (HMGB1) secreted out tumor cells, adenosine triphosphate (ATP) and heat shock proteins (HSP70, HSP90) released by cells. Coordination of TAAs with DAMPs is necessary to recruit and mature antigen-presenting cells such as dendritic cells (DCs). Exposure or release of DAMPs can be recognized by pattern recognition receptors (PRRs) on the DC cell surface, facilitating DCs recruitment and enhancing the uptake of tumor antigens, initiating a series of cytological responses and ultimately activating antitumor immune responses.

During traditional antitumor treatment, tumor cell apoptosis causes intracellular components to become hypoimmunogenic by activating apoptotic executioner caspase-3 to prevent autoimmunity. Meanwhile, DAMPs exposed to the microenvironment are subject to oxidative degradation and thus lose immunogenicity. Interestingly, partial cell death became more immunogenic during this treatment process by affecting necrosis or necrosis-like cell death (28). Necrosis is considered an inherently immunogenic form of cell death. The disintegration of the plasma membrane induced inflammatory response and antitumor immunoreaction. SDT has the potential to activate cell immunogenic death events. Due to DAMPs released without exposure to harsh conditions that lead to oxidation and proteolysis, the immunogenicity of DAMPs will not be significantly affected.

Hydrophobic sonosensitizers generally preferentially congregate in the hydrophobic inner layers of the plasma membrane, nucleus, endoplasmic reticulum, or mitochondrial membrane. During the ultrasound, the activated sonosensitizer degrades the plasma membrane by lipid peroxidation, thereby leaking intact or less denatured DAMPs to reverse hypoimmunogenicity. Notably, ROS produced can kill tumor cells, trigger endoplasmic reticulum pressure, and damage mitochondria. Endoplasmic reticulum oxidative stress can promote the high expression of CRT and HSPs. The destruction of mitochondria can promote the secretion of ATP and HMGB1. ICD outcomes have generally been accepted to correlate positively with ROS levels. Besides, the cavitation effect of ultrasound can also cause cell membrane cleavage and release of immunogenic DAMPs. Interestingly, it has been proved that ultrasonic cavitation can enhance the rate of ROS production and ICD induction (29, 30). In recent years, several studies related to SDT have demonstrated that SDT induces immunogenic death of tumor cells as an "*in situ* vaccine" that activates the body's immune response against tumors and has been verified *in vitro* and *in vivo* (31–33).

3 Strategies

3.1 SDT for ICD induction

Several studies have confirmed that SDT can transform the non-immunogenic "cold" TME into a "hot" TME under the effect of ultrasound, which helps to enhance the effect of antitumor immune response (Table 1) (53, 54).

3.1.1 Ultrasonic cavitation enhanced ICD

However, the efficiency of SDT-induced ICD generation remains a limitation. During apoptosis, the immunogenicity of TAAs and DAMPs is inhibited by protein kinase 3 (RIPK3). To improve the immunogenicity of SDT-triggered cell death, Parkp et al. (33) prepared a phase-change nano-sonosensitizer PFP@PEG-CMD-Ce6 (NBs) complex, which was able to cause tumor cell necrosis through bubble mediated cell membrane rupture, but not trigger RIPK3-dependent necrotizing apoptotic through the process of SDT. The expression of HMGB1 in cells was analyzed by Western blot and flow cytometry *in vitro*. The results showed that cancer cells treated with NBs released biologically active DAMPs compared to NPs. The results suggest that cell death induced by ultrasonic cavitation is more immunogenic. Similarly, Yuan et al. (34) constructed LIP-PFH phase-change nanoparticle-mediated

TABLE 1 Main strategy and characterizations of the sonodynamic therapy.

Therapy	Nanoparticles	Characterizations	Model	Refs.
SDT	HiPorfin (HPD)	Immunogenic sonodynamic therapy	Hep3b/H22/S180	(14)
	FA-MnPs	Stronger penetration ability of ultrasound	4T1	(21)
	PFP@PEG-CMD-Ce6 (NBs)	Ultrasound-triggered inertial cavitation (UIC)	CT26	(33)
	LIP-PFH	Ultrasound-triggered inertial cavitation (UIC)	4T1	(34)
	MON-PpIX-LA-CO_2	Ultrasound-triggered inertial cavitation (UIC)	4T1	(35)
	LMWHA-MPB	Catalyzing H_2O_2 to produce oxygen	4T1	(30)
	HABT-C@HA	Catalyzing H_2O_2 to produce oxygen	4T1	(36)
	PALF	Reducing oxygen consumption	4T1	(37)
	Mn-MOF	Relieve tumor hypoxia and decrease GSH	4T1	(38)
SDT+Chemotherapy	DTX/X-NPs	Delivery oxygen enhance immunity	B16F10	(39)
	CS–Rh–PFC	Delivering O_2 to tumor sites	B16F10	(40)
	Lipo-Ce6/TPZ@M_H	Tumor microenvironment response	B16F10	(20)
SDT+CDT	PEGylated $CoFe_2O_4$ nanoplatforms (CFP)	Catalyzing H_2O_2 to produce oxygen	4T1	(41)
SDT+Gas therapy	PIH-NO	Delivering O_2 to tumor sites	4T1	(42)
	N@CAu-BMSNs	Enhanced tumor-targeting ability	4T1	(43)
SDT+PTT	ZrO_2-x@PEG/cRGD (ZPR)	Photothermal-augmented SDT	4T1	(44)
SDT+PDT	PARN	Difunctional sono-/photo-sensitizers	B16/Hela	(45)
SDT+PDT+PTT	g-C_3N_4/Ce6	Difunctional sono-/photo-sensitizers	4T1	(46)
SDT+PDT+chemotherapy	OIX_NPs	Delivering O_2 to tumor sites	ID8	(47)
SDT+Immunotherapy	TiO_2-Ce6-CpG+aPD-L1	Combination with adjuvants	Hepa1-6	(48)
	HMME/R837@Lip+aPD-L1	Combination with adjuvants and checkpoint blockade	4T1/CT26	(49)
	PEG-CDMaPD-L1/Ce6	Combination with checkpoint blockade	B16F10	(50)
	PFCE@THPP$_{pf}$-COPs+antiCD47	Combination with checkpoint blockade	CT26	(51)
	SCN@B16F10M/PEG-aPD-L1	Combination with checkpoint blockade	B16F10	(52)

SDT to enhance the antitumor immune response by inducing ICD in breast cancer. These results suggest that ultrasonic cavitation-induced cell death is more immunogenic. Further, to amplify the cavitation-enhanced ICD effect, Zhang et al. (29) constructed a nano-sonosensitizer (MON-PpIX-LA-CO_2) with a continuous cavitation function. L-arginine (LA) has a good function of adsorption/desorption of CO_2. These complexes can continuously release CO_2 and induce ultrasound-triggered inertial cavitation (UIC) under ultrasound irradiation. That is conducive to producing abundant ROS, thus successfully inducing robust ICD, more antigen exposure, and presentation enhanced DCs maturation and more activated effector $CD8^+$ T cell infiltration *in vitro*. The results suggest that this strategy of ultrasonic cavitation-enhanced SDT-induced ICD successfully converts the "cold" TME into a "hot" one with significantly enhanced suppressive effects in primary and metastatic tumors.

3.1.2 Remodeling the undesirable TME

The TME, such as pH, glutathione (GSH), growth factors, oxygen levels, and immune cells, are closely related to the effect of SDT-induced antitumor therapy. Overcoming the hypoxic microenvironment is necessary to enhance the SDT immune response (35, 55). The breakdown of endogenous H_2O_2 to O_2 using H_2O_2 catalysts has been recognized as an effective strategy to alleviate tumor hypoxia and improve the efficacy of cancer therapy. Zhang et al. (56) constructed an *in situ* microenvironmental nano-regulator that can act as an *in situ* oxygen generator and macrophage transducer. LMWHA-MPB has excellent peroxidase activity and generates O_2 to alleviate tumor hypoxia through the catalytic breakdown of endogenous hydrogen peroxide (H_2O_2). In addition, LMWHA-MPB can remodel the phenotype of tumor-associated macrophages (TAMs) after being taken up by M2 macrophages (pro-tumor M2 → antitumor M1). Improving the TME inhibited 4T1 tumor proliferation and

metastasis, effectively. Liu et al. (36) constructed a cascade enzyme-based platform (HABT-C@HA) to regulate hypoxia and immunosuppressive factors in TME. The excellent enzyme cascade reaction of HABT-C@HA was utilized to achieve continuous O_2 production and abundant ROS generation, effectively overcoming hypoxic TME at tumor sites and enhancing the therapeutic effect. The RNA-seq results revealed that HABT-C@HA+US activated immune response and down-regulated MPP2, BHLHE40, and other negative related factors, which improved immune infiltration and reversed breast tumor immunosuppression.

In contrast, reducing oxygen consumption in tumor cells is also a strategy to alleviate tumor hypoxia. Dai et al. (37) constructed a metallic-phenol network-based nano-complex embedded with lactate oxidase (LOX) and atovaquone (ATO), a mitochondrial respiration inhibitor. The nano-complex reversed the tumor's immunosuppressive state by inhibiting mitochondrial respiration and assisting the lactate depletion process for alleviating tumor hypoxia and acidic TME. It exhibited effective immunostimulatory properties under US irradiation, such as releasing inflammatory factors (i.e., TNF-α, IL-6, IL-12), decreasing polarization of M2 macrophages, and increasing infiltration of activated T cells into tumor tissue, achieving a characteristic enhancement of SDT and inhibiting tumor proliferation and metastasis.

In addition to hypoxia, SDT is also severely limited by high glutathione (GSH) in TME. To improve the efficacy of SDT-induced antitumor immune response, Gan et al. (38) constructed a manganese porphyrin-based metal-organic framework. Mn-MOF exhibited peroxidase-like and GSH-lowering activities *in vitro*. Upon effective internalization into cancer cells, Mn-MOF catalyzed the generation of O_2 from tumor-overexpressed H_2O_2 to alleviate tumor hypoxia. Meanwhile, Mn-MOF reduced intracellular GSH content and GPX4 activity. In addition, Mn-MOF reduced the number of bone marrow-derived suppressor cells in tumor tissues by increasing the number of activated $CD8^+$ T cells and mature dendritic cells. Thus, research suggests that it has strong anticancer and antimetastatic activities in the *in vivo* treatment of H22 and 4T1 tumor-bearing mouse models.

3.2 SDT-based synergistic induction ICD

Although SDT is widely used for anticancer immunity, it still has some limitations, which are insufficient to elicit a robust immune response. Recently, multiple combination therapy strategies have been used to improve the efficiency of SDT. SDT-based synergistic induction of anticancer immunity is a potential strategy.

3.2.1 SDT combined with chemotherapy for ICD induction

Studies proved that chemotherapeutic drugs, including doxorubicin, oxaliplatin, cyclophosphamide, and paclitaxel, can also promote ICD in tumor cells and elicit host immune responses (53, 54). Chemo-SDT synergistic has produced a more excellent antitumor immune response than SDT alone. For instance, Zhai et al. (39) created a multi-responsive drug release nanoplatform (DTX/X-NPs) that enabled the release of the docetaxel DTX loaded with the cross-linked sonosensitizer chlorin e6 (Ce6) *via* redox/enzyme/ultrasound responsive for combined chemo-sonodynamic to initiate antitumor immune responses. Cytotoxic lymphocyte (CTL) infiltration increased in the TME following Chemo-SDT compared to the CTL percentage in the SDT group, and the CTL percentage increased by 1.3%. In addition, both SDT-NPs and Chemo-SDT treatment increased INF- expression, with a more pronounced treatment trend for Chemo-SDT. The aforementioned experimental findings show that chemo-SDT improves immune activation and the effectiveness of fighting *in-situ* cancers vs. metastasis.

The relationship between hypoxic tumor tissue and sustained oxygen depletion severely hampers the antitumor effect of oxygen-dependent Chemo-SDT. To enhance the Chemo-SDT antitumor immune response, Zhai et al. (40) designed a novel redox/ultrasound-responsive oxygen-carrying nanoplatform (CS–Rh–PFC). The CS–Rh–PFC encapsulated sonosensitizer Rhein (Rh), chemotherapeutic medication docetaxel (DTX) and perfluorocarbon. PFC transports oxygen and raises the oxygen concentration of B16F10 melanoma cells, finally enhancing the effectiveness of Chemo-SDT-induced ICD. Notably, DTX-loaded CS-Rh-PFC NPs elicited more "eat-me" signals and had higher CRT exposure on B16F10 cells. Increased secretion of IFN-γ, TNF-α, IL-2, and IL-6 cytokines and increased levels of $CD4^+$ and $CD8^+$ T cells infiltrating the tumor after treatment suggested that immunogenic chemotherapy-ultrasound kinetic treatment based on oxygen-carrying nanoparticles could significantly activate the immune system.

Utilizing the particular hypoxic tumor environment for SDT combined with hypoxia-induced chemotherapy is also an effective strategy. Wang et al. (20) constructed a biomimetic decoy, loaded the sonosensitizer Ce6 and hypoxia-activated tirapazamine (TPZ) in pH-sensitive liposomes, and fused them with PLT and RBC membranes to produce lipid Ce6/TPZ@M_H. Ce6 generates toxic ROS upon US irradiation, and the resulting hypoxia microenvironment activates TPZ for high-effective synergistic therapy. SDT combined with hypoxia-induced chemotherapy induces ICD synergistically, releasing the DAMPs (including CRT, HMGB1, etc.) and successfully promoting antitumor immunotherapy. Meanwhile, Lipo-Ce6/TPZ@M_H decoys maintain binding interactions with high levels of HMGB1 to prevent platelet-mediated tumor metastasis. Combined treatment with SDT and hypoxia-activated TPZ shows excellent potential in eliminating tumors *in situ* and inhibiting lung metastasis from melanoma.

3.2.2 SDT combined with other therapy for ICD induction

In addition, several other combination therapy modalities have been explored for synergistic induction of ICD, such as gas therapy, photothermal therapy (PTT), PDT, chemodynamic therapy (CDT), etc. Gas therapy delivers gases, e.g., carbon monoxide (CO) and nitric oxide (NO), to tumor sites to relieve and treat disease. Liu

et al. (43) developed an ultrasound-driven biomimetic nanosystem (N@CAu-BMSNs) to verify whether SDT/CO gas therapy could trigger burst ICD. In this study, the expression of CRT, as a biomarker during ICD, in 4T1 cells after N@CAu-BMSN treatment was detected. Compared to the control group, N@cau-BMSN+US-treated 4T1 tumor cells could more effectively increase CRT expression *in vitro* and *in vivo*. In addition, effective immune response and long-term immune memory were achieved by combining with indoleamine 2,3-dioxygenase (IDO) signaling blockade. Based on SDT/Gas therapy and IDO signaling inhibition may be promising strategies to prevent tumor recurrence and lung metastasis in future clinical translation. Ji et al. (42) designed a US-responsive oxygen and NO-loaded sonosensitive nanoparticle (PIH-NO) for combined SDT/NO gas therapy. The effectiveness of sensitization was validated on the breast cancer model *in vitro* and *in vivo*. PIH-NO preferentially accumulates in mitochondria, and the burst release of O_2 and NO under US treatment simultaneously generates large amounts of ROS and RNS, enhances SDT to inhibit tumor growth, and amplifies ICD. Furthermore, PIH-NO promoted the maturation of DCs and caused the clustering of M2 macrophages to M1 phenotype, reduced MDSC recruitment, reversed immunosuppression of TME *in vivo*, and enhanced immune response. Studies have demonstrated that O_2-enhanced SDT combined with NO treatment induces and amplifies ICD, triggering an antitumor immune response.

Most photosensitizers, such as Rose Bengal (RB), Ce6, and indocyanine green (ICG), are also sensitive to ultrasound. Liu et al. (45) designed a nano-sonosensitizer (PARN) consisting of difunctional sono-/photo-sensitizers (RB) for SDT combined with PDT, which has a good immune activating antitumor effect and a favorable prognosis. Chen et al. (46) developed a metal-free g-C_3N_4/Ce_6 nanohybrid.Metal-free g-C_3N_4 nanosheets loaded with Ce6 as a dual-function photo/sonosensitizer. Under ultrasound and NIR irradiation, the g-C3N4/Ce6 nanoplatform significantly combines PDT and SDT with pronounced antitumor effects. More importantly, the photothermal greatly promotes immunoreaction, significantly enhancing long-term immune responses and inhibiting tumor recurrence in 4T1 tumor-bearing mice. Chang et al. (47) prepared phase-changeable core-shell nanoparticles (OIX_NPs) with an oxygen-carrying core and the photosensitizer indocyanine green (ICG)/oxaliplatin (OXP) in the shell for PSDT (SDT/PDT) combined with chemodynamic therapy for ovarian cancer. This combined strategy can induce ICD through the passive release of HMGB1 and promote surface exposure of CRT. In a bilateral syngeneic mouse model, OIX_NPs mediated PSDT promoted infiltration of cytotoxic T lymphocytes within the tumor, inhibiting the primary tumor and the growth of distant tumors. The study suggests that PSDT combined with chemodynamic therapy is an effective therapeutic strategy to induce systemic antitumor immunity.

Similar to PDT, noninvasive PTT converts light into heat. PTT is based on near-infrared light (NIR-II) absorption-mediated photothermal conversion therapy. It has been shown that mild PTT could alleviate the hypoxic conditions in the tumor region and facilitate SDT-mediated ROS generation (59). Xue et al. (44) developed an oxygen-deficient zirconia-based nanoplatform with surface PEGylation and cyclic-Arg-Gly-Asp (cRGD) peptide functionalization (ZrO_2-x@PEG/cRGD, ZPR). It successfully induces ICD and promotes the photothermal enhancement of SDT antitumor effects in the NIR-II biological window. Upon confocal microscopy, SDT/PTT enhanced the CRT expression of ZPR+L/US. Compared with the control group, the intracellular CRT level in the ZPR+L/US group increased about 1.86-fold compared with the ZPR+US group, while the HMGB1 release decreased by about 55.7% and the intracellular ATP level decreased by about 60.5%, which was consistent with the extracellular decrease level. Overall, ZPR NPs promoted the ICD more significantly under NIR-II/US irradiation due to the crud-based ligand anchoring effect.

CDT utilizes Fenton or Fenton-like reagents (typically $Fe^{2+/3+}$) to catalyze excess H_2O_2 producing high ROS that kill tumor cells and have been shown to trigger ICD (58, 60). Xue et al. (41) synthesized a bioreactor PEGylated $CoFe_2O_4$ (CFP) for augmented SDT/CDT and elicit robust immune response by a typical solvothermal method. CFP is a novel and efficient SDT sonosensitizer with peroxidase-like activity, which can react with endogenous hydrogen peroxide to generate molecular oxygen. High O_2 levels may promote $^1O_2$ production during SDT. Besides, the fenton-like reaction can be produced by the $Co^{2+/3+}$ and $Fe^{2+/3+}$ redox pair by $CoFe_2O_4$ to produce ROS for CDT. The therapeutic effect of CFP-mediated SDT/CDT combined with anti-PD-L1 checkpoint blockade was also further evaluated in an aggressive lung metastasis model in BALB/c mice carrying bilateral 4T1 tumors. A few metastatic nodules were found in "CFP+US+aPD-L1" mice. CFP-enhanced SDT/CDT combined therapy effectively triggered ICD and promoted antitumor immunity while suppressing primary and distant tumors.

3.3 Multimodal immunotherapeutics on basis of SDT-induce ICD

Various strategies have been explored to enhance SDT and induce ICD in tumor cells to activate the host immune response to cancer. Based on the successful induction of the ICD, cancer immunotherapy can be triggered more effectively by fully activated antigen-presenting cells. However, the immunosuppression-related phenotype of tumor cells can interfere with the recognition of tumors by effector T cells, thus reducing the efficacy of tumor immunotherapy. Therefore, unimodal cancer immunotherapy based on SDT is insufficient for satisfactory treatment. Consequently, it is necessary to use immunotherapy on basis of SDT for multimodal cancer immunotherapy (57, 61, 62).

3.3.1 Combination with checkpoint blockade

Immune checkpoints are a class of immunosuppressive molecules that regulate immune responses, thereby avoiding damage and destruction of normal tissues, which become one of the main causes of immune tolerance during tumorigenesis and development. Immune checkpoint blocking (ICB) is a therapeutic

approach to regulate T-cell activity to kill tumor cells through pathways such as co-inhibition or co-stimulatory signaling (63). For example, Chen et al. (51) constructed perfluorocarbon-loaded fluorinated covalent organic polymers (PFCE@THPP$_{pf}$-COPs). When injected intratumorally, PFCE@THPP$_{pf}$-COPs alleviated tumor hypoxia and inhibited tumor growth by inducing ICD in cancer cells under ultrasound irradiation. Combined anti-CD47 immunotherapy can synergistically inhibit tumor growth and recurrence by increasing the efficiency of tumor infiltration by M1 macrophages and cytotoxic $CD3^+$ and $CD8^+$ T cells while decreasing the efficiency of immunosuppressive regulatory T cells.

To improve the delivery efficiency of immune checkpoint inhibitors and to reduce adverse immune reactions, Li et al. (52) prepared nano-sonosensitizers loaded with programmed cell death ligand 1 antibody (aPD-L1), and modified malignant melanoma cell membranes (B16F10M) for targeting melanoma. The bionanoparticle SCN@B16F10M/PEG-aPD-L1 was used for homologous and immune checkpoint dual targeting and enhanced sonodynamic tumor immunotherapy. The functionalized nano-sonosensitizers showed visible long-term retention in the tumor, which facilitated synergistic dual targeting of homologous and immune checkpoints and enhanced *in vivo* SDT-immunotherapy. A novel TME-responsive nano-sonosensitizers design strategy has high spatiotemporal specificity in the drug-controlled release. Shuai et al. (50) constructed pH and MMP-2 dual-responsive acoustic sensitizer PEG-CDMaPD-L1/Ce6 with low pH and high MMP-2 expression in the TME to trigger *in situ* release of aPD-L1. This strategy of *in situ* induction of ICD and release of aPD-L1 has better targeted therapeutic effects and can induce strong anticancer immunity and long-term immune memory.

3.3.2 Combination with adjuvants

In addition to SDT combined with immune checkpoint inhibition therapy, immune adjuvants are also used to enhance the antitumor immune response. Cytosinphospguanine (CpG), a toll-like receptor 9 (TLR9) agonist, is a significant antitumor immune adjuvant in clinical research (64). For example, Wang et al. (48) constructed TiO_2-Ce6-CpG using titanium dioxide (TiO_2) as a carrier loaded with the sonosensitizer Chlorin e6 (Ce6) and the immune adjuvant CpG oligonucleotide (CpG ODN). The emerging nano-sonosensitizer (TiO2-Ce6-CpG) effectively kills tumor cells and triggers ICD under ultrasound irradiation. The immune adjuvant CpG stimulates the immune system to activate adaptive immune responses. Combined aPD-L1 treatment showed superb inhibition against primary and metastatic tumors in mice's bilateral subcutaneous model of hepatocellular carcinoma. Besides, Chen et al. (49) designed a nanosonosensitizer, co-encapsulated HMME and immune adjuvant R837 in liposomes (HMME/R837@Lip). It has demonstrated that the nano-sonosensitizer can enhance the effect of SDT through applicating in multiple tumor models. SDT + PD-L1 blockade enhances the suppression of primary and distant tumors in the 4T1 breast cancer and CT26 colorectal cancer models. In addition, this combination therapy strategy provides a long-term immune memory function that can prevent tumor recurrence.

4 Discussion

More and more studies have confirmed the application value of SDT in antitumor immunotherapy. However, there are still various challenges in inducing immunotherapy during SDT. SDT-induced immune responses are of limited efficiency. In terms of treatment strategies, targeted delivery of sonosensitizers to specific organelles, such as the endoplasmic reticulum, and mitochondria, is expected to enhance the immunogenicity of tumor cells further. Endoplasmic reticulum (ER) is a crucial location for ROS production and ICD induction during SDT. The sonosensitizers accumulated in the ER significantly impact the activation of ICD (5). However, in most current studies, sonosensitizers are unable to the subcellular localization of ER, and can only produce ER stress response through indirect ROS activity. Therefore, a sononanoplatform that can directly target ER and effectively trigger ER stress is required. Peptides targeting ER, such as pardaxin peptides, and decorated nanomaterials are expected to solve the problem (65). Targeting peptides-modified nanoparticles could carry sonosensitizers accumulated specifically in the ER. The ER-localized SDT strategy improves primary ROS production and provides a promising modality for ICD-assisted immunotherapy (19). In terms of treatment mode, the effect of a single SDT treatment is often limited. Therefore, combining multiple modes is the treatment method to improve the efficiency of antitumor immunity. Many studies have confirmed that different strategies, such as SDT combined with chemotherapy, PDT, PTT, and SDT combined with immunoblockers are expected to improve the effect of tumor immunotherapy.

Although SDT-synergized immunotherapy has rapid development, several limitations associated with SDT and immunotherapy remain to be addressed. Combining immune checkpoint blockade therapy is often administered by systemic injection, leading to insufficient drug targeting, low drug utilization, and even susceptibility to immune-related adverse events. Targeting tumor delivery by loading immunotherapeutic drugs onto nanocarriers can solve these problems. The integration of sonosensitizers with various nanoplatform overcomes the challenges of SDT, such as hypoxia and poor targeting, and enhances SDT-based ICD induction and immunotherapy through synergistic delivery strategies. However, in clinical translations, the stability and biocompatibility of nano-sonosensitizers need to be evaluated.

In addition, even though tumor-derived HMGB1 is critical for SDT-related immunogenicity, researchers found that HMGB1 is also involved in tumor progression. Wang et al. proved that extracellular HMGB1 is an essential factor for TLR4 interaction with platelets and promotes melanoma tumor cells' interaction with aggregation, extravasation, and metastasis. Preventing HMGB1-mediated tumor growth and metastasis should be further studied (20).

In summary, the antitumor immune response is a highly complex process, and disruption of any of these steps can reduce the effectiveness of antitumor immunotherapy. In the future, it is necessary to design more effective multifunctional sonosensitizer nanoparticles rationally to obtain satisfied antitumor immunotherapy.

Author contributions

TW (First author): Conceptualization, investigation, writing - original draft. WP: Writing - Original draft. MD; ZC (Corresponding Author): Conceptualization, funding acquisition, resources, supervision, writing - review & editing. All authors contributed to the article and approved the submitted version.

Funding

This work was supported by National Key R&D Program of China (2019YFE0110400), National Natural Science Foundation of China (82272028, 81971621, 82102087), Key R&D Program of Hunan Province (2021SK2035), Natural Science Foundation of Hunan Province (2022JJ30039, 2022JJ40392), Natural Science Foundation of Guangdong Province (2021A1515011177, 2020A1515110628).

Conflict of interest

The authors declare that the research was conducted in the absence of any commercial or financial relationships that could be construed as a potential conflict of interest.

Publisher's note

References

1. Siddiqui I, Schaeuble K, Chennupati V, Fuertes Marraco SA, Calderon-Copete S, Pais Ferreira D, et al. Intratumoral Tcf1PD-1CD8 T cells with stem-like properties promote tumor control in response to vaccination and checkpoint blockade immunotherapy. *Immunity* (2019) 50(1):195–211. doi: 10.1016/j.immuni.2018.12.021

2. Hong M, Clubb JD, Chen YY. Engineering CAR-T cells for next-generation cancer therapy. *Cancer Cell* (2020) 38(4):473–88. doi: 10.1016/j.ccell.2020.07.005

3. Fucikova J, Kepp O, Kasikova L, Petroni G, Yamazaki T, Liu P, et al. Detection of immunogenic cell death and its relevance for cancer therapy. *Cell Death Dis* (2020) 11 (11):1013. doi: 10.1038/s41419-020-03221-2

4. Qian X, Zheng Y, Chen Y. Micro/Nanoparticle-augmented sonodynamic therapy (SDT): breaking the depth shallow of photoactivation. *Adv Mater* (2016) 28(37):8097–129. doi: 10.1002/adma.201602012

5. Song C, Ran J, Wei Z, Wang Y, Chen S, Lin L, et al. Organic near-Infrared-II nanophotosensitizer for safe cancer phototheranostics and improving immune microenvironment against metastatic tumor. *ACS Appl Mater Interfaces* (2021) 13 (3):3547–58. doi: 10.1021/acsami.0c18841

6. Bao Y, Chen J, Huang P, Tong W. Synergistic effects of acoustics-based therapy and immunotherapy in cancer treatment. *Bio Integration* (2021) 2(2):61–70. doi: 10.15212/bioi-2021-0007

7. Rengeng L, Qianyu Z, Yuehong L, Zhongzhong P, Libo L. Sonodynamic therapy, a treatment developing from photodynamic therapy. *Photodiagnosis Photodyn Ther* (2017) 19:159–66. doi: 10.1016/j.pdpdt.2017.06.003

8. Lin X, Song J, Chen X, Yang H. Ultrasound-activated sensitizers and applications. *Angew Chem Int Ed Engl* (2020) 59(34):14212–33. doi: 10.1002/anie.201906823

9. Wang H, Liu Q, Zhang K, Wang P, Xue Q, Li L, et al. Comparison between sonodynamic and photodynamic effect on MDA-MB-231 cells. *J Photochem Photobiol B* (2013) 127:182–91. doi: 10.1016/j.jphotobiol.2013.08.015

10. Wang X-Q, Wang W, Peng M, Zhang X-Z. Free radicals for cancer theranostics. *Biomaterials* (2021) 266:120474. doi: 10.1016/j.biomaterials.2020.120474

11. Nowak KM, Schwartz MR, Breza VR, Price RJ. Sonodynamic therapy: rapid progress and new opportunities for non-invasive tumor cell killing with sound. *Cancer Lett* (2022) 532:215592. doi: 10.1016/j.canlet.2022.215592

12. Wang S, Hu Z, Wang X, Gu C, Gao Z, Cao W, et al. 5-aminolevulinic acid-mediated sonodynamic therapy reverses macrophage and dendritic cell passivity in murine melanoma xenografts. *Ultrasound Med Biol* (2014) 40(9):2125–33. doi: 10.1016/j.ultrasmedbio.2014.05.007

13. Peng Y, Jia L, Wang S, Cao W, Zheng J. Sonodynamic therapy improves antitumor immune effect by increasing the infiltration of CD8+ T cells and altering tumor blood vessels in murine B16F10 melanoma xenograft. *Oncol Rep* (2018) 40 (4):2163–70. doi: 10.3892/or.2018.6612

14. Zhang Q, Bao C, Cai X, Jin L, Sun L, Lang Y, et al. Sonodynamic therapy-assisted immunotherapy: a novel modality for cancer treatment. *Cancer Sci* (2018) 109 (5):1330–45. doi: 10.1111/cas.13578

15. Wang X, Wang X, Zhong X, Li G, Yang Z, Gong Y, et al. V-TiO2 nanospindles with regulating tumor microenvironment performance for enhanced sonodynamic cancer therapy. *Appl Phys Rev* (2020) 7(4):041411. doi: 10.1063/5.0027606

16. Wang X, Zhong X, Bai L, Xu J, Gong F, Dong Z, et al. Ultrafine titanium monoxide (TiO(1+x)) nanorods for enhanced sonodynamic therapy. *J Am Chem Soc* (2020) 142(14):6527–37. doi: 10.1021/jacs.9b10228

17. Guo QL, Dai XL, Yin MY, Cheng HW, Qian HS, Wang H, et al. Nanosensitizers for sonodynamic therapy for glioblastoma multiforme: current progress and future perspectives. *Mil Med Res* (2022) 9(1):26. doi: 10.1186/s40779-022-00386-z

18. Yang Y, Wang X, Qian H, Cheng L. Titanium-based sonosensitizers for sonodynamic cancer therapy. *Appl Mater Today* (2021) 25:101215. doi: 10.1016/j.apmt.2021.101215

19. Xu M, Zhou L, Zheng L, Zhou Q, Liu K, Mao Y, et al. Sonodynamic therapy-derived multimodal synergistic cancer therapy. *Cancer Lett* (2021) 497:229–42. doi: 10.1016/j.canlet.2020.10.037

20. Zhao H, Zhao B, Li L, Ding K, Xiao H, Zheng C, et al. Biomimetic decoy inhibits tumor growth and lung metastasis by reversing the drawbacks of sonodynamic therapy. *Adv Healthc Mater* (2020) 9(1):e1901335. doi: 10.1002/adhm.201901335

21. Chen H, Liu L, Ma A, Yin T, Chen Z, Liang R, et al. Noninvasively immunogenic sonodynamic therapy with manganese protoporphyrin liposomes against triple-negative breast cancer. *Biomaterials* (2021) 269:120639. doi: 10.1016/j.biomaterials.2020.120639

22. Zhou J, Wang G, Chen Y, Wang H, Hua Y, Cai Z. Immunogenic cell death in cancer therapy: present and emerging inducers. *J Cell Mol Med* (2019) 23(8):4854–65. doi: 10.1111/jcmm.14356

23. Han L, Huang R, Liu S, Huang S, Jiang C. Peptide-conjugated PAMAM for targeted doxorubicin delivery to transferrin receptor overexpressed tumors. *Mol Pharm* (2010) 7(6):2156–65. doi: 10.1021/mp100185f

24. Huang L, Li Y, Du Y, Zhang Y, Wang X, Ding Y, et al. Mild photothermal therapy potentiates anti-PD-L1 treatment for immunologically cold tumors *via* an all-in-one and all-in-control strategy. *Nat Commun* (2019) 10(1):4871. doi: 10.1038/s41467-019-12771-9

25. Son S, Kim JH, Wang X, Zhang C, Yoon SA, Shin J, et al. Multifunctional sonosensitizers in sonodynamic cancer therapy. *Chem Soc Rev* (2020) 49(11):3244–61. doi: 10.1039/c9cs00648f

26. Li D, Yang Y, Li D, Pan J, Chu C, Liu G. Organic sonosensitizers for sonodynamic therapy: from small molecules and nanoparticles toward clinical development. *Small* (2021) 17(42):e2101976. doi: 10.1002/smll.202101976

27. Wang X, Zhong X, Gong F, Chao Y, Cheng L. Newly developed strategies for improving sonodynamic therapy. *Mater Horizons* (2020) 7(8):2028–46. doi: 10.1039/d0mh00613k

28. Aaes TL, Kaczmarek A, Delvaeye T, De Craene B, De Koker S, Heyndrickx L, et al. Vaccination with necroptotic cancer cells induces efficient antitumor immunity. *Cell Rep* (2016) 15(2):274–87. doi: 10.1016/j.celrep.2016.03.037

29. Yin Y, Jiang X, Sun L, Li H, Su C, Zhang Y, et al. Continuous inertial cavitation evokes massive ROS for reinforcing sonodynamic therapy and immunogenic cell death against breast carcinoma. *Nano Today* (2021) 36:101009. doi: 10.1016/j.nantod.2020.101009

30. Hu J, He J, Wang Y, Zhao Y, Fang K, Dong Y, et al. Ultrasound combined with nanobubbles promotes systemic anticancer immunity and augments anti-PD1 efficacy. *J Immunother Cancer* (2022) 10(3). doi: 10.1136/jitc-2021-003408

31. Yang G, Xu L, Xu J, Zhang R, Song G, Chao Y, et al. Smart nanoreactors for pH-responsive tumor homing, mitochondria-targeting, and enhanced photodynamic-immunotherapy of cancer. *Nano Lett* (2018) 18(4):2475–84. doi: 10.1021/acs.nanolett.8b00040

32. Li Y, Xie J, Um W, You DG, Kwon S, Zhang L, et al. Sono/Photodynamic nanomedicine-elicited cancer immunotherapy. *Advanced Funct Mater* (2020) 31 (12):2008061. doi: 10.1002/adfm.202008061

33. Um W, Ko H, You DG, Lim S, Kwak G, Shim MK, et al. Necroptosis-inducible polymeric nanobubbles for enhanced cancer sonoimmunotherapy. *Adv Mater* (2020) 32(16):e1907953. doi: 10.1002/adma.201907953

34. Si Y, Yue J, Liu Z, Li M, Du F, Wang X, et al. Phase-transformation nanoparticle-mediated sonodynamic therapy: an effective modality to enhance antitumor immune response by inducing immunogenic cell death in breast cancer. *Int J Nanomed* (2021) 16:1913–26. doi: 10.2147/IJN.S297933

35. Ning S, Dai X, Tang W, Guo Q, Lyu M, Zhu D, et al. Cancer cell membrane-coated c-TiO(2) hollow nanoshells for combined sonodynamic and hypoxia-activated chemotherapy. *Acta Biomater* (2022) 152:562–74. doi: 10.1016/j.actbio.2022.08.067

36. Tao N, Li H, Deng L, Zhao S, Ouyang J, Wen M, et al. A cascade nanozyme with amplified sonodynamic therapeutic effects through comodulation of hypoxia and immunosuppression against cancer. *ACS Nano* (2022) 16(1):485–501. doi: 10.1021/acsnano.1c07504

37. Zhang Z, Li B, Xie L, Sang W, Tian H, Li J, et al. Metal-phenolic network-enabled lactic acid consumption reverses immunosuppressive tumor microenvironment for sonodynamic therapy. *ACS Nano* (2021) 15(10):16934–45. doi: 10.1021/acsnano.1c08026

38. Xu Q, Zhan G, Zhang Z, Yong T, Yang X, Gan L. Manganese porphyrin-based metal-organic framework for synergistic sonodynamic therapy and ferroptosis in hypoxic tumors. *Theranostics* (2021) 11(4):1937–52. doi: 10.7150/thno.45511

39. Liu M, Khan AR, Ji J, Lin G, Zhao X, Zhai G. Crosslinked self-assembled nanoparticles for chemo-sonodynamic combination therapy favoring antitumor, antimetastasis management and immune responses. *J Control Release* (2018) 290:150–64. doi: 10.1016/j.jconrel.2018.10.007

40. Zhang Y, Qiu N, Zhang Y, Yan H, Ji J, Xi Y, et al. Oxygen-carrying nanoparticle-based chemo-sonodynamic therapy for tumor suppression and autoimmunity activation. *Biomater Sci* (2021) 9(11):3989–4004. doi: 10.1039/d1bm00198a

41. Fu S, Yang R, Ren J, Liu J, Zhang L, Xu Z, et al. Catalytically active CoFe2O4 nanoflowers for augmented sonodynamic and chemodynamic combination therapy with elicitation of robust immune response. *ACS Nano* (2021) 15(7):11953–69. doi: 10.1021/acsnano.1c03128

42. Ji C, Si J, Xu Y, Zhang W, Yang Y, He X, et al. Mitochondria-targeted and ultrasound-responsive nanoparticles for oxygen and nitric oxide codelivery to reverse immunosuppression and enhance sonodynamic therapy for immune activation. *Theranostics* (2021) 11(17):8587–604. doi: 10.7150/thno.62572

43. Zhang D, Lin Z, Zheng Y, Song J, Li J, Zeng Y, et al. Ultrasound-driven biomimetic nanosystem suppresses tumor growth and metastasis through sonodynamic therapy, CO therapy, and indoleamine 2,3-dioxygenase inhibition. *ACS Nano* (2020) 14(7):8985–99. doi: 10.1021/acsnano.0c03833

44. Jiao X, Sun L, Zhang W, Ren J, Zhang L, Cao Y, et al. Engineering oxygen-deficient ZrO2-x nanoplatform as therapy-activated "immunogenic cell death (ICD)" inducer to synergize photothermal-augmented sonodynamic tumor elimination in NIR-II biological window. *Biomaterials* (2021) 272:120787. doi: 10.1016/j.biomaterials.2021.120787

45. Liu Z, Li J, Jiang Y, Wang D. Multifunctional nanocapsules on a seesaw balancing sonodynamic and photodynamic therapies against superficial malignant tumors by effective immune-enhancement. *Biomaterials* (2019) 218:119251. doi: 10.1016/j.biomaterials.2019.119251

46. Chen MY, Zhang YL, Cui LF, Cao ZQ, Wang YW, Zhang W, et al. Protonated 2D carbon nitride sensitized with Ce6 as a smart metal-free nanoplatform for boosted acute multimodal photo-sono tumor inactivation and long-term cancer immunotherapy. *Chem Eng J* (2021) 422:15. doi: 10.1016/j.cej.2021.130089

47. Zheng J, Sun J, Chen J, Zhu S, Chen S, Liu Y, et al. Oxygen and oxaliplatin-loaded nanoparticles combined with photo-sonodynamic inducing enhanced immunogenic cell death in syngeneic mouse models of ovarian cancer. *J Control Release* (2021) 332:448–59. doi: 10.1016/j.jconrel.2021.02.032

48. Lin X, Huang R, Huang Y, Wang K, Li H, Bao Y, et al. Nanosonosensitizer-augmented sonodynamic therapy combined with checkpoint blockade for cancer immunotherapy. *Int J Nanomed* (2021) 16:1889–99. doi: 10.2147/IJN.S290796

49. Yue W, Chen L, Yu L, Zhou B, Yin H, Ren W, et al. Checkpoint blockade and nanosonosensitizer-augmented noninvasive sonodynamic therapy combination reduces tumour growth and metastases in mice. *Nat Commun* (2019) 10(1):2025. doi: 10.1038/s41467-019-09760-3

50. Huang J, Xiao Z, An Y, Han S, Wu W, Wang Y, et al. Nanodrug with dual-sensitivity to tumor microenvironment for immuno-sonodynamic anti-cancer therapy. *Biomaterials* (2021) 269:120636. doi: 10.1016/j.biomaterials.2020.120636

51. Yang Z, Tao D, Zhong W, Liu Z, Feng L, Chen M. Perfluorocarbon loaded fluorinated covalent organic polymers with effective sonosensitization and tumor hypoxia relief enable synergistic sonodynamic-immunotherapy. *Biomaterials* (2022) 280:121250. doi: 10.1016/j.biomaterials.2021.121250

52. Wei X, Feng Z, Huang J, Xiang X, Du F, He C, et al. Homology and immune checkpoint dual-targeted sonocatalytic nanoagents for enhancing sonodynamic tumor therapy. *ACS Appl Mater Interfaces* (2021) 13(28):32810–22. doi: 10.1021/acsami.1c08105

53. Xu H, Yu N, Zhang J, Wang Z, Geng P, Wen M, et al. Biocompatible fe-hematoporphyrin coordination nanoplatforms with efficient sonodynamic-chemo effects on deep-seated tumors. *Biomaterials* (2020) 257:120239. doi: 10.1016/j.biomaterials.2020.120239

54. Feng Q, Zhang W, Yang X, Li Y, Hao Y, Zhang H, et al. pH/Ultrasound dual-responsive gas generator for ultrasound imaging-guided therapeutic inertial cavitation and sonodynamic therapy. *Adv Healthc Mater* (2018) 7(5):1700957. doi: 10.1002/adhm.201700957

55. Carlson RD, Flickinger JC, Snook AE. Talkin' toxins: from coley's to modern cancer immunotherapy. *Toxins (Basel)* (2020) 12(4):241. doi: 10.3390/toxins12040241

56. Zhang H, Zhang X, Ren Y, Cao F, Hou L, Zhang Z. An *in situ* microenvironmental nano-regulator to inhibit the proliferation and metastasis of 4T1 tumor. *Theranostics* (2019) 9(12):3580–94. doi: 10.7150/thno.33141

57. Nesbitt H, Logan K, Thomas K, Callan B, Gao J, McKaig T, et al. Sonodynamic therapy complements PD-L1 immune checkpoint inhibition in a murine model of pancreatic cancer. *Cancer Lett* (2021) 517:88–95. doi: 10.1016/j.canlet.2021.06.003

58. Zhai T, Zhong W, Gao Y, Zhou H, Zhou Z, Liu X, et al. Tumor microenvironment-activated nanoparticles loaded with an iron-carbonyl complex for chemodynamic immunotherapy of lung metastasis of melanoma. *In Vivo ACS Appl Mater Interfaces* (2021) 13(33):39100–11. doi: 10.1021/acsami.1c11485

59. Wang X, Wang X, Yue Q, Xu H, Zhong X, Sun L, et al. Liquid exfoliation of TiN nanodots as novel sonosensitizers for photothermal-enhanced sonodynamic therapy against cancer. *Nano Today* (2021) 39:101170. doi: 10.1016/j.nantod.2021.101170

60. Xu Y, Guo Y, Zhang C, Zhan M, Jia L, Song S, et al. Fibronectin-coated metal-phenolic networks for cooperative tumor chemo-/Chemodynamic/Immune therapy *via* enhanced ferroptosis-mediated immunogenic cell death. *ACS Nano* (2022) 16 (1):984–96. doi: 10.1021/acsnano.1c08585

61. Jiang Q, Qiao B, Lin X, Cao J, Zhang N, Guo H, et al. A hydrogen peroxide economizer for on-demand oxygen production-assisted robust sonodynamic immunotherapy. *Theranostics* (2022) 12(1):59–75. doi: 10.7150/thno.64862

62. Tan X, Huang J, Wang Y, He S, Jia L, Zhu Y, et al. Transformable nanosensitizer with tumor microenvironment-activated sonodynamic process and calcium release for enhanced cancer immunotherapy. *Angew Chem Int Ed Engl* (2021) 60(25):14051–9. doi: 10.1002/anie.202102703

63. Pardoll DM. The blockade of immune checkpoints in cancer immunotherapy. *Nat Rev Cancer* (2012) 12(4):252–64. doi: 10.1038/nrc3239

64. Weiner GJ. CpG oligodeoxynucleotide-based therapy of lymphoid malignancies. *Adv Drug Delivery Rev* (2009) 61(3):263–7. doi: 10.1016/j.addr.2008.12.006

65. Lan G, Ni K, Xu Z, Veroneau SS, Song Y, Lin W. Nanoscale metal-organic framework overcomes hypoxia for photodynamic therapy primed cancer immunotherapy. *J Am Chem Soc* (2018) 140(17):5670–3. doi: 10.1021/jacs.8b01072

frontiers | Frontiers in Immunology

TYPE Systematic Review
PUBLISHED 12 May 2023
DOI 10.3389/fimmu.2023.1170569

OPEN ACCESS

EDITED BY
Sang T. Kim,
University of Texas MD Anderson Cancer Center, United States

REVIEWED BY
Yee Ung,
University of Toronto, Canada
Jianzhong Cao,
Shanxi Provincial Cancer Hospital, China

*CORRESPONDENCE
Wenbin Shen
wbshen1979@sina.com

RECEIVED 21 February 2023
ACCEPTED 02 May 2023
PUBLISHED 12 May 2023

CITATION
Wang H, Song C, Zhao X, Deng W, Dong J and Shen W (2023) Evaluation of neoadjuvant immunotherapy and traditional neoadjuvant therapy for resectable esophageal cancer: a systematic review and single-arm and network meta-analysis.
Front. Immunol. 14:1170569.
doi: 10.3389/fimmu.2023.1170569

Evaluation of neoadjuvant immunotherapy and traditional neoadjuvant therapy for resectable esophageal cancer: a systematic review and single-arm and network meta-analysis

Hesong Wang, Chunyang Song, Xiaohan Zhao, Wenzhao Deng, Jing Dong and Wenbin Shen*

Department of Radiation Oncology, Fourth Hospital of Hebei Medical University, Shijiazhuang, Hebei, China

Objective: This systematic review and meta-analysis aimed to investigate the role of neoadjuvant immunochemotherapy with or without radiotherapy [NIC(R)T] compared to traditional neoadjuvant therapies, without immunotherapy [NC(R)T].

Summary background data: NCRT followed by surgical resection is recommended for patients with early-stage esophageal cancer. However, it is uncertain whether adding immunotherapy to preoperative neoadjuvant therapy would improve patient outcomes when radical surgery is performed following neoadjuvant therapy.

Methods: We searched PubMed, Web of Science, Embase, and Cochrane Central databases, as well as international conference abstracts. Outcomes included R0, pathological complete response (pCR), major pathological response (mPR), overall survival (OS) and disease-free survival (DFS) rates.

Results: We included data from 5,034 patients from 86 studies published between 2019 and 2022. We found no significant differences between NICRT and NCRT in pCR or mPR rates. Both were better than NICT, with NCT showing the lowest response rate. Neoadjuvant immunotherapy has a significant advantage over traditional neoadjuvant therapy in terms of 1-year OS and DFS, with NICT having better outcomes than any of the other three treatments. There were no significant differences among the four neoadjuvant treatments in terms of R0 rates.

Conclusions: Among the four neoadjuvant treatment modalities, NICRT and NCRT had the highest pCR and mPR rates. There were no significant differences

in the R0 rates among the four treatments. Adding immunotherapy to neoadjuvant therapy improved 1-year OS and DFS, with NICT having the highest rates compared to the other three modalities.

Systematic Review Registration: https://inplasy.com/inplasy-2022-12-0060/, identifier INPLASY2022120060.

KEYWORDS

neoadjuvant therapy, immunotherapy, neoadjuvant immunotherapy, curative resection, esophageal carcinoma, meta-analysis

1 Introduction

Esophageal cancer is the seventh most common malignant tumor and the sixth leading cause of cancer-related mortality worldwide (1). Surgical resection has advocated for the treatment of early-stage esophageal cancer (2). The CROSS trial showed that neoadjuvant chemoradiation followed by surgical resection was more beneficial for esophageal cancer (3). Accordingly, the National Comprehensive Cancer Network guidelines recommend it as the standard therapy (4). Nevertheless, the treatment efficacy for esophageal cancer remains poor, with a 5-year survival rate of approximately 20% (5, 6).

Immunotherapy has become an effective treatment for many malignancies including esophageal cancer (7–9). By rescuing the immune checkpoint pathway to resist carcinoma, the anti-tumor action of T cells is blocked by immune checkpoint blockade. Immunotherapy has proven beneficial as a third-, second-, and even first-line treatment for patients with esophageal cancer. However, it remains unclear whether adding immunotherapy therapy to preoperative neoadjuvant confers an overall benefit to patient outcomes when radical surgery is performed after neoadjuvant therapy. Several studies have documented benefits when immunotherapy is added to neoadjuvant therapy (10, 11); on the other hand, adding immunotherapy to neoadjuvant therapy increases the severity of toxic side effects (12, 13).

Therefore, this systematic review and meta-analysis was conducted to evaluate the outcomes of patients treated with either of two neoadjuvant immunotherapies – neoadjuvant immunotherapy combined with chemoradiotherapy (NICRT) and neoadjuvant immunochemotherapy (NICT) – compared with two traditional neoadjuvant therapies – neoadjuvant chemoradiotherapy (NCRT) and neoadjuvant chemotherapy (NCT).

Abbreviations: NICRT, neoadjuvant immunotherapy combined with chemoradiotherapy; NICT, neoadjuvant immunochemotherapy; NCRT, neoadjuvant chemoradiotherapy; NCT, neoadjuvant chemotherapy; PRISMA, Preferred Reporting Items for Systematic Reviews and Meta-Analyses; PICOS, Population, Intervention, Comparison, Outcome, and Study Design; pCR, pathological complete response; mPR, major pathological response; OS, overall survival; DFS, disease-free survival; MINORS, Methodological Index for Non-randomized Studies; RR, risk ratio; CI, confidence interval; SCC, squamous cell carcinoma; AC, adenocarcinoma; CPS, combined positive score; TPS, tumor proportion score.

2 Methods

This study was conducted using the Preferred Reporting Items for Systematic Reviews and Meta-Analyses (PRISMA) 2020 (14). The present study was registered in the INPLASY (identifier: INPLASY2022120060).

2.1 Search strategy and eligibility criteria

We searched PubMed, Web of Science, Embase, and Cochrane Central databases, as well as international conference abstracts from American Society of Clinical Oncology, European Society for Medical Oncology and American Association for Cancer Research, along with various other resources, until December 16, 2022. The detailed search strategies are summarized in Supplementary Table 1. We searched for studies that explored patients with histologically confirmed-, resectable-, esophageal carcinoma who received either NICRT or NICT followed by surgery. Meanwhile, the patients treated with traditional neoadjuvant therapy (NCRT or NCT) were all derived from control patients in these studies, rather than from other studies that did not involve NICRT or NICT. We followed the Population, Intervention, Comparison, Outcome, and Study Design (PICOS) principles (Supplementary Table 2). The detailed inclusion and exclusion criteria are shown in Supplementary Table 3.

2.2 Study selection and data extraction

Two authors (CS and XZ) independently assessed each study and extracted the pertinent information therefrom. Another author (WD) resolved any differences that might have arisen in the process. Relevant parameters were extracted from each included study: author, year, country, study type, registration number, intervention model, type of article, treatment modalities and side

effects, sample size, age, sex, histologic subtype, relevant clinical characteristics, and outcome data of interest.

2.3 Outcomes

The outcome indicators in this study included direct measures of treatment efficacy – R0, pathological complete response (pCR), and major pathological response (mPR) rates – as well as survival-related indicators, including overall survival (OS), disease-free survival (DFS), and death within 30 days after surgery. We did not include treatment-related adverse events during neoadjuvant therapy or post-operative complications, as the evaluation criteria used to evaluate these indicators were not uniform across different studies. The primary goal of our study was to explore immediate post-treatment efficacy and subsequent survival outcomes, to investigate the effectiveness of neoadjuvant immunotherapy.

2.4 Quality assessment

Two authors (CS and XZ) independently evaluated the quality of each study. If there were any disagreements in the process, another author (JD) settled it. The Methodological Index for Non-randomized Studies (MINORS) was used to assess single-arm and retrospective dual-arm studies (15, 16). Each item was scored from 0 to 2. There were 8 items for non-comparative studies and 12 items for comparative studies. For non-comparative studies, an overall score > 12 was considered high, between 8 and 12 was considered intermediate, and < 8 was considered low. The Cochrane Risk of Bias tool was used to assess randomized controlled trials (RCT) (17, 18). The tool scores RCT studies according to five items. The overall bias included low risk of bias, some concerns, and high risk of bias. The quality of this systematic review and meta-analysis was evaluated according to the PRISMA 2020 Checklist (14) and the AMSTAR-2 Checklist (19).

2.5 Statistical analysis

All analyses were performed by STATA (STATA, version 14.0, College, TX),. Survival curve data from included studies which were not reported were extracted by Engauge Digitizer, version 12.1 (http://markummitchell.github.io/engauge-digitizer/). We performed a single-group meta-analysis of all included studies. In order to compare the four different neoadjuvant treatment modalities with each other and to rank their respective efficacies, we performed a network meta-analysis of the comparative studies among them. The significance level of the results was set at P <0.05, as per the convention. The combined risk ratio (RR) and 95% confidence interval (CI) were used as the outcome indicators. For OS and DFS rates, the number of events used to calculate the RR value was the number of survivors rather than the number of deaths. Therefore, in the present study, RR and 95% CI > 1 indicated that treatment was more conducive to survival, whereas RR and 95% CI < 1 indicated that treatment was more detrimental to survival (Detailed data synthesis are shown in Supplementary Table 4).

Subsequently, we merged NICRT and NICT into the neoadjuvant immunotherapy group and NCRT and NCT into the traditional neoadjuvant therapy group. We performed a traditional pairwise meta-analysis of these two groups, with head-to-head studies to explore the comparative advantages of neoadjuvant immunotherapy *vs.* traditional neoadjuvant therapy. Exploratory subgroup analyses were performed based on the study type (prospective or retrospective), intervention model (single-arm or dual-arm), immunotherapy drugs (PD-1 or PD-L1 inhibitors), and cancer type (squamous cell carcinoma [SCC] or adenocarcinoma [AC]). Additionally, sensitivity analyses were performed by omitting each study to evaluate the stability of the results. Publication bias was assessed using the Begg's funnel plot (20).

3 Results

3.1 Characteristics

From the 1,755 considered studies, we eventually selected 86 studies (10–13, 21–102) describing a total of 5,034 patients (Figure 1). This number consisted of 16 dual-arm studies and 70 single-arm studies, five RCTs and 81 non-RCTs.

All studies were published between 2019 and 2022, most of which were conducted in China. Among these studies, the number of patients who received NICRT, NICT, NCRT, and NCT were 427, 3508, 701, and 398, respectively. The median age of all patients ranged from 42.7 to 68.8. For cancer type, the studies included SCC only (n=73), AC only (n=6), mixed SCC and AC (n=5), and

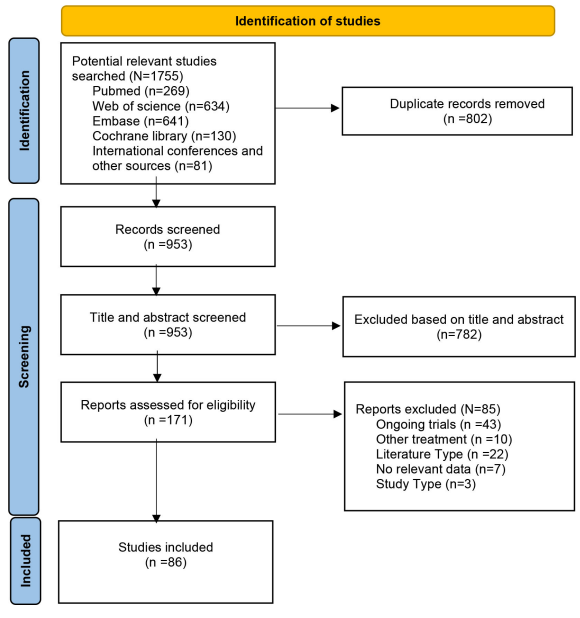

FIGURE 1
PRISMA flow diagram.

undetailed pathology (n=2). For neoadjuvant immunotherapy, PD-1 inhibitors were the most common, with only 6 studies using PD-L1 inhibitors. The radiation doses ranged from 30 Gy to 56 Gy. All neoadjuvant chemotherapy regimens were conventional treatment regimens. Detailed characteristics of each study are shown in Table 1 and Supplementary Tablea 5-8.

3.2 Clinical outcomes of NICRT, NICT, NCRT and NCT

A total of 56 trials reported R0 rates (pooled R0 rate and 95% CI: NICRT - 95.6% [91.8%-99.3%]; NICT - 97.5% [96.9%-98.2%]; NCRT - 94.9% [90.3%-99.5%]; NCT - 96.6% [93.5%-99.6%]) (Figure 2). Overall, 80 trials provided pCR rates (pooled pCR rate and 95% CI: NICRT - 38.9% [32.1%-45.6%]; NICT -27.2% [24.8%-29.6%]; NCRT - 35.5% [21.3%-49.7%]; NCT - 8.6% [2.9%-14.3%]) (Figure 2). Totally, 51 trials analyzed mPR rates (pooled mPR rate and 95% CI: NICRT - 64.2% [53.8%-74.7%]; NICT - 51.8% [46.7%-56.8%]; NCRT - 47.8% [10.5%-85.1%]; NCT - 43.6% [9.5%-77.7%]) (Figure 3). In terms of survival outcomes, 28 trials reported death within 30 days after surgery (pooled rate and 95% CI: NICRT - 2.0% [0.0%-4.2%]; NICT - 0.3% [0.0%-0.6%]; NCRT - 1.7% [0.6%-2.8%]; NCT - 1.3% [0.0%-2.7%]) (Figure 3). Thirteen trials provided 1-year OS rates (pooled 1-year OS rate and 95% CI: NICRT - 87.3% [80.9%-93.6%]; NICT - 96.2% [94.2%-98.1%]; NCRT - 86.2% [79.2%-93.1%]; NCT - 85.1% [74.9%-95.3%]) (Figure 4). And a total of 16 trials analyzed 1-year DFS rates (pooled 1-year DFS rate and 95% CI: NICRT - 77.7% [70.9%-84.6%]; NICT - 90.0% [86.2%-93.7%]; NCRT - 73.2% [64.4%-82.0%]; NCT - 76.6% [64.5%-88.7%]) (Figure 4).

To compare different neoadjuvant treatment modalities with each other, we included 16 dual-arm trials in the network meta-analysis. Network evidence plots and contribution plots are shown in Supplementary Figures 1, 2. The network estimates are shown in Figure 5 and Supplementary Figures 3, 4. There were no significant differences in pCR and mPR rates between NICRT and NCRT (pooled RR and 95% CI of pCR rate: NICRT *vs.* NCRT - 1.39 [0.82,2.37]; pooled RR and 95% of mPR rate: NICRT *vs.* NCRT - 1.02[0.87,1.19]). Both were superior to NICT (pooled RR and 95% CI of pCR rate: NICRT *vs.* NICT - 1.83 [1.10,3.05], NCRT *vs.* NICT - 1.32 [1.00,1.74]; pooled RR and 95% CI of mPR rate: NICRT *vs.* NICT - 1.17[1.05,1.31], NCRT *vs.* NICT - 1.15[1.01,1.31]), and NCT had the poorest results (pooled RR and 95% CI of pCR rate: NICRT *vs.* NCT - 5.43 [2.80,10.51], NCRT *vs.* NCT - 3.90 [2.36,6.47], NICT *vs.* NCT - 2.96 [1.93,4.54]; pooled RR and 95% CI of mPR rate: NICRT *vs.* NCT - 1.93 [1.56,2.39], NCRT *vs.* NCT - 1.90 [1.52,2.37], NICT *vs.* NCT - 1.65[1.35,2.00]). For 1-year OS and DFS rates, NICT showed the best rates compared to other three treatments (pooled RR and 95% CI of 1-year OS rate: NICT *vs.* NICRT - 1.10 [1.01,1.19], NICT *vs.* NCRT - 1.10 [1.01,1.20], NICT *vs.* NCT - 1.11 [1.00,1.26]; pooled RR and 95% CI of 1-year DFS rate: NICT *vs.* NICRT - 1.16 [1.05,1.27], NICT *vs.* NCRT - 1.22 [1.08,1.38], NICT *vs.* NCT - 1.16 [1.00,1.37]), with the other three treatments not having any statistically significant difference in these parameters amongst each other. None of the treatment modalities stood out from the others in terms of R0 rates or death within 30 days after surgery.

3.3 Neoadjuvant immunotherapy (NICRT and NICT) versus traditional neoadjuvant therapy (NCRT and NCT)

Next, we pooled the data for the NICRT and NICT cases into the neoadjuvant immunotherapy group and the NCRT and NCT cases into the traditional neoadjuvant therapy group. A total of 16 trials were included in this head-to-head pairwise meta-analysis. Patients in the neoadjuvant immunotherapy group exhibited significantly higher 1-year OS and DFS rates than those in the traditional neoadjuvant therapy group (pooled RR and 95% CI of the traditional group *vs.* immunotherapy group: 1-year OS rate - 0.90 [0.83-0.98]; 1-year DFS rate - 0.83 [0.74-0.93]) (Figure 6). However, there were no significant differences between the two groups in terms of R0, pCR, mPR, or death within 30 days after surgery (Figure 6).

3.4 Exploratory subgroup analysis

To explore the potential association of immunotherapy between NICRT and NICT, we conducted exploratory subgroup analysis based on study type (prospective or retrospective), intervention model (single-arm or dual-arm), immunotherapy drugs (PD-1 or PD-L1 inhibitors), and cancer type (SCC or AC), respectively. The results of the subgroup NICRT and NICT analyses were generally consistent with the above results in terms of R0, pCR, mPR, death within 30 days after surgery, 1-year OS, and 1-year DFS (Supplementary Figures 5–10).

3.5 Quality evaluation, sensitivity analysis and publication bias

The details of the risk of bias are provided in Supplementary Tables 9, 10. The MINORS was used to evaluate the 81 non-randomized studies. All the 81 studies were of high or intermediate quality. The Cochrane Risk of Bias tool was used to evaluate the five randomized studies, and it indicated that there was no high risk of bias in any of the evaluated categories among the five RCTs in our data set. Supplementary Tables 11, 12 show the quality evaluation of the present study using the PRISMA 2020 Checklist and AMSTAR-2 Checklist. Sensitivity analysis, conducted by omitting each study, indicated that all results were stable except for death within 30 days after surgery (Supplementary Figure 11). Similarly, there was no significant publication bias except for death within 30 days after surgery (Supplementary Figure 12).

4 Discussion

To the best of our knowledge, the present study is the first systematic review and meta-analysis to explore the effectiveness of four different neoadjuvant therapies (NICRT, NICT, NCRT, and NCT) followed by curative surgery for esophageal cancer, and then

TABLE 1 Study Characteristics.

Author	Year	Country	Study Type	Registration Number	Study Title	Intervention Model	Type of Article	Treatment	Sample Size, No	Age, y	Gender, No. (%)	Histologic Subtype, No. (%)	ICI Drugs	CT Regimen	RT Dose, Gy
M.Zhu	2022	USA	prospective	NCT02730546	MC1541	dual-arm	full text	NICRT	31	62.0 (44.0-76.0)	male:30 (96.8%) female:1 (3.2%)	AC:31 (100.0%)	Pembrolizumab	TC	41.4
								NCRT	93	–	–	–	–	TC	41.1-50.4
Y.Zhou	2022	China	retrospective	–	–	dual-arm	full text	NICT	14	>60:6 (42.9%) ≤60:8 (57.1%)	male:9 (64.3%) female:5 (35.7%)	SCC:14 (100.0%)	Toripalimab	TC	–
								NCRT	14	>60:9 (64.3%) ≤60:5 (35.7%)	male:14 (100%) female:0 (0%)	SCC:14 (100.0%)	–	TP	40.0
Zh.Zhang	2022	China	prospective	ChiCTR1900026593	–	single-arm	full text	NICT	47	66.0 (64.0-70.0)	male:36 (76.6%) female:11 (23.4%)	SCC:47 (100.0%)	Sintilimab	TC	–
Y.Zhang	2022	China	prospective	ChiCTR2000039170	–	single-arm	Conference abstract	NICT	166	62.9 (53.7-72.1)	male:140 (84.2%) female:26 (15.8%)	–	Camrelizumab	TP	–
X.K.Zhang	2022	China	retrospective	–	–	single-arm	full text	NICT	64	62.0	male:50 (78.1%) female:14 (21.9%)	SCC:64 (100.0%)	Camrelizumab	TP/FP	–
G.Q.Zhang	2022	China	prospective	–	–	single-arm	Conference abstract	NICT	54	–	–	SCC:54 (100.0%)	Toripalimab	T+S1	–
Y.Yu	2022	China	retrospective	–	–	single-arm	full text	NICT	79	62.0 (48.0-78.0)	male:58 (73.4%) female:21 (26.6%)	SCC:79 (100.0%)	Tislelizumab Camrelizumab Toripalimab Keytruda Sintilimab	TP	–

(Continued)

10.3389/fimmu.2023.1170569

TABLE 1 Continued

Author	Year	Country	Study Type	Registration Number	Study Title	Intervention Model	Type of Article	Treatment	Sample Size, No	Age, y	Gender, No. (%)	Histologic Subtype, No. (%)	ICI Drugs	CT Regimen	RT Dose, Gy
G.Yin	2022	China	retrospective	–	–	single-arm	full text	NICT	34	59.0 (52.0-69.0)	male:30 (88.2%) female:4 (11.8%)	SCC:34 (100.0%)	Camrelizumab	TC	–
Y.Yang	2022	China	retrospective	–	–	dual-arm	full text	NICRT	30	62.0 (42.0-68.0)	male:28 (93.3%) female:2 (6.7%)	SCC+AC	Pembrolizumab Camrelizumab Toripalimab Tislelizumab	TP/TC/FP	41.4
								NICT	299	64.0 (43.0-81.0)	male:249 (83.3%) female:50 (16.7%)	SCC+AC	Pembrolizumab Camrelizumab Sintilimab Toripalimab Tislelizumab	TP/TC/FP	–
W.Yang	2022	China	prospective	ChiCTR2000028900	–	single-arm	full text	NICT	23	58.6 (48.6-68.7)	male:22 (95.7%) female:1 (4.3%)	SCC:23 (100.0%)	Camrelizumab	TC	–
G.Yang	2022	China	retrospective	–	–	single-arm	Conference abstract	NICT	47	–	–	SCC:47 (100.0%)	Camrelizumab	T+capecitabine	–
X.Yan	2022	China	prospective	ChiCTR2000037488	TD-NICE	single-arm	full text	NICT	45	68.8 (56.9-70.7)	male:27 (60.0%) female:18 (40.0%)	SCC:45 (100.0%)	Tislelizumab	TC	–
X.Xu	2022	China	prospective	NCT04437212	–	single-arm	Conference abstract	NICRT	20	–	–	SCC:20 (100.0%)	Toripalimab	TP	41.4
W.Xu	2022	China	prospective	–	–	single-arm	Conference abstract	NICT	46	–	–	SCC:46 (100.0%)	Camrelizumab	TC	–
L.Xu	2022	China	retrospective	–	–	dual-arm	full text	NICT	314	>60:184 (58.6%) ≤60:130 (41.4%)	male:263 (83.8%) female:51 (16.2%)	SCC:314 (100.0%)	Camrelizumab Sintilimab Tislelizumab Pembrolizumab	TP/TC/DP/FP	–

(Continued)

10.3389/fimmu.2023.1170569

TABLE 1 Continued

Author	Year	Country	Study Type	Registration Number	Study Title	Intervention Model	Type of Article	Treatment	Sample Size, No	Age, y	Gender, No. (%)	Histologic Subtype, No. (%)	ICI Drugs	CT Regimen	RT Dose, Gy
								NCRT	154	>60:78 (50.6%) ≤60:76 (49.4%)	male:132 (85.7%) female:22 (14.3%)	SCC:154 (100.0%)	–	TP/TC/DP/FP	32.4-50.4
L.W.Xu	2022	China	prospective	NCT04506138	–	single-arm	full text	NICT	46	63.3 (57.6-70.0)	male:44 (95.7%) female:2 (4.3%)	SCC:46 (100.0%)	Camrelizumab	–	–
X.Xiao	2022	China	retrospective	–	–	dual-arm	full text	NICT	55	66.0 (61.0-71.0)	male:46 (83.6%) female:9 (16.4%)	SCC:55 (100.0%)	Pembrolizumab Sintilimab Tislelizumab Camrelizumab	TP	–
								NCRT	94	64.0 (57.0-69.0)	male:77 (81.9%) female:17 (18.1%)	SCC:94 (100.0%)	–	TP	40-50.4
P.Xia	2022	China	retrospective	–	–	single-arm	full text	NICT	66	67.5 (59.0-71.0)	male:60 (90.9%) female:6 (9.1%)	SCC:66 (100.0%)	Camrelizumab	TP/TC	–
X.Wang	2022	China	prospective	–	–	single-arm	full text	NICT	59	59.0 (43.0-79.0)	male:46 (79.3%) female:12 (20.7%)	SCC:59 (100.0%)	Camrelizumab	TC	–
W.Wang	2022	China	prospective	–	–	single-arm	Conference abstract	NICT	22	–	–	SCC:22 (100.0%)	Pembrolizumab	DP	–
R.Wang	2022	China	prospective	ChiCTR2000033252	–	single-arm	Conference abstract	NICT	30	–	–	SCC:30 (100.0%)	Camrelizumab	DP	–
N.V.Uboha	2022	USA	prospective	NCT03490292	–	single-arm	Conference abstract	NICRT	22	64.0	male:20 (90.9%) female:2 (9.1%)	SCC:3 (13.6%) ACC:19 (86.4%)	Avelumab	TC	41.4

(Continued)

10.3389/fimmu.2023.1170569

TABLE 1 Continued

Author	Year	Country	Study Type	Registration Number	Study Title	Intervention Model	Type of Article	Treatment	Sample Size, No	Age, y	Gender, No. (%)	Histologic Subtype, No. (%)	ICI Drugs	CT Regimen	RT Dose, Gy
Y.Qiao	2022	China	retrospective	–	–	dual-arm	full text	NICT	48	64.2 (56.9-71.4)	male:38 (79.2%) female:10 (20.8%)	SCC:48 (100.0%)	Camrelizumab	–	–
								NCT	206	62.2 (55.1-69.3)	male:147 (71.4%) female:59 (28.6%)	SCC:206 (100.0%)	–	–	–
Y.Qi	2022	China	prospective	NCT03917966	–	single-arm	Conference abstract	NICT	62	66.0	–	SCC:62 (100.0%)	Camrelizumab	DP	–
S. Matsuda	2022	Japan	prospective	NCT03914443	JCOG1804E	single-arm	Conference abstract	NICT	12	–	–	SCC:12 (100.0%)	Nivolumab	DCF	–
X.Ma	2022	China	retrospective	–	–	single-arm	full text	NICT	34	61.0 (47.0-74.0)	male:31 (91.2%) female:3 (8.8%)	SCC:34 (100.0%)	Pembrolizumab Camrelizumab Sintilimab Toripalimab Tislelizumab	TP	–
H.Lv	2022	China	retrospective	–	–	single-arm	full text	NICT	96	65.0 (60.0-69.0)	male:67 (69.8%) female:29 (30.2%)	SCC:96 (100.0%)	Sintilimab	TP/DP	–
Jun.Liu	2022	China	prospective	ChiCTR1900026240	NICE study	single-arm	full text	NICT	60	65.0 (48.0-74.0)	male:50 (83.3%) female:10 (16.7%)	SCC:60 (100.0%)	Camrelizumab	TC	–
J.Liu	2022	China	prospective	NCT04225364	NIC-ESCC2019	single-arm	full text	NICT	56	61.0 (40.0-70.0)	male:42 (75.0%) female:14 (25.0%)	SCC:56 (100.0%)	Camrelizumab	TP	–
Z.Li	2022	China	prospective	–	–	single-arm	Conference abstract	NICT	20	67.5 (47.0-75.0)	male:16 (80.0%) female:4 (20.0%)	SCC:20 (100.0%)	Sintilimab	TP	–

(Continued)

10.3389/fimmu.2023.1170569

TABLE 1 Continued

Author	Year	Country	Study Type	Registration Number	Study Title	Intervention Model	Type of Article	Treatment	Sample Size, No	Age, y	Gender, No. (%)	Histologic Subtype, No. (%)	ICI Drugs	CT Regimen	RT Dose, Gy
Y.Li	2022	China	prospective	NCT04460066	–	dual-arm	Conference abstract	NICT	32	–	–	SCC:32 (100.0%)	Socazolimab	TP	–
								NCT	32	–	–	SCC:32 (100.0%)	–	TP	–
A.H.Ko	2022	USA	prospective	NCT03165994	–	single-arm	Conference abstract	NICRT	34	–	–	SCC:8 (23.5%) AC:26 (76.5%)	Sotigalimab	TC	50.4
R.J.Kelly	2022	USA	prospective	NCT03044613	–	single-arm	Conference abstract	NICRT	32	65.0 (39.0-73.0)	male:26 (81.3%) female:6 (18.7%)	SCC:4 (12.5%) AC:28 (87.5%)	Nivolumab Relatlimab	TC	41.1
S.Jing	2022	China	retrospective	–	–	dual-arm	full text	NICT	47	>60:34 (72.3%) ≤60:13 (27.7%)	male:30 (63.8%) female:17 (36.2%)	SCC:47 (100.0%)	Pembrolizumab Camrelizumab Toripalimab Sintilimab	TP/FP	–
								NCT	47	>60:35 (74.5%) ≤60:12 (25.5%)	male:33 (70.2%) female:14 (29.8%)	SCC:47 (100.0%)	–	TP/FP	–
N.Jiang	2022	China	prospective	ChiCTR2100045104	SCALE-1	single-arm	Conference abstract	NICRT	23	–	–	SCC:23 (100.0%)	Toripalimab	TC	30.0
B.Jiang	2022	China	prospective	–	–	single-arm	Conference abstract	NICT	10	–	–	SCC:10 (100.0%)	Camrelizumab Sintilimab Tislelizumab	TP	–
S.J.Huang	2022	China	retrospective	–	–	single-arm	full text	NICT	51	60.0 (54.0-65.0)	male:41 (80.4%) female:10 (19.6%)	SCC:51 (100.0%)	Camrelizumab Nivolumab Pembrolizumab Sintilimab Tislelizumab	TP/DP	–

(Continued)

10.3389/fimmu.2023.1170569

TABLE 1 Continued

Author	Year	Country	Study Type	Registration Number	Study Title	Intervention Model	Type of Article	Treatment	Sample Size, No	Age, y	Gender, No. (%)	Histologic Subtype, No. (%)	ICI Drugs	CT Regimen	RT Dose, Gy
S.Huang	2022	China	retrospective	NCT04822103	RICE-Retro	single-arm	full text	NICT	155	61.0 (55.0-66.0)	male:121 (78.1%) female:34 (21.9%)	SCC:155 (100.0%)	Camrelizumab Pembrolizumab Sintilimab Tislelizumab Toripalimab Nivolumab	TP/DP	–
Z.Hong	2022	China	retrospective	–	–	dual-arm	full text	NICT	26	68.5 (51.1-65.9)	male:22 (84.6%) female:4 (15.4%)	SCC:26 (100.0%)	Camrelizumab Pembrolizumab Sintilimab	TP	–
								NCT	52	61.0 (54.6-67.4)	male:42 (80.8%) female:10 (19.2%)	SCC:48 (92.3%) non-SCC:4 (7.7%)	–	TP/FP	–
Z.N.Hong	2022	China	retrospective	–	–	dual-arm	full text	NICT	32	62.0 (55.0-67.0)	male:21 (65.5%) female:11 (34.5%)	SCC:32 (100.0%)	Camrelizumab Pembrolizumab Sintilimab	TP	–
								NCRT	32	60.0 (54.0-65.0)	male:27 (84.3%) female:5 (15.7%)	SCC:32 (100.0%)	–	TP/FP	40.0-56.0
W.He	2022	China	prospective	NCT04177797	–	single-arm	full text	NICT	20	62.1 (51.5-72.3)	male:15 (75.0%) female:5 (25.0%)	SCC:20 (100.0%)	Toripalimab	TC	–
J.Guo	2022	China	prospective	ChiCTR2000040345	–	single-arm	Conference abstract	NICT	15	–	–	SCC:15 (100.0%)	Sintilimab	TP	–
Y.M.Gu	2022	China	retrospective	–	–	single-arm	full text	NICT	38	66.0 (46.0-80.0)	male:27 (71.1%) female:11 (28.9%)	SCC:38 (100.0%)	Pembrolizumab Tislelizumab Camrelizumab Sintilimab Toripalimab	TP	–

(Continued)

10.3389/fimmu.2023.1170569

TABLE 1 Continued

Author	Year	Country	Study Type	Registration Number	Study Title	Intervention Model	Type of Article	Treatment	Sample Size, No	Age, y	Gender, No. (%)	Histologic Subtype, No. (%)	ICI Drugs	CT Regimen	RT Dose, Gy
T.Gong	2022	China	retrospective	–	–	single-arm	Conference abstract	NICT	37	62.0 (47.0-76.0)	male:30 (81.1%) female:7 (18.9%)	SCC:37 (100.0%)	Sintilimab	–	–
L.Gao	2022	China	prospective	ChiCTR2100052784	ESONICT-2	single-arm	full text	NICT	20	58.3 (49.0-69.0)	male:17 (85.0%) female:3 (15.0%)	SCC:20 (100.0%)	Toripalimab	DP	–
J.Feng	2022	China	retrospective	–	–	single-arm	full text	NICT	285	63.5 (56.9-70.1)	male:267 (93.7%) female:18 (6.3%)	SCC:285 (100.0%)	Nivolumab Pembrolizumab Camrelizumab Tislelizumab Sintilimab	TC	–
H.Duan	2022	China	prospective	ChiCTR2100048917	PEN-ICE	single-arm	full text	NICT	18	64.0 (35.0-78.0)	male:14 (77.8%) female:4 (22.2%)	SCC:18 (100.0%)	Pembrolizumab	TP/DP	–
Y.Dong	2022	China	prospective	ChiCTR2100050057	–	single-arm	Conference abstract	NICT	28	–	–	SCC:28 (100.0%)	Camrelizumab	TP	–
J.Cheng	2022	China	retrospective	–	–	dual-arm	full text	NICT	40	64.3 (55.4-73.2)	male:30 (75.0%) female:10 (25.0%)	SCC:40 (100.0%)	Pembrolizumab Tislelizumab Camrelizumab Sintilimab Toripalimab	TP/FP	–
								NCRT	109	62.7 (55.4-69.9)	male:93 (85.3%) female:16 (14.7%)	SCC:109 (100.0%)	–	TP/FP	40.0-50.0
F.Chen	2022	China	retrospective	–	–	single-arm	full text	NICRT	38	60.2 (54.4-66.0)	male:31 (81.6%) female:7 (18.4%)	SCC:38 (100.0%)	Camrelizumab	TC	–

(Continued)

10.3389/fimmu.2023.1170569

TABLE 1 Continued

Author	Year	Country	Study Type	Registration Number	Study Title	Intervention Model	Type of Article	Treatment	Sample Size, No	Age, y	Gender, No. (%)	Histologic Subtype, No. (%)	ICI Drugs	CT Regimen	RT Dose, Gy
L.Zhao	2021	China	prospective	–	–	single-arm	Conference abstract	NICT	30	–	–	SCC:30 (100.0%)	Toripalimab	TP	–
Z.Zhang	2021	China	prospective	–	–	single-arm	Conference abstract	NICT	40	–	–	SCC:40 (100.0%)	Sintilimab	TC	–
Z.Y.Zhang	2021	China	prospective	ChiCTR2100045659	ESONICT-1	single-arm	full text	NICT	30	58.3 (51.2-65.4)	male:26 (86.7%) female:4 (13.3%)	SCC:30 (100.0%)	Sintilimab	TP	–
X.Zhang	2021	China	prospective	ChiCTR2000029807	–	single-arm	Conference abstract	NICT	25	–	–	SCC:25 (100.0%)	Camrelizumab	T+S1	–
P.Yang	2021	China	prospective	ChiCTR2100051903	–	single-arm	full text	NICT	16	60.5 (56.0-67.3)	male:14 (87.5%) female:2 (12.5%)	SCC:16 (100.0%)	Camrelizumab	TC	–
G.Z.Yang	2021	China	retrospective	–	–	single-arm	full text	NICT	12	56.0 (50.0-65.0)	male:7 (58.3%) female:5 (41.7%)	SCC:12 (100.0%)	Camrelizumab	T+S1	–
S.Yamamoto	2021	Japan	prospective	NCT03914443	FRONTIER	single-arm	Conference abstract	NICT	13	62.0 (34.0-75.0)	–	–	Nivolumab	CF	–
W.Xing	2021	China	prospective	NCT03985670	–	single-arm	full text	NICT	30	63.8 (57.7-69.9)	male:22 (73.3%) female:8 (26.7%)	SCC:30 (100.0%)	Toripalimab	TP	–
Y.Xiao	2021	China	prospective	–	–	dual-arm	full text	NICT	30	42.7 (27.1-58.2)	male:15 (50.0%) female:15 (50.0%)	SCC:30 (100.0%)	Camrelizumab	Oxaliplatin + docetaxel	–
								NCT	30	43.6 (31.1-56.2)	male:14 (46.7%)	SCC:30 (100.0%)	–	Oxaliplatin + docetaxel	–

(Continued)

10.3389/fimmu.2023.1170569

TABLE 1 Continued

Author	Year	Country	Study Type	Registration Number	Study Title	Intervention Model	Type of Article	Treatment	Sample Size, No	Age, y	Gender, No. (%)	Histologic Subtype, No. (%)	ICI Drugs	CT Regimen	RT Dose, Gy
											female:16 (53.3%)				
Z.Wu	2021	China	retrospective	–	–	single-arm	full text	NICT	38	61.0 (57.0-75.0)	male:36 (94.7%) female:2 (5.3%)	SCC:38 (100.0%)	Pembrolizumab Camrelizumab Sintilimab	TP/TC	–
P.Wu	2021	China	retrospective	–	–	single-arm	Conference abstract	NICT	20	65.0	male:17 (85.0%) female:3 (15.0%)	SCC:20 (100.0%)	Toripalimab Sintilimab Pembrolizumab Camrelizumab Tislelizumab	TP	–
F.Wang	2021	China	prospective	–	–	single-arm	Conference abstract	NICT	26	63.0	male:17 (65.3%) female:9 (34.7%)	SCC:26 (100.0%)	Camrelizumab	DP	–
T.V.D.Ende	2021	Netherlands	prospective	NCT03087864	PERFECT	single-arm	full text	NICRT	40	63.0 (40.0-75.0)	male:35 (87.5%) female:5 (12.5%)	AC:40 (100.0%)	Atezolizumab	TC	41.4
S.Sihag	2021	USA	retrospective	NCT02962063	–	dual-arm	full text	NICRT	25	61.5 (53.0-67.0)	male:22 (88.0%) female:3 (12.0%)	AC:25 (100.0%)	Durvalumab	FOLFOX	–
								NCRT	143	64.0 (56.0-70.0)	male:123 (86.0%) female:20 (14.0%)	AC:143 (100.0%)	–	–	–
D.Shen	2021	China	prospective	–	–	single-arm	full text	NICT	28	62.2 (48.0-79.0)	male:27 (96.4%) female:1 (3.6%)	SCC:28 (100.0%)	Nivolumab Pembrolizumab Camrelizumab	TC	–
X.Shang	2021	China	prospective	NCT04389177	Keystone-001	single-arm	Conference abstract	NICT	42	–	–	SCC:42 (100.0%)	Pembrolizumab	TP	–

(Continued)

10.3389/fimmu.2023.1170569

TABLE 1 Continued

Author	Year	Country	Study Type	Registration Number	Study Title	Intervention Model	Type of Article	Treatment	Sample Size, No	Age, y	Gender, No. (%)	Histologic Subtype, No. (%)	ICI Drugs	CT Regimen	RT Dose, Gy
M.A.Shah	2021	USA	prospective	NCT02998268	–	dual-arm	Conference abstract	NICRT	40	68.0 (38.0-81.0)	male:32 (80.0%) female:8 (20.0%)	AC:40 (100.0%)	Pembrolizumab	TC	41.4
								NCRT	40	–	–	AC:40 (100.0%)	–	TC	41.4
J.Ma	2021	China	prospective	ChiCTR2000033761	ESPRIT	single-arm	Conference abstract	NICT	48	62.0	–	SCC:48 (100.0%)	Camrelizumab	TP	–
Lv	2021	China	retrospective	–	–	single-arm	Conference abstract	NICT	28	–	–	SCC:28 (100.0%)	Camrelizumab	TP	–
Hui.Lv	2021	China	retrospective	–	–	single-arm	Conference abstract	NICT	101	65.0 (43.0-78.0)	male:71 (70.3%) female:30 (29.7%)	SCC:101 (100.0%)	–	–	–
H.L.Lv	2021	China	retrospective	–	–	single-arm	Conference abstract	NICT	16	–	–	SCC:16 (100.0%)	Camrelizumab	TP	–
D.Liu	2021	China	prospective	ChiCTR1900025318	–	single-arm	Conference abstract	NICT	23	–	–	SCC:23 (100.0%)	Toripalimab	TP	–
C.Li	2021	China	prospective	NCT03792347	PALACE-1	single-arm	full text	NICRT	20	62.0 (42.0-66.0)	male:19 (95.0%) female:1 (5.0%)	SCC:20 (100.0%)	Pembrolizumab	TC	41.4
G.Y.Ku	2021	USA	prospective	–	–	single-arm	Conference abstract	NICRT	36	–	–	AC:36 (100.0%)	Durvalumab	mFOLFOX6	50.4
B.Huang	2021	China	prospective	–	–	dual-arm	full text	NICT	23	59.2 (51.9-66.5)	male:21 (91.3%) female:2 (8.7%)	SCC:23 (100.0%)	Pembrolizumab	DP	–
								NCT	31	58.9 (52.5-65.3)	male:30 (96.7%)	SCC:31 (100.0%)	–	DP	–

(Continued)

10.3389/fimmu.2023.1170569

TABLE 1 Continued

Author	Year	Country	Study Type	Registration Number	Study Title	Intervention Model	Type of Article	Treatment	Sample Size, No	Age, y	Gender, No. (%)	Histologic Subtype, No. (%)	ICI Drugs	CT Regimen	RT Dose, Gy
											female:1 (3.3%)				
Hong	2021	China	retrospective	–	–	single-arm	full text	NICT	38	58.8 (51.2-66.4)	male:22 (57.9%) female:16 (42.1%)	SCC:38 (100.0%)	Sintilimab Pembrolizumab Camrelizumab	TP	–
H.T.Duan	2021	China	prospective	–	SIN-ICE	single-arm	full text	NICT	23	63.5 (56.0-81.0)	male:21 (91.3%) female:2 (8.7%)	SCC:23 (100.0%)	Sintilimab	DP/TP	–
C.Cheng	2021	China	prospective	–	–	single-arm	Conference abstract	NICT	20	–	–	SCC:20 (100.0%)	Camrelizumab	TC	–
A.Athauda	2021	UK	prospective	NCT03399071	ICONIC	single-arm	Conference abstract	NICT	15	63.0 (25.0-73.0)	–	AC:15 (100.0%)	Avelumab	FLOT	–
G.Zhang	2020	China	prospective	ChiCTR1900027160	–	single-arm	Conference abstract	NICT	24	–	–	SCC:24 (100.0%)	Toripalimab	T+S1	–
W.Qi	2020	China	prospective	–	–	single-arm	Conference abstract	NICRT	40	61.2 (39.0-66.0)	male:19 (95.0%) female:1 (5.0%)	SCC:40 (100.0%)	Pembrolizumab	TC	41.4
S.Y.Park	2020	Korea	retrospective	NCT02844075	–	dual-arm	full text	NICRT	16	58.5 (56.5-66.0)	male:13 (81.3%) female:3 (18.7%)	SCC:16 (100.0%)	Pembrolizumab	TC	44.1
								NCRT	22	61.5 (56.3-66.0)	male:18 (81.8%) female:4 (18.2%)	SCC:22 (100.0%)	–	FP	44.1
K.Li	2020	China	prospective	–	–	single-arm	Conference abstract	NICT	17	–	–	SCC:17 (100.0%)	Toripalimab	TC	–

(Continued)

10.3389/fimmu.2023.1170569

10.3389/fimmu.2023.1170569

TABLE 1 Continued

Author	Year	Country	Study Type	Registration Number	Study Title	Intervention Model	Type of Article	Treatment	Sample Size, No	Age, y	Gender, No. (%)	Histologic Subtype, No. (%)	ICI Drugs	CT Regimen	RT Dose, Gy
H.Li	2020	China	prospective	NCT03604991	–	single-arm	Conference abstract	NICRT	20	–	–	SCC:20 (100.0%)	Pembrolizumab	TC	41.4
Y.Gu	2020	China	prospective	NCT03946969	KEEP-G 03	single-arm	Conference abstract	NICT	17	65.0 (42.0-69.0)	male:13 (76.4%) female:4 (23.6%)	SCC:17 (100.0%)	Sintilimab	TP+S1	–
S.Lee	2019	Korea	prospective	–	–	single-arm	Conference abstract	NICRT	28	60.0	–	SCC:28 (100.0%)	Pembrolizumab	TC	44.1

ICI, immune checkpoint inhibitor; CT, chemotherapy; RT, radiotherapy; NICRT, neoadjuvant immunotherapy combined with chemoradiotherapy; NICT, neoadjuvant immunochemotherapy; NCRT, neoadjuvant chemoradiotherapy; NCT, neoadjuvant chemotherapy; AC, adenocarcinoma; SCC, squamous cell carcinoma.

compare them with each other by not only postoperative outcome results but also survival-related efficacy outcomes. Drawing from data taken from 86 different studies, collectively describing 5,034 patients, we explored the comparison of R0, pCR, mPR, OS, DFS, and death within 30 days after surgery outcomes across treatment modalities. There were no significant differences in pCR and mPR rates between NICRT and NCRT; both were superior to NICT, and NCT had the poorest results. For 1-year OS and DFS rates, NICT showed the best rates compared to the other three treatments, with the other three treatments not having any statistically significant difference in these parameters amongst each other. No significant differences were observed among any of the four examined treatment modalities in terms of R0 rates or death within 30 days after surgery. As for the subgroup analyses based on the study type, intervention model, immunotherapy drugs, and cancer type, there were no significant differences between the subgroups, which is consistent with the above findings.

Although this is, to date, the largest meta-analysis to examine the role of four different neoadjuvant therapies after curative resection for esophageal cancer, previous studies on this subject have been conducted. A meta-analysis conducted by Wang et al. (103), which included 20 studies with 621 patients, explored the clinical outcomes of NICRT *vs.* NICT. Consistent with our findings, they reported that NICRT had an advantage over NICT in terms of mPR rates, but found no significant differences in R0 rates. However, they reported no significant differences in pCR rates between NICRT and NICT, whereas we found that NICRT had superior pCR rates to NICT (pooled RR and 95% CI: 1.83 [1.10, 3.05]). This discrepancy may be explained by Wang et al.'s smaller sample size, which included only two studies that involved NICRT. In contrast, our study included 14 studies of NICRT, including the two used by Wang et al. Additionally, the patients in the NCRT and NCT groups in their study were obtained from a meta-analysis by Li et al. (104), whereas the patients in our NCRT and NCT groups were extracted from dual-arm studies with direct head-to-head comparisons with NICRT or NICT. This significantly reduced error, increased comparability, and provided assurance of the quality of the results and conclusions. In addition, with the addition of follow-up parameters (OS and DFS), our study included more survival-related outcomes than previous studies. Our study showed greater 1-year OS and 1-year DFS rates in the NICT group, while the NICRT group showed no such results. This difference might be explained by the fact that concurrent administration of all three treatment modalities in the NICRT group significantly increased treatment-related adverse effects, resulting in patients showing no advantage in terms of survival. Wang et al. (103) reported that the incidence of preoperative grade 3-4 treatment-related adverse events was 51.2% in NICRT, which was much higher than the 19.4% in NICT. A multicenter dual-arm study conducted by Yang et al. (29) directly compared the safety of NICRT and NICT, noting that treatment-related adverse events, immune-related adverse events, and post-operative complications all had higher incidences in the NICRT group than in the NICT group. The toxicity of this treatment may ultimately result in a failure of NICRT to provide long-term survival benefits. Although this review concluded that there were no significant differences

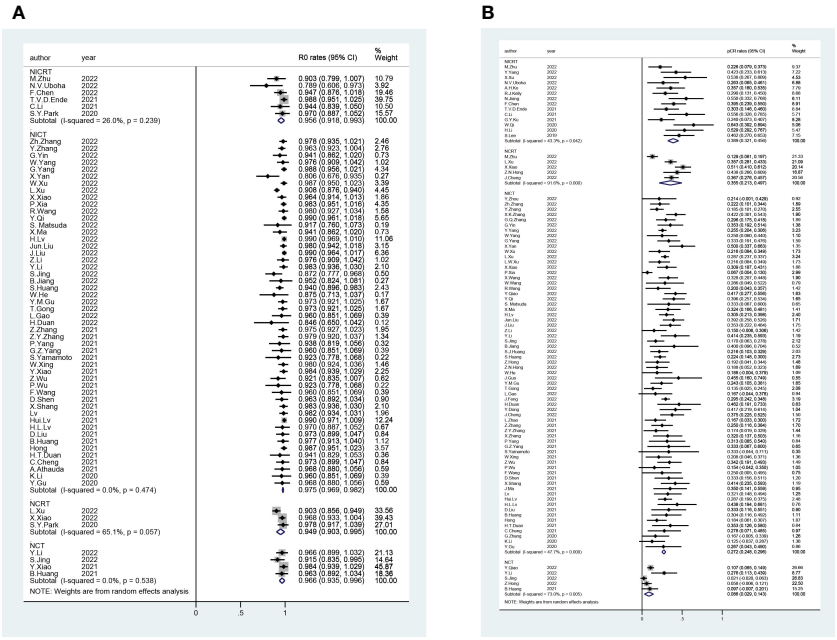

FIGURE 2
Forest Plot of **(A)** R0 and **(B)** Pathological Complete Response (pCR).

among the four different neoadjuvant treatments in terms of death within 30 days after surgery, this could be attributed to three reasons. First, the incidence of mortality within 30 days after surgery was low – close to zero, in fact – regardless of the treatment type, the differences they exhibited may not be statistically evident; second, the toxic effects of the treatment did not appear in such a short period of time and needed some time to manifest; And third, this outcome showed unstable results in both sensitivity analysis and publication bias analysis. A meta-analysis by Ge et al. (105) included 27 single-arm studies with 815 patients to explore the clinical outcomes of NICT. They reported pooled rates of R0, pCR and mPR were 98.6%, 31.4% and 48.9%, respectively, largely similar to the results obtained in our study (97.5%, 27.2%, and 51.8%, respectively). Compared to CROSS (3), which received NCRT, their R0 rate was 92.0%, which was not significantly different from the results obtained in our study and those of Ge et al. (105); however, their pCR rate was 49.0%, which was significantly higher than our results or those of Ge et al. That

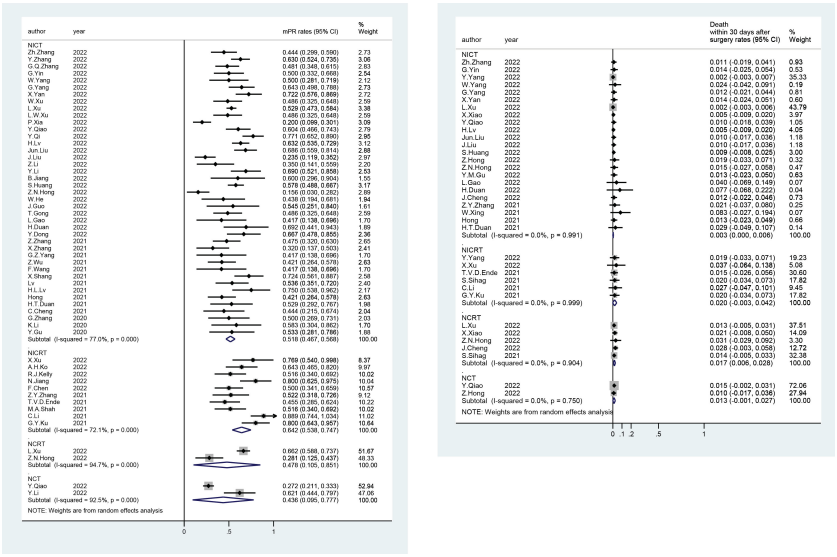

FIGURE 3
Forest Plot of **(A)** Major Pathological Response (mPR) and **(B)** Death within 30 Days after Surgery.

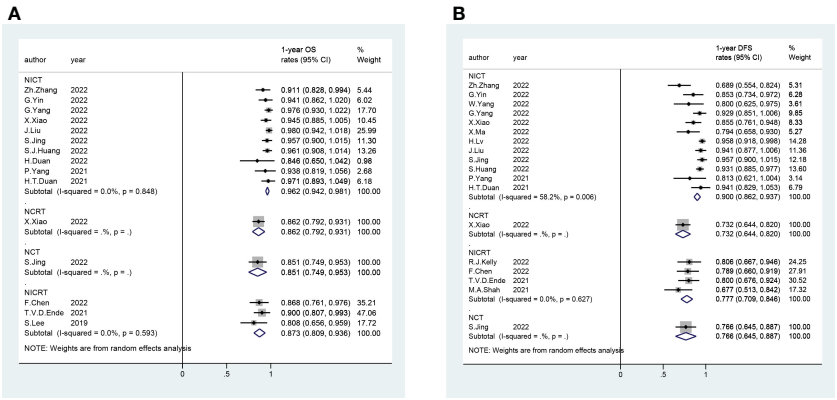

FIGURE 4
Forest Plot of **(A)** 1-year Overall Survival (OS) and **(B)** 1-year Disease Free Survival (DFS).

being said, this result is consistent with our conclusion that the pCR rate in the NCRT group was higher than that in the NICT group, while there were no significant differences in terms of R0 rate. A randomized controlled multicenter study conducted by Liu et al. (106) in 2022 reported that patients receiving NCT experienced a pCR rate of 20.8% and an mPR rate of 33.3%, consistent with our findings that the NCT group had the lowest pCR and mPR rates among the all four neoadjuvant treatments.

R0			
NICRT	1.01 (0.91,1.12)	1.01 (0.90,1.13)	1.00 (0.89,1.12)
0.99 (0.90,1.10)	NICT	1.00 (0.96,1.04)	0.99 (0.95,1.04)
0.99 (0.89,1.11)	1.00 (0.96,1.05)	NCRT	0.99 (0.93,1.06)
1.00 (0.89,1.12)	1.01 (0.96,1.05)	1.01 (0.95,1.07)	NCT
pCR			
NICRT	0.55 (0.33,0.91)	0.72 (0.42,1.22)	0.18 (0.10,0.36)
1.83 (1.10,3.05)	NICT	1.32 (1.00,1.74)	0.34 (0.22,0.52)
1.39 (0.82,2.37)	0.76 (0.58,1.00)	NCRT	0.26 (0.15,0.42)
5.43 (2.80,10.51)	2.96 (1.93,4.54)	3.90 (2.36,6.47)	NCT
mPR			
NICRT	0.85(0.76,0.95)	0.98(0.84,1.14)	0.52(0.42,0.64)
1.17(1.05,1.31)	NICT	1.15(1.01,1.31)	0.61(0.50,0.74)
1.02(0.87,1.19)	0.87(0.76,0.99)	NCRT	0.53(0.42,0.66)
1.93(1.56,2.39)	1.65(1.35,2.00)	1.90(1.52,2.37)	NCT
Death within 30 days after surgery			
NICRT	0.14 (0.01,1.90)	0.54 (0.05,6.49)	0.14 (0.00,4.60)
6.96 (0.53,91.99)	NICT	3.79 (0.86,16.77)	0.97 (0.09,10.28)
1.84 (0.15,21.91)	0.26 (0.06,1.17)	NCRT	0.25 (0.02,4.17)
7.21 (0.22,238.82)	1.04 (0.10,11.02)	3.92 (0.24,64.09)	NCT
1-year OS *			
NICRT	1.10(1.01,1.19)	1.00(0.89,1.11)	0.98(0.85,1.17)
0.91(0.84,0.99)	NICT	0.91(0.83,1.13)	0.90(0.79,1.00)
1.00(0.90,1.12)	1.10(1.01,1.20)	NCRT	0.99(0.85,1.14)
1.02(0.88,1.17)	1.11(1.00,1.26)	1.01(0.88,1.17)	NCT
1-year DFS *			
NICRT	1.16(1.05,1.27)	0.95(0.82,1.10)	0.99(0.83,1.19)
0.87(0.79,0.95)	NICT	0.82(0.73,0.93)	0.86(0.73,1.00)
1.05(0.91,1.23)	1.22(1.08,1.38)	NCRT	1.05(0.86,1.28)
1.01(0.84,1.21)	1.16(1.00,1.37)	0.96(0.78,1.17)	NCT

FIGURE 5
Results of Comparisons by Risk Ratio (RR) and 95% Confidence Interval (CI) among Four Neoadjuvant Therapies. (*The number of events in the calculation of the RR value is the number of survivors rather than the number of deaths. RR and 95% CI > 1 indicates that treatment is more conducive to survival, while RR and 95% CI < 1 indicates that treatment is more detrimental to survival.) Pathological Complete Response (pCR), Major Pathological Response (mPR), Overall Survival (OS), Disease Free Survival (DFS).

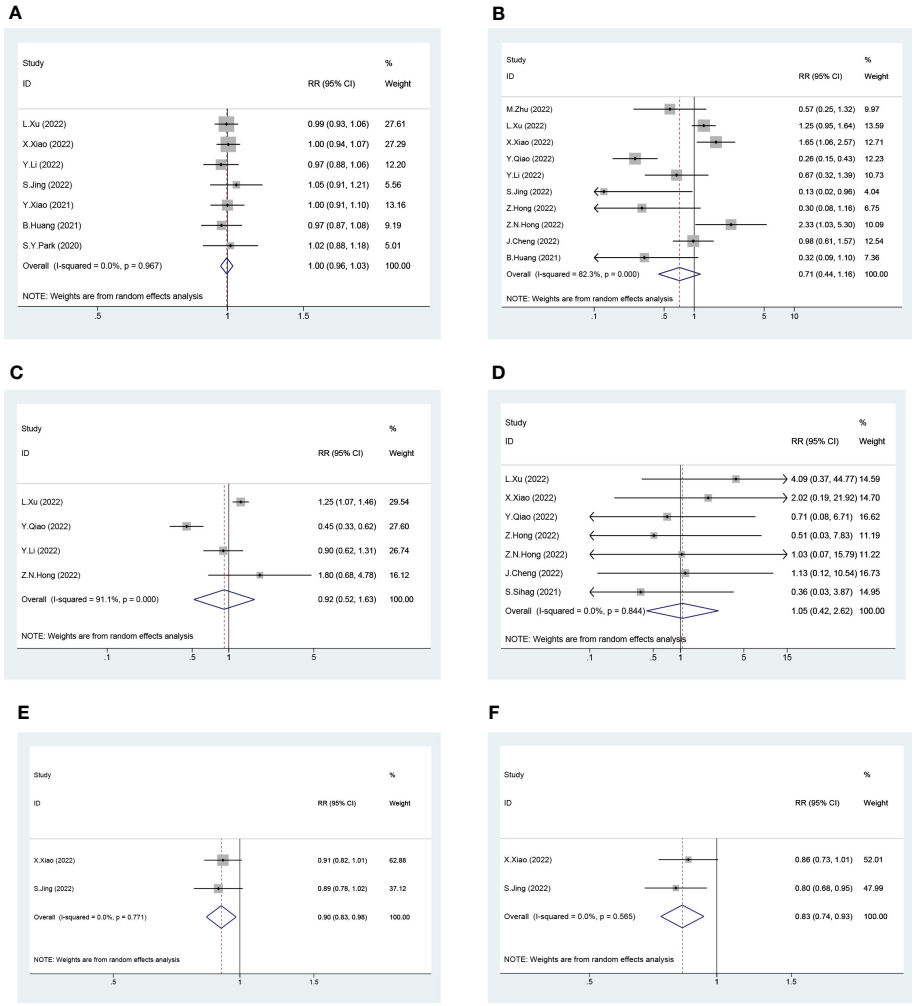

FIGURE 6
Forest Plot of Traditional Neoadjuvant Therapy (left) and Neoadjuvant Immunotherapy (right). **(A)** R0, **(B)** Pathological Complete Response (pCR), **(C)** Major Pathological Response (mPR), **(D)** Death within 30 Days after Surgery, **(E)** 1-year Overall Survival (OS) and **(F)** 1-year Disease Free Survival (DFS). (For 1-year OS and 1-year DFS, the number of events in the calculation of the RR value is the number of survivors rather than the number of deaths. RR and 95% CI > 1 indicates that treatment is more conducive to survival, while RR and 95% CI < 1 indicates that treatment is more detrimental to survival.).

When we combined treatment modalities based on the inclusion or absence of immunotherapy (regardless of the presence of radiation therapy), we found that the neoadjuvant immunotherapy group had a significant advantage over the traditional neoadjuvant therapy group in terms of 1-year OS and DFS rates, while there were no significant differences between the two groups in other outcomes. It can be seen that the addition of immunotherapy can significantly prolong the survival of patients. This adds further evidence to the growing pile attesting to the benefit of immunotherapy in neoadjuvant therapy. As for the other results of the same, because the results obtained in this study were that there were no significant differences among the four different neoadjuvant treatments in R0 rates and death within 30 days after surgery, there were also no differences in the comparison between the combined groups. Regarding pCR and mPR rates, since the incidences were highest in the NCRT cohort and lowest in the NCT cohort, when these two were combined together in the traditional group, it canceled out the difference that had been seen when the four cohorts were being compared individually. This systematic review and meta-analysis also had limitations. First, as most of the studies included in this review were single-armed, potential bias may arise; second, since immunotherapy is still in the process of exploration, some studies have not yet released their final results. Moreover, survival endings could only be extracted for 1 year, as for the follow-up of long-term survival, follow-up studies are needed to report; third, there were only five RCTs in this review, and the lack of RCTs may potentially lead to bias; fourth, as previously noted, both sensitivity and publication bias analysis indicated instability in the data used for death within 30 days after surgery in this review, which prohibits rigorous conclusions from being drawn therefrom; more studies and data

will be needed to verify the relevant findings of this study; fifth, due to the lack of available data, the role of effective biomarkers, for instance, combined positive score (CPS) and tumor proportion score (TPS), in neoadjuvant immunotherapy could not be investigated; Sixth, due to the inconsistent guidelines for and definitions of treatment-related adverse events in the different studies used in this meta-analysis, we were unable to properly compare them, instead focusing on the endpoints of efficacy and survival.

5 Conclusion

In conclusion, among the four neoadjuvant treatment modalities NICRT, NICT, NCRT, and NCT, NICRT and NCRT had the highest pCR and mPR rates. There were no significant differences in R0 rates among the four neoadjuvant treatment modalities. Adding immunotherapy to neoadjuvant therapy improved 1-year OS and DFS, with the NICT group having significantly higher longer survival according to both these metrics than any of the other three modalities. The results of this review provide a basis for future studies. Further, large multicenter RCTs and longer-term follow-ups are needed to refine these findings.

Data availability statement

The original contributions presented in the study are included in the article/Supplementary Material. Further inquiries can be directed to the corresponding author.

Author contributions

All authors read and approved the final manuscript prior to submission. WS are responsible for the conception and design of the study. HW are responsible for analysis and interpretation of data, and drafting the article and revising it. CS and XZ are responsible for acquisition of data. WD and JD is responsible for data check. All authors contributed to the article and approved the submitted version.

Acknowledgments

We would like to express our sincere thanks to Department of Radiation Oncology, Fourth Hospital of Hebei Medical University.

Conflict of interest

The authors declare that the research was conducted in the absence of any commercial or financial relationships that could be construed as a potential conflict of interest.

Publisher's note

All claims expressed in this article are solely those of the authors and do not necessarily represent those of their affiliated organizations, or those of the publisher, the editors and the reviewers. Any product that may be evaluated in this article, or claim that may be made by its manufacturer, is not guaranteed or endorsed by the publisher.

Supplementary material

The Supplementary Material for this article can be found online at: https://www.frontiersin.org/articles/10.3389/fimmu.2023.1170569/full#supplementary-material

References

1. Siegel RL, Miller KD, Fuchs HE, Jemal A. Cancer statistics, 2022. *CA Cancer J Clin* (2022) 72(1):7–33. doi: 10.3322/caac.21708

2. Paul S, Altorki N. Outcomes in the management of esophageal cancer. *J Surg Oncol* (2014) 110(5):599–610. doi: 10.1002/jso.23759

3. Eyck BM, van Lanschot JJB, Hulshof M, van der Wilk BJ, Shapiro J, van Hagen P, et al. Ten-year outcome of neoadjuvant chemoradiotherapy plus surgery for esophageal cancer: the randomized controlled CROSS trial. *J Clin Oncol* (2021) 39(18):1995–2004. doi: 10.1200/JCO.20.03614

4. Ajani JA, D'Amico TA, Bentrem DJ, Chao J, Corvera C, Das P, et al. Esophageal and esophagogastric junction cancers, version 2.2019, NCCN clinical practice guidelines in oncology. *J Natl Compr Canc Netw* (2019) 17(7):855–83. doi: 10.6004/jnccn.2019.0033

5. Baba NY Y, Kinoshita K, Iwatsuki M, Yamashita Y-I, Chikamoto A, Watanabe M, et al. And prognostic features of patients with esophageal cancer and multiple primary cancers: a retrospective single-institution study. *Ann Surg* (2018) 267(3):478–83. doi: 10.1097/SLA.0000000000002118

6. Huang LF TX. The immune landscape of esophageal cancer. *Cancer Commun (Lond)* (2019) 39(1):79. doi: 10.1186/s40880-019-0427-z

7. Janjigian JB YY, Calvo E, Kim JW, Ascierto PA, Sharma P, Ott PA, et al. CheckMate-032 study: efficacy and safety of nivolumab and nivolumab plus ipilimumab in patients with metastatic esophagogastric cancer. *J Clin Oncol* (2018) 36(28):2836–44. doi: 10.1200/JCO.2017.76.6212

8. Kojima MAS T, Muro K, Francois E, Adenis A, Hsu C-H, Doi T, et al. Randomized phase III KEYNOTE-181 study of pembrolizumab versus chemotherapy in advanced esophageal cancer. *J Clin Oncol* (2020) 38(35):4138–48. doi: 10.1200/JCO.20.01888

9. Ribas JDW A. Cancer immunotherapy using checkpoint blockade. *Science* (2018) 359(6382):1350–5. doi: 10.1126/science.aar4060

10. Li Y, Zhou A, Liu S, He M, Chen KN, Tian Z, et al. 1207P neoadjuvant PD-L1 inhibitor (socazolimab) plus chemotherapy in patients with locally advanced esophageal squamous cell carcinoma (ESCC): a multicenter, randomized, double-blind phase II study. *Ann Oncol* (2022) 33(S7):S1101. doi: 10.1016/j.annonc.2022.07.1325

11. Guo J, Qiao C, Lu J, Yang S, Zhang B. Neoadjuvant sintilimab combined with chemotherapy in patients with resectable esophageal squamous cell carcinoma (ESCC): preliminary results from a phase II study. *J Clin Oncol* (2022) 40(16):E16008–E. doi: 10.1200/JCO.2022.40.16_suppl.e16008

12. Li C, Zhao S, Zheng Y, Han Y, Chen X, Cheng Z, et al. Preoperative pembrolizumab combined with chemoradiotherapy for oesophageal squamous cell carcinoma (PALACE-1). *Eur J Cancer* (2021) 144:232–41. doi: 10.1016/j.ejca.2020.11.039

13. Kelly RJ, Zaidi AH, Van Liere Canzoniero J, Feliciano JL, Hales RK, Voong KR, et al. Multicenter phase II study of neoadjuvant nivolumab or nivolumab plus relatlimab (antiLAG3 antibody) plus chemoradiotherapy in stage II/III esophageal/gastroesophageal junction (E/GEJ) carcinoma. *J Clin Oncol* (2022) 40(4 SUPPL):321. doi: 10.1200/JCO.2022.40.4_suppl.321

14. Page MJ, McKenzie JE, Bossuyt PM, Boutron I, Hoffmann TC, Mulrow CD, et al. The PRISMA 2020 statement: an updated guideline for reporting systematic reviews. *J Clin Epidemiol* (2021) 134:178–89. doi: 10.1016/j.jclinepi.2021.03.001

15. Slim K, Nini E, Forestier D, Kwiatkowski F, Panis Y, Chipponi. J. Methodological index for non-randomized studies (minors): development and validation of a new instrument. *ANZ J Surg* (2003) 73(9):712–6. doi: 10.1046/j.1445-2197.2003.02748.x

16. Malgie J, Schoones JW, Pijls BG. Decreased mortality in coronavirus disease 2019 patients treated with tocilizumab: a rapid systematic review and meta-analysis of observational studies. *Clin Infect Dis* (2021) 72(11):e742–e9. doi: 10.1093/cid/ciaa1445

17. Higgins JP, Altman DG, Gotzsche PC, Juni P, Moher D, Oxman AD, et al. The cochrane collaboration's tool for assessing risk of bias in randomised trials. *BMJ* (2011) 343:d5928. doi: 10.1136/bmj.d5928

18. Sterne JAC, Savovic J, Page MJ, Elbers RG, Blencowe NS, Boutron I, et al. RoB 2: a revised tool for assessing risk of bias in randomised trials. *BMJ* (2019) 366:l4898. doi: 10.1136/bmj.l4898

19. Shea BJ, Reeves BC, Wells G, Thuku M, Hamel C, Moran J, et al. AMSTAR 2: a critical appraisal tool for systematic reviews that include randomised or non-randomised studies of healthcare interventions, or both. *BMJ* (2017) 358:j4008. doi: 10.1136/bmj.j4008

20. Mazumdar M, Begg CB. Operating characteristics of a rank correlation test for publication bias. *Biometrics* (1994) 50(4):1088–101.

21. Zhu M, Chen C, Foster NR, Hartley C, Mounajjed T, Salomao MA, et al. Pembrolizumab in combination with neoadjuvant chemoradiotherapy for patients with resectable adenocarcinoma of the gastroesophageal junction. *Clin Cancer Res* (2022) 28 (14):3021–31. doi: 10.1158/1078-0432.CCR-22-0413

22. Zhou YH, Li JY, Yan JX, Guo P, He WW, Liu Y. Alleviation of neoadjuvant immunochemotherapy for esophageal squamous cell carcinoma and its relationship with expression and changes of PD-L1. *Neoplasma* (2022) 69(4):785–93. doi: 10.4149/neo_2022_211223N1826

23. Zhang Z, Ye J, Li H, Gu D, Du M, Ai D, et al. Neoadjuvant sintilimab and chemotherapy in patients with resectable esophageal squamous cell carcinoma: a prospective, single-arm, phase 2 trial. *Front Immunol* (2022) 13:1031171. doi: 10.3389/fimmu.2022.1031171

24. Zhang Y, Shen G, Xu R, Huang G, Yang S, Zheng Q, et al. Real-world effectiveness and safety of camrelizumab-based neoadjuvant therapy in resectable esophageal cancer: initial results of a prospective multicenter observational study. *J Clin Oncol* (2022) 40(4_suppl):250–. doi: 10.1200/JCO.2022.40.4_suppl.250

25. Zhang X, Gari A, Li M, Chen J, Qu C, Zhang L, et al. Combining serum inflammation indexes at baseline and post treatment could predict pathological efficacy to anti–PD–1 combined with neoadjuvant chemotherapy in esophageal squamous cell carcinoma. *J Transl Med* (2022) 20(1):61. doi: 10.1186/s12967-022-03252-7

26. Zhang G, Yuan J, Pan C, Xu Q, Cui X, Zhang J, et al. Abstract CT544: multi-omics analysis uncovers prognostic biomarkers and tumor ecosystem dynamics during toripalimab combined with nab-paclitaxel and s-1 as neoadjuvant therapy for esophageal squamous carcinoma: a single-center, open-label, single-arm phase 2 trial. *Cancer Res* (2022) 82(12_Supplement):CT544–CT. doi: 10.1158/1538-7445.AM2022-CT544

27. Yu Y, Wang W, Qin Z, Li H, Liu Q, Ma H, et al. A clinical nomogram for predicting tumor regression grade in esophageal squamous-cell carcinoma treated with immune neoadjuvant immunotherapy. *Ann Transl Med* (2022) 10(2):102. doi: 10.21037/atm-22-78

28. Yin GQ, Li ZL, Li D. The safety and efficacy of neoadjuvant camrelizumab plus chemotherapy in patients with locally advanced esophageal squamous cell carcinoma: a retrospective study. *Cancer Manag Res* (2022) 14:2133–41. doi: 10.2147/CMAR.S358620

29. Yang Y, Tan L, Hu J, Li Y, Mao Y, Tian Z, et al. Safety and efficacy of neoadjuvant treatment with immune checkpoint inhibitors in esophageal cancer: real-world multicenter retrospective study in China. *Dis Esophagus* (2022) 35(11):1–8. doi: 10.1093/dote/doac031

30. Yang W, Xing X, Yeung SJ, Wang S, Chen W, Bao Y, et al. Neoadjuvant programmed cell death 1 blockade combined with chemotherapy for resectable esophageal squamous cell carcinoma. *J Immunother Cancer* (2022) 10(1):e003497. doi: 10.1136/jitc-2021-003497

31. Yang G, Sun X, Yang H, Luo G, Zheng Y, Huang M, et al. 1256P three courses of neoadjuvant camrelizumab combined with chemotherapy in locally advanced esophageal squamous cell carcinoma (ESCC): a prospective phase II clinical trial. *Ann Oncol* (2022) 33(S7):S1122. doi: 10.1016/j.annonc.2022.07.1374

32. Yan X, Duan H, Ni Y, Zhou Y, Wang X, Qi H, et al. Tislelizumab combined with chemotherapy as neoadjuvant therapy for surgically resectable esophageal cancer: a prospective, single-arm, phase II study (TD-NICE). *Int J Surg* (2022) 103:106680. doi: 10.1016/j.ijsu.2022.106680

33. Xu X, Sun Z, Zhang Y, Shen L, Liu Q, Zhang C, et al. Neoadjuvant chemoradiotherapy combined with perioperative toripalimab in locally advanced esophageal cancer. *J Clin Oncol* (2022) 40(16):E16065–E. doi: 10.1200/JCO.2022.40.16_suppl.e16065

34. Xu W, Jiang Y, Wang C, Wu J, Li J, Hu Y, et al. The efficacy and safety of neoadjuvant camrelizumab and chemotherapy for locally advanced thoracic esophageal squamous cell carcinoma. *J Clin Oncol* (2022) 40(4_suppl):278–. doi: 10.1200/JCO.2022.40.4_suppl.278

35. Xu L, Wei XF, Li CJ, Yang ZY, Yu YK, Li HM, et al. Pathologic responses and surgical outcomes after neoadjuvant immunochemotherapy versus neoadjuvant chemoradiotherapy in patients with locally advanced esophageal squamous cell carcinoma. *Front Immunol* (2022) 13:1052542. doi: 10.3389/fimmu.2022.1052542

36. Xu L, Qi Y, Jiang Y, Ji Y, Zhao Q, Wu J, et al. Crosstalk between the gut microbiome and clinical response in locally advanced thoracic esophageal squamous cell carcinoma during neoadjuvant camrelizumab and chemotherapy. *Ann Transl Med* (2022) 10(6):325. doi: 10.21037/atm-22-1165

37. Xiao X, Yang YS, Zeng XX, Shang QX, Luan SY, Zhou JF, et al. The comparisons of neoadjuvant chemoimmunotherapy versus chemoradiotherapy for oesophageal squamous cancer. *Eur J Cardiothorac Surg* (2022) 62(1):ezac341. doi: 10.1093/ejcts/ezac341

38. Xia P, Li P, Wu S, Wang Y, Ye P, Zhang C, et al. Evaluation of the safety and effectiveness of neoadjuvant combined chemoimmunotherapy in the treatment of locally advanced esophageal squamous cell carcinoma: a retrospective single-arm cohort study. *Ann Transl Med* (2022) 10(18):991. doi: 10.21037/atm-22-4268

39. Wang X, Yang W, Zhou Q, Luo H, Chen W, Yeung SJ, et al. The role of (18)F-FDG PET/CT in predicting the pathological response to neoadjuvant PD-1 blockade in combination with chemotherapy for resectable esophageal squamous cell carcinoma. *Eur J Nucl Med Mol Imaging* (2022) 49(12):4241–51. doi: 10.1007/s00259-022-05872-z

40. Wang W, Li L. Neoadjuvant pembrolizumab plus chemotherapy for resectable locally advanced esophageal squamous cell carcinoma (ESCC): interim results. *J Clin Oncol* (2022) 40(16):E16011–E. doi: 10.1200/JCO.2022.40.16_suppl.e16011

41. Wang R, Zhang G, Zhu Q, Ma T, Weng C, Zhang D, et al. 1234P neoadjuvant camrelizumab plus docetaxel and carboplatin in locally advanced esophageal squamous cell carcinoma (ESCC): a prospective study. *Ann Oncol* (2022) 33(S7):S1113. doi: 10.1016/j.annonc.2022.07.1352

42. Uboha NV, Eickhoff JC, Maloney JD, McCarthy D, De Camp M, Deming DA, et al. Phase I/II trial of perioperative avelumab in combination with chemoradiation (CRT) in the treatment of stage II/III resectable esophageal and gastroesophageal junction (E/GEJ) cancer. *J Clin Oncol* (2022) 40(16):4034. doi: 10.1200/JCO.2022.40.16_suppl.4034

43. Qiao Y, Zhao C, Li X, Zhao J, Huang Q, Ding Z, et al. Efficacy and safety of camrelizumab in combination with neoadjuvant chemotherapy for ESCC and its impact on esophagectomy. *Front Immunol* (2022) 13:953229. doi: 10.3389/fimmu.2022.953229

44. Qi Y, Meng X, Shan Z, Fan Q, Wang F. Camrelizumab combined with chemotherapy or apatinib as neoadjuvant therapy for locally advanced esophageal squamous cell carcinoma: A phase 2 trial. *Dis Esophagus* (2022) 35:62. doi: 10.1093/dote/doac051.355

45. Matsuda S, Yamamoto S, Kato K, Daiko H, Kojima T, Hara H, et al. FRONTiER: a feasibility trial of nivolumab with neoadjuvant CF or DCF, FLOT therapy for locally advanced esophageal carcinoma (JCOG1804E)–short-term results for cohorts c and d. *J Clin Oncol* (2022) 40(4_suppl):286–. doi: 10.1200/JCO.2022.40.4_suppl.286

46. Ma X, Zhao W, Li B, Yu Y, Ma Y, Thomas M, et al. Neoadjuvant immune checkpoint inhibitors plus chemotherapy in locally advanced esophageal squamous cell carcinoma: perioperative and survival outcomes. *Front Oncol* (2022) 12:810898. doi: 10.3389/fonc.2022.810898

47. Lv H, Tian Y, Li J, Huang C, Sun B, Gai C, et al. Neoadjuvant sintilimab plus chemotherapy in resectable locally advanced esophageal squamous cell carcinoma. *Front Oncol* (2022) 12:864533. doi: 10.3389/fonc.2022.864533

48. Liu J, Yang Y, Liu Z, Fu X, Cai X, Li H, et al. Multicenter, single-arm, phase II trial of camrelizumab and chemotherapy as neoadjuvant treatment for locally advanced esophageal squamous cell carcinoma. *J Immunother Cancer* (2022) 10(3):e004291. doi: 10.1136/jitc-2021-004291

49. Liu J, Li J, Lin W, Shao D, Depypere L, Zhang Z, et al. Neoadjuvant camrelizumab plus chemotherapy for resectable, locally advanced esophageal squamous cell carcinoma (NIC-ESCC2019): a multicenter, phase 2 study. *Int J Cancer* (2022) 151(1):128–37. doi: 10.1002/ijc.33976

50. Li Z, Xu PF, Mao WM, Kuang YK, Fan HY, Zou B, et al. A study of neoadjuvant sintilimab combined with chemotherapy TP for locally advanced esophageal squamous cell carcinoma (ESCC). *J Clin Oncol* (2022) 40(16):e16038. doi: 10.1200/JCO.2022.40.16_suppl.e16038

51. Ko AH, Noel M, Chao J, Sohal D, Crow M, Oberstein PE, et al. 1229P a multicenter phase II study of sotigalimab (CD40 agonist) in combination with neoadjuvant chemoradiation for resectable esophageal and gastroesophageal junction (GEJ) cancers. *Ann Oncol* (2022) 33(S7):S1111. doi: 10.1016/j.annonc.2022.07.1347

52. Jing SW, Zhai C, Zhang W, He M, Liu QY, Yao JF, et al. Comparison of neoadjuvant immunotherapy plus chemotherapy versus chemotherapy alone for patients with locally advanced esophageal squamous cell carcinoma: a propensity score matching. *Front Immunol* (2022) 13:970534. doi: 10.3389/fimmu.2022.970534

53. Jiang N, Jiang M, Zhu X, Ren B, Zhang J, Guo Z, et al. SCALE-1: safety and efficacy of short course neoadjuvant chemo-radiotherapy plus toripalimab for locally

advanced resectable squamous cell carcinoma of esophagus. *J Clin Oncol* (2022) 40 (16):4063. doi: 10.1200/JCO.2022.40.16_suppl.4063

54. Jiang B, Yang X, Zhang J, Huang M. Abstract 5230: neoadjuvant programmed cell death protein 1 inhibitors combined with chemotherapy in resectable esophageal squamous carcinoma: an open-label, single-arm study. *Cancer Res* (2022) 82 (12_Supplement):5230–. doi: 10.1158/1538-7445.AM2022-5230

55. Huang SJ, Tian D, Wang SC, Zeng RJ, Dong YJ, Hong LL, et al. Pathological responses of the primary tumor and locoregional lymph nodes after neoadjuvant immunochemotherapy in esophageal squamous cell cancer. *World J Oncol* (2022) 13 (4):195–204. doi: 10.14740/wjon1489

56. Huang S, Wu H, Cheng C, Zhou M, Xu E, Lin W, et al. Conversion surgery following immunochemotherapy in initially unresectable locally advanced esophageal squamous cell carcinoma-a real-world multicenter study (RICE-retro). *Front Immunol* (2022) 13:935374. doi: 10.3389/fimmu.2022.935374

57. Hong ZN, Zhang Z, Chen Z, Weng K, Peng K, Lin J, et al. Safety and feasibility of esophagectomy following combined neoadjuvant immunotherapy and chemotherapy for locally advanced esophageal cancer: a propensity score matching. *Esophagus* (2022) 19(2):224–32. doi: 10.1007/s10388-021-00899-x

58. Hong ZN, Gao L, Weng K, Huang Z, Han W, Kang M. Safety and feasibility of esophagectomy following combined immunotherapy and chemotherapy for locally advanced esophageal squamous cell carcinoma: a propensity score matching analysis. *Front Immunol* (2022) 13:836338. doi: 10.3389/fimmu.2022.836338

59. He W, Leng X, Mao T, Luo X, Zhou L, Yan J, et al. Toripalimab plus paclitaxel and carboplatin as neoadjuvant therapy in locally advanced resectable esophageal squamous cell carcinoma. *Oncologist* (2022) 27(1):e18–28. doi: 10.1093/oncolo/oyab011

60. Gu YM, Shang QX, Zhang HL, Yang YS, Wang WP, Yuan Y, et al. Safety and feasibility of esophagectomy following neoadjuvant immunotherapy combined with chemotherapy for esophageal squamous cell carcinoma. *Front Surg* (2022) 9:851745. doi: 10.3389/fsurg.2022.851745

61. Gong T, Song W, Lu J, Liu J, Fan B, Zhao J, et al. Efficacy and safety of neoadjuvant chemotherapy and immunotherapy in locally resectable advanced esophageal squamous cell carcinoma. *Dis Esophagus* (2022) 35:108–9. doi: 10.1093/dote/doac051.520

62. Gao L, Lu J, Zhang P, Hong ZN, Kang M. Toripalimab combined with docetaxel and cisplatin neoadjuvant therapy for locally advanced esophageal squamous cell carcinoma: a single-center, single-arm clinical trial (ESONICT-2). *J Gastrointest Oncol* (2022) 13(2):478–87. doi: 10.21037/jgo-22-131

63. Feng J, Wang L, Yang X, Chen Q, Cheng X. Pathologic complete response prediction to neoadjuvant immunotherapy combined with chemotherapy in resectable locally advanced esophageal squamous cell carcinoma: real-world evidence from integrative inflammatory and nutritional scores. *J Inflamm Res* (2022) 15:3783–96. doi: 10.2147/JIR.S367964

64. Duan H, Shao C, Pan M, Liu H, Dong X, Zhang Y, et al. Neoadjuvant pembrolizumab and chemotherapy in resectable esophageal cancer: an open-label, single-arm study (PEN-ICE). *Front Immunol* (2022) 13:849984. doi: 10.3389/fimmu.2022.849984

65. Dong Y, Luo J, Liu S, Lin Y, Han H. 1225P neoadjuvant therapy of camrelizumab combined with chemotherapy in patients (pts) with resectable esophageal squamous cell cancer (ESCC): preliminary results of a preoperative phase exploratory clinical trial. *Ann Oncol* (2022) 33(S7):S1119. doi: 10.1016/j.annonc.2022.07.1343

66. Cheng J, Guo M, Yang Y, Liu Y, Hu W, Shang Q, et al. Perioperative outcomes of minimally invasive esophagectomy after neoadjuvant immunotherapy for patients with locally advanced esophageal squamous cell carcinoma. *Front Immunol* (2022) 13:848881. doi: 10.3389/fimmu.2022.848881

67. Chen F, Qiu L, Mu Y, Sun S, Yuan Y, Shang P, et al. Neoadjuvant chemoradiotherapy with camrelizumab in patients with locally advanced esophageal squamous cell carcinoma. *Front Surg* (2022) 9:893372. doi: 10.3389/fsurg.2022.893372

68. Zhao L, Xing W, Yang Y, Zhang Y, Ma B, Fu X, et al. The sequence of chemotherapy and anti-PD-1 antibody influence the efficacy of neoadjuvant immunochemotherapy in locally advanced esophageal squamous cell cancer: a phase II study. *J Clin Oncol* (2021) 39(15_suppl):4051–. doi: 10.1200/JCO.2021.39.15_suppl.4051

69. Zhang Z, Ye J, Li H, Du M, Gu D, Zhang J, et al. 1378P a single-center, prospective, open-label, single-arm trial of sintilimab with paclitaxel and carboplatin as a neoadjuvant therapy for esophageal squamous carcinoma. *Ann Oncol* (2021) 32: S1042–S3. doi: 10.1016/j.annonc.2021.08.1487

70. Zhang Z, Hong ZN, Xie S, Lin W, Lin Y, Zhu J, et al. Neoadjuvant sintilimab plus chemotherapy for locally advanced esophageal squamous cell carcinoma: a single-arm, single-center, phase 2 trial (ESONICT-1). *Ann Transl Med* (2021) 9(21):1623. doi: 10.21037/atm-21-5381

71. Zhang X, Yang G, Su X, Luo G, Cai P, Zheng Y, et al. Neoadjuvant programmed death1 blockade plus chemotherapy in locally advanced esophageal squamous cell carcinoma. *J Clin Oncol* (2021) 39(15 SUPPL):e16076. doi: 10.1200/JCO.2021.39.15_suppl.e16076

72. Yang P, Zhou X, Yang X, Wang Y, Sun T, Feng S, et al. Neoadjuvant camrelizumab plus chemotherapy in treating locally advanced esophageal squamous cell carcinoma patients: a pilot study. *World J Surg Oncol* (2021) 19(1):333. doi: 10.1186/s12957-021-02446-5

73. Yang G, Su X, Yang H, Luo G, Gao C, Zheng Y, et al. Neoadjuvant programmed death-1 blockade plus chemotherapy in locally advanced esophageal squamous cell carcinoma. *Ann Transl Med* (2021) 9(15):1254. doi: 10.21037/atm-21-3352

74. Yamamoto S, Kato K, Daiko H, Kojima T, Hara H, Abe T, et al. FRONTiER: a feasibility trial of nivolumab with neoadjuvant CF or DCF therapy for locally advanced esophageal carcinoma (JCOG1804E)-the short-term results of cohort a and b. *J Clin Oncol* (2021) 39(3):202. doi: 10.1200/JCO.2021.39.3_suppl.202

75. Xing W, Zhao L, Zheng Y, Liu B, Liu X, Li T, et al. The sequence of chemotherapy and toripalimab might influence the efficacy of neoadjuvant chemoimmunotherapy in locally advanced esophageal squamous cell cancer-a phase II study. *Front Immunol* (2021) 12:772450. doi: 10.3389/fimmu.2021.772450

76. Xiao Y, Huo Q, Yang Y, Lu B, Wang X. Clinical trial of carrelizumab injection combined with operation in the treatment of patients with stage II/III esophageal squamous cell carcinoma. *Chin J Clin Pharmacol* (2021) 37(24):3323–5.

77. Wu Z, Zheng Q, Chen H, Xiang J, Hu H, Li H, et al. Efficacy and safety of neoadjuvant chemotherapy and immunotherapy in locally resectable advanced esophageal squamous cell carcinoma. *J Thorac Dis* (2021) 13(6):3518–28. doi: 10.21037/jtd-21-340

78. Wu P, Wang T, Chen B, Shi M, Zhou Y, Huang B, et al. Preoperative chemotherapy combined with PD-1 inhibitor in locally advanced operable or potentially resectable esophageal squamous cell carcinoma: a real world study. *J Clin Oncol* (2021) 39(15_suppl):e16010–e. doi: 10.1200/JCO.2021.39.15_suppl.e16010

79. Wang F, Qi Y, Meng X, Fan Q. Camrelizumab in combination with preoperative chemotherapy for locally advanced esophageal squamous cell carcinoma: a single-arm, open-label, phase II study. *J Clin Oncol* (2021) 39(15):222. doi: 10.1200/JCO.2021.39.15_suppl.e16072

80. van den Ende T, de Clercq NC, van Berge Henegouwen MI, Gisbertz SS, Geijsen ED, Verhoeven RHA, et al. Neoadjuvant chemoradiotherapy combined with atezolizumab for resectable esophageal adenocarcinoma: a single-arm phase II feasibility trial (PERFECT). *Clin Cancer Res* (2021) 27(12):3351–9. doi: 10.1158/1078-0432.CCR-20-4443

81. Sihag S, Ku GY, Tan KS, Nussenzweig S, Wu A, Janjigian YY, et al. Safety and feasibility of esophagectomy following combined immunotherapy and chemoradiotherapy for esophageal cancer. *J Thorac Cardiovasc Surg* (2021) 161 (3):836–43.e1. doi: 10.1016/j.jtcvs.2020.11.106

82. Shen D, Chen Q, Wu J, Li J, Tao K, Jiang Y. The safety and efficacy of neoadjuvant PD-1 inhibitor with chemotherapy for locally advanced esophageal squamous cell carcinoma. *J Gastrointest Oncol* (2021) 12(1):1–10. doi: 10.21037/jgo-20-599

83. Shang X, Zhang C, Zhao G, Zhang W, Liu L, Duan X, et al. LBA3 safety and efficacy of pembrolizumab combined with paclitaxel and cisplatin as a neoadjuvant treatment for locally advanced resectable (stage III) esophageal squamous cell carcinoma (Keystone-001): interim analysis of a prospective, single-arm, single-center, phase II trial. *Ann Oncol* (2021) 32:S1428–S9. doi: 10.1016/j.annonc.2021.10.218

84. Shah MA, Almhanna K, Iqbal S, Thakkar P, Schneider BJ, Yantiss R, et al. Multicenter, randomized phase II study of neoadjuvant pembrolizumab plus chemotherapy and chemoradiotherapy in esophageal adenocarcinoma (EAC). *J Clin Oncol* (2021) 39(15_suppl):4005–. doi: 10.1200/JCO.2021.39.15_suppl.4005

85. Ma J, Zhang J, Yang Y, Zheng D, Wang X, Liang H, et al. Camrelizumab combined with paclitaxel and nedaplatin as neoadjuvant therapy for locally advanced esophageal squamous cell carcinoma (ESPRIT): a phase II, single-arm, exploratory research. *Ann Oncol* (2021) 32:S1400–S. doi: 10.1016/j.annonc.2021.10.083

86. Lv H, Tian Y, Li Z, Huang C, Xu Y, Tian Z. 557 neoadjuvant camrelizumab in combination with albumin paclitaxel and cisplatin for patients with locally advanced esophageal squamous cell carcinoma (ESCC). *J ImmunoTher Cancer* (2021) 9(Suppl 2): A587–A. doi: 10.1136/jitc-2021-SITC2021.557

87. Lv H, Tian Y, Huang C, Sun B, Gai C, Li Z, et al. 110P neoadjuvant PD-1 blockade combined with chemotherapy for patients with resectable locally advanced esophageal squamous cell carcinoma (ESCC): a real world data analysis. *Ann Oncol* (2021) 32(S7):S1423. doi: 10.1016/j.annonc.2021.10.128

88. Lv H, Tian Y, Huang C, Li Z, Tian Z. Camrelizumab combined with albumin paclitaxel and cisplatin as neoadjuvant therapy for locally advanced esophageal squamous cell carcinoma (ESCC). *J Clin Oncol* (2021) 39(15):e16021. doi: 10.1200/JCO.2021.39.15_suppl.e16021

89. Liu D, Zhang Q, Zhu J, Qian T, Yin R, Fan Z, et al. Phase-II study of toripalimab combined with neoadjuvant chemotherapy for the treatment of resectable esophageal squamous cell carcinoma. *J Clin Oncol* (2021) 39(15):e16029. doi: 10.1200/JCO.2021.39.15_suppl.e16029

90. Ku GY, Wu AJ-C, Sihag S, Park BJ, Jones DR, Gu P, et al. Durvalumab (D) and PET-directed chemoradiation (CRT) after induction FOLFOX for esophageal adenocarcinoma. *J Clin Oncol* (2021) 39(3_suppl):226–. doi: 10.1200/JCO.2021.39.3_suppl.226

91. Huang B, Shi H, Gong X, Yu J, Xiao C, Zhou B, et al. Comparison of efficacy and safety between pembrolizumab combined with chemotherapy and simple chemotherapy in neoadjuvant therapy for esophageal squamous cell carcinoma. *J Gastrointest Oncol* (2021) 12(5):2013–21. doi: 10.21037/jgo-21-610

92. Hong ZN, Weng K, Peng K, Chen Z, Lin J, Kang M. Neoadjuvant immunotherapy combined chemotherapy followed by surgery versus surgery alone

for locally advanced esophageal squamous cell carcinoma: a propensity score-matched study. *Front Oncol* (2021) 11:797426. doi: 10.3389/fonc.2021.797426

93. Duan H, Wang T, Luo Z, Wang X, Liu H, Tong L, et al. A multicenter single-arm trial of sintilimab in combination with chemotherapy for neoadjuvant treatment of resectable esophageal cancer (SIN-ICE study). *Ann Transl Med* (2021) 9(22):1700. doi: 10.21037/atm-21-6102

94. Cheng C, Yang W, Chen W, Yeung S-CJ, Xing X, Wang X, et al. Neoadjuvant PD-1 blockade in combination with chemotherapy for patients with resectable esophageal squamous cell carcinoma. *J Clin Oncol* (2021) 39(3_suppl):220–. doi: 10.1200/JCO.2021.39.3_suppl.220

95. Athauda A, Starling N, Chau I, Cunningham D, Watkins DJ, Rao S, et al. Perioperative FLOT plus anti-PD-L1 avelumab (FLOT-a) in resectable oesophagogastric adenocarcinoma (OGA): interim safety analysis results from the ICONIC trial. *J Clin Oncol* (2021) 39(3_suppl):201–. doi: 10.1200/JCO.2021.39.3_suppl.201

96. Zhang G, Hu Y, Yang B, Xu Q, Li J, Sun S, et al. 1058P a single-centre, prospective, open-label, single-arm trial of toripalimab with nab-paclitaxel and s-1 as a neoadjuvant therapy for esophageal squamous cell carcinoma (ESCC). *Ann Oncol* (2020) 31(S4):S722. doi: 10.1016/j.annonc.2020.08.1178

97. Qi WX, Zhao S, Li H, Chen J. Safety and tolerability of neoadjuvant chemoradiotherapy combined with pembrolizumab for local advanced, resectable esophageal cancer: preliminary results of a prospective phase IB trial. *Int J Radiat OncologyBiologyPhysics* (2020) 108(3):e576–e7. doi: 10.1016/j.ijrobp.2020.07.1773

98. Park SY, Hong MH, Kim HR, Lee CG, Cho JH, Cho BC, et al. The feasibility and safety of radical esophagectomy in patients receiving neoadjuvant chemoradiotherapy with pembrolizumab for esophageal squamous cell carcinoma. *J Thorac Dis* (2020) 12 (11):6426–34. doi: 10.21037/jtd-20-1088

99. Li K, Yang X, Luo W, Ma Q, Wang Y, Xiong Y, et al. Toripalimab plus nab-paclitaxel and carboplatin as neoadjuvant therapy for patients with esophageal squamous cell carcinoma At clinical stage T2-T4/N0-N2/M0: a single-arm, single-center clinical study. *J Immunother Cancer* (2020) 8:A253–A. doi: 10.1136/jitc-2020-SITC2020.0415

100. Li H, Li C, Zheng Y, Zhao S, Chen X, Han Y, et al. Preoperative combination ofpembrolizumab withchemoradiation for patients withlocally advanced esophagealsquamous cell carcinoma:mid-termresults of NCT03604991. *Dis Esophagus* (2020) 33(SUPPL 1):14. doi: 10.1093/dote/doaa087.35

101. Gu Y, Chen X, Wang D, Ding M, Xue L, Zhen F, et al. 175P a study of neoadjuvant sintilimab combined with triplet chemotherapy of lipo-paclitaxel, cisplatin, and s-1 for resectable esophageal squamous cell carcinoma (ESCC). *Ann Oncol* (2020) 31:S1307–S8. doi: 10.1016/j.annonc.2020.10.196

102. Lee S, Ahn BC, Park SY, Kim DJ, Lee CG, Cho J, et al. A phase II trial of preoperative chemoradiotherapy and pembrolizumab for locally advanced esophageal squamous cell carcinoma (ESCC). *Ann Oncol* (2019) 30(Supplement 5):v754. doi: 10.1093/annonc/mdz266.018

103. Wang Z, Shao C, Wang Y, Duan H, Pan M, Zhao J, et al. Efficacy and safety of neoadjuvant immunotherapy in surgically resectable esophageal cancer: a systematic review and meta-analysis. *Int J Surg* (2022) 104:106767. doi: 10.1016/j.ijsu.2022.106767

104. Li F, Ding N, Zhao Y, Yuan L, Mao Y. The current optimal multimodality treatments for oesophageal squamous-cell carcinoma: a systematic review and meta-analysis. *Int J Surg* (2018) 60:88–100. doi: 10.1016/j.ijsu.2018.10.037

105. Ge F, Huo Z, Cai X, Hu Q, Chen W, Lin G, et al. Evaluation of clinical and safety outcomes of neoadjuvant immunotherapy combined with chemotherapy for patients with resectable esophageal cancer: a systematic review and meta-analysis. *JAMA Netw Open* (2022) 5(11):e2239778. doi: 10.1001/jamanetworkopen.2022.39778

106. Liu J, Wang Y, Cao B, Zhang S, Cao F, Gao L, et al. A randomized, controlled, multicenter study of nab-paclitaxel plus cisplatin followed by surgery versus surgery alone for locally advanced esophageal squamous cell carcinoma (ESCC). *J Clin Oncol* (2022) 40(4_suppl):310–. doi: 10.1200/JCO.2022.40.4_suppl.310

frontiers | Frontiers in Immunology

TYPE Original Research
PUBLISHED 23 May 2023
DOI 10.3389/fimmu.2023.1161538

OPEN ACCESS

EDITED BY
Yeonseok Chung,
Seoul National University,
Republic of Korea

REVIEWED BY
Frank Momburg,
German Cancer Research Center (DKFZ), Germany
Sébastien Wälchli,
Oslo University Hospital, Norway
Malcolm John Wyness Sim,
University of Oxford, United Kingdom

*CORRESPONDENCE
Nan Mou
nan.mou@genbase.com.cn
Chenlei Wen
tianzewcl@hotmail.com
Baiyong Shen
shenby@shsmu.edu.cn
Qian Zhan
zhanxi80@126.com

†These authors have contributed equally to this work and share first authorship

RECEIVED 08 February 2023
ACCEPTED 08 May 2023
PUBLISHED 23 May 2023

CITATION
Ai Q, Li F, Zou S, Zhang Z, Jin Y, Jiang L, Chen H, Deng X, Peng C, Mou N, Wen C, Shen B and Zhan Q (2023) Targeting KRAS^{G12V} mutations with HLA class II-restricted TCR for the immunotherapy in solid tumors.
Front. Immunol. 14:1161538.
doi: 10.3389/fimmu.2023.1161538

Targeting KRAS^{G12V} mutations with HLA class II-restricted TCR for the immunotherapy in solid tumors

Qi Ai[1,2,3†], Fanlu Li[1,2,3†], Siyi Zou[1,2,3], Zehui Zhang[1,2,3], Yangbing Jin[1,2,3], Lingxi Jiang[1,2,3], Hao Chen[1,2,3], Xiaxing Deng[1,2,3], Chenghong Peng[1,2,3], Nan Mou[4*], Chenlei Wen[1,2,3*], Baiyong Shen[1,2,3*] and Qian Zhan[1,2,3*]

[1]Department of General Surgery, Pancreatic Disease Center, Ruijin Hospital, Shanghai Jiao Tong University School of Medicine, Shanghai, China, [2]Research Institute of Pancreatic Diseases, Shanghai Jiao Tong University School of Medicine, Shanghai, China, [3]State Key Laboratory of Oncogenes and Related Genes, Institute of Translational Medicine, Shanghai Jiao Tong University, Shanghai, China, [4]Department of Cell Therapy, Shanghai Genbase Biotechnology Co., Ltd, Shanghai, China

KRAS mutation is a significant driving factor of tumor, and KRAS^{G12V} mutation has the highest incidence in solid tumors such as pancreatic cancer and colorectal cancer. Thus, KRAS^{G12V} neoantigen-specific TCR-engineered T cells could be a promising cancer treatment approach for pancreatic cancer. Previous studies had reported that KRAS^{G12V}-reactive TCRs originated from patients' TILs could recognized KRAS^{G12V} neoantigen presented by specific HLA subtypes and remove tumor persistently *in vitro* and *in vivo*. However, TCR drugs are different from antibody drugs in that they are HLA-restricted. The different ethnic distribution of HLA greatly limits the applicability of TCR drugs in Chinese population. In this study, we have identified a KRAS^{G12V}-specific TCR which recognized classII MHC from a colorectal cancer patient. Interestingly, we observed that KRAS^{G12V}-specific TCR-engineered CD4$^+$ T cells, not CD8$^+$ T cells, demonstrated significant efficacy *in vitro* and in xenograft mouse model, exhibiting stable expression and targeting specificity of TCR when co-cultured with APCs presenting KRAS^{G12V} peptides. TCR-engineered CD4$^+$ T cells were co-cultured with APCs loaded with neoantigen, and then HLA subtypes were identified by the secretion of IFN-γ. Collectively, our data suggest that TCR-engineered CD4$^+$ T cells can be used to target KRAS^{G12V} mutation presented by HLA-DPB1*03:01 and DPB1*14:01, which provide a high population coverage and are more suitable for the clinical transformation for Chinese, and mediate tumor killing effect like CD8$^+$ T cells. This TCR hold promise for precision therapy in immunotherapy of solid tumors as an attractive candidate.

KEYWORDS

KRAS G12V mutation, T cell receptor-engineered-T cell, immunotherapy, human leukocyte antigen-DPB*0301, human leukocyte antigen-DPB*1401, solid tumor

1 Introduction

Pancreatic ductal adenocarcinoma (PDAC) is mostly diagnosed in advanced stage, and the five-year survival rate is less than 9%, which is a difficult problem in human refractory cancer (1). Although immunotherapy has significant efficacy in many malignant tumors (2–5), for PDAC, many clinical trials such as immune checkpoint inhibitors, cancer vaccines, adoptive cellular immunotherapy and so on show unsatisfactory efficacy, and the key factor is its immunosuppressive tumor microenvironment (6, 7). T cell infiltration is positively correlated with the improvement of PDAC clinical outcome, and the overall survival time of PDAC patients with high effect T cell infiltration is longer (8–10). Preclinical studies have proved the feasibility of isolating and amplifying TIL from PDAC and other solid tumors *in vitro* (11, 12). Therefore, the therapeutic strategy of using antigen-specific recombinant T cells to accurately target tumor cells to overcome the problem of immunosuppressive microenvironment is a promising treatment. With the development of new antigen identification, single cell sequencing and recombinant TCR construction, adoptive cell therapy (ACT) has become a powerful strategy for the treatment of cancer (13–16). The infusion of a large number of tumor effector T cells specific to neoantigen can accurately clear the tumor. In addition, the injected T cells can also differentiate into memory T cells to maintain effective effector function and achieve the goal of long-term treatment (17). Compared with CAR, TCR can recognize almost all intracellular and cell surface antigens through MHC restriction system, and can detect lower levels of antigens to achieve hypersensitive recognition (18). In addition, under high antigen pressure, despite the restriction of HLA, TCR-T cells have higher expansion efficiency and lower expression of co-suppressor molecules than CAR-T cells (19). Clay TM et al. reported for the first time that transferring TCR gene into PBL of melanoma patients can produce CTL with anti-tumor response *in vitro* (20). Compared with peripheral blood T cells, natural TIL obtained from resected tumor suspensions or fragments has higher specific T cell concentration, but due to the malignant microenvironment of tumors, TIL is mostly aging, failure and sensitive to apoptosis, which weakens the long-term survival of functional T cells (21, 22). Therefore, the extraction of sensitive and effective effector T cells from TIL and T cell receptor modification may improve the tumor immunosuppressive microenvironment, which can greatly enhance the efficacy of ACT. Many TCR-T products based on $CD8^+$ T cells have been tested in clinical trials (23, 24), most of which are aimed at melanoma. Paul F Robbins et al. have demonstrated that adoptive autologous T cells ($CD8^+$ T cells account for more than 2/3) transduced by T cell receptor (TCR) targeting NY-ESO-1 can mediate tumor regression in patients with metastatic melanoma and synovial cell sarcoma, with response rates of 45% and 67% respectively (25). In addition to the fact that effector $CD8^+$ T cells can be used as the main killing effector cells of recombinant TCR-T cells, $CD4^+$T cells have also been shown to excrete cytokines IFN-γ and tumor necrosis factor (TNF) through a variety of mechanisms, thus eliminating tumor cells *in vivo* independently of $CD8^+$ T cells to play an anti-tumor effect (26–32). Therefore, it can also construct recombinant TCR as effective memory cells to kill tumor cells. Eric Tran et al. demonstrated that the tumor infiltrating lymphocytes (TIL) of metastatic lung tumors from patients with metastatic cholangiocarcinoma contain $CD4^+$ T cells that recognize ERBB2IP mutations expressed in the tumor, and reactive $CD4^+$ T cells are dominant. Tumor regression was observed in all lesions after transfusion of ERBB2IP mutation-specific $CD4^+$ T cells into the patient. Subsequent experiments showed that these $CD4^+$ T cells were effective memory $CD4^+$ T cells with cytolytic potential (33).

The selection of appropriate tumor antigens has always been a challenge to construct recombinant engineering T cell targets. KRAS gene is the most frequently mutated oncogene in cancer, 95% of PDAC patients show KRAS oncogene mutations, and KRAS mutations are often associated with poor prognosis and drug resistance of tumors (34, 35). Codon 12 of KRAS, such as G12V, G12D, G12C, etc, has the highest mutation frequency in pancreatic cancer, colorectal cancer and non-small cell lung cancer, accounting for about 90% of all KRAS mutations (35). Among them, KRAS G12V and G12D mutations are the most common, accounting for about 60% of pancreatic cancer, 20% of colorectal cancer, and 8% of non-small cell lung cancer (36, 37). Therefore, KRAS G12V and G12D mutations are ideal targets for PDAC (38–40). Eric Tran et al. found a polyclonal $CD8^+$ T cell response to mutant $KRAS^{G12D}$ from tumor infiltrating lymphocytes obtained from a patient with metastatic colorectal cancer, and infused HLA-C*08:02-restricted recombinant TCR-T cells targeting $KRAS^{G12D}$ into the patient, and observed the objective regression of the tumor (41). Rom Leidner et al. treated a patient who had progressive metastatic pancreatic cancer with a single infusion of 16.2×10^9 autologous HLA-C*08:02–restricted TCR-engineered T cells targeting mutant KRAS G12D, and mediated the objective regression of metastatic pancreatic cancer (42).

Here, we isolated and screened a $KRAS^{G12V}$-specific TCR derived from $CD4^+$ T cells of patient's TILs. Then we identified the HLA restriction of the TCR as HLA-DPB1*03:01 and DPB1*14:01, and tested the neoantigen epitopes and key amino acids of the $KRAS^{G12V}$ mutation. In order to validate that this neoantigen-reactive TCR could recognize $KRAS^{G12V}$ mutation, we constructed the $KRAS^{G12V}$-specific TCR-engineered $CD4^+$ T cells and $CD8^+$ T cells, and co-cultured them with APC cells and PDAC cell lines loaded with mutant peptides. Notably, we investigated the TCR specificity in functional assays of $CD4^+$ T cells but not $CD8^+$ T cells, indicating the restriction of this TCR for $CD4^+$ T cells. We then validated the antitumor activity of $KRAS^{G12V}$ specific TCR *in vivo* by xenograft mouse model, and found that treatment with $KRAS^{G12V}$-specific TCR could significantly reduce tumor growth. Taken together, we proved the effectiveness of this $KRAS^{G12V}$-specific TCR and expanded the available clinical subtypes of HLA for the development of TCR-based ACT.

2 Materials and methods

2.1 Cell lines and cell culture

SW620, CFPAC-1, 293T were purchased from ATCC. During the whole duration of this study, all cell lines were regularly tested negative for mycoplasma contamination. SW620 was cultured in RPMI1640 media (Gibco) supplemented with 10% fetal bovine serum (FBS, Gibco), 2 mM L-glutamine, and 1X penicillin/streptomycin (All

from Thermo Fisher Science). CFPAC-1 and 293T were cultured in DMEM media (Gibco) supplemented with 10% fetal bovine serum, 2 mM L-glutamine, and 1X penicillin/streptomycin. The cell lines usually kept in culture no more than two months.

2.2 Patients and HLA typing of patients

This study was approved by Ethics Committee of Ruijin Hospital of Shanghai Jiao Tong University. Written, informed consent was obtained from all patients. All patients studied were histologically diagnosed with CRC or PDAC and had a confirmed $KRAS^{G12V}$ mutation by whole-exome sequencing (Genergy Bio-Technology, Shanghai). B13 patient was diagnosed with CRC, and the tumor stage of B13 patient is IIIB (T3N1M0). Patient lymphocytes from peripheral blood were genotyped for HLA class II by high-resolution, high-throughput HLA genotyping with deep sequencing (Tissuebank, Shanghai) and found to be HLA-DPB1*03:01 (Supplementary Table S1).

2.3 Isolation and expansion of TILs

After being washed twice by the Dulbecco's Phosphate-Buffered Saline (DPBS, Thermo Fisher), fresh tumor samples were chopped into small pieces about 2-4 mm, and then cultured in 24-well plates, with Tumor infiltrating T Lymphocytes (TIL) media [X-Vivo15 (Lonza, BE02-060F) +25 mM Hepes+2% human AB Serum +6000 IU/ml IL2 (All from Thermo Fisher)]. Media would be changed every 2-3 days until Tumor infiltrating T Lymphocytes (TILs) converged to 60%-80% (containing about $0.5\text{-}3.0\times10^6$ TILs) of one 24-well plate. Amplified TILs were harvested and stored in CryoStor CS10 (Sigma-Aldrich, C2874) cryopreservation solution.

2.4 Antigen presentation mRNA or peptide preparation

The whole gene containing mutated KRAS genes (e. g. G12V, G12D) was synthesized and linked to LAMP3 signal peptide (leading sequence) to form LAMP3 LS-KRASmut, added with Xenopus globin UTR at both sides, and then cloned into a pcDNA3.1 plasmid containing prokaryotic T7 promotor, eukaryotic promotor and ORIP replication starting point. mRNA was transcribed by mMessage mMachine™ T7 Transcription Kit (Invitrogen, AM1344) as manufacturer's instructions *in vitro*, packed in 10 μg/tube, and stored at -80°C. A long peptide of 23-25 length (HPLC, purity > 95%) was synthesized from mutated KRAS, dissolved into 10mg/ml with DMSO, and stored at -80°C.

2.5 Antigen-presenting cells and $KRAS^{G12V}$ mRNA loading assay

Peripheral blood mononuclear cells (PBMCs) from patients were isolated by Ficoll-Paque gradient centrifugation and cryopreserved for generating LCLs and DCs. Specifically, $0.5\text{-}1.0\times10^7$ PBMCs were resuspended in RPMI media supplemented with 10% fetal bovine serum (FBS) and infected with EBV supernatant from the marmoset cell line B95.8 to be induced into immortalized B cells called lymphoblastoid cell line (LCL). During the induction period, half of the culture medium was changed every 7 days. After being cultured for 3 to 4 weeks, the induced LCL were amplified and cryopreserved in cell culture freezing medium. Monocyte-derived immature dendritic cells (DCs) were sorted by CD14 separate magnetic beads using MACS CD14 Isolation Kit (Miltenyi Biotec, 130050201) according to the manufacturer's instructions, and then cultured in DC induced media [AIM-V medium (Gibco, 12055091) +2% Human AB serum +1000 IU/ml IL4 + 1000 IU/ml granulocyte-macrophage colony-stimulating factor (GM-CSF) (All from Thermo Fisher)]. Induced DCs were cultured in fresh media on the third day and cryopreserved on days 5 to 6. Mature DCs were loaded with mRNA of KRAS G12V mutations by electroporation. In brief, messenger RNA coding KRAS G12V mutation was produced by CHINESE PEPTIDE as instructed by the manufacturer. Mature DCs or LCL were resuspended in Resuspension Buffer R at a finally density of 1.0×10^7 cells/ml by The Neon™ Kits (MPK10096, Invitrogen), and then added 100 μl cell suspension to the tube containing 5-8 μg mRNA and gently mix. Later, the cell-mRNA mixture was aspirated into the Neon™ Tip and electroporated at 1500 V for one pulse and 30 ms with the Neon™ device (MPK5000, Invitrogen) as instructed by Neon™ Transfection System User Guide. After that, transfected DCs or LCL were resuspended in the complete medium and transferred to the 24-well plate. GFP control was set to assess transfection efficiency by fluorescent microscopy.

2.6 Screening of neoantigen-specific T cells and Single-cell TCR sequencing

Transfected DCs or LCLs were used as APC to stimulate TILs for cytotoxic T lymphocyte (CTL) induction. 1.2×10^6 TILs were co-cultured with pulsed or non-pulsed 0.5×10^5 DCs cells or 4×10^5 LCLs in X-Vivo15 medium in 96-well plate. The supernatant of the culture medium was collected after 16 hours of culture, and the release of IFN-γ in supernatant was determined by Human IFN-γ Flex Set (BD Bioscience, 558269) to evaluate T cells' ability of specifically identifying and killing APCs. Neoantigen-specific T cells were stained with CD3, 41-BB, PI (propidium iodide solution) and analyzed by flow cytometry to sort out PI-/CD3-/41BB+ T cell group. Specifically, 1×10^6 TILs stimulated by APCs were re-suspended in flow buffer (DPBS solution containing 1% human AB serum and 2 mM EDTA), added with CD3/CD137 antibody and PI, incubated at 4 °C for 1 hour, then washed with flow buffer twice, and sorted by BD FACSAiraII flow sorter. The sorting population was PI-, CD3+ and CD137+. The selected cells were stored in RPMI1640 medium containing 10% human AB serum and placed on ice. The collected sorted cells (PI-, CD3+, CD137+) were centrifuged at 4 °C, 300 g for 10 minutes, then washed with DPBS twice, and re-suspended in DPBS. The sorted T cells were used for the following TCR sequencing analysis by 10X genomics Single Cell Sequencing. For the quality inspection and counting of

single cell suspension, the cell survival rate is generally required to be more than 80%. The qualified cells are washed and re-suspended to prepare suitable cell concentration at 700~1200 cells/μl for computer operation of 10X Genomics Chromium™ system. Using 10X Genomics Chromium™ system, gel Bead with sequence tags, sorted T cells and reagent premixed liquid and oil were loaded into their respective injection channels, a "double cross" cross system was formed through the microfluidic channel network to finally emerge a single-cell micro-reaction system GEMs wrapped by oil droplets. The single cell was isolated by gel beads, and then the mRNA molecule was released by cell cleavage and reverse-transcribed into cDNA by the polyT primer. The V (D) J region was amplified by a pair of primers near the 5-terminal UTR region of the V (D) J region and the gene C region. During the amplification process, the unique molecular tag (UMI) of the cell marker and transcript marker were introduced, and the amplified products were digested with restriction endonuclease to produce the second generation sequencing library. Finally, the high-throughput sequencing is carried out by using the double-ended sequencing mode of Illumina platform. The Cell Ranger- mkfastq subroutine was used to convert the sequencing data of BCL format into FastQ format. Using FastQC software to analyze the quality control of preprocessed data. Cell Ranger- VDJ subroutine was used to assemble the V (D) J region sequence of TCR gene of every single cell. IMGT database (https://support.10xgenomics.com/single-cell-vdj) and VDJ database (https://vdjdb.cdr3.net/) were used to analyze the results, and Loupe V (D) J Browser was used for the visualization of analysis results.

2.7 Synthesis and verification of recombinant TCR

Single cell sequencing data were analyzed and T cell clones were selected for verification. TCRVα and TCRVβ chains were synthesized and linked to mouse TCR constant region, and P2A (self-cleaving 2A peptide, 2A) sequence was used to link TCRα and TCRβ to form TCRVα-mTCRα-P2A-TCRVβ-mTCRβ structure, which was cloned into lentivirus shuttle vector (GV401) as manufacturer's instructions. Transfected 293T cells with lentivirus shuttle vector as manufacturer's instructions to package into lentiviral vector, and harvested supernatants after 24 h and 48 h of incubation. Human peripheral blood lymphocytes from different healthy donors (n=4) were used. PBMC (Sailybio, SLB-HP100B/200365) were activated in 6-well plate coated with CD3 (OKT3) and CD28 (15E8) antibody at 10^6 cells/ml for 24 hours, then were transduced with lentiviral vector containing TCR and cultured for 6-8 days for TCR screening. The transduced T cells were collected and washed with FACS buffer. 1×10^6 modified T cells were added with mouse TCRβ constant region antibody for staining to detect the expression of recombinant TCR. Antigen presenting cells and the prepared TCR-T cells were co-cultured as 1:1 in the RPMI1640 medium containing 2% FBS in 96Well-plate overnight. The specific IFN-γ release in the supernatant was determined to verify the specificity of recombinant TCR to Neoantigen.

2.8 HLA restriction assay of TCR

Engineered-TCR T cells were incubated with LCLs loaded with neoantigen. The LCLs were from LCL bank (from Shanghai Jikai Genome Medical Technology Co., Ltd) which have been identified HLA restriction for each LCL lines and used as the antigen presenting cell line (Supplementary Table S3). Specifically, LCLs from different donors were loaded with KRAS G12V-T15 peptide (TEYKLVVVGAVGV, 10 μg/ml) and co-cultured with Mock T cells and engineered-TCR T cells in RPMI1640 culture medium containing 2% fetal bovine serum at the ratio of 2×10^4: 2×10^4, and TCR-T specific IFN-γ release was used to determine HLA restriction.

CIITA gene (Genebank ID: 4261) was overexpressed in SW620 and CFPAC-1 cells by CIITA lentiviral transfection to construct SW620-CIITA and CFPAC-1-CIITA cell lines. After that, HLA-DPB1*03:01 and HLA-DPA1*02:02 was overexpressed in SW620 and CFPAC-1 cells by HLA lentiviral transfection to construct SW620/CFPAC1-CIITA-DPB1*03:01 cell lines and SW620/CFPAC1-CIITA- DPA1*02:02-DPB1*03:01 cell lines. The above cells were collected and suspended in RPMI1640 medium and cultured at 37 °C for 2 hours, then washed twice with DPBS. Antigen presenting cells (modified SW620 or CFPAC-1) and B13.14.1 TCR-T cells were cultured overnight in RPMI1640 medium containing 2% fetal bovine serum as the ratio of 2×10^4: 2×10^4, and the release of IFN-γ in the supernatant was determined.

2.9 Determination of neoantigen epitopes and key amino acids

Synthetic peptides containing G12V mutant sites (TEYKLVVVGAVG, G12V-T3; YKLVVVGAVGVG, G12V-T6; EYKLVVVGAVG, G12V-T9; YKLVVVGAVG, G12V-T10; KLVVVGAVG, G12V-T11; TEYKLVVVGAV, G12V-T12; EYKLVVVGAV, G12V-T13; YKLVVVGAV, G12V-T14; TEYKLVVVGAVGV, G12V-T15; EYKLVVVGAVGV, G12V-T16; YKLVVVGAVGV, G12V-T17) and alanine substitution (Supplementary Table S4) were loaded into autologous LCL cells and co-cultured with TCR-T cells. Neoantigen epitopes and key amino acids were determined by IFN-γ release assay in the supernatant. Specifically, the 9-23 peptides were synthesized and then dissolved in DMSO. The autologous LCL cells of B13 patients were re-suspended in the RPMI1640 culture medium, adding the above peptides to the final concentration of 1 μg/ml. After incubating for 2 hours, they were washed twice with DPBS solution, and then re-suspended with RPMI1640 culture medium containing 2% fetal bovine serum to $2\times10^{5/}$ml. The antigen presenting cells loaded with peptides and B13.14.1 TCR-T cells were cultured overnight according to the ratio of 2×10^4: 2×10^4. The release of IFN γ in the supernatant was measured by the Human IFN-γ Flex Set (BD Bioscience, 558269).

By replacing the peptides of $KRAS^{G12V}$ epitopes with alanine one by one, the key amino acids involved in antigen presentation in $KRAS^{G12V}$ epitopes can be screened. Specifically, peptides of

$KRAS^{G12V}$ epitopes with alanine replaced were synthesized (Supplementary Table S4). IFN-γ or IL2 in the supernatant of antigen presenting cells co-cultured with B13.14.1 TCR-T were determined by the Human IFN-γ Flex Set (BD Bioscience, 558269).

2.10 Killing assay of Engineered-TCR T cells

SW620-CIITA-DPB1*03:01 or CFPAC-1-CIITA-DPB1*03:01 cells were re-suspended in RPMI1640 medium containing 2% FBS and inoculated in 96-well plates as 10^{4}/well. Mock-T, Engineered-TCR-$CD4^+$ T cells and Engineered-TCR-$CD8^+$ T cells were added separately according to the proportion of 10:1, 3:1, 1:1, 0.3:1, 0.1:1. After 48 hours of co-incubation, the medium was removed and washed with 200 µl DPBS solution per well. 100 µl RPMI1640 medium containing 2% FBS and 10 µl CCK8 detection reagent (Cell Counting Kit-8, Sigma Aldrich, 96992) were added to each well and incubated at 37 °C for 1 hour to detect 450nm light absorption. Killing rate was:

Specific Lysis%= 1 - (light absorption value/control hole light absorption value)

2.11 Engineered-TCR-T cells functional avidity determination

Autologous LCL cells or the SW620-DPB1*03:01 were loaded with different concentrations of $KRAS^{G12V}$-T15 peptide (TEYKLVVVGAVGV) and corresponding wild type peptide (TEYKLVVVGAGGV) (10 µg/ml, 1 µg/ml, 0.1 µg/ml, 0.01 µg/ml, 0.001 µg/ml) at 37 °C for 2 hours, then washed twice with DPBS. The antigen-presenting cells or the SW620-DPB1*03:01 and the engineered-TCR-T cells were co-cultured overnight in RPMI1640 medium containing 2% fetal bovine serum according to the ratio of 2×10^{4}: 2×10^{4}, and the release of IFN-γ or IL-2 in the supernatant was determined.

2.12 IFN-γ and IL-2 determination assay

Antigen presenting cells were loaded with or without mRNA of KRAS G12V mutations, or a range of indicated concentrations of synthetic peptides as previously described. Neoantigen-reactive $CD4^+$ T cells clones were incubated with the antigen presenting cells at a ratio of 1:1-1:4 in X-Vivo15 medium overnight. The release of IFN-γ and IL-2 in the supernatant were determined by the Human IFN-γ Flex Set (BD Bioscience, 558269) and Human IL-2 Flex Set (BD Bioscience, 558270). Specifically, the IFN-γ or IL-2 standard (2500 pg/ml) was added with Assay Diluent to dilute by gradient (1: 2, 1: 4, 1: 8, 1: 16, 1: 32, 1: 64, 1: 128, 1: 256), and using 500 µl Assay Diluent as negative control tube (0 pg/ml). The total amount of capture microspheres and antibodies detected by diluted PE markers needed to be diluted in the test were determined according to 50 µl/sample, respectively. The volume of each captured microsphere and PE labeling antibody detection reagent were determined according to 1 µl/sample, respectively. Mix the capture microsphere with the capture microsphere diluent in a tube and mark "mixed capture microsphere". Dilute the PE antibody detection reagent with the detection antibody diluent, mix it in a tube, and label "mixed PE to detect antibody". Use the first 4°C to avoid light. 50 µl gradient diluted standard substance was added to each tube of standard quality control, and 50 µl supernatant to be tested in each sample tube. Scrolled mixed microspheres for at least 5 seconds, and added 50 µl mixed microspheres per tube. Mixed gently and incubated at room temperature for 1 hour. Then 50 µl PE labeled antibody was added to each tube and mixed gently and incubated at room temperature for 2 hours. Added 1ml lotion to each tube and centrifuged 200 g for 5 minutes. Carefully absorbed or gently poured out the supernatant, and add 300 µl lotion per tube to resuscitate cells. Samples should be tested as soon as possible after the instrument is adjusted. After the sample was collected (FCS2.0 format), the standard curve was drawn and the data was analyzed by CBA special analysis software FCAPArrayv1.0.

2.13 Mouse xenograft models

SW620-CIITA-DPB1-Luc single clone was generated (SW620 was transfected with CIITA, HLA-DPB1*03:01 and firefly luciferase) and then was injected subcutaneously into NOD-scid $IL2r\gamma^{null}$ (NSG) mice to establish xenograft. TCR-T cells treatment that intravenous injections of 1×10^{7} engineered $CD4^+$, $CD8^+$ or mixed T cells ($CD4^+$: $CD8^+$= 1:1) expressing B13.14 TCR separately was given when the tumor size reached about 50 mm^3 after tumor inoculation. Control mice received no treatment (Mock) T cells. The tumor size was determined by measuring the vertical diameter of each tumor with a caliper, and the calculation formula was as follows: tumor volume (mm^3) = [(length) × (width) × (width)]/2. On day 9, 16 and 34, the mice were anesthetized by intraperitoneal injection of 0.7% pentobarbital sodium according to the dose of 10 µl/g and were imaged under the living imager to observe the fluorescence.

2.14 Statistics

Data analysis was performed using GraphPad Prism v8.0 (GraphPad Software, CA). Data represent mean ± SD of triplicates. Statistical comparison was conducted with Student's test, and two-way ANOVA.

3 Results

3.1 Isolation of $KRAS^{G12V}$-reactive T cells from TIL and TCR sequencing of sorted $KRAS^{G12V}$-reactive T cells

To obtain $KRAS^{G12V}$-reactive T cells, we collected surgically resected tumor tissues of 16 patients who were diagnosed with CRC and 15 patients who were diagnosed with PDAC as experimental

samples for TIL, and obtained their peripheral blood mononuclear cells (PBMCs) for DCs and LCLs (Figure 1). PBMCs were induced to lymphoblastoid cell line (LCL) by EBV (Figure 2A). TIL clones were subsequently isolated and assessed with their activity and specificity. To screen tumor-reactive TILs, TILs from different tumor specimens were separately co-cultured with mature dendritic cells (DCs) and LCLs loaded with $KRAS^{G12V}$ mRNA. As a result, we found that tumor fractions TIL-B13.1, TIL-B13.4 and TIL-B13.14 from B13 patient who was diagnosed with colorectal cancer produced a significantly higher level of IFN-γ than other TIL fractions and its control group (Figure 2B).

B13.1 TILs, B13.4 TILs and B13.14 TILs stimulated by APC cells were sorted by BD FACSAirall flow sorter and then were sequenced their TCRα and TCRβ chains by 10X genomics Single Cell Sequencing. Top three TIL clonotypes were identified, and the percentages of the first ranked TIL clonotypes were 36.55% in B13.1 TILs group, 87.98% in B13.4 TILs group, 47.98% in B13.14 TILs group, respectively (Figure 2C). Dominant TCRα and dominant TCRβ chains were identified, TRAV26-1*01-J12*01 was paired with TRBV3-1*01-D1*01-J2-7*01 in B13.1 TILs group, TRAV5*01-J6*01 was paired with TRBV7-9*01-D1*01-J2-1*01 in B13.4 TILs group, and TRAV3*01-J10*01 was paired with TRBV19*01-D1*01-J1-6*02 in B13.14 TILs (Table 1), which suggested that the first ranked TCR could be most likely tumor-reactive TCR.

3.2 $KRAS^{G12V}$-reactive TCR-engineered T cells recognized and killed HLA-DPB1*03:01 tumor cells loaded with $KRAS^{G12V}$

To obtain $KRAS^{G12V}$-reactive TCR-T cells, the first ranked TCRs were used for function validation for each TIL group (Table 1). $KRAS^{G12V}$-reactive TCR gene were synthesized in the order of TRAVmCa-P2A-TRBVmCb as the results of 10X genomics Single Cell Sequencing (Table 2) to construct recombinant TCR modified T cells. The modified TCR-T cells were added with mouse TCRβ constant region antibody for staining to detect the expression of recombinant TCR, and the results showed that all 6 recombined TCRs from patient B13 could indeed be expressed in allogeneic T cells (Supplementary Figure S1).

To evaluate the ability of these TCR-T cells to specifically identify and mediate killing functions in response to $KRAS^{G12V}$ *in vitro*, We performed a co-culture of recombinant TCR modified T cells with autologous LCL cells which were electroporated with $KRAS^{G12V}$ mRNA, and the results showed that B13.14.1 TCRs could specifically recognize KRAS G12V mutation but not wild type KRAS (Figures 3A, B).

The patient was genotyped and found to be HLA-DPB1*03:01 (Supplementary Table S1). SW620 (colorectal cancer lymph node metastasis) contains $KRAS^{G12V}$ homozygous mutation, and CFPAC-1 cell line (pancreatic cancer) contains $KRAS^{G12V}$ heterozygous mutation. Their HLA-DP matching is shown in the table (Supplementary Table S2). In order to verify the HLA restriction, we performed a co-culture experiment using EBV-LCL cells (Supplementary Table S3) from LCL bank with B13.14.1 TCR-engineered T cells or mock T cells, the results suggested that the B13.14.1 TCR can recognize the $KRAS^{G12V}$ antigenic peptides presented not only by HLA-DPB1*03:01 but also by HLA-DPB1*14:01 (Figure 3C). To verify that the $KRAS^{G12V}$ peptides are endogenously processed and presented on the cells with corresponding HLA molecules, we overexpressed CIITA gene and HLA gene in SW620 and CFPAC1 (Supplementary Table S2, Supplementary Figure S2), and then co-cultured B13.14.1 TCR-engineered T cells or mock T cells with SW620, SW620-CIITA, SW620-CIITA-DPB1*03:01, SW620-CIITA-DPA1*02:02-DPB1*03:01, CFPAC-1, CFPAC1-CIITA, CFPAC1-CIITA-DPB1*03:01 and CFPAC1-CIITA-DPA1*02:02-DPB1*03:01, respectively. We here demonstrated that B13.14.1 TCR can recognize the restricted G12V mutation presented by HLA-DPB1*03:01, and can be presented better with both HLA-DPB1*03:01 and HLA-DPA1*02:02 (Figures 3D, E).

To further evaluate the killing efficiency and characteristics of B13.14.1 TCR-engineered T cells, SW620/CFPAC1-CIITA-DPA1*02:02-DPB1*03:01 were co-cultured with Mock T cells, B13.14.1 TCR-engineered $CD4^+$ T cells, and B13.14.1 TCR-engineered $CD8^+$ T cells, respectively, with different effector/target cell ratios, i.e., 10:1, 3:1, 1:1, 1:3, and 1:10. The results showed that B13.14.1 TCR-engineered T cells could kill tumor cells in a dose-dependent manner and the killing effect of $CD4^+$ T cells was superior to $CD8^+$ T cells, indicating its dependence on CD4 (Figures 3F, G).

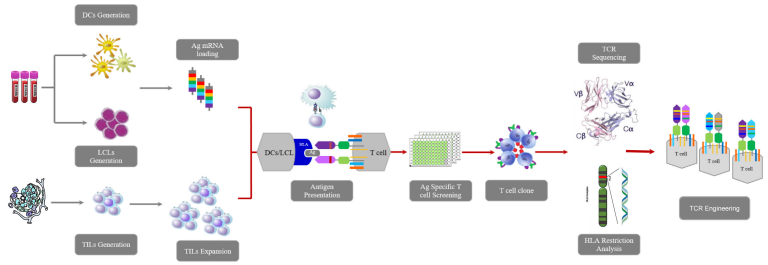

FIGURE 1
Workflow of this research including TILs isolation, TCR sequencing, tumor-reactive TCR-engineered T cells construction, determination of HLA restriction, tumor killing assay *in vivo and vitro*.

10.3389/fimmu.2023.1161538

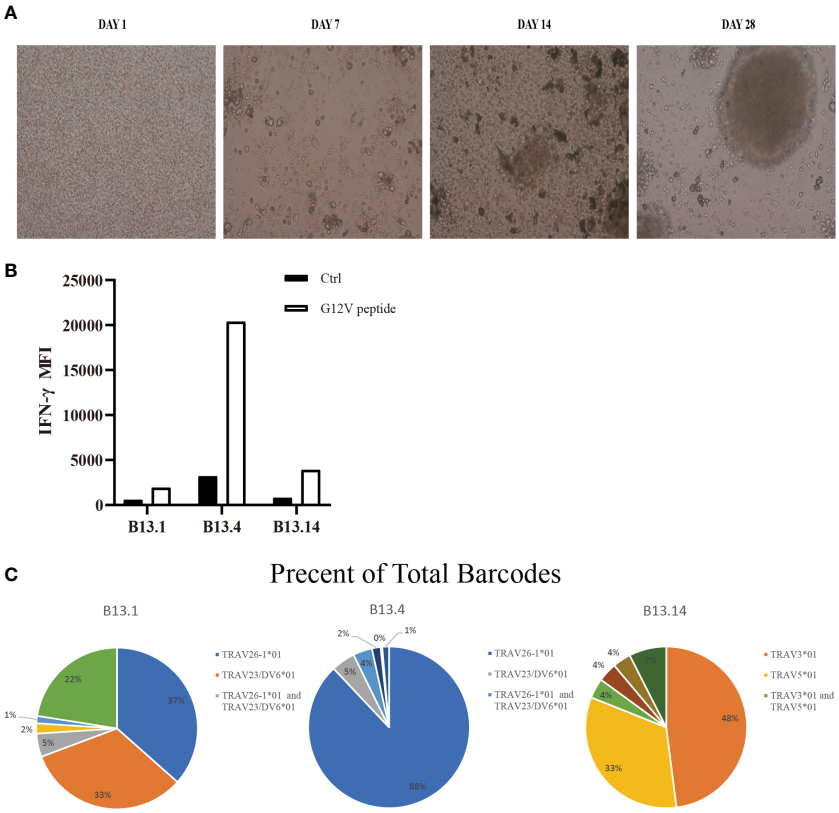

FIGURE 2
Screen of tumor-reactive TILs and identification of TCRα and TCRβ sequences of sorted $CD4^+$ T cells. **(A)** Representative images of the process of LCLs inducement by EBV. **(B)** Flow Cytometry measuring secretion of INF-γ from B13.1, B13.4, B13.14 TILs following the co-culture with LCLs loaded with G12V peptide or wild type peptide. **(C)** Frequencies of top five TILs clonotypes of B13.1, B13.4, B13.14 TILs, respectively.

3.3 Identification of $KRAS^{G12V}$ mutation epitopes and key amino acids

To further characterize the $KRAS^{G12V}$ mutation epitopes, 9-23 peptides containing G12V mutation were synthesized (Table 3) and loaded in the autologous LCLs to present the antigen to the B13.14.1 TCR-engineered T cells. The results of the release of the IFN-γ and IL-2 showed that G12V-T3, G12V-T9, G12V-T15 and G12V-T16 peptides could effectively induce IFN-γ release from B13.14.1 TCR-engineered T cells, of which G12V-T15 is the most effective, indicating that HLA-DPB1*03:01 could present the above peptides (Figures 4A, B). The results also suggested that the

TABLE 1 Top three TCR sequences of B13.1 TILs, B13.4 TILS and B13.14 TILs.

Clonotype	TRAV	TRAJ	TRBV	TRBJ	CDR3α	CDR3β	Clonotype Frequency
B13.1	TRAV26-1*01	TRAJ12*01	TRBV3-1*01	TRBJ2-7*01	CIVRVEGSSYKLIF	CASSQGGSYEQYF	36.55%
	TRAV23/DV6*01	TRAJ58*01	TRBV5-6*01	TRBJ2-7*01	CAASEETSGSRLTF	CASSWNLQASYEQYF	32.75%
	TRAV26-1*01 TRAV23/DV6*01	TRAJ12*01 TRAJ58*01	TRBV3-1*01 TRBV5-6*01	TRBJ2-7*01 TRBJ2-7*01	CIVRVEGSSYKLIF CAASEETSGSRLTF	CASSQGGSYEQYF CASSWNLQASYEQYF	4.68%
B13.4	TRAV5*01	TRAJ6*01	TRBV7-9*01	TRBJ2-1*01	CAEDAGGSYIPTF	CASSLEENEQFF	87.98%
	–	–	TRBV7-9*01	TRBJ2-1*01	–	CASSLEENEQFF	4.79%
	TRAV12-1*01 TRAV5*01	TRAJ7*01 TRAJ6*01	TRBV7-9*01	TRBJ2-1*01	CVVNSLWEQQTRF CAEDAGGSYIPTF	CASSLEENEQFF	3.82%
B13.14	TRAV3*01	TRAJ10*01	TRBV19*01	TRBJ1-6*02	CAVRDGRGGGNKLTF	CASSPGQRDNSPLHF	47.98%
	TRAV5*01	TRAJ6*01	TRBV7-9*01	TRBJ2-1*01	CAEDAGGSYIPTF	CASSLEENEQFF	33.06%
	TRAV3*01 TRAV5*01	TRAJ10*01 TRAJ6*01	TRBV7-9*01	TRBJ2-1*01	CAVRDGRGGGNKLTF CAEDAGGSYIPTF	CASSLEENEQFF	4.00%

10.3389/fimmu.2023.1161538

TABLE 2 TCR sequences of recombinant TCR modified T cells.

Clone Name	TCRα	TCRβ
B13.1.1	TRAV26-1*01, TRAJ12*01	TRBV3-1*01, TRBJ2-7*01
B13.1.2	TRAV23/DV6*01, TRAJ58*01	TRBV5-6*01, TRBJ2-7*01
B13.4.1	TRAV5*01, TRAJ6*01	TRBV7-9*01, TRBJ2-1*01
B13.4.2	TRAV12-1*01, TRAJ7*01	TRBV7-9*01, TRBJ2-1*01
B13.14.1	TRAV3*01, TRAJ10*01	TRBV19*01, TRBJ1-6*02
B13.14.2	TRAV5*01, TRAJ6*01	TRBV7-9*01, TRBJ2-1*01

peptide containing amino acid residues E (position 2) and G (position12) of the KRAS^{G12V} mutant peptides were essential for G12V epitope presentation and could effectively activate T lymphocytes and induce immune response to tumors with KRAS^{G12V} mutations.

Next, the key amino acids involved in antigen presentation in KRAS^{G12V} epitopes was screened by replacing the peptides of KRAS^{G12V} epitopes sequentially with alanine (i.e., "A") from position 1 to 13 (Supplementary Table S4). Investigation of the reactivity of B13.14 TCR-T cells against the autologous LCL cells loaded with these peptides revealed that the ability of B13.14.1 TCR-T cells to recognize KRAS G12V epitopes decreased after p3Y, p4K, p5L and p8V were mutated to alanine, especially p3Y, p4K and p5L (Figures 4C, D). Thus, these amino acid (p3Y, p4K, p5L and p8V) may be critical for DPB1*03:01 binding or TCR recognition to DPB1*03:01 and KRAS^{G12V} peptide complex, but the binding of the peptides to the MCH II remains to be verified.

3.4 High functional avidity of the KRAS^{G12V}-reactive TCR-engineered T cells to KRAS^{G12V} mutants

To further investigate the functional characteristics of B13.14.1 TCR-engineered T cells, we carried out a tumor cell line killing assay with autologous LCL cells or SW620-CIITA-DPB1*03:01 loaded with different concentrations of KRAS G12V-T15 peptide (TEYKLVVVGAVGV) and corresponding wild type peptide (TEYKLVVVGAGGV), i.e., 10 μg/ml, 1 μg/ml, 0.1 μg/ml, 0.01 μg/ml, 0.001 μg/ml. The killing efficacy is positively correlated with the concentrations of the peptide, and the B13.14.1 TCR-engineered T cells can recognize KRAS^{G12V} peptide loaded on autologous LCL cells and SW620-CIITA-DPB1*03:01 at a low concentration of <10 ng/ml (Figures 5A–C). Therefore, B13.14.1 TCR-engineered T cell could specifically secrete IFN-γ and IL-2 on encountering the antigen presenting cells in a dose-dependent manner, and it had high functional avidity and high specificity for KRAS^{G12V} mutants.

3.5 Treatment efficacy of KRAS^{G12V}-reactive TCR-engineered T cells in xenograft model

To test whether B13.14.1 TCR-engineered T cells had antitumor functions *in vivo*, we implanted subcutaneously the KRAS^{G12V}-positive SW620-CIITA-DPB1-luc into NOD-scid IL2rγ^{null} (NSG) mice. When tumor size reached about 50 mm^3, we treated them with B13.14.1 TCR transduced human CD4 T cells, CD8 T cells and the mixture of CD4 T cells and CD8 T cells intravenously, and set intravenous injection of Mock-T (untransduced T cell) and PBS as control groups. Recombinant TCR expression was determined by mTCRβ expression (Supplementary Figure S3). The results showed that the growth of tumors in mice treated with B13.14.1 TCR-engineered CD4$^+$ T cells was significantly suppressed compared with all control groups (compared with treatment with Mock T cells; $P < 0.0001$; Figures 6A, D). Through tacking B13.14.1 TCR-engineered T cells using human CD3 and mouse TCR constant region TCRβ antibody, we found that B13.14.1 TCR transduced CD4 T cell showed significantly higher expansion *in vivo* than other groups (compared with treatment with B13.14.1 TCR-engineered mix T cells; $P = 0.0024$; Figures 6B, C). The results indicated that B13.14.1 TCR-engineered T cells could inhibit the growth of SW620-DPB1*03:01 tumor, and exhibited the dependence on CD4.

4 Discussion

Adoptive TILs and CAR-T transfer-based immunotherapy is a promising therapeutic approach to eliminate a variety of tumors (43–45). However, the validity of adoptive cell therapy for most patients with solid tumors has not yet been fully proved (46, 47). PDAC is a highly immunosuppressive cancer type, and its TILs in the tumor immune microenvironment is often depleted and senile. Hence, the generation *in vitro* of TCR-engineered T cells targeting tumor-specific neoantigens would be a promising strategy to overcome the immunosuppressive status. Recent clinical researches on TCR-T therapy have promising results for curative tumor regression in solid tumors (25, 41, 42, 48). Currently, the choice of tumor-specific neoantigens for antitumor TILs is still a challenge. RAS mutations are the most frequent proto-oncogene mutations, in which KRAS mutation has the highest incidence in solid tumors (about 86% of the three RAS mutations), i.e., approximately 90% in pancreatic cancer and 40% in colorectal cancer (49, 50). About 60%-80% of KRAS mutations are found to be G12V and G12D in pancreatic cancer, and 20%-30% in colorectal cancer (51, 52). Therefore, KRAS^{G12V} may be a good target for pancreatic cancer. It has been reported that the frequency of the HLA-DPB1*03:01 in the Chinese Han population is approximately 3.5913% (N=4845), which ranks the 7th in frequency of DPB1 (53). HLA-DPB1*03:01 and DPB1*14:01 is 3rd rank of HLA-DPB1 alleles in Asian and Caucasian with 20-30% frequency. Also, HLA-DPB1*14:01 is the highest DPB1 alleles found in south Americans (>50%). In this study, we isolated and identified the

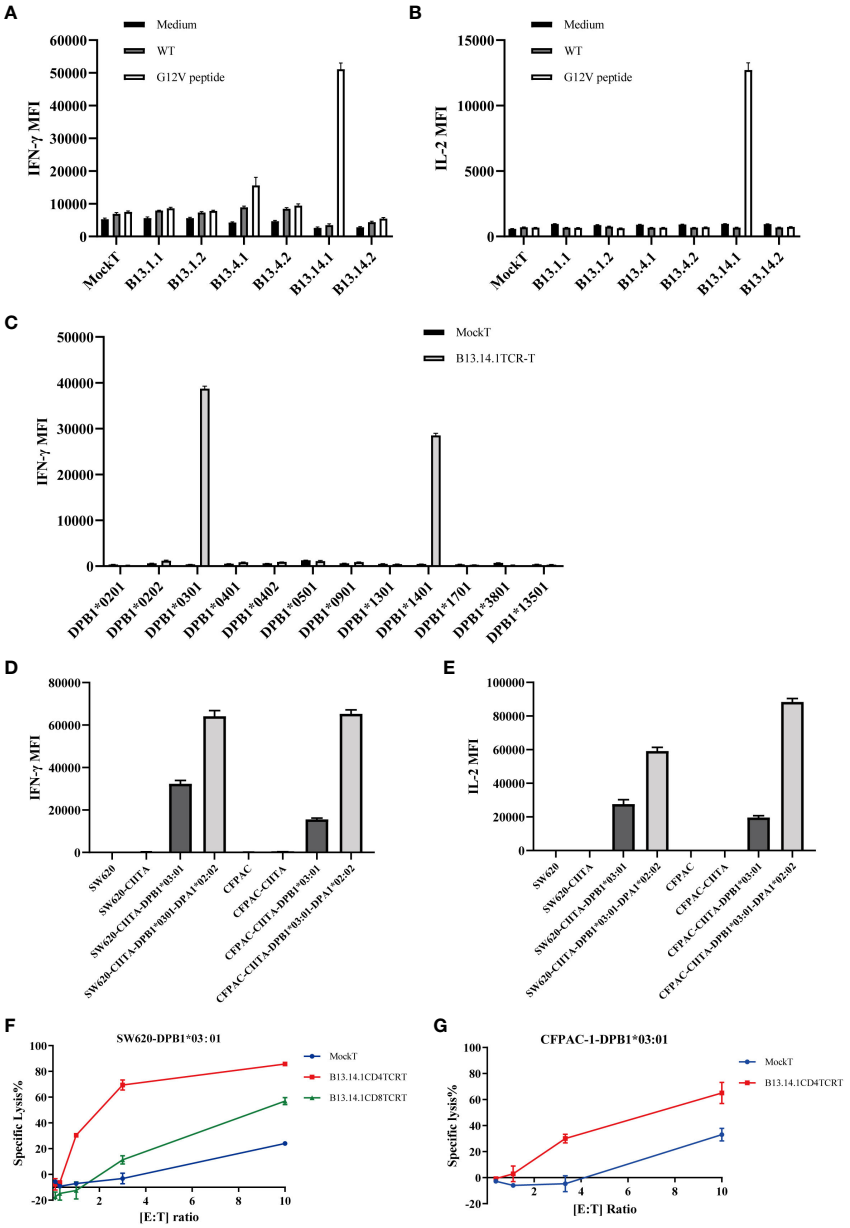

FIGURE 3
Function evaluation and HLA restriction determination of B13.14.1 TCR-CD4$^+$ T cells. **(A, B)** Flow Cytometry measuring secretion of INF-γ and IL-2 from B13.14.1 TCR-engineered T cells or Mock T cells stimulated by autologous LCLs electroporated with KRAS^{G12V} mRNA. **(C)** Flow Cytometry measuring secretion of INF-γ from B13.14.1 TCR-CD4$^+$ T cells or Mock T cells stimulated by EBV-LCLs from LCL bank loaded with KRAS^{G12V} mRNA. **(D, E)** Flow Cytometry measuring secretion of INF-γ and IL-2 from B13.14.1 TCR-CD4$^+$ T cells or Mock T cells stimulated by SW620, SW620-CIITA, SW620-CIITA-DPB1*03:01, SW620-CIITA-DPA1*02:02-DPB1*03:01, CFPAC-1, CFPAC1-CIITA, CFPAC1-CIITA-DPB1*03:01 and CFPAC1-CIITA-DPA1*02:02-DPB1*03:01, respectively. For **(A–E)**, each graph shows the mean results of three technical replicates from one donor, and each experiment has been performed with a different donor. **(F, G)** Specific lysis of SW620-DPB1*03:01 and CFPAC-1-DPB1*03:01 induced by B13.14.1 TCR-CD4$^+$ T cells under different effector cell/target cell ratios. Five different ratios (10:1, 3:1, 1:1, 1:3, and 1:10) were examined.

HLA-DPB1*03:01-restricted human TILs from patient's tumor tissue that recognize natural processed and presented epitopes in KRAS^{G12V} mutants, and cloned the TCRs to construct KRAS^{G12V}-reactive TCR-engineered CD4$^+$ T cells. The reason why the specific reaction TCR of KRAS^{G12V} mutation was not isolated in other tumor tissue samples may be that the infiltration density of TIL in tumor tissue samples is too low or the TIL itself is in a suppressed state with low activity, which is not enough to exert anti-tumor killing effect.

Our study not only obtained KRAS^{G12V}-reactive TILs but identified and isolated corresponding KRAS^{G12V}-reactive TCRs by single-cell TCR sequencing. In addition, B13.14.1 TCR could express stably in primary T cells and mediate the specific recognition of KRAS^{G12V}-HLA-DPB1*03:01 complex, leading to stronger antitumor response of efficient killing of target cells. However, the recombined TCR-T cells from B13.1 TILs and B13.4 TILs showed low secretion of IFN-γ, the reason may be that the sequences of reactive TCRs were not be founded by the 10X

10.3389/fimmu.2023.1161538

TABLE 3 List of KRAS G12V mutation peptides.

No.	Length	Amino acid sequences
G12V-T1	23	TEYKLVVVGAVGVGKSALTIQLI
G12V-T2	15	AVGVGKSALTIQLI
G12V-T3	12	TEYKLVVVGAVG
G12V-T4	11	VVVGAVGVGKS
G12V-T5	15	VGAVGVGKSALTIQ
G12V-T6	12	YKLVVVGAVGVG
G12V-T7	15	VVVGAVGVGKSALT
G12V-T8	12	LVVVGAVGVGKS
G12V-T9	11	EYKLVVVGAVG
G12V-T10	10	YKLVVVGAVG
G12V-T11	9	KLVVVGAVG
G12V-T12	11	TEYKLVVVGAV
G12V-T13	10	EYKLVVVGAV
G12V-T14	9	YKLVVVGAV
G12V-T15	13	TEYKLVVVGAVGV
G12V-T16	12	EYKLVVVGAVGV
G12V-T17	11	YKLVVVGAVGV
G12V-T18	14	TEYKLVVVGAVGVG
G12V-T19	16	TEYKLVVVGAVGVGK
G12V-T20	16	TEYKLVVVGAVGVGKS
G12V-T21	17	TEYKLVVVGAVGVGKSA

genomics Single Cell Sequencing. We also demonstrated that B13.14.1 TCR could recognized an additional HLA-DPB1 allele, HLA-DPB1*14:01, which can therefore broaden application of our TCR. The sequences of HLA-DPB1*14:01 and DPB1*03:01 differ by only one amino acid, which may explain why the TCR can respond to these two allotypes. The results of the high functional avidity of our TCR further supported its clinical efficacy. Besides, we compared the functional avidity of B13.14.1 TCR with 6F9 TCR which recognizes MAGEA3 p243-258 in HLA-DPB1*04:01 restricted manner (54) and founded that functional avidity of B13.14.1TCR is comparable with 6F9 TCR in the same assay format (peptide titrated on autologous LCL line). Interestingly, we found that the B13.14.1 TCR-engineered $CD4^+$ T cells had higher killing effect than $CD8^+$ T cells *in vivo and vitro*. In the immunodeficient mouse models, we found that the response of engineered-TCR $CD4^+$ T cells were more effective in antitumor immunity than $CD8^+$ T cells or mix T cells. The reason may be that the B13.14.1 TCR is derived from $CD4^+$ T cells.

Unlike MHC I which is broadly expressed in majority of tissues and tumor types, expression of MHC II is limited to antigen presenting cell, such as DC and B cell reported in previous publications. Some researches have showed the evidence of MHC II expression in normal tissue and different tumor types. Evidence of MHC II expression in normal tissue was concluded from that HLA-A, B, C, DRB1 and DQB1 matched unrelated hematopoietic cell transplantation patients with HLA-DPB1 mismatch informs risk of GVHD development (55). HLA-DPB1-mismatched donor-derived TCRs can recognize human autoantigens presented in recipient tissue HLA-DPB1, implying that HLA-DPB1 is expressed to a certain extent in recipient normal tissues. MHCII expression was reported in various tumor types originated from different tissues, such as melanoma, breast cancer, colorectal cancer, ovarian cancer, prostate cancer and NSCLC (56). In recent studies, expression of MHC II expression was reported in 77.7% of PDAC (49/63) using immunohistochemistry and half of tumor cells are expressing MHC II at moderate or high levels (57).

Previous studies on TCR-T cell therapy mostly developed MHC class I-restricted TCRs (58) and applied $CD8^+$ T cells for killing cells. However, immunotherapies based on $CD8^+$ T cells have shown the transient and weak immune response in most patients (59). Some studies showed evident clinical adverse events of $CD8^+$ T cell-therapies despite of its remarkable clinical responses (60, 61). In the meanwhile, the last 5 years have seen many reports recognizing the critical role of $CD4^+$ T cells driving anti-tumor immunity and in supporting anti-tumor $CD8^+$ T cell responses (62). $CD4^+$ T cell can infiltrate and recognize autologous tumor in a MHC II-restricted manner (28). High infiltration of $CD4^+$ T cell was associated with improved survival in pancreatic cancer patients while $CD8^+$ T cell infiltration didn't have an impact on overall survival (63). Furthermore, cytotoxic $CD4^+$ T cells in tumors predicts a clinical response in 244 metastatic bladder cancer patients with anti PDL1 therapy (64). Besides, single cell analysis reveals a $CD4^+$ T cell cluster is correlated with efficacy of PD1 blockade in NSCLC (65).

Neoantigen specific T cell may be the main player against human cancer, for example PD1/PDL1 blockade can restore antitumor activity of neoantigen specific tumor infiltrating lymphocytes in solid tumor. Evidence of antitumor activity of neoantigen specific $CD4^+$ T cell has been reported in different tumor types including breast cancer (33), melanoma (66), pancreatic cancer (42). Moreover, adoptive $CD4^+$ T cell therapy using HLA-DPB1*0401 restricted TCR recognizing MAGEA3 has been proved to be effective in 17 patients with metastatic cancer and 4/17 patients treated with DPB1*0401 restricted TCR-T cells showed durable clinical response (1CR, 3PR) (67). Proteasome processing of tumor antigens and presentation in MHC II are critical for tumor recognition by $CD4^+$ T cells. Lysosomal processing and presenting on MHC II of acquired exogenous antigen by tumor cells were considered to be the major antigen presentation pathway of human $CD4^+$ T cells (68). However, some studies showed that MHC II can efficiently present intracellular protein to human $CD4^+$ T cell in non-classical antigen processing pathways (69, 70). Interestingly, 80% of neoantigen specific TCRs can recognize autologous tumor cells in MHC II restricted manner which were isolated from 62 of 75 gastrointestinal cancer patients (71). A high proportion of MHC II-restricted neoantigen-specific TCRs can be isolated in more than 80% of different tumor types, suggesting that MHC II-presented neoantigens may be more prevalent in human cancers than previously realized. These studies have shown that $CD4^+$ T cells can promote the killing of tumor cells in various ways.

10.3389/fimmu.2023.1161538

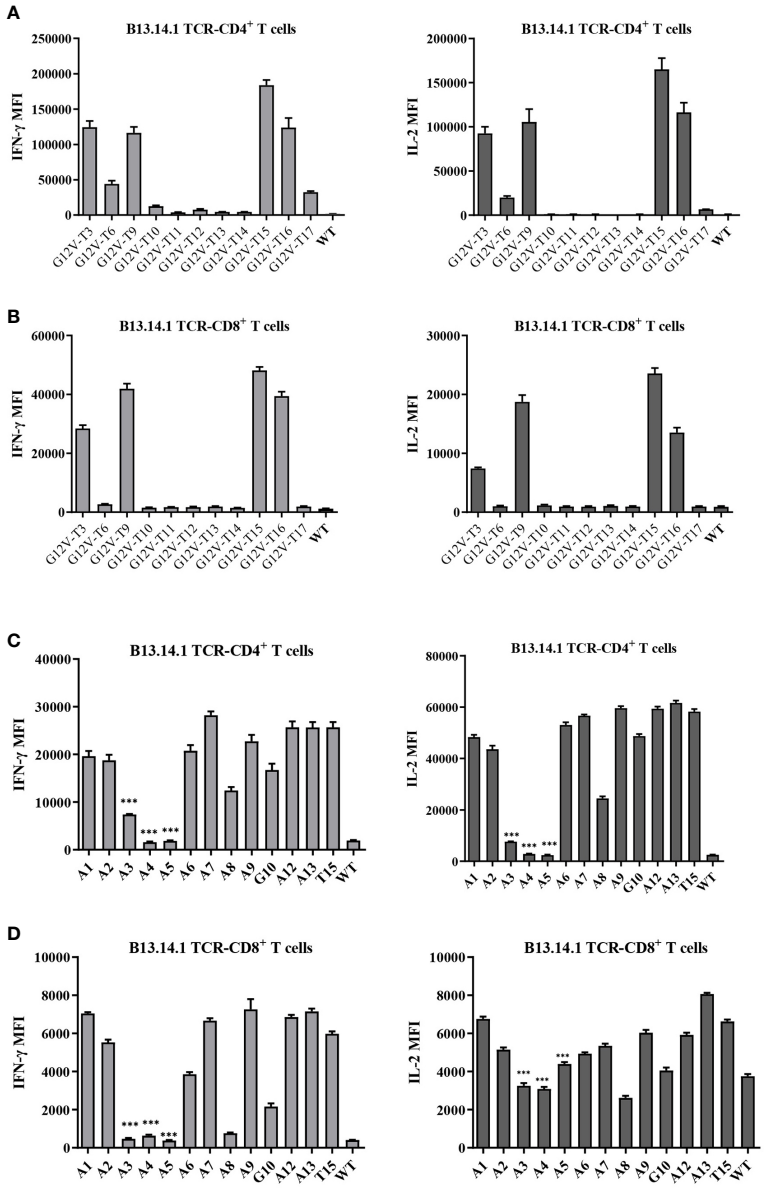

FIGURE 4
Amino acid residues E (position 2) and G (position12) of the KRAS^{G12V} mutant peptides were essential for G12V epitope presentation and immunoreactivity. **(A, B)** Flow Cytometry measuring secretion of INF-γ and IL-2 from B13.14.1 TCR-CD4$^+$/CD8$^+$ T cells stimulated by autologous LCLs loaded with 12 peptides. **(C, D)** Flow Cytometry measuring secretion of INF-γ and IL-2 from B13.14.1 TCR-CD4$^+$/CD8$^+$ T cells stimulated by autologous LCLs loaded with G12V-T15 peptides which were sequentially replaced with alanine (i.e., "A") from position 1 to 13. Data represent mean ± SD of triplicates. ***p ≤ 0.001.

In addition to the KRAS^{G12V} mutation, we also conducted experiments on the reactivity of B13.14.1 TCR to other KRAS mutants (G12A, G12D, G12I, G12V, G12S). The result turned out that B13.14.1 TCR showed specific reactivity to KRAS^{G12V} and KRAS^{G12I} but not to other KRAS mutants. It seems that longer methyl group of Isoleucine may enhance interaction of TCR and pMHC complex compared with Valine residue. KRAS^{G12D} accounts for the top one KRAS mutation in solid tumor. We also tried to screen KRAS^{G12D} reactive TCR clone from TIL of patients. However, none of screened T cell clone showed specific KRAS^{G12D} recognition. Dr Steven Rosenberg's group reported isolation of KRAS^{G12D} specific TCR from CRC patients which was HLA-C*0802 restricted (41), but HLA-C*0802 restricted TCR is not that of valuable for further development because of low frequency of HLA-C*0802 in most countries.

We reported here that B13.14.1 TCR-engineered CD4$^+$ T cells were able to recognize and kill MHC class II expressing target cells such as SW620-CIITA-DPB1*03:01 and CFPAC-1-CIITA-DPB1*03:01, in a dose-dependent manner, independent of APCs, which was the same as described in other studies (28, 32). Besides, CD4$^+$ T cells can secret multiple cytokines to mediate anti-tumor effects, for instance, the secretion of IL-2 from Th1 cells is essential for the function of CD8$^+$ T cells such as the initiation of the immune response and its growth (72). Thus, it is significant to strength the study of the mechanism of

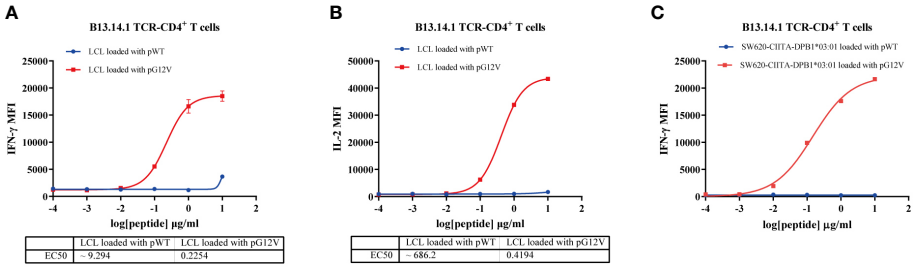

FIGURE 5
Functional avidity analysis of B13.14.1 TCR-CD4$^+$T cells. **(A, B)** Flow Cytometry measuring secretion of INF-γ and IL-2 from B13.14.1 TCR-CD4$^+$T cells stimulated by autologous LCLs loaded with different concentrations of KRAS G12V-T15 peptide (TEYKLVVVGAVGV) and corresponding wild type peptide (TEYKLVVVGAGGV), i.e., 10 μg/ml, 1 μg/ml, 0.1 μg/ml, 0.01 μg/ml, 0.001 μg/ml. **(C)** Flow Cytometry measuring secretion of INF-γ from B13.14.1 TCR-CD4$^+$ T cells stimulated by SW620-CIITA-DPB1*03:01 with different concentrations of KRAS G12V-T15 peptide (TEYKLVVVGAVGV) and corresponding wild type peptide (TEYKLVVVGAGGV), i.e., 10 μg/ml, 1 μg/ml, 0.1 μg/ml, 0.01 μg/ml, 0.001 μg/ml. Data represent mean ± SD of triplicates.

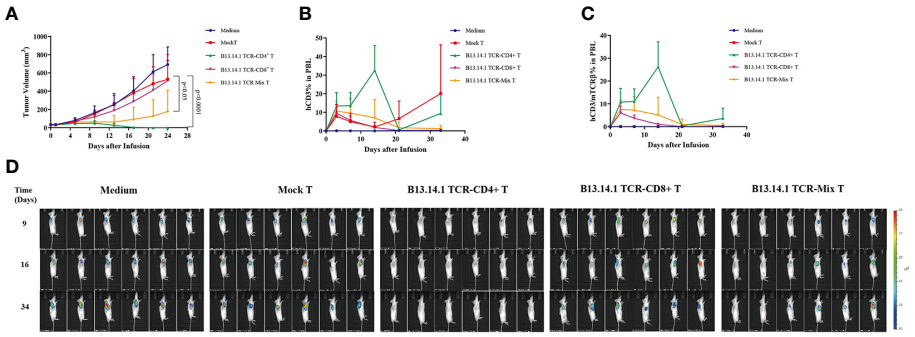

FIGURE 6
Evaluation of the activities of B13.14.1 TCR-engineered T cells *in vivo*. SW620-CIITA-DPB1*03:01 were implanted into immunodeficient NSG mice and treated them with intravenous injection of PBS, human CD4$^+$ T cells, CD8$^+$ T cells and the mixture of CD4$^+$ T cells and CD8$^+$ T cells (CD4$^+$ T cells: CD8$^+$ T cells = 1:1) transduced with B13.14.1 TCR (TRAV3*01-J10*01/TRBV19*01-D1*01-J1-6*02) when tumor size reached about 50 mm^3. The results showed **(A)** tumor sizes, **(B)** proportions of human CD3$^+$ T cells in the peripheral blood, **(C)** proportions of human CD3$^+$ T cells/mouse TCRβ in the peripheral blood. **(D)** Micrographs obtained from IVIS of mice inoculated with SW620-CIITA-DPB1*03:01 and were treated or untreated with Mock T cells or B13.14.1 TCR-engineered T cells.

CD4$^+$ T cells recognizing and killing tumor cell to obtain optimal antitumor responses. The identification of CD4$^+$ TCR specific for KRAS mutations provides the foundation for applying the CD4$^+$ T-cell immunity to the adoptive transfer therapy and deepens the mechanism of CD4$^+$ T cells in human anti-tumor immunity. In the future studies, we would enroll patients with advanced PDAC for clinical researches to validate our approach. However, it is still a challenge to improve the anti-tumor efficacy of TCR-T immunotherapy, including how to expand the range of available TCRs in more patients, how to increase the safety and the functional avidity of therapeutic TCRs, and how to overcome the immunosuppressive effects of suppressor cell subsets in CD4$^+$ T cells. With the development of next-generation sequencing technology, TCR-T immunotherapy for personalized neoantigens will become more and more mature in the future and become a viable and ideal cancer treatment.

Data availability statement

The original contributions presented in the study are publicly available. This data can be found here: GSE232897 (GEO).

Ethics statement

The studies involving human participants were reviewed and approved by Ethics Committee of Ruijin Hospital of Shanghai Jiao Tong University. The patients/participants provided their written informed consent to participate in this study. The animal study was reviewed and approved by Ethics Committee of Ruijin Hospital of Shanghai Jiao Tong University.

Author contributions

QZ, BS and CW planned the research and contributed to conception and design of the study, and provided funding support. QA and FL contributed to conception and design of the study, execution of the experiments, data collection, data analysis, and preparation of the manuscript. QA and FL contributed equally to this work and should be considered as co-first authors. SZ, ZZ, YJ, HC, CP and XD have involved in the interpretation of data. LJ and NM guided the revision of this article. NM provided experimental platform and technical support. QZ, CW and BS contributed to the review of the manuscript. All authors contributed to the article and approved the submitted version.

Funding

This study was supported by National Natural Science Foundation of China (grant numbers 82103482, 82273356, and 82073326), the Shanghai Sailing Program (grant number 20YF1426900), Medical-Engineering Cross Foundation of Shanghai Jiao Tong University (ZH2018ZDA01), Shanghai Collaborative Innovation Center for Translational Medicine (TM201903) and Innovative research team of high-level local universities in Shanghai.

Conflict of interest

Author NM was employed by the company Shanghai Genbase Biotechnology Co.,Ltd.

The remaining authors declare that the research was conducted in the absence of any commercial or financial relationships that could be construed as a potential conflict of interest

Publisher's note

Supplementary material

The Supplementary Material for this article can be found online at: https://www.frontiersin.org/articles/10.3389/fimmu.2023.1161538/full#supplementary-material

References

1. Qin C, Yang G, Yang J, Ren B, Wang H, Chen G, et al. Metabolism of pancreatic cancer: paving the way to better anticancer strategies. *Mol Cancer* (2020) 19(1):50. doi: 10.1186/s12943-020-01169-7

2. Robert C, Long GV, Brady B, Dutriaux C, Maio M, Mortier L, et al. Nivolumab in previously untreated melanoma without braf mutation. *New Engl J Med* (2015) 372 (4):320–30. doi: 10.1056/NEJMoa1412082

3. Sharma P, Callahan MK, Bono P, Kim J, Spiliopoulou P, Calvo E, et al. Nivolumab monotherapy in recurrent metastatic urothelial carcinoma (Checkmate 032): a multicentre, open-label, two-stage, multi-arm, phase 1/2 trial. *Lancet Oncol* (2016) 17(11):1590–8. doi: 10.1016/S1470-2045(16)30496-X

4. Borghaei H, Paz-Ares L, Horn L, Spigel DR, Steins M, Ready NE, et al. Nivolumab versus docetaxel in advanced nonsquamous non-Small-Cell lung cancer. *New Engl J Med* (2015) 373(17):1627–39. doi: 10.1056/NEJMoa1507643

5. Brahmer JR, Tykodi SS, Chow LQM, Hwu W-J, Topalian SL, Hwu P, et al. Safety and activity of anti-Pd-L1 antibody in patients with advanced cancer. *New Engl J Med* (2012) 366(26):2455–65. doi: 10.1056/NEJMoa1200694

6. Morrison AH, Byrne KT, Vonderheide RH. Immunotherapy and prevention of pancreatic cancer. *Trends Cancer* (2018) 4(6):418–28. doi: 10.1016/j.trecan.2018.04.001

7. Schizas D, Charalampakis N, Kole C, Economopoulou P, Koustas E, Gkotsis E, et al. Immunotherapy for pancreatic cancer: a 2020 update. *Cancer Treat Rev* (2020) 86:102016. doi: 10.1016/j.ctrv.2020.102016

8. Fukunaga A, Miyamoto M, Cho Y, Murakami S, Kawarada Y, Oshikiri T, et al. Cd8+ tumor-infiltrating lymphocytes together with Cd4+ tumor-infiltrating lymphocytes and dendritic cells improve the prognosis of patients with pancreatic adenocarcinoma. *Pancreas* (2004) 28(1):e26–31. doi: 10.1097/00006676-200401000-00023

9. Balachandran VP, Łuksza M, Zhao JN, Makarov V, Moral JA, Remark R, et al. Identification of unique neoantigen qualities in long-term survivors of pancreatic cancer. *Nature* (2017) 551(7681):512–6. doi: 10.1038/nature24462

10. Ino Y, Yamazaki-Itoh R, Shimada K, Iwasaki M, Kosuge T, Kanai Y, et al. Immune cell infiltration as an indicator of the immune microenvironment of pancreatic cancer. *Br J Cancer* (2013) 108(4):914–23. doi: 10.1038/bjc.2013.32

11. Hall M, Liu H, Malafa M, Centeno B, Hodul PJ, Pimiento J, et al. Expansion of tumor-infiltrating lymphocytes (Til) from human pancreatic tumors. *J Immunother Cancer* (2016) 4:61. doi: 10.1186/s40425-016-0164-7

12. Meng Q, Liu Z, Rangelova E, Poiret T, Ambati A, Rane L, et al. Expansion of tumor-reactive T cells from patients with pancreatic cancer. *J Immunother* (2016) 39 (2):81–9. doi: 10.1097/CJI.0000000000000111

13. Zhao Q, Jiang Y, Xiang S, Kaboli PJ, Shen J, Zhao Y, et al. Engineered tcr-T cell immunotherapy in anticancer precision medicine: pros and cons. *Front Immunol* (2021) 12:658753. doi: 10.3389/fimmu.2021.658753

14. Lowery FJ, Krishna S, Yossef R, Parikh NB, Chatani PD, Zacharakis N, et al. Molecular signatures of antitumor neoantigen-reactive T cells from metastatic human cancers. *Science* (2022) 375(6583):877–84. doi: 10.1126/science.abl5447

15. Malekzadeh P, Pasetto A, Robbins PF, Parkhurst MR, Paria BC, Jia L, et al. Neoantigen screening identifies broad Tp53 mutant immunogenicity in patients with epithelial cancers. *J Clin Invest* (2019) 129(3):1109–14. doi: 10.1172/JCI123791

16. Til transcriptomic states enable successful tcr prediction. *Cancer Discovery* (2022) 12(4):884. doi: 10.1158/2159-8290.CD-RW2022-031

17. Choi BD, Maus MV, June CH, Sampson JH. Immunotherapy for glioblastoma: adoptive T-cell strategies. *Clin Cancer Res* (2019) 25(7):2042–8. doi: 10.1158/1078-0432.CCR-18-1625

18. Harris DT, Kranz DM. Adoptive T cell therapies: a comparison of T cell receptors and chimeric antigen receptors. *Trends In Pharmacol Sci* (2016) 37(3):220–30. doi: 10.1016/j.tips.2015.11.004

19. Wachsmann TLA, Wouters AK, Remst DFG, Hagedoorn RS, Meeuwsen MH, van Diest E, et al. Comparing car and tcr engineered T cell performance as a function of tumor cell exposure. *Oncoimmunology* (2022) 11(1):2033528. doi: 10.1080/2162402X.2022.2033528

20. Clay TM, Custer MC, Sachs J, Hwu P, Rosenberg SA, Nishimura MI. Efficient transfer of a tumor antigen-reactive tcr to human peripheral blood lymphocytes confers anti-tumor reactivity. *J Immunol* (1999) 163(1):507–13. doi: 10.4049/jimmunol.163.1.507

21. van der Leun AM, Thommen DS, Schumacher TN. Cd8 T cell states in human cancer: insights from single-cell analysis. *Nat Rev Cancer* (2020) 20(4):218–32. doi: 10.1038/s41568-019-0235-4

22. Blank CU, Haining WN, Held W, Hogan PG, Kallies A, Lugli E, et al. Defining 'T cell exhaustion'. *Nat Rev Immunol* (2019) 19(11):665–74. doi: 10.1038/s41577-019-0221-9

23. Duval L, Schmidt H, Kaltoft K, Fode K, Jensen JJ, Sorensen SM, et al. Adoptive transfer of allogeneic cytotoxic T lymphocytes equipped with a hla-A2 restricted mart-1 T-cell receptor: a phase I trial in metastatic melanoma. *Clin Cancer Res* (2006) 12 (4):1229–36. doi: 10.1158/1078-0432.CCR-05-1485

24. Johnson LA, Morgan RA, Dudley ME, Cassard L, Yang JC, Hughes MS, et al. Gene therapy with human and mouse T-cell receptors mediates cancer regression and targets normal tissues expressing cognate antigen. *Blood* (2009) 114(3):535–46. doi: 10.1182/blood-2009-03-211714

25. Robbins PF, Morgan RA, Feldman SA, Yang JC, Sherry RM, Dudley ME, et al. Tumor regression in patients with metastatic synovial cell sarcoma and melanoma using genetically engineered lymphocytes reactive with ny-Eso-1. *J Clin Oncol* (2011) 29(7):917–24. doi: 10.1200/JCO.2010.32.2537

26. Mumberg D, Monach PA, Wanderling S, Philip M, Toledano AY, Schreiber RD, et al. Cd4(+) T cells eliminate mhc class ii-negative cancer cells in vivo by indirect effects of ifn-gamma. *Proc Natl Acad Sci USA* (1999) 96(15):8633–8. doi: 10.1073/pnas.96.15.8633

27. Qin Z, Blankenstein T. Cd4+ T cell–mediated tumor rejection involves inhibition of angiogenesis that is dependent on ifn gamma receptor expression by nonhematopoietic cells. *Immunity* (2000) 12(6):677–86. doi: 10.1016/S1074-7613(00)80218-6

28. Xie Y, Akpinarli A, Maris C, Hipkiss EL, Lane M, Kwon E-KM, et al. Naive tumor-specific Cd4(+) T cells differentiated in vivo eradicate established melanoma. *J Exp Med* (2010) 207(3):651–67. doi: 10.1084/jem.20091921

29. Ding Z-C, Huang L, Blazar BR, Yagita H, Mellor AL, Munn DH, et al. Polyfunctional $Cd4^+$ T cells are essential for eradicating advanced b-cell lymphoma after chemotherapy. *Blood* (2012) 120(11):2229–39. doi: 10.1182/blood-2011-12-398321

30. Corthay A, Skovseth DK, Lundin KU, Røsjø E, Omholt H, Hofgaard PO, et al. Primary antitumor immune response mediated by Cd4+ T cells. *Immunity* (2005) 22(3):371–83. doi: 10.1016/j.immuni.2005.02.003

31. Braumüller H, Wieder T, Brenner E, Aßmann S, Hahn M, Alkhaled M, et al. T-Helper-1-Cell cytokines drive cancer into senescence. *Nature* (2013) 494(7437):361–5. doi: 10.1038/nature11824

32. Quezada SA, Simpson TR, Peggs KS, Merghoub T, Vider J, Fan X, et al. Tumor-reactive Cd4(+) T cells develop cytotoxic activity and eradicate Large established melanoma after transfer into lymphopenic hosts. *J Exp Med* (2010) 207(3):637–50. doi: 10.1084/jem.20091918

33. Tran E, Turcotte S, Gros A, Robbins PF, Lu Y-C, Dudley ME, et al. Cancer immunotherapy based on mutation-specific Cd4+ T cells in a patient with epithelial cancer. *Science* (2014) 344(6184):641–5. doi: 10.1126/science.1251102

34. Buscail L, Bournet B, Cordelier P. Role of oncogenic kras in the diagnosis, prognosis and treatment of pancreatic cancer. *Nat Rev Gastroenterol Hepatol* (2020) 17(3):153–68. doi: 10.1038/s41575-019-0245-4

35. Haigis KM. Kras alleles: the devil is in the detail. *Trends Cancer* (2017) 3(10):686–97. doi: 10.1016/j.trecan.2017.08.006

36. Stephen AG, Esposito D, Bagni RK, McCormick F. Dragging ras back in the ring. *Cancer Cell* (2014) 25(3):272–81. doi: 10.1016/j.ccr.2014.02.017

37. Cox AD, Fesik SW, Kimmelman AC, Luo J, Der CJ. Drugging the undruggable ras: mission possible? *Nat Rev Drug Discovery* (2014) 13(11):828–51. doi: 10.1038/nrd4389

38. Sim MJW, Lu J, Spencer M, Hopkins F, Tran E, Rosenberg SA, et al. High-affinity oligoclonal tcrs define effective adoptive T cell therapy targeting mutant kras-G12d. *Proc Natl Acad Sci USA* (2020) 117(23):12826–35. doi: 10.1073/pnas.1921964117

39. Dillard P, Casey N, Pollmann S, Vernhoff P, Gaudernack G, Kvalheim G, et al. Targeting kras mutations with hla class ii-restricted tcrs for the treatment of solid tumors. *Oncoimmunology* (2021) 10(1):1936757. doi: 10.1080/2162402X.2021.1936757

40. Deniger DC, Pasetto A, Robbins PF, Gartner JJ, Prickett TD, Paria BC, et al. T-Cell responses to "Hotspot" mutations and unique neoantigens expressed by human ovarian cancers. *Clin Cancer Res* (2018) 24(22):5562–73. doi: 10.1158/1078-0432.CCR-18-0573

41. Tran E, Robbins PF, Lu Y-C, Prickett TD, Gartner JJ, Jia L, et al. T-Cell transfer therapy targeting mutant kras in cancer. *New Engl J Med* (2016) 375(23):2255–62. doi: 10.1056/NEJMoa1609279

42. Leidner R, Sanjuan Silva N, Huang H, Sprott D, Zheng C, Shih Y-P, et al. Neoantigen T-cell receptor gene therapy in pancreatic cancer. *New Engl J Med* (2022) 386(22):2112–9. doi: 10.1056/NEJMoa2119662

43. Dudley ME, Wunderlich JR, Robbins PF, Yang JC, Hwu P, Schwartzentruber DJ, et al. Cancer regression and autoimmunity in patients after clonal repopulation with antitumor lymphocytes. *Science* (2002) 298(5594):850–4. doi: 10.1126/science.1076514

44. Rosenberg SA, Dudley ME. Cancer regression in patients with metastatic melanoma after the transfer of autologous antitumor lymphocytes. *Proc Natl Acad Sci USA* (2004) 101(Suppl 2):14639–45. doi: 10.1073/pnas.0405730101

45. Wang H, Song X, Shen L, Wang X, Xu C. Exploiting T cell signaling to optimize engineered T cell therapies. *Trends Cancer* (2022) 8(2):123–34. doi: 10.1016/j.trecan.2021.10.007

46. Shafer P, Kelly LM, Hoyos V. Cancer therapy with tcr-engineered T cells: current strategies, challenges, and prospects. *Front Immunol* (2022) 13:835762. doi: 10.3389/fimmu.2022.835762

47. Wang S, Sun J, Chen K, Ma P, Lei Q, Xing S, et al. Perspectives of tumor-infiltrating lymphocyte treatment in solid tumors. *BMC Med* (2021) 19(1):140. doi: 10.1186/s12916-021-02006-4

48. Tsimberidou A-M, Van Morris K, Vo HH, Eck S, Lin Y-F, Rivas JM, et al. T-Cell receptor-based therapy: an innovative therapeutic approach for solid tumors. *J Hematol Oncol* (2021) 14(1):102. doi: 10.1186/s13045-021-01115-0

49. Che Y, Siprashvili Z, Kovalski JR, Jiang T, Wozniak G, Elcavage L, et al. Kras regulation by small non-coding rnas and snare proteins. *Nat Commun* (2019) 10(1):5118. doi: 10.1038/s41467-019-13106-4

50. Zhu G, Pei L, Xia H, Tang Q, Bi F. Role of oncogenic kras in the prognosis, diagnosis and treatment of colorectal cancer. *Mol Cancer* (2021) 20(1):143. doi: 10.1186/s12943-021-01441-4

51. Tan C, Du X. Kras mutation testing in metastatic colorectal cancer. *World J Gastroenterol* (2012) 18(37):5171–80. doi: 10.3748/wjg.v18.i37.5171

52. Hobbs GA, Wittinghofer A, Der CJ. Selective targeting of the kras G12c mutant: kicking kras when it's down. *Cancer Cell* (2016) 29(3):251–3. doi: 10.1016/j.ccell.2016.02.015

53. Jiang X, Yuan X, Li Y, Zhang T, Chen L, Bao X, et al. Use of next-generation sequencing to detect polymorphism of 11 hla allele loci in the Chinese han population and variance from other common and well-documented lists. *HLA* (2022). 101:222–227 doi: 10.1111/tan.14932

54. Yao X, Lu Y-C, Parker LL, Li YF, El-Gamil M, Black MA, et al. Isolation and characterization of an hla-Dpb1*04: 01-restricted mage-A3 T-cell receptor for cancer immunotherapy. *J Immunother* (2016) 39(5):191–201. doi: 10.1097/CJI.0000000000000123

55. Petersdorf EW, Bengtsson M, De Santis D, Dubois V, Fleischhauer K, Gooley T, et al. Role of hla-dp expression in graft-Versus-Host disease after unrelated donor transplantation. *J Clin Oncol* (2020) 38(24):2712–8. doi: 10.1200/JCO.20.00265

56. Axelrod ML, Cook RS, Johnson DB, Balko JM. Biological consequences of mhc-ii expression by tumor cells in cancer. *Clin Cancer Res* (2019) 25(8):2392–402. doi: 10.1158/1078-0432.CCR-18-3200

57. Baleeiro RB, Bouwens CJ, Liu P, Di Gioia C, Dunmall LSC, Nagano A, et al. Mhc class ii molecules on pancreatic cancer cells indicate a potential for neo-Antigen-Based immunotherapy. *Oncoimmunology* (2022) 11(1):2080329. doi: 10.1080/2162402X.2022.2080329

58. Wolf B, Zimmermann S, Arber C, Irving M, Trueb L, Coukos G. Safety and tolerability of adoptive cell therapy in cancer. *Drug Saf* (2019) 42(2):315–34. doi: 10.1007/s40264-018-0779-3

59. Wang RF. The role of mhc class ii-restricted tumor antigens and Cd4+ T cells in antitumor immunity. *Trends Immunol* (2001) 22(5):269–76. doi: 10.1016/S1471-4906(01)01896-8

60. Linette GP, Stadtmauer EA, Maus MV, Rapoport AP, Levine BL, Emery L, et al. Cardiovascular toxicity and titin cross-reactivity of affinity-enhanced T cells in myeloma and melanoma. *Blood* (2013) 122(6):863–71. doi: 10.1182/blood-2013-03-490565

61. Cameron BJ, Gerry AB, Dukes J, Harper JV, Kannan V, Bianchi FC, et al. Identification of a titin-derived hla-A1-Presented peptide as a cross-reactive target for engineered mage A3-directed T cells. *Sci Trans Med* (2013) 5(197):197ra03. doi: 10.1126/scitranslmed.3006034

62. Tay RE, Richardson EK, Toh HC. Revisiting the role of Cd4+ T cells in cancer immunotherapy-new insights into old paradigms. *Cancer Gene Ther* (2021) 28(1-2):5–17. doi: 10.1038/s41417-020-0183-x

63. Brouwer T, Ijsselsteijn M, Oosting J, Ruano D, van der Ploeg M, Dijk F, et al. A paradoxical role for regulatory T cells in the tumor microenvironment of pancreatic cancer. *Cancers* (2022) 14(16):3862. doi: 10.3390/cancers14163862

64. Oh DY, Kwek SS, Raju SS, Li T, McCarthy E, Chow E, et al. Intratumoral Cd4+ T cells mediate anti-tumor cytotoxicity in human bladder cancer. *Cell* (2020) 181(7):1612-1625. doi: 10.1016/j.cell.2020.05.017

65. Kagamu H, Yamasaki S, Kitano S, Yamaguchi O, Mouri A, Shiono A, et al. Single-cell analysis reveals a Cd4+ T-cell cluster that correlates with pd-1 blockade efficacy. *Cancer Res* (2022) 82(24):4641–53. doi: 10.1158/0008-5472.CAN-22-0112

66. Veatch JR, Lee SM, Fitzgibbon M, Chow IT, Jesernig B, Schmitt T, et al. Tumor-infiltrating Brafv600e-specific Cd4+ T cells correlated with complete clinical response in melanoma. *J Clin Invest* (2018) 128(4):1563–8. doi: 10.1172/JCI98689

67. Lu Y-C, Parker LL, Lu T, Zheng Z, Toomey MA, White DE, et al. Treatment of patients with metastatic cancer using a major histocompatibility complex class ii-restricted T-cell receptor targeting the cancer germline antigen mage-A3. *J Clin Oncol* (2017) 35(29):3322–9. doi: 10.1200/JCO.2017.74.5463

68. Pishesha N, Harmand TJ, Ploegh HL. A guide to antigen processing and presentation. *Nat Rev Immunol* (2022) 22(12):751–64. doi: 10.1038/s41577-022-00707-2

69. Hegde NR, Dunn C, Lewinsohn DM, Jarvis MA, Nelson JA, Johnson DC. Endogenous human cytomegalovirus Gb is presented efficiently by mhc class ii molecules to Cd4+ ctl. *J Exp Med* (2005) 202(8):1109–19. doi: 10.1084/jem.20050162

70. Matsuzaki J, Tsuji T, Luescher I, Old LJ, Shrikant P, Gnjatic S, et al. Nonclassical antigen-processing pathways are required for mhc class ii-restricted direct tumor recognition by ny-Eso-1-Specific Cd4(+) T cells. *Cancer Immunol Res* (2014) 2(4):341–50. doi: 10.1158/2326-6066.CIR-13-0138

71. Parkhurst MR, Robbins PF, Tran E, Prickett TD, Gartner JJ, Jia L, et al. Unique neoantigens arise from somatic mutations in patients with gastrointestinal cancers. *Cancer Discovery* (2019) 9(8):1022–35. doi: 10.1158/2159-8290.CD-18-1494

72. Schoenberger SP, Toes RE, van der Voort EI, Offringa R, Melief CJ. T-Cell help for cytotoxic T lymphocytes is mediated by Cd40-Cd40l interactions. *Nature* (1998) 393(6684):480–3. doi: 10.1038/31002

frontiers | Frontiers in Immunology

TYPE Original Research
PUBLISHED 06 June 2023
DOI 10.3389/fimmu.2023.1176370

OPEN ACCESS

EDITED BY
Sang T Kim,
University of Texas MD Anderson Cancer Center, United States

REVIEWED BY
Moses Donkor,
BioXcel Therapeutics, Inc., United States
Firas Hamdan,
University of Helsinki, Finland

*CORRESPONDENCE
Anthony David Sandler
ASandler@childrensnational.org

RECEIVED 28 February 2023
ACCEPTED 25 May 2023
PUBLISHED 06 June 2023

CITATION
Wu X, Srinivasan P, Basu M, Zimmerman T, Li S, Wang Y, Zheng P, Liu Y and Sandler AD (2023) CD24-Fc suppression of immune related adverse events in a therapeutic cancer vaccine model of murine neuroblastoma.
Front. Immunol. 14:1176370.
doi: 10.3389/fimmu.2023.1176370

CD24-Fc suppression of immune related adverse events in a therapeutic cancer vaccine model of murine neuroblastoma

Xiaofang Wu[1], Priya Srinivasan[1], Mousumi Basu[1], Talia Zimmerman[1], Samuel Li[1], Yin Wang[2], Pan Zheng[3], Yang Liu[3] and Anthony David Sandler[1]*

[1]The Joseph E. Robert Jr. Center for Surgical Care and The Sheikh Zayed Institute for Pediatric Surgical Innovation, Children's National Hospital, George Washington University, Washington, DC, United States, [2]University of Maryland Medical Center, University of Maryland, Baltimore, MD, United States, [3]OncoC4. Inc, Rockville, MD, United States

Introduction: The combination of Myc-suppressed whole tumor cells with checkpoint inhibitors targeting CTLA-4 and PD-L1 generates a potent therapeutic cancer vaccine in a mouse neuroblastoma model. As immunotherapies translate from pre-clinical to clinical trials, the potential immune-related adverse events (irAEs) associated with induction of potent immunity must be addressed. The CD24-Siglec 10/G interaction is an innate checkpoint that abrogates inflammatory responses to molecules released by damaged cells, but its role in cancer immunology is not well defined. We investigate irAEs of an effective whole cell neuroblastoma vaccine and subsequently the effect of CD24-Fc, a CD24 and Fc fusion protein, on both the vaccine efficacy and induced irAEs in a mouse neuroblastoma model.

Methods: To test whether the whole tumor cell vaccination leads to autoimmune responses in other organ systems we harvested lung, heart, kidney and colon from naïve mice (n=3), unvaccinated tumor only mice (n=3), and vaccinated mice with CD24 Fc (n=12) or human IgG-Fc control (n=12) after tumor inoculation and vaccination therapy at day 30. The Immune cell infiltrates and immunogenic pathway signatures in different organ systems were investigated using NanoString Autoimmune Profiling arrays. Nanostring RNA transcript results were validated with immunohistochemistry staining.

Results: The whole tumor cell vaccine combined with immune checkpoint therapy triggers occult organ specific immune cell infiltrates, primarily in cardiac tissue and to a lesser extent in the renal and lung tissue, but not in the colon. CD24-Fc administration with vaccination partially impedes anti-tumor immunity but delaying CD24-Fc administration after initial vaccination reverses this effect. CD24-Fc treatment also ameliorates the autoimmune response induced by effective tumor vaccination in the heart.

Discussion: This study illustrates that the combination of Myc suppressed whole tumor cell vaccination with checkpoint inhibitors is an effective therapy, but occult immune infiltrates are induced in several organ systems in a mouse neuroblastoma model. The systemic administration of CD24-Fc suppresses autoimmune tissue responses, but appropriate timing of administration is critical for maintaining efficacy of the therapeutic vaccine.

KEYWORDS

CD24Fc, tumor cell vaccine, neuroblastoma, immune-related adverse events, autoimmune profiling

Introduction

Cancer immunotherapy in the form of checkpoint inhibitors targeting CTLA-4, PD-L1 and PD-1 has made significant impact in the treatment of solid tumors. However, immune-related adverse events associated with immunotherapy are and will be a significant problem as even more effective immunotherapeutic approaches are developed (1–3). Immune related adverse events (irAEs) are reported in multiple organ systems, often leading to profound pathology. Hypophysitis is observed in patients treated with ipilimumab (an anti-CTLA-4 inhibitor) (4), thyroid dysfunction is noted following pembrolizumab (a PD-1 receptor antibody) treatment (5) and gastrointestinal irAEs are common with any check-point inhibitor (CPI) (6). The specific presentation of the irAE and the severity of the event during treatment are unpredictable which in some cases can be fatal. The mechanism of irAE is not clearly understood and the ability to reduce these events without impeding anti-tumor immunity is and will be critical. Success in reducing irAE could have a transformative impact on the field of cancer immunotherapy.

Immunotherapy is thought to promote immunogenic tumor cell death that initiates antitumor immunity, but cell death may also induce damage-associated molecular patterns (DAMPs). These DAMP molecules recruit and activate dendritic cells (DCs) that present tumor-specific antigens to T cells for elimination of neoplastic cells, but may also lead to severe tissue damage (7). In order to limit non-specific tissue damage, the CD24-Siglec signaling pathway suppresses inflammation triggered by DAMPs through blockade of NF-κB activation (8). CD24 is a multifunctional molecule, with a wide distribution in diverse cell lineages including tumor cells and immune cells. It partners with its receptor, Siglec-10 in humans or Siglec-G in mice to abrogate inflammatory responses to molecules released by damaged cells (9–11). Recently a CD24-Fc fusion protein composed of the extracellular part of CD24 and human IgG1Fc has been administered to prevent acute graft-versus-host disease (GVHD) in a Phase 2a clinical trial in adult leukemic patients who underwent hematopoietic cell transplantation (12). In another clinical trial CD24-Fc successfully improved overall survival and reduced multiple organ autoimmune injury in treating severe COVID-19 patients (13). Thus, engaging CD24-signaling may provide protection from inflammation and/or autoimmune disease following acute tissue injury induced by effective cancer immunotherapy. In contrast to these potential beneficial effects, CD24 is overexpressed in ovarian cancer and breast cancer, and acts as a "don't eat me" signal to protect cancer cells from phagocytosis that in turn promotes immune evasion (14). CD24 is thought to induce tumor progression by activating signaling molecules involved in proliferation and survival of cancer cells (15) and by increasing tumor suppressor activity of p53 (16). Blockade of CD24 and its receptor Siglec-10 reduces tumor growth and extends patient survival (14). Furthermore, CD24 on antigen presenting cells can act as a CD28 independent costimulatory molecule for activation of both CD4 and CD8-T cell responses (17–19). These conflicting observations in innate and acquired immunity highlight the crossover between tumor proliferation, antitumor immunity and autoimmunity suggesting that the predominant effects may be determined by the context in which CD24 is engaged as well as by glycosylation of CD24 (16).

Amplification of the Myc oncogene is associated with immune privilege in neuroblastoma (20). Targeting Myc *in vitro* with small molecule inhibitors induced Neuro2a tumor cell immunogenicity and enabled the production of a whole cell tumor vaccine in mouse tumor models (20). When the vaccine is combined with immune checkpoint inhibitors (anti-CTLA4 and anti-PD-L1 antibodies) potent tumor specific immunity is induced in the neuroblastoma mouse model (20). Although mice appear well and survive both the tumor challenge and the vaccine treatment, it is unknown if this tumor vaccine strategy induces autoimmune disorders in the host mice. In this study, we examined the autoimmune consequences of effective tumor vaccination on multiple organ systems and tested the impact of targeting the CD24-Siglec signaling pathway on both the vaccine therapy and autoimmune effects in the mouse neuroblastoma model. Nanostring autoimmune profiling of several organ systems indicated that the vaccine strategy induced moderate to severe lymphocytic infiltration and enhanced autoimmune signals in cardiac tissue and to a lesser extent in renal tissue. The lungs also demonstrated limited autoimmunity, but surprisingly the colon was essentially spared from the autoimmune effect of the vaccine therapy. Administration of CD24-Fc

with the initial tumor vaccine dampened the therapeutic effect of the vaccine. When CD24-Fc administration lagged several days behind initial vaccination, vaccine efficacy was not altered and treatment resulted in excellent tumor free survival. Notably, CD24-Fc administration suppressed the autoimmune response detected in cardiac and renal tissues. These findings suggest that an effective whole cell vaccine in a mouse neuroblastoma model induces organ specific autoimmune responses and when CD24- Fc is appropriately administered, the irAE can be reduced without exacerbating tumor growth or impeding tumor immunity.

Materials and methods

Animals

Female C57BL/6 and A/J mice aged 6 weeks were purchased from Jackson Laboratories (Bar Harbor, Maine, USA). All procedures were approved by the Institutional Animal Care and Use Committee (IACUC) of Children's National Hospital, Washington, DC.

Cells

The mouse neuroblastoma Neuro2a cell line (Sigma, St. Louis, Missouri, USA) was cultured using DMEM supplemented with 10% heat-inactivated fetal bovine serum (FBS, Sigma) and 100 IU/mL penicillin, 100 µg/mL streptomycin. All media and supplements were purchased from Thermo Fisher Scientific (Waltham, Massachusetts, USA).

Antibodies and reagents

Anti (α)-mouse CTLA-4, α-mouse programmed death-ligand 1 (PD-L1), and mouse IgG2b isotype antibodies were purchased from BioXCell (West Lebanon, New Hampshire, USA). I-BET726 was purchased from Millipore Sigma (Burlington, Massachusetts, USA) and JQ1 was purchased from Tocris (Minneapolis, Minnesota, USA). TLR7/8 ligand (Resiquimod, R848) was purchased from InvivoGen (San Diego, California). CD24-Fc and human IgG1-Fc were supplied by OncoImmune, Inc.

Mouse tumor therapeutic models

As described previously (20), the right flanks of A/J mice were injected (subcutaneously) with 2×10^6 Neuro2a cells on day 0. For vaccination, 2×10^6 Myc inhibitor (BET/JQ1) treated and irradiated (40 Gy) Neuro2a cells were injected (subcutaneously) into the left flank of each mouse on day 7, 10 and 13 as a whole tumor cell vaccine along with anti-CTLA-4 (aCTLA4) and anti-PD-L1 (aPD-L1) antibodies (100 µg/mouse) administered intraperitoneally. TLR7/8 agonist (25 µg/mouse) was used on day 7 in an attempt to enhance immunity induced by the vaccine. CD24-Fc (100 µg/mouse) or IgG-Fc (100 µg/mouse) was administered intraperitoneally on day 7, 10 and 13 (immediate model) or on day 10, 13 and 16 (delayed model). Mice were monitored daily following tumor inoculation and tumor growth was recorded in two dimensions. Tumor volume was calculated using the following formula: largest diameter^2 × smaller diameter × 0.52. A tumor size of 20 mm in any dimension was designated as the endpoint, and mice were euthanized at that time. All the procedures are approved by the IACUC at Children's National Hospital and are in accordance with the humane care of research animals.

Nanostring

Lung, heart, colon and kidney were harvested from mice in four groups: 1.) naïve, 2.) unvaccinated tumor only, 3.) vaccinated with CD24-Fc or 4.) vaccinated with IgG-Fc on day 30 after tumor cell inoculation. RNA was extracted and gene expression was directly measured via counts of corresponding mRNA in each sample using an nCounter murine AutoImmune Profiling Panel (NanoString, Seattle, WA, USA). For full details, see our previous publication (20). Briefly, 100 ng of high-quality total RNA was hybridized with reporter probes, and then biotinylated capture probes at 65°C for 16–18 hr before being placed into the nCounter Prep station in which samples were affixed to a cartridge. Cartridges were then read by the nCounter Digital Analyzer optical scanner. Further advanced immune-profiling analysis was performed using nSolver 4.0 analysis software with nCounter advanced analysis package (NanoString Technologies). Genes were grouped into 14 immune cell types and 35 immune functions according to the manufacturer's designation (20).

Characterization of mouse cardiac tissue by immunohistochemistry

Mouse hearts were fixed in 10% neutral buffered formalin (pH 6.8–7.2; Richard-Allan Scientific, Kalamazoo, Michigan, US) for paraffin embedding and sectioning. Five µm tissue sections were cut with a microtome, and sample processing and IHC staining were performed as previously described (20) using rabbit polyclonal to CD45 antibodies (1:200. Abcam, Cambridge, Massachusetts, US). Isotype-matched antibodies were used for negative controls. Optical density (mean gray value) was obtained by color deconvolution analysis with Image J.

Statistical analysis

Statistical analysis of nanostring gene expression, normalization, clustering, Pathview plots and fold-changes were performed using the Advanced Analysis Module in the nSolver™ Analysis Software version 4.0 from NanoString Technologies (NanoString Technologies, WA, USA) following our published

method (20). Briefly, raw data for each sample were normalized to the geometric mean of housekeeping genes using the geNorm algorithm. Pathway scores were calculated as the first principal component (PC) scores for each sample based on the individual gene expression levels for all the measured genes within a specific pathway. The cell type score is calculated as the mean of the log2 expression levels for all the probes included in the final calculation for that specific cell type. An increase of 1 corresponds to a doubling in abundance (nanostring.com). All differentially expressed genes were subjected to KEGG term analysis, with significance accepted at $p < 0.05$. The Benjamini-Yekutieli method was used to control the false discovery rate. All statistical analyses of nanostring data were carried out in R v3.4.3 software.

Statistical significance for each set of experiments was determined by the unpaired 2-tailed Student's t-test, and the specific tests were indicated in the figure legends. The data are expressed as the mean (± SD), with $p<0.05$ considered statistically significant. For the survival analysis, we calculated and compared the median survival time and the cumulative survival probability using the Kaplan-Meier survival estimator followed by a log-rank test, and calculated hazard ratio (HR) using the Cox proportional-hazards regression model.

Results

Inoculation of a whole tumor cell vaccine combined with immune checkpoint therapy triggers autoimmune responses and immune cell infiltrates primarily in cardiac tissue and with limited infiltrates in renal and lung tissue

Prior work from our laboratory shows that a neuroblastoma vaccine strategy containing BET/JQ1 treated cancer cells combined with anti-CTLA4 and anti-PDL-1 checkpoint inhibitors induced robust anti-tumor immunity and cured mice with established tumors (20). To test whether this whole tumor cell vaccination leads to autoimmune responses in other organ systems, we injected 2×10^6 WT Neuro2a cells subcutaneously on day 0 on the right leg of A/J mice. For vaccination, 2×10^6 Myc inhibitor (BET/JQ1) treated and irradiated (40 Gy) Neuro2a cells were injected (subcutaneously) into the left flank of each mouse on day 7, 10 and 13 as a whole tumor cell vaccine along with anti-CTLA-4 and anti-PD-L1 antibodies (100 µg/mouse) administered intraperitoneally. TLR7/8 agonist (25 µg/mouse) was used on day 7. The Schematic experimental design was shown in

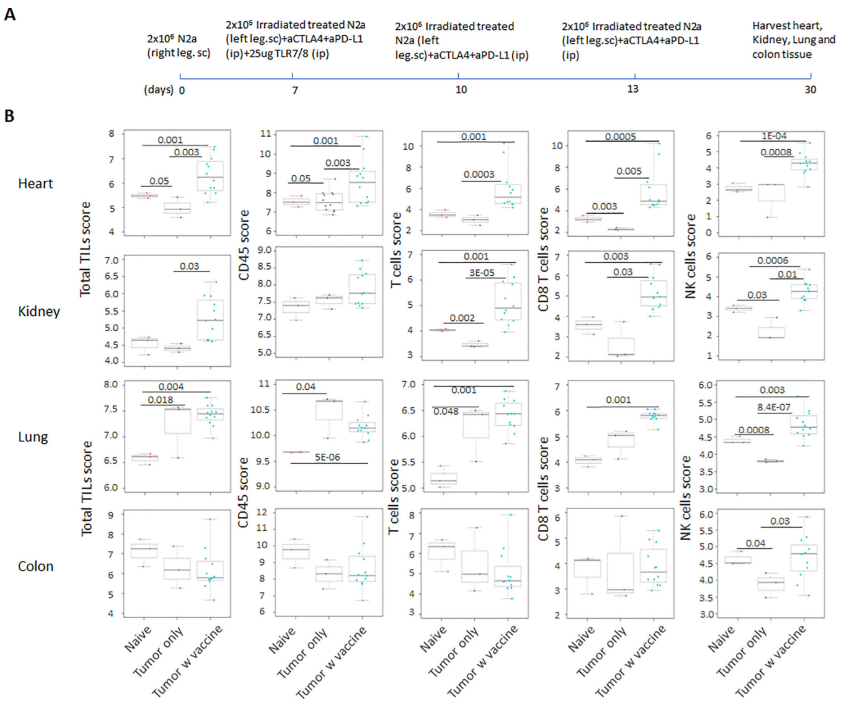

FIGURE 1
(A) Schematic design of tumor cell vaccination. To test whether whole tumor cell vaccination leads to autoimmune responses in other organ systems, we injected (subcutaneously) the right flanks of A/J mice with 2×10^6 Neuro2a cells on day 0. For vaccination, 2×10^6 Myc inhibitor (BET/JQ1) treated and irradiated (40Gy) Neuro2a cells were injected (subcutaneously) into the left flank of each mouse on day 7, 10 and 13 as a whole tumor cell vaccine along with anti-CTLA-4 and anti-PD-L1 antibodies (100 µg/mouse) administered intraperitoneally. TLR7/8 agonist (25 µg/mouse) was used on day 7. **(B)** The lung, heart, kidney and colon were harvested from naïve mice (n=3), unvaccinated tumor baring mice (n=3), and vaccinated mice (n=12) after tumor inoculation at day 30. The global expression of mRNA from each organ was investigated using NanoString Autoimmune Profiling arrays. Nanostring Autoimmune Profiling analysis revealed that heart, kidney and lung from the vaccination group demonstrated a moderate to severe increase in signature markers for total TIL, CD45 cells, T cells, CD8+ cells and NK cells when compared to naïve and tumor only control mice. Box plots show distribution of immune cells by relative number present within mouse heart, kidney, lung and colon calculated by gene expression. ($p<0.05$). As abundance estimates (cell type scores) are calculated in log2 scale, an increase of 1 on the vertical axis corresponds to a doubling in abundance. The horizontal black line on the box plot represents the median expression, and each symbol represents a single individual. Statistical significance was determined by unpaired two-tailed Student's t-test, and $p<0.05$ was considered statistically significant.

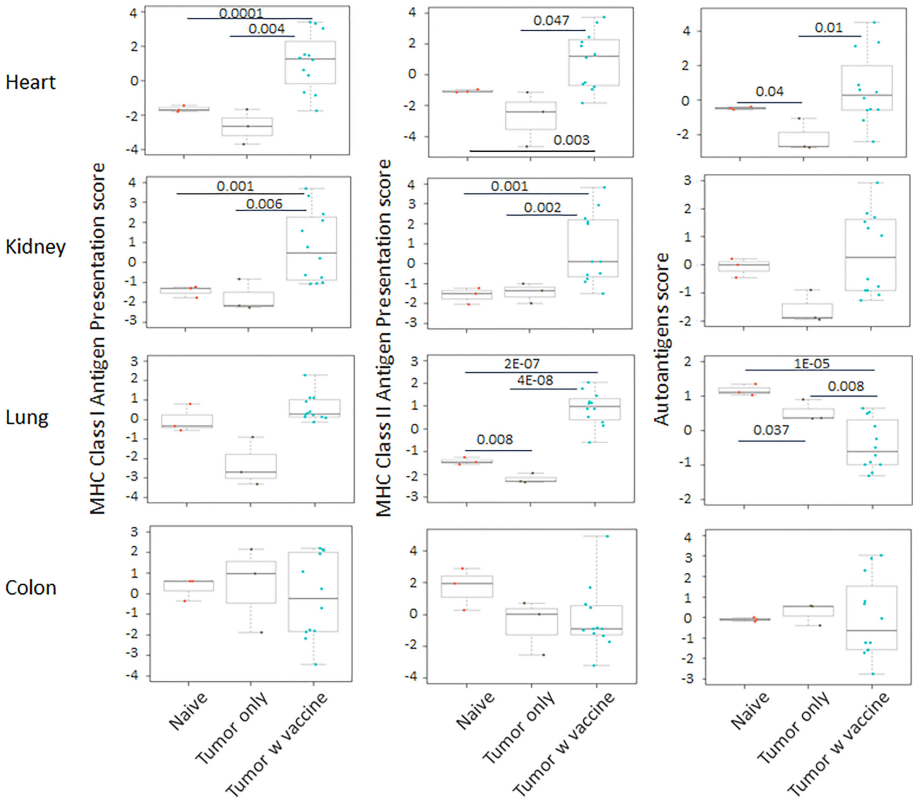

FIGURE 2
The pathway scores of multiple autoimmune signals that relate to antigen presentation were markedly enhanced in the tumor vaccinated group (n=12) in heart, kidney and lung, but not in the colon when compared with the organs that were collected from unvaccinated tumor only mice (n=3) and naïve mice (n=3) at day 30 after tumor inoculation. The vaccination strategy is described in Figure 1. Unpaired two-tailed Student's t-test was performed for the statistical analysis, and $p<0.05$ was considered statistically significant.

Figure 1A. We harvested lung, heart, kidney and colon from naïve mice (n=3), unvaccinated tumor only mice (n=3), and vaccinated mice after tumor inoculation and vaccination therapy at day 30 (n=12). The global expression of mRNA was investigated using NanoString Autoimmune Profiling arrays. Nanostring analysis revealed that the heart, kidney and lung from the vaccination group demonstrated a moderate to severe level of upregulation in the expression of signature markers for total TIL, CD45 cells, T cells, CD8+ cells, NK cells, dendritic cells, neutrophils, macrophages, and B cells when compared with naïve and tumor only control mice (Figure 1B; Supplement Figure 1). In addition, the scores of multiple autoimmune signaling pathways that related to antigen presentation (Figure 2), lymphocyte trafficking (Figure 3), chemokines and cytokines (Figure 4), and major inflammatory signaling pathways (Supplemental Figure 2), were all enhanced in the tumor vaccinated group. Interestingly, there was no significant autoimmune response detected following vaccination in the colons of the mice tested.

CD24-Fc administration with vaccination can partially impede anti-tumor immunity, but delaying CD24-Fc therapy until after initial vaccination reverses this effect

CD24 signaling is reported to promote immune evasion and tumor progression (14), yet this pathway is also thought to suppress autoimmunity through down regulation of DAMP signaling. In order to determine the effect on tumor immunity, we tested two neuroblastoma mouse models in which CD24-Fc was administered either at the time of tumor vaccination or three days following the initial vaccination to determine if the timing of CD24 signaling altered immunity. Briefly, 2×10^6 WT Neuro2a cells were subcutaneously administered on day 0 on the right leg of AJ mice, then two treatment models were used. In the *immediate* vaccine model, CD24-Fc or human IgG-Fc control was injected simultaneously with the whole cell vaccine plus anti-PD-L1/CTLA4 antibodies at day 7, 10 and 13 post tumor inoculation (Figure 5A). In the second *delayed* vaccine model, vaccine and anti-PD-L1/CTLA4 antibodies were injected on day 7, 10 and 13, while CD24-Fc or IgG-Fc was administered three days after the first dose of vaccine, which was injected on day 10, 13 and 16 (Figure 5C). The methods and timelines are shown in Figures 5A, C. The individual tumor growth in various treatment groups from the early vaccine model and the delayed vaccine model were monitored and compared (Figures 5B, D). None of the mice developed tumor at the site of the vaccine cell injection. Significant therapeutic survival benefit was observed in vaccine groups either with CD24-Fc or with IgG-Fc when compared with tumor only control groups in both models, but the anti-tumor effect was more profound in the model of delayed CD24-Fc treatment (Figure 6). In the vaccine model, eight out of ten mice (80%) of the IgG/vac group were cured of the

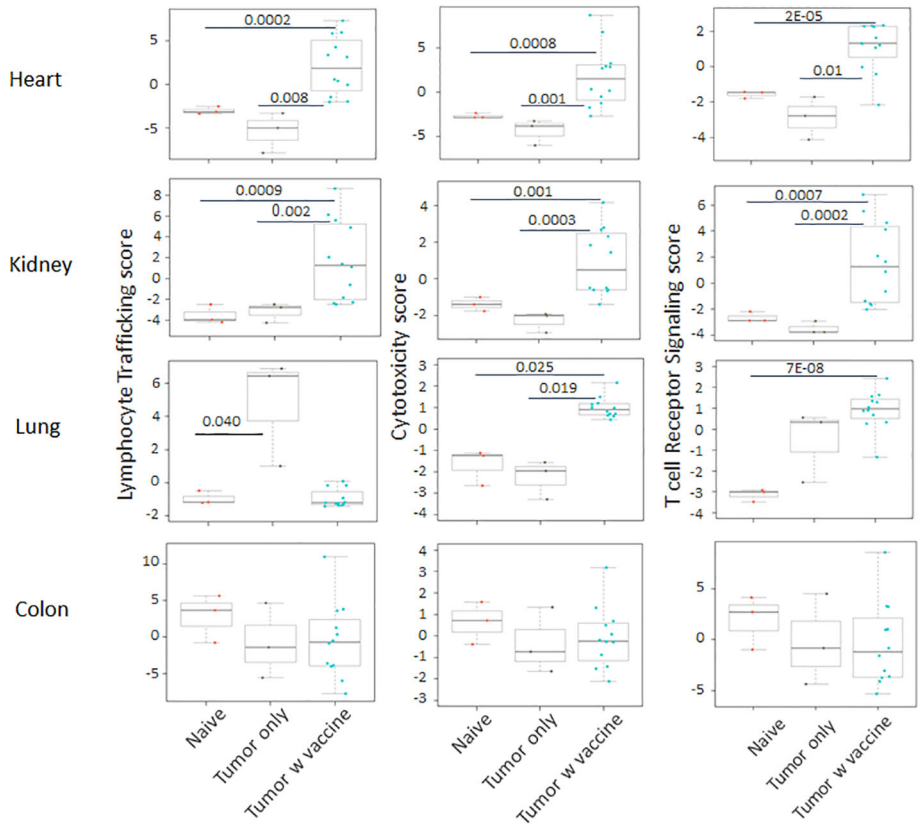

FIGURE 3
The autoimmune signaling pathway scores that relate to lymphocyte trafficking were all significantly increased in the tumor vaccinated group in heart, kidney and lung, but not in colon when compared with the organs collected from unvaccinated tumor only mice (n=3) and naïve mice (n=3) at day 30 after tumor inoculation. The vaccination strategy is described in Figure 1. Unpaired two-tailed Student's t-test was performed for the statistical analysis and $p<0.05$ was considered statistically significant.

high dose 7 day established tumors, compared with tumor only control (p=0.009), whereas administration of CD24-Fc at the start of vaccination resulted in 55% cure, which was better than controls (13% cure) without vaccine, but was not statistically significant (p=0.1) (Figure 6A). In the second model of delayed CD24-Fc administration, there was no difference in tumor free survival between the mice that received IgG or CD24-Fc treatment (93% versus 94%), in which the tumor control group (no vaccine) had no survivors at day 30 (Figure 6B). In summary, these results suggest that CD24-Fc administration at the time of initial tumor vaccination can impair tumor immunity, but if the administration of CD24-Fc is delayed after the initial vaccination and administered with the boosters, the effect on tumor immunity induced by the vaccine does not appear to be hindered.

CD24-Fc treatment with vaccination can ameliorate the autoimmune responses induced by effective tumor vaccination

We analyzed auto-immune responses in lung, heart, kidney and colon tissues of mice in the various groups, including naïve mice (n=3), vaccinated mice administered IgG-Fc with vaccination (n=12) and vaccinated mice administered CD24-Fc with vaccination (n=12) at day 30 after tumor inoculation and vaccination therapy following delayed vaccine model. The global expression of mRNA was compared using NanoString Autoimmune Profiling arrays. The upregulated autoimmune signatures were broadly suppressed by CD24-Fc in heart tissue. Concurrent with changes in immune cell profiles (Figure 7; Supplement Figure 3), CD24-Fc repressed multiple genes that include antigen presentation (Figure 8), lymphocyte differentiation and trafficking (Supplement Figure 4), and chemokines and cytokines (Supplement Figure 5), major inflammatory signaling pathways (Supplement Figure 6) in the cardiac tissue assayed. Most genes that were significantly upregulated by tumor vaccine therapy were dampened by CF24-Fc. The top 28 up-regulated immune genes expressed in the heart tissue of vaccinated mice compared to naïve controls, were also amongst the most dampened genes suppressed by CD24-Fc (fold change>3 and p value<0.05). These genes are listed in Table 1. These results suggest that CD24-Fc can efficiently suppress the autoimmune response that was induced by vaccination therapy in cardiac tissue. There are also variable degrees of autoimmune response following vaccination in kidney and lung tissue samples, in which CD24-Fc suppressed specific targets, but without the broad impact it seemed to have in the cardiac tissues. (Supplement Figures 4–6). No significant

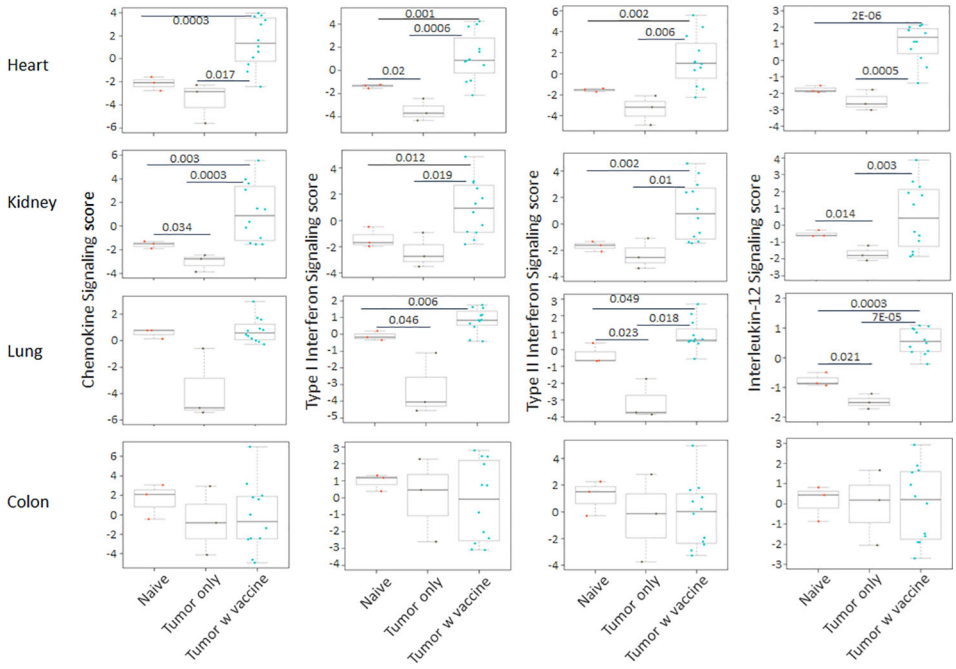

FIGURE 4
The autoimmune signaling pathway scores that related to chemokines and cytokines were also markedly augmented in the heart, kidney and lung tissue collected from the tumor vaccinated mouse group, but this change was absent in the colon when compared with the organs that were collected from unvaccinated tumor only mice (n=3) and naïve mice (n=3) at day 30 after tumor inoculation. The vaccination strategy is described in Figure 1. Unpaired two-tailed Student's t-test was performed for the statistical analysis and $p<0.05$ was considered statistically significant.

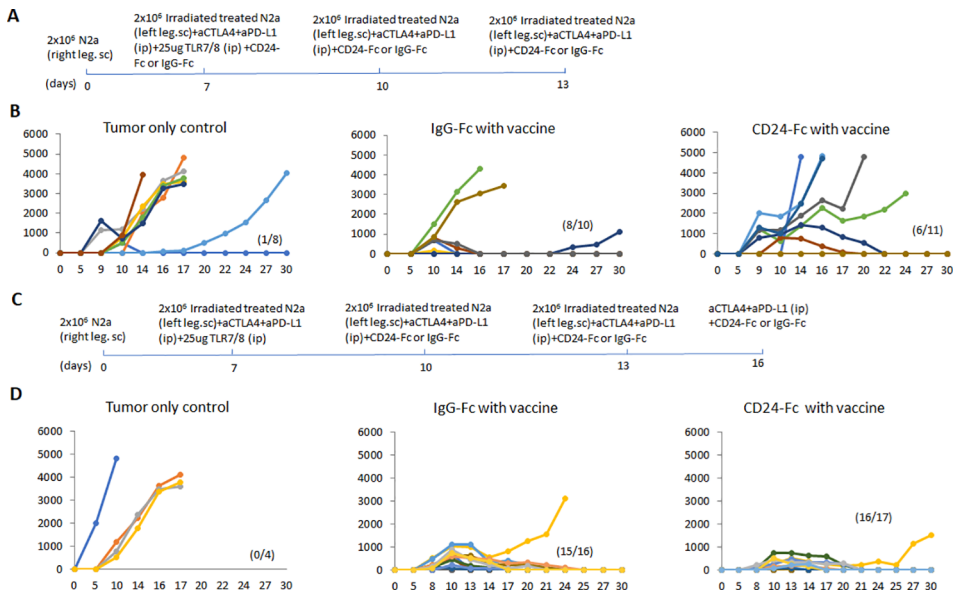

FIGURE 5
(A) The immediate vaccine model in which the vaccine protocol and timeline are depicted. $2x10^6$ Neuro2a cells were injected (subcutaneously) in the right flanks of A/J mice on day 0. CD24-Fc or human IgG-Fc control was injected simultaneously with the whole cell vaccine plus anti-PD-L1/CTLA4 antibodies on day 7, 10 and 13 post tumor inoculation. **(B)** The graphs reflect individual tumor growth in various treatment groups. Absence of tumor in individual mice is recorded in parenthesis. **(C)** The delayed vaccine model in which the vaccine protocol and timeline are depicted. The vaccination protocol and anti-PD-L1/CTLA4 antibodies were injected on day 7, 10 and 13, while CD24-Fc or IgG-Fc was administered three days after the first dose of vaccine on day 10, 13 and 16. **(D)** The graphs reflect individual tumor growth in the various treatment groups. Absence of tumor in individual mice is recorded in parenthesis.

10.3389/fimmu.2023.1176370

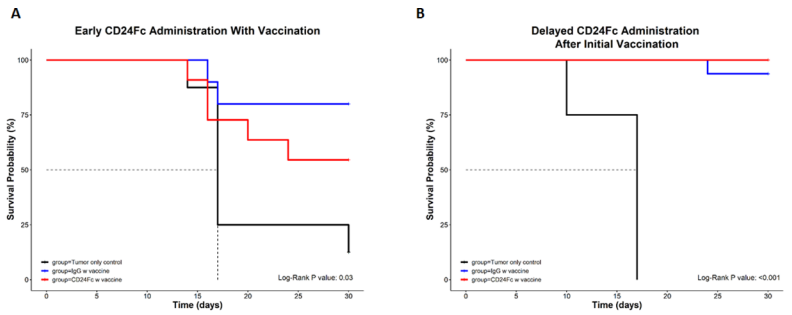

Groups	Median Survival time (days)	Hazard Ratio (95% CI)	Log-Rank P value
Tumor-only control vs. IgG w vaccine	17 vs. NA	0.15 (0.03, 0.73)	0.009
Tumor-only control vs. CD24Fc w vaccine	17 vs. NA	0.38 (0.12, 1.21)	0.100
IgG w vaccine vs. CD24Fc w vaccine	NA	2.60 (0.50, 13.40)	0.200

Groups	Median Survival time (days)	Hazard Ratio (95% CI)	Log-Rank P value
Tumor-only control vs. IgG w vaccine	17 vs. NA	-	<0.0001
Tumor-only control vs. CD24Fc w vaccine	17 vs. NA	-	<0.0001
IgG w vaccine vs. CD24Fc w vaccine	NA	-	0.300

FIGURE 6
In this survival analysis, we compared survival and tumor growth between the three study groups (tumor-only control vs. IgG w vaccine vs. CD24-Fc w vaccine) **(A)** depicts the immediate (early) administration of CD24-Fc, while **(B)** depicts the delayed administration of CD24-Fc with vaccine. For the survival analysis, we calculated and compared the median survival time and the cumulative survival probability using the Kaplan-Meier survival estimator followed by a log-rank test, and calculated hazard ratio (HR) using the Cox proportional-hazards regression model. The comparison between the groups is shown in the tables below the graphs. * NA= median survival time could not be calculated since at least 50% of the subjects in that group didn't have the outcome event (death) ** Hazard ratios could not be calculated due to a lack of adequate outcome events.

autoimmune responses were detected in colon tissue following vaccination and CD24-Fc did not change autoimmune profiles in these tissue specimens either.

To validate nanostring RNA transcript results, we performed immunohistochemistry staining of the immune cell marker CD45 on the same heart samples that were used for nanostring analysis. Results showed that the IgG-Fc group had significantly more CD45 (Figure 9) positive immune cell infiltrates than unvaccinated tumor only controls and naïve controls. Adding CD24-Fc significantly reduced the infiltration of CD45 positive cells in the cardiac tissue.

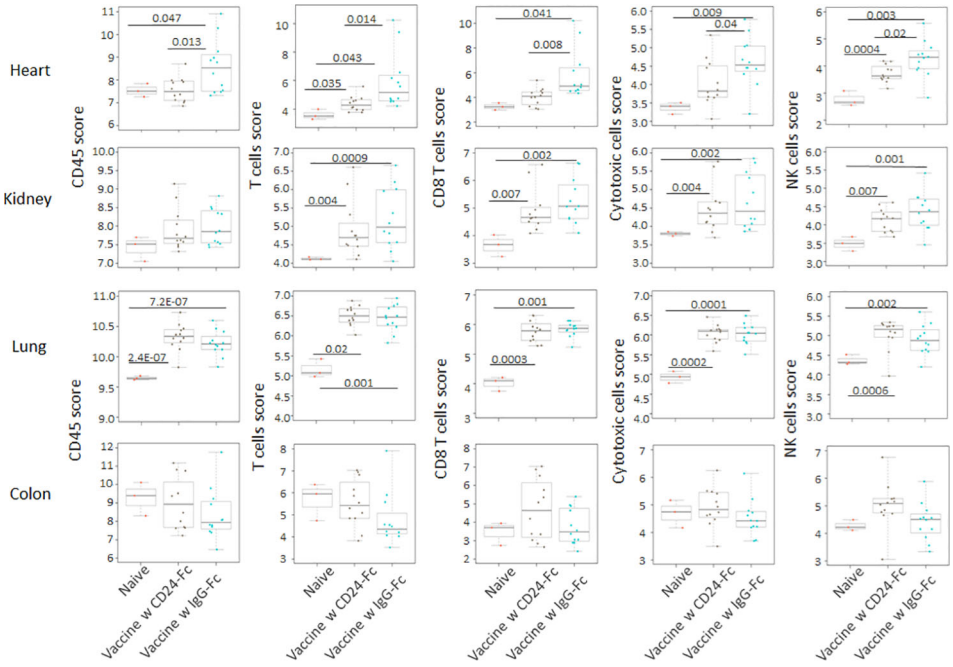

FIGURE 7
Following the delayed vaccination model in which the CD24-Fc or IgG-Fc was administered three days after the first dose of vaccine, the auto-immune responses in lung, heart, kidney and colon tissues of mice in the various groups, including naïve mice (n=3), vaccinated mice administered IgG-Fc with vaccination (n=12) and vaccinated mice administered CD24-Fc with vaccination (n=12) at day 30 after tumor inoculation were compared using NanoString Autoimmune Profiling arrays. Cell type analysis reveals that the influx of several immune cell subtypes was suppressed by delayed CD24-Fc treatment in cardiac tissue. Statistical significance was determined by unpaired two-tailed Student's t-test and $p<0.05$ was considered statistically significant.

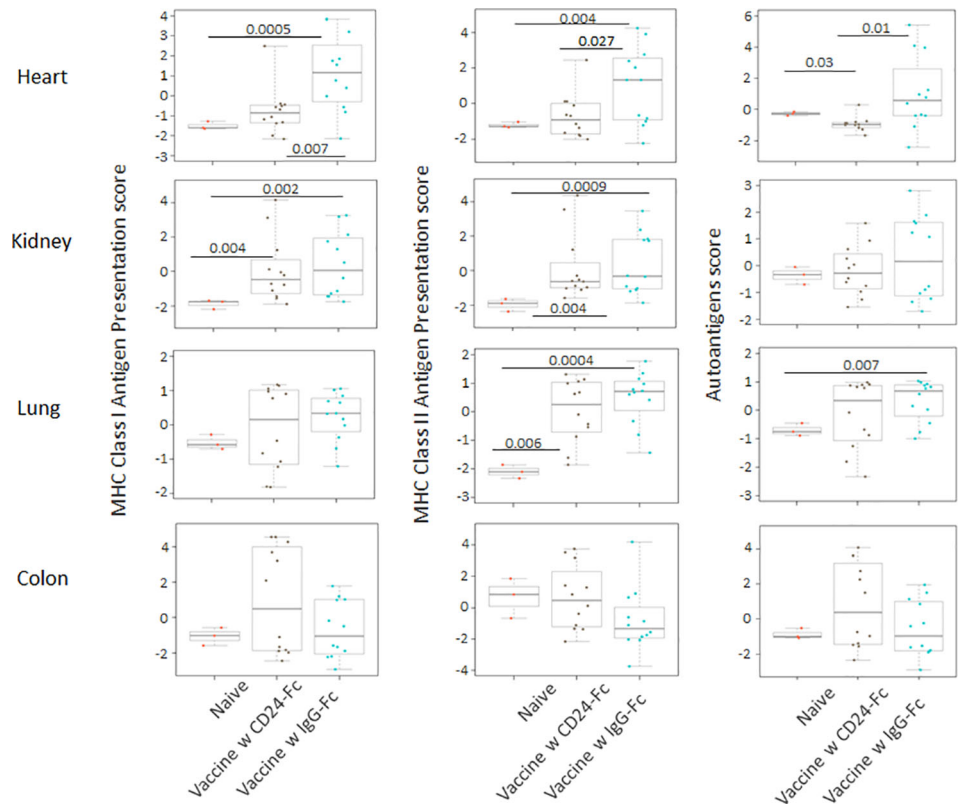

FIGURE 8
Delayed CD24-Fc treatment repressed the pathway scores of multiple autoimmune signaling that related to antigen presentation in cardiac tissue. Statistical significance was determined by unpaired two-tailed Student's t-test and $p<0.05$ was considered statistically significant.

Taken together, these data demonstrate that autoimmunity occurs to a different extent in various organ systems and the administration of CD24-Fc alleviates much of the autoimmune response observed. Despite dampening these immune related adverse tissue specific events, appropriate timing of CD24-Fc administration can still maintain sufficient immunotherapeutic effect of vaccination in the mouse neuroblastoma model.

Discussion

The combination of Myc-inhibited tumor cells with checkpoint inhibition generates a potent therapeutic cancer vaccine in the mouse neuroblastoma model. We previously noted that a combination of both vaccination and checkpoint inhibitors cured 75% of mice and significantly improved long-term survival despite a large initial tumor cell challenge (20). To consider translating this therapeutic strategy from pre-clinical studies to clinical trials, knowledge of auto-immune side effects is essential. The great progress made by cancer immunotherapy is tempered by the occurrence of irAE. The immune related toxicities can be unpredictable, effect multiple organ systems and can be of variable severity. Managing these adverse events is a major challenge for the continued success of current immunotherapies or for the application of potent combined immunotherapeutic approaches. Several other aspects of irAE remain clinically concerning in that: i.) there may be an association between the efficacy of an anti-tumor immunotherapeutic response and the severity of the irAE (21, 22); ii.) many diagnostic challenges persist in patients with irAE in which some of the consequences of organ injury may be clinically occult; and iii.) the management of irAE is unclear as potential drugs suppressing these events may also suppress the effectiveness of the immunotherapy itself.

In the current study, we tested autoimmune responses in mouse lung, heart, kidney and colon tissues thirty days following an effective tumor vaccination combined with immune checkpoint inhibitors. Nanostring AutoImmune mouse gene profiling and immunohistochemistry staining were used to analyze signaling pathways, immune cell infiltrates and changes in gene profiles. We found that there were varying levels of immune cell infiltration in the heart, lungs and kidneys. In addition, multiple autoimmune signaling pathways were significantly upregulated, especially in the heart and kidneys. Surprisingly, there was no obvious autoimmune response in the colon of mice tested, which was unexpected considering the higher incidence of colitis seen in patients receiving immune therapy. Speculatively, the colitis may be pre-conditioned in patients and exacerbated by immunotherapy which does not seem to be the case in the mouse model. These results suggest that the tumor vaccine model induced organ specific autoimmune responses, that were clinically occult and preferentially detected in cardiac and renal tissues. The results are based on 770 human genes encompassing 35 pathways and

TABLE 1 Top statistically significantly up-regulated genes in heart tissue of vaccinated mice compared with naïve control, which are the most dampened genes by CD24 Fc (fold change>3 and p value<0.05,).

Gene ID	Fold change (Vaccinated vs Naïve)	P-value	Fold change (CD24Fc vs IgG w vaccination)	P-value	Gene Function
Cd8b1	71.4	9E-05	-11.7	6E-05	Lymphocyte Trafficking, T-cell Receptor Signaling
Cd6	31.7	7E-04	-17.3	2E-05	Lymphocyte Trafficking
Cd3d	26.9	2E-04	-12.5	1E-05	T-cell Checkpoint Signaling, T-cell Receptor Signaling
Cd27	24.0	6E-04	-16.7	7E-06	T-cell Checkpoint Signaling
Cd5	23.9	0.003	-19.4	3E-05	T-cell Checkpoint Signaling
Lat	21.9	0.003	-31.9	3E-06	Fc Receptors and Phagocytosis, Growth Factor Signaling, NF-kB Signaling, T-cell Receptor Signaling
Cxcl10	20.0	0.002	-4.1	0.009	Chemokine Signaling, Cytosolic DNA Sensing, Endothelial Activation, Th17 Mediated Biology, TNF Family Signaling, Toll Like Receptor Signaling
Cd4	19.5	0.003	-19.8	2E-05	Lymphocyte Trafficking, T-cell Checkpoint Signaling, T-cell Receptor Signaling
Zap70	19.2	0.003	-14.7	5E-05	NF-kB Signaling, T-cell Receptor Signaling
Cd3g	18.2	5E-04	-12.3	1E-05	T-cell Checkpoint Signaling, T-cell Receptor Signaling
Cd3e	17.1	5E-04	-11.4	1E-05	T-cell Checkpoint Signaling, T-cell Receptor Signaling
Itk	14.9	0.003	-7.6	5E-04	Chemokine Signaling, Fc Receptors and Phagocytosis, Lymphocyte Trafficking, T-cell Receptor Signaling
Xcl1	12.2	0.002	-4.9	3E-04	Chemokine Signaling
Ccl8	8.6	0.003	-3.5	0.005	Chemokine Signaling
Il2ra	8.2	0.019	-11.9	9E-05	Other Interleukin Signaling, Th2 Differentiation
Cd7	7.1	0.003	-3.1	0.002	Lymphocyte Trafficking
Lrr1	5.8	0.025	-9.6	7E-05	MHC Class I Antigen Presentation
Hist1h4k	5.1	0.008	-7.0	1E-05	Autoantigens
Slamf6	5.0	0.016	-3.0	0.007	Cytotoxicity
Gata3	4.5	0.02	-4.0	0.001	Th2 Differentiation
Hist1h3b	4.4	0.009	-5.6	2E-05	Autoantigens, Epigenetics and Transcriptional Regulation
Pycard	4.4	0.046	-3.2	0.013	Cytosolic DNA Sensing, Inflammasomes, NLR Signaling
Il18	4.0	0.044	-4.3	0.002	Cytosolic DNA Sensing, NLR Signaling, Other Interleukin Signaling
Kif22	3.9	0.036	-5.9	1E-04	MHC Class II Antigen Presentation
Ikzf1	3.8	0.026	-5.1	1E-04	Epigenetics and Transcriptional Regulation
Casp1	3.8	0.017	-3.3	0.001	Cytosolic DNA Sensing, Inflammasomes, NLR Signaling
Ikzf3	3.6	0.037	-5.1	2E-04	Epigenetics and Transcriptional Regulation
Hist1h2bk	3.6	0.013	-4.4	5E-05	Autoantigens

processes, that are involved in immune system dysfunction and autoimmune disease. The cell profiling feature included in the panel allows for the relative quantification of 14 different immune cell types (23). The score of total lymphocytes (CD45+ cells), cytotoxic T cells (CD8α+ cells), exhausted T cells, Treg, neutrophils, DCs and mature NK cells are all significantly increased in the cardiac tissue collected from vaccinated mice when compared to naïve and tumor only controls. The scores of B cells, mast cells and macrophages didn't change significantly. The ratio of CD8+ T cells/Total TIL, and CD8+ T cells/CD4+ T cells were also enhanced following vaccination. Similar trends of T cells (cytotoxic, exhausted and Treg) and NK cells to a lesser degree were observed in kidney and lung tissue after vaccination. In addition, the score of macrophages and B cells were significantly increased in lung tissue. The signature scores are determined using the Inflammation Signature Algorithm across all RNA input levels. The leukocyte marker CD45 was evaluated using IHC in cardiac tissue from the same animals. Staining confirmed the findings of the nanostring analysis in which the pro-inflammatory infiltration of CD45 following vaccination was detected in the heart tissue which was inhibited

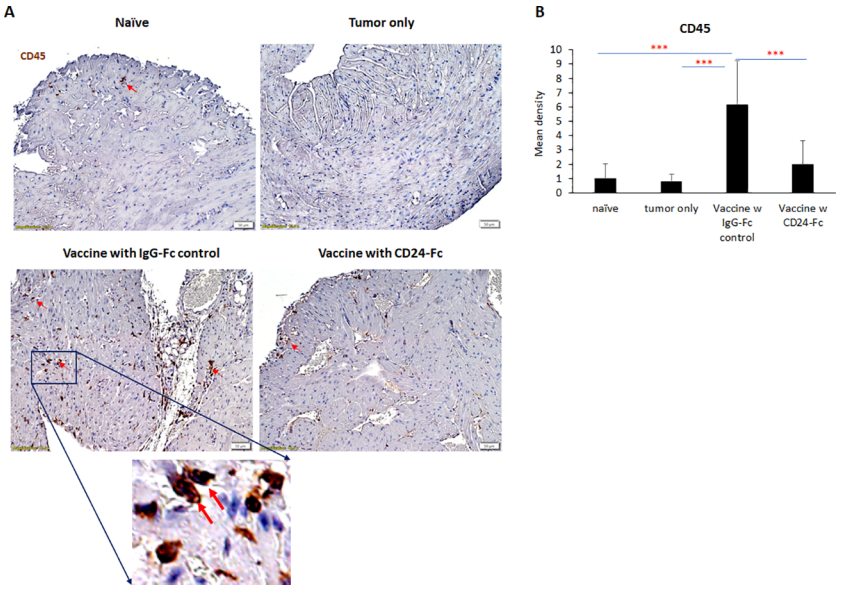

FIGURE 9
To validate nanostring results, CD45 expression was evaluated with immunohistochemical staining in heart tissue from naïve, tumor only control, and vaccination groups combined with either IgG-Fc or with CD24-Fc. **(A)** Representative images of CD45 staining visualized with diaminobenzidine **(DAB)** (brown) and hematoxylin (blue, nuclei) counter staining. Area in the blue box was enlarged and the CD45 staining of corresponding area was shown. **(B)** Optical density (mean gray value) obtained by color deconvolution analysis. Optical density graph bars represent the mean ± SD (n = 20 images). ***p<0.001, determined by unpaired two-tailed Student's t-test.

by CD24-Fc administration. Although there is moderate lymphocytic infiltration in the major organs examined and immune signatures were upregulated, no obvious life-threatening cardiac or renal side effects were noted in the mice at 30 days, nor were any seen in prior mouse models with long term survival at the carefully selected doses of immune checkpoints.

A CD24-Fc fusion protein composed of the extracellular part of CD24 and the human IgG-Fc portion has shown encouraging results in clinical trials as a specific modulator of auto-inflammatory syndromes. The current study evaluates whether CD24-Fc could be used to prevent or treat irAE while evaluating the effect on T cell anti-tumor immunity with tumor vaccine therapy. We studied two vaccine strategies in mouse neuroblastoma models to evaluate the influence of CD24-Fc on the therapeutic effect of the vaccine. We compared the treatment of CD24-Fc administered at the onset of vaccination (initial) or administered with follow-up booster vaccination (delayed). When CD24-Fc was used at the onset of vaccination, it appeared to have dampened the anti-tumor efficacy of the cancer vaccine. However, when we delayed administration of CD24-Fc for three days at the time of booster vaccination, there was no impact on survival rate in which tumor rejection was similar to controls. The impact on vaccination of initial administration may be explained by the potential immune checkpoint inhibitory and anti-inflammatory function of CD24. Upon administration, CD24-Fc immediately binds to injured tumor cell components and prevents the interaction of DAMPs with toll-like receptors (TLRs) inhibiting both nuclear factor-kappa B (NFkB) activation and secretion of inflammatory cytokines, which may dampen tumor immunity induced by the vaccine (24). In addition, CD24-Fc could bind to and activate Siglec G/10, stimulate SHP-1-mediated inhibitory signaling, and prevent NFkB activation and secretion of inflammatory mediators, which may further prevent lymphocytic infiltration (25). Moreover, CD24-Fc may also initiate tumor cell proliferation and behave as a "don't eat me" signal to assist in tumor evasion from phagocytosis. On the other hand, using CD24-Fc later with booster vaccination would avoid the initial suppressive effect, thus allowing the vaccine to activate immune pathways and boost immune cell infiltrates in the tumor. Delaying CD24-Fc administration at the time of the booster would theoretically have the desired effect of suppressing DAMPs, limiting non-specific tissue damage and suppressing inflammation through blockade of NF-κB activation (8) without suppressing the anti-tumor effect. Further optimizing the dose and timing of administration of CD24-Fc with vaccination is important for suppressing auto-immunity.

Another interesting finding from this study is the variable effect of CD24-Fc as it was more efficient in suppressing the auto-immune response in the heart when compared to other organs. A caveat to this observation is that the auto-immunity in the heart was most prominent in comparison, thus any suppressive effect would be more obvious. Alternatively, the strong suppressive effect could be due to CD24 receptor engagement. CD24 can interact with Siglecs, a class of sialic acid binding receptors on immune cells and selectively repress tissue damage-induced immune responses. DAMPs such as HMGB1, HSP70 and -90 are presented to Siglec by binding to their high affinity ligand CD24, which leads to the activation of

immunoreceptor tyrosine-based inhibitory motifs (ITIM) and the subsequent abrogation of inflammatory cytokine signals through a blockade of NF-κB activation (26). Siglec-G is the major receptor for CD24-Fc in mice (27), and is primarily expressed on immune cells including monocytes, granulocytes and lymphocytes. Our tumor vaccine induced the most abundant immune cell infiltrate in cardiac tissue, which provides CD24-Fc with the most Siglec binding sites and thus a positive feedback loop for CD24-Fc to inhibit the autoimmune response. CD24 Fc can bind to multiple Siglec receptors, and each Siglec has a unique specificity for sialylated ligands, making it more probable that additional signaling pathways, including but not limited to the axis of the CD24-Fc-siglec G may be recruited. It will be of interest to define which ligands and Siglecs are present and able to interact with CD24-Fc in the various organs systems.

Taken together, our data demonstrates that the combination of Myc-overexpressing tumor cell vaccine with check point inhibitors is an efficient and relatively safe therapeutic strategy for treating neuroblastoma in a mouse model. Despite this seemingly safe therapy, occult auto-immune effects are detected in the cardiac, renal and pulmonary tissue evaluated thirty days after vaccination. The systemic administration of CD24-Fc, is sufficient to suppress autoimmune responses in the heart, but appropriate timing of administration is critical in order to avoid suppression of the vaccine therapy effect as noted in this mouse neuroblastoma tumor model.

Data availability statement

The datasets presented in this study can be found in online repositories. The names of the repository/repositories and accession number(s) can be found in the article/Supplementary Material.

Ethics statement

The animal study was reviewed and approved by the IACUC at Children's National Hospital.

Author contributions

AS conceived the idea and acquired funding for the study. AS and XW wrote the original draft, and all authors reviewed and edited the manuscript; XW, MB, PS, TZ, SL, PZ, YL and AS interpreted the data, made the figures, planned the experiments, performed and analyzed the experiments. All authors reviewed, edited, and approved the final manuscript.

Funding

This work has been supported in part by NIH R01CA227671 Authors receiving (PZ, AS), the EVAN Foundation, the Catherine Blair foundation, and the Michael Sandler Research Fund as well as the Sheikh Zayed Institute for Pediatric Surgical Innovation. Author receiving: AS.

Acknowledgments

We thank Mrs Karuna Panchapakesan and Dr Susan Knoblach from the Children's National Genetic and Bioinformatics Core for helping with Nanostring experimental setup, and the Pathology department at the Children's National Hospital for their assistance in tissue sample processing.

Conflict of interest

Authors PZ and YL were employed by the company OncoC4. Inc.

The remaining authors declare that the research was conducted in the absence of any commercial or financial relationships that could be construed as a potential conflict of interest.

Publisher's note

Supplementary material

The Supplementary Material for this article can be found online at: https://www.frontiersin.org/articles/10.3389/fimmu.2023.1176370/full#supplementary-material

SUPPLEMENTARY FIGURE 1
The lung, heart, kidney and colon were harvested from naïve mice (n=3), unvaccinated tumor only mice (n=3), and vaccinated mice (n=12) after tumor inoculation at day 30. The global expression of mRNA from each organ was investigated using NanoString Autoimmune Profiling arrays. Profiling analysis revealed that heart, kidney and lung from the vaccination group demonstrated a moderate to severe increase in signature markers for dendritic cells, neutrophils, macrophages, and B cells when compared to naïve and tumor only control mice. Statistical significance was determined by unpaired two-tailed Student's t-test, and $p<0.05$ was considered statistically significant.

SUPPLEMENTARY FIGURE 2
The autoimmune signaling pathway scores that related to major inflammatory signaling pathways were all significantly augmented in the heart, kidney and lung tissue collected from tumor vaccinated mice, but these were not observed in the colon. Unpaired two-tailed Student's t-test was performed for the statistical analysis and $p<0.05$ was considered statistically significant.

SUPPLEMENTARY FIGURE 3
Delayed CD24Fc treatment did not have significant impact on infiltration of dendritic cells, neutrophils, macrophages, and B cells in heart, kidney, lung and colon tissue. Statistical significance was determined by unpaired two-tailed Student's t-test and $p<0.05$ was considered statistically significant.

SUPPLEMENTARY FIGURE 4
Delayed CD24Fc treatment repressed the pathway scores of multiple autoimmune signals related to lymphocyte differentiation and trafficking in heart tissue. Statistical significance was determined by unpaired two-tailed Student's t-test and p<0.05 was considered statistically significant.

SUPPLEMENTARY FIGURE 5
Delayed CD24Fc treatment repressed the pathway scores of multiple autoimmune signals related to chemokines and cytokines in heart tissue. Statistical significance was determined by unpaired two-tailed Student's t-test and p<0.05 was considered statistically significant.

SUPPLEMENTARY FIGURE 6
Delayed CD24Fc treatment repressed the pathway scores of multiple autoimmune signals that related to major inflammatory pathways in heart tissue. Statistical significance was determined by unpaired two-tailed Student's t-test and p<0.05 was considered statistically significant.

References

1. Boutros C, Tarhini A, Routier E, Lambotte O, Ladurie FL, Carbonnel F, et al. Safety profiles of anti-CTLA-4 and anti-PD-1 antibodies alone and in combination. *Nat Rev Clin Oncol* (2016) 13(8):473–86. doi: 10.1038/nrclinonc.2016.58

2. Young A, Quandt Z, Bluestone JA. The balancing act between cancer immunity and autoimmunity in response to immunotherapy. *Cancer Immunol Res* (2018) 6 (12):1445–52. doi: 10.1158/2326-6066.CIR-18-0487

3. Horvat TZ, Adel NG, Dang TO, Momtaz P, Postow MA, Callahan MK, et al. Immune-related adverse events, need for systemic immunosuppression, and effects on survival and time to treatment failure in patients with melanoma treated with ipilimumab at memorial Sloan Kettering cancer center. *J Clin Oncol* (2015) 33(28):3193–8. doi: 10.1200/JCO.2015.60.8448

4. Faje AT, Lawrence D, Flaherty K, Freedman C, Fadden R, Rubin K, et al. High-dose glucocorticoids for the treatment of ipilimumab-induced hypophysitis is associated with reduced survival in patients with melanoma. *Cancer* (2018) 124 (18):3706–14. doi: 10.1002/cncr.31629

5. Osorio JC, Ni A, Chaft JE, Pollina R, Kasler MK, Stephens D, et al. Antibody-mediated thyroid dysfunction during T-cell checkpoint blockade in patients with non-small-cell lung cancer. *Ann Oncol* (2017) 28(3):583–9. doi: 10.1093/annonc/mdw640

6. Wang Y, Abu-Sbeih H, Mao E, Ali N, Ali FS, Qiao W, et al. Immune-checkpoint inhibitor-induced diarrhea and colitis in patients with advanced malignancies: retrospective review at MD Anderson. *J Immunother Cancer.* (2018) 6(1):37. doi: 10.1186/s40425-018-0346-6

7. Hernandez C, Huebener P, Schwabe RF. Damage-associated molecular patterns in cancer: a double-edged sword. *Oncogene* (2016) 35(46):5931–41. doi: 10.1038/onc.2016.104

8. Liu Y, Chen GY, Zheng P. CD24-siglec G/10 discriminates danger- from pathogen-associated molecular patterns. *Trends Immunol* (2009) 30(12):557–61. doi: 10.1016/j.it.2009.09.006

9. Chen GY, Tang J, Zheng P, Liu Y. CD24 and siglec-10 selectively repress tissue damage-induced immune responses. *Science* (2009) 323(5922):1722–5. doi: 10.1126/science.1168988

10. Chen GY, Chen X, King S, Cavassani KA, Cheng J, Zheng X, et al. Amelioration of sepsis by inhibiting sialidase-mediated disruption of the CD24-SiglecG interaction. *Nat Biotechnol* (2011) 29(5):428–35. doi: 10.1038/nbt.1846

11. Chen W, Han C, Xie B, Hu X, Yu Q, Shi L, et al. Induction of siglec-G by RNA viruses inhibits the innate immune response by promoting RIG-I degradation. *Cell* (2013) 152(3):467–78. doi: 10.1016/j.cell.2013.01.011

12. Zheng P, Yang L, Chen H, Devenport M, Reddy P, Farag SS, et al. Targeting danger associated molecular pattern (DAMP) with CD24-fc to reduce acute gvhd: study design on a randomized double blind placebo controlled phase III clinical trial (CATHY study). *Biol Blood Marrow Transplant* (2020) 26(3):S180–S1. doi: 10.1016/j.bbmt.2019.12.741

13. Welker J, Pulido JD, Catanzaro AT, Malvestutto CD, Li Z, Cohen JB, et al. Efficacy and safety of CD24-fc in hospitalised patients with COVID-19: a randomised, double-blind, placebo-controlled, phase 3 study. *Lancet Infect Dis* (2022) 22(5):611–21. doi: 10.1016/S1473-3099(22)00058-5

14. Barkal AA, Brewer RE, Markovic M, Kowarsky M, Barkal SA, Zaro BW, et al. CD24 signalling through macrophage siglec-10 is a target for cancer immunotherapy. *Nature* (2019) 572(7769):392–6. doi: 10.1038/s41586-019-1456-0

15. Yin SS, Gao FH. Molecular mechanism of tumor cell immune escape mediated by CD24/Siglec-10. *Front Immunol* (2020) 11:1324. doi: 10.3389/fimmu.2020.01324

16. Wang L, Liu R, Ye P, Wong C, Chen GY, Zhou P, et al. Intracellular CD24 disrupts the ARF-NPM interaction and enables mutational and viral oncogene-mediated p53 inactivation. *Nat Commun* (2015) 6:5909. doi: 10.1038/ncomms6909

17. Liu Y, Jones B, Aruffo A, Sullivan KM, Linsley PS, Janeway CAJr. Heat-stable antigen is a costimulatory molecule for CD4 T cell growth. *J Exp Med* (1992) 175 (2):437–45. doi: 10.1084/jem.175.2.437

18. Liu Y, Wenger RH, Zhao M, Nielsen PJ. Distinct costimulatory molecules are required for the induction of effector and memory cytotoxic T lymphocytes. *J Exp Med* (1997) 185(2):251–62. doi: 10.1084/jem.185.2.251

19. Wu Y, Zhou Q, Zheng P, Liu Y. CD28-independent induction of T helper cells and immunoglobulin class switches requires costimulation by the heat-stable antigen. *J Exp Med* (1998) 187(7):1151–6. doi: 10.1084/jem.187.7.1151

20. Wu X, Nelson M, Basu M, Srinivasan P, Lazarski C, Zhang P, et al. MYC oncogene is associated with suppression of tumor immunity and targeting myc induces tumor cell immunogenicity for therapeutic whole cell vaccination. *J Immunother Cancer* (2021) 9(3):e001388. doi: 10.1136/jitc-2020-001388

21. Zou W, Chen L. Inhibitory B7-family molecules in the tumour microenvironment. *Nat Rev Immunol* (2008) 8(6):467–77. doi: 10.1038/nri2326

22. Sjoblom T, Jones S, Wood LD, Parsons DW, Lin J, Barber TD, et al. The consensus coding sequences of human breast and colorectal cancers. *Science* (2006) 314 (5797):268–74. doi: 10.1126/science.1133427

23. Danaher P, Warren S, Dennis L, D'Amico L, White A, Disis ML, et al. Gene expression markers of tumor infiltrating leukocytes. *J Immunother Cancer.* (2017) 5:18. doi: 10.1186/s40425-017-0215-8

24. Piccinini AM, Midwood KS. DAMPening inflammation by modulating TLR signalling. *Mediators Inflamm* (2010) 2010:672395. doi: 10.1155/2010/672395

25. Lin CH, Yeh YC, Yang KD. Functions and therapeutic targets of siglec-mediated infections, inflammations and cancers. *J Formos Med Assoc* (2021) 120(1 Pt 1):5–24. doi: 10.1016/j.jfma.2019.10.019

26. Royster W, Wang P, Aziz M. The role of siglec-G on immune cells in sepsis. *Front Immunol* (2021) 12:621627. doi: 10.3389/fimmu.2021.621627

27. Toubai T, Hou G, Mathewson N, Liu C, Wang Y, Oravecz-Wilson K, et al. Siglec-G-CD24 axis controls the severity of graft-versus-host disease in mice. *Blood* (2014) 123(22):3512–23. doi: 10.1182/blood-2013-12-545335

frontiers | Frontiers in Immunology

TYPE Original Research
PUBLISHED 07 June 2023
DOI 10.3389/fimmu.2023.1175960

OPEN ACCESS

EDITED BY
Sang T. Kim,
University of Texas MD Anderson Cancer Center, United States

REVIEWED BY
Justin Jagodinsky,
University of Wisconsin-Madison, United States
Eric Chi-ching Ko,
University of Massachusetts Medical School, United States

*CORRESPONDENCE
Xianling Liu
liuxianling@csu.edu.cn
Nong Yang
yangnong0217@163.com
Fang Ma
fangma@csu.edu.cn

†These authors have contributed equally to this work and share first authorship

RECEIVED 28 February 2023
ACCEPTED 18 May 2023
PUBLISHED 07 June 2023

CITATION
Liu C, Zeng L, Deng C, Jiang W, Wang Y, Zhou Y, Liu L, Wang S, Zhou C, Qiu Z, Zeng F, Wu F, Weng J, Liu X, Yang N and Ma F (2023) Hypofractionated radiotherapy with immunochemotherapy for extensive-stage small-cell lung cancer. *Front. Immunol.* 14:1175960. doi: 10.3389/fimmu.2023.1175960

Hypofractionated radiotherapy with immunochemotherapy for extensive-stage small-cell lung cancer

Chaoyuan Liu[1†], Liang Zeng[2†], Chao Deng[1], Wenjuan Jiang[2], Yapeng Wang[1], Yiguang Zhou[1], Li Liu[2], Sisi Wang[1], Chunhua Zhou[2], Zhenhua Qiu[1], Fanxu Zeng[2], Fang Wu[1], Jie Weng[3], Xianling Liu[1,4*], Nong Yang[2*] and Fang Ma[1*]

[1]Department of Oncology, The Second Xiangya Hospital, Central South University, Changsha, Hunan, China, [2]Department of Medical Oncology, Lung Cancer and Gastrointestinal Unit, Hunan Cancer Hospital/The Affiliated Cancer Hospital of Xiangya School of Medicine, Central South University, Changsha, China, [3]Department of Oncology, Yueyang Center Hospital, Yueyang, China, [4]Department of Oncology, Guilin Hospital of the Second Xiangya Hospital, Central South University, Guilin, China

Introduction: The combination of a PD-L1 inhibitor plus carboplatin/cisplatin and etoposide (EC/EP) has become a new standard first-line treatment for extensive-stage small-cell lung cancer (ES-SCLC). Combining concurrent palliative hypofractionated radiotherapy of the thorax (HFRT) and immunochemotherapy may have a synergistic effect. In this study, we explored an optimal model of combination radiotherapy with immunochemotherapy as first-line treatment of ES-SCLC.

Patients and methods: In this multicenter single-arm phase 2 trial, patients with ES-SCLC received atezolizumab with EC/EP for two cycles (induction phase), then, those who did not progress received concurrent palliative HFRT and two cycles of atezolizumab with EC/EP (combination phase). Afterward they received atezolizumab every 3 weeks for a maximum of 2 years after study enrolment (maintenance phase). Prophylactic cranial irradiation (PCI) was recommended. The primary endpoints were safety and tolerance; the second endpoints were progression-free survival (PFS).

Results: Forty patients were enrolled, and all had completed palliative HFRT and four cycles of immunochemotherapy. There were seven grade 3 adverse events (3 decreased neutrophil count, 1 anemia, 2 pneumonitis, 1 esoenteritis), two grade 4 adverse events (2 decreased white cell count) and no grade 5 toxicities. The pneumonitis rate was 12.5% (three grade 2 and two grade 3 events). At the median follow-up of 14.2 months (range, 6.8–28.7), the median PFS was 8.6 months (95%CI, 6.1–11.1).

Conclusion: The addition of concurrent hypofractionated thoracic radiotherapy to first-line immunochemotherapy for ES-SCLC was well tolerated and showed promising clinical efficacy. Additional randomized trials are needed to validate benefits.

Clinical trial registration: https://clinicaltrials.gov/ (NCT 04636762).

KEYWORDS

extensive-stage small-cell lung cancer, thoracic radiation, immunochemotherapy, safety, progression free survival

Introduction

Small cell lung cancer (SCLC) accounts for 15% of lung cancer cases and is an aggressive cancer characterized by rapid growth, early metastasis, and a poor prognosis (1). Approximately 75% of SCLC patients present with extensive-stage disease at the time of diagnosis, which is classically defined as a disease that cannot be encompassed by a single radiation field (2). Before the era of immunotherapy, the standard first-line therapy for ES-SCLC was platinum-based chemotherapy with etoposide (3); Once complete remission (CR) or partial remission (PR) was achieved after chemotherapy, consolidative thoracic radiation was recommended (4). Despite this standard treatment, the median overall survival (OS) of ES-SCLC is about 8–11 months, which has not changed for about 40 years (5).

Significant progress has been achieved in the treatment of ES-SCLC in recent years. Based on the results of the IMPOWER 133 study and the Caspian study, the PD-L1 inhibitor (Atezolizumab or Durvalumab) with EC/EP has become the new first-line treatment for ES-SCLC (6, 7). However, the results of ES-SCLC remain poor, with a median OS of only approximately 12–13 months (6, 7). There is therefore an urgent need for the development of long-lasting effective treatments for ES-SCLC.

Radiation could induce immunogenic cell death and enhance the antitumor immune response; therefore, synergizing with α-PD-1/PD-L1 inhibitor and can create an abscopal effect (8–10). Previous studies have shown that hypofractionated radiotherapy and immune checkpoint therapy might generate synergistic effects (9, 11). The addition of HFRT to immunochemotherapy may enhance antitumor immunity and improve outcomes (11, 12). The safety and efficacy of combining α-PD-1/PD-L1 inhibitor plus thoracic radiotherapy have been tested in several clinical trials in lung cancer. For example, an international double-blind, placebo-controlled phase III trial PACIFIC showed that adjuvant durvalumab treatment after chemoradiotherapy improved both PFS and OS in patients with stage III NSCLC (13). Some phase 1/2 studies (NCT02621398, NCT02434081, NCT02402920, NCT03585998) also revealed that the α-PD-1/PD-L1 inhibitor plus concurrent chemoradiotherapy combination was tolerable in patients with advanced NSCLC and limited stage SCLC, with promising clinical efficacy (14–16). However, the optimal model for combining immunochemotherapy and radiotherapy remains unknown (17), and there is no report on the safety and efficacy of the combination of concurrent HFRT and immunochemotherapy in ES-SCLC. Therefore, we designed this trial (NCT04636762) to explore a preferred model of combining immunochemotherapy and radiation and to evaluate the safety and efficacy of adding palliative HFRT to standard first-line immunochemotherapy treatment in patients with ES-SCLC. We present a safety profile and a final analysis of PFS.

Abbreviations: PCI, Prophylactic cranial irradiation;CR, complete remission; PR, partial remission; SD, stable disease; PD, progressive disease; EC, carboplatin and etoposide; EP, cisplatin and etoposide; SCLC, Small cell lung cancer; ES-SCLC, extensive-stage small-cell lung cancer; HFRT, hypofractionated radiotherapy of the thorax; PFS, progression-free survival; RECIST 1.1, Response Evaluation Criteria in Solid Tumors, version 1.1.

Methods

Patients

The patients were screened at the second Xiangya Hospital, the Hunan Cancer Hospital, and the Yueyang Central Hospital in Hunan province. Inclusion criteria were: 1) adults with histologically confirmed ES-SCLC (the Veterans Administration Lung Study Group staging system) with an Eastern Cooperative Oncology Group (ECOG) performance status score of 0 or 1 (on a 5-point scale, with higher numbers reflecting greater disability); 2) patients with adequate organ function and with no history of previous systemic treatment for ES-SCLC; 3) patients with no disease progression after two cycles of EC/EP with atezolizumab; and 4) patients treated for asymptomatic central nervous system metastases.

The key exclusion criteria were the following: 1) patients with another malignancy that is progressing or requires active treatment; 2) patients with active autoimmune disease or other condition requiring systemic steroids or immunosuppressive agents within the previous 3 months (except for physiological steroid replacement); 3) patients with carcinomatous meningitis; and 4) patients with a history of active Bacillus tuberculosis (TB) or other active infection requiring systemic therapy. Efficacy assessments

were performed according to Response Evaluation Criteria in Solid Tumors, version 1.1 (RECIST 1.1).

Trial design and interventions

The trial was an open, single arm, multicenter, phase 2 trial. The treatment process was divided into three phases: induction, combination, and maintenance phase. The recruited eligible patients received two 21-day cycles of the investigator's choice of cisplatin (75 mg/m^2) or carboplatin (area under the curve [AUC] of 5 mg/ml/minute, administered intravenously on day 1 of each cycle) and etoposide (100 mg per square meter of body-surface area, administered intravenously on days 1 through day 3 of each cycle) with concurrent atezolizumab (at a dose of 1200 mg, administered intravenously on day 1 of each cycle) in the induction phase. Cranial irradiation was completed in the induction phase as needed at the discretion of the investigator. If the disease did not progress after the induction phase, the patients were enrolled and the treatment moved to the combination phase. In the combination phase, we added thoracic palliative-hypofractionated radiation therapy to the third cycle of immunochemotherapy. The thoracic radiotherapy protocol involved intensity-modulated radiation therapy based on CT planning, which entailed administering a total dose of 30-45Gy over 10-15 treatment days (equivalent to 14-21 calendar days). The therapy was delivered once daily, with a dose of 3Gy per session. The radiation therapy to the metastatic lesions was permitted at the discretion of the investigators. All radiotherapy procedures were managed by a radiotherapy quality assurance program designed by the Radiation Oncology Department of the Second Xiangya Hospital, Central South University. After the concurrent radiotherapy and the third cycle of immunochemotherapy, the fourth cycle of immunochemotherapy was given without delay. The combination phase was followed by a maintenance phase, in which patients received atezolizumab every 3 weeks for a maximum of 2 years after study enrolment until the appearance of unacceptable toxic effects or disease progression according to RECIST 1.1. During the maintenance phase, prophylactic cranial irradiation (PCI, 25 Gy, 10 fractions) was allowed.

End points and assessments

The primary endpoints were safety and tolerance. The key secondary endpoint was PFS assessed by the investigator (the time from initial immunochemotherapy to disease progression according to RECIST 1.1 or death from any cause, whichever occurred first) in the population with intention of treatment.

Tumor evaluations were performed at the time of diagnosis, every 6 weeks for the first 18 weeks (starting from day 1 of the first cycle), and every 9 weeks thereafter until the appearance of disease progression according to RECIST 1.1. Adverse events were assessed according to the National Cancer Institute Common Terminology Criteria for Adverse Events, version 4.0. The investigators determined whether adverse events were related to the trial regimen.

Statistical analysis

Primary and secondary endpoints were evaluated in the intention-to-treat population. The PFS was calculated from the date of immunochemotherapy of the first protocol to the date of progression, death, or the last follow-up, whichever came first. The PFS was estimated by Kaplan–Meier analysis. Summary statistics were calculated along with confidence intervals. The small sample size precluded formal statistical comparison with historical control.

Results

Patients

Between 6 June 2020 and 31 November 2021, a total of 40 patients were enrolled at three sites in China. The eligibility and analysis flow chart is shown in Figure 1.

The demographics of the baseline patient and the characteristics of the disease are shown in Table 1. Most of the participants were males (97.5%), current or former smokers (92.5%), and the median age was 58 years old (range, 47 to 75). Most had metastatic disease with an ECOG score of 1.

Treatment

The treatment exposure in the 40 enrolled patients is shown in Table 2. The median number of atezolizumab doses received was 9 (range, 4 to 29). Eight (20%) patients received 12 or more doses of atezolizumab. All patients received four cycles of platinum–etoposide, half received cisplatin, and the remainder received carboplatin. Six (15%) patients received PCI in the maintenance phase.

Safety

The safety of all 40 patients was evaluated. Adverse events related to any component of the trial regimen occurred in 39

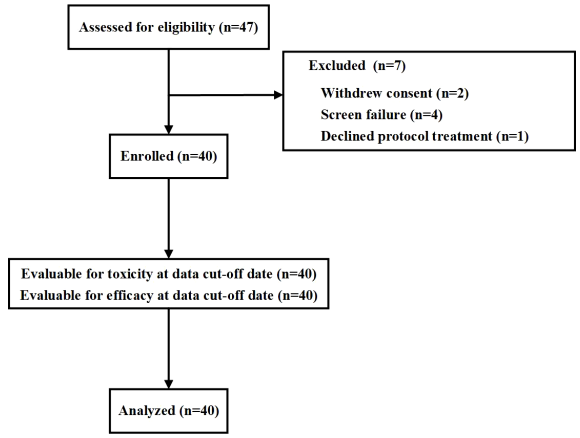

FIGURE 1
Flowchart showing study eligibility and analysis.

TABLE 1 Baseline characteristics of all enrolled patients (Intention-to-Treat Population).

Characteristics	no. (%)
Mean age (min, max) – years	58 (47,75)
Age group, years	
<65	27 (67.5%)
≥65	13 (32.5%)
Sex	
female	1 (2.5%)
male	39 (97.5%)
Smoking status	
Never smoked	3 (7.5%)
Current smoker	32 (80%)
Former smoker	5 (12.5%)
Disease stage	
III	9 (22.5%)
IV	31 (77.5%)
ECOG score	
0	7 (17.5%)
1	33 (82.5%)
Brain metastasis at enrollment	3 (7.5%)
Liver metastases at enrollment	6 (15%)

patients (97.5%). The most common grade 3 or 4 adverse events related to the trial regimen were a decrease in white blood cell count (Table 3). No death related to the trial regimen occurred. Thyroid dysfunction was the most common immune-related adverse event; it appeared in 10 patients (25%), with grade 1–2 hypothyroidism. Treatment-associated pneumonitis occurred in 5 patients (12.5%); only two of them were grade 3 (5%); the remainder were grades 1 or 2. Of these immune-related adverse events, only 3 patients discontinued maintenance treatment with atezolizumab due to grade 3 esoenteritis (1 patient) or grade 3 pneumonitis (2 patients, who recovered after active treatment with corticosteroids).

TABLE 2 Treatment exposure (safety population).

Atezolizumab (N=40)	
Median number of atezolizumab doses, median (min, max)	9 (4, 29)
Patients receiving 12 or more atezolizumab doses	8 (20%)
Platinum	
Cisplatin	20 (50%)
Carboplatin	20 (50%)
Patients receiving PCI	6 (15%)

PCI, Prophylactic cranial irradiation.

TABLE 3 The incidence of Adverse events of any cause (safety population).

Adverse events	Any Grade – (no,(%))	Grade 3 – (no,(%))	Grade 4 – (no,(%))
Any event	39 (97.5%)	7 (17.5%)	2 (5%)
Any event leading to discontinuation	3 (7.5%)	3 (7.5%)	0
Decreased white cell count	21 (52.5%)	3 (7.5%)	2 (5%)
Decreased platelet count	4 (10%)	0	0
Anemia	25 (62.5%)	1 (2.5%)	0
Alopecia	14 (35%)	0	0
Nausea	12 (30%)	0	0
Fatigue	8 (20%)	0	0
Decreased appetite	9 (22.5%)	0	0
Vomiting	5 (12.5%)	0	0
Constipation	4 (10%)	0	0
Diarrhea	3 (7.5%)	0	0
Hypo-albuminemia	2 (5%)	0	0
Pneumonitis	5 (12.5%)	2 (5%)	0
Thyroid dysfunction	10 (25%)	0	0
Myocarditis	1 (2.5%)	0	0
Esoenteritis	1 (2.5%)	1 (2.5%)	0
Esophagitis	12 (30%)	0	0

Multiple occurrences of the same adverse event in one patient were counted once at the highest grade for the preferred term. The incidence of treatment-related adverse events associated with any component of the trial regimen is shown. no. (%): "no" means the number of patients who have the according adverse events, and "%" means the incidence of the according adverse events.

Progression-free survival analysis

The data cutoff date was 26 October 2022. The median follow-up time was 14.2 months (range, 6.8–28.7), the median PFS was 8.6 months (95%CI, 6.1–11.1) (Figure 2). The PFS rate at 12 months was 27.5%. PFS according to baseline characteristics is shown in Table 4.

Confirmed objective response rate

The investigator-assessed confirmed objective response rates (from the start of the screening to the time of enrollment) are shown in Table 5. In total, 32 (32/44,72.7%) patients achieved a partial response (PR) and 40 (40/44,90.9%) patients achieved disease control. A waterfall map of the best response of the enrolled patients is shown in Figure 3. In total, the lesions of 39 (39/40,97.5%) patients decreased, and 25 (25/40,62.5%) patients achieved PR.

10.3389/fimmu.2023.1175960

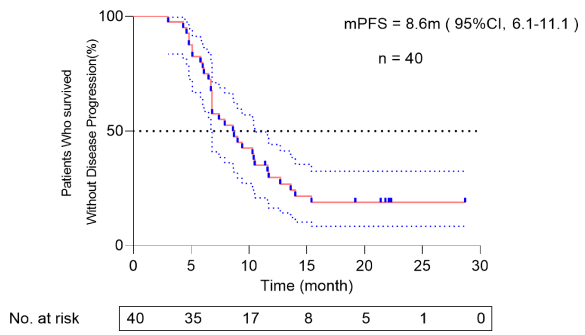

FIGURE 2
Kaplan–Meier plots of progression-free survival. The blue dot lines represent 95% CI of PFS.

Discussion

Radiotherapy plays an important role in ES-SCLC. A large phase 3 randomized controlled trial CREST showed that the addition of thoracic radiotherapy prolonged progression-free survival at 6 months (24% vs. 7%, P=0.001) and the 2-year OS (13% vs. 3%, P=0.004) significantly. Thoracic radiotherapy was thus recommended for all patients with ES-SCLC who respond to chemotherapy (18). The NCCN guidelines also recommend thoracic radiotherapy if ES-SCLC achieves CR or PR after chemotherapy. However, in the era of immunotherapy, the optimal timing, radiation schedule, safety, and efficacy of thoracic radiotherapy in ES-SCLC have yet to be evaluated. In limited-stage SCLC, concurrent chemoradiotherapy is more effective than sequential chemoradiotherapy (19), and thoracic radiation should be initiated in the first or second cycle of chemotherapy (20–22). Thus, earlier radiation may be beneficial for SCLC. Furthermore, some studies have shown that compared to post-immunotherapy radiation, pre-immunotherapy or concurrent radiation could induce more potent abscopal responses (23, 24). Our study added hypofractionated thoracic radiation after two cycles of immunochemotherapy in ES-SCLC patients who responded. There are two similar ongoing trials registered on the ClinicalTrials website. These trials were designed to explore the safety and efficacy of concurrent radiation and immunochemotherapy in recurrent ES-SCLC or in ES-SCLC refractory to initial platinum-based chemotherapy (NCT03262454, NCT04562337), and did not investigate the first-line treatment evaluated in our study. To our

TABLE 4 PFS according to baseline characteristics.

	No. of Patients (%)	Median PFS (months)	HR (95%CI)
Age group			
<65 years	27 (67.5%)	7.90	0.98 (0.94-1.03)
≥65 years	13 (32.5%)	10.30	
Sex			
Female	1 (2.5%)	Undefined	Undefined
Male	39 (97.5%)	8.60	
Smoking status			
Never smoked	3 (7.5%)	11.60	1.61 (0.80-3.24)
Current smoker	32 (80%)	6.80	
Former smoker	5 (12.5%)	11.70	
Disease stage			
III	9 (22.5%)	9.40	1.596 (0.66-3.89)
IV	31 (77.5%)	7.90	
ECOG score			
0	7 (17.5%)	7.40	1.041 (0.40-2.71)
1	33 (82.5%)	8.70	
Brain metastasis at enrollment			
YES	3 (7.5%)	6.67	2.66 (0.28-24.97)
NO	37 (92.5%)	8.63	
Liver metastases at enrollment			
YES	6 (15%)	6.70	1.69 (0.53-5.42)
NO	34 (85%)	9.37	

TABLE 5 Summary of tumor responses.

Best response after first two cycles of immunochemotherapy	
CR	0
PR	32
SD	8
PD	4

CR, complete remission; PR, partial remission; SD, stable disease; PD, progressive disease.

knowledge, this study is the first report of a prospective trial evaluating the safety and efficacy of concurrent thoracic palliative-hypofractionated radiation plus immunochemotherapy in patients with ES-SCLC.

The addition of concurrent thoracic palliative-hypofractionated radiotherapy after two cycles of immunochemotherapy is the key difference between the regimen adopted in the present study and the atezolizumab regimens in the IMPOWER 133 trial. The follow-up time was about 14 months (ours vs. IMPOWER 133, 14.2 months vs. 13.9 months). The median number of atezolizumab doses used was comparable between the present study and the IMPOWER 133 study: 9 (range, 4 to 29) vs. 7 (range, 1 to 30), respectively. Adverse events related to any component of the trial regimen occurred in 97.5% of the patients (in IMPOWER 133, 94.9%). The most common all-grade adverse events were anemia and decreased white blood cell count. The shared grade 3 or 4 adverse events related to the trial regimen were a reduced white blood cell count. Unlike IMPOWER133, there was no Grade 5 adverse event in the present study. The most immune-related adverse event in both studies was hypothyroidism. Some studies reported increased pneumonitis when combining immunochemotherapy and thoracic radiation (9, 25). All-grade and grade 3-5 pneumonitis was higher in the present study compared to the IMPOWER 133 study, 12.5% (5/40) vs. 4% (8/198) and 5% (2/40) vs. 2.5% (5/198), respectively. Nevertheless, there was no grade 5 pneumonitis in our study. The incidence of all-grade or grade 3-5 pneumonitis in our study is comparable to those reports that combined immunochemotherapy and thoracic radiotherapy in NSCLC (25, 26). In SCLC, a Phase I/II Trial reported the incidence of all-grade pneumonitis of the regimen of pembrolizumab and concurrent chemoradiation therapy for limited-stage small cell lung cancer was 15% (6/40), grade 1-2 and grade 3 effects were half-to-half (15), which was more or less similar to those observed in our study. In the present study, although more patients experienced pneumonitis than those in the IMPOWER 133 trial, all patients recovered after active treatment with corticosteroids. In summary, the addition of thoracic radiation to immunotherapy leads to a higher incidence of pneumonitis, but it is manageable. Due to the short follow-up time in the current study, it is not possible to assess long-term toxic effects such as pulmonary fibrosis and esophageal stricture or fistula. In summary, first-line concurrent thoracic palliative-hypofractionated radiation plus immunochemotherapy for ES-SCLC has an acceptable safety profile, at least in the short term.

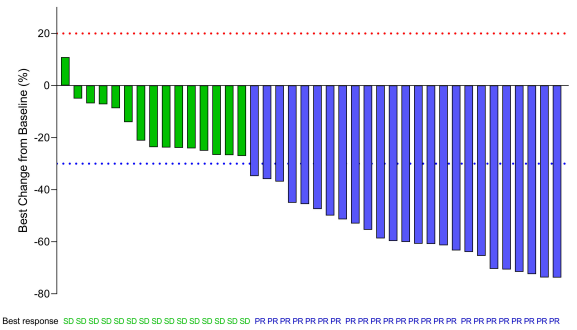

FIGURE 3
Waterfall map showing the best response of enrolled patients. The waterfall plots display an individual patient's best response data expressed as the percent change in the sum of the longest diameter of target lesions as measured at baseline and the best response during the whole treatment period. (SD, PR) is indicated by the color of the data bar. SD, stable disease; PR, partial response. The red dot line represents 20% increase in the sum of the longest diameter of target lesions than baseline according to RECIST 1.1. The green dot line represents 30% decrease in the sum of the longest diameter of target lesions than baseline according to RECIST 1.1.

The PFS in the present study is approximately 3.4 months longer than that of IMPOWER 133(8.6 months (95%CI, 6.1–11.1)) vs. 5.2 m (95% CI, 4.4–5.6)). The PFS rate at 12 months is 27.5%. An abstract in the 2021 ESMO congress (Abstract NO.#2568) reported a retrospective study that showed a significant improvement in PFS for patients with ES-SCLC undergoing atezolizumab and consolidating thoracic radiotherapy, which is consistent with our study. In the retrospective study mentioned above, consolidating thoracic radiation therapy was performed during the atezolizumab maintenance phase; the detailed radiation dose and fractionation schedules remained unknown, which differed from our study. The previous study did not report any benefit in overall survival (OS) for patients undergoing the combination of atezolizumab and consolidating thoracic radiotherapy. Whether the PFS benefit revealed in our study could convert into an OS benefit requires further follow-up.

Unlike in the IMPOWER 133 trial, the PFS in patients with treated brain or liver metastases was shorter than in those without brain or liver metastases in our study. However, no conclusions can be drawn due to the small number of patients with brain or liver metastases enrolled in the trial. Similar to the IMPOWER 133 trial, we also noticed that older patients had a longer PFS than younger patients. Further analyses are needed to explore the potential mechanisms.

This phase II trial has its limitations. First, the sample size was small. Second, the follow-up time was relatively short and we did not have the final analysis of OS. Third, this study was a single-arm and open trial, some inevitable biases included selection bias, differential and non-differential reporting bias, and confounding effects. However, these limitations could not obscure its contributions to exploring an optimal model of first line treatment for ES-SCLC.

In summary, this open, single-arm, multicenter, phase 2 trial showed that the addition of concurrent thoracic palliative-hypofractionated radiation therapy to first-line standard immunochemotherapy resulted in significantly longer PFS than immunochemotherapy, with a manageable safety profile. Our findings laid a foundation for further randomized investigations.

Data availability statement

The raw data supporting the conclusions of this article will be made available by the authors, without undue reservation.

Ethics statement

The studies involving human participants were reviewed and approved by the Declaration of Helsinki and Good Clinical Guidelines and ethics committee and the institutional review board of the Second Xiangya Hospital of Central South University (2020–089). All patients provided their written informed consent to participate in this study.

Author contributions

Main contribution: XL: Conceptualization, Methodology. NY: Conceptualization, Methodology. FM: Conceptualization, Methodology. CL: Data curation, Writing- Original draft preparation. LZ: Data curation, Writing- Original draft preparation. CD: Investigation, Supervision. WJ: Investigation, Writing- Reviewing and Editing. YZ, Data curation. YW: Formal analysis, Investigation. LL: Investigation. SW: Investigation, Validation. CZ: Investigation. ZQ: Investigation. FZ: Formal analysis, Investigation. FW: Investigation, Supervision. JW: Investigation, Supervision. All authors contributed to the article and approved the submitted version.

Funding

The study was sponsored by grant S2020SFYLJS0412 from the Department of Science and Technology of Hunan Province and grant 2023JJ40837 from the Natural Science Foundation of Hunan Province and the Scientific Research Launch Project for new employees of the Second Xiangya Hospital of Central South University.

Acknowledgments

We thank all the patients, their families and all the investigators.

Conflict of interest

The authors declare that the research was conducted in the absence of any commercial or financial relationships that could be construed as a potential conflict of interest.

Publisher's note

References

1. Cristea S, Sage J. Is the canonical RAF/MEK/ERK signaling pathway a therapeutic target in SCLC? *J Thorac Oncol* (2016) 11(8):1233–41. doi: 10.1016/j.jtho.2016.04.018

2. Hellmann MD, Callahan MK, Awad MM, Calvo E, Ascierto PA, Atmaca A, et al. Tumor mutational burden and efficacy of nivolumab monotherapy and in combination with ipilimumab in small-cell lung cancer. *Cancer Cell* (2018) 33:853–861.e4. doi: 10.1016/j.ccell.2018.04.001

3. Owonikoko TK, Dahlberg SE, Sica GL, Wagner LI, Wade JL3rd, Srkalovic G, et al. Randomized phase II trial of cisplatin and etoposide in combination with veliparib or placebo for extensive-stage small-cell lung cancer: ECOG-ACRIN 2511 study. *J Clin Oncol* (2019) 37:222–229. doi: 10.1200/JCO.18.00264

4. Wang S, Zimmermann S, Parikh K, Mansfield AS, Adjei AA. Current diagnosis and management of small-cell lung cancer. *Mayo Clin Proc* (2019) 94:1599–1622. doi: 10.1016/j.mayocp.2019.01.034

5. Seckl MJ, Ottensmeier CH, Cullen M, Schmid P, Ngai Y, Muthukumar D, et al. Multicenter, phase III, randomized, double-blind, placebo-controlled trial of pravastatin added to first-line standard chemotherapy in small-cell lung cancer (LUNGSTAR). *J Clin Oncol* (2017) 35:1506–14. doi: 10.1200/JCO.2016.69.7391

6. Horn L, Mansfield AS, Szczesna A, Havel L, Krzakowski M, Hochmair MJ, et al. First-line atezolizumab plus chemotherapy in extensive-stage small-cell lung cancer. *N Engl J Med* (2018) 379(23):2220–9. doi: 10.1056/NEJMoa1809064

7. Paz-Ares L, Dvorkin M, Chen Y, Reinmuth N, Hotta K, Trukhin D, et al. Durvalumab plus platinum–etoposide versus platinum–etoposide in first-line treatment of extensive-stage small-cell lung cancer (CASPIAN): a randomised, controlled, open-label, phase 3 trial. *Lancet* (2019) 394(10212):1929–39. doi: 10.1016/S0140-6736(19)32222-6

8. Yi M, Zheng X, Niu M, Zhu S, Ge H, Wu K. Combination strategies with PD-1/PD-L1 blockade: current advances and future directions. *Mol Cancer* (2022) 21(1):28. doi: 10.1186/s12943-021-01489-2

9. Shang S, Liu J, Verma V, Wu M, Welsh J, Yu J, et al. Combined treatment of non-small cell lung cancer using radiotherapy and immunotherapy: challenges and updates. *Cancer Commun (Lond)* (2021) 41(11):1086–99. doi: 10.1002/cac2.12226

10. Arina A, Gutiontov SA-O, Weichselbaum RA-O. Radiotherapy and immunotherapy for cancer: from "Systemic" to "Multisite". *Clin Cancer Res* (2020) 26:2777–2782. doi: 10.1158/1078-0432.CCR-19-2034

11. Ye H, Pang H, Shi X, Ren P, Huang S, Yu H, et al. Nivolumab and hypofractionated radiotherapy in patients with advanced lung cancer: ABSCOPAL-1 clinical trial. *Front Oncol* (2021) 11:657024. doi: 10.3389/fonc.2021.657024

12. Miyasaka Y, Sato H, Okano N, Kubo N, Kawamura H, Ohno T. A promising treatment strategy for lung cancer: a combination of radiotherapy and immunotherapy. *Cancers (Basel)* (2021) 14(1):203. doi: 10.3390/cancers14010203

13. Antonia SJ, Villegas A, Daniel D, Vicente D, Murakami S, Hui R, et al. Durvalumab after chemoradiotherapy in stage III non-Small-Cell lung cancer. *N Engl J Med* (2017) 377(20):1919–29. doi: 10.1056/NEJMoa1709937

14. Jabbour SK, Berman AT, Decker RH, Lin Y, Feigenberg SJ, Gettinger SN, et al. Phase 1 trial of pembrolizumab administered concurrently with chemoradiotherapy for locally advanced non-small cell lung cancer: a nonrandomized controlled trial. *JAMA Oncol* (2020) 6:848–855. doi: 10.1001/jamaoncol.2019.6731

15. Welsh JW, Heymach JV, Guo C, Menon H, Klein K, Cushman TR, et al. Phase 1/2 trial of pembrolizumab and concurrent chemoradiation therapy for limited-stage SCLC. *J Thorac Oncol* (2020) 15(12):1919–27. doi: 10.1016/j.jtho.2020.08.022

16. Durm GA-OX, Jabbour SK, Althouse SK, Liu Z, Sadiq AA, Zon RT, et al. A phase 2 trial of consolidation pembrolizumab following concurrent chemoradiation for patients with unresectable stage III non-small cell lung cancer: Hoosier cancer research network LUN 14-179. *Cancer* (2020) 126:4353–4361. doi: 10.1002/cncr.33083

17. Kordbacheh T, Honeychurch J, Blackhall F, Faivre-Finn C, Illidge T. Radiotherapy and anti-PD-1/PD-L1 combinations in lung cancer: building better translational research platforms. *Ann Oncol* (2018) 29:301–310. doi: 10.1093/annonc/mdx790

18. Slotman BJ, van Tinteren H, Praag JO, Knegjens JL, El Sharouni SY, Hatton M, et al. Use of thoracic radiotherapy for extensive stage small-cell lung cancer: a phase 3 randomised controlled trial. *Lancet* (2015) 385(9962):36–42. doi: 10.1016/S0140-6736(14)61085-0

19. Takada M, Fukuoka M, Kawahara M, Sugiura T, Yokoyama A, Yokota S, et al. Phase III study of concurrent versus sequential thoracic radiotherapy in combination with cisplatin and etoposide for limited-stage small-cell lung cancer: results of the Japan clinical oncology group study 9104. *J Clin Oncol Off J Am Soc Clin Oncol* (2002) 20 (14):3054–60. doi: 10.1200/JCO.2002.12.071

20. Stinchcombe TE, Gore EM. Limited-stage small cell lung cancer: current chemoradiotherapy treatment paradigms. *Oncologist* (2010) 15(2):187–95. doi: 10.1634/theoncologist.2009-0298

21. Fried DB, Morris DE, Poole C, Rosenman JG, Halle JS, Detterbeck FC, et al. Systematic review evaluating the timing of thoracic radiation therapy in combined modality therapy for limited-stage small-cell lung cancer. *J Clin Oncol Off J Am Soc Clin Oncol* (2004) 22(23):4837–45. doi: 10.1200/JCO.2004.01.178

22. Murray N, Coy P, Pater JL, Hodson I, Arnold A, Zee BC, et al. Importance of timing for thoracic irradiation in the combined modality treatment of limited-stage small-cell lung cancer. the national cancer institute of Canada clinical trials group. *J Clin Oncol* (1993) 11:336–44. doi: 10.1200/JCO.1993.11.2.336

23. Janopaul-Naylor JR, Shen Y, Qian DC, Buchwald ZS. The abscopal effect: a review of pre-clinical and clinical advances. *Int J Mol Sci* (2021) 22(20):11061. doi: 10.3390/ijms222011061

24. Wei JA-O, Montalvo-Ortiz WA-O, Yu L, Krasco AA-O, Ebstein SA-O, Cortez C, et al Sequence of αPD-1 relative to local tumor irradiation determines the induction of abscopal antitumor immune responses. *Sci Immunol* (2021) 6(58):eabg0117. doi: 10.1126/sciimmunol.abg0117

25. Li B, Jiang C, Pang L, Zou B, Ding M, Sun X, et al. Toxicity profile of combining PD-1/PD-L1 inhibitors and thoracic radiotherapy in non-small cell lung cancer: a systematic review. *Front Immunol* (2021) 12:627197. doi: 10.3389/fimmu.2021.627197

26. Li M, Gan L, Song A, Xue J, Lu Y. Rethinking pulmonary toxicity in advanced non-small cell lung cancer in the era of combining anti-PD-1/PD-L1 therapy with thoracic radiotherapy. *Biochim Biophys Acta Rev Cancer* (2019) 1871(2):323–30. doi: 10.1016/j.bbcan.2019.02.004

frontiers | Frontiers in Immunology

TYPE Case Report
PUBLISHED 07 July 2023
DOI 10.3389/fimmu.2023.1160586

OPEN ACCESS

EDITED BY
Yeonseok Chung,
Seoul National University, Republic of Korea

REVIEWED BY
Wendi Kang,
Chinese Academy of Medical Sciences and Peking Union Medical College, China
Valeria Maffeis,
Ospedale di Treviso, Italy
André Filipe Oliveira,
Hospital do Divino Espírito Santo, Portugal

*CORRESPONDENCE
Leyla Özer
leylahmet@gmail.com

RECEIVED 07 February 2023
ACCEPTED 21 June 2023
PUBLISHED 07 July 2023

CITATION
Mutlu AU, Aytaç E, Gülmez M, Erdamar S and Özer L (2023) Case Report: Chemoimmunotherapy in microsatellite-instability-high advanced goblet cell carcinoma of the colon.
Front. Immunol. 14:1160586.
doi: 10.3389/fimmu.2023.1160586

Case Report: Chemoimmunotherapy in microsatellite-instability-high advanced goblet cell carcinoma of the colon

Arda Ulaş Mutlu[1], Erman Aytaç[2], Mehmet Gülmez[3], Sibel Erdamar[4] and Leyla Özer[5]*

[1]Faculty of Medicine, Acibadem University, Istanbul, Türkiye, [2]Department of General Surgery, Faculty of Medicine, Acıbadem University, Istanbul, Türkiye, [3]Department of Surgery, Grossman School of Medicine, New York University, New York City, United States, [4]Department of Pathology, Faculty of Medicine, Acıbadem University, Istanbul, Türkiye, [5]Department of Medical Oncology, Faculty of Medicine, Acıbadem University, Istanbul, Türkiye

Background: Mismatch repair (MMR) deficiency is a fundamental factor affecting the management treatment outcomes of colorectal cancer (CRC). MMR status can be diagnosed by both immunohistochemistry (IHC) polymerase chain reaction (PCR). Since tumors with MMR deficiency are prone to respond to immunotherapy immune checkpoint inhibitors are used to treat such tumors.

Case presentation: A 69-year-old male patient presented to an outside clinic with weight loss and abdominal pain. Radiological investigations detected a mesenteric mass of 10 cm, peritoneal implants, and mediastinal lymphadenopathy. The eventual biopsy result from the mesenteric mass was mucinous adenocarcinoma with a goblet cell pattern. Since the IHC result was unclear for deficiency in mismatch repair (dMMR) metastatic CRC (mCRC), the diagnosis was confirmed with PCR. The patient received 8 cycles of FOLFIRINOX + bevacizumab followed by FOLFOX combined with pembrolizumab. No adverse effect was reported related to immunotherapy which resulted in radiologic and metabolic regression. The patient underwent cytoreductive surgery and hyperthermic intraperitoneal chemotherapy (HIPEC). The final pathology results revealed a pathological complete response and R0 resection. In the 6th month follow-up, no recurrence or metastasis was reported.

Conclusion: Chemotherapy and immunotherapy combination is a promising treatment modality which can also be used for mCRC. This is the index case who received chemotherapy in combination with immunotherapy for mucinous adenocarcinoma of the colon with a goblet cell pattern and had pCR.

KEYWORDS

chemoimmunotherapy, metastatic colon cancer (mCRC), complete response, MSI-H, microsatellite unstable (high), goblet cell

Introduction

Colorectal cancer (CRC) with a deficiency in mismatch repair (dMMR) is characterized by a strong mutator phenotype known as high microsatellite instability (MSI-H) and tumor mutation burden (1). The vast majority of MSI-H/dMMR colon cancers exhibit distinctive features, such as the tendency to arise in the proximal colon and comprise a poorly differentiated, mucinous, or signet ring cell component (2). Almost 15% of all CRCs harbor MSI-H/dMMR phenotype.

Microsatellite instable (MSI) disease is characterized by an obvious antitumor immune response, with increased lymphocyte infiltrate that entails the basis for the improved prognosis of especially stage II CRC with MSI. An explanation for the lack of benefit of fluoropyrimidine (FP)-based chemotherapy in these patients is the antagonization of antitumor response by the immunosuppressive effects of chemotherapy (3). Fortunately, MSI has been established as a strong predictor of efficacy in blocking the immune checkpoint, leading to the approval of programmed death 1 inhibitors such as nivolumab ± ipilimumab and pembrolizumab for MSI patients with metastatic CRC (mCRC) (4, 5).

There is no data about the utility of the combination of chemotherapy and immunotherapy in mCRC patients, although it has been the standard of care for many types of advanced cancers, such as head and neck, gastric, cervical, and non-small cell lung cancer (6, 7). We represent a case of MSI-H mCRC whose indeterminate MMR findings were confirmed by PCR and who was treated successfully with chemoimmunotherapy.

Case

A 69-year-old male patient presented to an outside clinic with weight loss and abdominal pain. Radiological investigations detected a mesenteric mass of 10 cm, which was supposed to be originating from the right colon. Diagnostic laparoscopy revealed a retroperitoneal mass with peritoneal implants. Biopsies' results were carcinoma and its peritoneal metastasis. Then, the patient was referred to our center. A colonoscopy was performed, revealing a 3 cm diameter mass at the base of the cecum. Mucinous adenocarcinoma with a goblet cell pattern and widespread extracellular mucin secretion was detected (Figure 1). Abdomen magnetic resonance imaging (MRI) showed a 14x5.5x5 cm conglomerate mass and implants extending to the root of the superior mesenteric vein and attaching to the duodenum with minimal ascites in the pelvis (Figure 2A). Thorax computed tomography (CT) pointed at 15x10 mm lymphadenopathy in the mediastinum with no other abnormal finding. Molecular analysis of the primary tumor revealed BRAF V600E mutant, KRAS, NRAS wild, and HER-2 (-) disease. Positron emission tomography/computed tomography (PET/CT) scan revealed conglomerated lesion in the mesentery (SUVMax 23.5), wall thickening in the ascending colon (SUVMax: 26.1), and hypermetabolic areas in the abdomen thought to be due to the spread of the disease in the peritoneum (Figure 2B). The systemic treatment of the patient was started with 5-fluorouracil, folinic acid, irinotecan, oxaliplatin (FOLFIRINOX), and bevacizumab while waiting for the MSI results.

A control CT after 4 cycles of treatment with FOLFIRINOX + bevacizumab regimen showed partial regression, and the treatment was completed to 8 cycles. A PET/CT scan following 8 cycles of FOLFIRINOX + bevacizumab showed a 90% metabolic response (SUVMax: 3). Meanwhile, immunohistochemical evaluation of the MSI panel from the primary tumor showed nuclear dot-like staining patterns for MLH1 (Figure 3A) and PMS2 (Figure 3B). Molecular analysis with PCR was performed due to suspicious staining patterns for MLH-1 and PMS-2. It revealed MSI-H phenotype (Figure 3C). MLH-1 methylation analysis was also performed; hypermethylation in the promoter region of the MLH-1 gene was detected (Figure 3D). The systemic treatment was converted to folinic acid, fluorouracil, and oxaliplatin (FOLFOX) combined with pembrolizumab after the status of MSI-H was confirmed. The rationale behind this strategy was the assumption that the primary tumor, metastatic lymph nodes, and

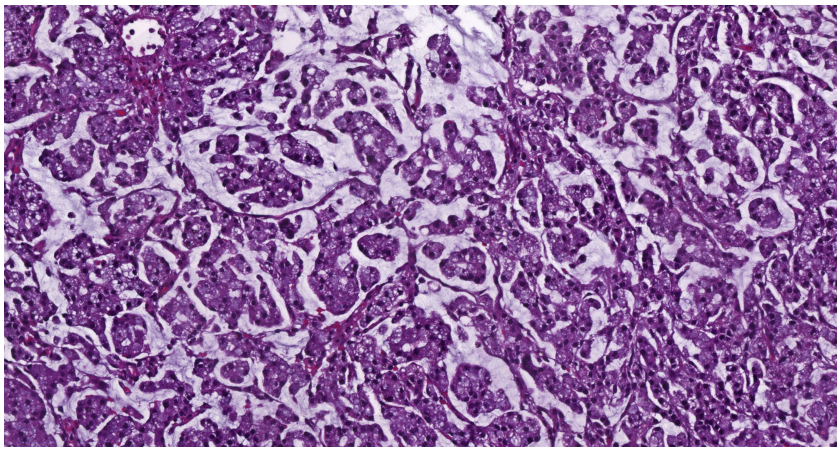

FIGURE 1
Mucinous adenocarcinoma with a goblet cell pattern, H&E x22.3.

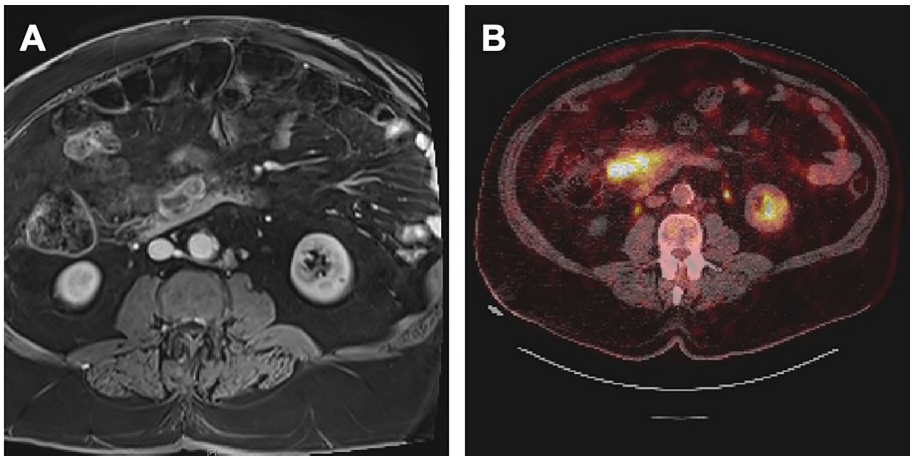

FIGURE 2
(A) MRI at the diagnosis. **(B)** PET/CT at the diagnosis.

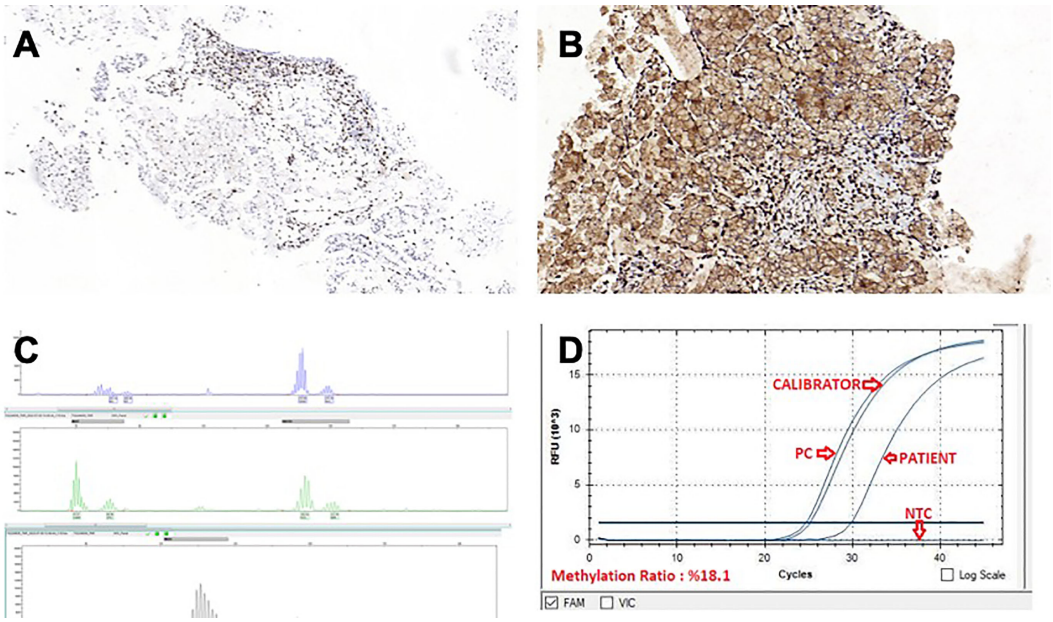

FIGURE 3
(A) MLH-1, IHC x10.0 **(B)** PMS-2, IHC x15.5 **(C)** MSI-H phenotype molecular analysis with PCR **(D)** MLH-1 methylation analysis.

peritoneal implants had responded dramatically to triplet chemotherapy + bevacizumab.

The patient was treated with additional 4 cycles of FOLFOX concurrently with pembrolizumab with no adverse effects. The MRI prior to surgery showed that the cecal mass regressed and was limited to the mesocolon. The patient underwent a right hemicolectomy, a pelvic and lower abdominal peritonectomy, a total omentectomy, and a diverting loop ileostomy. Hyperthermic intraperitoneal chemotherapy with mitomycin-C was administered for 90 minutes. No major surgical complications occurred, and the stoma was reversed a month after the surgery. The pathology results revealed ypT0N0 (60 lymph nodes). There were no tumor cells in the peritoneal fluid cytology. Pembrolizumab as maintenance treatment was continued after curative resection. The patient was tumor free in his postoperative 6th-month follow-up. The treatment was planned to be continued for 24 months if no toxicity or adverse effects were seen. The timeline of the patient is summarized in Figure 4.

Discussion

This case presents a successful treatment of a patient with metastatic MSI mucinous colonic adenocarcinoma with immunotherapy in combination with 5-FU and oxaliplatin based chemotherapy. MSI status is one of the critical factors affecting the

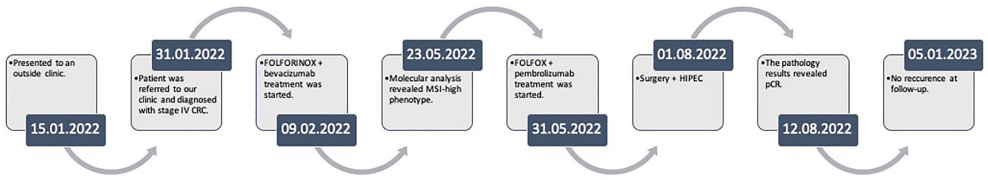

FIGURE 4
Timeline of the patient's management.

treatment approach in mCRC patients (4). While IHC is a more available, cost-effective, rapid, and concordant way to detect MSI status, PCR is a crucial next step to diagnose MSI for inconclusive, borderline cases such as nuclear dot-like staining patterns, as in our patient (8, 9).

Management of mCRC with microsatellite stable status depends on the tumor and patient-related factors, such as performance status and comorbidities, and the aim of the treatment, such as conversion to a resectable state. Usually, a combination of chemotherapy with biological agents like anti-VEGF or anti-EGFR therapy is considered depending on tumor-related factors, including RAS, RAF status, and tumor-sidedness. For MSI-H mCRC patients, pembrolizumab or nivolumab -/+ ipilimumab is recommended as a first-line therapy depending on the results of the KEYNOTE-177 and CM-142 studies (10–12). The Keynote-177 trial revealed 11.1% of complete response and 29.4% of progressive disease in stage IV colorectal patients treated with single-agent pembrolizumab (13). Since the response of BRAF mutant patients to chemotherapy is lower than the wild type, we preferred to start with combination chemotherapy as FOLFIRINOX + bevacizumab until the MSI results were confirmed. Our patient had been a candidate for single-agent pembrolizumab treatment based on the MSI status. However, the MSI tumor's sensitivity to FOLFIRINOX chemotherapy has been confirmed after 4 months of treatment, and a dramatic response had already been demonstrated in PET-CT even before the commencement of pembrolizumab. Due to the 30% risk of progression with single-agent pembrolizumab in the KEYNOTE-177 trial and our patient's *in vivo* confirmed sensitivity to chemotherapy, we preferred to continue FOLFOX regimen concurrently with immunotherapy.

Even though chemotherapy and immunotherapy combination is a widely used treatment approach in non-colorectal cancers in both early and advanced settings with satisfactory long-term results, there is no phase III data supporting the use of this combination for mCRC yet (6, 7).

The hypotheses to explain the biological mechanisms underlying resistance to chemotherapy of MSI-associated diseases primarily concern adjuvant fluorouracil-based treatments in non-metastatic CRC. Studies cited in literature often point at the antitumor immune response characterized by the lymphocyte infiltrate of MSI diseases, constituting the basis for the improved prognosis of these patients in early stages. This advantage is supposed to be antagonized by the immunosuppressive effects of chemotherapy that explain the lack of benefit of single agent fluoropyrimidine-based chemotherapy (3). It is important to emphasize that these studies refer to stage II CRCs. According to some authors, adding irinotecan or oxaliplatin counteracts resistance to fluorouracil in MSI tumors (14, 15). However, these hypotheses have not been confirmed in randomized studies. Two phase III randomized trials for resected stage III MSI CRC have been initiated: the ATOMIC study, which is evaluating FOLFOX (5-FU/LV + oxaliplatin) ± atezolizumab for 6 months plus maintenance with atezolizumab or placebo for 6 months (NCT02912559), and the POLEM study (NCT03827044), which aimed to evaluate the efficacy of 24 weeks of FP versus 12 weeks of FP plus oxaliplatin ± avelumab for MSI or patients with POLE mutation. However, the POLEM study has been terminated due to challenges in patient recruitment.

A phase Ib trial evaluating the effect of chemoimmunotherapy, pembrolizumab, in combination with a modified FOLFOX regimen in metastatic colorectal patients has been completed (16). In this trial, 6.7% of the patients had a complete response, and patients with advanced disease at the time of diagnosis had reduced tumor burden and became eligible for definitive surgery. 6.7% of the patients had grade 3 or 4 toxicity; the remaining patients tolerated the treatment well. Similar to our case, Copur et al. (17) published a case of a locally advanced colon cancer treated with FOLFOX + pembrolizumab, resulting in a pathologically complete response.

BRAF mutation is seen in 38.9% of the patients with MSI, while only 9.3% of patients with MSS CRC have a BRAF mutation, and 20.4% of the patients with BRAF mutation were MSI (8). In the subgroup analysis of KEYNOTE-177 study, BRAF wild type patients seem to have better survival with immunotherapy compared to chemotherapy (for OS; HR 0.72 vs. 0.55 for BRAF mutant and wild type, respectively).

BRAF mutation is associated with poor prognosis reducing the benefits derived from MSI even in the earlier disease setting. The BRAFV600E mutation has been a poor prognostic factor in both MSI and MSS patients underlining the importance of these biomarkers for the management of patients at recurrence (18). Thus, chemoimmunotherapy may be explicitly considered for patients with BRAF mutant and MSI-H tumors since it's a promising approach with a tolerable toxicity.

While being a case report, the major limitation to propose chemotherapy in combination with immunotherapy as a novel treatment for MSI mCRC with in general, this index case can be didactic to plan future studies of this promising approach.

Data availability statement

The original contributions presented in the study are included in the article/supplementary material. Further inquiries can be directed to the corresponding author.

Ethics statement

Written informed consent was obtained from the individual(s) for the publication of any potentially identifiable images or data included in this article. Written informed consent was obtained from the participant/patient(s) for the publication of this case report.

Author contributions

Writing original draft: AM, EA, LO. Supervision: LO, EA, SE. All authors participated in the revision of the manuscript. All authors contributed to the article and approved the submitted version.

Conflict of interest

The authors declare that the research was conducted in the absence of any commercial or financial relationships that could be construed as a potential conflict of interest.

Publisher's note

All claims expressed in this article are solely those of the authors and do not necessarily represent those of their affiliated organizations, or those of the publisher, the editors and the reviewers. Any product that may be evaluated in this article, or claim that may be made by its manufacturer, is not guaranteed or endorsed by the publisher.

References

1. Sinicrope FA. Lynch syndrome–associated colorectal cancer. *New Engl J Med* (2018) 379(8):764–73. doi: 10.1056/nejmcp1714533

2. Boland CR, Goel A. Microsatellite instability in colorectal cancer. *Gastroenterology* (2010) 138(6):2073–2087.e3. doi: 10.1053/j.gastro.2009.12.064

3. Phillips SM, Banerjea A, Feakins R, Li SR, Bustin SA, Dorudi S. Tumour-infiltrating lymphocytes in colorectal cancer with microsatellite instability are activated and cytotoxic. *Br J Surg* (2004) 91(4):469–75. doi: 10.1002/bjs.4472

4. Sherman SK, Schuitevoerder D, Chan CHF, Turaga KK. Metastatic colorectal cancers with mismatch repair deficiency result in worse survival regardless of peritoneal metastases. *Ann Surg Oncol* (2020) 27(13):5074–83. doi: 10.1245/s10434-020-08733-x

5. Le DT, Uram JN, Wang H, Bartlett BR, Kemberling H, Eyring AD, et al. PD-1 blockade in tumors with mismatch-repair deficiency. *New Engl J Med* (2015) 372 (26):2509–20. doi: 10.1056/nejmoa1500596

6. Paz-Ares L, Luft A, Vicente D, Tafreshi A, Gümüş M, Mazières J, et al. Pembrolizumab plus chemotherapy for squamous non–Small-Cell lung cancer. *New Engl J Med* (2018) 379(21):2040–51. doi: 10.1056/nejmoa1810865

7. Gandhi L, Rodríguez-Abreu D, Gadgeel S, Esteban E, Felip E, De Angelis F, et al. Pembrolizumab plus chemotherapy in metastatic non–Small-Cell lung cancer. *New Engl J Med* (2018) 378(22):2078–92. doi: 10.1056/nejmoa1801005

8. Bartley AN, Luthra R, Saraiya DS, Urbauer DL, Broaddus RR. Identification of cancer patients with lynch syndrome: clinically significant discordances and problems in tissue-based mismatch repair testing. *Cancer Prev Res* (2012) 5(2):320–7. doi: 10.1158/1940-6207.capr-11-0288

9. Zhang X, Li J. Era of universal testing of microsatellite instability in colorectal cancer. *World J Gastrointestinal Oncol* (2013) 5(2):12. doi: 10.4251/wjgo.v5.i2.12

10. Benson AB, Venook AP, Al-Hawary MM, Arain MA, Chen YJ, Ciombor KK, et al. Colon cancer, version 2.2021, NCCN clinical practice guidelines in oncology. *J Natl Compr Cancer Network* (2021) 19(3):329–59. doi: 10.6004/jnccn.2021.0012

11. Lenz HJ, Van Cutsem E, Luisa Limon M, Wong KYM, Hendlisz A, Aglietta M, et al. First-line nivolumab plus low-dose ipilimumab for microsatellite instability-High/Mismatch repair-deficient metastatic colorectal cancer: the phase II CheckMate 142 study. *J Clin Oncol* (2022) 40(2):161–70. doi: 10.1200/jco.21.01015

12. Andre T, Amonkar M, Norquist JM, Shiu KK, Kim TW, Jensen BV, et al. Health-related quality of life in patients with microsatellite instability-high or mismatch repair deficient metastatic colorectal cancer treated with first-line pembrolizumab versus chemotherapy (KEYNOTE-177): an open-label, randomised, phase 3 trial. *Lancet Oncol* (2021) 22(5):665–77. doi: 10.1016/s1470-2045(21)00064-4

13. André T, Shiu KK, Kim TW, Jensen BV, Jensen LH, Punt C, et al. Pembrolizumab in Microsatellite-Instability–high advanced colorectal cancer. *New Engl J Med* (2020) 383(23):2207–18. doi: 10.1056/nejmoa2017699

14. Bertagnolli MM, Niedzwiecki D, Compton CC, Hahn HP, Hall M, Damas B, et al. Microsatellite instability predicts improved response to adjuvant therapy with irinotecan, fluorouracil, and leucovorin in stage III colon cancer: cancer and leukemia group b protocol 89803. *J Clin Oncol* (2009) 27(11):1814–21. doi: 10.1200/JCO.2008.18.2071

15. Zaanan A, Cuilliere-Dartigues P, Parc Y, Louvet C, Tiret E, Gayet B, et al. Impact of microsatellite instability and p53 expression on stage III colon cancer disease-free survival in patients treated by fluorouracil and leucovorin with or without oxaliplatin. *J Clin Oncol* (2008) 26(Suppl. 15):15017. doi: 10.1200/jco.2008.26.15_suppl.15017

16. Herting CJ, Farren MR, Tong Y, Liu Z, O'Neil B, Bekaii-Saab T, et al. A multi-center, single-arm, phase ib study of pembrolizumab (MK-3475) in combination with chemotherapy for patients with advanced colorectal cancer: HCRN GI14-186. *Cancer Immunol Immunother* (2021) 70(11):3337–48. doi: 10.1007/s00262-021-02986-5

17. Copur MS, Schroeder CW, Ly Q, Wedel W, Kelly JR, Rodriguez P, et al. Complete pathologic response to neoadjuvant chemoimmunotherapy and oxaliplatin-induced fever associated with IL-6 release in a patient with locally advanced colon cancer. *Oncol (Williston Park)* (2022) 36(2):115–9. doi: 10.46883/2022.25920944

18. Zaanan A, Shi Q, Taieb J, Alberts SR, Meyers JP, Smyrk TC, et al. Role of deficient DNA mismatch repair status in patients with stage III colon cancer treated with FOLFOX adjuvant chemotherapy: a pooled analysis from 2 randomized clinical trials. *JAMA Oncol* (2018) 4(3):379–83. doi: 10.1001/jamaoncol.2017.2899

frontiers | Frontiers in Immunology

TYPE Original Research
PUBLISHED 06 September 2023
DOI 10.3389/fimmu.2023.1188831

OPEN ACCESS

EDITED BY
Yeonseok Chung,
Seoul National University, Republic of Korea

REVIEWED BY
Kai Zhang,
Zhengzhou University, China
Dapeng Zhou,
Tongji University, China

*CORRESPONDENCE
Preethi H. Gunaratne
phgunaratne@uh.edu
Isabelle Bedrosian
ibedrosian@mdanderson.org

†These authors have contributed equally to this work and share first authorship

RECEIVED 17 March 2023
ACCEPTED 27 July 2023
PUBLISHED 06 September 2023

CITATION
Mistretta B, Rankothgedera S, Castillo M, Rao M, Holloway K, Bhardwaj A, El Noafal M, Albarracin C, El-Zein R, Rezaei H, Su X, Akbani R, Shao XM, Czerniecki BJ, Karchin R, Bedrosian I and Gunaratne PH (2023) Chimeric RNAs reveal putative neoantigen peptides for developing tumor vaccines for breast cancer.
Front. Immunol. 14:1188831.
doi: 10.3389/fimmu.2023.1188831

Chimeric RNAs reveal putative neoantigen peptides for developing tumor vaccines for breast cancer

Brandon Mistretta[1†], Sakuni Rankothgedera[1†], Micah Castillo[1†], Mitchell Rao[1], Kimberly Holloway[1], Anjana Bhardwaj[2], Maha El Noafal[3], Constance Albarracin[4], Randa El-Zein[3], Hengameh Rezaei[1], Xiaoping Su[5], Rehan Akbani[5], Xiaoshan M. Shao[6], Brian J. Czerniecki[7], Rachel Karchin[6], Isabelle Bedrosian[2*] and Preethi H. Gunaratne[1,8,9*]

[1]Department of Biology & Biochemistry, University of Houston, Houston, TX, United States, [2]Department of Breast Surgical Oncology, University of Texas, MD Anderson Cancer Center, Houston, TX, United States, [3]Department of Medicine, Houston Methodist Research Institute, Houston, TX, United States, [4]Department of Pathology, The UT MD Anderson Cancer Center, Houston, TX, United States, [5]Department of Bioinformatics & Computational Biology, University of Texas, MD Anderson Cancer Center, Houston, TX, United States, [6]Biomedical Engineering Department, Institute for Computational Medicine, Johns Hopkins School of Medicine, Baltimore, MD, United States, [7]Department of Molecular & Cellular Biology, Baylor College of Medicine, Houston, TX, United States, [8]Human Genome Sequencing Center, Baylor College of Medicine, Houston, TX, United States, [9]Department of Breast Oncology, H. Lee Moffitt Cancer Center, Tampa, FL, United States

Introduction: We present here a strategy to identify immunogenic neoantigen candidates from unique amino acid sequences at the junctions of fusion proteins which can serve as targets in the development of tumor vaccines for the treatment of breastcancer.

Method: We mined the sequence reads of breast tumor tissue that are usually discarded as discordant paired-end reads and discovered cancer specific fusion transcripts using tissue from cancer free controls as reference. Binding affinity predictions of novel peptide sequences crossing the fusion junction were analyzed by the MHC Class I binding predictor, MHCnuggets. CD8+ T cell responses against the 15 peptides were assessed through in vitro Enzyme Linked Immunospot (ELISpot).

Results: We uncovered 20 novel fusion transcripts from 75 breast tumors of 3 subtypes: TNBC, HER2+, and HR+. Of these, the NSFP1-LRRC37A2 fusion transcript was selected for further study. The 3833 bp chimeric RNA predicted by the consensus fusion junction sequence is consistent with a read-through transcription of the 5'-gene NSFP1-Pseudo gene NSFP1 (NSFtruncation at exon 12/13) followed by trans-splicing to connect withLRRC37A2 located immediately 3' through exon 1/2. A total of 15 different 8-mer neoantigen peptides discovered from the NSFP1 and LRRC37A2 truncations were predicted to bind to a total of 35 unique MHC class I alleles with a binding affinity of IC50<500nM.); 1 of which elicited a robust immune response.

Conclusion: Our data provides a framework to identify immunogenic neoantigen candidates from fusion transcripts and suggests a potential vaccine strategy to target the immunogenic neopeptides in patients with tumors carrying the NSFP1-LRRC37A2 fusion.

KEYWORDS

RNA fusions, chimeric RNAs, neoantigens, immunopeptides, tumor peptide vaccines

1 Introduction

Tumor vaccines capable of promoting immune response have the potential to make significant contributions to the treatment and prevention of cancer. The antigenic repertoire that arises during tumorigenesis through somatic alterations in tumors provides a plethora of non-self-antigens (neoantigens) that can form the basis of vaccination-based cancer immunotherapies. Many of the neoantigens discovered have been shown to be capable of inducing anti-tumor immune responses with minimal side effects in the treatment setting (1, 2). Neoantigen load has been reported to be strongly correlated with clinical response to immunotherapy (3) and high somatic mutational burden. A high density of candidate neoantigens have also been shown to improve survival in patients treated with immune checkpoint blockades in non-small cell lung cancer (NSCLC) (4) and melanoma (5, 6). However, many neoantigens caused by non-synonymous mutations are patient specific, thus can only be used as personalized vaccines and not available as an 'off the shelf' option for treatment that would facilitate widespread adoption (7). Therefore, identification of shared neoantigens generated through aberrant transcripts which are prevalent in cancer patients would help overcome one of the current challenges in the advancement of vaccination-based cancer immunotherapies.

Much of the work on neoantigens relates to single nucleotide variants (SNV) and small insertions and deletions (indel) (8). However, for cancers with a low to moderate mutation burden, such as breast cancer, these approaches provide a limited neoantigen repertoire that can be harnessed for therapeutic cancer vaccines. Non-mutated, over-expressed peptides have thus been of interest in this context, with much of the clinical research focused on peptides derived from HER2-Neu (9, 10). Additional approaches that expand the available immunogenic peptides for use in cancer vaccines in these tumors with a limited repertoire of neoantigens derived from non-synonymous mutations is needed if this promising immunotherapy strategy is to be fully utilized clinically.

Here, we focused on identifying neoantigens in fusion transcripts from two separate genes identified from RNA-sequencing (RNA-seq) data of breast cancer samples. The unique sequences at the fusion junctions form new open reading frames (ORFs) that can result in fusion proteins representing a hybrid of the two founding genes and/or truncated versions of the two wild type proteins due to premature termination of the 5'-gene yielding a unique amino acid sequence in the C-terminus and novel N-terminal region in the 3'gene. Our main objective was to discover whether such intergenic spliced chimeric mRNA can provide novel neoantigens that can be processed and presented by the major histocompatibility complex (MHC) Class I peptides to target $CD8^+$ T cells. The ultimate goal of this work is to establish a framework for using immunogenic neopeptides generated from the novel amino acids at the fusion junctions of chimeric RNAs for the development of "off the shelf" tumor vaccines for breast cancer.

2 Materials and methods

2.1 Samples and controls

All tissue samples were obtained from archival formalin fixed, paraffin embedded (FFPE) blocks under a protocol approved by the MD Anderson Cancer Center Institutional Review Board. Tumor samples were obtained from women who met the following criteria: i) newly diagnosed breast cancer, ii) no prior history of breast cancer (primary disease), iii) undergoing surgery as the initial treatment modality, iv) no prior receipt of chemotherapy. In addition, only tumors from women with no known germline mutations and without a significant family history were included in order to enrich for sporadic cancers. Stage was not specifically selected for, however all patients had non-metastatic disease. Seventy-five cases from cancer patients were used, 25 from each of the 3 main clinical subtypes: i) estrogen and/or progesterone positive and HER2 negative (referred to as hormone receptor [HR] positive), ii) HER2 positive regardless of HR status and iii) HR negative and HER2 negative (TNBC; triple negative). Four breast tissue samples from women without a cancer diagnosis were used as controls.

2.2 RNA extraction

RNA extraction was conducted using the Ambion Recoverall Total Nucleic Acid isolation kit (cat# AM19750, ThermoFisher) following the manufacturer's recommendations. Briefly, tissue cores were crushed, placed in 1.5ml tubes and washed three times with 100% xylene for 10 min. Tissues were then washed in 100% ethanol twice for 10 min followed by one wash in 95% ethanol for 10 min

and another wash in 10% PBS, then allowed to air dry for 5 min. Tissues were then incubated in protease digestion buffer at 50°C for 3 hours followed by a 15 min incubation at 80°C after which tissues were stored in -20°C until RNA isolation. At the time of RNA extraction, isolation additive and ethanol mix were added to each sample and placed into the filter cartridge followed by centrifugation for 30 sec at 10,000xg. This was repeated 3 times followed by the addition of wash solutions and centrifugation. DNase was then added to the filter cartridge and incubated at room temperature for 30 min. RNA was then eluted by adding nuclease free water to the center of the filter cartilage, incubating for 5 min and centrifugation at maximum speed for 1 min. RNA was then stored at -80°C.

2.3 FFPE RNA quality control

Extracted RNA samples underwent quality control assessment using the RNA tape on a Tapestation 4200 (Agilent, RRID : SCR_019398). DV200 was calculated as the percentage of RNA fragments that are >200 nucleotides in size. All samples had a DV200 >30% which is the recommended cutoff for RNA sequencing (Illumina Technical Pub. No. 470-2014-001,2016). Samples were then quantified with Qubit Fluorometer (ThermoFisher) for input into library preparation.

2.4 Transcriptome sequencing

The RNA libraries were prepared and sequenced at the University of Houston Seq-N-Edit Core per standard protocols. RNA libraries were prepared with the TruSeq RNA Exome kit (Illumina) using 30 ng input RNA. RNA was fragmented, reverse transcribed into cDNA and ligated with sequence adaptors. The size selection for libraries was performed using SPRIselect beads (Beckman Coulter). Enrichment for coding RNA was performed by coding region specific biotinylated capture probes and selected by streptavidin magnetic beads. Library purity was analyzed using the DNA 1000 tape on a Tapestation 4200 (Agilent, RRID : SCR_019398) and quantified with Qubit Fluorometer 2.0 (ThermoFisher, RRID : SCR_020553). The prepared libraries were pooled and sequenced using the NextSeq 500 (Illumina, RRID : SCR_016381); generating ~15 million 2×76 bp paired end reads per sample.

2.5 RNA fusion detection

The RNA-seq raw fastq data was processed with CLC Genomics Workbench 20 (Qiagen). The Illumina sequencing adaptors were trimmed, and reads were mapped to the human reference genome hg38 Refseq GRCh38.p9 from the Biomedical Genomics Analysis Plugin 20.0.1 (Qiagen). Read alignment was represented as integer counts by using parameters of mismatch cost 2, insertion cost 3, deletion cost 3, length fraction 0.8, similarity fraction 0.8, max of 10 hits for a read. Integer read counts were normalized by Trimmed Means of M-values (TMM) algorithm (11). RNA fusions were detected using the detect fusion gene algorithm under the parameters of minimum length of unaligned sequence 15, maximum distance to exon boundary 10, maximum distances for broken pair fusions 1,000, assumed error rate 0.001, promiscuity threshold 7. The algorithm identifies fusion events based on the number of fusion crossing reads and fusion spanning reads. Refine fusion gene tool was used to re-count the number of fusion crossing reads and the novel RNA seq reads mapped against the fusion reference created in detect fusion genes. The fusion list was further refined by excluding those that were detected in both normal breast tissue controls and in paired adjacent normal tissue samples. Details of the false positive and negative filters applied are shown below.

False Positive filter: To reduce the false positive rates of ~50% associated with the majority of fusion callers that rely only on discordant paired end reads we introduced a filter that first extracts fusion candidates based on discordant paired end reads and then filter out fusion candidates that are not supported by at least 1 junction crossing read that has to be split to map on two different genes on the reference genome.

False Negative filter: To capture fusions associated with small sub populations of cells in pre-cancerous lesions and/or 'cancer stem cells' driving drug resistance and disease recurrence we relaxed filters that eliminate candidates based on read numbers and included fusions supported by junction crossing split reads mapping on two different genes supported by at least 1 read in three independent patients across the 3 subtypes studies. Additionally, using the CLC Genomics Workbench, we included a secondary alignment of unmapped RNA-seq reads to a fusion reference sequence created in the initial detect fusion genes pipeline. This decreased the number of false negatives discovered in other fusion callers.

2.6 Validation of junction sequence

cDNA from whole transcriptome sequencing underwent PCR amplification across the *NSFP1-LRRC37A2* fusion junction site using Forward Primer (5'-GCCTGCAAGTGACGAGAG-3) and Reverse Primer (5'-CGGTCCAACTGTATGCTTTC-3'). DreamTaq DNA polymerase (ThermoFisher Scientific; Cat.# EP0701) was used in a 30-cycle PCR reaction. Amplicon size was analyzed using the High Sensitivity DNA 1000 tape on a Tapestation 4200 (Agilent, RRID : SCR_019398).

2.7 Validation of junction sequence: cloning & sanger sequencing

The PCR amplicon was inserted in to a pJET1.2 vector as per the sticky-end cloning protocol provided by the manufacturer (CloneJET PCR Cloning Kit; ThermoFisher Scientific; Cat.# K1232). The ligation mixture was directly transformed to provided competent cells and plated on Ampicillin-LB agar plates. Plates were incubated overnight at 37°C. After incubation, 4 colonies were selected per plate to confirm the DNA insert. A PCR

was performed to validate the junction sequence using the primers for *NSFP1-LRRC37A2*. Colonies expressing the amplicon were grown in Ampicillin LB broth at 37°C in a shaking incubator overnight. Plasmids extraction from the bacterial cultures was carried out using manufacturer supplied protocols (QIAprep Spin Miniprep Kit; Qiagen; Cat.# 27104) and were verified using Sanger sequencing.

2.8 Neoantigen predictions

Our neoantigen prediction pipeline is described in Shao et al. (12). Neopeptide regions were delineated from the 2 major ORFs predicted from the *NSFP1* [Exon 1-13] - *LRRC37A2* [Exon 2-14] fusion. To assess the immunogenicity of our predicted neopeptides in relation to 118 MHC class I haplotypes found in humans, we utilized a neoantigen prediction platform, MHCNuggets. Peptides of 8 amino acids encompassing two major ORFs generated from the *NSFP1-LRRC37A2* fusion were analyzed. The HLA genotypes extracted from RNASeq fusion caller from the 75 samples served as input to MHCnuggets to predict the MHC class I binding potential (IC50 nM) of each peptide region from wild-type and neoantigen peptide regions of two truncated proteins. Neoantigen candidates meeting an IC50 affinity < 500 nM were subsequently ranked based on MHC binding. Anchor and auxiliary anchor residues for neopeptide-HLA class I allele pairs were evaluated by the SYFPEITHI online tool (13).

2.9 Peptide library generation

The peptide library consisted of 15 neoantigenic 8-mer peptides discovered from the *NSFP1*- Exon 1-13 truncation ORF and *LRRC37A2*-Exon 2-14 truncation ORF and was synthesized and purified using standard solid-phase synthetic peptide chemistry and Reverse Phase High Performance Liquid Chromatography (ThermoFisher Scientific PEPotec). These peptides were reconstituted to 1 mg/mL concentrations under sterile conditions. An 8-mer peptide used by the manufacturer to standardize the peptide library which was confirmed to be a peptide of no biological significance was used as a Negative Peptide Control (NCP) to validate the effect of stimulation by a synthetic peptide. A commercially available Cytomegalovirus (CMV) peptide pool (MabTech; Cat.# 3619-1) containing 42 peptides from the Cytomegalovirus where 28 of the peptides are MHC class I restricted and 14 are MHC class II restricted was used as the positive control.

2.10 Human primary cells

The HLA class C07:02 matched human Peripheral Blood Mononuclear Cells (PBMCs) from a healthy donor were acquired (STEMCELL Technologies) and were stored in liquid nitrogen until use.

2.11 Culture medium

Complete media consisted of RPMI-1640 growth media with L-glutamine (Gibco; Cat.# 61870036) supplemented with 10% heat-inactivated fetal bovine serum (GenDEPOT; Cat.# F0601-050), 0.1 mmol/L nonessential amino acids (Corning; Cat.# 25-025-CI), 10ug/ml Cellmaxin (GenDEPOT; Cat.# C3319-006), and 0.5 mg/mL Amphotericin B (Gibco; Cat.# 15290026).

2.12 *In vitro* stimulation of PBMCs using peptides

PBMCs were retrieved from liquid nitrogen, thawed in a water bath at 37°C, and washed with culture medium warmed to 37°C, as previously described in the primary cell thawing protocol by Stem Cell Technologies. Cells were incubated at 37°C, 5% CO_2 for 24 hours (Cell Resting). After resting, cells were seeded at a concentration of 1×10^6/mL in 6-well plates with culture medium containing IL-2 (10 IU/ml), IL-7 (10 ng/ml), and IL-15 (10 ng/ml). The cells of the Negative (Unstimulated) control (NC) wells not treated with any peptides but were supplemented with the growth medium and cytokines required for growth and proliferation and were maintained at the same growth conditions as the cells of wells treated with the neoantigenic peptides. The cells of the CMV positive control wells were treated with 1µg/ml of the CMV peptide pool and were supplemented with media and growth conditions identical to that of the test peptide wells. The 15 neaoantigenic 8-mer test peptides were added to the respective wells at 2 µg/ml and the plates were incubated at 37°C, 5% CO_2 for 4 days On day 5, 50% of the medium was replaced with fresh medium, and cells were cultured for an additional 5 days. A second round of peptide restimulation was carried out with the corresponding peptides coupled with the cytokine medium before the cells were used for the ELISpot assay.

2.13 Isolation of CD8+ T cells from PBMCs

On Day 13, untouched $CD8^+$ T cells were isolated from PBMCs by magnetic negative selection using the MojoSort™ Human $CD8^+$ T Cell Isolation Kit (BioLegend; Cat.# 480012) following the manufacturer's instructions.

2.14 IFN-γ ELISpot assay

To evaluate peptide stimulated $CD8^+$ T cell immune response, IFN-γ production by cells stimulated with the predicted neoantigenic peptides was quantified using a commercially available Human IFN-γ- ELISpot kit (CTL ImmunoSpot, Cellular Technology Ltd), following the instructions of the manufacturer. The plate was read with an ELISpot reader (CTL counter, Cellular

Technology Ltd). The cell culture medium used to incubate the cells in the ELISpot plate was augmented with anti-CD28 antibody (1µg/ml) and corresponding peptides (2µg/ml).

2.15 Statistical analysis

Positive response to the assay was defined using a threshold minimum of 20 Spot Forming Colony Units (SFC)/10^6 cells in experimental wells after subtracting the unstimulated background (Mean number of SFUs generated by the NC wells). To compare immune responses generated by the neonatigenic peptides, SFUs generated by the wells stimulated with the neoantigenic peptides were compared with that of the wells stimulated with CMV peptide pool. ELISpot data were analyzed by Mann-Whitney U Test, without correction for multiple comparisons, using GraphPad Prism 9.0 (RRID : SCR_002798). Each row was analyzed individually, without assuming consistent standard deviation. Data are represented as mean ± SEM. For all analyses, significance threshold was considered as *, $P \leq 0.05$.

3 Results

3.1 Twenty highly prevalent fusion transcripts were discovered across 3 breast cancer subtypes

With the goal of discovering RNA-fusions that can be targeted for neoantigen peptide candidates, we performed RNA-Sequencing of triple negative (TNBC), HER2+ and hormone receptor positive (HR+) breast cancer samples (n=25 each). Mining the sequence reads (i) that were discarded due to discordant paired-end reads and (ii) that were supported by split-reads (junction crossing reads) we found a large number of chimeric fusion RNAs. These were then cross referenced with the TCGA Multi-Center Breast Cancer Dataset. We uncovered 20 fusion RNAs with high prevalence across the set of 75 tumor samples and also detected in 1 or more of the TCGA samples. To eliminate false positives, we also required a given fusion to be present within more than one dataset discovered by an independent fusion caller (CLC Genomics Workbench and University of Chicago fusion caller). Table 1 shows the comprehensive list of fusion

TABLE 1 Top 20 novel prevalent chimeric RNAs discovered in TNBC, HER2+, and HR+ patient sample gene fusions after comparison to normal samples.

RNA FUSIONS (BREAST CANCER)	EXON Boundaries	TNBC Fusions		HER2+ Fusions		HR+ Fusions		TCGA (Breast Tumors)
		# of Fusion Positive Samples	Avg. # Junction Crossing Reads	# of Fusion Positive Samples	Avg. # Junction Crossing Reads	# of Fusion Positive Samples	Avg. # Junction Crossing Reads	# Samples
NSFP1-LRRC37A2	Exon 1-13| Exon 2-14	2	218	2	274	5	217	5
F8-CLIC2	Exon 1|Exon 2-6	1	50	4	6	3	2	1
KIAA0753-PITPNM3	Exon 1-16 | Exon 2-20	0	25	3	2	4	3	1
PRKCH-FLJ22447	Exon 1-12 | Exon 2-3	3	24	5	1	3	1	26
PACSIN2-ARFGAP3	Exon 1-11 | Exon 2-6	2	15	2	1	3	1	1
UBE3C-DNAJB6	Exon 1 | Exon 2-8	1	13	0	0	1	2	2
NCOR2-UBC	Exon 1-15 | Exon 1	0	13	1	1	2	2	3
GALK2-FGF7	Exon 1-10 | Exon 3-4	1	11	1	4	2	3	1
ARIH2-SLC25A20	Exon 1-5 | Exon 5-9	0	8	0	0	1	2	2
B4GALT1-SMU1	Exon 1-2,3| Exon 2-12	2	7	1	2	1	2	1
WNK1-ERC1	Exon 1-24| Exon 6-18	1	7	0	0	0	0	1

(Continued)

10.3389/fimmu.2023.1188831

TABLE 1 Continued

RNA FUSIONS (BREAST CANCER)	EXON Boundaries	TNBC Fusions		HER2+ Fusions		HR+ Fusions		TCGA (Breast Tumors)
		# of Fusion Positive Samples	Avg. # Junction Crossing Reads	# of Fusion Positive Samples	Avg. # Junction Crossing Reads	# of Fusion Positive Samples	Avg. # Junction Crossing Reads	# Samples
SCCPDH-CNST	Exon 1-5| Exon 4-9	1	6	0	0	0	0	1
NOXRED1-TMED8	Exon 1-5 | Exon 2-6	1	3	1	1	0	0	1
ACAP2-XXYLT1	Exon 1-21 | Exon 3-4	0	3	1	1	0	0	1
MBD5-ORC4	Exon 1-2| Exon 2-14	1	2	1	2	0	0	2
UBE2G1-ANKFY1	Exon 1-3 | Exon 3-25	1	2	6	0	1	1	1
AKT3-SDCCAG8	Exon 1|Exon 7-18	0	1	0	0	1	1	3
BACE2-FAM3B	Exon 1-8| Exon 2-7	0	1	0	0	1	1	3
ADCY9-SRL	Exon 1-2 | Exon 2-6	0	1	1	2	0	0	6
TMCO3-TFDP1	Exon 1-7 | Exon 3-12	1	7	0	0	0	0	6

To remove false positive discoveries the fusions was required to be found in an independent dataset (TCGA Breast Cancer dataset). Exon boundaries from the fusion junction site between the 2 genes, the number of tumor samples positive for each fusion (n=25) for each subtype, and the average number of junction crossing reads identified from the positive sample are shown.

transcripts with the number of samples in each subtype that was found to carry the fusion in the tumor.

The average number of junction crossing reads as well as the exon boundaries of the 5' and 3' genes in both our dataset and TCGA are also presented. Of the 20 novel fusions found, 4 were identified with a frequency of 10% or greater in the MD Anderson Cancer Center (MDACC) cohort. The *NSFP1- LRRC37A2* fusion transcript was selected for further study based on the fact that it was associated with the highest number of junction crossing reads (TNBC=218, HER2 +=274, HR+=217), and detected with highest frequency across the 75 tumor samples (9/75 = 12%), (TNBC=2 samples, Her2+=2 samples and HR+=5 samples). Furthermore, it was also present in 5 samples in the TCGA breast cancer dataset previously analyzed with filters that traditionally exclude fusions found in adjacent normal tissue. TCGA, however, did not remove fusions from cancer free controls similar to what was done in this study.

3.2 Exon boundaries of *NSFP1-LRRC37A2* Fusion Maps to Exon 13 of *NSFP1* (5'-boundary) and Exon 2 of *LRRC37A2* (3'-boundary)

NSFP1 (N-ethylmaleimide sensitive factor, vesicle fusing ATPase, transcript variant 1 pseudogene) and LLRC37A2 (Leucine Rich Repeat Containing 37 Member A2) are located in 17q21.31. To compile the *NSFP1-LRRC37A2* fusion junction, we mapped the consensus junction sequence compiled from the complete set of junction crossing reads extracted from fusion positive samples to hg38 Refseq GRCh38.p9. The 5'-boundary of *NSFP1-LRRC37A2* was found to be located on Exon 13 of *NSFP1* (NR_033799.1) and the 3' – boundary mapped to Exon 2 (NM_001006607.3) of *LRRC37A2* located immediately 3' to NSP1 on the coding strand of both genes. The boundaries were consistent and supported by 986 junction-crossing reads (TNBC=218, HER2 +=274 and HR+=217) with the breakpoint sequence always **AAACCA-3'** on the *NSFP1* gene and **5'-AAATTC** on LRRC37A2. The 5 samples found to be positive for *NSFP1-LRRC37A2* fusion in the TCGA dataset (an independent set of samples) also contained the same exon boundaries. The fusion junction and the exon boundaries model for the *NSFP1-LRRC37A2* fusion are shown in Figure 1. The consensus junction sequence and the cDNA for the fusion transcript are shown in Supplemental Figure 1. The fusion junction supported by 986 junction crossing reads was validated by amplicon PCR assay as shown in Figure 2. We expected a 121bp PCR fragment from the PCR amplicon generated using a Forward Primer located on *NSFP1* (5'-GCCTGCAAGTGACGAGAG-3) and Reverse Primer located on *LRRC37A2* (5'-CGGTCCAACTGTATGCTTTC-3'). The PCR amplicons of 121bp cloned to the positive selection cloning vector were Sanger sequenced to further validate the presence of the fusion junction. The chromatogram acquired through Sanger sequencing

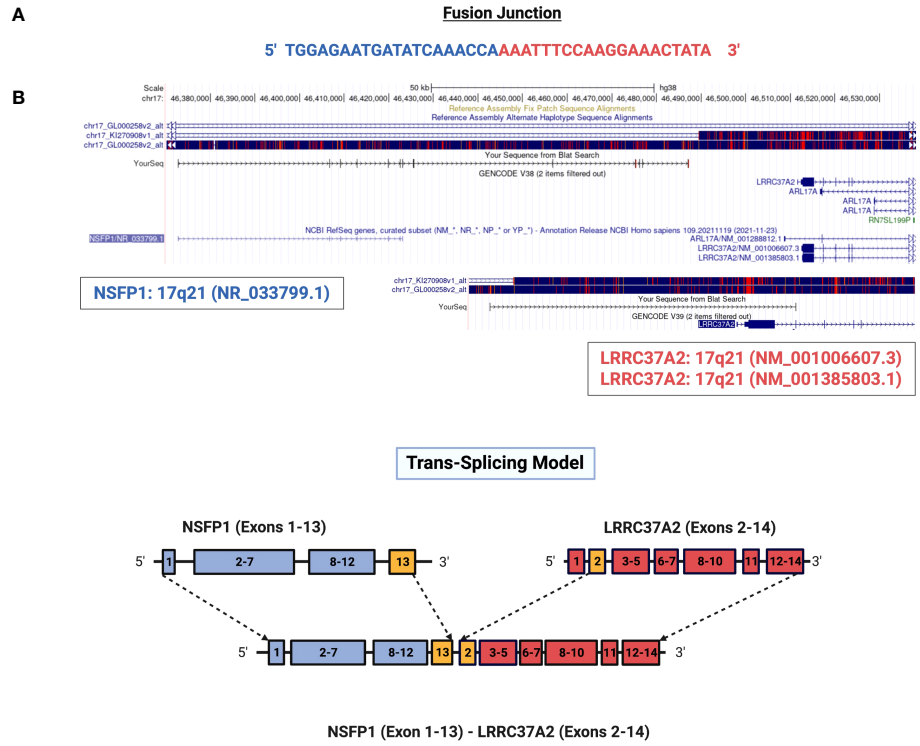

FIGURE 1
Genomic mapping of junction crossing reads for *NSFP1-LRRC37A2*. **(A)** The fusion junction sequence. The sequence of the junction-crossing read extracted from 986 sequence reads from 75 samples (25 Tumor samples – 3 subtypes) is shown. The segment of the reads that map to *NSFP1* and *LRRC37A2* is shown in Blue and Red respectively. **(B)** A model of the novel fusion transcript *NSFP1-LRRC37A2*. The junction site is shown in green between exon 13 of *NSFP1* and exon 2 of *LRRC37A2*.

is also shown in Figure 2. The same exon boundary of *NSFP1* Exon 13 *LRRC37A2* Exon 2 identified by the CLC Genomics workbench 20.0 (Qiagen) on the breast cancer dataset presented here was also found in the fusions uncovered TCGA and MDACC datasets.

3.3 Novel fusion junctions from the *NSFP1-LRRC37A2* fusion transcript variants contain two major ORFs generating two truncated proteins

The major open reading frames (ORFs) predicted from the *NSFP1* [Exon 1-13] -*LRRC37A2* [Exon 2-14] fusion are shown in Figure 3. Two regions of unique amino acid residues carrying neopeptides were uncovered from the 2 major ORFs predicted from the *NSFP1* [Exon 1-13] - *LRRC37A2* [Exon 2-14] fusion. The truncated *NSFP1* protein yielded the unique peptide fragment KFPRKLYFLH at the C-terminal end of *NSFP1* Exon 13 fused with the beginning of *LRRC37A2* Exon 2. The truncated *LRRC37A2* protein yielded the unique peptide fragment MISNQN at the N-terminal end of *LRRC37A2* Exons 2-14 (unique amino acids contributed by Exon 13 of *NSFP1*). To assess the immunogenicity of our predicted neoantigens a total 15 peptides of 8–11 amino acids extracted from the 2 major ORFs generated from the *NSFP1-LRRC37A2* fusion were processed through the neoantigen prediction platform, MHCnuggets, which evaluates binding of somatic peptides to MHC class I, antigen processing, self-similarity and gene expression (12). A total of 106 HLA genotypes served as input to MHCnuggets to predict the MHC class I binding potential (IC50nM) of each peptide region. Neoantigen candidates meeting an IC50 affinity < 500nM were subsequently ranked based on MHC binding. Anchor and auxiliary anchor residues for neopeptide-HLA class I allele pairs were evaluated by the SYFPEITHI online tool (13). These peptides were then rank ordered for binding affinity to the greatest number of MHC class I alleles (promiscuity), antigen processing, and self-similarity. To identify the most promiscuous peptides, which have been shown to be strong vaccine candidates (14), we ranked the peptides by number of HLA Class I alleles that each peptide bound to at a binding affinity threshold of IC50 <500nM. The promiscuity distribution plot for the complete set of peptides generated from the *NSFP1-LRRC37A2* fusion is shown in Figure 4. While many of the peptides bind to less than 10 MHC class 1 alleles, a small fraction does bind to >20 MHC alleles which were further investigated. We uncovered 10 and 5 immunogenic neoantigen peptides from the truncated NFS protein variant and the truncated *LRRC37A2* protein variant respectively. Table 2 presents data from the selected neoepitopic regions with HLA class I IC50 affinities of < 1000nM, < 500nM and < 50nM. Previous studies have reported that predicted antigens with IC50<50 nM bind too strongly and do not initiate an immune response, so we chose to pursue MHC class I alleles with a binding affinity of IC50<500nM (15). A total of 10

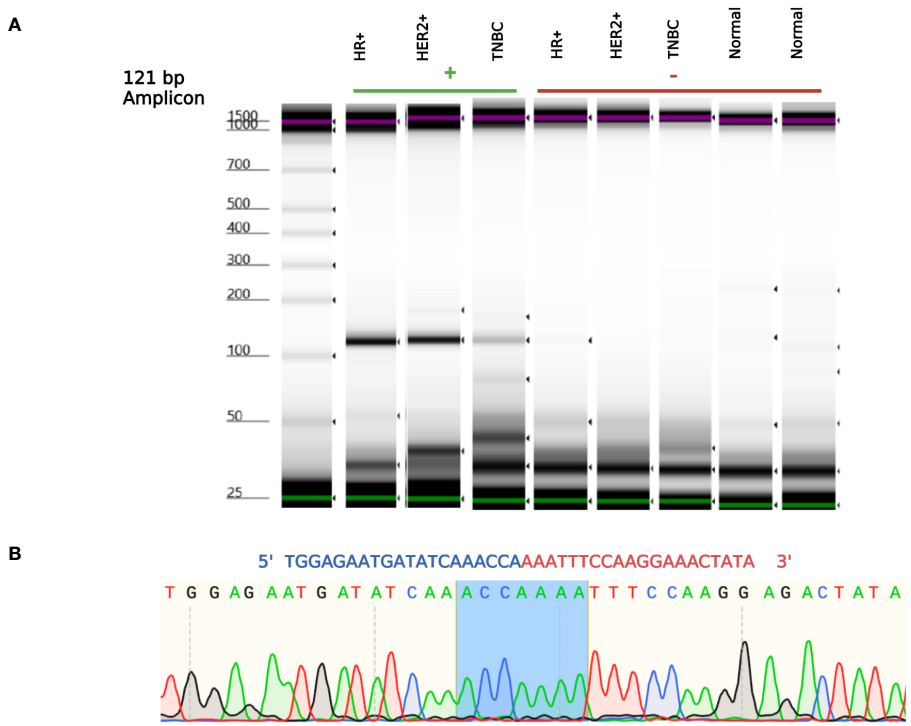

FIGURE 2
NSFP1-LRRC37A2 Fusion PCR validation. **(A)** One fusion junction positive sample from each subtype, was chosen to be validated by PCR. Capillary gel electrophoresis was used to detect the 121 bp amplicon fragment, representing the *NSFP1-LRRC37A2* fusion. **(B)** The sanger sequencing chromatogram of the PCR amplicons cloned into plasmids and sequenced. The junction site of the fusion between exon 13 of *NSFP1* and exon 2 of *LRRC37A2* is shown in blue in the chromatogram.

different 8-mer neoantigen peptides discovered from the *NSFP1*-Exon 1-13 truncation ORF were predicted to bind to a total of 28 unique MHC class I alleles with a binding affinity of IC50<500nM (Table 3). A total of 5 different 8-mer neoantigen peptides discovered from the *LRRC37A2*-Exon 2-14 truncation ORF were predicted to bind to a total of 7 unique MHC class I alleles with a binding affinity of IC50<500nM. The unique set of MHC Class I alleles binding the immunogenic neoantigens from *NSFP1* and *LRRC37A2* truncations are shown in Supplementary Table 1.

3.4 CD8+ T cell immune responses were elicited by 1 out of 15 candidate fusion neopeptides

To determine if the predicted neopeptides induced CD8+ T cell immune responses *in vitro*, IFN-γ secretion of PBMCs was evaluated through ELISpot. The IFN-γ secretion of the cells stimulated with the 15 neopeptides were compared to that of PBMCs stimulated with a CMV peptide pool as a positive control. The Negative (Unstimulated) Control is an essential component of an ELISpot assay as it helps determine the non-specific signal or background caused by cytokines necessary for the growth and proliferation of PBMCs. To accurately account for this non-specific effect, a subtraction method is employed. To quantify the specific immune response, the mean Spot Forming Units (SFUs) generated by the Negative control wells are subtracted from the SFUs generated by all the wells on the plate. This subtraction allows for the distinction between the specific immune response induced by the antigen of interest and the background signal resulting from cytokines present in the unstimulated control wells. A Mann-Whitney Test was performed to compare the mean no. of SFUs/10^6 cells developed for each experimental peptide with that of the CMV positive control. The peptide ENDIKPKF ($p=0.0417$) was identified as the only neoantigenic peptide candidate that satisfied the set parameters for a positive response including $p<0.05$. This peptide (ENDIKPKF) exhibits a response which is approximately 2 folds greater than the response shown by the CMV positive control and 5 folds greater than the response shown by the unrelated peptide stimulated cells (Figure 5).

4 Discussion

Chimeric RNAs generated through chromosomal rearrangements (translocations, deletions, duplications and inversions), trans-splicing or read-through transcription have been proposed as reagents for developing tumor vaccines (16). Neoantigens generated from fusion transcripts have been reported to be better candidates for developing tumor vaccines because they are usually associated with significantly higher immunogenic potential than point mutation, SNV or in-del based neoantigens

NSFP1: [Exon 1-13] C-Terminal Truncation

>lcl|ORF1

MAGRSMQAARCPTDELSLTNCAVVNEKDFQSGQHVIVRTSPNHRYTFTLKT
HPSVVPGSIAFSLPQRKWAGLSIGQEIEVSLYTFDKAKQCIGTMTIEIDFLQKK
SIDSNPYDTDKMAAEFIQQFNNQAFSVGQQLVFSFNEKLFGLLVKDIEAMDP
SILKGEPATGKRQKIEVGLVVGNSQVAFEKAENSSLNLIGKAKTKENRQSIINP
DWNFEKMGIGGLDKEFSDIFRRAFASRVFPPEIVEQMGCKHVKGILLYGPPG
CGKTLLARQIGKMLNAREPKVVNGPEILNKYVGESEANIRKLFADAEEEQRRL
GANSGLHIIIFDEIDAICKQRGSMAGSTGVHDTVVNQLLSKIDGVEQLNNILVI
GMTNRPDLIDEALLRPGRLEVKMEIGLPDEKGRLQILHIHTARMRGHQLLSA
DVDIKELAVETKNFSGAELEGLVRAAQSTAMNRHIKASTKVEVDMEKAESL
QVMRGDFLASLENDIKP**KFPRKLYFLH**

LRRC37A2: [Exon 2-14] N-Terminal Truncation

>lcl|ORF5

MISNQNFQGNYISYIDGNVWKAYSWTEKLILRENNLTELHKDSFEGLLSL
QYLDLSCNKIQSIERHTFEPLPFLKFINLSCNVITELSFGTFQAWHGMQF
LHKLILNHNPLTTVEDPYLFKLPALKYLDMGTTLVPLTTLKNILMMTVEL
EKLILPSHMACCLCQFKNSIEAVCKTVKLHCNSACLTNTTHCPEEASVGN
PEGAFMKVLQARKNYTSTELIVEPEEPSDSSGINLSGFGSEQLDTNDESD
FISTLSYILPYFSAVNLDVKSLLLPFIKLPTTGNSLAKIQTVGQNRQRVK
RVLMGPRSIQKRHFKEVGRQSIRREQGAQASVENAAEEKRLGSPAPREV
EQPHTQQGPEKLAGNAVYTKPSFTQEHKAAVSVLKPFSKGAPSTSSPAK
ALPQVRDRWKDLTHAISILESAKARVTNTKTSKPIVHARKKYRFHKTRSHVT
HRTPKVKKSPKVRKKSYLSRLMLANRLPFSAAKSLINSPSQGAFSSLGDL
SPQENPFLEVSAPSEHFIENNNTKHTTARNAFEENDFMENTNMPEGTISE
NTNYNHPHEADSAGTAFNLGPTVKQTETKWEYNNVGTDLSPEPKSFNY
PLLSSPGDQFEIQLTQQLQSLIPNNNVRRLIAHVIRTLKMDCSGAHVQVTCA
KLISRTGHLMKLLSGQQEVKASKIEWDTDQWKIENYINESTEAQSEQKEK
SLELKKEVPGYGYTDKLILALIVTGILTILIILFCLIVICCHRRSLQEDEEGFSR
GIFRFLPWRGCSSRRESQDGLSSFGQPLWFKDMYKPLSATRINNHAWKL
HKKSSNEDKILNRDPGDSEAPTEEEESEALP

FIGURE 3
NSFP1- LRRC37A2 fusion transcript predicted ORFs. The cDNA sequence generated from the *NSFP1-LRRC37A2* fusion model was analyzed through the NCBI-Open Reading Frame (ORF) Finder. Two major ORFs consistent with two truncated proteins that are predicted from the *NSFP1* [Exon 1-13] - *LRRC37A2* [Exon 2-14] fusion transcript were uncovered. The *NSFP1* [Exon 1-13] 3'-end truncation yielded an ORF of 500 amino acids. The *LRRC37A2* [Exon 2-14] 5'-end truncation yielded an ORF of 835 amino acids.

(3). Unique junctions formed in the chimeric RNAs that are translated can generate tumor-specific neoantigens, which can be exploited to design tumor vaccines for peptide-mediated T-cell activation and immunotherapies targeting cancer cells (3, 16). Our data suggests that chimeric RNAs are prevalent in breast tumors, provide a large number of novel fusions and generate immunogenic peptides that can elicit CD8+T cell responses, thus providing an expanded repertoire for development of breast cancer vaccines.

Breast cancer has low mutational burden, and therefore provides limited opportunities for peptide vaccine development. The chimeric RNAs that we uncovered, and the relatively large number of associated immunogenic peptides, open the door for cancer vaccines in these tumors with relatively fewer somatic mutations. The majority of the fusions discovered in our set of 75 cancer cases showed low frequency (present in 1-2 patients, ≤ 3% of the MDACC cohort). This is consistent with data from the TCGA Pan Cancer dataset that similarly noted that the overwhelming majority of fusions were private (17). Using computational approaches, the TCGA Pan Cancer study also determined the relative immunogenicity of neoantigens generated from fusions and reported that neopeptides derived from private fusions appeared to be more immunogenic than candidate neoantigens derived from highly frequent fusion events. While intriguing, these data lack direct *in vitro*/*in vivo* validation and thus the relationship between the frequency with which neoantigens are identified in the population and the ability to elicit a robust immune response remains unclear. Our data shows that some chimeric RNAs, such as *NSFP1*-LRRC37A2, occur at frequency in line with other therapeutic targets such as HER2/neu in breast cancer and EGFR in lung cancer, opening the door to an "off the shelf" peptide vaccine targeting tumors with these alterations, similar to targeted therapeutic strategies in breast and lung cancer.

In order to increase sensitivity and specificity of fusion discovery, we employed a unique strategy that incorporated two filters to significantly decrease the false positive and false negative rates of fusion detection. Focusing exclusively on the split reads crossing fusion junctions that are associated with discordant paired end reads bringing together two independent genes to extract

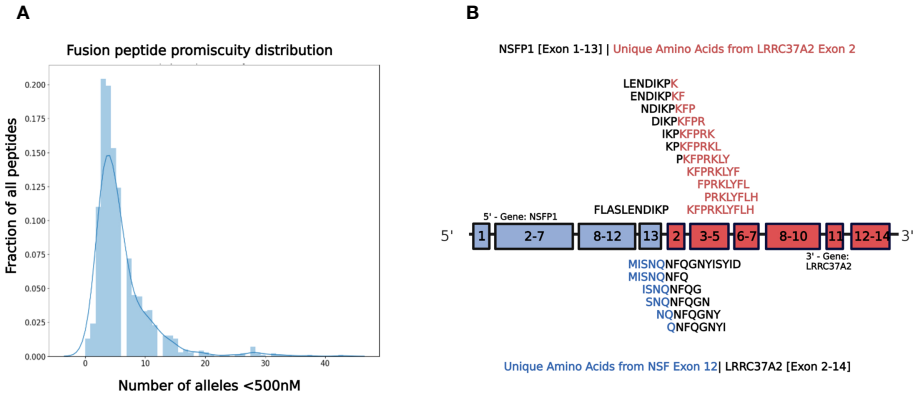

FIGURE 4
NSFP1-LRRC37A2 Fusion Model and Immunogenic Neoantigen Peptide Fragments. **(A)** The distribution model shows the promiscuity of peptides binding to MHC Class 1 alleles. The X-axis is the number of MHC Class 1 alleles and the Y-axis is the number of total peptides found. While a majority of peptides bind less than 10 MHC Class 1 alleles, a small fraction binds to >20, which are considered to be highly promiscuous. **(B)** The unique peptide junction regions predicted from the *NSFP1* [Exon 1-13] -*LRRC37A2* [Exon 2-14] fusion transcript are shown here. The immunogenic peptides generated through MHC Class I binding predictor (MHCnuggets) from the *NSFP1* [Exon 1-13]-C-Terminal truncation are shown above the fusion transcript model and the *LRRC37A2* [Exon 2-14]-N-Terminal truncation are shown below. Amino acid residues from *NSFP1* and *LRRC37A2* are shown in (blue) and (red) respectively. The unique amino acids formed at the fusion junction are shown in (black).

TABLE 2 Predicted immunogenic neo-antigen peptide fragments from the *NSFP1* [Exon 1-13]-*LRRC37A2* [Exon 2-14] Fusion with MHC Class I partners.

Unique Peptide Region *NSFP1* [Exon 1-13] C-Terminal Truncation			
FLASLENDIKPKFPRKLYFLH			
NSFP1 Exon 1-13 | Unique from *LRRC37A2* Exon 2	# of alleles<1000nM	# of alleles<500nM	# of alleles<50nM
FPRKLYFL	18	15	6
KFPRKLYF	15	13	5
NDIKP**KFP**	6	6	1
KP**KFPRKL**	5	5	2
ENDIKP**KF**	6	5	1
DIKP**KFPR**	6	5	1
IKP**KFPRK**	5	4	0
PRKLYFLH	5	3	3
LENDIKP**K**	3	2	0
PKFPRKLY	2	1	0
Unique Peptide Region *LRRC37A2* [Exon 2-14] N-Terminal Truncation			
MISNQNFQGNYISYID			
Unique from *NSFP1* Exon 13 | *LRRC37A2* Exon 2-14	# of alleles<1000nM	# of alleles<500nM	# of alleles<50nM
MISNQNFQ	4	4	2
QNFQGNYI	4	3	2
NQNFQGNY	6	5	1
ISNQNFQG	4	4	1
SNQNFQGN	3	2	0

Peptide fragments predicted to bind multiple MHC Class 1 alleles at IC50<1000nm, IC50<500nm, and IC50<50nm. Unique amino acids derived from the NSFP1-LRRC37A2 fusion are represented in red and blue respectively.

10.3389/fimmu.2023.1188831

TABLE 3 Immunogenic neo-antigen peptide fragments from the *NSFP1* [Exon 1-13]-*LRRC37A2* [Exon 2-14] Fusion predicted to bind with MHC Class I alleles at IC50<500nM.

Unique Peptide Region *NSFP1* [Exon 1-13] C-Terminal Truncation				Unique Peptide Region *LRRC37A2*[Exon 2-14] N-Terminal Truncation	
FLASLENDIKPKFPRKLYFLH				MISNQNFQGNYISYID	
FPRKLYFL	IC50	PKFPRKLY	IC50	MISNQNFQ	IC50
HLA-B*42:01	4	HLA-C*07:02	75	HLA-A*68:23	8
HLA-B*08:01	10	**KPKFPRKL**	**IC50**	HLA-A*32:07	32
HLA-A*32:07	16	HLA-B*42:01	44	HLA-A*32:15	168
HLA-A*68:23	20	HLA-C*07:02	50	HLA-C*03:03	492
HLA-B*44:01	24	HLA-B*07:02	125	**ISNQNFQG**	**IC50**
HLA-B*07:02	43	HLA-B*07:01	326	HLA-A*68:23	30
HLA-C*14:02	51	HLA-A*32:07	477	HLA-A*32:07	59
HLA-B*53:01	62	**DIKPKFPR**	**IC50**	HLA-C*12:03	132
HLA-C*08:02	70	HLA-A*33:01	7	HLA-A*32:15	209
HLA-B*07:01	93	HLA-C*07:02	100	**SNQNFQGN**	**IC50**
HLA-B*15:02	146	HLA-A*68:23	127	HLA-A*68:23	132
HLA-C*07:02	152	HLA-A*68:01	210	HLA-A*32:07	156
HLA-A*32:15	169	HLA-A*32:07	362	**NQNFQGNY**	**IC50**
HLA-C*03:04	260	**PRKLYFLH**	**IC50**	HLA-A*30:02	13
HLA-C*03:03	279	HLA-A*68:23	25	HLA-A*68:23	94
KFPRKLYF	**IC50**	HLA-C*14:02	35	HLA-B*15:01	139
HLA-A*24:03	2	HLA-A*32:07	48	HLA-A*32:07	141
HLA-A*68:23	10	**NDIKPKFP**	**IC50**	HLA-A*32:15	335
HLA-A*32:07	15	HLA-B*44:01	40	**QNFQGNYI**	**IC50**
HLA-C*14:02	16	HLA-A*68:23	84	HLA-A*68:23	23
HLA-C*03:03	41	HLA-A*32:07	115	HLA-A*32:07	36
HLA-B*15:02	53	HLA-C*08:02	262	HLA-A*32:15	160
HLA-C*07:02	56	HLA-C*07:02	271		
HLA-A*32:15	71	HLA-A*32:15	332		
HLA-B*15:03	161	**ENDIKPKF**			
HLA-A*23:01	203	HLA-C*07:02	39		
HLA-B*44:01	279	HLA-B*44:01	75		
HLA-A*24:01	407	HLA-C*08:02	81		
HLA-B*27:02	410	HLA-A*32:07	169		
LENDIKPK		HLA-A*68:23	203		
HLA-A*68:23	250				
HLA-C*07:02	316				
IKPKFPRK					
HLA-A*68:23	69				
HLA-C*07:02	124				

(Continued)

TABLE 3 Continued

Unique Peptide Region *NSFP1* [Exon 1-13] C-Terminal Truncation				Unique Peptide Region *LRRC37A2*[Exon 2-14] N-Terminal Truncation	
FLASLENDIKPKFPRKLYFLH				MISNQNFQGNYISYID	
FPRKLYFL	IC50	PKFPRKLY	IC50	MISNQNFQ	IC50
HLA-A*32:07	159				
HLA-A*30:01	260				

Wild-type amino acids are colored (black), amino acid residues from the NSFP1-Truncation are colored (red) and residues from the LRRC37A2-truncation are colored (blue) respectively.

chimeric RNAs that are not present in normal breast tissue we reduced the false positive rate. Including fusions that are present in adjacent normal samples (typically excluded by other 'fusion callers') and absent in normal breast tissue from cancer free patients, we significantly decreased the false negative rates of fusion detection. Additionally, this approach excludes chimeric RNAs that may be found in normal cells that have no impact on tumorigenesis or cancer progression (18). A number of fusion callers have been developed and published to extract fusion junctions from chimeric RNAs from RNAseq. Brian et al. and Trung et al. have each compared and benchmarked 15 gene fusion identification tools which are contingent on the accuracy of the transcriptome mapping (19, 20). Read length, quality scores and number of reads supporting each fusion were reported as the top limitations associated with fusion callers using short reads (21). *De-novo* assembly-based approaches yielding longer contigs have been reported to reduce limitations of short-read alignment but are computationally intensive (20–22). SeekFusion, developed by Balan et al. is designed to leverage *de-novo* assembly and alignment based approaches to increase the accuracy utilizing PCR-UMI-based amplicon RNA-Seq (23). Taking in to account the extensive body of prior work on fusion callers we used a multi-layered strategy to minimize false positives and false negatives. The key elements used include 1) de-novo assembly of RNA-seq data using the CLC Genomics Workbench 20 (Qiagen) to reduced false positives from shared repeat sequences on the genome; 2) utilized filters for removal of false positives from mis-mapping of reads to shared sequences in gene family members and/or pseudogenes when they exist (3, 24); and 3) relied heavily on fusions supported by split reads in multiple samples reported through other fusion callers from independent datasets (i.e. TCGA).

With an ultimate goal of identifying immunogenic peptides antigens that are broadly shared in breast cancer patients, we selected the *NSFP1-LRRC37A2* fusion transcript based on its frequency in tumor samples (found in 12% of samples tested) and 5 samples in the TCGA breast cancer dataset. *LRRC37A2* and *NSFP1* were previously predicted by the ChimeRScope pipeline to generate a fusion transcript in the opposite orientation (*LRRC37A2-NSFP1*) in a

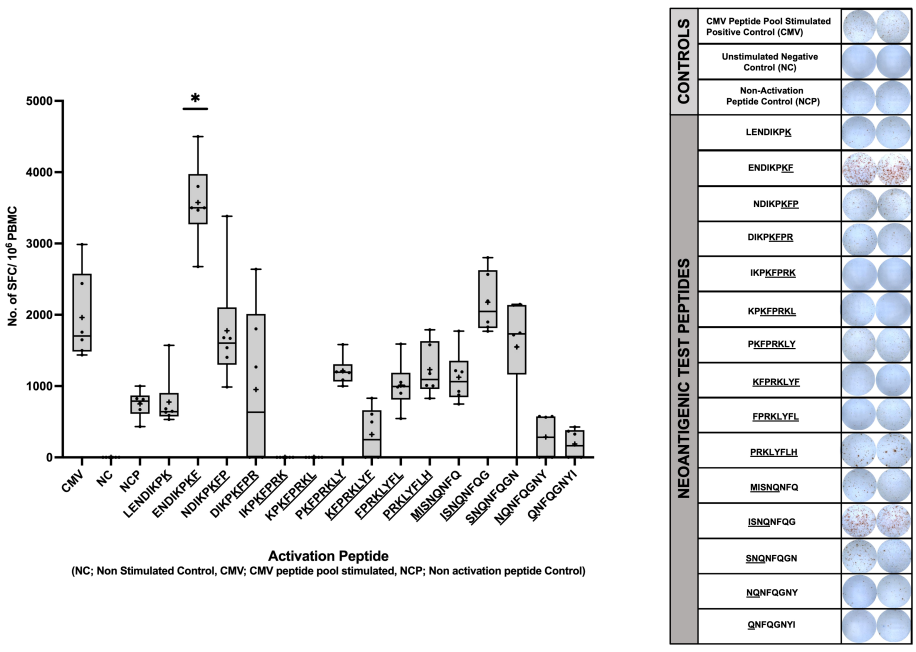

FIGURE 5
Human IFN-g ELISpot Assay using predicted immunogenic peptides of NSFP1-LRRC37A2. PBMCs from an HLA matched healthy donor were stimulated with the 15 predicted immunogenic peptides and analyzed via IFN-g ELISpot. Data represented as mean ± SEM. For the analysis, significance threshold was considered as *, $P \leq 0.05$.

natural killer cell line (25). However, the data did not report the fusion junction site or exon boundaries due to poor sequence quality of the amplified PCR product (25). Increased read-depths made possible by decreased costs for RNA-seq applications have uncovered an increasing number of non-genetic gene fusions arising from intergenic cis- or trans-splicing that are emerging as new biomarkers and therapeutic targets for cancer (26). The *NSFP1-LRRC37A2* fusion is consistent with a transcriptional read through of the *NSFP1*-pseudo gene truncated at Exon 13 into *LRRC37A2* located immediately 3' followed by a Cis-splicing event between *NSFP1* [Exon 13] and Exon 2 of *LRRC37A2* (Figure 1; Supplemental Figure 1). The relatively high degree of recurrence (12% in 75 patients) in 3 subtypes of breast cancer in our study and 5 subjects in TCGA breast tumor cohort makes it a highly attractive candidate for targeted therapies. The relatively low read numbers supporting the *LRRC37A2-NSFP1* fusion junction (average of 217-274 reads across the 75 samples) validated through PCR suggests that the fusion is likely present in a small subpopulation of cells in the tumor samples. Cai et al. and Carter et al. (27, 28) using clonal mutation analysis also report that tumor purity, heterogeneity and ploidy can result in variable cancer cell fractions in samples from cancer patients. However, if the fusion resulted from non-genetic fusions such as the one reported here they will not have corresponding DNA changes that are needed to compute CCF (cancer cell fraction) for each mutation.

Gene fusions have been reported to function as tumorigenic events in 16.5% of cancers and appear to be druggable in 6% of cases. The recurrent fusions commonly found associated with breast cancer and the potential impact of these in the development of new therapies for cancer is discussed by Loo et al. Gao et al. (29, 30). The most significant recurrent fusions reported from breast malignancies that could be benefit from targeted therapies as therapeutic vulnerabilities include *ESR1-CCDC170*, ESR1 exon 6 fusions, *BCL2L14-ETV6*, *ETV6-NTRK3* and *MYB-NFIB*. *ESR1-CCDC170* and ESR1 exon 6, have been reported to result in estrogen resistance and metastatic transformation in Luminal B breast cancer (31–33). *BCL2L14-ETV6* found in 6-12% of TNBC (34). *BCL2L14-ETV6* fusions reported in TNBC has been shown to result in EMT and paclitaxel resistance (35). 83% of a rare type of TNBS (adenoid cystic carcinomas (ACC) of the breast) carry the *MYB-NFIB* fusion (36). *ETV6-NTRK4* has been reported in secretory breast carcinoma (SBC). ETV6-NTRK3 and MYB-NFIB have been established to be cancer drivers (37, 38). Kinase fusions are currently being evaluated in breast cancer clinical trials and on-going mechanistic investigation is exposing therapeutic vulnerabilities in patients with fusion positive disease.

The *NSFP1*-[Exon-1-13]-KFPRKLYFLH C-terminal truncation and MISNQ-*LRRC37A2*-[Exon-2-14] N-terminal truncation together was found to generate 15 predicted immunogenic neoantigens with the potential to be processed and presented by 28 different MHC Class I alleles with a binding affinity of IC50<500nM. Out of the 15 peptides predicted to be immunogenic from the fusion junction, 8 peptides showed binding affinity (IC50<500nM) to the tested HLA Class of HLA-C*07:02. The peptide ENDIKPKF which showed the highest binding affinity (IC50 = 39) among all the peptides predicted to bind to HLA-C*07:02 was the only candidate which, satisfied the $p<0.05$ cutoff in the ELISpot assay (39).

In summary, we describe an untapped framework for discovery of neoantigens in breast cancer, generated through novel ORFs created from intergenically spliced mRNA transcripts. This novel pool of neopeptides broadens the opportunities for development of vaccines in breast cancer.

Data availability statement

The original contributions presented in the study are publicly available. This data can be found here: NCBI, accession number PRJNA1004862.

Ethics statement

The studies involving humans were approved by Institutional Review Board at MD Anderson Cancer Center under the protocol PA-16-0112. The studies were conducted in accordance with the local legislation and institutional requirements. Written informed consent for participation in this study was provided by the participants' legal guardians/next of kin.

Author contributions

BM, IB and PG conceptualized and designed the study. BM, SR, MC, AB, MR and HR contributed to the data acquisition and interpretation as well as in methodology and analysis. CA selected patient samples and oversaw the assembly of patient sample cores that were used for RNA extraction. BM, SR, MC, MR, AB, RK, IB and PG were major contributors in writing, review and editing the manuscript. All authors listed have made a substantial, direct, and intellectual contribution to the work and approved it for publication.

Funding

This work was supported by funds from the Moores Professorship to PG; 1U01CA189240-01 grant to IB and RE-Z (M-PI). BM, SR, MC and HR were supported in part by a grant from the McCammon Foundation.

Acknowledgments

We would like to acknowledge bioinformatics and sequencing support from the UH-Sequencing & Gene Editing Core and the contributions from the USAEOP/REAP funded internship program participants for exon-boundary analysis of the RNA fusions led by mentors Dr. Kimberly Holloway, Sudhili Fernando, Abhinav Vadassery, and interns Tanya Roysam, Fernando Peraza and Aprameya Sudharsan.

Conflict of interest

The authors declare that the research was conducted in the absence of any commercial or financial relationships that could be construed as a potential conflict of interest.

Publisher's note

All claims expressed in this article are solely those of the authors and do not necessarily represent those of their affiliated organizations, or those of the publisher, the editors and the reviewers. Any product that may be evaluated in this article, or claim that may be made by its manufacturer, is not guaranteed or endorsed by the publisher.

Supplementary material

The Supplementary Material for this article can be found online at: https://www.frontiersin.org/articles/10.3389/fimmu.2023.1188831/full#supplementary-material

References

1. Li L, Goedegebuure SP, Gillanders WE. Preclinical and clinical development of neoantigen vaccines. *Ann Oncol* (2017) 28(suppl_12):xii11–xii7. doi: 10.1093/annonc/mdx681

2. Tran E, Robbins PF, Rosenberg SA. 'Final common pathway' of human cancer immunotherapy: targeting random somatic mutations. *Nat Immunol* (2017) 18(3):255–62. doi: 10.1038/ni.3682

3. Wei Z, Zhou C, Zhang Z, Guan M, Zhang C, Liu Z, et al. The landscape of tumor fusion neoantigens: A pan-cancer analysis. *iScience* (2019) 21:249–60. doi: 10.1016/j.isci.2019.10.028

4. Anagnostou V, Smith KN, Forde PM, Niknafs N, Bhattacharya R, White J, et al. Evolution of neoantigen landscape during immune checkpoint blockade in non-small cell lung cancer. *Cancer Discov* (2017) 7(3):264–76. doi: 10.1158/2159-8290.CD-16-0828

5. Gartner JJ, Parker SC, Prickett TD, Dutton-Regester K, Stitzel ML, Lin JC, et al. Whole-genome sequencing identifies a recurrent functional synonymous mutation in melanoma. *Proc Natl Acad Sci USA* (2013) 110(33):13481–6. doi: 10.1073/pnas.1304227110

6. Ott PA, Hu Z, Keskin DB, Shukla SA, Sun J, Bozym DJ, et al. An immunogenic personal neoantigen vaccine for patients with melanoma. *Nature* (2017) 547 (7662):217–21. doi: 10.1038/nature22991

7. Aldous AR, Dong JZ. Personalized neoantigen vaccines: A new approach to cancer immunotherapy. *Bioorg Med Chem* (2018) 26(10):2842–9. doi: 10.1016/j.bmc.2017.10.021

8. Turajlic S, Litchfield K, Xu H, Rosenthal R, McGranahan N, Reading JL, et al. Insertion-and-deletion-derived tumour-specific neoantigens and the immunogenic phenotype: a pan-cancer analysis. *Lancet Oncol* (2017) 18(8):1009–21. doi: 10.1016/S1470-2045(17)30516-8

9. Disis ML, Wallace DR, Gooley TA, Dang Y, Slota M, Lu H, et al. Concurrent trastuzumab and HER2/neu-specific vaccination in patients with metastatic breast cancer. *J Clin Oncol Off J Am Soc Clin Oncol* (2009) 27(28):4685–92. doi: 10.1200/JCO.2008.20.6789

10. Lowenfeld L, Zaheer S, Oechsle C, Fracol M, Datta J, Xu S, et al. Addition of anti-estrogen therapy to anti-HER2 dendritic cell vaccination improves regional nodal immune response and pathologic complete response rate in patients with ER(pos)/HER2(pos) early breast cancer. *Oncoimmunol* (2017) 6(9):e1207032. doi: 10.1080/2162402X.2016.1207032

11. Robinson MD, Oshlack A. A scaling norMalization method for differential expression analysis of RNA-seq data. *Genome Biol* (2010) 11(3):R25. doi: 10.1186/gb-2010-11-3-r25

12. Shao XM, Bhattacharya R, Huang J, Sivakumar IKA, Tokheim C, Zheng L, et al. High-throughput prediction of MHC class I and II neoantigens with MHCnuggets. *Cancer Immunol Res* (2020) 8(3):396–408. doi: 10.1158/2326-6066.CIR-19-0464

13. Hundal J, Kiwala S, McMichael J, Miller CA, Xia H, Wollam AT, et al. pVACtools: A computational toolkit to identify and visualize cancer neoantigens. *Cancer Immunol Res* (2020) 8(3):409–20. doi: 10.1158/2326-6066.CIR-19-0401

14. Almeida RR, Rosa DS, Ribeiro SP, Santana VC, Kallas EG, Sidney J, et al. Broad and cross-clade CD4+ T-cell responses elicited by a DNA vaccine encoding highly conserved and promiscuous HIV-1 M-group consensus peptides. *PloS One* (2012) 7(9): e45267. doi: 10.1371/journal.pone.0045267

15. Van der Auwera I, Bovie C, Svensson C, Trinh XB, Limame R, van Dam P, et al. Quantitative methylation profiling in tumor and matched morphologically normal tissues from breast cancer patients. *BMC Cancer* (2010) 10:97. doi: 10.1186/1471-2407-10-97

16. Yang W, Lee KW, Srivastava RM, Kuo F, Krishna C, Chowell D, et al. Immunogenic neoantigens derived from gene fusions stimulate T cell responses. *Nat Med* (2019) 25(5):767–75. doi: 10.1038/s41591-019-0434-2

17. Vellichirammal NN, Albahrani A, Banwait JK, Mishra NK, Li Y, Roychoudhury S, et al. Pan-cancer analysis reveals the diverse landscape of novel sense and antisense fusion transcripts. *Mol Ther Nucleic Acids* (2020) 19:1379–98. doi: 10.1016/j.omtn.2020.01.023

18. Singh S, Qin F, Kumar S, Elfman J, Lin E, Pham LP, et al. The landscape of chimeric RNAs in non-diseased tissues and cells. *Nucleic Acids Res* (2020) 48(4):1764–78. doi: 10.1093/nar/gkz1223

19. Vu TN, Deng W, Trac QT, Calza S, Hwang W, Pawitan Y. A fast detection of fusion genes from paired-end RNA-seq data. *BMC Genomics* (2018) 19(1):786. doi: 10.1186/s12864-018-5156-1

20. Haas BJ, Dobin A, Li B, Stransky N, Pochet N, Regev A. Accuracy assessment of fusion transcript detection via read-mapping and *de novo* fusion transcript assembly-based methods. *Genome Biol* (2019) 20:213. doi: 10.1186/s13059-019-1842-9

21. Carrara M, Beccuti M, Lazzarato F, Cavallo F, Cordero F, Donatelli S, et al. State-of-the-art fusion-finder algorithms sensitivity and specificity. *Biomed Res Int* (2013) 2013:340620. doi: 10.1155/2013/340620

22. Davidson NM, Majewski IJ, Oshlack A. JAFFA: high sensitivity transcriptome-focused fusion gene detection. *Genome Med* (2015) 7(1):43. doi: 10.1186/s13073-015-0167-x

23. Balan J, Jenkinson G, Nair A, Saha N, Koganti T, Voss J, et al. SeekFusion - A clinically validated fusion transcript detection pipeline for PCR-based next-generation sequencing of RNA. *Front Genet* (2021) 12:739054. doi: 10.3389/fgene.2021.739054

24. Kumar S, Razzaq SK, Vo AD, Gautam M, Li H. Identifying fusion transcripts using next generation sequencing. *Wiley Interdiscip Rev RNA* (2016) 7(6):811–23. doi: 10.1002/wrna.1382

25. Li Y, Heavican TB, Vellichirammal NN, Iqbal J, Guda C. ChimeRScope: a novel alignment-free algorithm for fusion transcript prediction using paired-end RNA-Seq data. *Nucleic Acids Res* (2017) 45(13):e120. doi: 10.1093/nar/gkx315

26. Jia Y, Xie Z, Li H. Intergenically spliced chimeric RNAs in cancer. *Trends Cancer* (2016) 2(9):475–84. doi: 10.1016/j.trecan.2016.07.006

27. Carter SL, Cibulskis K, Helman E, McKenna A, Shen H, Zack T, et al. Absolute quantification of somatic DNA alterations in human cancer. *Nat Biotechnol* (2012) 30 (5):413–21. doi: 10.1038/nbt.2203

28. Cai W, Zhou D, Wu W, Tan WL, Wang J, Zhou C, et al. MHC class II restricted neoantigen peptides predicted by clonal mutation analysis in lung adenocarcinoma patients: implications on prognostic immunological biomarker and vaccine design. *BMC Genomics* (2018) 19(1):582. doi: 10.1186/s12864-018-4958-5

29. Loo SK, Yates ME, Yang S, Oesterreich S, Lee AV, Wang X. Fusion-associated carcinomas of the breast: Diagnostic, prognostic, and therapeutic significance. *Genes Chromosomes Cancer* (2022) 61(5):261–73. doi: 10.1002/gcc.23029

30. Gao Q, Liang WW, Foltz SM, Mutharasu G, Jayasinghe RG, Cao S, et al. Driver fusions and their implications in the development and treatment of human cancers. *Cell Rep* (2018) 23(1):227–238.e3. doi: 10.1016/j.celrep.2018.03.050

31. Veeraraghavan J, Tan Y, Cao XX, Kim JA, Wang X, Chamness GC, et al. Recurrent ESR1–CCDC170 rearrangements in an aggressive subset of oestrogen receptor-positive breast cancers. *Nat Commun* (2014) 5(1):4577. doi: 10.1038/ncomms5577

32. Liu CC, Veeraraghavan J, Tan Y, Kim JA, Wang X, Loo SK, et al. A novel neoplastic fusion transcript, *RAD51AP1-DYRK4* , confers sensitivity to the MEK inhibitor trametinib in aggressive breast cancers. *Clin Cancer Res* (2021) 27(3):785–98. doi: 10.1158/1078-0432.CCR-20-2769

33. Hartmaier RJ, Trabucco SE, Priedigkeit N, Chung JH, Parachoniak CA, Vanden Borre P, et al. Recurrent hyperactive ESR1 fusion proteins in endocrine therapy-resistant breast cancer. *Ann Oncol* (2018) 29(4):872–80. doi: 10.1093/annonc/mdy025

34. Guo B, Godzik A, Reed JC. Bcl-G, a novel pro-apoptotic member of the bcl-2 family. *J Biol Chem* (2001) 276(4):2780–5. doi: 10.1074/jbc.M005889200

35. Lee S, Hu Y, Loo SK, Tan Y, Bhargava R, Lewis MT, et al. Landscape analysis of adjacent gene rearrangements reveals BCL2L14–ETV6 gene fusions in more aggressive

triple-negative breast cancer. *Proc Natl Acad Sci* (2020) 117(18):9912–21. doi: 10.1073/pnas.1921333117

36. Martelotto LG, De Filippo MR, Ng CK, Natrajan R, Fuhrmann L, Cyrta J, et al. Genomic landscape of adenoid cystic carcinoma of the breast. *J Pathol* (2015) 237 (2):179–89. doi: 10.1002/path.4573

37. Persson M, Andrén Y, Mark J, Horlings HM, Persson F, Stenman G. Recurrent fusion of MYB and NFIB transcription factor genes in carcinomas of the breast and head and neck. *Proc Natl Acad Sci USA* (2009) 106(44):18740–4. doi: 10.1073/pnas.0909114106

38. Bishop JA, Yonescu R, Batista D, Begum S, Eisele DW, Westra WH. Utility of mammaglobin immunohistochemistry as a proxy marker for the ETV6-NTRK3 translocation in the diagnosis of salivary mammary analogue secretory carcinoma. *Hum Pathol* (2013) 44(10):1982–8. doi: 10.1016/j.humpath.2013.03.017

39. Currier JR, Kuta EG, Turk E, Earhart LB, Loomis-Price L, Janetzki S, et al. A panel of MHC class I restricted viral peptides for use as a quality control for vaccine trial ELISPOT assays. *J Immunol Methods* (2002) 260(1-2):157–72. doi: 10.1016/S0022-1759(01)00535-X

frontiers | Frontiers in Immunology

TYPE Original Research
PUBLISHED 15 September 2023
DOI 10.3389/fimmu.2023.1264929

OPEN ACCESS

EDITED BY
Roberto Gramignoli,
Karolinska Institutet (KI), Sweden

REVIEWED BY
Jinzhang Chen,
Southern Medical University, China
Xiaoxiang Rong,
Southern Medical University, China

*CORRESPONDENCE
Hong Qiu
qiuhong@hust.edu.cn
Henghui Cheng
hhcheng2007@hust.edu.cn

RECEIVED 21 July 2023
ACCEPTED 25 August 2023
PUBLISHED 15 September 2023

CITATION
Dai Y, Liu Y, Gong Z, He L, Wang L, Yang W, Qiu P, Zhang F, Yuan X, Cheng H and Qiu H (2023) Revalidation of the ATTRACTION-4 study in a real-world setting: a multicenter, retrospective propensity score matching study in China. *Front. Immunol.* 14:1264929. doi: 10.3389/fimmu.2023.1264929

Revalidation of the ATTRACTION-4 study in a real-world setting: a multicenter, retrospective propensity score matching study in China

Yuhong Dai[1], Yongqing Liu[1], Zhimin Gong[2], Lilin He[3], Lei Wang[2], Wenjie Yang[3], Ping Qiu[4], Fangyuan Zhang[1], Xianglin Yuan[1], Henghui Cheng[5]* and Hong Qiu[1]*

[1]Department of Oncology, Tongji Hospital Affiliated to Tongji Medical College of Huazhong University of Science & Technology, Wuhan, Hubei, China, [2]Department of Oncology, Xiangyang Central Hospital, Affiliated Hospital of Hubei University of Arts and Science. Institute of Oncology, Hubei University of Arts and Science, Xiangyang, Hubei, China, [3]Department of Oncology, The First People's Hospital of Tianmen, Tianmen, Hubei, China, [4]Department of Oncology, Jingzhou Central Hospital, Jingzhou, Hubei, China, [5]Institution of Pathology, Tongji Hospital Affiliated to Tongji Medical College of Huazhong University of Science & Technology, Wuhan, Hubei, China

Background: Immune-checkpoint inhibitors (ICIs) combined with chemotherapy have been successfully used in clinical trials to treat advanced gastric cancer. However, the efficacy and safety of first-line immunotherapy combined with chemotherapy in Chinese patients are unknown.

Methods: This multicenter retrospective study included patients with human epidermal growth factor receptor-2 (HER-2) negative advanced gastric cancer treated with first-line chemotherapy or chemotherapy with an ICI between January 2019 and December 2022. Propensity score matching was used to compare progression-free survival (PFS), overall survival, objective response rates, and adverse reactions between cohorts.

Results: After propensity score matching, 138 patients, who had balanced baseline characteristics, were included in the chemotherapy and combination treatment groups. The median follow-up duration was 16.90 months, and the median PFS was 8.53 months (95% confidence interval [CI] 7.77-9.28) in the combination treatment group and 5.97 months (95% CI 4.56-7.37) in the chemotherapy group. The median survival duration was 17.05 months (95% CI 14.18-19.92) in the combination treatment group and 16.46 months (95% CI 12.99-19.93) in the chemotherapy group. The PFS subgroup analysis revealed that age ≥65 years, women, Eastern Cooperative Oncology Group performance status of 1, non-signet ring cell carcinoma, esophagogastric junction, liver metastasis, peritoneal metastasis, no massive ascites, only one metastatic organ, and combined platinum-based chemotherapy correlated with treatment benefit. The incidences of adverse events above grade 3 were comparable between groups.

Conclusions: Our study confirmed the ATTRACTION-4 trial results. Compared with chemotherapy, first-line ICIs combined with chemotherapy prolonged PFS but did not improve overall survival in patients with HER-2-negative advanced gastric cancer.

KEYWORDS

immune checkpoint inhibitors, advanced gastric cancer, propensity score matching, progression free survival, overall survival

1 Introduction

Gastric cancer is a notable global health problem and the third leading cause of mortality and the sixth leading cause of morbidity (1). In China, approximately 679,000 new cases of gastric cancer and 498,000 deaths occurred in 2015, with gastric cancer ranking second in the mortality rate among malignant tumors (2). Currently, treatment methods for advanced gastric cancer are limited, and comprehensive treatment based on chemotherapy is the main strategy for advanced gastric cancer. The recommended chemotherapeutic agents for advanced gastric cancer include platinum, fluorouracil, and taxane drugs, as well as anti- human epidermal growth factor receptor-2 (HER-2) or anti-angiogenic drugs in specific populations. At present, the treatment outcome of advanced gastric cancer is unsatisfactory, and the median survival time is approximately only 1 year (3).

Recently, several clinical studies have revealed the survival benefits of immune- checkpoint inhibitor (ICI) therapy in select populations with gastric cancer. Compared with chemotherapy alone, combined immunotherapy can increase the overall response rate (ORR) while prolonging progression free survival (PFS) and overall survival (OS) in specific populations (4–7). Multiple guidelines, including those of the National Comprehensive Cancer Network, European Society for Medical Oncology, and Chinese Society of Clinical Oncology, recommend the first-line use of ICIs in combination with chemotherapy in patients with advanced gastric cancer with a high combined positive score (CPS) (3, 8, 9).

Currently, ICIs are highly accessible and widely used for the treatment of advanced gastric cancer in China. Here, we analyzed the short- and long-term outcomes and adverse reactions of patients with advanced gastric cancer treated with chemotherapy or chemotherapy combined with ICIs, to explore the efficacy and safety of immunotherapy in this patient population.

2 Materials and methods

2.1 Study design and participants

This retrospective, multicenter study involved patients diagnosed with HER-2 negative local advanced or metastatic gastric adenocarcinoma. The protocol of this study was reviewed and approved by the ethics committee of Tongji Hospital of Huazhong University of Science and Technology (Ethical approval no: TJ-IRB 20230303). All patients were fully informed about the objectives of the study, and the requirement for informed consent was waived due to this study's observational retrospective design. This study retrospectively analyzed the clinical data of patients with advanced gastric cancer from six cancer centers across China, between January 2019 and December 2022. Data were collected from the first chemotherapy session until patient death.

All eligible patients had histologically or cytologically confirmed unresectable, locally advanced, relapsed, or metastatic gastric adenocarcinoma; had received at least one cycle of doublet or triplet chemotherapy or doublet or triplet chemotherapy combined with immunotherapy; and had been evaluated for efficacy at least once. Patients with recurrent gastric cancer were included when at least six months had elapsed from the end of adjuvant or neoadjuvant therapy. Patients were excluded if their clinical data were incomplete, survival follow-up data were not available, their HER-2 status was positive, or if they received single-agent chemotherapy.

After screening 3190 patients according to the above criteria, we excluded 2093 patients with no clear evidence of tumor recurrence and metastasis, 35 patients with positive HER-2 expression, 64 patients who received single-agent chemotherapy, 96 patients without tumor evaluation, and 586 patients with no readily accessible clinical data. In the final analysis, 316 patients were included (Figure 1).

2.2 Study procedures

All patients included in the final analysis received first-line oxaliplatin- or taxane-based chemotherapy and some patients received a treatment combined with ICIs, at the discretion of the clinician.

The following baseline characteristics were collected for each patient: age, sex, Eastern Cooperative Oncology Group (ECOG) performance status (PS), primary tumor location, involved organs, CPS, microsatellite instability status, and chemotherapy regimen, if available. Computed tomography scans were conducted every 6-8 weeks after the initiation of first-line chemotherapy, to evaluate the clinical response using the Response Evaluation Criteria in Solid Tumors (RECIST) version 1.1 (10).

10.3389/fimmu.2023.1264929

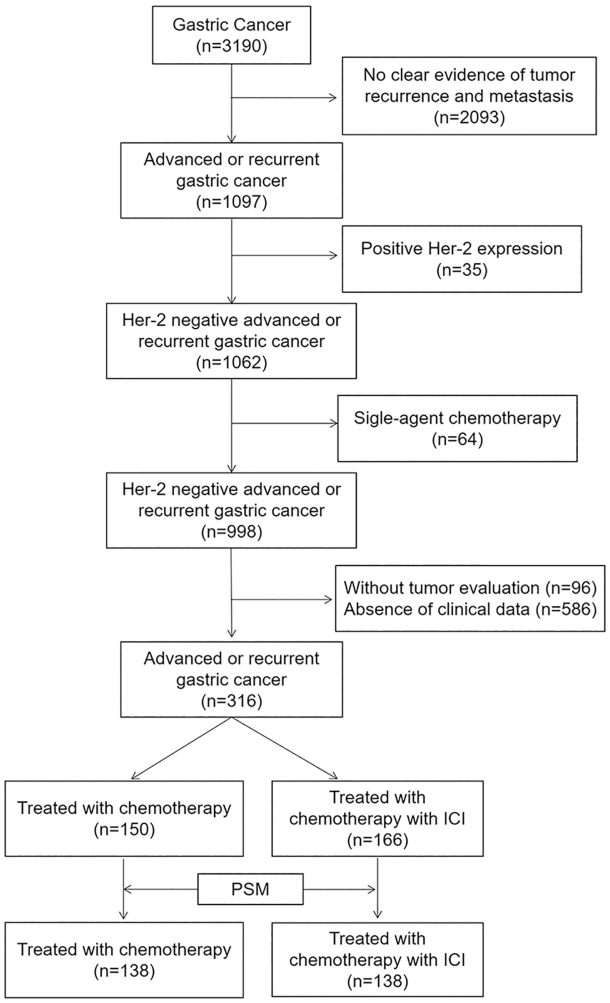

FIGURE 1
Flow diagram of the study.

2.3 Outcomes

The primary endpoint was first-line PFS, which was estimated from treatment initiation to progression or death. The secondary endpoints included OS, defined as the duration from treatment initiation to death due to any reason; ORR, defined as the number of patients with a best overall response of complete response or partial response (PR); and disease control rate (DCR), defined as the proportion of patients who achieved a complete response, PR, stable disease, or non-PR/non-Progression Disease and safety. Adverse events (AEs) were monitored and classified according to the Common Terminology Criteria for Adverse Events version 5.0.

2.4 Statistical analysis

Continuous and categorical data were reported as medians (interquartile range [IQR]) and percentages. PFS and OS were estimated using Kaplan-Meier analysis and expressed as median values with corresponding two-sided 95% confidence intervals (CIs), and differences between treatment groups were compared by log-rank tests with two-sided significance levels of p=0.05. The ORR and DCR were compared using the chi-square test. Hazard ratios (HRs) and corresponding 95% CIs were calculated using the Cox proportional hazards model. Univariate and multivariate analyses were performed to evaluate the effects of immunotherapy on PFS and OS.

A 1:1 propensity score matching (PSM) algorithm with a caliper of 0.1 was conducted to adjust for the non-random design of the study. The propensity score was estimated by multivariate logistic regression, with combined immunotherapy as the dependent variable, and age, sex, ECOG PS, primary tumor location, liver metastasis, signet-ring cell status, peritoneum metastasis, massive ascites, first-line chemotherapy regimen, and number of organs involved as covariables.

All statistical analyses were performed using SPSS (version 27.0, IBM Corp., Armonk, NY) and GraphPad Prism (version 9.0; GraphPad Software, San Diego, CA).

3 Results

3.1 Patient characteristics

The median age of the included patients was 55 years (IQR 48-63); 180 (57.0%) of the 316 patients were men, and all patients had an ECOG PS of 0-1. The patients received a median of five cycles (IQR 4-6) of first-line fluoropyrimidine-based (5-fluorouracil, capecitabine, S-1, etc.) chemotherapy. The majority (65.5%) of patients received platinum drug regimens (oxaliplatin, cisplatin, etc.) and 41.5% received taxane drug regimens (docetaxel, paclitaxel, nap-paclitaxel, etc.), among whom 7% received platinum combined with taxane regimens (DCF, DOX, FLOT, etc.) A total of 166 patients (52.2%) received first-line chemotherapy combined with ICIs, including nivolumab, sintilimab, tislelizumab, camrelizumab, and pembrolizumab. Because CPS values were not available for more than 90% of the enrolled patients, no analysis was performed for this indicator. Patients who received up to eight cycles of first-line treatment without disease progression and with tolerable adverse event profiles were treated with maintenance therapy, which consisted of single-agent chemotherapy (S-1 or capecitabine) combined with or without immunotherapy.

3.2 PSM results

After performing PSM using the procedures described in the Methods section, 138 patients who received first-line chemotherapy alone and 138 matched patients who received first-line chemotherapy combined with immunotherapy were included in the final analysis. The baseline characteristics of patients before matching revealed statistically significant differences between the groups in terms of age and proportion of first-line platinum-based chemotherapy regimens. However, the post-matching analysis revealed well-balanced characteristics between the two groups (Table 1).

10.3389/fimmu.2023.1264929

3.3 Efficacy

At the cutoff date of January 9, 2023, 236 of 316 patients (74.7%) had disease progression, and 207 of the 276 matched patients (75.0%) had PFS. After a median follow-up duration of 16.90 months, the median PFS (mPFS) durations before matching were 5.84 months (95% CI 4.69-6.98) in the chemotherapy group and 8.56 months (95% CI 7.86-9.26) in the combination treatment group (HR 0.64 [95% CI 0.45-0.83], p<0.001). The post-match analysis revealed that the mPFS duration in the chemotherapy group was 5.97 months (95% CI 4.56-7.37), and that in the combination treatment cohort was 8.53 months (95% CI 7.77-9.28) (HR 0.68 [95% CI 0.52-0.91], p=0.008). The PFS curves before and after matching are shown in Figure 2. The 6-month PFS rate was 46.4% (95% CI 38-55) with chemotherapy and 58.7% (95% CI 50-67) with combined therapy.

At the cutoff date, 150 of the 316 patients had died, with a median OS (mOS) duration of 16.39 months (95% CI 12.90-19.89) in the chemotherapy group and 17.05 months (95% CI 14.12-19.97) in the combination treatment group (HR 0.78 [95% CI 0.56-1.09], p=0.147). The matched data analysis showed that 135 (48.9%) of the 276 patients had died, with mOS durations of 16.46 months (95% CI 12.99-19.93) in the chemotherapy group and 17.05 months (95% CI 14.18-19.92) in the combination treatment group (HR 0.88 [95% CI 0.62-1.26], p=0.481), with no statistical difference in OS between the two groups, either before or after matching (Figure 3).

TABLE 1 Demographic and clinical characteristics of patients before and after PSM.

	Before PSM			After PSM		
Variable	CT (n=150)	CT+ICI (n=166)	*p* value	CT (n=138)	CT+ICI (n=138)	*p* value
Sex			0.136			0.543
Male	92(61.3%)	88(53.0%)		81(58.7%)	76(55.1%)	
Female	58(38.7%)	78(47.0%)		57(41.3%)	62(44.9%)	
Age	56.5(51.0-64.0)	53.0(44.8-63.0)	0.011	55.0(49.8-63.0)	54.0(47.5-64.0)	0.395
ECOG PS			0.813			0.185
0	73(48.7%)	83(50.0%)		73(52.9%)	62(44.9%)	
1	77(51.3%)	83(50.0%)		65(47.1%)	76(55.1%)	
Primary tumor location						
EGJ	29(19.3%)	18(10.8%)		24(17.4%)	14(10.1%)	0.204
GC	119(79.3%)	145(87.3%)		112(81.2%)	121(87.7%)	
residue	2(1.3%)	3(1.8%)		2(1.4%)	3(2.2%)	
Signet-ring cell			0.413			0.457
Yes	27(18.0%)	36(21.7)		26(18.8%)	31(22.5%)	
No	123(82.5)	130(78.3%)		112(81.2%)	107(77.5%)	
Metastatic site						
Liver	42(28.0%)	44(26.5%)	0.766	37(26.8%)	36(26.1%)	0.891
Peritoneum	82(54.7%)	80(48.2%)	0.250	73(52.9%)	71(50.7%)	0.718
Number of organs involved						
1	49(32.7%)	63(38.0%)	0.327	45(32.6%)	52(37.7%)	0.377
≥2	101(67.3%)	103(62.0%)		93(67.4%)	86(62.3%)	
Massive ascites			0.312			0.651
Yes	32(21.3%)	28(16.9%)		29(21.0%)	26(18.8%)	
No	118(78.7%)	138(83.1%)		109(79.0%)	112(81.2%)	
First-line chemotherapy regimen						
Taxane-based	68(45.3%)	63(38.0%)	0.184	59(42.8%)	54(39.1%)	0.541
Platinum-based	87(58.0%)	120(72.3%)	0.008	84(60.9%)	92(66.7%)	0.316

PSM, propensity score matching; CT, chemotherapy; ICI, immune-checkpoint inhibitors; ECOG PS, Eastern Cooperative Oncology Group performance status; GC, gastric cancer; EGJ, esophagogastric junction.

In the matched population, according to RECIST1.1 criteria, one patient in the chemotherapy group achieved complete response, 41 patients (29.7%) achieved PR, and the ORR was 30.4%. In the combined treatment group, 51 patients achieved PR, no patients achieved complete response, and the ORR was 37.0%. There was no statistically significant difference in ORR between the two groups (p=0.252). The DCR in the chemotherapy group was 84.8%, which was significantly lower than that in the combination treatment group (93.5%) (p=0.020). Supplementary Table 1 shows the tumor responses during first-line treatment in each study cohort.

3.4 Subgroup analysis

In the *post-hoc* subgroup analysis of PFS based on baseline characteristics, women aged 65 years or older, ECOG PS of 1, non-signet ring cell carcinoma, esophagogastric junction, liver metastasis, peritoneal metastasis, no massive ascites, and only one metastatic organ were associated with benefits from combination therapy. Moreover, in the choice of chemotherapy regimen, immunotherapy combined with a platinum-based chemotherapy regimen appeared to provide more PFS benefits. The results of the subgroup analysis of PFS and OS are shown in Figure 4.

This study included 59 patients without measurable target lesions who presented with peritoneal metastases or ascites. In the cohort with measurable target lesions(n=217), chemotherapy combined with immunotherapy improved the DCR by 13.5% compared to chemotherapy alone (93.7% versus 80.2%; p=0.003; Supplementary Table 2), while there was no significant difference in ORR (45.9% versus 39.6%; p=0.347) between the treatments. In the cohorts with no measurable target lesions, there was no difference in DCR (92.6% versus 100.0%, p=0.398) between treatments. The survival analysis showed no significant differences in PFS (7.77 m *vs.* 8.72 m, HR 0.75 [95% CI 0.53-1.04], p=0.081) and OS (15.93 m *vs.* 20.75 m, HR 0.80 [95% CI 0.54-1.21], p=0.297) between patients with or without target lesions. The corresponding PFS and OS results are shown in Online Supplementary Figures 1, 2.

3.5 Expansion follow-up

Of the matched patients, 77 (55.8%) of 138 patients receiving chemotherapy, and 57 (41.3%) of 138 patients receiving combination therapy received at least one subsequent anticancer therapy following progression after first-line treatment. Of the patients in the chemotherapy group, 59.7% (46/77) received immunotherapy after first-line treatment progression, and 70.2% (40/57) of the patients in the combination treatment group received continued immunotherapy after disease progression. The subgroup analysis showed that in the first-line chemotherapy group, combined immunotherapy after disease progression reduced the risk of death by 53.6%, compared with chemotherapy (HR 0.46 [95% CI 0.26-0.84], p=0.010), with an associated mOS of 24.07 months and 14.07 months, respectively. In the first-line combination treatment group, sequential immunotherapy beyond progression had no significant impact on OS (17.97 m *vs.* 13.28 m, HR 0.80 [95% CI 0.36-1.79], p=0.590) (Supplementary Figures 3, 4). Patients who had been treated with ICIs during first-line or sequential treatment had a significantly longer OS durations compared with patients who had never been treated with ICI [19.97 m *vs.* 11.34 m, HR 0.60 (95% CI 0.43-0.84, p=0.003)]. The associated survival curves are shown in Figure 5.

Of the 276 patients, 59 (21.4%) received palliative radiotherapy at various treatment stages. The corresponding treatments included radiotherapy for primary foci, liver metastases, metastatic lymph nodes, or metastatic bone lesions. The survival analysis revealed that compared to patients who did not receive palliative radiotherapy, patients who underwent palliative radiotherapy had significantly longer survival, with respective median OS durations of 21.80 months *vs.* 15.12 months (HR, 0.55 [95% CI 0.35-0.87], p=0.010). The corresponding survival curves for palliative radiotherapy are shown in Supplementary Figure 5.

3.6 Safety

The main AEs identified after matching are presented in Table 2. In the chemotherapy group, 92.8% (128/138) of the patients experienced some grade of AE, as did 98.6% (136/138) of patients in the combination treatment group. The most common AEs included anemia, leukopenia, neutropenia, elevated alanine aminotransferase or aspartate aminotransferase, and thrombocytopenia, most of which were of grade 1-2 and manageable.

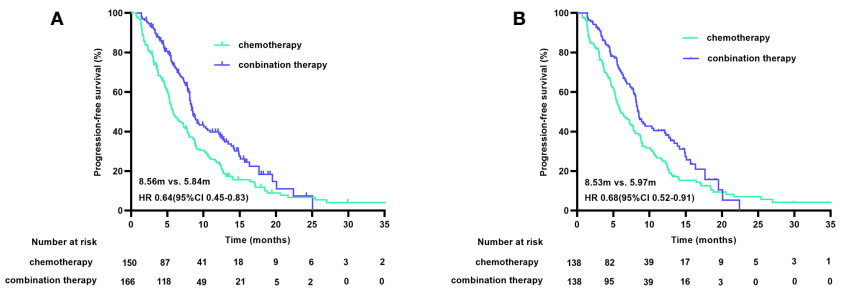

FIGURE 2
PFS curves before **(A)** and after **(B)** PSM. PFS, progression free survival; PSM, propensity score matching.

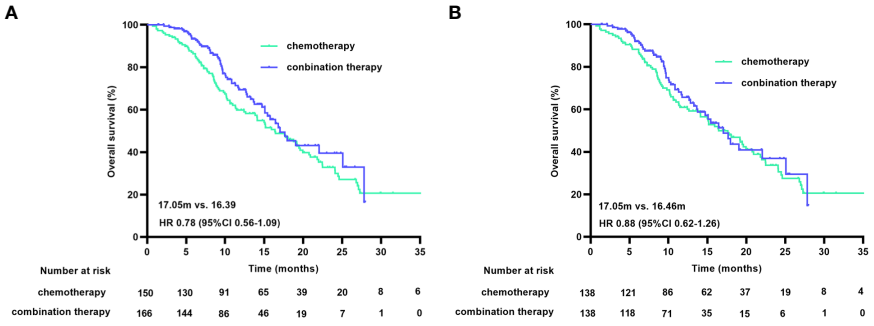

FIGURE 3
OS curves before **(A)** and after **(B)** PSM. OS, overall survival; PSM, propensity score matching.

Any grade thrombocytopenia and elevated alanine aminotransferase or aspartate aminotransferase were significantly more frequent in the combination treatment group; however, there was no difference in the incidence of AEs above grade 2 between the two cohorts. ICI-related thyroid dysfunction occurred in 15.9% of the patients, most of whom had hypothyroidism. Overall, hyperthyroidism occurred in 2.9% of the patients, all of whom eventually developed hypothyroidism. Two patients developed myocarditis, one of whom developed cardiogenic shock, and ICI therapy was discontinued in both patients. Acute renal failure occurred in one patient; however, it was difficult to determine whether the adverse reaction was an immune-related AE. The remaining immune-related AEs were grade 1-2.

4 Discussion

In this multicenter, retrospective, real-world study, chemotherapy combined with ICI therapy was found to significantly improve PFS in previously untreated HER-2 negative patients with advanced gastric adenocarcinoma. This regimen reduced the risk of disease progression by 32% compared with chemotherapy. Consistent with the results of previous clinical studies, our results reveal that ICIs combined with chemotherapy provide clinical benefits to patients with advanced HER-2 negative gastric adenocarcinoma (4–7).

However, our results showed no significant difference in OS between the groups, which is inconsistent with the results of some previous clinical studies. In the CheckMate 649 and Orient 16 studies, chemotherapy combined with immunotherapy was associated with a significant improvement in OS in all randomly assigned patients and was more pronounced in patients with high CPS expression. In our study, 64.7% of the patients received sequential treatment after disease progression following first-line treatment, which was similar to the incidence reported in the ATTRACTION-4 study, whereas the incidence was only 39% in the CM649 study. It is widely accepted that patients who received subsequent anticancer pharmacotherapy had better survival. More than 60% of the patients who received sequential therapy chose combination immunotherapy, and patients who received immunotherapy throughout the course of their treatment had a 40% lower risk of death than those who did not. This finding suggests that the use of immunotherapy as a sequential therapy may provide survival benefits, even if first-line immunotherapy is not used. This finding can be explained by the fact that patients in the first-line chemotherapy group, chemotherapy combined with immunotherapy after disease progression significantly prolongs OS and increases HR benefits.

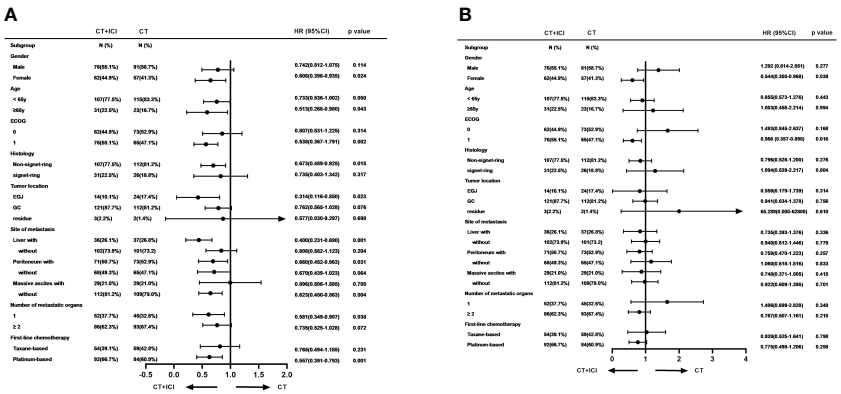

FIGURE 4
Subgroup analyses of PFS **(A)** and OS **(B)** based on baseline characteristics. PFS, progression free survival; OS, overall survival.

10.3389/fimmu.2023.1264929

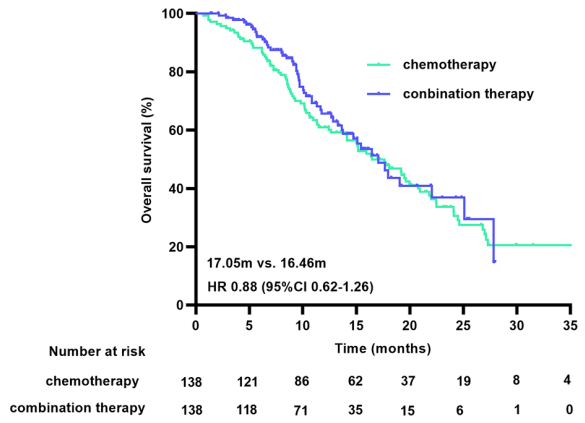

FIGURE 5
OS curve for the treatment with or without ICI. OS, overall survival; ICI, immune checkpoint inhibitors.

In the KEYNOTE-062 study, pembrolizumab plus chemotherapy was not superior to chemotherapy alone in terms of OS and PFS; however, immunotherapy combined with chemotherapy has been associated with significant improvements in both parameters in multiple studies, including CheckMate 649, ATTRACTION-4, and Orient 16 (11). Cisplatin-based chemotherapy was used in the KEYNOTE-062 study, whereas oxaliplatin-based chemotherapy was used in other clinical studies. Programmed cell death protein 1 (PD-1) inhibitors combined with oxaliplatin-based chemotherapy may be a better first-line treatment option for patients with advanced gastric cancer (12). In our study, 60.9% of the matched patients in the combination therapy group received platinum-based chemotherapy, but only four patients received a cisplatin-containing regimen, with the remainder receiving oxaliplatin, and 36.2% of the patients were treated with taxane-based chemotherapy. Preclinical studies have shown that paclitaxel can activate antitumor immunity by inducing immunogenic cell death, which increases PD-L1 expression within the tumor microenvironment, stimulates natural killer cells and T lymphocytes, and affects macrophage polarization, thereby enhancing PD-1 antibody efficacy (13–21). This combination may be more effective than other chemotherapeutic agents, such as cisplatin and oxaliplatin (13).

A previous clinical study conducted by our research team showed that first-line chemotherapy with albumin-paclitaxel plus S-1 resulted in prolonged PFS in patients with HER-2-negative advanced gastric cancer, compared with first-line chemotherapy with oxaliplatin plus S-1 (22). However, the results of the survival analysis in this study showed that when combined with immunotherapy, patients who received taxanes as first-line chemotherapy had slightly longer PFS and OS than those who received platinum-based drugs, although the differences were not statistically significant. Interestingly, the results of the PFS subgroup analysis suggested that patients benefited more from the addition of immunotherapy when platinum-based chemotherapy was selected as first-line treatment. The effects of chemotherapeutic agents on

TABLE 2 Summary of adverse events.

	CT (N=138)				CT+ICI (N=138)				*p*	
	Any		≥3 Grade		Any		≥3 Grade		Any	≥3 Grade
Hematological										
Leucopenia	74	53.6	20	14.5	82	59.4	15	10.9	0.331	0.366
Neutropenia	72	52.2	34	24.6	81	58.7	23	16.7	0.276	0.102
Anemia	118	85.5	24	17.4	116	84.1	18	13.0	0.738	0.315
Thrombocytopenia	49	35.5	8	5.8	66	47.8	6	4.3	0.038	0.583
Non-hematological										
ALT/AST increase	49	35.5	1	0.7	76	55.1	2	1.4	0.001	0.583
Creatinine increase	9	6.5	0	0	8	5.8	1	0.7	0.830	1.000
Total bilirubin increase	14	10.1	1	0.7	13	9.4	0	0	0.839	0.316
Albumin decrease	36	26.1	1	0.7	48	34.8	0	0	0.116	0.316
hypothyroidism	NA	NA	NA	NA	18	13.0	0	0	NA	NA
Hyperthyroidism	NA	NA	NA	NA	4	2.9	0	0	NA	NA
Hypophysitis	NA	NA	NA	NA	2	1.4	0	0	NA	NA
Amylase/lipase evaluation	NA	NA	NA	NA	7	5.1	0	0	NA	NA
myocarditis	NA	NA	NA	NA	2	1.4	1	0.7	NA	NA
pneumonitis	NA	NA	NA	NA	2	1.4	0	0	NA	NA

CT, chemotherapy; ICI, immune checkpoint inhibitors; ALT/AST, alanine aminotransferase/aspartate aminotransferase; NA, not available.

the immune microenvironment are complex and subtle, and further studies are needed to confirm which chemotherapeutic agents are the best combinations for immunotherapy.

Previous randomized clinical trial results have revealed that patients with liver metastases, ECOG PS of 1, and non-signet ring cell carcinoma were more likely to benefit from immunotherapy, which is consistent with the results of this study (5–7). In the subgroup analysis of the RATIONAL305 study, immunotherapy combined with chemotherapy significantly prolonged OS in patients without peritoneal metastasis, while no significant survival benefit was shown in patients with peritoneal metastasis (7). Our study included 59 patients without target lesions who presented with peritoneal metastases or massive ascites, a population that was excluded from prospective randomized controlled trials but represents a substantial proportion of patients in the real world. Our results showed no difference in PFS and OS between patients with and without target lesions, and the subgroup analysis results suggested that immunotherapy could impact survival benefit to patients with peritoneal metastasis but could not impact obvious benefits to patients with massive ascites. However, owing to the small sample size of only 59 patients, the accuracy of this result needs to be verified in a larger, diverse patient population. Notably, this population, which was excluded from prospective studies, is worthy of specific attention, and further studies are needed to investigate the efficacy of immunotherapy. Previous studies have confirmed that palliative radiotherapy plays an important role in relieving bleeding, obstruction, and pain and in improving the quality of life of patients with advanced gastric cancer; however, the relationship between palliative radiotherapy and survival is unclear (23–25). A total of 59 patients with advanced gastric cancer who received palliative radiotherapy during the course of the disease were included in this study, and the corresponding results showed that palliative radiotherapy improved their OS. Due to the small sample size, further subgroup analyses were not performed to explore whether radiotherapy could increase the efficacy of immunotherapy; however, it is well known that radiotherapy may increase the benefits of immunotherapy (26, 27). Whether palliative radiotherapy combined with chemotherapy and immunotherapy can provide survival benefits for patients with advanced gastric cancer warrants further investigation.

As this was a retrospective real-world study, clinical data collection was based on the extraction of electronic medical records and patient follow-up. Data for the safety analysis mainly came from medical records and objective laboratory and imaging examinations. Data on subjective AEs, such as rash, diarrhea, and peripheral neurotoxicity were partly missing; therefore, these subjective AEs were not included in the final safety analysis. Cardiotoxicity occurred in 1.4% of the patients in our study, which were consistent with the results of the previous studies (28, 29). One patient developed cardiogenic shock with a marked elevation in cardiac troponin levels, which resolved after treatment with high-dose corticosteroids. Overall, although chemotherapy combined with immunotherapy was associated with a low incidence of grade 3 or higher AEs and was generally well tolerated, patients with serious immune-related AEs, including cardiac and renal injuries, should be closely monitored.

A major limitation of this study was the absence of PD-L1 CPS expression results in most patients. Owing to the obvious heterogeneity of CPS detection, many pathology centers, including ours, do not perform routine CPS detection, which results in a large amount of missing data (30). Although high PD-L1 expression has been confirmed to be a good independent prognostic factor for survival in previous clinical studies, CPS was not further analyzed in this study due to missing data (31, 32). In this study, four patients had deficient mismatch repair/microsatellite instability-high tumors, and only one patient achieved PFS. Therefore, the relationship between the mismatch repair status and survival was not analyzed. Despite the use of PSM, the potential biases caused by the retrospective, non-randomized design remains a limitation of this study.

5 Conclusion

The findings of this PSM study showed that first-line treatment with chemotherapy combined with ICIs significantly improved PFS in patients with HER-2 negative advanced gastric cancer; however, there was no significant improvement in OS, and the side effects were tolerable. The results of this study are consistent with those of ATTRACTION-4 and confirm the efficacy and safety of immunotherapy in combination with chemotherapy in a real-world setting.

Data availability statement

The original contributions presented in the study are included in the article/Supplementary Material. Further inquiries can be directed to the corresponding authors.

Ethics statement

The studies involving humans were approved by the ethics committee of Tongji Hospital of Huazhong University of Science and Technology. The studies were conducted in accordance with the local legislation and institutional requirements. The ethics committee/institutional review board waived the requirement of written informed consent for participation from the participants or the participants' legal guardians/next of kin because the requirement for informed consent was waived due to this study's observational retrospective design.

Author contributions

YD: Data curation, Investigation, Software, Writing – original draft. YL: Data curation, Writing – original draft. ZG: Resources, Writing – original draft. LH: Resources, Writing – original draft. LW: Data curation, Writing – original draft. WY: Data curation, Writing – original draft. PQ: Resources, Writing – original draft. FZ: Data curation, Writing – original draft. XY: Conceptualization, Methodology, Writing – review & editing. HC: Conceptualization, Methodology, Writing – review & editing. HQ: Conceptualization, Methodology, Writing – review & editing.

Acknowledgments

We acknowledge the patients and their families for participating in the study, we thank the physicians and staff at the hospitals that participated in this study.

Conflict of interest

The authors declare that the research was conducted in the absence of any commercial or financial relationships that could be construed as a potential conflict of interest.

Publisher's note

All claims expressed in this article are solely those of the authors and do not necessarily represent those of their affiliated organizations, or those of the publisher, the editors and the reviewers. Any product that may be evaluated in this article, or claim that may be made by its manufacturer, is not guaranteed or endorsed by the publisher.

Supplementary material

The Supplementary Material for this article can be found online at: https://www.frontiersin.org/articles/10.3389/fimmu.2023.1264929/full#supplementary-material

References

1. Sung H, Ferlay J, Siegel RL, Laversanne M, Soerjomataram I, Jemal A, et al. Global cancer statistics 2020: GLOBOCAN estimates of incidence and mortality worldwide for 36 cancers in 185 countries. *CA Cancer J Clin* (2021) 71(3):209–49. doi: 10.3322/caac.21660

2. Chen W, Zheng R, Baade PD, Zhang S, Zeng H, Bray F, et al. Cancer statistics in China, 2015. *CA Cancer J Clin* (2016) 66(2):115–32. doi: 10.3322/caac.21338

3. Wang FH, Zhang XT, Li YF, Tang L, Qu XJ, Ying JE, et al. The Chinese Society of Clinical Oncology (CSCO): Clinical guidelines for the diagnosis and treatment of gastric cancer, 2021. *Cancer Commun (Lond)* (2021) 41(8):747–95. doi: 10.1002/cac2.12193

4. Kang YK, Chen LT, Ryu MH, Oh DY, Oh SC, Chung HC, et al. Nivolumab plus chemotherapy versus placebo plus chemotherapy in patients with HER2–negative, untreated, unresectable advanced or recurrent gastric or gastro–oesophageal junction cancer (ATTRACTION–4): a randomised, multicentre, double–blind, placebo–controlled, phase 3 trial. *Lancet Oncol* (2022) 23(2):234–47. doi: 10.1016/S1470-2045(21)00692-6

5. Xu J–M, Jiang H, Pan Y, Gu K, Cang S, Han L, et al. Abstract CT078: First–line treatment with sintilimab (sin) vs placebo in combination with chemotherapy (chemo) in patients (pts) with unresectable gastric or gastroesophageal junction (G/GEJ) cancer: Final overall survival (OS) results from the randomized, phase III ORIENT–16 trial. *Cancer Res* (2023) 83:CT078–CT. doi: 10.1158/1538-7445

6. Janjigian YY, Shitara K, Moehler M, Garrido M, Salman P, Shen L, et al. First–line nivolumab plus chemotherapy versus chemotherapy alone for advanced gastric, gastro–oesophageal junction, and oesophageal adenocarcinoma (CheckMate 649): a randomised, open–label, phase 3 trial. *Lancet.* (2021) 398(10294):27–40. doi: 10.1016/S0140-6736(21)00797-2

7. Moehler MH, Kato K, Arkenau HT, Oh DY, Tabernero J, Cruz-Correa M, et al. Rationale 305: Phase 3 study of tislelizumab plus chemotherapy vs placebo plus chemotherapy as first–line treatment (1L) of advanced gastric or gastroesophageal junction adenocarcinoma (GC/GEJC). *J Clin Oncol* (2023) 41:286. doi: 10.1200/JCO.2023.41.4_suppl.286

8. Ajani JA, D'Amico TA, Bentrem DJ, Chao J, Cooke D, Corvera C, et al. Gastric cancer, version 2.2022, NCCN clinical practice guidelines in oncology. *J Natl Compr Canc Netw* (2022) 20(2):167–92. doi: 10.6004/jnccn.2022.0008

9. Pavel M, Oberg K, Falconi M, Krenning EP, Sundin A, Perren A, et al. Gastroenteropancreatic neuroendocrine neoplasms: ESMO Clinical Practice Guidelines for diagnosis, treatment and follow–up. *Ann Oncol* (2020) 31(7):844–60. doi: 10.1016/j.annonc.2020.03.304

10. Eisenhauer EA, Therasse P, Bogaerts J, Schwartz LH, Sargent D, Ford R, et al. New response evaluation criteria in solid tumours: revised RECIST guideline (version 1.1). *Eur J Cancer* (2009) 45(2):228–47. doi: 10.1016/j.ejca.2008.10.026

11. Shitara K, Van Cutsem E, Bang YJ, Fuchs C, Wyrwicz L, Lee KW, et al. Efficacy and safety of pembrolizumab or pembrolizumab plus chemotherapy vs chemotherapy alone for patients with first–line, advanced gastric cancer: the KEYNOTE–062 phase 3 randomized clinical trial. *JAMA Oncol* (2020) 6(10):1571–80. doi: 10.1001/jamaoncol.2020.3370

12. Guo X, Yang B, He L, Sun Y, Song Y, Qu X. PD–1 inhibitors plus oxaliplatin or cisplatin–based chemotherapy in first–line treatments for advanced gastric cancer: A network meta–analysis. *Front Immunol* (2022) 13:905651. doi: 10.3389/fimmu.2022.905651

13. Yang Q, Shi G, Chen X, Lin Y, Cheng L, Jiang Q, et al. Nanomicelle protects the immune activation effects of Paclitaxel and sensitizes tumors to anti–PD–1 Immunotherapy. *Theranostics.* (2020) 10(18):8382–99. doi: 10.7150/thno.45391

14. Chen Q, Xia R, Zheng W, Zhang L, Li P, Sun X, et al. Metronomic paclitaxel improves the efficacy of PD–1 monoclonal antibodies in breast cancer by transforming the tumor immune microenvironment. *Am J Transl Res* (2020) 12(2):519–30.

15. Kubo M, Morisaki T, Matsumoto K, Tasaki A, Yamanaka N, Nakashima H, et al. Paclitaxel probably enhances cytotoxicity of natural killer cells against breast carcinoma cells by increasing perforin production. *Cancer Immunol Immunother.* (2005) 54(5):468–76. doi: 10.1007/s00262-004-0617-6

16. Vicari AP, Luu R, Zhang N, Patel S, Makinen SR, Hanson DC, et al. Paclitaxel reduces regulatory T cell numbers and inhibitory function and enhances the anti–tumor effects of the TLR9 agonist PF–3512676 in the mouse. *Cancer Immunol Immunother.* (2009) 58(4):615–28. doi: 10.1007/s00262-008-0586-2

17. Zhang L, Dermawan K, Jin M, Liu R, Zheng H, Xu L, et al. Differential impairment of regulatory T cells rather than effector T cells by paclitaxel–based chemotherapy. *Clin Immunol* (2008) 129(2):219–29. doi: 10.1016/j.clim.2008.07.013

18. Wanderley CW, Colon DF, Luiz JPM, Oliveira FF, Viacava PR, Leite CA, et al. Paclitaxel reduces tumor growth by reprogramming tumor–associated macrophages to an M1 profile in a TLR4–dependent manner. *Cancer Res* (2018) 78(20):5891–900. doi: 10.1158/0008-5472.CAN-17-3480

19. Yamaguchi T, Fushida S, Yamamoto Y, Tsukada T, Kinoshita J, Oyama K, et al. Low–dose paclitaxel suppresses the induction of M2 macrophages in gastric cancer. *Oncol Rep* (2017) 37(6):3341–50. doi: 10.3892/or.2017.5586

20. Paz–Ares L, Luft A, Vicente D, Tafreshi A, Gumus M, Mazieres J, et al. Pembrolizumab plus chemotherapy for squamous non–small–cell lung cancer. *N Engl J Med* (2018) 379(21):2040–51. doi: 10.1056/NEJMoa1810865

21. Zhang F, Huang D, Zhao L, Li T, Zhang S, Zhang G, et al. Efficacy and safety of PD–1/PD–L1 inhibitors plus nab–paclitaxel for patients with non–small cell lung cancer who have progressed after platinum–based chemotherapy. *Ther Adv Med Oncol* (2020) 12:1758835920936882. doi: 10.1177/1758835920936882

22. Dai YH, Yu XJ, Xu HT, Zhuang L, Zhang MS, Zou YM, et al. Nab–paclitaxel plus S–1 versus oxaliplatin plus S–1 as first–line treatment in advanced gastric cancer: results of a multicenter, randomized, phase III trial (GAPSO study). *Ther Adv Med Oncol* (2022) 14:17588359221118020. doi: 10.1177/17588359221118020

23. Tey J, Zheng H, Soon YY, Leong CN, Koh WY, Lim K, et al. Palliative radiotherapy in symptomatic locally advanced gastric cancer: A phase II trial. *Cancer Med* (2019) 8(4):1447–58. doi: 10.1002/cam4.2021

24. Yu J, Jung J, Park SR, Ryu MH, Park JH, Kim JH, et al. Role of palliative radiotherapy in bleeding control in patients with unresectable advanced gastric cancer. *BMC Cancer.* (2021) 21(1):413. doi: 10.1186/s12885-021-08145-4

25. Merchant SJ, Kong W, Mahmud A, Booth CM, Hanna TP. Palliative radiotherapy for esophageal and gastric cancer: population–based patterns of utilization and outcomes in ontario, Canada. *J Palliat Care* (2023) 38(2):157–66. doi: 10.1177/08258597211072946

26. Yu WD, Sun G, Li J, Xu J, Wang X. Mechanisms and therapeutic potentials of cancer immunotherapy in combination with radiotherapy and/or chemotherapy. *Cancer Lett* (2019) 452:66–70. doi: 10.1016/j.canlet.2019.02.048

27. Arina A, Gutiontov SI, Weichselbaum RR. Radiotherapy and immunotherapy for cancer: from "Systemic" to "Multisite". *Clin Cancer Res* (2020) 26(12):2777–82. doi: 10.1158/1078-0432.CCR-19-2034

28. Mahmood SS, Fradley MG, Cohen JV, Nohria A, Reynolds KL, Heinzerling LM, et al. Myocarditis in patients treated with immune checkpoint inhibitors. *J Am Coll Cardiol* (2018) 71(16):1755–64. doi: 10.1016/j.jacc.2018.02.037

29. Salem JE, Manouchehri A, Moey M, Lebrun–Vignes B, Bastarache L, Pariente A, et al. Cardiovascular toxicities associated with immune checkpoint inhibitors: an

observational, retrospective, pharmacovigilance study. *Lancet Oncol* (2018) 19 (12):1579–89. doi: 10.1016/S1470-2045(18)30608-9

30. Yeong J, Lum HYJ, Teo CB, Tan BKJ, Chan YH, Tay RYK, et al. Choice of PD–L1 immunohistochemistry assay influences clinical eligibility for gastric cancer immunotherapy. *Gastric Cancer.* (2022) 25(4):741–50. doi: 10.1007/s10120-022-01301-0

31. Yoon HH, Jin Z, Kour O, Kankeu Fonkoua LA, Shitara K, Gibson MK, et al. Association of PD–L1 expression and other variables with benefit from immune checkpoint inhibition in advanced gastroesophageal cancer: systematic review and meta–analysis of 17 phase 3 randomized clinical trials. *JAMA Oncol* (2022) 8(10):1456–65. doi: 10.1001/jamaoncol.2022.3707

32. Zhao JJ, Yap DWT, Chan YH, Tan BKJ, Teo CB, Syn NL, et al. Low programmed death–ligand 1–expressing subgroup outcomes of first–line immune checkpoint inhibitors in gastric or esophageal adenocarcinoma. *J Clin Oncol* (2022) 40(4):392–402. doi: 10.1200/JCO.21.01862

frontiers | Frontiers in Immunology

TYPE Original Research
PUBLISHED 29 September 2023
DOI 10.3389/fimmu.2023.1249511

OPEN ACCESS

EDITED BY
Wei Guo,
Shandong University, China

REVIEWED BY
Qiang Wen,
Shandong Provincial Hospital, China
Gilles Defraene,
KU Leuven, Belgium

*CORRESPONDENCE
Jia Wu
jwu11@mdanderson.org

†These authors share senior authorship

RECEIVED 28 June 2023
ACCEPTED 12 September 2023
PUBLISHED 29 September 2023

CITATION
Aminu M, Daver N, Godoy MCB, Shroff G, Wu C, Torre-Sada LF, Goizueta A, Shannon VR, Faiz SA, Altan M, Garcia-Manero G, Kantarjian H, Ravandi-Kashani F, Kadia T, Konopleva M, DiNardo C, Pierce S, Naing A, Kim ST, Kontoyiannis DP, Khawaja F, Chung C, Wu J and Sheshadri A (2023) Heterogenous lung inflammation CT patterns distinguish pneumonia and immune checkpoint inhibitor pneumonitis and complement blood biomarkers in acute myeloid leukemia: proof of concept. *Front. Immunol.* 14:1249511. doi: 10.3389/fimmu.2023.1249511

Heterogenous lung inflammation CT patterns distinguish pneumonia and immune checkpoint inhibitor pneumonitis and complement blood biomarkers in acute myeloid leukemia: proof of concept

Muhammad Aminu[1], Naval Daver[2], Myrna C. B. Godoy[3], Girish Shroff[3], Carol Wu[3], Luis F. Torre-Sada[4], Alberto Goizueta[4], Vickie R. Shannon[4], Saadia A. Faiz[4], Mehmet Altan[5], Guillermo Garcia-Manero[2], Hagop Kantarjian[2], Farhad Ravandi-Kashani[2], Tapan Kadia[2], Marina Konopleva[2], Courtney DiNardo[2], Sherry Pierce[2], Aung Naing[6], Sang T. Kim[7], Dimitrios P. Kontoyiannis[8], Fareed Khawaja[8], Caroline Chung[9], Jia Wu[1*†] and Ajay Sheshadri[4†]

[1]Departments of Imaging Physics, University of Texas MD Anderson Cancer Center, Houston, TX, United States, [2]Departments of Leukemia, University of Texas MD Anderson Cancer Center, Houston, TX, United States, [3]Departments of Diagnostic Imaging, University of Texas MD Anderson Cancer Center, Houston, TX, United States, [4]Departments of Pulmonary Medicine, University of Texas MD Anderson Cancer Center, Houston, TX, United States, [5]Departments of Thoracic/Head and Neck Medical Oncology, University of Texas MD Anderson Cancer Center, Houston, TX, United States, [6]Departments of Investigational Cancer Therapeutics, University of Texas MD Anderson Cancer Center, Houston, TX, United States, [7]Departments of Rheumatology and Infectious Diseases, University of Texas MD Anderson Cancer Center, Houston, TX, United States, [8]Departments of Infectious Diseases, University of Texas MD Anderson Cancer Center, Houston, TX, United States, [9]Departments of Radiation Oncology, University of Texas MD Anderson Cancer Center, Houston, TX, United States

Background: Immune checkpoint inhibitors (ICI) may cause pneumonitis, resulting in potentially fatal lung inflammation. However, distinguishing pneumonitis from pneumonia is time-consuming and challenging. To fill this gap, we build an image-based tool, and further evaluate it clinically alongside relevant blood biomarkers.

Materials and methods: We studied CT images from 97 patients with pneumonia and 29 patients with pneumonitis from acute myeloid leukemia treated with ICIs. We developed a CT-derived signature using a habitat imaging algorithm, whereby infected lungs are segregated into clusters ("habitats"). We validated the model and compared it with a clinical-blood model to determine whether imaging can add diagnostic value.

Results: Habitat imaging revealed intrinsic lung inflammation patterns by identifying 5 distinct subregions, correlating to lung parenchyma, consolidation, heterogenous ground-glass opacity (GGO), and GGO-consolidation transition. Consequently, our proposed habitat model (accuracy of 79%, sensitivity of 48%, and specificity of 88%) outperformed the clinical-blood model (accuracy of 68%, sensitivity of 14%, and specificity of 85%) for classifying pneumonia versus pneumonitis. Integrating imaging and blood achieved the optimal performance (accuracy of 81%, sensitivity of 52% and specificity of 90%). Using this imaging-blood composite model, the post-test probability for detecting pneumonitis increased from 23% to 61%, significantly (p = 1.5E − 9) higher than the clinical and blood model (post-test probability of 22%).

Conclusion: Habitat imaging represents a step forward in the image-based detection of pneumonia and pneumonitis, which can complement known blood biomarkers. Further work is needed to validate and fine tune this imaging-blood composite model and further improve its sensitivity to detect pneumonitis.

KEYWORDS

habitat analysis, immune checkpoint inhibitor, acute myeloid leukemia, non-small cell lung cancer, pneumonitis

Introduction

Immune checkpoint inhibitors (ICIs) have been a transformative force in oncology and have become a key part of the therapeutic arsenal for numerous cancers (1). Acute myeloid leukemia (AML), a highly lethal cancer (2) which often requires allogeneic hematopoietic transplantation (allo-HCT) (3) to achieve a durable remission, may sometimes respond to ICIs given in combination with hypomethylating agents (4). However, the use of ICIs to treat AML is associated with high rates of pneumonitis, which significantly increases mortality (5).

A major barrier to diagnosing pneumonitis is the difficulty in distinguishing pneumonitis from other pulmonary conditions, especially pneumonia (6). Bronchoalveolar lavage biomarkers show clonal expensive of Th17.1 cells, but do not necessarily distinguish between pneumonia and pneumonitis (7). Culture-based identification of pathogens can identify up to 60% of infections (8), but these results may require up to 48 hours and are more useful for ruling infection in, and not out. Metagenomic approaches may increase the yield for the detection of bacterial organisms in immunocompromised hosts (9), but the diagnostic yield remains suboptimal for certain infections, and distinguishing colonization from true infection is challenging. The prompt diagnosis of pneumonitis and pneumonia is necessary to ensure the appropriate administration of corticosteroids, both to promptly treat pneumonitis and to be withheld in cases of infection.

Radiomic approaches may allow for the prompt identification of pulmonary disease, as has been shown in interstitial lung diseases (10). However, these approaches have not been tested to distinguish infectious pneumonia from ICI pneumonitis. The classical radiomics approach profiles the infected lung region as a whole entity and may fall short when characterizing phenotypically heterogeneous subareas of the lung that are infected or inflamed. Habitat imaging is an emerging technology that aims to address this challenge by explicitly dividing the region-of-interest (ROI) into coherent subregions termed as habitats (11–13).

Pilot studies from our group and others have demonstrated the added value of habitat imaging analysis in profiling intratumor heterogeneity and predicting treatment response in several cancer types (13–16). In this study, we tested whether our habitat analyses could accurately distinguish pneumonia and pneumonitis in a retrospective cohort of AML patients who received ICIs therapies between 2016-2018 (5).

Methods

Participants

We reviewed imaging from a group of 258 patients with AML who were started on ICI therapies (ipilimumab, n=40; nivolumab, n=175; ipilimumab and nivolumab, n=43). between 2016 and 2018. 126 patients with confirmed episodes of pneumonia (n=97) or pneumonitis (n=29) with CT scans available for analysis were included (Supplementary Figure 1). All cases were reviewed by a multidisciplinary adjudication committee, who reviewed the clinical history, including the time course of symptoms, representative laboratory, imaging, and microbiological data, and response to antimicrobial or anti-inflammatory therapies (Table 1). Pneumonia was diagnosed in episodes with 1) consistent

10.3389/fimmu.2023.1249511

TABLE 1 Characteristics of the study cohort.

Variable	Pneumonia (n=97)	Pneumonitis (n=29)
Median age at enrollment (years)	64.01	69.14
Female sex, n (%)	37(38%)	17(58.6%)
Race, n (%)		
White/Caucasian	84(86.6)	25(86.2%)
Non-white	13(13.4%)	4(13.8%)
AML Diagnosis, n (%)		
De novo AML	67(69.1%)	21(72.4%)
Secondary/therapy-related AML	30(30.9%)	8(27.6%)
Prior SCT	17(17.5%)	1(3.4%)
ECOG, n (%)		
0	8(8.25%)	7(24.1%)
1	82(84.54%)	21(72.4%)
2	7(7.21%)	1(3.4%)
Symptoms at baseline, n (%)		
Cough	22(22.7%)	6(20.7%)
Fever	18(18.6%)	7(24.1%)
Shortness of breath	22(22.7%)	8(27.6%)
Symptoms at syndrome, n (%)		
Cough	72(74.2%)	19(65.5%)
Fever	77(79.4%)	21(72.4%)
Shortness of breath	63(64.9%)	22(75.9%)
Median cell counts at baseline		
Bone marrow blasts (%)	20	15
Total WBC (10^3 cells/μL)	2.5	2.3
NC (cells/μL) %	23	19
LC (cells/μL) %	40	40.1
Platelets (10^3 cells/μL)	34	29
Median cell counts at syndrome		
Total WBC (10^3 cells/μL)	2.4	1.4
NC (cells/μL) %	22	30
LC (cells/μL) %	25	25
Platelets (10^3 cells/μL)	22	14
Smoking status, n (%)		
Never	46(47.4%)	21(72.4%)
Former	48(49.5%)	8(27.6%)
Current	3(3.1%)	
Pneumonia within 30 days of ICI initiation, n (%)	21(21.7%)	6(20.7%)
Viral infection within 30 days of ICI initiation, n (%)	4(4.1%)	1(3.4%)

(Continued)

TABLE 1 Continued

Variable	Pneumonia (n=97)	Pneumonitis (n=29)
Prior lung disease, n (%)		
COPD	11(11.3%)	1(3.4%)
Asthma	5(5.2%)	1(3.4%)
Prior autoimmune disease, n (%)	5(5.2%)	2(6.9%)
Chest radiation prior to ICI, n (%)	5(5.2%)	2(6.9%)

ICI, immune checkpoint inhibitor; AML, acute myeloid leukemia; ECOG, Eastern Cooperative Oncology Group; WBC, white blood cell; NC, neutrophil count; LC, lymphocyte count; COPD, chronic obstructive pulmonary disease; ILD, interstitial lung disease; SCT, stem cell transplantation.

symptoms (e.g. fevers, cough) and consistent imaging (for example, lobar consolidation, nodular opacities, centrilobular or tree-in-bud opacities, cavitary opacities, halo sign) and 2) had a clear response to antibiotics but not corticosteroids or had microbiological confirmation from a lower respiratory tract specimen of an organism known to cause pneumonia (7). Pneumonitis was diagnosed in episodes with 1) consistent symptoms (e.g. cough, shortness of breath) and consistent imaging and 2) a clear response to corticosteroids but not antibiotics or had histopathological confirmation of pneumonitis. Based on CT appearance, pneumonitis cases were classified into the following patterns (17): nonspecific interstitial pneumonitis (NSIP), organizing pneumonia (OP), hypersensitivity pneumonitis (HP), acute interstitial pneumonia (AIP)-acute respiratory distress syndrome (ARDS), or indeterminate/mixed (i.e., nonspecific patchy ground-glass or consolidative opacities or a mixture of patterns without clear dominant pattern). Pneumonitis was graded according to the Common Terminology Criteria for Adverse Events (CTCAE) 5.0 (18). Because symptoms of pneumonitis and pneumonia may often be similar, the multidisciplinary committee weighted imaging, clinical course, and response to therapies heavily in their final diagnoses. The MD Anderson Institutional Review Board approved the study (PA18-0802).

Overall design

Our overall approach is summarized in Figure 1A. In brief, we performed patient and imaging curation, then trained and tested a CT-derived signature using habitat imaging to determine whether a patient was more likely to have pneumonia or pneumonitis. In parallel, we derived a clinical-blood benchmark model by selecting informative clinical and blood metrics to fit into a classification model. Ultimately, we integrated the two approaches (imaging and benchmark features) to evaluate the prediction performance.

Image acquisition and preprocessing

The CT scans of the 126 patients enrolled in this study were obtained using both Siemens and GE medical systems CT scanners at MD Anderson Cancer Center at the time of the event. CT scans had a slice thickness of 2.5mm and an in-plane spatial resolution of 0.98 to 1.2 mm. A deep learning-based segmentation model (19) was used to extract the left and right lung parenchyma, followed by a morphological dilation and erosion to smoothen the boundaries of the extracted lung regions. An in-house radiologist reviewed and manually corrected the lung ROI segmentations.

Habitat imaging analysis

The architecture of the habitat imaging technique (16) is a unified approach containing several key steps as illustrated in Figure 1B. First, a contrast-enhancing method was applied to filter both the lung and mediastinum window images from the original input images. The extracted lung and mediastinum images were then further processed using a local entropy filter to generate filtered images that capture subtle variations in the texture of the images under different window settings. An image fusion approach was then utilized to combine (fuse) the lung, mediastinum, and their corresponding filtered images to form the final composite image.

Second, the habitat detection has a patient- and population-level clustering blocks. For the patient-level clustering step, the simple linear iterative clustering (SLIC) algorithm (20) is used to oversegment the individual patients' composite images of lung ROI into a large number of superpixels. Then, the extracted superpixels across the whole patient are aggregated to identify the similar ones inside one patient and across different patients. Specifically, the superpixels from the patient-level clustering step are considered as individual samples. In particular, we characterized individual superpixels by extracting ten features separately on four image channels (CT image normalized by lung window or mediastinal window, as well as two corresponding entropy maps for local texture). Ten different features include skewness, kurtosis, mean, median, 1 quantile, 3 quantile, interquartile range, standard deviation, variance, and energy. These features characterized different aspects of the lung, including the intensity, the symmetricity of intensity and texture, the intensity uniformity, the texture of CT images, and the texture of entropy maps. The superpixels were subsequently clustered using the hierarchical clustering algorithm to identify subregions with similar imaging patterns. The optimal number of subregions was determined using both the gap criterion and hierarchical structure of the clusters dendrogram.

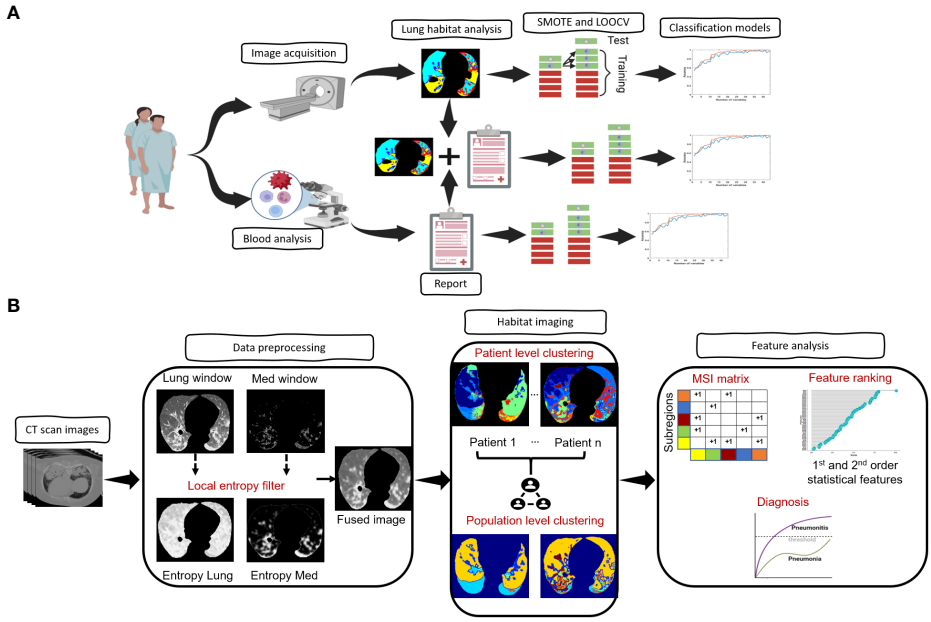

FIGURE 1
Architecture of the proposed framework. **(A)**, Overview of the overall proposed approach starting from image acquisition, habitat analysis and diagnostic model prediction. **(B)**, Overview of the steps involved in the habitat analysis.

Feature extraction and machine learning model construction

After the lesion/subregion segmentation, forty-four multiregional spatial interaction (MSI) features were measured from the habitat maps to quantify overall lung parenchyma. In addition, we quantified the symmetric difference (Δ_{Sym}) between left and right lungs by:

$$\Delta_{Sym}(\boldsymbol{L},\boldsymbol{R}) = |\boldsymbol{MSI_L} - \boldsymbol{MSI_W}| \times |\boldsymbol{MSI_R} - \boldsymbol{MSI_W}| \quad (1)$$

where MSI_W, MSI_L, and MSI_R denotes the MSI features computed on the whole, left and right lungs, respectively. One strength of the MSI features is their clear interpretations. These features are designed to quantify the spatial heterogeneity of infected lung patterns. Specifically, the MSI features captures information such as the absolute burden and relative percentage of individual habitat as well as their interactions. More detailed explanation regarding the extracted MSI features is presented in Table 2.

After feature extraction, the correlation among the extracted features was explored. Also, the univariate Chi-square test statistics approach was applied to examine feature association with infection types. Each feature was tested independently, and the output of the univariate Chi-square model is the probability (p-value) that the patient had been diagnosed with either pneumonia or pneumonitis for each feature. The computed p-values of all the features are then used to rank the individual features by computing feature importance (score) as:

$$\boldsymbol{score} = -\log(\boldsymbol{p})$$

where p is the corresponding p-value for each feature, and higher score denotes greater importance. Next, we iteratively increase the number of selected features based on their importance in order to identify the optimal diagnostic model. Specifically, the top-ranked features were used to build an ensemble model of 100 boosted classification trees. To avoid biased classification to the pneumonitis class due to data imbalance (i.e., significantly larger number of samples in the pneumonia class), we employed synthetic minority oversampling technique (SMOTE) nested with leave-one-out cross validation (LOOCV) approach together to validate model performance. To avoid information leakage, we first left out one sample as the test set before applying SMOTE on the training set to train a prediction model. This process is repeated n -times (n equals to total number of samples) until every data sample is left out as a test sample.

In parallel, we also built a benchmark model using clinical and blood-based measures. For clinical variables, we included cough, fever, shortness of breath at both baseline and at time of syndrome together with age and sex. For blood-based variables, we used five blood-based measurements including absolute white blood cells (WBC) count, absolute neutrophils count (ANC), absolute lymphocyte count (ALC) and platelet count at both baseline and time of syndrome together with bone marrow blast cells count at baseline. Using similar strategy as our earlier work (5), we considered the log transformation of WBC and platelets at both baseline and at time of syndrome. Given the clinical and blood measures, we adopted a similar SMOTE and LOOCV machine learning strategy to build the benchmark model. The diagnostic performance of the benchmark model was compared to the habitat

10.3389/fimmu.2023.1249511

TABLE 2 Multiregional spatial interaction features interpretation.

Feature name	Feature description
MSI 1 – MSI 4	2^{nd} order statistics features (contrast, correlation, Homogeneity and energy)
MSI 5 – MSI 9	absolute subregions volume (SR1 – SR5)
MSI 10 – MSI 14	interaction (absolute) between subregions and border
MSI 15 – MSI 18	interaction (absolute) between SR1 and the remaining subregions, i.e., MSI 15 = SR1 ∩ SR2, MSI 16 = SR1 ∩ SR3, …, MSI 18 = SR1 ∩ SR5.
MSI 19 – MSI 21	interaction (absolute) between SR2 and SR3, SR4 and SR5, i.e., MSI 19 = SR2 ∩ SR3, MSI 20 = SR2 ∩ SR4, MSI 21 = SR2 ∩ SR5.
MSI 22 – MSI 23	interaction (absolute) between SR3 and SR4, SR5, i.e., MSI 22 = SR3 ∩ SR4, MSI 23 = SR3 ∩ SR5.
MSI 24	interaction (absolute) between SR4 and SR5, i.e., MSI 24 = SR4 ∩ SR5.
MSI 25 – MSI 29	normalized percentage of subregions volume (SR1 – SR5)
MSI 30 – MSI 34	normalized interaction (percentage) between subregions and border
MSI 35 – MSI 38	normalized interaction (percentage) between SR1 and the remaining subregions, i.e., MSI 35 = SR1 ∩ SR2, MSI 36 = SR1 ∩ SR3, …, MSI 38 = SR1 ∩ SR5.
MSI 39 – MSI 41	normalized interaction (percentage) between SR2 and SR3, SR4 and SR5, i.e., MSI 39 = SR2 ∩ SR3, MSI 40 = SR2 ∩ SR4, MSI 41 = SR2 ∩ SR5.
MSI 42 – MSI 43	normalized interaction (percentage) between SR3 and SR4, SR5, i.e., MSI 42 = SR3 ∩ SR4, MSI 43 = SR3 ∩ SR5.
MSI 44	normalized interaction (percentage) between SR4 and SR5, i.e., MSI 44 = SR4 ∩ SR5.
MSI 45 – MSI 48	symmetric difference (left vs right lung) of the 2^{nd} order statistics features
MSI 49 – MSI 53	symmetric difference (left vs right lung) of absolute subregions volume (SR1 – SR5)
MSI 54 – MSI 58	symmetric difference (left vs right lung) of the interaction (absolute) between tumor subregions and border
MSI 59 – MSI 62	symmetric difference (left vs right lung) of the interaction (absolute) between SR1 and the remaining subregions, i.e., MSI 59 = $\lvert MSI_L\ 15 - MSI_W\ 15\rvert \times \lvert MSI_R\ 15 - MSI_W\ 15\rvert$, …, MSI 62 = $\lvert MSI_L\ 18 - MSI_W\ 18\rvert \times \lvert MSI_R\ 18 - MSI_W\ 18\rvert$.
MSI 63 – MSI 65	symmetric difference (left vs right lung) of the interaction (absolute) between SR2 and SR3, SR4 and SR5, i.e., MSI 63 = $\lvert MSI_L\ 19 - MSI_W\ 19\rvert \times \lvert MSI_R\ 19 - MSI_W\ 19\rvert$, …, MSI 65 = $\lvert MSI_L\ 21 - MSI_W\ 21\rvert \times \lvert MSI_R\ 21 - MSI_W\ 21\rvert$.
MSI 66 – MSI 67	symmetric difference (left vs right lung) of the interaction (absolute) between SR3 and SR4, SR5, i.e., MSI 66 = $\lvert MSI_L\ 22 - MSI_W\ 22\rvert \times \lvert MSI_R\ 22 - MSI_W\ 22\rvert$, MSI 67 = $\lvert MSI_L\ 23 - MSI_W\ 23\rvert \times \lvert MSI_R\ 23 - MSI_W\ 23\rvert$.
MSI 68	symmetric difference (left vs right lung) of the interaction (absolute) between SR4 and SR5, i.e., MSI 68 = $\lvert MSI_L\ 24 - MSI_W\ 24\rvert \times \lvert MSI_R\ 24 - MSI_W\ 24\rvert$
MSI 69 – MSI 73	symmetric difference (left vs right lung) of the percentage of subregions volume (SR1 – SR5)
MSI 74 – MSI 78	symmetric difference (left vs right lung) of the normalized interaction (percentage) between subregions and border
MSI 79 – MSI 82	symmetric difference (left vs right lung) of the normalized interaction (percentage) between SR1 and the remaining subregions, i.e., MSI 79 = $\lvert MSI_L\ 35 - MSI_W\ 35\rvert \times \lvert MSI_R\ 35 - MSI_W\ 35\rvert$, MSI 82 = $\lvert MSI_L\ 38 - MSI_W\ 38\rvert \times \lvert MSI_R\ 38 - MSI_W\ 38\rvert$.
MSI 83 – MSI 85	symmetric difference (left vs right lung) of the normalized interaction (percentage) between SR2 and SR3, SR4 and SR5, i.e., MSI 83 = $\lvert MSI_L\ 39 - MSI_W\ 39\rvert \times \lvert MSI_R\ 39 - MSI_W\ 39\rvert$, MSI 85 = $\lvert MSI_L\ 41 - MSI_W\ 41\rvert \times \lvert MSI_R\ 41 - MSI_W\ 41\rvert$.
MSI 86 – MSI 87	symmetric difference (left vs right lung) of the normalized interaction (percentage) between SR3 and SR4, SR5, i.e., MSI 86 = $\lvert MSI_L\ 42 - MSI_W\ 42\rvert \times \lvert MSI_R\ 42 - MSI_W\ 42\rvert$, MSI 87 = $\lvert MSI_L\ 43 - MSI_W\ 43\rvert \times \lvert MSI_R\ 43 - MSI_W\ 43\rvert$.
MSI 88	symmetric difference (left vs right lung) of normalized interaction (percentage) between SR4 and SR5, i.e., MSI 88 = $\lvert MSI_L\ 44 - MSI_W\ 44\rvert \times \lvert MSI_R\ 44 - MSI_W\ 44\rvert$.

MSI_L, multi regional spatial interaction feature extracted from the left lung; MSI_R, multi regional spatial interaction feature extracted from the right lung; MSI_W, multi regional spatial interaction feature extracted from the whole lung.

imaging model. Furthermore, we evaluated the performance when integrating clinical-blood benchmark and habitat in a composite model. For comparison purposes, we also extracted the classical radiomics features from the whole lung regions and built a prediction model.

Statistical analysis

The ability to separate pneumonia (coded as 0) from pneumonitis (coded as 1) was assessed by the accuracy, specificity, and sensitivity in the leave-one-out cross-validation. For this work, sensitivity means the true positive rate of pneumonitis, while specificity represents true negative rate of pneumonitis. To mitigate the imbalance in the distribution of pneumonia and pneumonitis, Synthetic Minority Oversampling Technique (SMOTE) algorithm was applied. Furthermore, we applied Bayesian theorem to compute the pre-test and post-test probability (21), which referred to the probability of detecting pneumonitis before a diagnostic model was performed (pre-test probability) and after a model is performed (post-test probability). The feature correlation analysis was done using the Pearson's correlation test with the R software. The Chi-square test statistics was used to evaluate the predictive value of individual features and the t-test statistics was used to compare the prediction performance of the different models.

Results

Study participants

Table 1 shows the characteristics of the overall study cohort (n=126) who developed pneumonia or pneumonitis. Most patients had *de novo* AML, but ICI was usually given after frontline therapy was initiated. 86 patients received nivolumab without ipilimumab, either alone (n=11), or with azacitidine (n=58) or idarubicin (n=17). 15 patients received ipilimumab without nivolumab, either alone (n=9) or with azacitidine (n=6). 25 patients received nivolumab and ipilimumab together, with (n = 17) or without (n=8) azacitidine. We identified 97 distinct patients of pneumonia and 29 distinct patients of pneumonitis in which a CT was available for analysis. No patients had more than one pneumonia or pneumonitis. All cases of pneumonia and pneumonitis were independently reviewed by blinded expert thoracic radiologists who reviewed feature characteristics in the current study. Representative cases of pneumonia and pneumonitis are shown in Supplementary Figure 2. Supplementary Table 1 shows a list of organisms isolated in cases of microbiologically-proven pneumonia. Of the patients with pneumonitis, 19 had an indeterminate/mixed pattern, 7 had an organizing pneumonia pattern, and 3 had an acute interstitial pneumonia (AIP)-acute respiratory distress syndrome (ARDS) pattern. The median time to pneumonitis was 109 days after ICI initiation (range 1-484 days).

Habitat imaging reveals intrinsic infection patterns of lung parenchyma

We applied our proposed habitat imaging method (Figure 1B) and determined the optimal number of intra-lung subregions. As shown in Figure 2A, there are five distinct clusters (i.e, habitats) according to hierarchical structure of the dendrogram. We then investigated the imaging parameters that underline and differentiate these habitats. Figure 2A shows the detailed distributions of the representative features from five types of imaging parameters (intensity uniformity, Intensity, texture of lung window, texture of entropy map, symmetricity of intensity and texture) in each of these habitats. The detailed phenotypical patterns of CT imaging associated with each habitat were summarized in Figure 2B. We observed that subregions 1 corresponds to the uninfected lung parenchyma, subregion 3 corresponds to ground glass opacity (GGO) with elevated texture heterogeneity and low CT number, subregion 4 corresponds to the consolidation, subregions 2 and 5 correspond to the transition zone to GGO at different degrees. The detailed partitioning results of entire lung region after habitat analysis were presented in Figure 3 for four selected pneumonia and pneumonitis patients, where detailed habitats were consistently defined to quantify the infection patterns.

Habitat model outperforms benchmark model of clinical and blood metrics

Given the clinical variables and blood metrics both at baseline and at time of infection (their correlation in Supplementary Figure 3A), we built a benchmark model with the feature importance presented in Figure 4A and model performance in Figure 4B. The top ranked features include sex; cough at time of event; baseline platelets; and ANC (at both baseline and at time of event). This benchmark model had an accuracy of 68%, sensitivity (i.e., true positive of pneumonitis) of 14%, and specificity (true negative of pneumonitis) of 85%. Then, based on the habitat map for individual patients, we extracted MSI features to characterize the overall infection patterns as well as their symmetricity between left and right lungs, which resulted in a total of 88 features. The correlation among these habitat features was presented in Supplementary Figures 3B, C. Next, we built a classifier to differentiate pneumonia from pneumonitis using LOOCV, and the feature importance was presented in Figure 4C. For the prediction model, interestingly the top ranked habitat features were MSI30 which measures the infected area on the lung surface and MSI37, which relates to the interaction between habitat 1 (normal lung parenchyma) and habitat 4 (consolidation). Using this approach, we found that pneumonia had elevated asymmetric interaction, suggesting more asymmetry in the CT pattern between left and right lung. The habitat model achieved an accuracy of 79%, sensitivity of 48%, and specificity of 88%, based on the cross-validated confusion matrix in Figure 4D. For comparison purposes, we also built a conventional radiomics model (Supplementary Figure 4), which we

A

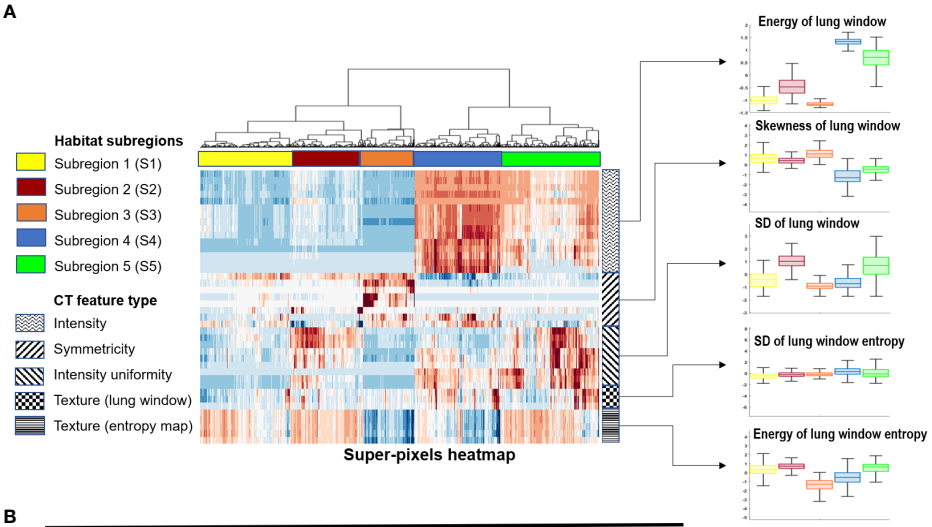

B

	Intensity	Intensity and texture symmetricity	Intensity uniformity	Texture (Lung window)	Texture (Entropy map)
S1	Low	Positive	Uniform	Homogeneous	Mixed
S2	Intermediate	Positive	Non-uniform	Mixed	Heterogeneous
S3	Low	Positive	Uniform	Mixed	Homogeneous
S4	High	Negative	uniform	Heterogeneous	Mixed
S5	High	Negative	Non-uniform	Heterogeneous	Heterogeneous

FIGURE 2
Habitat subregions identification. **(A)**, Heatmap of the five identified subregions together with distribution plot (boxplot) of five representative features from the feature types grouped by habitat subregions. **(B)**, Characteristics of the five habitat subregions in relation to the CT feature types.

found to have a significantly lower performance (accuracy, 60%; sensitivity, 17%; specificity, 72%) to the habitat model ($p = 5E - 19$).

Imaging-blood composite model achieves the optimal performance

Next, we integrated the prediction results from both the habitat model and the benchmark model (Figure 5A). Based on the cascading model with clinical and blood model in the first layer and habitat model in the second, we simulated the predicted infection type stratification as shown in Figure 5B. If we set up the rule as following: we will make a diagnosis if both models agree and will label the cases as ambiguous cases if both models disagree. This has achieved 87.1% accuracy in predicting pneumonia, a greater than 10% increase than clinical model. Of note, 0% accuracy in predicting pneumonitis, indicating imaging and blood are capturing different and non-overlapping pneumonitis cases. For

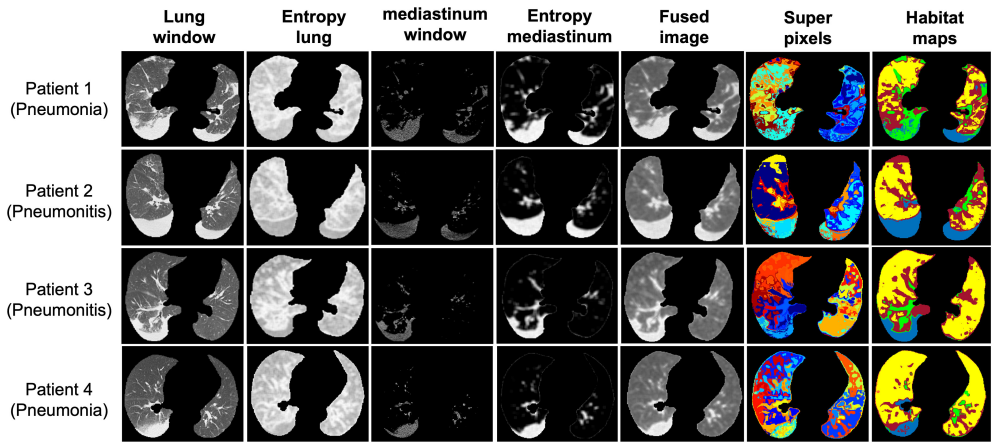

FIGURE 3
Representative habitat maps of four subjects from both the pneumonia and pneumonitis categories.

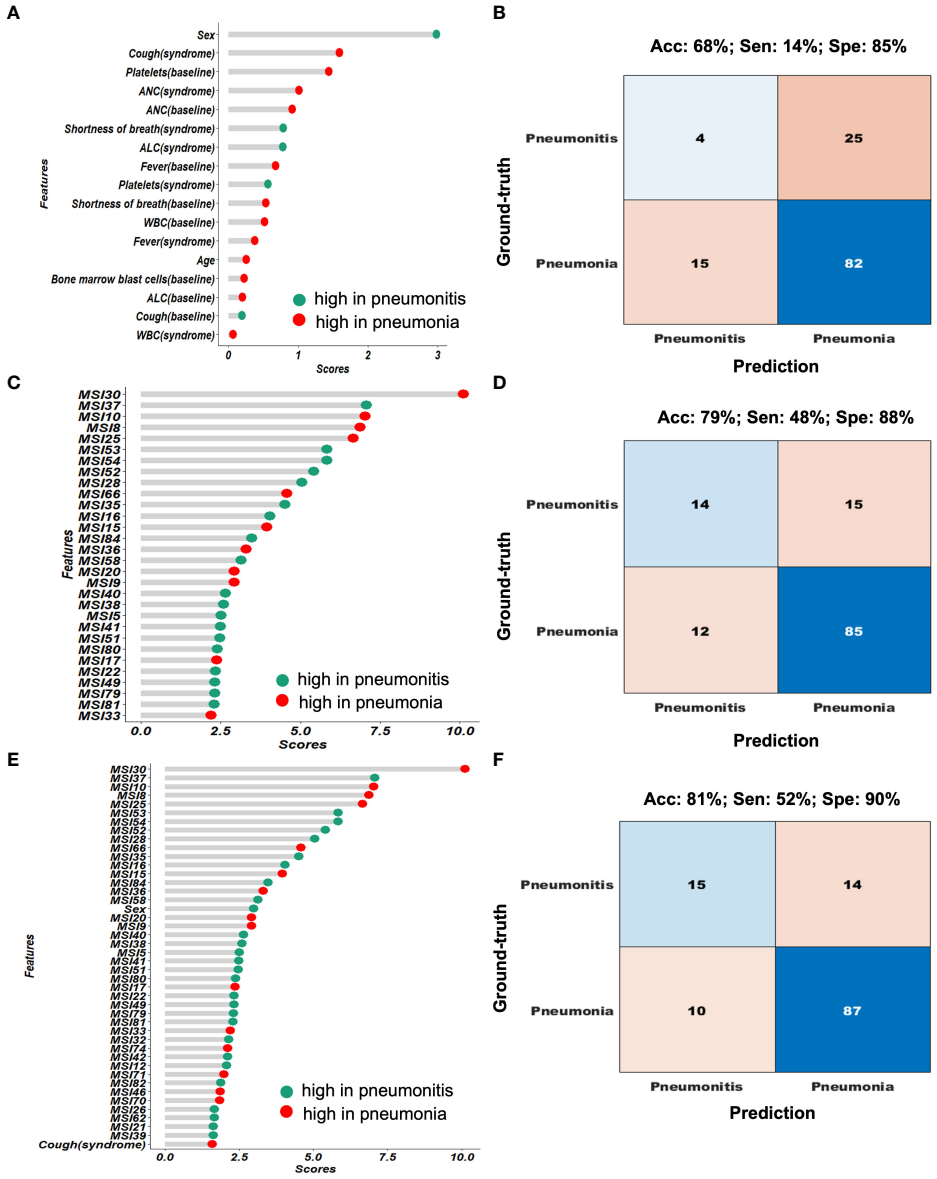

FIGURE 4
Performance comparison of the different diagnostic models. **(A, B)** shows the feature importance and confusion matrix for the clinical-blood (benchmark model). **(C, D)** shows the feature importance and confusion matrix for the habitat-based model. **(E, F)** shows the feature importance and confusion matrix for the composite (clinical-blood plus habitat models).

these 37 conflicting cases that imaging and blood model disagreed, imaging model had an accuracy of 59% and the blood model had an accuracy of 41%.

In addition, we mixed the habitat features with clinical and blood metrics together to re-fit a prediction model, and the ranked feature importance table was shown in Figure 4E. In general, the habitat features were consistently more important than the clinical and blood measures. The composite model achieved the optimal performance with an overall accuracy of 81%, sensitivity of 52% and specificity of 90% (Figure 4F).

Further, we compared the post-test probability of detecting pneumonitis based on different models when the various models diagnosed pneumonitis (Table 3). The pre-test probability (i.e., prevalence) of pneumonitis was observed to be 23%. With the benchmark prediction model using clinical and blood metrics, the post-test probability degraded to 22% if the model diagnosed pneumonitis. When using our habitat model, the post-test probability increased to 55% if the model diagnosed pneumonitis. We observed synergistic effects when combining habitat imaging with clinical and blood metrics into a composite model, which achieved the best post-test probability of 61% if the model diagnosed pneumonitis, more than a 2-fold increase from pre-test probability. By contrast, the classical radiomics model had the worst performance with post-test probability of 15%.

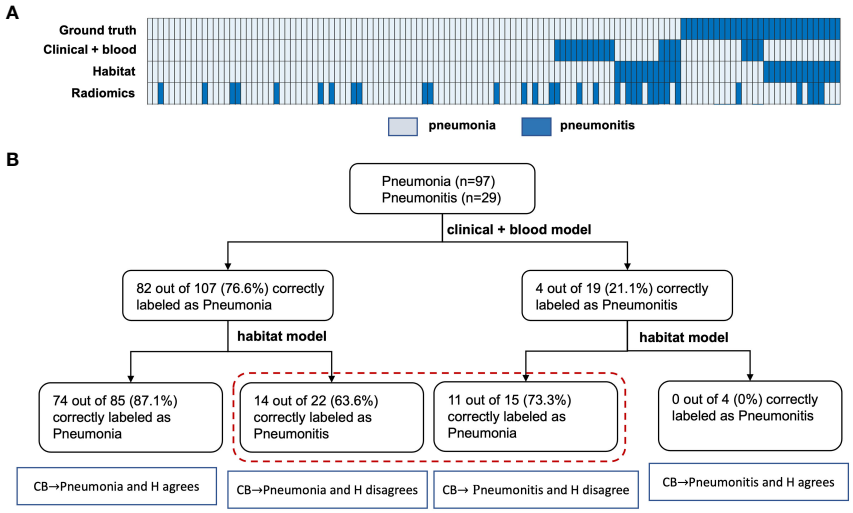

FIGURE 5
Evaluation of the benefit of the habitat model in improving baseline model prediction. **(A)**, shows the heatmap of the different model's prediction. **(B)**, shows how the cascading model improves the benchmark models predictions in both the pneumonia and pneumonitis group. Notes that CB and H here represents the clinical-blood and habitat models, respectively.

Discussion

Recognizing the difficulty in distinguishing pneumonia and pneumonitis in the absence of definitive biomarkers, we developed an imaging-based pipeline that could distinguish these two entities with a much-improved accuracy using a well-characterized cohort of patients with AML undergoing ICI therapy. Our proposed imaging marker has significantly outperformed a benchmark model based on clinical-blood metrics. Further, we observed a synergy between our imaging markers and blood markers, and their integration into a joint model has achieved the best prediction. All in all, our pilot study serves as proof-of-concept to demonstrate that machine learning of computed tomography (CT) scans can offer complementary values on top of existing clinical biomarkers for improved management of immune-related adverse events (irAE).

Diagnosing pneumonitis in real-time is challenging, and the prompt differentiation of pneumonitis from other conditions, such as pneumonia or cancer progression, is not always possible from imaging information alone. Additional tests may be required, but these results may further delay the prompt administration of definitive therapy toward pneumonia or pneumonitis, potentially leading to patient harm. For example, prompt administration of antibiotics for community acquired pneumonia decreases in-hospital mortality (22). Improving the ability of interpreting radiologists to diagnose pneumonitis may lead to improved patient outcomes. Tools such as the one we highlight in this work can potentially augment the capabilities of interpreting so to help radiologists make definitive image-based diagnoses. Approaches that combine artificial intelligence imaging tools with clinical radiologists often exceed the accuracy seen with human evaluations, as has been shown when determining the probability that a lung nodule is malignant (23) or whether reticular abnormalities represent interstitial lung disease (24). We envision that this tool may reduce the uncertainty seen when trying to differentiate pneumonia and pneumonitis in real time, but further studies are needed to validate this.

Pneumonitis is a serious complication of checkpoint inhibitor immunotherapy, and the mortality ranges from 10-20% in non-small cell lung cancer cohorts (NSCLC), where ICIs are frequently used (25–27) to nearly 50% in AML (5). Pneumonitis is likely to be more amenable to treatment if detected early and distinguished from pneumonia. The treatments for pneumonitis, namely immunosuppressive therapies of appropriate intensity and duration, are substantively different from the treatments for pneumonia. Furthermore, overuse of antimicrobial agents in patients without pneumonia may alter the intestinal microbiome, potentially reducing the efficacy of ICIs (28). In our original report,

TABLE 3 Pretest and posttest probability comparison among different diagnostic models.

Model	Pre-test Probability	Post-test Probability
Benchmark (clinical-blood)	23%	22%
Habitat		55%
Refitted composite model		61%
Classical Radiomics		15%

28/31 cases of pneumonitis were treated with both corticosteroids and antibiotic therapies. While pneumonia was fivefold more common in our cohort than pneumonitis, promptly distinguishing these two conditions will benefit all patients undergoing ICI therapy for cancer, regardless of the underlying rates of these two conditions. Further, diagnosis of pneumonitis with histopathology in nearly all cases due to the concern for bleeding due to thrombocytopenia or the concern for pulmonary deterioration after a biopsy procedure.

Computed tomography (CT) patterns associated with immune checkpoint inhibitor related pneumonitis may resemble interstitial lung diseases seen in the general population, including organizing pneumonia, interstitial pneumonitis, and others (29). The patterns that may be seen in these diseases is highly variable from case to case, as others have shown (30, 31). Radiomics has been used to predict the risk of developing ICI-induced pneumonitis based on baseline CT scans from 2 patients who developed pneumonitis and 30 who did not (32), but not to differentiate pneumonitis from other lung diseases. In this study, we have implemented the habitat imaging algorithm to differentiate pneumonia and pneumonitis. Compared to conventional radiomics, the key strength of our habitat imaging analysis is that it explicitly accounts for the spatial heterogeneity of the infected lung and partitions the whole lung regions into phenotypically distinct subregions. By analyzing these subregions individually as well as their interactions, we have demonstrated its superior performance in separating pneumonitis from pneumonia. Analogous to the superior multiregional gene sequencing over conventional cocktail sequencing (33), a fine grained spatial analysis enabled by habitat imaging can reveal new insights to improve the pneumonitis diagnosis. By contrast, traditional radiomics extracts features (including texture) from the entire lung region but cannot capture the degree of intra-lung infection heterogeneity. This may explain why our habitat imaging approach outperformed conventional radiomics.

Our study has several strengths. This is the first tool of its kind and is positioned to address a significant problem that hinders the treatment of all patients undergoing ICI therapy. The tool was developed by incorporating CT images that used diverse acquisition protocols, and thus can be more easily applied and validated in external cohorts. Also, another strength of our study is the strict selection of patients with AML under immunotherapy. AML patients do not have solid malignancies in their lung regions to confound the imaging analysis, which is different from solid tumors (e.g. NSCLC).

Several limitations must be considered. First, the results presented in this manuscript would benefit from an external cohort for model validation. Second, while all cases of pneumonia and pneumonitis in this study were confirmed by an expert multidisciplinary cohort at MD Anderson, the accuracy of this tool needs to be confirmed in a prospective cohort where the appropriate testing, especially CT imaging of the chest and universal BAL, are performed promptly and systematically. Third, it is likely that blood and clinical markers that associate with pneumonitis will vary from cohort to cohort, which would make an approach that only utilizes imaging more attractive. Fourth, other lung processes such as disease progression or radiation injury are more applicable to solid tumors but not seen in the current cohort treated for AML, and therefore this tool must be validated before applying in patients with solid tumors such as non-small cell lung cancer. Fifth, it is possible that pneumonia and pneumonitis may co-exist in some patients, and it is not uncommon for more than one serious adverse event to manifest concurrently in AML patients (34). Therefore, a test that determines the probability of one or the other as mutually exclusive results may not be appropriate in all cases. Sixth, there is no "gold standard" to diagnose pneumonia, and it remains a clinical diagnosis. Therefore, it is possible that the multidisciplinary adjudication of pneumonia and pneumonitis were erroneous in some instances. Finally, because ICIs are not currently approved to treat AML, there is not a possibility to expand the number of cases with pneumonitis in a similar cohort.In conclusion, we developed a tool that could accurately distinguish pneumonia and pneumonitis in AML patients treated with ICI inhibitors. If validated, our approach holds great promise to improve the clinical care of cancer patients treated with ICIs by improving our ability to differentiate pneumonitis from other lung diseases in a prompt fashion.

Data availability statement

The data of this study are available through signed data access agreement from the corresponding author. De-identified blood and clinical data will be provided on reasonable request. The CT image data are not publicly available since they contain sensitive information that could compromise patient privacy.

Ethics statement

The studies involving humans were approved by MD Anderson Institutional Review Board. The studies were conducted in accordance with the local legislation and institutional requirements. The ethics committee/institutional review board waived the requirement of written informed consent for participation from the participants or the participants' legal guardians/next of kin because Waiver of consent for this study. Original study consented patients for the trial. Written informed consent was not obtained from the individual(s) for the publication of any potentially identifiable images or data included in this article because Waiver of consent for this study. Original study consented patients for the trial.

Author contributions

AS and JW conceived the study. All authors participated in data collection. MuA performed primary data analyses with the guidance of AS and JW. MuA, JW, and AS wrote the manuscript. All authors contributed to the article and approved the submitted version.

Funding

This work was supported by the NIH/NIAID (K23 AI117024; to AS), NIH/NIAMS (K08 AR079587 to SK) and NIH/NCI grant (R00 CA218667; to JW). This work was supported by the Tumor Measurement Initiative through the MD Anderson Strategic Initiative Development Program (STRIDE).

Conflict of interest

The authors declare that the research was conducted in the absence of any commercial or financial relationships that could be construed as a potential conflict of interest.

Publisher's note

Supplementary material

The Supplementary Material for this article can be found online at: https://www.frontiersin.org/articles/10.3389/fimmu.2023.1249511/full#supplementary-material

References

1. Haslam A, Prasad V. Estimation of the percentage of US patients with cancer who are eligible for and respond to checkpoint inhibitor immunotherapy drugs. *JAMA Netw Open* (2019) 2(5):e192535. doi: 10.1001/jamanetworkopen.2019.2535

2. Shah A, Andersson TM, Rachet B, Bjorkholm M, Lambert PC. Survival and cure of acute myeloid leukaemia in England, 1971-2006: a population-based study. *Br J Haematol* (2013) 162(4):509–16. doi: 10.1111/bjh.12425

3. Knipp S, Hildebrand B, Kundgen A, Giagounidis A, Kobbe G, Haas R, et al. Intensive chemotherapy is not recommended for patients aged >60 years who have myelodysplastic syndromes or acute myeloid leukemia with high-risk karyotypes. *Cancer* (2007) 110(2):345–52. doi: 10.1002/cncr.22779

4. Daver N, Garcia-Manero G, Basu S, Boddu PC, Alfayez M, Cortes JE, et al. Efficacy, safety, and biomarkers of response to azacitidine and nivolumab in relapsed/refractory acute myeloid leukemia: A nonrandomized, open-label, phase II study. *Cancer Discovery* (2019) 9(3):370–83. doi: 10.1158/2159-8290.CD-18-0774

5. Sheshadri A, Goizueta AA, Shannon VR, London D, Garcia-Manero G, Kantarjian HM, et al. Pneumonitis after immune checkpoint inhibitor therapies in patients with acute myeloid leukemia: A retrospective cohort study. *Cancer* (2022) 128 (14):2736–45. doi: 10.1002/cncr.34229

6. Garcia JB, Lei X, Wierda W, Cortes JE, Dickey BF, Evans SE, et al. Pneumonia during remission induction chemotherapy in patients with acute leukemia. *Ann Am Thorac Soc* (2013) 10(5):432–40. doi: 10.1513/AnnalsATS.201304-097OC

7. Kim ST, Sheshadri A, Shannon V, Kontoyiannis DP, Kantarjian H, Garcia-Manero G, et al. Distinct immunophenotypes of T cells in bronchoalveolar lavage fluid from leukemia patients with immune checkpoint inhibitors-related pulmonary complications. *Front Immunol* (2020) 11:590494. doi: 10.3389/fimmu.2020.590494

8. Choo R, Naser NSH, Nadkarni NV, Anantham D. Utility of bronchoalveolar lavage in the management of immunocompromised patients presenting with lung infiltrates. *BMC Pulm Med* (2019) 19(1):51. doi: 10.1186/s12890-019-0801-2

9. Azar MM, Schlaberg R, Malinis MF, Bermejo S, Schwarz T, Xie H, et al. Added diagnostic utility of clinical metagenomics for the diagnosis of pneumonia in immunocompromised adults. *Chest* (2021) 159(4):1356–71. doi: 10.1016/j.chest.2020.11.008

10. Choe J, Hwang HJ, Seo JB, Lee SM, Yun J, Kim MJ, et al. Content-based image retrieval by using deep learning for interstitial lung disease diagnosis with chest CT. *Radiol* (2022) 302(1):187–97. doi: 10.1148/radiol.2021204164

11. Wu J, Mayer AT, Li R. Integrated imaging and molecular analysis to decipher tumor microenvironment in the era of immunotherapy. In: *Seminars in Cancer Biology*. Amsterdam, The Netherlands: Elsevier (2020).

12. Gillies RJ, Kinahan PE, Hricak H. Radiomics: images are more than pictures, they are data. *Radiol* (2016) 278(2):563–77. doi: 10.1148/radiol.2015151169

13. Aminu M, Yadav D, Hong L, Young E, Edelkamp P, Saad M, et al. Habitat imaging biomarkers for diagnosis and prognosis in cancer patients infected with COVID-19. *Cancers* (2022) 15(1):275. doi: 10.3390/cancers15010275

14. Tomaszewski MR, Gillies RJ. The biological meaning of radiomic features. *Radiol* (2021) 202553:505–16. doi: 10.1148/radiol.2021202553

15. Wu J, Gensheimer MF, Zhang N, Guo M, Liang R, Zhang C, et al. Tumor subregion evolution-based imaging features to assess early response and predict prognosis in oropharyngeal cancer. *J Nucl Med* (2020) 61(3):327–36. doi: 10.2967/jnumed.119.230037

16. Wu J, Cao G, Sun X, Lee J, Rubin DL, Napel S, et al. Intratumoral spatial heterogeneity at perfusion MR imaging predicts recurrence-free survival in locally advanced breast cancer treated with neoadjuvant chemotherapy. *Radiol* (2018) 288 (1):26–35. doi: 10.1148/radiol.2018172462

17. Kalisz KR, Ramaiya NH, Laukamp KR, Gupta A. Immune checkpoint inhibitor therapy–related pneumonitis: patterns and management. *Radiographics* (2019) 39 (7):1923–37. doi: 10.1148/rg.2019190036

18. program Cte. *Common Terminology Criteria for Adverse Events (CTCAE) NIH*. United States: Division of cancer treatment and diagnosis: NIH (2018). Available at: https://ctep.cancer.gov/protocoldevelopment/electronic_applications/ctc.htm#ctc_50.

19. Ronneberger O, Fischer P, Brox T. U-net: convolutional networks for biomedical image segmentation. *Lect Notes Comput Sc.* (2015) 9351:234–41. doi: 10.1007/978-3-319-24574-4_28

20. Achanta R, Shaji A, Smith K, Lucchi A, Fua P, Susstrunk S. SLIC superpixels compared to state-of-the-art superpixel methods. *IEEE Trans Pattern Anal Mach Intell* (2012) 34(11):2274–82. doi: 10.1109/TPAMI.2012.120

21. Akobeng AK. Understanding diagnostic tests 2: likelihood ratios, pre-and post-test probabilities and their use in clinical practice. *Acta paediatrica* (2007) 96(4):487–91. doi: 10.1111/j.1651-2227.2006.00179.x

22. Houck PM, Bratzler DW, Nsa W, Ma A, Bartlett JG. Timing of antibiotic administration and outcomes for Medicare patients hospitalized with community-acquired pneumonia. *Arch Intern Med* (2004) 164(6):637–44. doi: 10.1001/archinte.164.6.637

23. Kim RY, Oke JL, Pickup LC, Munden RF, Dotson TL, Bellinger CR, et al. Artificial intelligence tool for assessment of indeterminate pulmonary nodules detected with CT. *Radiol* (2022) 304(3):683–91. doi: 10.1148/radiol.212182

24. Kim W, Lee SM, Kim JI, Ahn Y, Park S, Choe J, et al. Utility of a deep learning algorithm for detection of reticular opacity on chest radiography in patients with interstitial lung disease. *AJR Am J Roentgenol* (2022) 218(4):642–50. doi: 10.2214/AJR.21.26682

25. Cho JY, Kim J, Lee JS, Kim YJ, Kim SH, Lee YJ, et al. Characteristics, incidence, and risk factors of immune checkpoint inhibitor-related pneumonitis in patients with non-small cell lung cancer. *Lung Cancer (Amsterdam Netherlands)* (2018) 125:150–6. doi: 10.1016/j.lungcan.2018.09.015

26. Suresh K, Naidoo J. Lower survival in patients who develop pneumonitis following immunotherapy for lung cancer. *Clin Lung Cancer* (2020) 21(3):e169–e70. doi: 10.1016/j.cllc.2019.10.009

27. Tone M, Izumo T, Awano N, Kuse N, Inomata M, Jo T, et al. High mortality and poor treatment efficacy of immune checkpoint inhibitors in patients with severe grade checkpoint inhibitor pneumonitis in non-small cell lung cancer. *Thorac Cancer* (2019) 10(10):2006–12. doi: 10.1111/1759-7714.13187

28. Derosa L, Hellmann MD, Spaziano M, Halpenny D, Fidelle M, Rizvi H, et al. Negative association of antibiotics on clinical activity of immune checkpoint inhibitors in patients with advanced renal cell and non-small-cell lung cancer. *Ann Oncol* (2018) 29(6):1437–44. doi: 10.1093/annonc/mdy103

29. Travis WD, Costabel U, Hansell DM, King TE Jr., Lynch DA, Nicholson AG, et al. An official American Thoracic Society/European Respiratory Society statement: update of the international multidisciplinary classification of the idiopathic interstitial

pneumonias. *Am J Respir Crit Care Med* (2013) 188(6):733–48. doi: 10.1164/rccm.201308-1483ST

30. Nishino M, Ramaiya NH, Awad MM, Sholl LM, Maattala JA, Taibi M, et al. PD-1 inhibitor–related pneumonitis in advanced cancer patients: radiographic patterns and clinical coursePD-1 inhibitor–related pneumonitis in advanced cancer. *Clin Cancer Res* (2016) 22(24):6051–60. doi: 10.1158/1078-0432.CCR-16-1320

31. Huang A, Xu Y, Zang X, Wu C, Gao J, Sun X, et al. Radiographic features and prognosis of early- and late-onset non-small cell lung cancer immune checkpoint inhibitor-related pneumonitis. *BMC Cancer* (2021) 21(1):634. doi: 10.1186/s12885-021-08353-y

32. Colen RR, Fujii T, Bilen MA, Kotrotsou A, Abrol S, Hess KR, et al. Radiomics to predict immunotherapy-induced pneumonitis: proof of concept. *Investigational New Drugs* (2018) 36(4):601–7. doi: 10.1007/s10637-017-0524-2

33. Gerlinger M, Rowan AJ, Horswell S, Larkin J, Endesfelder D, Gronroos E, et al. Intratumor heterogeneity and branched evolution revealed by multiregion sequencing. *N Engl J Med* (2012) 366:883–92. doi: 10.1056/NEJMoa1113205

34. Hersh EM, Bodey GP, Nies BA, Freireich EJ. Causes of death in acute leukemia: A ten-year study of 414 patients from 1954-1963. *JAMA* (1965) 193:105–9. doi: 10.1001/jama.1965.03090020019005

frontiers | Frontiers in Immunology

TYPE Case Report
PUBLISHED 06 October 2023
DOI 10.3389/fimmu.2023.1274449

OPEN ACCESS

EDITED BY
Simona Kranjc Brezar,
Institute of Oncology Ljubljana, Slovenia

REVIEWED BY
Shaolai Zhou,
Fudan University, China
Liang He,
University of California, San Francisco, United States
Jingxia Liu,
Southwest Jiaotong University, China

*CORRESPONDENCE
Ze-yang Ding
zyding@tjh.tjmu.edu.cn
Xin Luo
lx56960201@outlook.com

†These authors have contributed equally to this work

RECEIVED 08 August 2023
ACCEPTED 26 September 2023
PUBLISHED 06 October 2023

CITATION
Gao H, Chang R-z, Chen X-p, Zhang W-g, Zhang B, Luo X and Ding Z-y (2023) Case Report: Durable complete response of metastatic hepatocellular carcinoma with asymptomatic hyperamylasemia to combined immunotherapy of anti-cytotoxic T lymphocyte-associated antigen 4 plus anti-programmed cell death-1 antibodies.
Front. Immunol. 14:1274449.
doi: 10.3389/fimmu.2023.1274449

Case Report: Durable complete response of metastatic hepatocellular carcinoma with asymptomatic hyperamylasemia to combined immunotherapy of anti-cytotoxic T lymphocyte-associated antigen 4 plus anti-programmed cell death-1 antibodies

Han Gao[1,2,3†], Rui-zhi Chang[1,2,3†], Xiao-ping Chen[1,2,3], Wan-guang Zhang[1,2,3], Bixiang Zhang[1,2,3], Xin Luo[1,2,3*] and Ze-yang Ding[1,2,3*]

[1]Hepatic Surgery Center, Tongji Hospital, Tongji Medical College, Huazhong University of Science and Technology, Wuhan, Hubei, China, [2]Clinical Medicine Research Center for Hepatic Surgery of Hubei Province, Tongji Hospital, Tongji Medical College, Huazhong University of Science and Technology, Wuhan, Hubei, China, [3]Hubei Key Laboratory of Hepato-Pancreatic-Biliary Diseases, Tongji Hospital, Tongji Medical College, Huazhong University of Science and Technology, Wuhan, Hubei, China

Background: Combined immunotherapy has shown promising results in the treatment of advanced HCC, whereas the priority population that would respond to the combined immunotherapy is still elusive. In addition, HCC with asymptomatic hyperamylasemia was not reported previously.

Case presentation: An aged patient was diagnosed as HCC with BCLC stage C (bone metastasis). Notably, this patient showed asymptomatic hyperamylasemia. The patient was then enrolled in a trial evaluating combined immunotherapy of anti-PD-1 antibody sintilimab (IBI308) plus anti-CTLA-4 antibody (IBI310) in advanced HCC. After being treated with combined immunotherapy, this patient rapidly achieved complete response (CR) according to mRECIST criteria or immune partial response (iPR) according to iRECIST criteria and maintain the CR state for more than 12 months. Interestingly, serum levels of amylase and lipase in this patient were reduced after treatment.

Conclusion: We reported, for the first time, a case of metastatic HCC with asymptomatic hyperamylasemia, and suggested that HCC patients with asymptomatic hyperamylasemia may benefit from combined immunotherapy of anti-CTLA-4 and PD-1 antibodies.

KEYWORDS

hepatocellular carcinoma, asymptomatic hyperamylasemia, PD-1 inhibitor, CTLA-4 inhibitor, combined immunotherapy

Introduction

Hepatocellular carcinoma (HCC) is the sixth most commonly diagnosed cancer and is currently the fourth leading cause of cancer-related death worldwide (1). Currently, immune-checkpoint inhibitors (ICIs) based systemic therapies showed promising effects in treating advanced HCC. Combined immunotherapy of Nivolumab Plus Ipilimumab has been approved as a second-line systemic therapy for advanced HCC, based on the results of the CheckMate 040 trial (2). In addition, the HIMALAYA trial found that the tremelimumab plus durvalumab improved overall survival (16.43 months, 95% CI, 14.16 to 19.58) versus sorafenib (13.77 months, 95% CI, 12.25 to 16.13) (3). In China, a phase 3 trial comparing the effectiveness and safety of anti-cytotoxic T lymphocyte-associated antigen 4 (CTLA-4) antibody (IBI310) combined with sintilimab (IBI308) versus sorafenib in the first-line treatment of advanced HCC is ongoing.

Paraneoplastic syndrome (PNS) was found in 20–40% of HCC patients, and 8–17% of patients having more than one PNS. The most common PNS in HCC are hypercholesterolemia, hypoglycemia, hypercalcemia, and erythrocytosis, whereas rheumatic, neuromuscular, dermatological, hematological, and endocrine syndromes were less commonly found. HCC patients with PNS showed worse prognosis than those without PNS (4), and the best treatment for HCC patients with PNS, especially for those with unresectable, advanced HCC, is still exploring.

In this study, we report a case of metastatic HCC with asymptomatic hyperamylasemia, a PNS that has never been reported in HCC before. This patient showed a significant response to combined immunotherapy of sintilimab plus anti-CTLA-4 antibody.

Case presentation

In August 2021, an elderly patient was admitted to Tongji Hospital (Wuhan, China) for a mass at the right chest wall with tenderness for 1 month. At admission, this patient received a computed tomography (CT) scan, and results of abdominal CT revealed abnormally enhancing nodules of 92mm and 16 mm in the right posterior lobe and right anterior lobe of the liver respectively. Chest CT revealed a mass in the right anterior chest wall with bone destruction on the right side of the sternum. In addition, the serum level of AFP was 2075 ng/ml at admission. Based on these findings, this patient was diagnosed with HCC according to the clinical diagnostic criteria of AASLD and EASL. The patient's Eastern Cooperative Oncology Group performance status (PS) score was 0 and liver blood tests at admission showed the patient's Child-pugh score was 5 (grade A). The patient refused to undergo a biopsy of the tumor for pathological diagnosis. We evaluated the patient's China Liver Cancer stage (CNLC IIIb: PS 0, Child-Pugh A and extrahepatic metastasis), BCLC stage (BCLC C, PS 0, Child-Pugh A and extrahepatic metastasis) and TNM stage IV (cT3N0M1, multiple tumors, tumor diameter>5cm and distant metastasis), which are critical for treatment choice and prognosis assessment.

After discussion in a multidisciplinary team board meeting based on the evaluation, radical resection was not applicable and systemic therapy with atezolizumab and bevacizumab was recommended to the patient. However, the patient refused this therapy due to its high cost that they could not afford since atezolizumab is not on the list of drugs covered by medical insurance in China. The patient was then recommended to participate in a trial designed to evaluate the efficacy and safety of combined immunotherapy using sintilimab (IBI308) and anti-CTLA-4 antibody (IBI310) versus sorafenib in first-line treatment of advanced HCC (NCT04720716). After signing informed consent form, it was confirmed through screening that this patient met eligibility criteria for trial participation. At screening, it was found that this patient had hyperamylasemia with serum levels of amylase at 892 U/L, pancreatic amylase at 510 U/L, and lipase at 67.7 IU/L. The patient was confirmed to have no symptoms of abdominal pain. The dynamic changes in serum levels of AFP, amylase and lipase are shown in Figures 1A–C. The abdominal CT scan revealed no signs of enlargement or inflammation in this patient's pancreas (Figure 1D), and the serum levels of creatinine and eGFR were within normal range. After the screen, this patient was randomized to the group of combined immunotherapy, and began the first dose of combined immunotherapy on August 31st, 2021.The flowchart of the treatment and the changes of the imaging examination is in Figure 2. After receiving four cycles of combined immunotherapy, the patient was evaluated as having achieved CR according to mRECIST criteria, iPR according to iRECIST criteria or PR according to RECIST 1.1 criteria. Accordingly, AFP levels decreased rapidly until they eventually returned to normal range. In addition, sternal metastasis was found to have disappeared on

10.3389/fimmu.2023.1274449

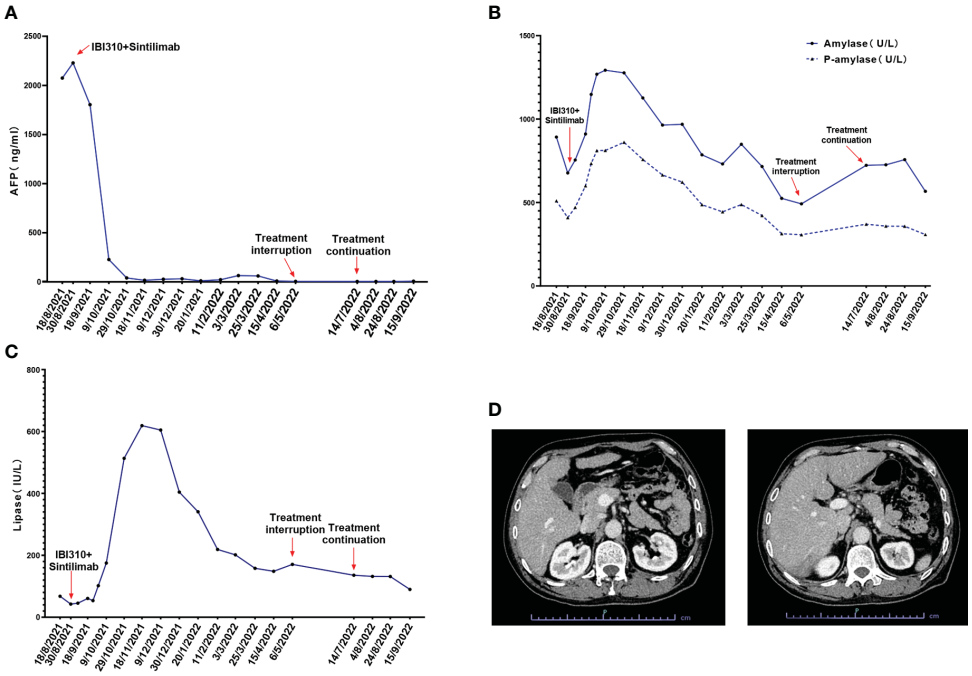

FIGURE 1
(A) The alpha fetoprotein (AFP) levels of the patient during the treatment of sintilimab combined with IBI310; **(B)** The total amylase and P-amylase levels of the patient during the treatment; **(C)** The lipase levels of the patient during the treatment; **(D)** The abdominal CT scan of the patient at admission which revealed no signs of enlargement or inflammation of the pancreas.

physical examination after the third cycle of treatment. Levels of amylase and lipase remained high at the beginning of treatment (1293 U/L and 618.9 IU/L). Interestingly, as the duration of treatment, the levels of amylase and lipase decreased significantly (492 U/L and 89.8 IU/L). Although levels of amylase and pancreatic amylase increased at the first two cycles of immunotherapy, the abdominal CT scan did not reveal any signs of enlargement or inflammation in the pancreas (Figure 2).

After beginning combined immunotherapy, the patient subsequently developed a series of adverse events (AEs) (grade 1, CTCAE 5.0), such as fatigue, pruritus, loss of appetite, and hyperglycemia. The patient then developed hypothyroidism and erythema nodosum on both lower limbs (grade 2, CTCAE 5.0) and was treated with levothyroxine and mucopolysaccharide polysulfate cream. At the 12th cycle of treatment (May 9th, 2022), the treatment was delayed, since the fatigue and loss of appetite were exacerbated to the grade 3 of CTCAE 5.0 criteria. Treatment continued after these adverse effects were improved to the grade 2 (July 14th, 2022). Noticeably, amylase levels rebounded to 723 U/L after the treatment was interrupted. As treatment continued, amylase levels eventually decreased to 567 U/L.

In October 2022, the treatment was delayed again due to a COVID-19 outbreak in Wuhan. After the lift lockdown of the hospital, this patient was informed to continue the treatment, but he refused because he was tired of repeating SARS-CoV-2 tests before every admission, and did not feel any discomfort. The patient received the last dose of combined therapy on September 15th, 2022. As of July 2023, telephone follow-ups are still being performed and the patient is surviving without any symptoms.

Discussion

To the best of our knowledge, this is the first reported case of a patient with advanced HCC and asymptomatic hyperamylasemia. Asymptomatic hyperamylasemia is rarely found in non-pancreatic tumors (5, 6). We performed a literature review of neoplasms associated with hyperamylasemia (Supplementary Table 1), and found that it was occasionally present in lung cancer, ovarian cancer, pheochromocytoma, and hematological malignancies including multiple myeloma, MALT lymphoma, AML and ALL (7). Considering that amylase levels are not routinely measured in blood tests during screening and follow-up of HCC, the incidence of HCC with hyperamylasemia might be underestimated. In ALL, hyperamylasemia is usually associated with L-asparaginase toxicity and leukemic infiltration of the pancreas. Besides these situations, amylase-producing tumor cells appear to be the major source of hyperamylasemia in malignancies. In human, α-amylase is encoded by AMY1 (salivary type) and AMY2 (pancreatic type) genes. α-Amylase can be produced by the liver and is encoded by the AMY-2B, an isogene of AMY2 (7, 8). In this case, evidence indicates that elevated levels of amylase may be produced by the tumor. Firstly, both serum levels of amylase and pancreatic amylase were elevated in this case. Secondly, dynamic changes in serum levels of amylase and pancreatic amylase were observed after starting combined immunotherapy. Specifically, levels of amylase and pancreatic amylase increased during the first two cycles of immunotherapy, suggesting that amylase was released from necrotic tumor cells. Levels of amylase decreased during subsequent cycles of immunotherapy. Unfortunately, since the patient refused to undergo a tumor biopsy and

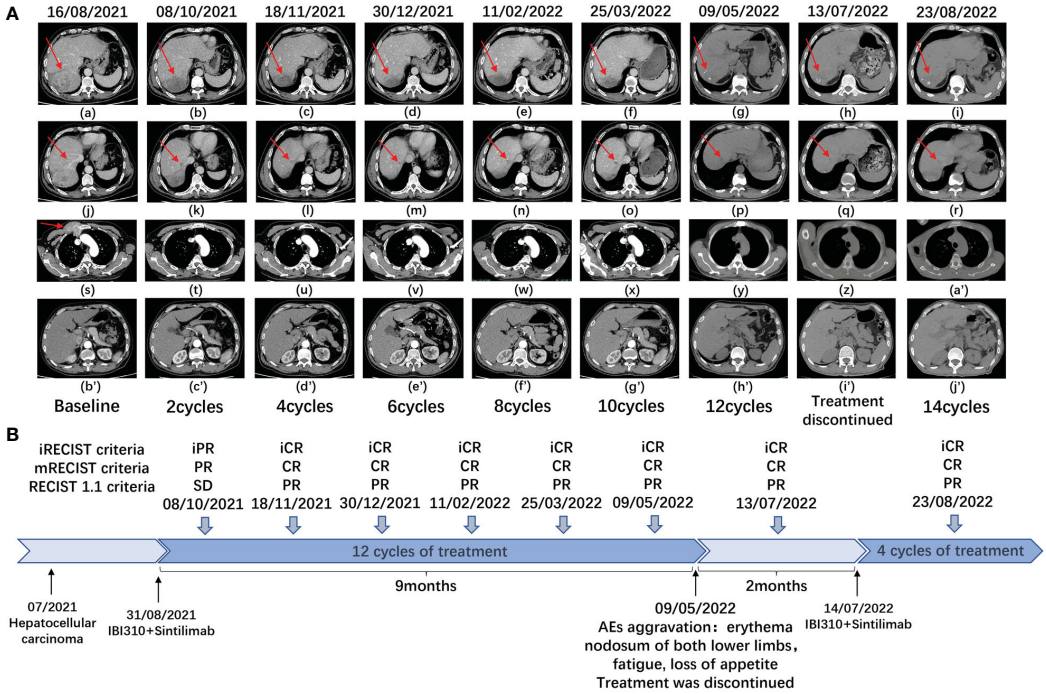

FIGURE 2
(A) Plain and enhanced CT of main lesions of the patient in different periods. a-i: right posterior lobe of the liver; j-r: right anterior lobe of the liver; s-a' the right anterior chest wall; b'j': the pancreas with no signs of any inflammation and enlargement. **(B)** This is a flowchart of the treatment of the patient. At different times, the patient received combination immunotherapy (sintilimab plus IBI310). CR, complete response, PR, partial response, SD, stable disease, AEs, adverse events.

histopathological detection of amylase in tumor tissue was unavailable, it was impossible to provide definite evidence for an amylase-producing HCC. Interestingly, levels of amylase behaved like a specific tumor biomarker for predicting efficacy and recurrence in different cancers since its dramatic decrease reflected tumor response to treatment.

In this study, we reported that this case, metastatic HCC with hyperamylasemia showed a quick and durable response to combined immunotherapy. In addition, previous studies have reported that cases of lung cancer, ovarian cancer, and ALL with hyperamylasemia were highly sensitive to chemotherapy (9–11). These results shed light on the association between hyperamylasemia and the sensitivity of cancer patients to systemic therapy including chemotherapy or immunotherapy. Further research is required to understand the underlying mechanisms. Furthermore, this is the first time that combined immunotherapy has been used for the treatment of a malignant tumor with asymptomatic hyperamylasemia. This has shown great predictive potential and efficacy. It remains to be explored whether combined immunotherapy can be generalized to other cancers with asymptomatic hyperamylasemia and whether cancers with asymptomatic hyperamylasemia are more sensitive to immunotherapy.

In conclusion, we reported for the first time a case of metastatic HCC with asymptomatic hyperamylasemia that was highly sensitive to combined immunotherapy using anti-CTLA-4 and anti-PD-1 antibodies. Our report suggests that despite being rarely found in HCC, hyperamylasemia might serve as a marker for reflecting the efficacy of immunotherapy. This association is worth validating in a large HCC cohort in the future.

Data availability statement

The original contributions presented in the study are included in the article/Supplementary Material. Further inquiries can be directed to the corresponding authors.

Ethics statement

The studies involving humans were approved by ethics committee of Huazhong University of Science and Technology. The studies were conducted in accordance with the local legislation and institutional requirements. The participants provided their written informed consent to participate in this study. Written informed consent was obtained from the individual(s) for the publication of any potentially identifiable images or data included in this article. Written informed consent was obtained from the participant/patient(s) for the publication of this case report.

Author contributions

HG: Writing – original draft, Writing – review & editing, Methodology. R-ZC: Investigation, Writing – original draft, Writing – review & editing. X-PC: Supervision, Writing – review & editing. W-GZ: Supervision, Writing – review & editing. BZ: Supervision, Writing – review & editing. XL: Supervision, Writing – review & editing. Z-YD: Funding acquisition, Supervision, Writing – review & editing.

Funding

The authors declare financial support was received for the research, authorship, and/or publication of this article. This work was funded by the National Natural Science Foundation of China (82273441), Special Project on Knowledge Innovation (Shuguang Project) of Wuhan city (2022020801020456), and the first level of the Public Health Youth Top Talent Project of Hubei province (2022SCZ051).

Conflict of interest

The authors declare that the research was conducted in the absence of any commercial or financial relationships that could be construed as a potential conflict of interest.

Publisher's note

Supplementary material

The Supplementary Material for this article can be found online at: https://www.frontiersin.org/articles/10.3389/fimmu.2023.1274449/full#supplementary-material

References

1. Islami F, Ward EM, Sung H, Cronin KA, Tangka FKL, Sherman RL, et al. Annual report to the nation on the status of cancer, part 1: national cancer statistics. *J Natl Cancer Inst* (2021) 113(12):1648–69. doi: 10.1093/jnci/djab131

2. Yau T, Kang YK, Kim TY, El-Khoueiry AB, Santoro A, Sangro B, et al. Efficacy and safety of nivolumab plus ipilimumab in patients with advanced hepatocellular carcinoma previously treated with sorafenib: the checkMate 040 randomized clinical trial. *JAMA Oncol* (2020) 6(11):e204564. doi: 10.1001/jamaoncol.2020.4564

3. Abou-Alfa GK, Lau G, Kudo M, Chan SL, Kelley RK, Furuse J, et al. Tremelimumab plus durvalumab in unresectable hepatocellular carcinoma. *NEJM Evidence* (2022) 1(8):EVIDoa2100070. doi: 10.1056/EVIDoa2100070

4. Qu Q, Wang S, Chen S, Zhou L, Rui JA. Prognostic role and significance of paraneoplastic syndromes in hepatocellular carcinoma. *Am Surg* (2014) 80(2):191–6. doi: 10.1177/000313481408000230

5. Gallucci F, Buono R, Ferrara L, Madrid E, Miraglia S, Uomo G. Chronic asymptomatic hyperamylasemia unrelated to pancreatic diseases. *Adv Med Sci* (2010) 55(2):143–5. doi: 10.2478/v10039-010-0049-9

6. Crook M. Hyperamylasaemia: don't forget undiagnosed carcinoma. *Ann Clin Biochem* (2014) 51(Pt 1):5–7. doi: 10.1177/0004563213510490

7. Seyama K, Nukiwa T, Takahashi K, Takahashi H, Kira S. Amylase mRNA transcripts in normal tissues and neoplasms: the implication of different expressions of amylase isogenes. *J Cancer Res Clin Oncol* (1994) 120(4):213–20. doi: 10.1007/BF01372559

8. Koyama I, Komine S, Iino N, Hokari S, Igarashi S, Alpers DH, et al. alpha-Amylase expressed in human liver is encoded by the AMY-2B gene identified in tumorous tissues. *Clin Chim Acta* (2001) 309(1):73–83. doi: 10.1016/S0009-8981(01)00501-0

9. Guruprasad CS, Reghu KS, Nair M, Kumary PK. Asymptomatic hyperamylasemia/hyperlipasemia due to pancreatic infiltration in acute lymphoblastic leukemia. *Indian J Pediatr* (2016) 83(1):81–2. doi: 10.1007/s12098-015-1754-y

10. Tohya T, Shimajiri S, Onoda C, Yoshimura T. Complete remission of ovarian endometrioid adenocarcinoma associated with hyperamylasemia and liver metastasis treated by paclitaxel and carboplatin chemotherapy: a case report. *Int J Gynecol Cancer* (2004) 14(2):378–80. doi: 10.1136/ijgc-00009577-200403000-00029

11. Akinosoglou K, Siagris D, Geropoulou E, Kosmopoulou O, Velissaris D, Kyriazopoulou V, et al. Hyperamylasaemia and dual paraneoplastic syndromes in small cell lung cancer. *Ann Clin Biochem* (2014) 51(Pt 1):101–5. doi: 10.1177/0004563213500658

frontiers | Frontiers in Immunology

TYPE Original Research
PUBLISHED 11 October 2023
DOI 10.3389/fimmu.2023.1178060

OPEN ACCESS

EDITED BY
Steven Fiering,
Dartmouth College, United States

REVIEWED BY
Simon Völkl,
University Hospital Erlangen, Germany
Niels Schaft,
University Hospital Erlangen, Germany
Theresa L. Whiteside,
University of Pittsburgh, United States

*CORRESPONDENCE
Dominik Lock
dominiklo@miltenyi.com

RECEIVED 02 March 2023
ACCEPTED 28 September 2023
PUBLISHED 11 October 2023

CITATION
Teppert K, Winter N, Herbel V, Brandes C, Lennartz S, Engert F, Kaiser A, Schaser T and Lock D (2023) Combining CSPG4-CAR and CD20-CCR for treatment of metastatic melanoma.
Front. Immunol. 14:1178060.
doi: 10.3389/fimmu.2023.1178060

Combining CSPG4-CAR and CD20-CCR for treatment of metastatic melanoma

Karin Teppert, Nora Winter, Vera Herbel, Caroline Brandes, Simon Lennartz, Fabian Engert, Andrew Kaiser, Thomas Schaser and Dominik Lock*

Miltenyi Biotec B.V. & Co. KG, Bergisch Gladbach, Germany

The prognosis for patients with metastatic melanoma is poor and treatment options are limited. Genetically-engineered T cell therapy targeting chondroitin sulfate proteoglycan 4 (CSPG4), however, represents a promising treatment option, especially as both primary melanoma cells as well as metastases uniformly express CSPG4. Aiming to prevent off-tumor toxicity while maintaining a high cytolytic potential, we combined a chimeric co-stimulatory receptor (CCR) and a CSPG4-directed second-generation chimeric antigen receptor (CAR) with moderate potency. CCRs are artificial receptors similar to CARs, but lacking the CD3ζ activation element. Thus, T cells expressing solely a CCR, do not induce any cytolytic activity upon target cell binding, but are capable of boosting the CAR T cell response when both CAR and CCR engage their target antigens simultaneously. Here we demonstrate that co-expression of a CCR can significantly enhance the anti-tumor response of CSPG4-CAR T cells *in vitro* as well as *in vivo*. Importantly, this boosting effect was not dependent on co-expression of both CCR- and CAR-target on the very same tumor cell, but was also achieved upon trans activation. Finally, our data support the idea of using a CCR as a powerful tool to enhance the cytolytic potential of CAR T cells, which might open a novel therapeutic window for the treatment of metastatic melanoma.

KEYWORDS

immunotherapy, adoptive T cell therapy, chimeric antigen receptor, chimeric costimulatory receptor, melanoma

Introduction

Great clinical success has been achieved with the implementation of CAR T cells, especially for treatment of hematological malignancies (1–3). However, liquid tumors only represent 8-10% of all adult human cancers and certain characteristics of solid tumors such as strong physical barriers inhibiting T cell infiltration and a highly immunosuppressive tumor microenvironment have been demonstrated to weaken adoptive T cell therapies (4–6). In addition, one major challenge represents the selection of a suitable tumor antigen to

be targeted, since most of the identified tumor-associated antigens are also expressed on healthy tissues, carrying the risk for on-target/off-tumor toxicity and severe side effects (7). This is for instance the case for the target antigen CSPG4, first identified in melanoma and thus also referred to as melanoma-associated-chondroitin-sulfate-proteoglycan (MCSP) (8). Although expression levels are clearly lower than in tumor cells, CSPG4 is also found on non-malignant tissue, such as pericytes and small intestine (9, 10). Nonetheless, CSPG4 represents a promising target for adoptive T cell therapies, as it is not only overexpressed in melanoma but also in a broad range of other malignancies such as triple-negative breast cancers, various types of gliomas, head and neck squamous-cell carcinomas, soft-tissue sarcomas, tumor-associated vasculature and also leukemia (11–13). In line with this, CSPG4 was described to promote multiple steps of cancer development such as angiogenesis, dissemination, metastasis, proliferation, and survival (14, 15). The expression in not only primary but also metastatic melanoma cells further underlines the great therapeutic potential of targeting CSPG4, especially for treatment of metastatic melanoma, which is generally associated with poor prognosis and a median survival of less than one year (9, 10, 16). Traditional approaches such as chemotherapy, radiotherapy and surgical removal are ineffective in late-stage metastasized melanoma (17). Targeted immunotherapies such as MEK- or BRAF-inhibitors have led to promising results, but the high mutational rate in melanoma strongly promotes the development of secondary resistances (18). The implementation of immune checkpoint blockade (ICB) has yielded a groundbreaking outcome, marking the first successful extension of survival for metastatic melanoma (19, 20). However, latest reports from clinical trials (NCT01844505) showed that long-lasting effects can only be expected in approximately half of the patients (21, 22). Adoptive T-cell based immunotherapies targeting for instance VEGFR-2 (NCT01218867), GD2 (NCT02107963, NCT03635632), CD70 (NCT02830724), gp100 (NCT03649529) or CD20 (NCT03893019) are currently assessed in several clinical trials and were suggested to be especially helpful in case of treatment-resistant melanomas (23). Particularly combinatorial approaches were suggested to increase efficiency and to minimize the risk for therapy-accompanied adverse events such as on-target/off-tumor toxicity (23). This aspect of increasing tumor cell specificity is also highly relevant in the context of targeting CSPG4, due to its role in multiple physiological processes and the expression on healthy tissues (24). To this end, our approach was focused on combining a low-affinity CSPG4-CAR, which by itself only showed weak activity and cytotoxicity, with a chimeric co-stimulatory co-receptor (CCR). CCRs are artificial receptors, which comprise an extracellular binding moiety, a spacer, a transmembrane region and defined intracellular signaling domains that differ from conventional CAR designs. As the CD3ζ signaling domain is typically absent in CCRs, no cytolytic activity is induced upon antigen engagement. However, CCRs are capable of boosting a simultaneously activated CAR T cell response, which results in an enhanced release of inflammatory cytokines and increased cytotoxicity. Due to the low functional avidity, the risk for CAR-binding to healthy target cells expressing low levels of CSPG4 is reduced. We show that CSPG4-expressing target cells were only effectively lysed when both CCR and CAR engaged their target antigens. This means that the CCR could either simply target a second tumor-associated antigen, or an antigen, which is not expressed by the tumor cell but found in close proximity, as for example in the tumor microenvironment (TME). In this study, CD20 was selected as CCR target; on the one hand to guarantee omnipresent expression in B cells, and on the other hand, due to the clinical success by targeting $CD20^+$ cell subsets in melanoma (9, 10, 24–26).

Results

Generation of a panel of CCR variants expressing different co-stimulatory domains

With the primary goal to improve the safety of CSPG4-targeting CAR T cell therapies, we used a low-affinity antibody-derived CSPG4-CAR, which showed low cytotoxic activity, consequently entailing a minimized risk for on-target/off-tumor toxicity. As expected, comparison of CAR T cells, either expressing the conventional Leu16-derived CD20-CAR or a CSPG4-CAR, revealed more than 20-fold lower levels of IFN-γ release with the novel low-affinity CSPG4-CAR (Figure 1A). Aiming to boost the activity of this CSPG4-CAR, various CD20-targeting CCR constructs with different combinations of 4-1BB and/or CD28 co-stimulatory domains were generated (Figure 1B). CD20 was selected as CCR target in order to guarantee omnipresent expression through bystanding or tumor-infiltrating B cells (9, 10, 24–26). The hypothesized mechanism is illustrated in Figure 1C, showing that target cell lysis is only successfully facilitated by CSPG4-CAR T cells, when both CAR and the co-expressed CCR engage their target antigens simultaneously. As depicted, CAR- and CCR-target can either be expressed in cis (on the same target cell) or in trans (on two different target cells).

CCRs boost the cytolytic potential of CSPG4-directed CAR T cells

In order to test whether a CCR boosts the cytolytic potential of the CSPG4-CAR, activated T cells were co-transduced with the CSPG4-CAR and with one of the engineered CD20-CCR variants. Prior to functionality analysis, the T cells were enriched via the surface markers ΔLNGFR and/or ΔEGFR (exemplarily shown in Figure S1A). To initially study the approach in trans and to assess whether the boosting effect is dependent on CCR engagement with its target antigen, T cells co-expressing the CSPG4-CAR and a specific CCR construct were co-cultured with $CSPG4^+$ Mel526 cells *in vitro*, in presence or absence of $CD20^+$ JeKo-1^{WT} cells. After 24 hours, the level of pro-inflammatory cytokines in the supernatant was determined. Since strong 4-1BB signaling supports survival and persistence of CAR T cells, we focused on two different CCR constructs with either two sequential 4-1BB endodomains or the combination of 4-1BB and CD28 co-stimulatory domain, termed CCR-(4-1BB_4-1BB) and CCR-(CD28_4-1BB), respectively.

10.3389/fimmu.2023.1178060

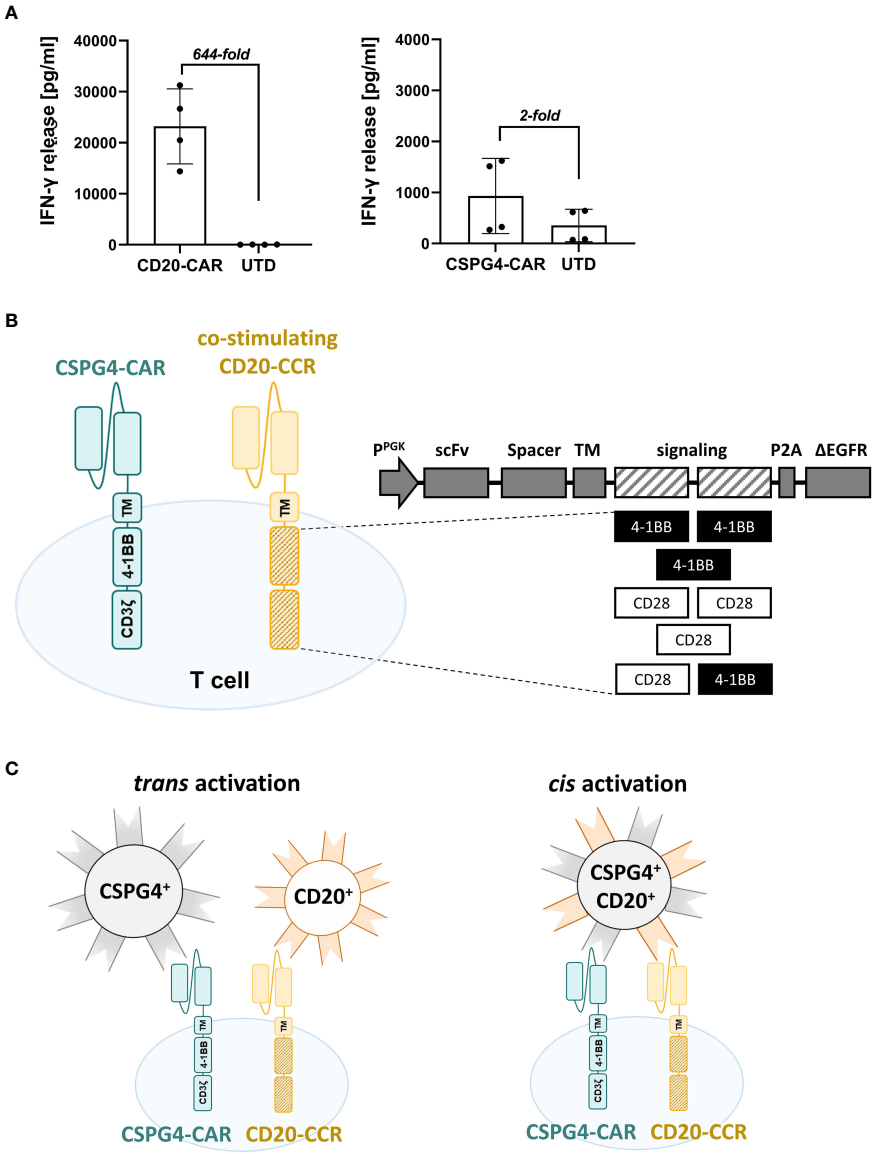

FIGURE 1
Co-expressing CD20-targeting Chimeric Co-stimulation Receptor (CCR) to boost CSPG4 CAR functionality. **(A)** Fold-increase in IFN-γ release by high-performing CD20-CAR T cells (right graph) in comparison to low-affinity antibody-derived CSPG4-CAR T cells (left graph) upon 24 hours co-culture with CD20$^+$ JeKo-1 cells or CSPG4$^+$ Mel526 cells, respectively. Data shows mean and individual values for four different donors (± SD). **(B)** Schematic representation of a T cell co-expressing a 4-1BB-co-stimulated second-generation CSPG4-CAR and a chimeric CD20-CCR, containing one or two co-stimulatory domains (4-1BB_4-1BB; 4-1BB, CD28_CD28; CD28; CD28_4-1BB) and lacking the CD3ζ signaling domain. **(C)** Mechanism of boosting the performance of the low-performing CSPG4-CAR (blue) by co-expression of a CD20-CCR (yellow), either achieved through cis (left) or trans (right) activation, meaning that CCR- and CAR- target are expressed on the same target cell or on different target cells, respectively.

Strongest effect upon dual stimulation was observed with CSPG4-CAR T cells co-expressing CCR-(4-1BB_4-1BB), resulting in significantly increased IFN-γ and TNF-α production compared to CSPG4-CAR T cells only (Figure 2A). In general, all CCR variants led to increase in cytokine secretion with more than 10- and 100-fold higher IFN-γ and TNF-α release, respectively, whereas control groups with T cells expressing only CAR or only CCR did not show noticeable release of pro-inflammatory cytokines (exemplarily shown in Figures S1B, C). The data demonstrated that the functionality of the CSPG4-CAR was significantly increased through co-expression of a CCR and, as previously hypothesized, that the combination of CAR and CCR only facilitated increased potency when both CAR and CCR were engaging their target antigens.

In order to simplify the engineering process, to ensure purity of the final T cell product (containing neither CAR-only nor CCR-only T cells), we designed a polycistronic lentiviral construct, encoding for both CSPG4-CAR and CD20-directed CCR-(4-1BB_4-BB), termed CSPG4-CAR_CD20-CCR (Figure 2B). CCR and CAR co-expressing T cells were engineered using the newly designed polycistronic lentiviral vector and subsequently enriched via the transduction marker ΔLNGFR, reaching comparable transgene expression above 75% (Figure 2C). After 24 hours of co-culture in trans, CSPG4-CAR_CD20-CCR T cells demonstrated

10.3389/fimmu.2023.1178060

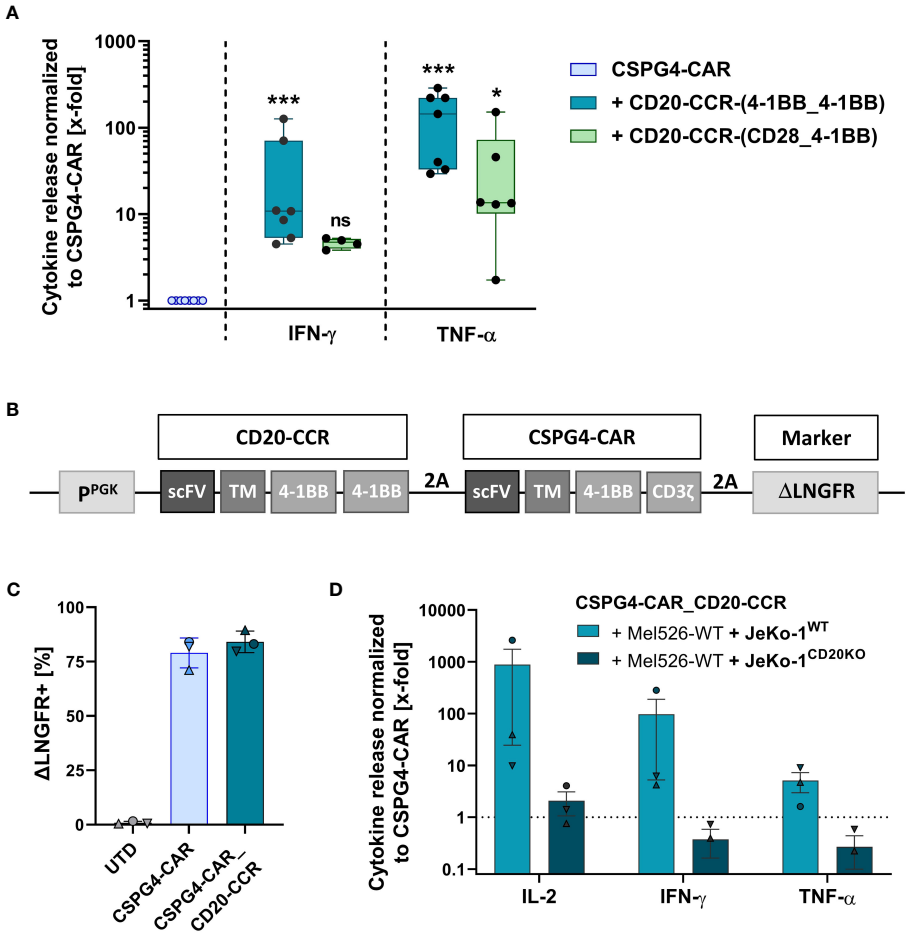

FIGURE 2
Co-expression of CSPG4-CAR and CD20-CCR significantly increases cytokine release upon trans activation and can be achieved through transduction with a polycistronic lentiviral construct. **(A)** T cells were lentivirally transduced with a CSPG4-CAR and/or a CD20-CCR, either containing 4-1BB_4-1BB or CD28_4-1BB costimulatory domains. Cytokine secretion of IFN-γ and TNF-α was determined after 24 hours of co-culture with CSPG4$^+$ Mel526 and CD20$^+$ JeKo-1^{WT} cells. Box and whiskers plots show median and individual values (normalized to CSPG4-CAR) for eight different donors from four individual experiments. Significance was determined using nonparametric one-way ANOVA (ns, not significant; *$p \leq 0.05$, ***$p \leq 0.001$). **(B)** Gene schematics of CD20-CCR_CSPG4-CAR T cells, poly-cistronically expressing CSPG4-CAR and CD20-specific CCR-(4-1BB_4-1BB). **(C)** Frequency of magnetically enriched ΔLNGFR$^+$, measured before co-culture with target cells. Mean and individual values are shown for four different donors from two independent experiments (± SD). **(D)** Cytokine secretion (IL-2, IFN-γ, TNF-α) after 24 hours of co-culture with a mixture of CSPG4$^+$ Mel526 and either CD20$^+$ JeKo-1^{WT} cells or CD20$^-$ JeKo-1^{CD20KO} cells at an E:T ratio of 5:1. Bar graph shows mean and individual values for three different donors (± SEM).

strongly enhanced secretion of IL-2, IFN-γ and TNF-α, compared to CSPG4-CAR T cells only (Figure 2D). As expected, this boosting effect was dependent on the presence of CD20$^+$ JeKo-1^{WT} cells. Co-culture with a mixture of Mel526^{WT} and JeKo-1^{CD20KO} cells led to comparable cytokine release between CSPG4-CAR T cells and dual-specific CSPG4-CAR_CD20-CCR cells.

After proving the applicability of the boosting system in the trans setting, we next aimed to assess, whether cytokine secretion of CSPG4-CAR_CD20-CCR T cells is also enhanced upon cis activation, using CD20$^+$ CSPG4$^+$ Mel526 cells. In accordance with the results obtained in trans, CSPG4-CAR_CD20-CCR T cells led to significantly increased, more than 5-fold higher, IFN-γ and GM-CSF secretion than CSPG4-CAR T cells without CCR (Figure 3A). Particularly, the IL-2 secretion was strongly increased in CSPG4-CAR_CD20-CCR T cells, demonstrating more than 100-fold higher production than CSPG4-CAR T cells. Moreover, co-expression of CCR-(4-1BB_4-1BB) significantly enhanced the *in vitro* cytolytic potential and recovered functionality of the CSPG4-CAR (Figure 3B). Lysis of CD20$^+$ CSPG4$^+$ Mel526 target cells was comparable between untransduced T cells and CSPG4-CAR T cells, whereas only dual-stimulated CSPG4-CAR_CD20-CCR T cells demonstrated significant cytotoxicity.

CCR boosts CAR in a dose-dependent manner

As hypothesized, we were able to show that the cytotoxic potential of our low-affinity antibody-derived CAR, which on its own only showed moderate activity and consequently also

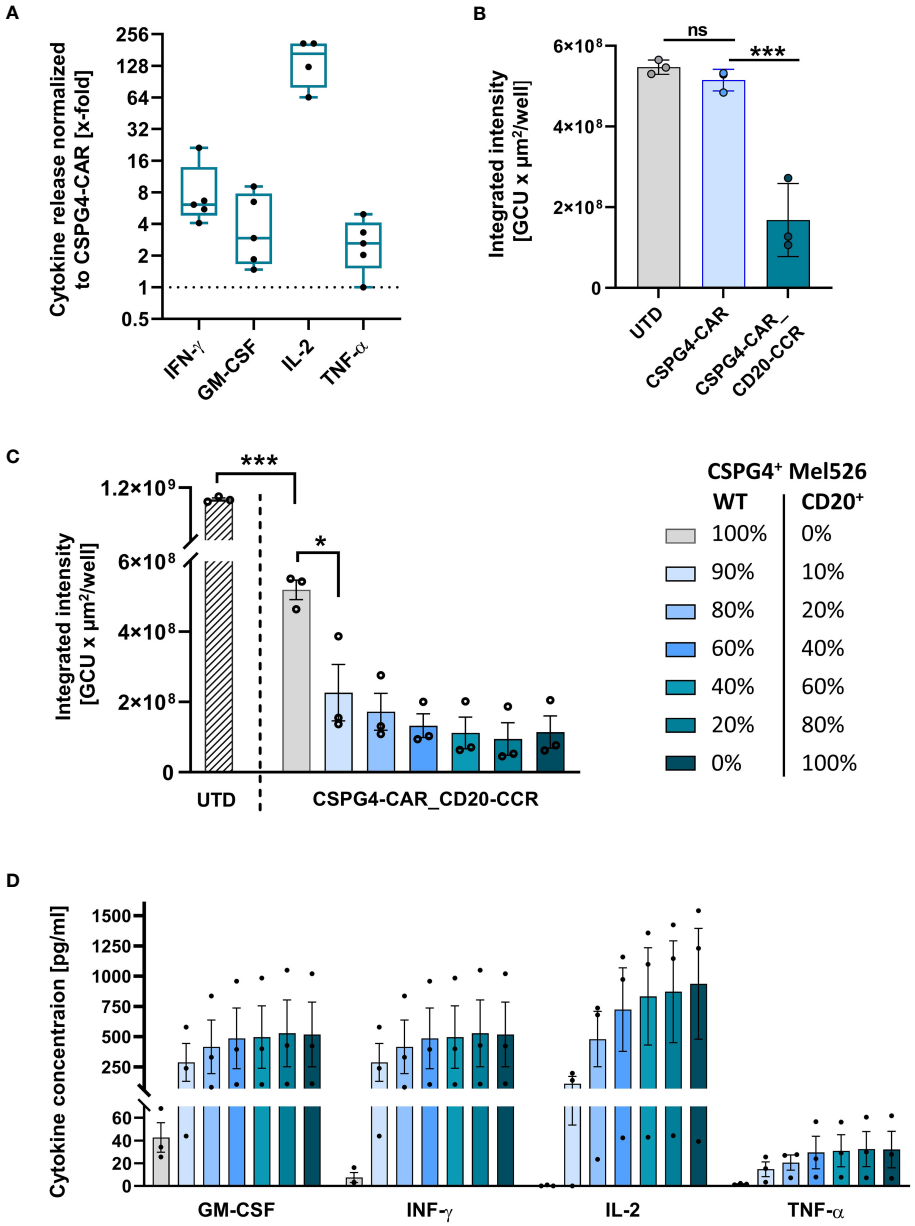

FIGURE 3
CSPG4-CAR_CD20-CCR T cells demonstrate significantly enhanced cytotoxicity upon cis stimulation and respond in a dose-dependent manner. **(A)** Cytokine release by CD20-CCR_CSPG4-CAR T cells after 24 hours of co-culture with CD20$^+$ CSPG4$^+$ Mel526^{CD20} target cells an E:T ratio of 1:1. Box and whiskers plots show median and individual x-fold values, normalized to CSPG4-CAR T cells, for five different donors from two individual experiments. **(B)** Integrated intensity of GFP$^+$ CD20-CCR_CSPG4-CAR T cells after 94 hours co-culture with UTD (untransduced) T cells, CSPG4-CAR T cells, or CD20-CCR_CSPG4-CAR T cells at an E:T ratio of 1:1. Displayed are mean and individual values (± SD). Significance was determined using ordinary one-way ANOVA (ns, not significant; *p ≤ 0.05, ***p ≤ 0.001). **(C)** UTD T cells and CD20-CCR_CSPG4-CAR T cells were co-cultured for 94 hours with varying percentages of Mel526^{WT} and Mel526^{CD20} target cells at an E:T ratio of 2:1. Displayed is the integrated intensity of GFP$^+$ target cells, showing mean and individual values of three different donors (± SEM). Significance was determined using ordinary one-way ANOVA (*p ≤ 0.05, ***p ≤ 0.001). **(D)** Cytokine concentrations in the supernatant were determined after 24 hours.

minimized risk for on-target/off-tumor toxicity, can be recovered in a target-specific manner by co-expression of the CD20-targeting CCR-(4-1BB_4-1BB). To assess whether this boosting effect through the CCR in this artificial system is dependent on the CCR-target antigen level, we co-cultured CSPG4-CAR_CD20-CCR T cells with CSPG4$^+$ Mel526^{WT} target cells and spiked in defined percentages of CD20-expressing CSPG4$^+$ Mel526^{CD20} cells. This titration experiment, which is especially relevant in case of reduced CCR-target antigen availability, revealed that only 10% of CCR antigen expressing target cells were already sufficient to significantly induce lysis of CSPG4$^+$ target cells with CSPG4-CAR_CD20-CCR T cells in a dose-dependent manner. The higher the frequency of CD20$^+$ cells, the stronger the CAR-induced cytotoxicity and clearance of Mel526 cells (Figure 3C).

Consistently, engagement of CD20 via the CCR was required for full cytokine secretion, shown by the dose-dependent increase in GM-CSF, IFN-γ, IL-2 and TNF-α in the supernatant after 24 hours of co-culture (Figure 3D).

Considering this relatively low CCR-activation threshold and the potential on-target/off-target toxicity against CSPG4^{low}-expressing healthy cells through CD20^{+} bystander cells, we performed a side-by-side comparison of CSPG4-CAR_CD20-CCR T cells co-cultured with either CSPG4^{high} or CSPG4^{low} target cells (exemplarily shown in Figures S2A–C). As hypothesized, we observed that co-culture with CSPG4^{low} A-431 cells (in presence of CCR-stimulating JeKo-1^{WT} cells) did not induce proliferation nor increase cytotoxicity of CSPG4-CAR_CD20-CCR T cells.

CCR boosts CAR *in vivo* and mediates robust tumor regression in a melanoma model

In order to study the cytolytic potential of CSPG4-CAR_CD20-CCR T cells *in vivo* with solid tumors, a melanoma xenograft model was established with CD20^{+} Mel526 tumor cells (Figure 4A). After tumor engraftment, mice were randomized according to tumor size. Subsequently, 1 × 10^{6} UTD T cells, CSPG4-CAR T cells, CD20-CCR T cells, or CSPG4-CAR_CD20-CCR T cells were injected intravenously (Figure 4B). In line with the *in vitro* findings, CSPG4 CAR T cells led to outgrowth of tumor cells, while tumor clearance was only observed in the group with CCR-expressing CSPG4-CAR

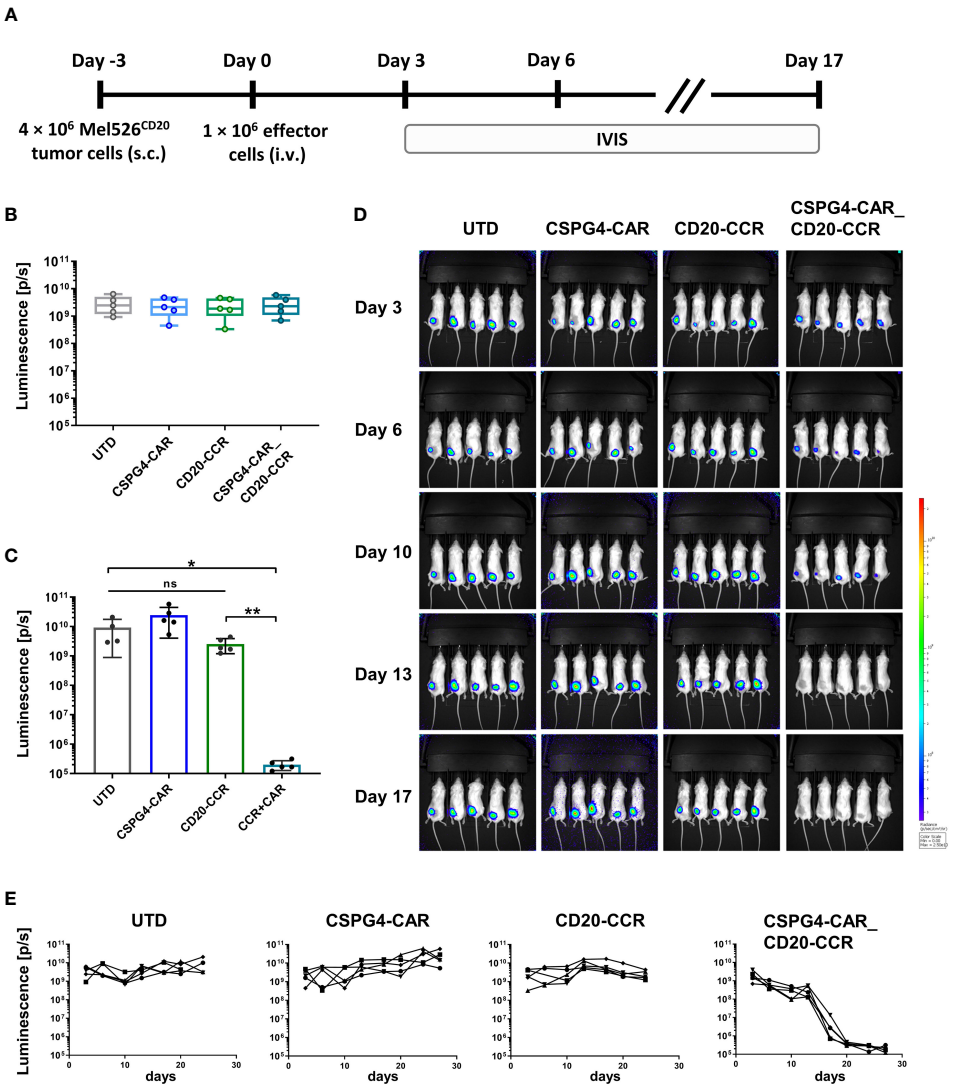

FIGURE 4
In vivo tumor clearance only successfully achieved upon treatment with CSPG4-CAR_CD20-CCR T cells. **(A)** Experimental timeline comparing antitumor efficacy of CSPG4-CAR, CD20-CCR and CSPG4-CAR_CD20-CCR in mice bearing Mel526FFluc_CD20_eGFP cells. **(B)** Randomization of different treatment groups with 5 mice each. **(C)** Endpoint-analysis of the anti-tumor reactivity of UTD, CSPG4-CAR, CD20-CCR or CSPG4-CAR_CD20-CCR was assessed using *in vivo* imaging systems (IVIS) measurement. **(D)** IVIS measurements displaying tumor burden on day 3, 6, 10, 13 and 17. **(E)** Luminescence measured over the course of the whole study displayed for mouse treated with UTD T cells, CSPG4-CAR T cells, CD20-CCR T cells and CSPG4-CAR_CD20-CCR co-expressing T cells. Significance was determined using nonparametric Mann-Whitney t-test (ns = not significant, *p ≤ 0.05, **p ≤ 0.01).

T cells (Figures 4C–E). Mice treated with CSPG4-CAR T cells showed continuous outgrowth of the engrafted melanoma cells, similar as observed for groups treated with UTD or CCR-only T cells. In summary, this study showed that the moderate cytotoxic potential of the low-affinity antibody-derived CSPG4-CAR could successfully be recovered *in vitro* as well as *in vivo* by co-expression of a 4-1BB_4-1BB-costimulated CD20-CCR.

Discussion

The rather poor prognosis for patients with metastatic malignant melanoma is associated with a median survival of less than one year (16, 27). CSPG4-targeting adoptive T cell therapy, however, might represent a powerful treatment option, especially as CSPG4 is not only expressed in primary but also metastatic melanoma cells (11, 13). Moreover, CSPG4 was also found in a broad range of other malignancies such as triple-negative breast cancer, various types of gliomas, head and neck squamous cell carcinoma, soft-tissue sarcomas, tumor-associated vasculature and also leukemia (9, 10). This is in line with the reported role of CSPG4 in several cancer-associated pathways, including angiogenesis, dissemination, metastasis, proliferation and survival (13, 14). It is important to keep in mind that low levels of CSPG4 were also found in non-malignant tissue, which might cause severe side effects due to on-target/off-tumor toxicity (28–30). For this reason, our approach was focused on combining a low-affinity CSPG4-targeting CAR, which by itself only showed weak anti-tumor cytotoxicity, with an anti-CD20 chimeric co-stimulatory co-receptor (CCR). As hypothesized, CSPG4-expressing tumor cells were only efficiently lysed when both CCR and CAR engaged their target antigens simultaneously. Interestingly, boosting of the CAR T cell response was not only observed upon cis activation (both targets expressed on same tumor cell) but also in case of trans activation (targets on two different tumor cells). This is a very promising finding for clinical application as targeting of $CSPG4^+$ primary and metastatic melanoma cells can be facilitated via trans stimulation through abundantly available bystanding or even tumor-infiltrating CD20-expressing B cells (31). Additionally, boosting through cis activation allows the targeting of tumor-initiating $CD20^+$ $CSPG4^+$ melanoma cancer stem cells, which is supported by the clinical success using the anti-CD20 antibody Rituximab for treatment of melanoma (25, 26, 32–34).

We demonstrated that the co-expression of a CD20-CCR, encoding two sequential 4-1BB co-stimulatory domains, led to significantly increased target cell-specific cytotoxicity of the CSPG4-CAR *in vitro* and *in vivo*. Although the superiority of this CCR was not very pronounced, aiming to ensure survival and persistency of our gene-engineered T cells, we specifically focused on a strong 4-1BB signaling which is known – in contrast to CD28 signaling - to specifically upregulate transcription factors associated with memory differentiation and anti-apoptotic pathways (35). The melanoma xenograft model with $CD20^+$ Mel526 tumor cells clearly demonstrated that treatment with CSPG4-CAR T cells led to continuous tumor outgrowth, while robust tumor regression was only achieved upon treatment with dual-specific CSPG4-CAR_CD20-CCR T cells. This again substantiates the need for simultaneous target antigen engagement through both CAR and CCR, which highly increases the safety and tumor cell restriction of CSPG4-targeted T cell therapy. Aiming for the same goal of reducing the risk for on-target/off-tumor toxicity, Kloss *et al.* showed that also a first-generation CD19-CAR can be functionally rescued through combination with a PSMA-targeting CCR (36). While validating this finding for the target antigen CSPG4, we were also able to successfully extend the understanding by analyzing multiple CCR molecules with various co-stimulatory domains, the influence of the CCR target antigen level, and the applicability of this combinatorial approach in cis and in trans. In this context, the finding that even low frequencies of CCR antigen-expressing target cells were sufficient to significantly enhance the cytolytic capacity is of particular importance for potential clinical applications, where the CCR target might be the limiting factor. Further studies, though, are required to assess whether this low CCR-activation threshold – despite the combination with low-affinity antibody-derived CARs - would then also increase the risk for on-target/off-tumor toxicity. In-depth validation is required to assess the extent of bystander lysis of $CD20^+$ cells. However, since the CD20-targeting CCR by itself was shown to be non-functional, only minor depletion of non-malignant bystander B cells is expected, while the side effects should be clinically tolerable, especially considering the success of leukemia or lymphoma treatment with CD20- or CD19-targeting CAR T cells (37).

A clinical study using Her2-targeting CAR T cells drastically demonstrated the necessity to increase safety of CAR T cell therapies, as already low levels of target antigen expression on healthy tissue led to on-target/off-tumor toxicity causing lethal adverse effects (7). Novel technologies such as the adCAR, UniCAR, or inducible CAR allow for temporal "on-/off-switching" and a controllable CAR T cell response (28–30). However, all of those systems require regular re-injection of the respective stimulus and the clinical long-term efficacy still needs to be evaluated. Wiesinger *et al.* used mRNA electroporation in order to achieve transient expression of the CSPG4-CAR and to minimize the risk for side effects in the clinical trial (38). Again, this approach necessitates complete tumor clearance and might have insufficient long-term effect to prevent recurrence. Another approach for safer adoptive cell therapy is based on Boolean logic AND gates, in which an affinity-reduced first-generation CAR containing only the CD3ζ activation signal is combined with a CCR providing the co-stimulatory domain (39). Similar to this, it was also our goal to achieve a perfectly calibrated and balanced split antigen recognition in order to only induce full T cell response, when both CAR and CCR are stimulated simultaneously. However, our CAR is not necessarily dependent on CCR stimulation and shows functionality by itself. Despite of the very low potency of our CAR, this might still represent a safety problem, which needs to be clinically evaluated. The use of a second-generation CAR with reduced potency offers the advantage of minimizing the risk of antigen escape, whereas target cell lysis is only expected in malignant tissues with sufficient CSPG4 expression levels to induce CAR-T cell activation.

In regard to clinical applicability, we also demonstrated that T cells expressing CAR and CCR can be successfully manufactured by

using only one polycistronic lentiviral vector, even showing slightly higher anti-tumor activity compared to co-transduction. In order to apply our approach to other clinically relevant settings, it would also be interesting to study the functionality of CAR T cells co-expressing a CCR, targeting the tumor microenvironment. Especially in the context of solid tumors, various studies demonstrated the beneficial effect of CARs targeting components of the TME such as TGF-β (15) or fibroblast activating protein (40–42). Moreover, the efficacy and functional persistence of CSPG4-CAR_CD20-CCR T cells could further be amplified through combination with ICB, especially considering its great clinical progress in treatment of advanced melanoma (43) and the encouraging results of combining ICB and adoptive cell therapy observed in preclinical and clinical studies (44–47).

Finally, our *in vitro* and *in vivo* findings confirm that co-expression of a CD20-directed CCR successfully potentiated the anti-tumor cytotoxicity of CSPG4-CAR T cells in a CCR- and CAR-target antigen-dependent manner. In light of the fact that this boosting effect was achieved upon cis and trans activation, this approach opens a novel therapeutic window by targeting not only primary and metastatic tumor cells but also tumor-promoting melanoma cancer stem cells (25, 26, 32–34, 48). However, this combinatorial adoptive T cell-based approach might be of particular relevance in case of advanced late-stage melanomas, when traditional therapy such as chemotherapy, radiotherapy or surgical removal are ineffective (17, 23).

Conclusion

We showed that our CD20-targeting CCRs enhance the cytolytic potential and polyfunctionality of the co-expressed CSGP4-CAR, not only upon a simultaneous activation but also in a CCR-target antigen-dependent manner. Depending on target antigen expression, safety and toxicity might vary for different CCR and CAR combinations and need to be evaluated individually. However, our data suggests that especially the combination of CCRs with low-affinity antibody-derived CARs, which depend on high-level target antigen expression and consequently spare basal tissues, represents a promising therapeutic concept for the treatment of a wide range of solid tumors.

Methods

Unless mentioned to the contrary, kits were used according to the manufacturer´s protocol.

Generation of engineered cell lines

Mel526 cells (CVCL_8051) were lentivirally transduced to express a PGK promotor-driven construct encoding FFluc_CD20_eGFP. After 72 hours, $CD20^+$ cells were enriched using anti-CD20 Biotin (Miltenyi Biotec, #130-113-372) and anti-Biotin-Microbeads (Miltenyi Biotec, #130-105-637) and LS columns (Miltenyi Biotec, #130-122-729). Subsequently, cells were seeded in a limiting dilution for 2 weeks. Individual clones were analyzed using flow cytometry and frozen. Mel526FFluc_CD20_eGFP cells are referred to as $Mel526^{CD20}$.

JeKo-1 CD20 knock-out cells ($JeKo\text{-}1^{CD20KO}$) were generated as previously described (49). In brief, 1 µg gRNAs targeting 5´-CACGCAAAGCTTCTTCATGA-3´ (Metabion) were co-transfected with 1 µg Cas9 (Integrated DNA Technologies, Coralville, USA) encoding plasmid using Nucleofector 2b Device and the Cell line Nucleofector Kit V VCA-1003 (Lonza Group, Basel, Switzerland). After seven days, $CD20^+$ cells were depleted using LD columns (Miltenyi Biotec, #130-042-901) and anti-CD20 Biotin (Miltenyi Biotec, #130-113-372) and anti-Biotin-Microbeads (Miltenyi Biotec, #130-105-637). Hereafter, 0.3 cells/well were seeded in a 96-well culture plate (Corning, #3598) and a single cell expansion was performed for two weeks. $JeKo\text{-}1^{CD20KO}$ cells were analyzed by flow cytometry and frozen.

Cloning and generation of engineered CSPG4-CAR, CD20-CCR and CSPG4-CAR_CD20-CCR CAR T cells

The CSPG4-specific second-generation CAR sequence encodes a 225.28s-derived scFv linked to an IgG4 Hinge_CH2_CH3 spacer, a 4-1BB co-stimulatory, CD3ζ signaling domain and a P2A-connected ΔLNGFR. The CD20-directed CCR library contained a Leu-16-derived scFv, a spacer domain, different combinations of 4-1BB and CD28 as co-stimulatory domains and P2A-linked ΔEGFR. In the PGK-promotor-driven construct encoding CCR as well as CAR, the CCR-(4-1BB_4-1BB) was P2A element-linked to the CSPG4-CAR followed by a T2A element-linked ΔLNGFR.

T cells were isolated from healthy donor-derived Buffy coats using the PAN T cell isolation Kit (Miltenyi Biotec, #130-096-535). T cells were activated using T Cell TransAct™, human (Miltenyi Biotec, #130-111-160). After 24 hours, T cells were transduced with lentiviral particles and cultured in TexMACS (Miltenyi Biotec, #130-097-196), supplemented with 12.5 ng/ml human IL-7 (Miltenyi Biotec, #130-095-367) and human IL-15 (Miltenyi Biotec, #130-095-760), respectively. CAR and/or CCR (co-) expressing T cells were enriched after 7 days via their co-expressed marker genes ΔLNGFR and ΔEGFR using either anti-ΔLNGFR-Biotin (Miltenyi Biotec, #130-112-797) anti-Biotin MultiSort-MB Kit (Miltenyi Biotec, #130-091-256) or anti-ΔEGFR-PE (Miltenyi Biotec, #130-115-505) and anti-PE-MB (Miltenyi Biotec, #130-105-639), respectively.

Functionality testing of engineered T cells

Cytolytic activity was assessed by co-culturing either untransduced or modified effector cells with 1×10^4 GFP^+ target cells. Trans stimulation was facilitated through co-culture with a mixture of $Mel526^{WT}$ and either $CD20^+$ $JeKo\text{-}1^{WT}$ or $CD20^-$ $JeKo\text{-}1^{CD20KO}$ cells. Cis stimulation was achieved through co-culture with CD20-transduced $Mel526^{CD20}$ target cells. Effector-to-target ratios and time of co-culture are indicated in the figure legends. All

experiments were performed using technical duplicates. Specific killing was calculated based on the number of residual target cells measured by flow cytometry using MACSQuant Analyzer 10 (Miltenyi Biotec, Bergisch Gladbach, Germany) or using the IncuCyte S3 Live-Cell Analysis Systems (Essen BioScience, Michigan, USA), determining the integrated intensity of GFP^+ target cells in GCU x µm/well. Cytokine concentrations were determined in supernatant after 24 hours of co-culture using the human MACSPlex Cytokine 12 Kit (Miltenyi Biotec, #130-099-169).

All experiments performed on animals follow institutional guidelines and regulations. 6- to 8-week-old female NOD.Cg-PrkdcscidIl2rgtm1Wjl/SzJ NSG mice were purchased from Charles River and kept under specific pathogen-free conditions. Mice were kept at 12:12 light/dark cycles with unrestricted food and water supply. 4×10^6 $Mel526^{CD20}$ cells were injected subcutaneously in the flanks. When a tumor size of 0.5 cm^2 was reached, mice were randomized into treatment groups, each containing 5 mice. 1×10^6 effector cells were infused intravenously (i.v.). Tumor burden was monitored twice a week using an *in vivo* Imaging System IVIS Lumina III (Perkin Elmer, Waltham, USA) after intraperitoneal D-Luciferin (Gold Biotechnology, #LUCK-1G) injection.

Statistical analysis

Statistical significance was determined using GraphPad Prism version 8.1.2. The used test is described in the figure legends. The ρ-values are indicated by following criteria: ns, not significant; *ρ ≤ 0.05, **ρ ≤ 0.01, ***ρ ≤ 0.001, ****ρ ≤ 0.0001).

Data availability statement

The raw data supporting the conclusions of this article will be made available by the authors, without undue reservation.

Ethics statement

Ethical approval was not required for the studies involving humans because Buffy coats were provided by Klinikum Dortmund with written informed consent before sample collection. The studies were conducted in accordance with the local legislation and institutional requirements. The human samples used in this study were acquired from Buffy coats were provided by Klinikum Dortmund with written informed consent before sample collection. Written informed consent to participate in this study was not required from the participants or the participants' legal guardians/next of kin in accordance with the national legislation and the institutional requirements. The animal study was approved by Landesamt für Natur, Umwelt und Verbraucherschutz Nordrhein-Westfalen. The study was conducted in accordance with the local legislation and institutional requirements.

Author contributions

DL and AK conceptualized the study; KT, NW, VH, CB, SL, FE and DL generated and analyzed data; AK supervised defined aspects of the project; KT and DL wrote a first draft of the manuscript. TS reviewed and edited the manuscript. All authors contributed to the article and approved the submitted version.

Acknowledgments

The authors acknowledge the technical assistance of Sandra Dapa and Janina Brauner as well as the scientific advice of Jörg Mittelstät and Ian Johnston. The authors also thank Xueting Wang for revising and editing the manuscript.

Conflict of interest

KT, NW, VH, CB, SL, FE, AK, TS and DL are employees of Miltenyi Biotec B.V. & Co. KG.

Publisher's note

Supplementary material

The Supplementary Material for this article can be found online at: https://www.frontiersin.org/articles/10.3389/fimmu.2023.1178060/full#supplementary-material

SUPPLEMENTARY FIGURE 1
Co-expression of CSPG4-CAR and CD20-CCRs, containing various co-stimulatory domains, significantly increases cytokine release upon trans activation. **(A)** T cells were lentivirally transduced with a CSPG4-CAR, CD20-CCRs (different variants with alternative endodomains displayed in parenthesis) or a combination of both CSPG4-CAR and CD20-CCR (blue bars). The level of (co-)expression is shown pre- and post-enrichment. CAR and CCR expression was determined via co-expression of surface markers ΔLNGFR and ΔEGFR, respectively. Exemplarily shown are mean and individual values of two different donors (± SD). **(B, C)** Dual-specific T cells co-expressing CSPG4-CAR and CD20-CCR and T cells only expressing CD20-CCR were co-cultured with $CSPG4^+$ Mel526 with our without $CD20^+$ $JeKo\text{-}1^{wt}$ cells. Displayed is the IFN-γ secretion after 24 hours of co-culture. Significance was determined using ordinary one-way ANOVA (ns, not significant; *ρ ≤ 0.05, **ρ ≤ 0.01, ***ρ ≤ 0.001, ****ρ ≤ 0.0001). Shown are mean and individual values of two different donors (± SD). **(D, E)** Dual-specific T cells co-expressing CSPG4-CAR and CD20-CCR and T cells only expressing CD20-CCR or CSPG4-CAR were co-cultured with $CSPG4^+$

Mel526 with our without CD20^{+} JeKo-1^{wt} cells. Displayed is the TNF-α secretion after 24 hours of co-culture. Box and whiskers plots display values of two different donors. **(F)** CSPG4-CAR T cells, either co-expressing 4-1BB_4-1BB-co-stimulated CCR (green bars) or CD28_4-1BB-co-stimulated CCR (blue bars), were co-cultured with CSPG4^{+} Mel526 and CD20^{+} JeKo-1^{WT} (trans) or CD20^{+} CSPG4^{+} Mel526^{CD20} (cis). Shown are mean and individual values of two different donors (± SD).

SUPPLEMENTARY FIGURE 2

Proliferative capacity and cytotoxicity of CSPG4-CAR_CD20-CCR T cells upon co-culture with CSPG low-expressing target cells. **(A)** CSPG4 MFI of SupT1 (negative control), A-431 (CSPG4^{low}) and Mel526^{WT} (CSPG4^{high}) cells. **(B)** Proliferation of CSPG4-CAR_CD20-CCR T cells upon 5 days of co-culture with CSPG4^{low} A-431 or CSPG4^{high} Mel526 target cells, both with or without CCR-stimulating CD20^{+} JeKo-1 cells at an E:T ratio of 1:1. Shown are mean values of two donors (± SD), normalized to proliferation of non-stimulated effector cells. **(C)** CSPG4-CAR_CD20-CCR T cells co-cultured with either A-431 (CSPG4^{low}) or Mel526 (CSPG4^{high}) cells (in presence of CD20^{+} JeKo-1 cells). Shown are mean values of two donors (± SD) and x-fold change of target cell lysis after 24 hours normalized to start of co-culture.

SUPPLEMENTARY FIGURE 3

Mel526^{WT} target cell lysis upon co-culture with CSPG4-CAR_CD20-CCR T cells in presence of JeKo-1^{WT} or JeKo-1^{CD20} cells at an E:T ratio of 5:1. Data shows mean values of two donors. Integrated intensity of GFP^{+} Mel526^{WT} target cells was determined over the course of 64 hours of co-culture.

References

1. Maude SL, Frey N, Shaw PA, Aplenc R, Barrett DM, Bunin NJ, et al. Chimeric antigen receptor T cells for sustained remissions in leukemia. *N Engl J Med* (2014) 371 (16):1507–17. doi: 10.1056/NEJMoa1407222

2. Davila ML, Riviere I, Wang X, Bartido S, Park J, Curran K, et al. Efficacy and toxicity management of 19-28z CAR T cell therapy in B cell acute lymphoblastic leukemia. *Sci Transl Med* (2014) 6(224):224ra25. doi: 10.1126/scitranslmed.3008226

3. Brentjens RJ, Davila ML, Riviere I, Park J, Wang X, Cowell LG, et al. CD19-targeted T cells rapidly induce molecular remissions in adults with chemotherapy-refractory acute lymphoblastic leukemia. *Sci Transl Med* (2013) 5(177):177ra38. doi: 10.1126/scitranslmed.3005930

4. Mak TW, Saunders ME, Jett BD eds. Chapter 20 - hematopoietic cancers. In: *Primer to the immune response*, *2nd ed.*. Boston: Academic Cell. p. 553–85.

5. Hou AJ, Chen LC, Chen YY. Navigating CAR-T cells through the solid-tumour microenvironment. *Nat Rev Drug Discov* (2021) 20(7):531–50. doi: 10.1038/s41573-021-00189-2

6. Huynh D, Winter P, Märkl F, Endres S, Kobold S. Beyond direct killing—novel cellular immunotherapeutic strategies to reshape the tumor microenvironment. *Semin Immunopathol* (2022) 45(2):215–27. doi: 10.1007/s00281-022-00962-4

7. Morgan RA, Yang JC, Kitano M, Dudley ME, Laurencot CM, Rosenberg SA. Case report of a serious adverse event following the administration of T cells transduced with a chimeric antigen receptor recognizing ERBB2. *Mol Ther* (2010) 18(4):843–51. doi: 10.1038/mt.2010.24

8. Wilson BS, Imai K, Natali PG, Ferrone S. Distribution and molecular characterization of a cell-surface and a cytoplasmic antigen detectable in human melanoma cells with monoclonal antibodies. *Int J Cancer* (1981) 28(3):293–300. doi: nbsp;10.1002/ijc.2910280307

9. Harrer DC, Dörrie J, Schaft N. CSPG4 as target for CAR-T-cell therapy of various tumor entities-merits and challenges. *Int J Mol Sci* (2019) 20(23):5942. doi: 10.3390/ijms20235942

10. Beard RE, Zheng Z, Lagisetty KH, Burns WR, Tran E, Hewitt SM, et al. Multiple chimeric antigen receptors successfully target chondroitin sulfate proteoglycan 4 in several different cancer histologies and cancer stem cells. *J ImmunoTher Cancer* (2014) 2(1):25. doi: 10.1186/2051-1426-2-25

11. Geldres C, Savoldo B, Hoyos V, Caruana I, Zhang M, Yvon E, et al. T lymphocytes redirected against the chondroitin sulfate proteoglycan-4 control the growth of multiple solid tumors both in *vitro* and in vivo. *Clin Cancer Res* (2014) 20 (4):962–71. doi: 10.1158/1078-0432.CCR-13-2218

12. CheKenya M, Enger P, Thorsen F, Tysnes BB, Al-Sarraj S, Read TA, et al. The glial precursor proteoglycan, NG2, is expressed on tumour neovasculature by vascular pericytes in human Malignant brain tumours. *Neuropathol Appl Neurobiol* (2002) 28 (5):367–80. doi: 10.1046/j.1365-2990.2002.00412.x

13. Ilieva KM, Cheung A, Mele S, Chiaruttini G, Crescioli S, Griffin M, et al. Chondroitin sulfate proteoglycan 4 and its potential as an antibody immunotherapy target across different tumor types. *Front Immunol* (2018) 8. doi: 10.3389/fimmu.2017.01911

14. Tamburini E, Dallatomasina A, Quartararo J, Cortelazzi B, Mangieri D, Lazzaretti M, et al. Structural deciphering of the NG2/CSPG4 proteoglycan multifunctionality. *FASEB J* (2019) 33(3):3112–28. doi: 10.1096/fj.201801670R

15. Werchau N, Kotter B, Criado-Moronati E, Gosselink A, Cordes N, Lock D, et al. Combined targeting of soluble latent TGF-ß and a solid tumor-associated antigen with adapter CAR T cells. *Oncoimmunology* (2022) 11(1):2140534. doi: 10.1080/2162402X.2022.2140534

16. Franken MG, Leeneman B, Aarts MJB, van Akkooi ACJ, van den Berkmortel FWPJ, Boers-Sonderen MJ, et al. Trends in survival and costs in metastatic melanoma in the era of novel targeted and immunotherapeutic drugs. *ESMO Open* (2021) 6 (6):100320. doi: 10.1016/j.esmoop.2021.100320

17. Davis LE, Shalin SC, Tackett AJ. Current state of melanoma diagnosis and treatment. *Cancer Biol Ther* (2019) 20(11):1366–79. doi: 10.1080/15384047.2019.1640032

18. Rager T, Eckburg A, Patel M, Qiu R, Gantiwala S, Dovalovsky K, et al. Treatment of metastatic melanoma with a combination of immunotherapies and molecularly targeted therapies. *Cancers (Basel)* (2022) 14(15):3779. doi: 10.3390/cancers14153779

19. Hodi FS, O'Day SJ, McDermott DF, Weber RW, Sosman JA, Haanen JB, et al. Improved survival with ipilimumab in patients with metastatic melanoma. *N Engl J Med* (2010) 363(8):711–23. doi: 10.1056/NEJMoa1003466

20. Robert C, Thomas L, Bondarenko I, O'Day S, Weber J, Garbe C, et al. Ipilimumab plus dacarbazine for previously untreated metastatic melanoma. *N Engl J Med* (2011) 364(26):2517–26. doi: 10.1056/NEJMoa1104621

21. SChadendorf D, Hodi FS, Robert C, Weber JS, Margolin K, Hamid O, et al. Pooled analysis of long-term survival data from phase II and phase III trials of ipilimumab in unresectable or metastatic melanoma. *J Clin Oncol: Off J Am Soc Clin Oncol* (2015) 33(17):1889–94. doi: 10.1200/JCO.2014.56.2736

22. Wolchok JD, Chiarion-Sileni V, Gonzalez R, Grob JJ, Rutkowski P, Lao CD, et al. Long-term outcomes with nivolumab plus ipilimumab or nivolumab alone versus ipilimumab in patients with advanced melanoma. *J Clin Oncol* (2022) 40(2):127–37. doi: 10.1200/JCO.21.02229

23. Razavi A, Keshavarz-Fathi M, Pawelek J, Rezaei N. Chimeric antigen receptor T-cell therapy for melanoma. *Expert Rev Clin Immunol* (2021) 17(3):209–23. doi: 10.1080/1744666X.2021.1880895

24. Vergilis IJ, Szarek M, Ferrone S, Reynolds SR. Presence and prognostic significance of melanoma-associated antigens CYT-MAA and HMW-MAA in serum of patients with melanoma. *J Invest Dermatol* (2005) 125(3):526–31. doi: 10.1111/j.0022-202X.2005.23798.x

25. Pinc A, Somasundaram R, Wagner C, Hörmann M, Karanikas G, Jalili A, et al. Targeting CD20 in melanoma patients at high risk of disease recurrence. *Mol Ther* (2012) 20(5):1056–62. doi: 10.1038/mt.2012.27

26. Schmidt P, Kopecky C, Hombach A, Zigrino P, Mauch C, Abken H. Eradication of melanomas by targeted elimination of a minor subset of tumor cells. *Proc Natl Acad Sci USA* (2011) 108(6):2474–9. doi: 10.1073/pnas.1009069108

27. Hodi FS, O'Day SJ, McDermott DF, Weber RW, Sosman JA, Haanen JB, et al. Improved survival with ipilimumab in patients with metastatic melanoma. *N Engl J Med* (2010) 363(8):711–23. doi: 10.1056/NEJMoa1003466

28. Seitz CM, Mittelstaet J, Atar D, Hau J, Reiter S, Illi C, et al. Novel adapter CAR-T cell technology for precisely controllable multiplex cancer targeting. *OncoImmunology* (2021) 10(1):2003532. doi: 10.1080/2162402X.2021.2003532

29. Bachmann M. The UniCAR system: A modular CAR T cell approach to improve the safety of CAR T cells. *Immunol Lett* (2019) 211:13–22. doi: 10.1016/j.imlet.2019.05.003

30. Zhang R-Y, Wei D, Liu Z-K, Yong Y-L, Wei W, Zhang Z-Y, et al. Doxycycline inducible chimeric antigen receptor T cells targeting CD147 for hepatocellular carcinoma therapy. Frontiers in cell and developmental biology. *Front Cell Dev Biol* (2019) 7:233. doi: 10.3389/fcell.2019.00233

31. Willsmore ZN, Harris RJ, Crescioli S, Hussein K, Kakkassery H, Thapa D, et al. B cells in patients with melanoma: implications for treatment with checkpoint inhibitor antibodies. *Front Immunol* (2020) 11:622442. doi: 10.3389/fimmu.2020.622442

32. Fang D, Nguyen TK, Leishear K, Finko R, Kulp AN, Hotz S, et al. A tumorigenic subpopulation with stem cell properties in melanomas. *Cancer Res* (2005) 65(20):9328–37. doi: 10.1158/0008-5472.CAN-05-1343

33. Schlaak M, Schmidt P, Bangard C, Kurschat P, Mauch C, Abken H. Regression of metastatic melanoma in a patient by antibody targeting of cancer stem cells. *Oncotarget* (2012) 3(1):22–30. doi: 10.18632/oncotarget.437

34. Yin Q, Shi X, Lan S, Jin H, Wu D. Effect of melanoma stem cells on melanoma metastasis. *Oncol Lett* (2021) 22(1):566. doi: 10.3892/ol.2021.12827

35. Long AH, Haso WM, Shern JF, Wanhainen KM, Murgai M, Ingaramo M, et al. 4-1BB costimulation ameliorates T cell exhaustion induced by tonic signaling of chimeric antigen receptors. *Nat Med* (2015) 21(6):581–90. doi: 10.1038/nm.3838

36. Kloss CC, Condomines M, Cartellieri M, Bachmann M, Sadelain M. Combinatorial antigen recognition with balanced signaling promotes selective tumor eradication by engineered T cells. *Nat Biotechnol* (2013) 31(1):71–5. doi: 10.1038/nbt.2459

37. Kalos M, Levine BL, Porter DL, Katz S, Grupp SA, Bagg A, et al. T cells with chimeric antigen receptors have potent antitumor effects and can establish memory in patients with advanced leukemia. *Sci Transl Med* (2011) 3(95):95ra73. doi: 10.1126/scitranslmed.3002842

38. Wiesinger M, März J, Kummer M, Schuler G, Dörrie J, Schuler-Thurner B, et al. Clinical-Scale Production of CAR-T Cells for the Treatment of Melanoma Patients by mRNA Transfection of a CSPG4-Specific CAR under Full GMP Compliance. *Cancers* (2019) 11(8):1198. doi: 10.3390/cancers11081198

39. Savanur MA, Weinstein-Marom H, Gross G. Implementing logic gates for safer immunotherapy of cancer. *Front Immunol* (2021) 12. doi: 10.3389/fimmu.2021.780399

40. Wang LC, Lo A, Scholler J, Sun J, Majumdar RS, Kapoor V, et al. Targeting fibroblast activation protein in tumor stroma with chimeric antigen receptor T cells can inhibit tumor growth and augment host immunity without severe toxicity. *Cancer Immunol Res* (2014) 2(2):154–66. doi: 10.1158/2326-6066.CIR-13-0027

41. Pircher M, Schuberth P, Gulati P, Sulser S, Weder W, Curioni A, et al. FAP-specific re-directed T cells first in-man study in Malignant pleural mesothelioma: experience of the first patient treated. *J Immunother Cancer* (2015) 3(Suppl 2):P120. doi: 10.1186/2051-1426-3-S2-P120

42. Adusumilli PS, Zauderer MG, Rivière I, Solomon SB, Rusch VW, O'Cearbhaill RE, et al. A phase I trial of regional mesothelin-targeted CAR T-cell therapy in patients with Malignant pleural disease, in combination with the anti-PD-1 agent pembrolizumab. *Cancer Discov* (2021) 11(11):2748–63. doi: 10.1158/2159-8290.CD-21-0407

43. Huang AC, Zappasodi R. A decade of checkpoint blockade immunotherapy in melanoma: understanding the molecular basis for immune sensitivity and resistance. *Nat Immunol* (2022) 23(5):660–70. doi: 10.1038/s41590-022-01141-1

44. Cherkassky L, Morello A, Villena-Vargas J, Feng Y, Dimitrov DS, Jones DR, et al. Human CAR T cells with cell-intrinsic PD-1 checkpoint blockade resist tumor-mediated inhibition. *J Clin Invest* (2016) 126(8):3130–44. doi: 10.1172/JCI83092

45. Wang H, Kaur G, Sankin AI, Chen F, Guan F, Zang X. Immune checkpoint blockade and CAR-T cell therapy in hematologic Malignancies. *J Hematol Oncol* (2019) 12(1):59. doi: 10.1186/s13045-019-0746-1

46. Liu X, Zhang Y, Cheng C, Cheng AW, Zhang X, Li N, et al. CRISPR-Cas9-mediated multiplex gene editing in CAR-T cells. *Cell Res* (2017) 27(1):154–7. doi: 10.1038/cr.2016.142

47. Li AM, Hucks GE, Dinofia AM, Seif AE, Teachey DT, Baniewicz D, et al. Checkpoint inhibitors augment CD19-directed chimeric antigen receptor (CAR) T cell therapy in relapsed B-cell acute lymphoblastic leukemia. *Blood* (2018) 132:556. doi: 10.1182/blood-2018-99-112572

48. Price MA, Colvin Wanshura LE, Yang J, Carlson J, Xiang B, Li G, et al. CSPG4, a potential therapeutic target, facilitates Malignant progression of melanoma. *Pigment Cell melanoma Res* (2011) 24(6):1148–57. doi: 10.1111/j.1755-148X.2011.00929.x

49. Cong L, Ran FA, Cox D, Lin S, Barretto R, Habib N, et al. Multiplex genome engineering using CRISPR/Cas systems. *Sci (New York NY)* (2013) 339(6121):819–23. doi: 10.1126/science.1231143

frontiers | Frontiers in Immunology

TYPE Original Research
PUBLISHED 22 November 2023
DOI 10.3389/fimmu.2023.1268090

OPEN ACCESS

EDITED BY
Christoph Schaniel,
Icahn School of Medicine at Mount Sinai, United States

REVIEWED BY
Ezhilarasi Chendamarai,
Washington University in St. Louis, United States
Fang-Min Zhong,
Second Affiliated Hospital of Nanchang University, China
Marjanu Hikmah Elias,
Universiti Sains Islam Malaysia, Malaysia

*CORRESPONDENCE
Chao Lin
linch26@mail2.sysu.edu.cn
Bo Lu
lubo5@mail.sysu.edu.cn
Tian-Tian Sun
suntt6@mail.sysu.edu.cn

†These authors have contributed equally to this work

RECEIVED 27 July 2023
ACCEPTED 06 November 2023
PUBLISHED 22 November 2023

CITATION
Wang Y, Bin T, Tang J, Xu X-J, Lin C, Lu B and Sun T-T (2023) Construction of an acute myeloid leukemia prognostic model based on m6A-related efferocytosis-related genes. *Front. Immunol.* 14:1268090. doi: 10.3389/fimmu.2023.1268090

Construction of an acute myeloid leukemia prognostic model based on m6A-related efferocytosis-related genes

Ying Wang[1†], Ting Bin[1†], Jing Tang[1†], Xiao-Jun Xu[1], Chao Lin[2*], Bo Lu[1*] and Tian-Tian Sun[1*]

[1]Department of Haematology. The Seventh Affiliated Hospital, Sun Yat-Sen University, Shenzhen, China, [2]Pediatric Hematology Laboratory, Division of Hematology/Oncology, Department of Pediatrics. The Seventh Affiliated Hospital, Sun Yat-Sen University, Shenzhen, China

Background: One of the most prevalent hematological system cancers is acute myeloid leukemia (AML). Efferocytosis-related genes (ERGs) and N6-methyladenosine (m6A) have an important significance in the progression of cancer, and the metastasis of tumors.

Methods: The AML-related data were collected from The Cancer Genome Atlas (TCGA; TCGA-AML) database and Gene Expression Omnibus (GEO; GSE9476, GSE71014, and GSE13159) database. The "limma" R package and Venn diagram were adopted to identify differentially expressed ERGs (DE-ERGs). The m6A related-DE-ERGs were obtained by Spearman analysis. Subsequently, univariate Cox and Least Absolute Shrinkage and Selection Operator (LASSO) were used to construct an m6A related-ERGs risk signature for AML patients. The possibility of immunotherapy for AML was explored. The pRRophetic package was adopted to calculate the IC50 of drugs for the treatment of AML. Finally, the expression of characterized genes was validated by quantitative reverse transcription-PCR (qRT-PCR).

Results: Based on m6A related-DE-ERGs, a prognostic model with four characteristic genes (UCP2, DOCK1, SLC14A1, and SLC25A1) was constructed. The risk score of model was significantly associated with the immune microenvironment of AML, with four immune cell types, 14 immune checkpoints, 20 HLA family genes and, immunophenoscore (IPS) all showing differences between the high- and low-risk groups. A total of 56 drugs were predicted to differ between the two groups, of which Erlotinib, Dasatinib, BI.2536, and bortezomib have been reported to be associated with AML treatment. The qRT-PCR results showed that the expression trends of DOCK1, SLC14A1 and SLC25A1 were consistent with the bioinformatics analysis.

Conclusion: In summary, 4 m6A related- ERGs were identified and the corresponding prognostic model was constructed for AML patients. This prognostic model effectively stratified the risk of AML patients.

KEYWORDS

acute myeloid leukemia, N6-methyladenosine, efferocytosis, prognostic risk model, bioinformatics, drug prediction

1 Introduction

Acute myeloid leukemia (AML) refers to a kind of malignant disease originated from haemopoietic stem cells and features clonal expansion of blasts of myeloid lineage under abnormal differentiation. Upon the proliferation of immature myeloid cells, immature progenitors (blasts) are accumulated and normal hemopoiesis is impaired, resulting in the occurrence of serious infection, anemia and hemorrhage (1). AML accounts for 1.3% of newly diagnosed cancer cases in the U.S (2). The rising AML incidences are partially a result of rising prevalence of AML related to therapy, because the primary malignancy of increasing numbers of cancer patients who received cytotoxic chemotherapy have been cured (3). AML is one of the most fatal type of hematologic malignancy, with the 5-year survival rate < 30%. Hence, new prognostic biomarkers shall be urgently identified for well monitoring patient outcomes as well as more deeply explaining the AML pathogenesis.

Recent researchers have identified reversible N6-methyladenosine (m6A) RNA methylation regulators as a new way to achieve the post-transcriptional regulation (4). Geneticists confirmed that m6A was methylated in eukaryotic messenger RNA (mRNA). RNA methylation modification takes up over 60% of all the RNA modifications, of which the representative type on higher biological mRNAs is the m6A RNA methylation (5). When m6A regulators are dysregulated, the cell reproductive capacity weakens, and the self-renewal capacity losses, together with developmental defects and apoptosis (6). m6A RNA methylation regulators play roles in the cancer occurrence and development, involving liver cancer (7, 8), glioblastoma (9), osteosarcoma (10), and colorectal cancer (11).

Macrophages critically impact the remodeling of tissues in normal physiology and the way inflammation and tissue injury are resolved (12). The key step in the resolution process lies in the elimination of apoptotic cells (ACs) (13). The elimination of apoptotic cells by professional and non-professional phagocytes, a process that is essential for maintaining tissue homeostasis called "efferocytosis" (13, 14). Such process has been informed in recent studies, together with the roles it plays in maintaining tissue homeostasis and repair as well as the organism health. Our study stresses on the mechanisms regarding efferocytosis (dying cell recognition, phagocytic engulfment and homeostatic resolution), as well as explains the resulting pathological and physiological consequences upon the abrogation of the efferocytosis process (13). As we all know, m6A regulates gene expression and thus cellular processes such as cellular self-renewal, differentiation, invasion, and apoptosis (15). For example, Mettl14-mediated m6A modification could induce apoptosis of spinal cord neurons in spinal cord injury by promoting miRNA translation (16). Apoptosis and its subsequent clearance by efferocytosis occur in virtually all tissues during development, homeostasis, and disease. However, the prognostic value of m6A-related efferocytosis related-genes (ERGs) in AML has not been systematically investigated.

AML is an aggressive blood cancer among adults, and the existing techniques fail to obviously improve most patients' survival rate. In the situation, it is necessary to find potential markers for enhancing AML patients' diagnosis, treatment and prognosis. According to previous studies, we inferred m6A RNA methylation regulators and efferocytosis were inextricably linked to the onset and progression of AML. Our study adopts AML-related data from public database and the comprehensive biological informatics approach for mining the m6A-related ERGs in AML. The prognostic model related to m6A and ERGs was constructed to predict the prognosis of the AML patients. In addition, the exploration of potential molecular mechanisms and therapeutic approaches will contribute to the treatment and prognosis of AML.

2 Materials and methods

2.1 Acquirement of the data of the AML patients

Bone marrow samples of 132 TCGA-AML (Illumina platform) patients were downloaded from the Cancer Genome Atlas (TCGA) (https://portal.gdc.cancer.gov/), and these AML patients with complete clinical information and survival data were used as the training set for the follow-up analysis. Three independent cohorts (GSE9476, GSE71014, and GSE13159) were acquired from the Gene Expression Omnibus (GEO) database (https://www.ncbi.nlm.nih.gov/geo/). The GSE71014 dataset (Illumina HumanHT-12 V4.0 expression beadchip) containing the RNA-seq and survival data of 104 AML patients was used as the validation set. The GSE9476 dataset (Affymetrix Human Genome U133A Array) contains 10 normal samples and 7 AML bone marrow samples for differential expression analysis. Peripheral blood samples from the GSE13159 dataset (Affymetrix Human Genome U133 Plus 2.0 Array) were excluded, and 73 normal samples and 501 AML bone marrow samples were obtained for expression validation of characteristic genes. Based on the previous paper, 74 efferocytosis-related genes (ERGs) were acquired (17, 18).

2.2 Identification of m6A -related differentially expressed ERGs

The data annotations in the GSE9476 dataset were performed based on the Symbol conversions corresponding to the chips in the GPL96 file. The raw count is converted to FPKM mainly by the following formula:

$$\mathrm{FPKM} = \mathrm{ExonMappedFragments} * 10^9 / \mathrm{TotalMappedFragments} * \mathrm{ExonLength}$$

CEL files were generated using MAS 5.0 software (Affymetrix) with target signals for probe sets scaled to 500. Log2 expression values for individual probe sets were generated from. CEL files via robust multi-array average (gcRMA). The "limma" package, a package for analyzing gene expression data generated by microarray or RNA-seq technology (19), was used to obtain the DEGs in the GSE9476 dataset. The screening criteria was: p value < 0.05 and $|\log_2\mathrm{FoldChange}| > 0.5$ (20, 21). The "VennDiagram" package (22) was applied to visualize the differentially expressed ERGs (DE-ERGs). Spearman and Wilcoxon.test

were applied to screen for m6A-related DE-ERGs (|cor| > 0.3 and p < 0.05). Prediction of miRNAs for m6A-related DE-ERGs was performed using TargetScan, miRTarBase, and starBase databases. Based on lncbase, starbase, and miRNet database, lncRNAs were subsequently predicted based on miRNAs common to the three databases. Cytoscape software was adopted to visualize the lncRNA-miRNA-mRNA network.

2.3 Acquirement of m6A-related DE-ERGs-related subtypes in the training set

Consensus Clustering, an unsupervised clustering method, can divide samples into subtypes based on different datasets, resulting the discovery of new disease subtypes. The R package "ConsensusClusterPlus" (23) was utilized to identify the subtypes based on the expression of m6A -related DE-ERGs. Additionally, the overall survival (OS) among different subtypes was explored by the "Survival" package (24). Enrichment pathways for inter-subtype differences were assessed using Gene Set Variation Analysis (GSVA) (25). The Cell-type identification by estimating relative subsets of RNA transcripts (CIBERSORT) algorithm (26) was utilized to analyze the abundance of immune cell infiltration for all samples between the subtypes. To examine the variations in immune cells between two subtypes, the Wilcoxon test was used.

2.4 Constructing a new AML prognostic risk model based on m6A -related DE-ERGs

The data of TCGA-AML were transformed based on the hg38 human reference genome. After transforming the data in the form of count into the form of FPKM, the FPKM was then $\log_2$(fpkm+1) computed to get the final FPKM value, which was our normalization method. By using univariate Cox analysis of m6A -related DE-ERGs in the TCGA-AML dataset, the prognosis-related genes were acquired (P < 0.05). Subsequently, the most predictive characteristic genes were identified by the least absolute shrinkage and selection operator (LASSO) (27). Subsequently, the risk score of each AML patient was calculated based on the formula:

$$\text{Riskscore} = \sum_1^n coef(gene_i) * expr(gene_i)$$

Based on the median risk score, the AML patients were divided into two groups. The difference in OS between the two groups was then displayed using Kaplan-Meier (KM) curves. The "survROC" (28) was applied to display the receiver operating characteristic (ROC) curves to perform an assessment of the prognostic capability of the prognostic risk model. At last, the stability of this prognostic risk model was investigated in the external GSE71014 dataset. Meanwhile, the wilcoxon test was applied to evaluate the expression of characteristic genes in the training and validation sets.

2.5 Assessment of prognostic risk model

In order to explore the differences in biological functions between high- and low-risk groups, we performed Gene Set Variation Analysis (GSVA). The "GSVA" package (25) was used to calculated the score of the pathways in samples, and "limma" package (19) was used to implement the differential analysis of pathways (|t value| > 2). Since somatic mutations play a critical role in tumor development, we investigated the tumor body mutations of samples in the two groups by "maftools" package (29), and showed the top20 mutated genes, respectively. Clinicopathological characteristics of TCGA-AML included cytogenetic risk, age, M subtype, bone marrow (BM) blasts (%), invasiveness, and Platelets (x10^9/L). To determine if clinicopathological characteristics and risk scores were independent predictive factors for AML patients, univariate and multifactorial Cox analyses were performed. The "rms" (30) was adopted to construct the nomogram to predict survival probability based on independent prognostic criteria. The calibration curve was adopted to validate whether the nomogram has good predictive power.

2.6 Relationship between AML patients' risk scores and tumor microenvironment

The "estimate" package (31) was adopted to compare the stroma, immune, estimate score, and tumor purity between the high/low-risk groups. Spearman's rank correlation was used to analyze the correlation between TME and risk score. The CIBERSORT (32) was utilized to analyze the abundance of immune cell infiltration for all samples in the TCGA-AML dataset. To examine the variations in immune cells between the two groups of AML, the Wilcoxon test was used. Subsequently, 48 immune checkpoint and HLA family genes were analyzed for differences in expression between the two groups. The Cancer Immunome Atlas framework (https://www.tcia.at/home) was adopted to calculate immunophenoscore (IPS) of each TCGA-AML patient sample. IPS predicts patient response to immunotherapy, with higher scores associated with greater immunogenicity (33). Calculation of mRNA expression-based stemness index (mRNAsi) scores of TCGA-AML patients was performed by "glmnet" package (34), and then the correlation between mRNAsi scores and risk scores was analyzed by Spearman.

2.7 Prediction of chemotherapy drug

Using the "pRRophetic", the chemotherapy medicines for AML were predicted based on GDSC (https://www.cancerrxgene.org/) (35). To compare the two groups' differences in drug sensitivity, we adopted the Wilcoxon.test.

2.8 Validation of expression of characterized genes

The AML and normal samples were collected form Seventh Affiliated Hospital, Sun Yat-Sen University according to the following inclusion criteria: (1) aged 18-60 years; (2) bone marrow; (3) initial diagnosed AMI patients and healthy donor. The exclusion criteria of AMI samples were M3 and therapeutic interventions (such as chemotherapeutic agents), and bone marrow stimulated by granulocyte colony-stimulating factor. The clinical information of AML and normal samples in qRT-PCR (Supplementary Table 1). This study was approved by Sanming Project of Medicine in Shenzhen (No.SZSM201911004), Ethics Committee of Seventh Affiliated Hospital, Sun Yat-Sen University. The expression of characterized genes was verified using quantitative reverse transcription-polymerase chain reaction (qRT-PCR). Total RNA was extracted from bone marrow samples (6 AML samples and 5 normal samples) with TRIzol method. The reverse transcription reactions were performed using SureScript-First-strand-cDNA-synthesis-kit (Servicebio, China), and then used to perform qRT-PCR with Universal Blue SYBR Green qPCR Master Mix. The qRT-PCR thermocycling protocol was as follows: initial denaturation at 95°C for 60 s, denaturation at 95°C for 20 s, annealing at 55°C for 20 s, extension 72°C for 30s, and amplification for 40 cycles. GAPDH was used as the housekeeping gene. The primer sequences were shown in Table 1. The $2^{-\triangle\triangle CT}$ method was applied to calculate the expression level of genes and normalized to GAPDH.

3 Result

3.1 The m6A-related DE-ERGs for AML

There were 2482 DEGs (up=1192 and down=1290) (Figures 1A, B) and a total of 14 ERGs were differentially expressed in the GSE9476 dataset (Figure 1C). And then 14 m6A related-DE-ERGs were obtained by Spearman's correlation analysis (Figure 1D). A total of 27 predicted miRNAs based on 14 m6A-associated DE-ERGs were common across the 3 databases (Supplementary Table 2). Subsequently, based on shared miRNAs, 7 of the predicted lncRNAs were common across the 3 databases (Supplementary Table 3). Finally, 7 m6A-DE-ERGs, 27 miRNAs, and 7 lncRNAs of the lncRNA-miRNA-mRNA network were constructed (Figure 1E). It was known from the network that DLEU1 could only affect HIF1A by regulating hsa-miR-381-3p, while HIF1A could be affected by multiple miRNAs.

TABLE 1 The primer sequences of characteristic genes.

Primers	Sequence
DOCK1 F	GTTTGCTGCAACCCCTTCTCT
DOCK1 R	GACCAGCGAACCAGGTAGT
SLC14A1 F	TGGCTGTTACTCCCTGTATGTGC
SLC14A1 R	ATGGATTGTAATGTCCTGTGGC
SLC25A1 F	CCGTCAGGTTTGGAATGTTCG
SLC25A1 R	TAACCCCGTGGAAGAATCCTC
UCP2 F	GGAGGTGGTCGGAGATACCAA
UCP2 R	ACAATGGCATTACGAGCAACAT
GAPDH F	CGAAGGTGGAGTCAACGGATTT
GAPDH R	ATGGGTGGAATCATATTGGAAC

3.2 The m6A-related ERGs related-subtypes for AML

Based on the expression of 14 m6A related-DE-ERGs, 132 AML patients were classified into two subtypes (Figures 2A–C). The cluster1 had a worse prognosis than cluster2 ($p < 0.05$) (Figure 2D). Figure 2E showed that ERGs associated with m6A may be regulated through various amino acid metabolic pathways and some down-regulated pathways (chemokine signaling pathway, B-cell receptor signaling pathway, and Fc gamma R-mediated phagocytosis). 22 immune cells were present in some abundance between the two subtypes (Figure 2F). Figure 2G revealed that 14 immune cell types were differentially expressed between the two subtypes, of which the proportion of naive B cells, eosinophils, resting mast cells, resting NK cells, plasma cells, resting CD4 memory T cells, and CD8 T cells was significantly higher in cluster 2 than cluster 1. Moreover, the proportion of monocytes was notably higher in the cluster 1. In summary, we speculated that the activity in terms of immune response, immune surveillance, and cellular immunity was stronger in cluster 2, whereas the increase in the proportion of monocytes may imply that the effects of immunomodulation are stronger in cluster 1.

3.3 The m6A-related ERGs prognostic risk model for AML

According to m6A related-DE-ERGs, four genes with $p < 0.05$ were screened in the training set (Figure 3A). After that, LASSO regression analysis was carried out to obtain four characteristic genes (UCP2, DOCK1, SLC14A1, and SLC25A1) (Figures 3B, C). Risk score = 0.5890×UCP2 + 0.2590×DOCK1 -0.2193×SLC14A1 + 0.2553×SLC25A1. Based on median risk score = 4.864, patients were classified into two groups (Figure 3D). Patients with low-risk scores had significantly higher OS than those with high-risk scores (Figure 3E). The ROC curve for OS was computed to further evaluate the validity of the risk signature, and the AUC values at 1, 3, and 5 years were larger than 0.70, demonstrating improved efficacy of the prognostic risk model (Figure 3F). The prognostic risk model still had strong predictive power in the GSE71014 datasets (Figures 3D–F). The expression trends of DOCK1 and SLC25A1 were increased in AML, while the opposite was true for SLC14A1 and UCP2 in the GSE9476 and GSE13159 datasets (Supplementary Figure S1).

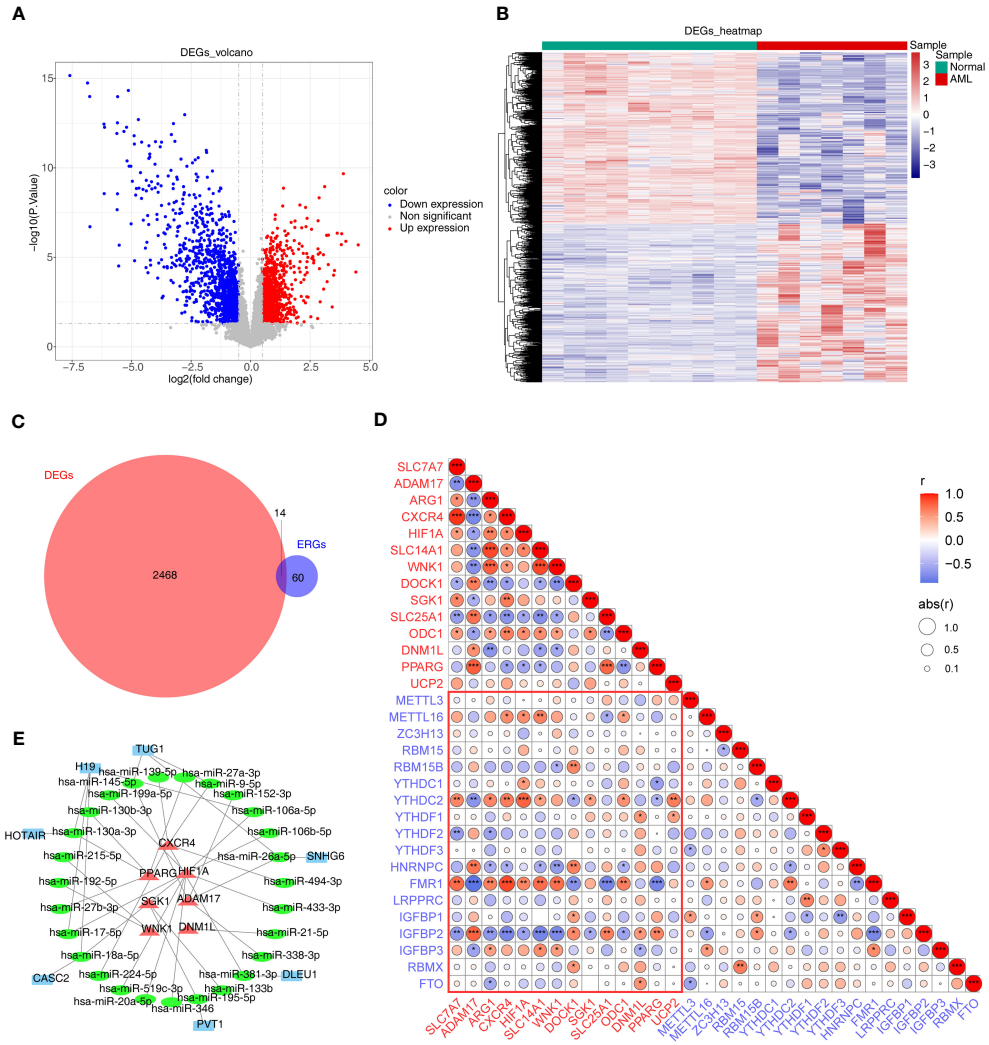

FIGURE 1
Differential expression analysis. **(A, B)** The volcano map **(A)** and heat map **(B)** of up- and down-regulated DEGs. **(C)** The Venn diagram of 14 DE-ERGs obtained by overlapping ERGs and DEGs. **(D)** The relevance of DE-ERGs and m6A-related genes. Genes in red text are DE-ERGs and genes in blue text are m6A regulators. The color and size of the circles indicate the direction and size of the correlation. *p<0.05; ** p<0.01; ***p<0.001. **(E)** The network constructed based on m6A-DE-ERGs, miRNAs, and lncRNAs. Red represents m6A-DE-ERGs, green represents miRNAs, and blue represents lncRNAs. DEGs, differentially expressed genes; AML, acute myeloid leukemia; ERGs, efferocytosis-related genes; DE-ERGs, differentially expressed ERGs; miRNA, microRNA; lncRNA, long non-coding RNA.

3.4 The biological and mutational changes in AML

A total of 4083 GO entries and 117 pathways now differ between the high/low-risk groups (|t|>2). Figure 4A displayed the top10 up-regulated and top4 down-regulated KEGG pathways that were significantly different between high- and low-risk groups, e.g., biosynthesis of unsaturated fatty acids, antigen processing and presentation, and pantothenate and CoA biosynthesis. Moreover, the top10 up- and down-regulated GO terms (including biological progress (BP), cellular component (CC), and molecular function (MF)) that were notably different between two risk groups were shown in Figures 4B–D. Interestingly, some immune-related biological functions, such as T cell extravasation, MHC protein complex, T cell receptor binding, and MHC class I protein binding, were significantly up-regulated in GO terms that differed significantly between high- and low-risk groups. Figures 4E, F showed the top20 mutated genes in the high- and low-risk groups, of which ASXL1, NPM1, and TP53 were mutated between both groups.

3.5 The independent predictors and nomogram in AML

Clinicopathological variables and risk scores from 132 patients were combined to perform univariate and multivariate Cox analyses (Figures 5A, B). The risk scores and Cytogenetic risk was the prognostic factor for AML patients. Construction of a nomogram model on the basis of independent prognostic factors (Figure 5C), it was found that the survival rate decreases as the overall score increases. The slope of the calibration curve of the model is close to

10.3389/fimmu.2023.1268090

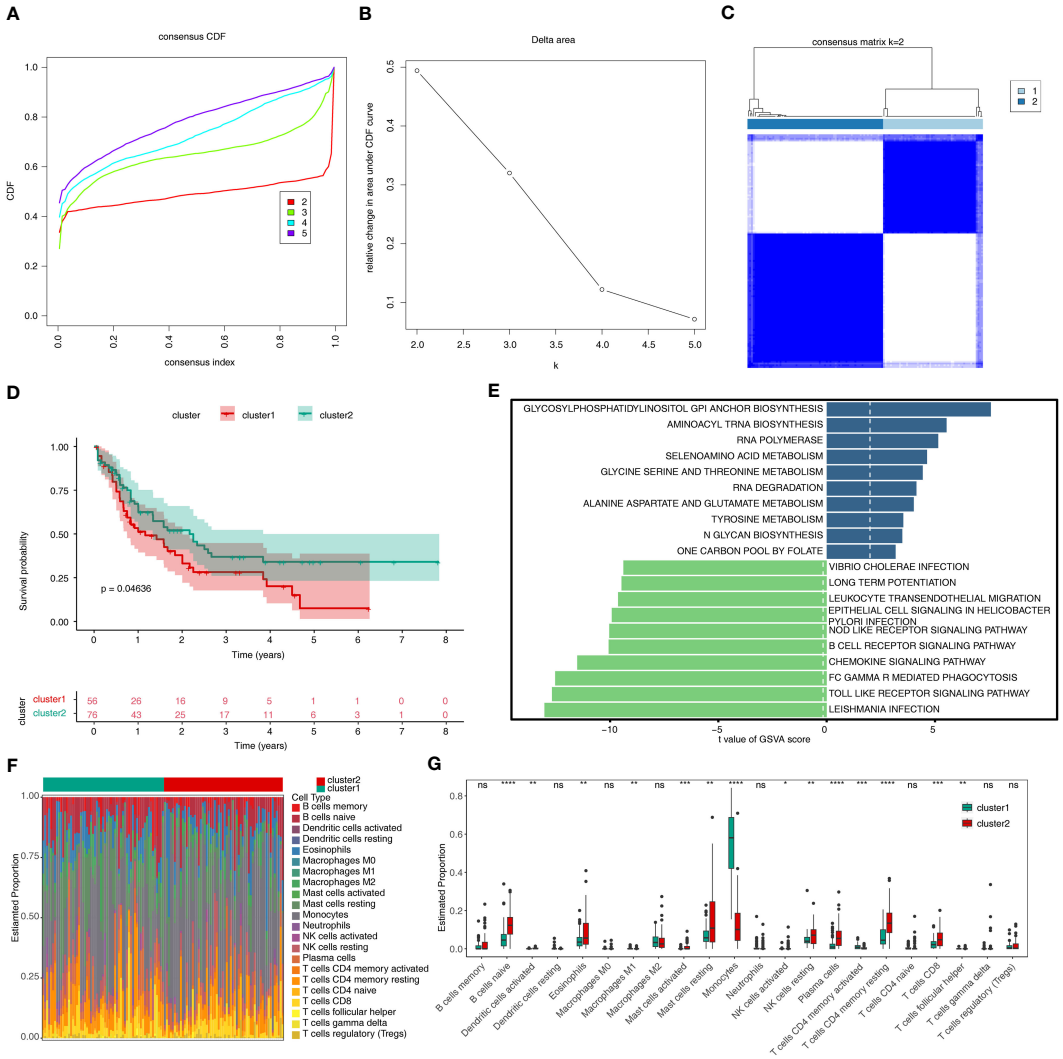

FIGURE 2
Results of consensus clustering of 132 AML patients. **(A)** Consensus clustering CDF for k = 2 to k = 5. **(B)** The corresponding relative change in area under the CDF curves when cluster number changed from k to k + 1. **(C)** Consensus clustering matrix of 132 AMI samples for k = 2. **(D)** The survival difference between cluster1 and cluster2, which are shown below the survival graph, are the number of samples corresponding to that survival time. **(E)** The top10 up- and down-regulated pathways enriched in two sub-types. **(F)** The heat map of 22 immune cells in cluster1 and cluster2. **(G)** Discrepancies of the proportion of immune cells in two sub-types. CDF, cumulative distribution function; GSVA, Gene Set Variation Analysis. ns, not significant; *p<0.05; ** p<0.01; ***p<0.001; ****p<0.0001.

1, indicating that the predictions of the model are true and reliable (Figure 5D).

3.6 The differences of immune microenvironment and immunotherapy between two risk groups

The ImmuneScore, StromalScore, and Estimate score of samples in the high-risk group were significantly higher than in the low-risk group ($p < 0.05$) (Figure 6A). Figure 6B revealed that ImmuneScore, StromalScore, and EstimateScore were positively associated with risk score. The proportion of 22 immune cell types was present in some abundance (Figure 6C) and 4 immune cell types (activated dendritic cells, monocytes, resting CD4 memory T cells, and gamma delta T cells) were significantly different between the two groups (Figure 6D). In addition, 14 immune checkpoints, 20 HLA family genes were significantly differentially expressed between the high/low-risk groups, and most factors were upregulated in the high-risk group (Figures 6E, F), and there was a negative correlation between risk score and mRNAsi score (R=-0.2 and $p<0.05$) (Figure 6G). Moreover, the IPS score was notably different between high- and low-risk groups, and the low-risk group was accompanied by higher score (Figure 6H).

10.3389/fimmu.2023.1268090

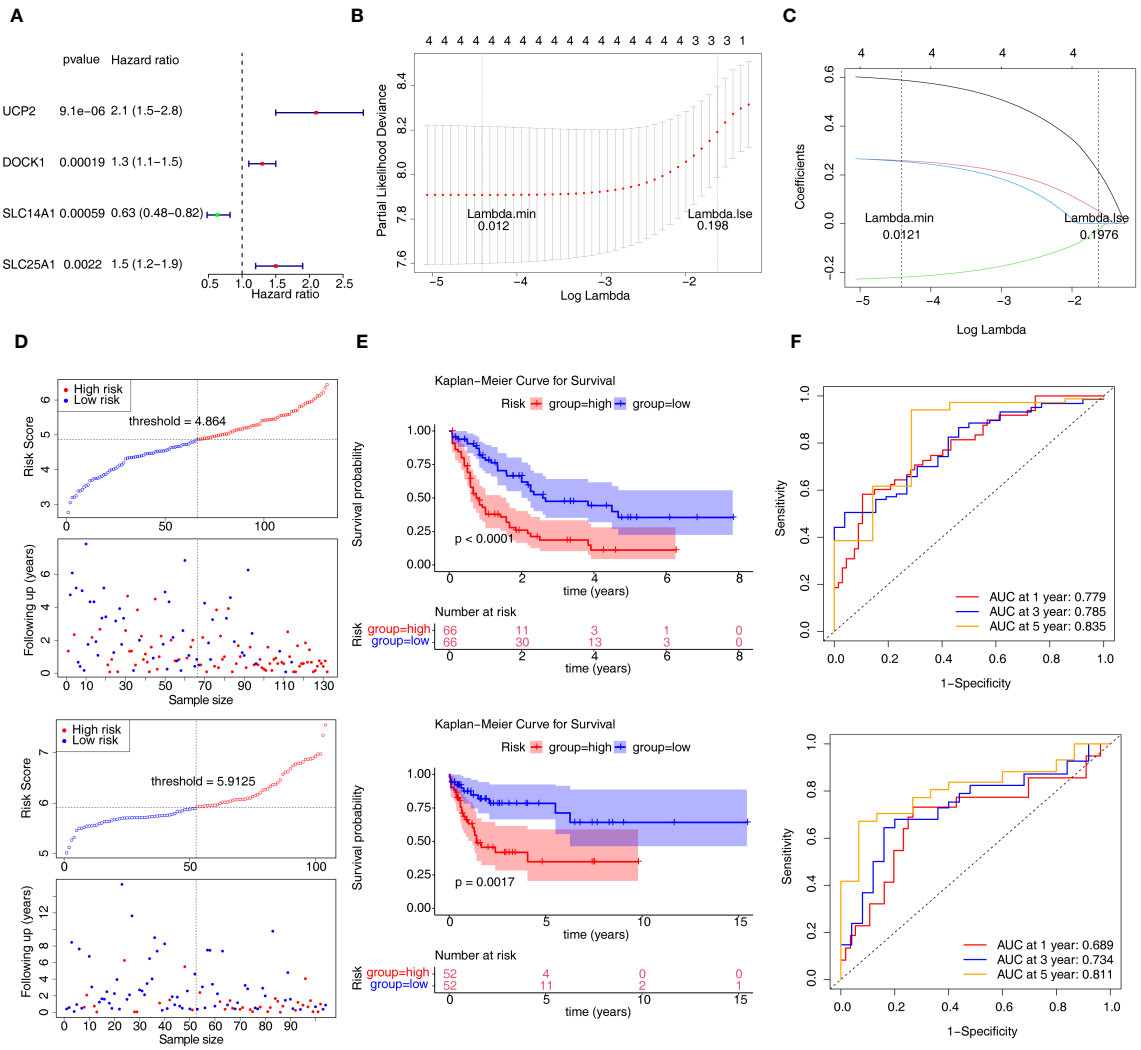

FIGURE 3
Construction and validation of the prognostic risk model. **(A)** Univariate Cox analysis of four genes. **(B, C)** The error plots for 10-fold cross-validation **(B)** and the plot of gene coefficients **(C)** in least absolute shrinkage and selection operator (LASSO) analysis. Each line **(C)** represents a gene. **(D)** The risk curve of prognostic risk model in the training set and GSE71014 dataset. **(E)** The Kaplan-Meier curves of high- and low-risk groups in two datasets. **(F)** The ROC curves of 1/3/5-year in the training set and GSE71014 dataset. ROC, receiver operating characteristic; AUC, area under the curve.

This showed that the prognostic risk model was linked to the immune microenvironment of AML, which provides some theoretical basis for immunotherapy of AML.

3.7 The differences of drug sensitivity between two risk groups

IC50 was calculated for each AML patient in the two groups, yielding a total of 56 drugs with significantly different IC50s (Supplementary Table 4). Figure 7 displayed box plots of the IC50 values for the top 10 significantly different treatment-sensitive drugs. The findings demonstrated that the low-risk group's IC50 was much higher than the high-risk groups. Among them, Erlotinib, Dasatinib, BI.2536, and Bortezomib have been reported to be associated with the treatment of AML. Therefore, we believed that risk scores could be used to predict sensitivity to the above drugs for AML patients, where drug inhibitors might be more effective against organisms or cell lines in samples from high-risk group.

3.8 The expression of m6A-related ERGs by qRT-PCR

The qRT-PCR analysis was performed to further verify characterized genes in AML and normal samples (Table 2; Figures 8A–D). The expression level of DOCK1 and SLC25A1 was higher in AML samples than in normal samples (Figures 8A, C). UCP2 mRNA expression was increased in AML patient samples as compare to healthy control samples, however the difference was not statistically significant (Figure 8D). The expression of SLC14A1 was higher in normal samples than in AML samples (Figure 8B).

10.3389/fimmu.2023.1268090

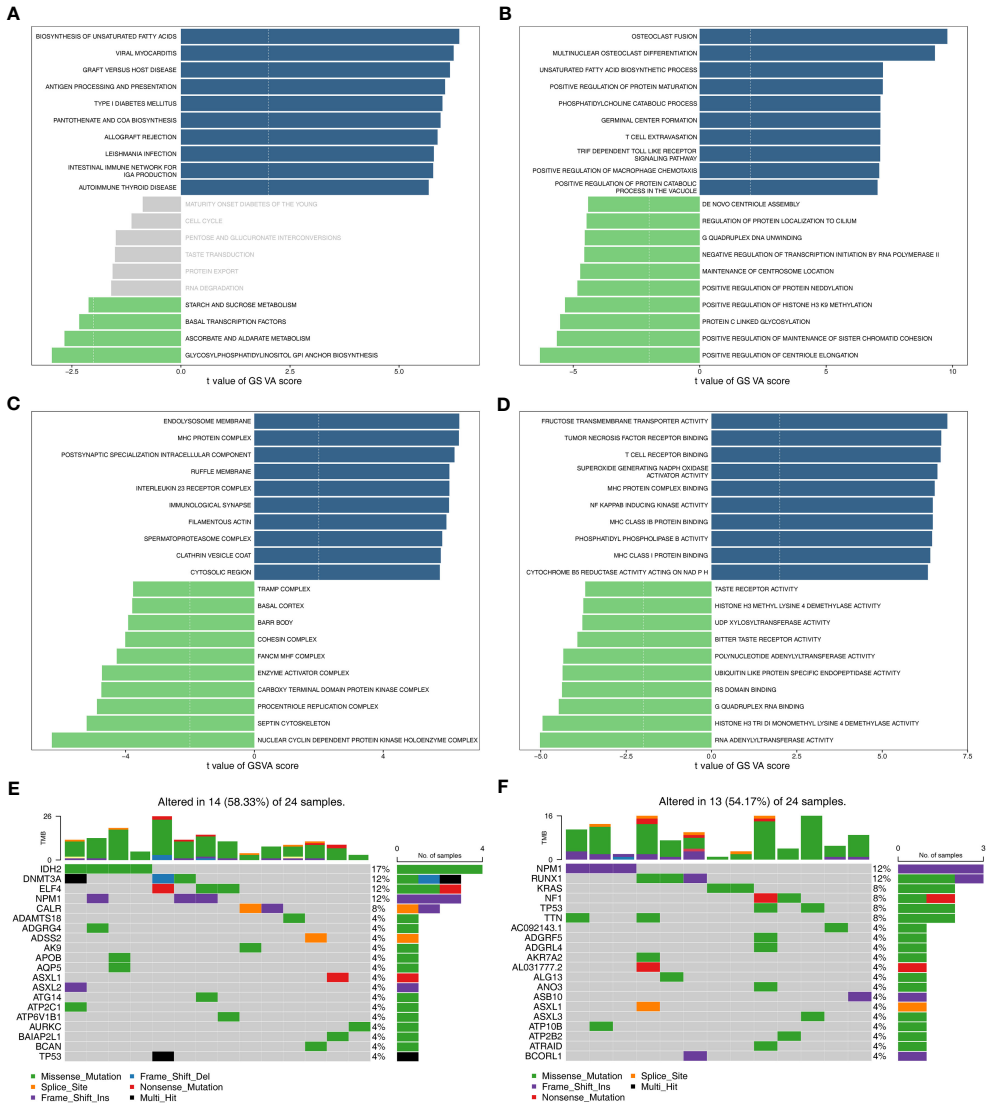

FIGURE 4
Functional enrichment analysis and somatic mutation analysis. **(A)** The KEGG pathways enriched in high- and low-risk groups. **(B–D)** The GO terms enriched in two risk groups. B: BP; C: CC; D: MF. **(E)** Top 20 genes with the highest mutation frequency in the high-risk group. **(F)** Top 20 genes with the highest mutation frequency in the low-risk group. GO, gene ontology; KEGG, Kyoto Encyclopedia of Genes and Genomes; BP, biological progress; CC, cellular component; MF, molecular function.

4 Discussion

The m6A methyltransferase METTL3 can impact the way AML is initiated and maintained. STM2457 is a high-efficiency selective first-in-class catalytic inhibitor specific to METTL3, and using it for tumor treatment can weaken the AML growth, and enhance the cell differentiation and apoptosis (36). In the study by Joselyn Cruz Cruz et al. (37), MerTK inhibition by small molecule tyrosine kinase, MRX2843, could change the leukemia microenvironment from tumor-permissive toward immune responsiveness to leukemia, as well as enhance the AML clearance mediated by immune. And the MerTK (or other vesicular cell receptors) on macrophages play an important role in mediating efferocytosis. m6A and genes related to efferocytosis can mediate the immune system, thereby affecting the AML development. Nevertheless, seldom studies have reported their joint roles. On that account, our study investigates m6A-related ERGs, aiming at contributing to new prognostic models and treatment strategies for AML patients.

In this study, we identified 7 m6A-DE-ERGs (CXCR4, PPARG, SGK1, WNK1, DNM1L, ADAM17, HIF1A), 27 miRNAs, and 7 lncRNAs, which were used to construct the lncRNA-miRNA-mRNA network. Some studies have reported the close association between SGK1, CXCR 4, PPARG, and ADAM17 and HIF1A and AML (38–42). DLEU1 can only exert impact on HIF1A through regulating hsa-miR-381-3p, while HIF1A can be impacted by various miRNAs. According to Abdul-Aziz AM et al. (42), PARP14 regulated the expression of HIF1A, thereby enhancing AML cell growth and glycolysis. On that account, applying miRNAs and 7 lncRNAs to regulate m6A-related DE-ERGs can impact the AML development.

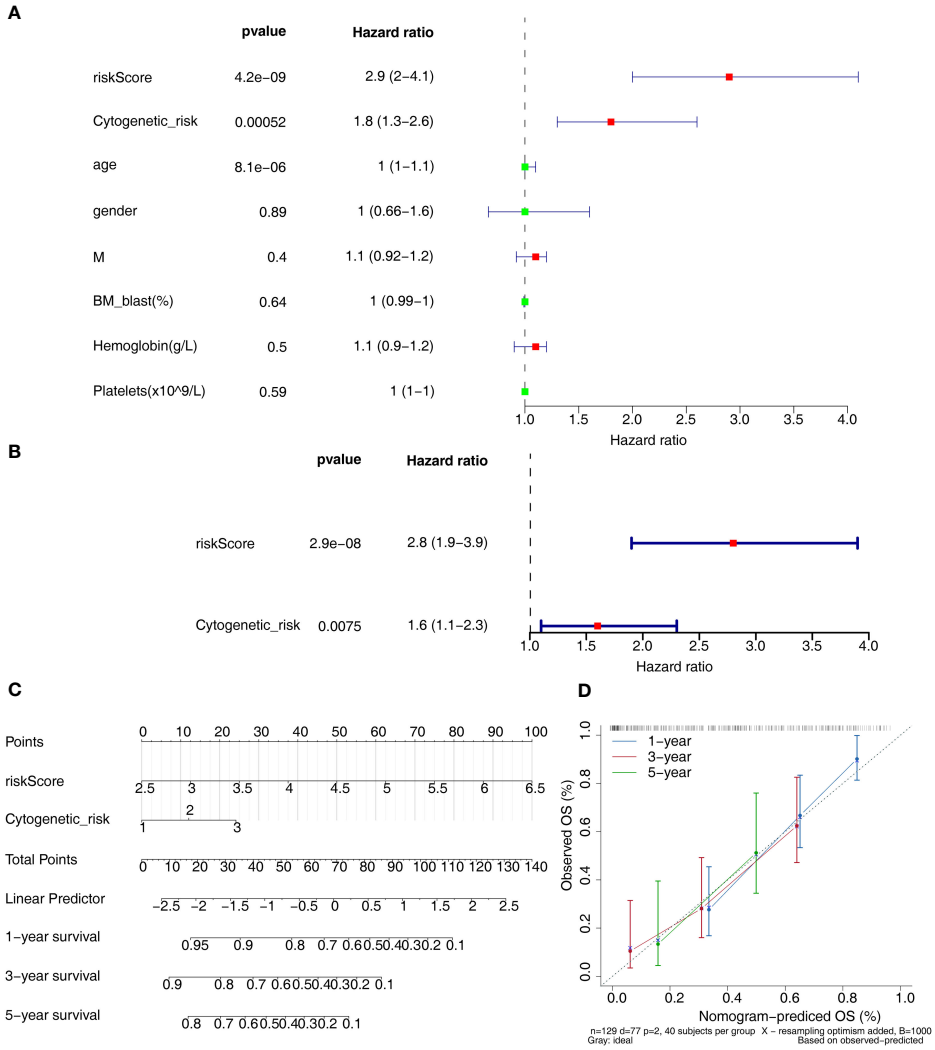

FIGURE 5
Independent prognostic analysis. **(A, B)** The independent prognostic predictors obtained by univariate **(A)** and multivariate **(B)** Cox analyses. **(C)** The nomogram of risk score and cytogenetic risk. **(D)** The calibration curve of the nomogram.

Amino acids not only constitute proteins, but also serve as the intermediate metabolites for various biosynthetic pathways. The study by Yoko Tabe et al. (43) summed up the amino acid metabolism occurring in hematologic malignancy, and assisted in reclassifying amino acid-depleting enzymes into targeted therapeutic agents. In our study, amino acid metabolic pathways significantly impact AML development. According to Courtney L Jones et al. (44), the leukemia stem cell (LSC) population presented elevated amino acid uptake, steady-state levels, and catabolism, and drugs targeting LSC metabolic vulnerabilities could serve for eradicating LSCs in clinical practice. Hence, m6A-related DE-ERGs may regulate the AML occurrence and development through various amino acid metabolic pathways. Our study also reveals the close association between chemokine signaling pathway and AML. Chemokine refers to a family of small cytokines with chemotactic properties, consisted by 8-10 kilodaltons. Chemokine can traffic and regulate the proliferative, migratory, differentiative and homing activities of immune cells. The CXCR4 chemokine receptor can enhance the survival rate of various cell types. According to the study of Kimberly N Kremer et al. (45), CXCR4 chemokine receptor signaling regulated many of the Bcl-2 family members (Bcl-XL, Noxa, and Bak), thereby inducing AML cell apoptosis. Taken together, m6A-related DE-ERGs may be involved in AML progression by downregulating chemokine signaling pathway.

In the 14 m6A-related ERGs related-subtypes analysis, different subpopulations present obviously different monocytes, plasma cells and naive B cells, with more infiltrated in the worse prognosis cluster1. Clinical experiments in the study confirmed the significant role of monocytes, plasma cells and naive B cells in the AML pathogenesis, and its close association with myeloid tumor cell progression. Monocyte is the innate immune cell in the mononuclear phagocyte system and can remarkably regulate tumor development and progression. Plasma cell that secretes antibody serves as the core pillar of the humoral immunity, generated during the basic cellular restructuration from the naive

10.3389/fimmu.2023.1268090

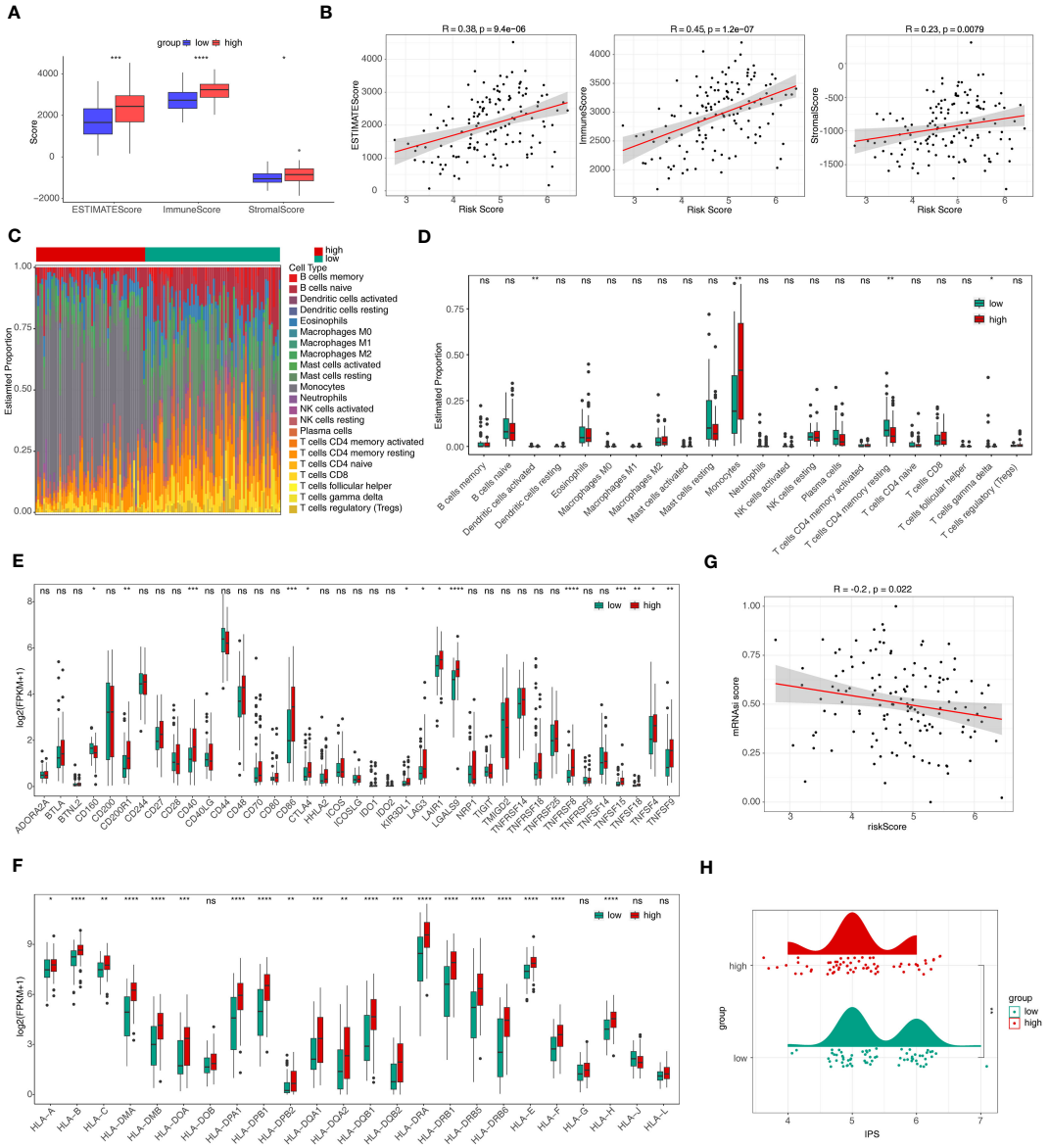

FIGURE 6
Immune infiltration and immune correlation analyses. **(A)** The discrepancies of immune score, stromal score, and estimate score between high- and low-risk groups. *p<0.05; ** p<0.01; ***p<0.001; ****p<0.0001. **(B)** The relevance of risk score to immune score, stromal score, and estimate score. **(C)** The heat map of abundance of 22 immune cells in two risk groups. **(D)** The discrepancies of immune cells between two risk groups. ns, not significant; *p<0.05; ** p<0.01. **(E, F)** The discrepancies of immune checkpoints **(E)** and HLA family genes **(F)** between high- and low-risk groups. ns, not significant; *p<0.05; ** p<0.01; ***p<0.001; ****p<0.0001. **(G)** The relevance of risk score and mRNAsi score. **(H)** Discrepancies of IPS between high- and low-risk groups. HLA, human leukocyte antigen; mRNAsi, stemness index based on mRNA expression; IPS, immunophenoscores. ns, not significant; *p<0.05; ** p<0.01; ***p<0.001; ****p<0.0001.

B cells-antigen contact. When naive B cells are differentiated into extrafollicular B cells, antibody-secreting cells with weaker affinity and short life can be generated. Claire E Olingy et al. (46) made a comprehensive explanation of the monocyte heterogeneity in the homeostasis process, highlighted the role played by monocyte in the cancer development, as well as gave effective monocyte-targeted cancer treatment strategies. In the study by Maartje C A Wouters et al. (47), substantial evidences, by virtue of a comprehensive PubMed search, had proved that plasma cells positively impact the antitumor immunity, and it is suggested to enhance these responses in designing cancer immunotherapies. Helmink BA et al. (48) used mass cytometry for interrogating various surface proteins, finding the existence of naive B cells, memory B cells, activated memory B cells, and plasmablasts. Therefore, we speculated that different subtypes suggested the possible mediating roles played by monocytes, plasma cells and naive B cells in the prognosis of patients with different AML subtypes.

Our study constructed the prognosis model and the prognostic genes of UCP 2, DOCK 1, SLC14A1, and SLC25A1. Uncoupling protein 2 (UCP2), and mitochondrial uncoupling proteins belong to the family of mitochondrial anion carrier proteins (MACP). AML patients showed elevated UCP2 expression. Dongxu Gang

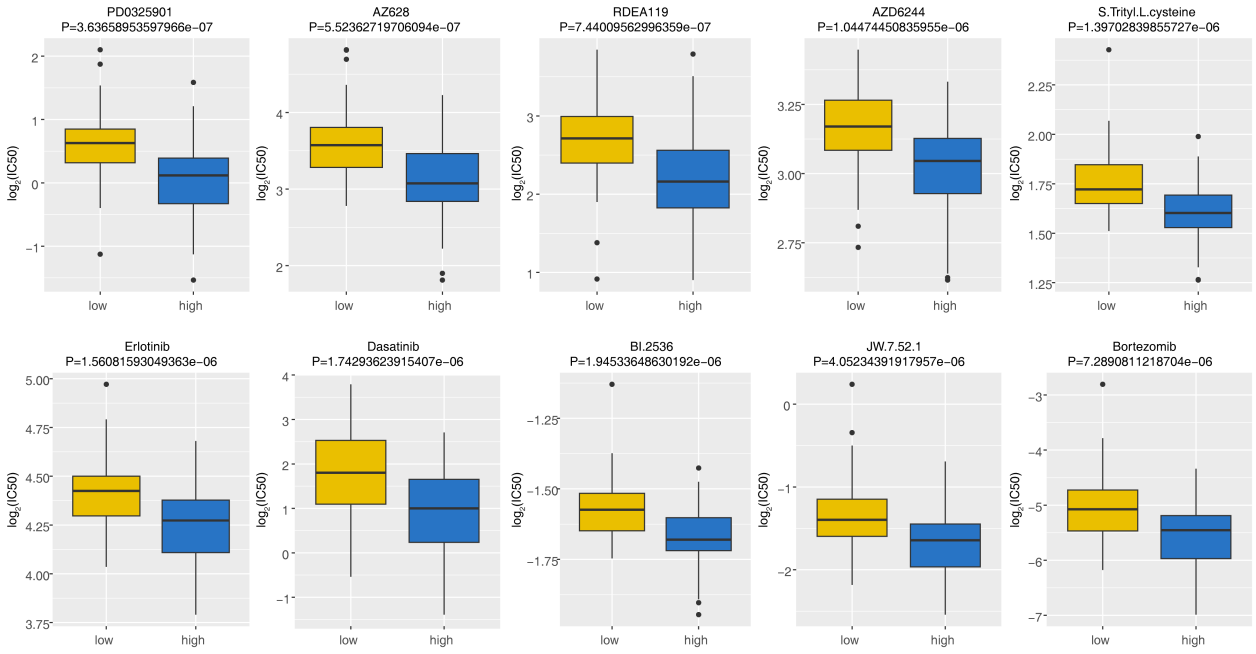

FIGURE 7
The discrepancies of drug sensitivity between high- and low-risk groups. The lower the log_2(IC50) value, the more sensitive the groups of patient was to the drug. IC50, half-maximal inhibitory concentration.

et al. (49) found that UCP2 inhibition could lead to weakened AML cell line proliferation, cell cycle alternation, and apoptosis enhancement *in vitro*. Dedicator of cytokinesis 1(DOCK1) is the dedicator of cytokinesis proteins and the guanine nucleotide exchange factors specific to small Rho family G proteins. According to Sze-Hwei Lee et al. (50), highly expressed DOCK1 led to worse AML prognosis, and higher DOCK1 expression exhibited an obvious relevance to older age, higher platelet and peripheral blast counts, intermediate-risk cytogenetics, FLT3-ITD, MLL-PTD and PTPN11, NPM1, RUNX1, ASXL1 and DNMT3A mutations. Solute carrier family 14 member 1 (SLC14A1) is a gene that encodes a protein that mediates urea transport in erythrocytes (51). Through targeting SLC14A1, ARHGAP5 and PIK3CA, miR-10a-3p may be involved in the development of FLT3 mutation in adult AML (52). Solute carrier family 25 member 1(SLC25A1) is a mitochondrial carrier that facilitates the flow of citrate/isocitrate in mitochondria in exchange for the entry of malate in the cytoplasm (53, 54). According to a report, prognostic signature associated with SLC25A1 denotes AML patients worse prognosis (55). On that account, UCP 2, DOCK 1, SLC14A1, and SLC25A1 show important prognostic value in AML, but subsequent studies are still needed to explore their functions in AML.

TABLE 2 The results of qRT-PCR.

	Normal	AML	P value
DOCK1	1.2828 ± 0.6249	4.4652 ± 1.4656	0.0072
SLC14A1	1.7453 ± 1.0774	0.208. ± 0.1413	0.03
SLC25A1	1.1357 ± 0.5504	3.5250 ± 1.1734	0.0102
UCP2	1.0428 ± 0.2490	1.6593 ± 0.6231	0.1158

The HLA correlation analysis revealed the highly expressed HLA in the high-risk group, which had a worse prognosis, and the two risk groups presented obvious difference in the expressions of the 14 immune checkpoints, 20 HLA family genes, and IPS. Immune checkpoint molecules, inhibitory and stimulatory, refer to ligand-receptor pairs that inhibit or stimulate the immune responses (56). Luca Vago et al. (57) conducted studies to test the latest immunotherapies for the specific targeting of AML cells (antibody therapy and cellular therapy, etc.) or the broader reactivation of antileukemia immunity (vaccines and checkpoint blockade, etc.), which combines complementary immunotherapeutic strategies with chemotherapeutics or other pharmacotherapies. Rikako Tabata et al. (58) demonstrated the underlying clinical benefits exhibited by immuno-oncology (IO) therapy specific to AML and ICIs with or without conventional chemotherapy. These prove the certain efficacy of immunotherapy in AML. Immune checkpoint, HLA and IPS are different in the two risk groups, suggesting their mediating roles in AML prognosis. Hence, the immune microenvironment of AML offers theoretical basis for immunotherapy of AML.

In the study, the predicted drugs are Erlotinib, Dasatinib, BI.2536, and Bortezomib, etc. Erlotinib, as a type of tyrosine kinase inhibitor, did not achieve a good response in AML patients in pilot study (59). Dasatinib is a type of kinase inhibitor, and has the function of inhibiting BCR-ABL, Src family kinases, c-Kit, and platelet-derived growth factor receptor kinase. Due to the inhibitory effect on BCR-ABL, it is usually used for treating chronic myeloid leukemia (CML) and Philadelphia chromosome-positive

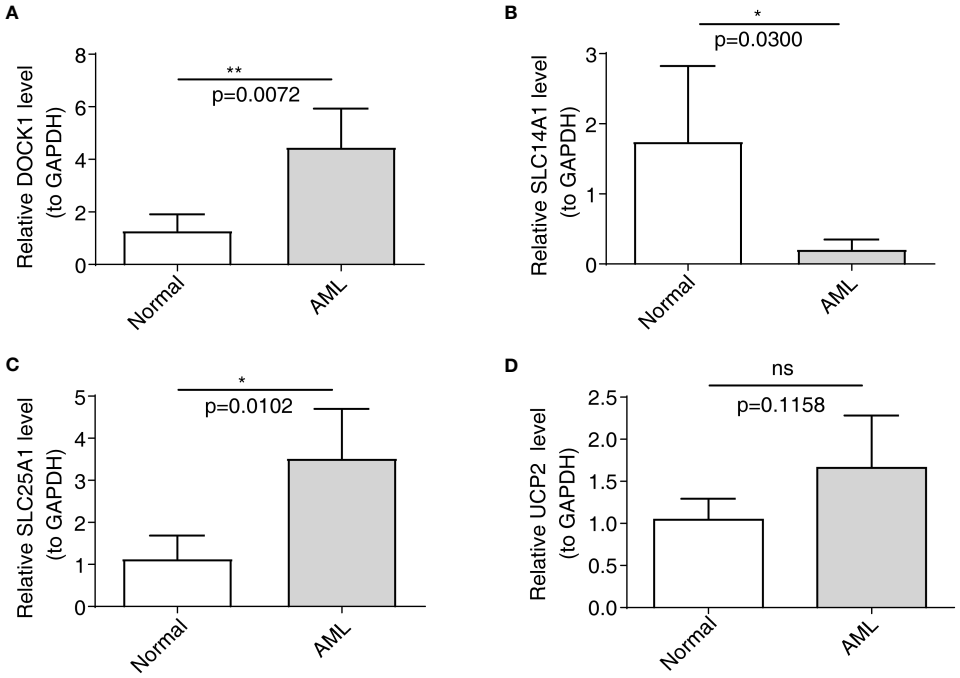

FIGURE 8
Validation of the expression of characterized genes by quantitative reverse transcriptase PCR. **(A)**: DOCK1; **(B)**: SLC14A1; **(C)**: SLC25A1; **(D)**: UCP2. ns, not significant; *p<0.05; **p<0.01.

acute lymphoblastic leukemia. A subpopulation of AML patients show BCR-ABL expression. Patients with unselected AML present remarkably mixed clinical responses to dasatinib, which shall be validated in larger-scale studies (60). BI.2536 is a newly discovered Plk inhibitor capable of inducing mitotic arrest and apoptosis. According to the randomized, open-label, phase I/II trial, clinical activity in patients treated with single-agent BI 2536 provides the first evidence of the potential therapeutic value of targeted Plk in patients with relapsed refractory AML (61). Bortezomib, proteasome inhibitor, is the mainstream drug for treating various myeloma and mantle cell lymphoma. AML patients give a series of different clinical responses to the chemotherapy regimens that combine bortezomib, and some cases show a complete remission rate over 80% (62). On these account, dasatinib, BI.2536, and bortezomib may be applicable for treating AML, which shall be more deeply concerned in future studies.

In summary, using bioinformatic methods, this study has identified prognostic genes for AML and constructed a prognostic model associated with m6A and ERGs. Differential analyses were conducted between high and low-risk groups, evaluating immune cell infiltration, immune therapy response, functional enrichment, and drug sensitivity. However, the study has discernible limitations. The analysis predominantly relies on a constrained number of samples from public databases, highlighting the imperative need for an expanded sample size. While gene expression levels have been validated through qRT-PCR, the requisite further verification and elucidation of potential molecular mechanisms necessitate animal experiments. Moreover, the analyses pertaining to immune therapy and drug sensitivity in the study require clinical validation to ascertain their clinical value further. Such exploration will constitute the main thrust of our ensuing research efforts. Ultimately, our findings furnish researchers with a novel theoretical framework for delving deeper into the relationship between m6A regulatory factors, efferocytosis, and AML, thereby providing new targets for enhancing the prognosis and treatment of AML.

Data availability statement

The datasets presented in this study can be found in online repositories. The names of the repository/repositories and accession number(s) can be found in the article/Supplementary Material.

Ethics statement

The studies involving humans were approved by Seventh Affiliated Hospital, Sun Yat-Sen University. The studies were conducted in accordance with the local legislation and institutional requirements. The participants provided their written informed consent to participate in this study. The manuscript presents research on animals that do not require ethical approval for their study.

Author contributions

YW: Validation, Writing – original draft. TB: Resources, Writing – review & editing. JT: Conceptualization, Data curation, Writing – review & editing. X-JX: Formal analysis, Writing – review

& editing. CL: Project administration, Software, Writing – original draft. BL: Funding acquisition, Investigation, Writing – review & editing. T-TS: Methodology, Visualization, Writing – review & editing.

Funding

The author(s) declare financial support was received for the research, authorship, and/or publication of this article. We thank Sanming Project of Medicine in Shenzhen (No.SZSM201911004) for supporting the manuscript preparation and publication.

Acknowledgments

Thanks to all authors for their contributions to this manuscript.

Conflict of interest

The authors declare that the research was conducted in the absence of any commercial or financial relationships that could be construed as a potential conflict of interest.

Publisher's note

Supplementary material

The Supplementary Material for this article can be found online at: https://www.frontiersin.org/articles/10.3389/fimmu.2023.1268090/full#supplementary-material

SUPPLEMENTARY FIGURE 1
The expression of prognostic genes. **(A, B)** The discrepancies of the expression of four prognostic genes in the GSE9476 **(A)** and GSE13159 **(B)** datasets. *p<0.05; ** p<0.01; ***p<0.001; ****p<0.0001.

SUPPLEMENTARY TABLE 1
The clinical information of AML and normal samples in qRT-PCR.

SUPPLEMENTARY TABLE 2
27 miRNAs targeting 14 m6A-associated DE-ERGs.

SUPPLEMENTARY TABLE 3
7 lncRNAs targeting miRNAs.

SUPPLEMENTARY TABLE 4
The IC50 value for 138 drugs in patients in the high and low-risk groups.

References

1. Ganzel C, Manola J, Douer D, Rowe JM, Fernandez HF, Paietta EM, et al. Extramedullary disease in adult acute myeloid leukemia is common but lacks independent significance: analysis of patients in ECOG-ACRIN cancer research group trials, 1980-2008. *J Clin Oncol* (2016) 34(29):3544–53. doi: 10.1200/JCO.2016.67.5892

2. *Cancer stat facts: leukemia—acute myeloid leukemia (AML)* (2017). National Cancer Institute (Accessed Sept 21, 2017).

3. McNerney ME, Godley LA, Le Beau MM. Therapy-related myeloid neoplasms: when genetics and environment collide. *Nat Rev Cancer* (2017) 17(9):513–27. doi: 10.1038/nrc.2017.60

4. Zhao BS, Roundtree IA, He C. Post-transcriptional gene regulation by mRNA modifications. *Nat Rev Mol Cell Biol* (2017) 18(1):31–42. doi: 10.1038/nrm.2016.132

5. Dubin DT, Taylor RH. The methylation state of poly A-containing messenger RNA from cultured hamster cells. *Nucleic Acids Res* (1975) 2(10):1653–68. doi: 10.1093/nar/2.10.1653

6. Liu N, Pan T. N6-methyladenosine–encoded epitranscriptomics. *Nat Struct Mol Biol* (2016) 23(2):98–102. doi: 10.1038/nsmb.3162

7. Zhao X, Chen Y, Mao Q, Jiang X, Jiang W, Chen J, et al. Overexpression of YTHDF1 is associated with poor prognosis in patients with hepatocellular carcinoma. *Cancer biomark* (2018) 21(4):859–68. doi: 10.3233/CBM-170791

8. Cheng X, Li M, Rao X, Zhang W, Li X, Wang L, et al. KIAA1429 regulates the migration and invasion of hepatocellular carcinoma by altering m6A modification of ID2 mRNA. *Onco Targets Ther* (2019) 12:3421–8. doi: 10.2147/OTT.S180954

9. Cui Q, Shi H, Ye P, Li L, Qu Q, Sun G, et al. m(6)A RNA methylation regulates the self-renewal and tumorigenesis of glioblastoma stem cells. *Cell Rep* (2017) 18(11):2622–34. doi: 10.1016/j.celrep.2017.02.059

10. Miao W, Chen J, Jia L, Ma J, Song D. The m6A methyltransferase METTL3 promotes osteosarcoma progression by regulating the m6A level of LEF1. *Biochem Biophys Res Commun* (2019) 516(3):719–25. doi: 10.1016/j.bbrc.2019.06.128

11. Li T, Hu PS, Zuo Z, Lin JF, Li X, Wu QN, et al. METTL3 facilitates tumor progression *via* an m(6)A-IGF2BP2-dependent mechanism in colorectal carcinoma. *Mol Cancer* (2019) 18(1):112. doi: 10.1186/s12943-019-1038-7

12. Wynn TA, Chawla A, Pollard JW. Macrophage biology in development, homeostasis and disease. *Nature* (2013) 496(7446):445–55. doi: 10.1038/nature12034

13. Boada-Romero E, Martinez J, Heckmann BL, Green DR. The clearance of dead cells by efferocytosis. *Nat Rev Mol Cell Biol* (2020) 21(7):398–414. doi: 10.1038/s41580-020-0232-1

14. Doran AC, Yurdagul A Jr., Tabas I. Efferocytosis in health and disease. *Nat Rev Immunol* (2020) 20(4):254–67. doi: 10.1038/s41577-019-0240-6

15. He L, Li H, Wu A, Peng Y, Shu G, Yin G. Functions of N6-methyladenosine and its role in cancer. *Mol Cancer* (2019) 18(1):176. doi: 10.1186/s12943-019-1109-9

16. Wang H, Yuan J, Dang X, Shi Z, Ban W, Ma D, et al. Mettl14-mediated m6A modification modulates neuron apoptosis during the repair of spinal cord injury by regulating the transformation from pri-mir-375 to miR-375. *Cell Biosci* (2021) 11(1):52. doi: 10.1186/s13578-020-00526-9

17. Trzeciak A, Wang YT, Perry JSA. First we eat, then we do everything else: The dynamic metabolic regulation of efferocytosis. *Cell Metab* (2021) 33(11):2126–41. doi: 10.1016/j.cmet.2021.08.001

18. Mehrotra P, Ravichandran KS. Drugging the efferocytosis process: concepts and opportunities. *Nat Rev Drug Discov* (2022) 21(8):601–20. doi: 10.1038/s41573-022-00470-y

19. Ritchie ME, Phipson B, Wu D, Hu Y, Law CW, Shi W, et al. limma powers differential expression analyses for RNA-sequencing and microarray studies. *Nucleic Acids Res* (2015) 43(7):e47. doi: 10.1093/nar/gkv007

20. Ji Y, Yan T, Zhu S, Wu R, Zhu M, Zhang Y, et al. The integrative analysis of competitive endogenous RNA regulatory networks in coronary artery disease. *Front Cardiovasc Med* (2021) 8:647953. doi: 10.3389/fcvm.2021.647953

21. Chen G, Li L, Tao H. Bioinformatics identification of ferroptosis-related biomarkers and therapeutic compounds in ischemic stroke. *Front Neurol* (2021) 12:745240. doi: 10.3389/fneur.2021.745240

22. Chen H, Boutros PC. VennDiagram: a package for the generation of highly-customizable Venn and Euler diagrams in R. *BMC Bioinf* (2011) 12:35. doi: 10.1186/1471-2105-12-35

23. Wilkerson MD, Hayes DN. ConsensusClusterPlus: a class discovery tool with confidence assessments and item tracking. *Bioinformatics* (2010) 26(12):1572–3. doi: 10.1093/bioinformatics/btq170

24. Wang K, Guan C, Shang X, Ying X, Mei S, Zhu H, et al. A bioinformatic analysis: the overexpression and clinical significance of FCGBP in ovarian cancer. *Aging (Albany NY)* (2021) 13(5):7416–29. doi: 10.18632/aging.202601

25. Hänzelmann S, Castelo R, Guinney J. GSVA: gene set variation analysis for microarray and RNA-seq data. *BMC Bioinf* (2013) 14:7. doi: 10.1186/1471-2105-14-7

26. Zhou S, Lu H, Xiong M. Identifying immune cell infiltration and effective diagnostic biomarkers in rheumatoid arthritis by bioinformatics analysis. *Front Immunol* (2021) 12:726747. doi: 10.3389/fimmu.2021.726747

27. Friedman J, Hastie T, Tibshirani R. Regularization paths for generalized linear models *via* coordinate descent. *J Stat Softw* (2010) 33(1):1–22. doi: 10.18637/jss.v033.i01

28. Hebert PD, Cywinska A, Ball SL, deWaard JR. Biological identifications through DNA barcodes. *Proc Biol Sci* (2003) 270(1512):313–21. doi: 10.1098/rspb.2002.2218

29. Mayakonda A, Lin DC, Assenov Y, Plass C, Koeffler HP. Maftools: efficient and comprehensive analysis of somatic variants in cancer. *Genome Res* (2018) 28(11):1747–56. doi: 10.1101/gr.239244.118

30. Pan X, Jin X, Wang J, Hu Q, Dai B. Placenta inflammation is closely associated with gestational diabetes mellitus. *Am J Transl Res* (2021) 13(5):4068–79.

31. Yoshihara K, Shahmoradgoli M, Martínez E, Vegesna R, Kim H, Torres-Garcia W, et al. Inferring tumour purity and stromal and immune cell admixture from expression data. *Nat Commun* (2013) 4:2612. doi: 10.1038/ncomms3612

32. Kawada JI, Takeuchi S, Imai H, Okumura T, Horiba K, Suzuki T, et al. Immune cell infiltration landscapes in pediatric acute myocarditis analyzed by CIBERSORT. *J Cardiol* (2021) 77(2):174–8. doi: 10.1016/j.jjcc.2020.08.004

33. Xu Q, Chen S, Hu Y, Huang W. Landscape of immune microenvironment under immune cell infiltration pattern in breast cancer. *Front Immunol* (2021) 12:711433. doi: 10.3389/fimmu.2021.711433

34. Engebretsen S, Bohlin J. Statistical predictions with glmnet. *Clin Epigenet* (2019) 11(1):123. doi: 10.1186/s13148-019-0730-1

35. Geeleher P, Cox N, Huang RS. pRRophetic: an R package for prediction of clinical chemotherapeutic response from tumor gene expression levels. *PloS One* (2014) 9(9):e107468. doi: 10.1371/journal.pone.0107468

36. Yankova E, Blackaby W, Albertella M, Rak J, De Braekeleer E, Tsagkogeorga G, et al. Small-molecule inhibition of METTL3 as a strategy against myeloid leukaemia. *Nature* (2021) 593(7860):597–601. doi: 10.1038/s41586-021-03536-w

37. Cruz Cruz J, Allison KC, Page LS, Jenkins AJ, Wang X, Earp HS, et al. Inhibiting efferocytosis reverses macrophage-mediated immunosuppression in the leukemia microenvironment. *Front Immunol* (2023) 14:1146721. doi: 10.3389/fimmu.2023.1146721

38. Chae YC, Jung H, Kim JY, Lee DH, Seo SB. Ubiquitin-specific peptidase 3 induces TPA-mediated leukemia cell differentiation *via* regulating H2AK119ub. *Anim Cells Syst (Seoul)* (2019) 23(5):311–7. doi: 10.1080/19768354.2019.1661283

39. Núñez Y, Garcia-León A, Falgàs A, Serna N, Sánchez-García L, Garrido A, et al. T22-PE24-H6 nanotoxin selectively kills CXCR4-high expressing AML patient cells *in vitro* and potently blocks dissemination *in vivo*. *Pharmaceutics* (2023) 15(3):727. doi: 10.3390/pharmaceutics15030727

40. Esmaeili S, Salari S, Kaveh V, Ghaffari SH, Bashash D. Alteration of PPAR-GAMMA (PPARG; PPARγ) and PTEN gene expression in acute myeloid leukemia patients and the promising anticancer effects of PPARγ stimulation using pioglitazone on AML cells. *Mol Genet Genomic Med* (2021) 9(11):e1818. doi: 10.1002/mgg3.1818

41. Bouchet S, Tang R, Fava F, Legrand O, Bauvois B. Targeting CD13 (aminopeptidase-N) in turn downregulates ADAM17 by internalization in acute myeloid leukaemia cells. *Oncotarget* (2014) 5(18):8211–22. doi: 10.18632/oncotarget.1788

42. Abdul-Aziz AM, Shafat MS, Sun Y, Marlein CR, Piddock RE, Robinson SD, et al. HIF1α drives chemokine factor pro-tumoral signaling pathways in acute myeloid leukemia. *Oncogene* (2018) 37(20):2676–86. doi: 10.1038/s41388-018-0151-1

43. Tabe Y, Lorenzi PL, Konopleva M. Amino acid metabolism in hematologic Malignancies and the era of targeted therapy. *Blood* (2019) 134(13):1014–23. doi: 10.1182/blood.2019001034

44. Jones CL, Stevens BM, D'Alessandro A, Reisz JA, Culp-Hill R, Nemkov T, et al. Inhibition of amino acid metabolism selectively targets human leukemia stem cells. *Cancer Cell* (2018) 34(5):724–740.e4. doi: 10.1016/j.ccell.2018.10.005

45. Kremer KN, Peterson KL, Schneider PA, Meng XW, Dai H, Hess AD, et al. CXCR4 chemokine receptor signaling induces apoptosis in acute myeloid leukemia cells *via* regulation of the Bcl-2 family members Bcl-XL, Noxa, and Bak. *J Biol Chem* (2013) 288(32):22899–914. doi: 10.1074/jbc.M113.449926

46. Olingy CE, Dinh HQ, Hedrick CC. Monocyte heterogeneity and functions in cancer. *J Leukoc Biol* (2019) 106(2):309–22. doi: 10.1002/JLB.4RI0818-311R

47. Wouters MCA, Nelson BH. Prognostic significance of tumor-infiltrating B cells and plasma cells in human cancer. *Clin Cancer Res* (2018) 24(24):6125–35. doi: 10.1158/1078-0432.CCR-18-1481

48. Helmink BA, Reddy SM, Gao J, Zhang S, Basar R, Thakur R, et al. B cells and tertiary lymphoid structures promote immunotherapy response. *Nature* (2020) 577(7791):549–55. doi: 10.1038/s41586-019-1922-8

49. Gang D, Jiang Y, Wang X, Zhou J, Zhang X, He X, et al. Aging-related genes related to the prognosis and the immune microenvironment of acute myeloid leukemia. *Clin Transl Oncol* (2023) 25(10):2991–3005. doi: 10.21203/rs.3.rs-2245364/v1

50. Lee SH, Chiu YC, Li YH, Lin CC, Hou HA, Chou WC, et al. High expression of dedicator of cytokinesis 1 (DOCK1) confers poor prognosis in acute myeloid leukemia. *Oncotarget* (2017) 8(42):72250–9. doi: 10.18632/oncotarget.19706

51. Wan Z, Wang Y, Li C, Zheng D. SLC14A1 is a new biomarker in renal cancer. *Clin Transl Oncol* (2023) 25(8):2607–23. doi: 10.1007/s12094-023-03140-6

52. Chen S, Chen Y, Zhu Z, Tan H, Lu J, Qin P, et al. Identification of the key genes and microRNAs in adult acute myeloid leukemia with FLT3 mutation by bioinformatics analysis. *Int J Med Sci* (2020) 17(9):1269–80. doi: 10.7150/ijms.46441

53. Fernandez HR, Gadre SM, Tan M, Graham GT, Mosaoa R, Ongkeko MS, et al. The mitochondrial citrate carrier, SLC25A1, drives stemness and therapy resistance in non-small cell lung cancer. *Cell Death Differ* (2018) 25(7):1239–58. doi: 10.1038/s41418-018-0101-z

54. Palmieri F. Mitochondrial transporters of the SLC25 family and associated diseases: a review. *J Inherit Metab Dis* (2014) 37(4):565–75. doi: 10.1007/s10545-014-9708-5

55. Liu F, Deng S, Li Y, Du J, Zeng H. SLC25A1-associated prognostic signature predicts poor survival in acute myeloid leukemia patients. *Front Genet* (2022) 13:1081262. doi: 10.3389/fgene.2022.1081262

56. Zhang Y, Zheng J. Functions of immune checkpoint molecules beyond immune evasion. *Adv Exp Med Biol* (2020) 1248:201–26. doi: 10.1007/978-981-15-3266-5_9

57. Vago L, Gojo I. Immune escape and immunotherapy of acute myeloid leukemia. *J Clin Invest* (2020) 130(4):1552–64. doi: 10.1172/JCI129204

58. Tabata R, Chi S, Yuda J, Minami Y. Emerging immunotherapy for acute myeloid leukemia. *Int J Mol Sci* (2021) 22(4):1944. doi: 10.3390/ijms22041944

59. Sayar H, Czader M, Amin C, Cangany M, Konig H, Cripe LD. Pilot study of erlotinib in patients with acute myeloid leukemia. *Leuk Res* (2015) 39(2):170–2. doi: 10.1016/j.leukres.2014.11.022

60. Amrein PC. The potential for dasatinib in treating chronic lymphocytic leukemia, acute myeloid leukemia, and myeloproliferative neoplasms. *Leuk Lymphoma* (2011) 52(5):754–63. doi: 10.3109/10428194.2011.555890

61. Müller-Tidow C, Bug G, Lübbert M, Krämer A, Krauter J, Valent P, et al. A randomized, open-label, phase I/II trial to investigate the maximum tolerated dose of the Polo-like kinase inhibitor BI 2536 in elderly patients with refractory/relapsed acute myeloid leukaemia. *Br J Haematol* (2013) 163(2):214–22. doi: 10.1111/bjh.12518

62. Csizmar CM, Kim DH, Sachs Z. The role of the proteasome in AML. *Blood Cancer J* (2016) 6(12):e503. doi: 10.1038/bcj.2016.112

frontiers | Frontiers in Immunology

TYPE Systematic Review
PUBLISHED 01 December 2023
DOI 10.3389/fimmu.2023.1273220

OPEN ACCESS

EDITED BY
Jiaxi He,
First Affiliated Hospital of Guangzhou Medical University, China

REVIEWED BY
Zhenzhou Yang,
Chongqing Medical University, China
Luis Mas,
Auna Oncosalud, Peru

*CORRESPONDENCE
Liting You
youlitin_med@163.com

†These authors have contributed equally to this work

RECEIVED 05 August 2023
ACCEPTED 21 November 2023
PUBLISHED 01 December 2023

CITATION
Zheng Y, Feng B, Chen J and You L (2023) Efficacy, safety, and survival of neoadjuvant immunochemotherapy in operable non-small cell lung cancer: a systematic review and meta-analysis.
Front. Immunol. 14:1273220.
doi: 10.3389/fimmu.2023.1273220

Efficacy, safety, and survival of neoadjuvant immunochemotherapy in operable non-small cell lung cancer: a systematic review and meta-analysis

Yue Zheng[1†], Baijie Feng[1†], Jingyao Chen[2†] and Liting You[3*]

[1]West China School of Medicine, Sichuan University, Chengdu, Sichuan, China, [2]Precision Medicine Research Center, West China Hospital, Sichuan University, Chengdu, Sichuan, China, [3]Department of Laboratory Medicine, West China Hospital, Sichuan University, TCM Regulating Metabolic Diseases Key Laboratory of Sichuan Province, Hospital of Chengdu University of Traditional Chinese Medicine, Chengdu, Sichuan, China

Background: Neoadjuvant immunochemotherapy may benefit patients with non-small cell lung cancer (NSCLC), but its impact requires further investigation.

Methods: A meta-analysis was conducted. PubMed, Embase, Web of Science, and the Cochrane Library were searched. The study was registered in PROSPERO (registration no. CRD42022360893).

Results: 60 studies of 3,632 patients were included. Comparing with neoadjuvant chemotherapy, neoadjuvant immunochemotherapy showed higher pCR (RR: 4.71, 95% CI: 3.69, 6.02), MPR (RR, 3.20, 95% CI: 2.75, 3.74), and ORR (RR, 1.46, 95% CI: 1.21, 1.77), fewer surgical complications (RR: 0.67, 95%CI: 0.48, 0.94), higher R0 resection rate (RR: 1.06, 95%CI: 1.03, 1.10, I^2 = 52%), and longer 1-year and 2-year OS, without affecting TRAEs. For neoadjuvant immunochemotherapy in NSCLC, the pooled pCR rate was 0.35 (95% CI: 0.31, 0.39), MPR was 0.59 (95% CI: 0.54, 0.63), and ORR was 0.71 (95% CI: 0.66, 0.76). The pooled incidence of all grade TRAEs was 0.70 (95% CI: 0.60, 0.81), and that of >= grade 3 TRAEs was 0.24 (95% CI: 0.16, 0.32). The surgical complications rate was 0.13 (95% CI: 0.07, 0.18) and R0 resection rate was 0.98 (95% CI: 0.96, 0.99). The pooled 1-year OS was 0.97 (95%CI: 0.96, 0.99), and 2-year OS was 0.89 (95%CI: 0.83, 0.94). Patients with squamous cell carcinoma, stage III or higher PD-L1 performed better. Notably, no significant differences were observed in pCR, MPR, and ORR between 2 or more treatment cycles. Pembrolizumab-, or toripalimab-based neoadjuvant immunochemotherapy demonstrated superior efficacy and tolerable toxicity.

Conclusion: According to our analysis, reliable efficacy, safety, and survival of neoadjuvant immunochemotherapy for operable NSCLC were demonstrated.

Systematic review registration: https://www.crd.york.ac.uk/prospero/display_record.php?ID=CRD42022360893, identifier CRD42022360893.

KEYWORDS

non-small cell lung cancer, neoadjuvant immunochemotherapy, efficacy, safety, survival

1 Introduction

Non-small cell lung cancer (NSCLC) remains the main reason of tumor-related deaths (1). Of patients with NSCLC, 20-25% are surgically resectable, but 30-55% of patients treated with surgery still experience cancer relapse, metastasis, or death (2, 3). Due to the large tumor burden in advanced NSCLC, direct surgical treatment is challenging, while neoadjuvant therapy can shrink the tumor and make unresectable tumors resectable (4, 5). As a result, the NCCN guidelines recommend preoperative neoadjuvant therapy and postoperative adjuvant therapy as the standard therapy for NSCLC (6). But neoadjuvant chemotherapy may only provide a 5-6% benefit of 5-year overall survival (OS) and few patients achieve pathologic complete response (pCR) (7).

Immune checkpoint inhibitor (ICI) plays an important role in the first-line and second-line therapy of patients with NSCLC, showing a better survival benefit than chemotherapy (8–12). A growing view is that earlier immunotherapy may provide greater benefits. Several clinical studies have shown that neoadjuvant immunotherapy can was crucial in the comprehensive treatment of NSCLC, with controllable adverse events and less surgical delay (13, 14). CheckMate 159 showed that the pCR and MPR rates of nivolumab were 10% and 45%, respectively (15). The LCCMC 3 study revealed that the MPR rate of patients receiving 2 cycles of atezolizumab neoadjuvant therapy was 20.4%, and the pCR rate was 6.8% (16). These results were superior to those of previous neoadjuvant chemotherapy.

In the NADIM study, neoadjuvant immunochemotherapy for operable NSCLC had a pCR rate of 69.2% and an MPR rate of 84.6% (17, 18). In the NeoTPD01, and NCT02716038, and SAKK 16/14 studies, the MPR was around 60% (19–21). CheckMate 816, the first successful phase III trial of neoadjuvant immunochemotherapy versus chemotherapy in operable stage IB-III NSCLC, showed that MPR (36.9% *vs*. 8.9%) and pCR (24% *vs*. 2.2%) were significantly improved (22, 23). Updated data from the NADIM II study also revealed that neoadjuvant immunochemotherapy can effectively shrink tumors, increase pCR (36.8% *vs*. 6.9%), MPR (52.6% *vs*. 13.8%), and ORR (75.4% *vs*. 48.2%), and help patients obtain better survival in locally advanced IIIA-IIIB resectable NSCLC (24, 25). These studies provide encouraging results of neoadjuvant immunochemotherapy in patients with NSCLC.

Despite the promising results, concerns about the efficacy, safety, and survival of neoadjuvant immunochemotherapy remain. To address these concerns, we conducted a meta-analysis to combine all related trials and evaluate the efficacy, safety, and survival rates of neoadjuvant immunochemotherapy in operable NSCLC. Additionally, we compared the results among different subgroups, such as age, gender, smoking history, histology, stage, treatment cycles, pretreatment programmed death-ligand 1 (PD-L1), and ICI type. Our goal was to provide guidance for the clinical treatment of NSCLC.

2 Methods

To ensure the accuracy and transparency of our study, we followed the PRISMA (Preferred Reporting Items for Systematic Reviews and Meta-Analyses) and AMSTAR (Assessing the methodological quality of systematic reviews) guidelines (26, 27). This study was registered in PROSPERO (registration no.CRD42022360893, available at: https://www.crd.york.ac.uk/prospero/display_record.php?ID=CRD42022360893).

2.1 Data search

We searched PubMed, Embase, Web of Science, and Cochrane Library, using keywords such as “neoadjuvant”, “immunotherapy”, “chemotherapy”, and “non-small cell lung cancer”. The search was conducted independently by two authors and included papers updated until July 2023. Language restrictions were not applied.

2.2 Study criteria

To be eligible for our study, trials were required to have administered neoadjuvant immunochemotherapy to patients diagnosed with operable NSCLC and acquired radiological or pathological response data. Enrolled patients should not have received any prior systemic anti-neoplastic treatment for NSCLC, must have had no history of lung radiotherapy, and should have undergone surgical resection for NSCLC. Excluded were trials involving patients with concurrent progressive or actively treated additional malignancies, those who had received previous systemic antineoplastic therapy for NSCLC, or those with a history of lung radiotherapy. Studies falling into categories such as reviews, comments, case reports, trial protocols, or animal experiments were also eliminated. In the context of randomized controlled trials (RCTs), preference was given to those that compared non-combination therapy with combination therapy, establishing a basis for a comparison group. In cases where multiple publications reported results from the same study population across different journals, the most comprehensive or most current study was selected for inclusion.

2.3 Data extraction and quality assessment

We screened these literatures based on pre-determined inclusion and exclusion criteria. Two authors independently screened the records, read the full-text papers, and extracted details from the included studies. The primary endpoints were pCR (no residual vital cancer cells), major pathologic response (MPR, <= 10% residual vital cancer cells), the incidence of grade 3 or higher treatment-related adverse events (TRAEs), and 1-year and 2-year OS (the duration from randomization to death from any reason). The secondary endpoints were objective response rate (ORR, proportion of patients with a partial or complete response), total grade TRAEs, R0 resection rate, and the incidence of surgical complications. We assessed the quality of RCTs using the Cochrane Collaboration’s tool (28). For dual-arm non-RCTs, we used the Newcastle-Ottawa scale, and for single-arm non-RCTs, we used the Methodological Index for Non-Randomized Studies

criteria (MINORS) to assess quality (29, 30). We consulted a third referee to resolve discrepancies.

2.4 Data synthesis and statistical analysis

For single-arm studies, we combined the proportion of each endpoint with a 95% confidence interval (95% CI) to draw forest plots. For dual-arm studies, we calculated the risk ratio (RR) and 95% CI. We used the Cochrane Q test and I^2 test to determine statistical heterogeneity. If $I^2 > 50\%$ or $p < 0.05$, we used the random effects model. If $I^2 < 50\%$ or $p > 0.05$, we used the fixed effects model. We carried out subgroup analysis according to age, gender, smoking history, histology, stage, treatment cycles, pretreatment PD-L1, and ICI type. The sensitivity analysis evaluated the stability of the results by ruling out each trial separately. We evaluated publication bias using funnel plots. We used R 4.3.1 software and the meta_v6.2-1 package for the analysis.

3 Results

3.1 Study selection

Totally, 1,601 studies were screened. After eliminating duplicates and irrelevant studies based on their titles and abstracts, 1,416 were excluded, and the remaining 185 studies were reviewed in detail. Out of these, 125 studies were further excluded due to reasons such as incorrect study type, insufficient data, non-targeted outcomes, duplicated cohorts, trial protocol, and treatment combined with radiotherapy. Ultimately, 60 studies comprising 4 RCTs, 13 dual-arm cohorts, and 43 single-arm studies were selected for analysis, with a total of 3,632 eligible patients included. Figure 1; Supplementary Table 1 provides details of this literature search. Tables 1, 2 suggest the characteristics of the eligible studies. All the included studies were considered moderately or highly credible, and Supplementary Figure 3 provides funnel plots. The quality scores of each eligible study are presented in Supplementary Tables 2-4.

3.2 Efficacy of neoadjuvant immunochemotherapy

The efficacy of neoadjuvant immunochemotherapy was assessed based on pCR, MPR, and ORR rates, with neoadjuvant immunochemotherapy showing significantly better efficacy than neoadjuvant chemotherapy. The estimated RR was 4.71 (95% CI: 3.69, 6.02, $I^2 = 0\%$) for pCR, 3.20 (95% CI: 2.75, 3.74, $I^2 = 26\%$) for MPR, and 1.46 (95% CI: 1.21, 1.77, $I^2 = 62\%$) for ORR (Figures 2A, B; Supplementary Figure 1A). For neoadjuvant immunochemotherapy in NSCLC, the pooled pCR rate was 0.35 (95% CI: 0.31, 0.39, $I^2 = 78\%$), the MPR rate was 0.59 (95% CI: 0.54, 0.63, $I^2 = 85\%$), and the ORR rate was 0.71 (95% CI: 0.66, 0.76, $I^2 = 82\%$) (Figure 3).

3.3 Safety of neoadjuvant immunochemotherapy

In the comparison of safety and surgical outcomes between neoadjuvant immunochemotherapy and neoadjuvant chemotherapy, the estimated RR for >= grade 3 TRAEs was 1.14 (95%CI: 0.99, 1.31, $I^2 = 21\%$) (Figure 2C) and for all grade TRAEs, the RR was 1.00 (95%CI: 0.96, 1.03, $I^2 = 19\%$), suggesting no significant difference (Supplementary Figure 1B). However, neoadjuvant immunochemotherapy may result in fewer surgical complications (RR: 0.67, 95%CI: 0.48, 0.94, $I^2 = 0\%$) and higher R0 resection rate (RR: 1.06, 95%CI: 1.03, 1.10, $I^2 = 52\%$) (Supplementary Figures 1C, D). The pooled incidence of >= grade 3 TRAEs was 0.24 (95%CI: 0.16, 0.32, $I^2 = 96\%$) (Figure 4A). The pooled incidence of all grade TRAEs was 0.70 (95%CI: 0.60, 0.81, $I^2 = 97\%$) and that of surgical complications was 0.13 (95%CI: 0.07, 0.18, $I^2 = 82\%$), and the R0 resection rate was 0.98 (95%CI: 0.96, 0.99, $I^2 = 61\%$) (Supplementary Figure 2).

3.4 Survival of neoadjuvant immunochemotherapy

When compared with neoadjuvant chemotherapy, neoadjuvant immunotherapy may significantly enable long survival for patients, with a RR of 1.18 (95%CI: 1.04, 1.34, $I^2 = 0\%$) for 1-year OS, and 1.08 (95%CI: 1.02, 1.14, $I^2 = 53\%$) for 2-year OS (Figures 2D, E). Among the studies that reported specific survival data for patients with NSCLC receiving neoadjuvant immunochemotherapy, the pooled results were 0.97 (95%CI: 0.96, 0.99, $I^2 = 46\%$) for 1-year OS, and 0.89 (95%CI: 0.83, 0.94, $I^2 = 84\%$) for 2-year OS (Figures 4B, C).

3.5 Sensitivity analysis and subgroup analysis

To test the stability, we performed sensitivity analyses by removing each individual trial, and found that our selected studies were reliable (Supplementary Figure 4). We also performed subgroup analyses, and the results are presented in Figure 5; Supplementary Figures 5-7.

As basic clinical characteristics may contribute to heterogeneity, we conducted subgroup analyses based on age, gender, and smoking history in the neoadjuvant immunochemotherapy group. However, no significant differences were found in these subgroups (all p values > 0.05).

Among the included patients, the histology subtypes were divided into squamous and non-squamous. Neoadjuvant immunochemotherapy treatment in patients with squamous lung cancer performed significantly higher rates of MPR ($p = 0.03$) and ORR ($p < 0.01$), and a tendency towards better pCR without reaching statistical significance ($p = 0.09$). Stage is also a key factor of heterogeneity, so we further explored subgroups based on stage (II, IIIA, IIIB, IIIC). We found that patients with stage II

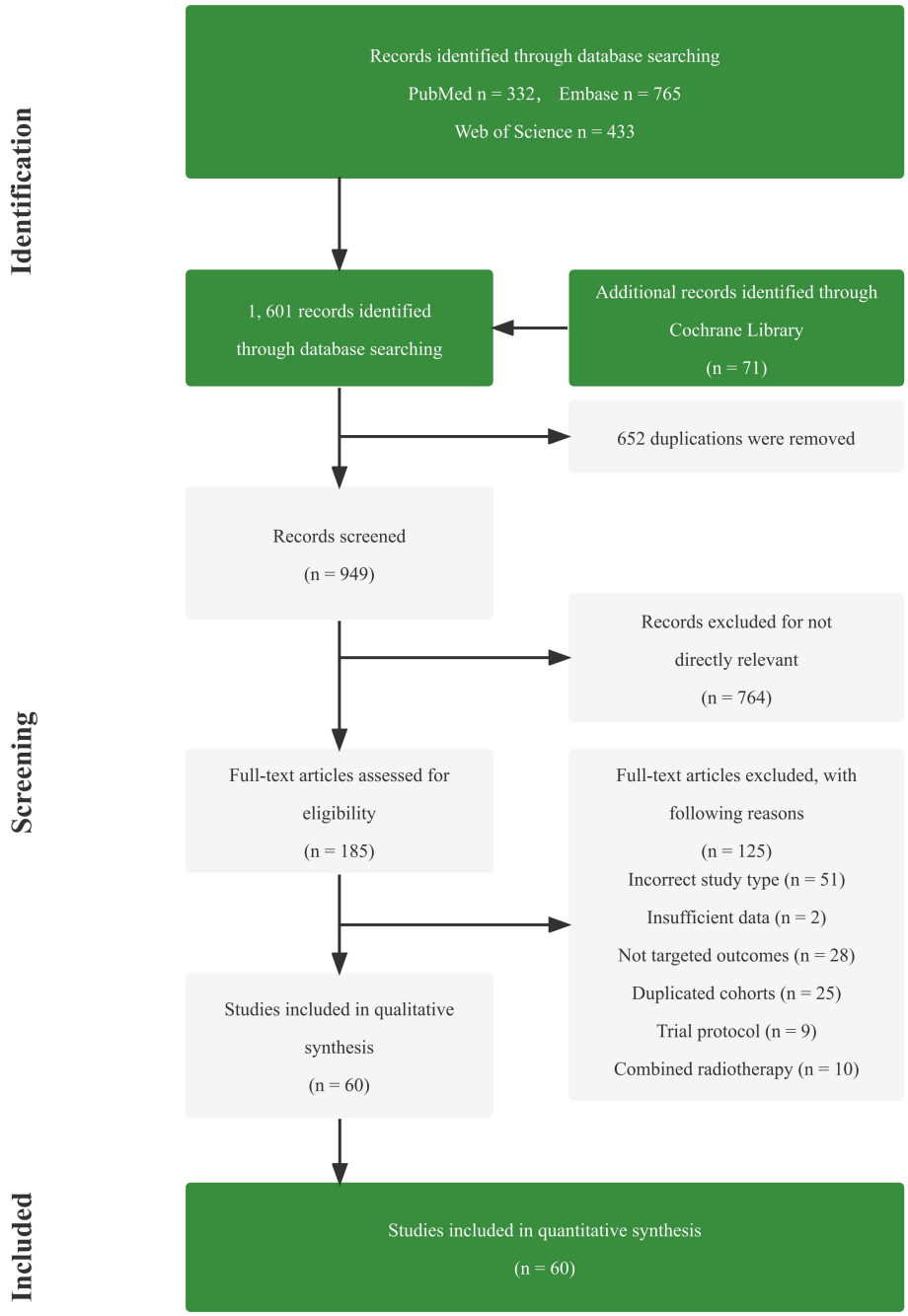

FIGURE 1
PRISMA diagram of identifying eligible studies.

NSCLC experienced less benefit in terms of pCR ($p < 0.01$) and ORR ($p = 0.05$) than those with advanced stage.

The optimal treatment cycle for neoadjuvant immunochemotherapy remains uncertain, with no clear evidence indicating whether 2 or more cycles are superior. To investigate this, we conducted a subgroup analysis of treatment cycles (2 cycles *vs.* >2 cycles) and found no significant discrepancies in pCR ($p = 0.92$), MPR ($p = 0.80$), or ORR ($p = 0.61$) between these subgroups. We also examined the effect of pretreatment PD-L1 expression and found that patients with higher PD-L1 (TPS ≥ 50% or TPS = 1-49%) had significantly improved pCR, MPR, and ORR compared to those with lower PD-L1 (TPS < 1%). Patients who achieved partial response (PR) or complete response (CR) had higher MPR rates than those with stable disease (SD) ($p < 0.01$).

We observed significant differences among subgroups in pCR, MPR, ORR, and 3 or higher grade TRAEs for different ICI types ($p < 0.01$). Pembrolizumab-based neoadjuvant immunochemotherapy demonstrated higher pCR (0.49, 95% CI: 0.37-0.61), MPR (0.69, 95% CI: 0.57-0.80), and ORR (0.86, 95% CI: 0.71-0.95) rates. Toripalimab-based neoadjuvant immunochemotherapy showed higher pCR (0.44, 95% CI: 0.31-0.57) and MPR (0.61, 95% CI: 0.48-0.73) rates. Nivolumab-based neoadjuvant immunochemotherapy had

TABLE 1 Main characteristics of dual-arm studies included in the meta-analysis.

Author (Year)	Study (Phase, Design)	Registered ID (Randomization)	Study type	Sample size	Stage	Median age	Gender (M/F)	Smoking history (%)	Median follow-up (month)	Neoadjuvant therapy of intervention Arm	Neoadjuvant therapy of control Arm	Surgery	Outcomes
Provencio (2022) (24, 25)	NADIM II (II, open-label)	NCT03838159 (1:1)	RCT	86 (57/29)	IIIA-IIIB	_	_	_	_	nivolumab + paclitaxel + carboplatin	paclitaxel + carboplatin	53/20	pCR, MPR, ORR, TRAE
Forde (2023) (23)	CheckMate 816 (III, open-label)	NCT02998528 (1:1)	RCT	358 (179/179)	IB-IIIA	64.5	255/103	88.8	41.4	nivolumab + cisplatin or carboplatin	cisplatin or carboplatin	149/135	pCR, MPR, ORR, TRAE, OS, R0 resection rate
Wakelee (2023) (31)	KEYNOTE-671 (III, double-blind)	NCT03425643 (1:1)	RCT	797 (397/400)	II-III	63.5	563/234	87.3	25.2	pembrolizumab + chemo	cisplatin-based chemo	325/317	pCR, MPR, TRAE
Alì (2023) (32)	_	(12:14)	Retro	26 (12/14)	I-IV	69	18/8	_	29	ICI + chemo	platinum based doublet chemo	26	pCR, MPR
Cesur (2022) (33)	_	_	Retro	65 (17/48)	_	_	_	_	_	ICI + chemo	chemo	17/48	MPR, OS
Sun (2022) (34)	_	_	Retro	81(40/41)	II-IIIA	_	57/24	77.8	24	ICI + chemo	chemo	40/41	pCR, MPR
Dai (2022) (35)	_	ChiCTR2200060433 (20:42)	Retro	62 (20/42)	IB-IIIB	_	53/9	74.2	24	ICI + chemo	chemo	20/42	pCR, MPR, R0 resection rate
Sun (2022) (36)	_	_	Retro	168 (79/89)	II-IIIA	61	136/32	92.9	18	ICI + chemo	chemo	79/89	pCR, MPR
Feng (2022) (37)	_	(8:13)	Pro	21 (8/13)	IIA-IIIB	64	20/1	95.2	20.53	pembrolizumab or toripalimabd + gemcitabine, paclitaxel or nab-paclitaxel + cisplatin or carboplatin	gemcitabine, paclitaxel or nab-paclitaxel + cisplatin or carboplatin	8/13	pCR, MPR, ORR, TRAE, R0 resection rate
Hou (2022) (38)	_	(31:25)	Pro	56 (31/25)	IIIA-IIIB	60.7	43/13	82.1	11.8	camrelizumab + paclitaxel + carboplatin	paclitaxel + carboplatin	31/25	pCR, MPR, ORR, TRAE, OS

(Continued)

10.3389/fimmu.2023.1273220

TABLE 1 Continued

Author (Year)	Study (Phase, Design)	Registered ID (Randomization)	Study type	Sample size	Stage	Median age	Gender (M/F)	Smoking history (%)	Median follow-up (month)	Neoadjuvant therapy of intervention Arm	Neoadjuvant therapy of control Arm	Surgery	Outcomes
Liu (2022) (39)	_	(79:91)	Retro	170 (79/91)	IB–IIIB	_	141/29	82.9	17.0	pembrolizumab or nivolumab or sintilimab or camrelizumab + paclitaxel or pemetrexed or docetaxel or gemcitabine + platinum	paclitaxel or pemetrexed or docetaxel or gemcitabine + platinum	79/91	pCR, MPR, ORR, R0 resection rate
Yue (2022) (40)	_	(1:1)	Retro	18 (12/6)	I-III	62.5	17/5	81.8	17.7	ICI + chemo	chemo	12/6	pCR, MPR
Zhang (2022) (41)	_	(1:2)	Retro	190 (69/121)	IB-IIIB	_	175/15	85.3	ICI + chemo: 18.6 chemo: 22.4	PD-1 + cisplatin or carboplatin	cisplatin or carboplatin	69/121	pCR, MPR, ORR, TRAE, OS, R0 resection rate, surgical complications
Zhao (2022) (42)	_	(42:98)	Retro	140 (42/98)	IB-IIIB	_	123/17	50	ICI + chemo: 18 chemo: 24	ICI + chemo	chemo	42/98	pCR, MPR, ORR, R0 resection rate, surgical complications
Liang (2021) (43)	_	(1:1)	Retro	20 (10/10)	IIB-IIIB	60.89	14/6	70	ICI + chemo: 13.5 chemo: 20.8	pembrolizumab or nivolumab or sintilimab + platinum-based doublet chemo	platinum-based doublet chemo	10/10	pCR, MPR, ORR, OS, surgical complications
Sun (2021) (44)	_	(1:1)	Retro	168 (79/89)	II-IIIA	_	136/32	79.7		nivolumab or camrelizumab or tislelizumab + chemo	chemo	79/89	pCR, MPR
Lei (2020) (45)	(II, open-label)	NCT04338620 (1:1)	RCT	27 (14/13)	IIIA-IIIB	_	_	_	_	camrelizumab + ab-Pac + cisplatin	ab-Pac + cisplatin	13 (7/6)	pCR, MPR, ORR, TRAE

RCT, randomized controlled trials; pCR, pathologic complete response; MPR, major pathologic response; ORR, objective response rate; TRAE, treatment related adverse events; EFS, event free survival; OS, overall survival; Pro, prospective study; DFS, disease free survival; Retro, retrospective study; ICI, immune checkpoint inhibitors; chemo, chemotherapy; PD-1, programmed death 1; ab-Pac, albumin-bound paclitaxel.

10.3389/fimmu.2023.1273220

TABLE 2 Main characteristics of single-arm studies included in the meta-analysis.

Author (Year)	Study (Phase, Design)	Registered ID	Study type	Sample size	Stage	Median age (Years)	Gender (M/F)	Smoking history (%)	Median follow-up (month)	Neoadjuvant therapy of intervention Arm	Surgery	Outcomes
Henick (2023) (46)	(I, open-label)	_	Pro	30	_	_	_	_	39.5	atezolizumab +carboplatin+ nab-paclitaxel	29	pCR, MPR, OS, R0 resection rate
Tao (2023) (47)	(II, open-label)	NCT04606303	Pro	55	IIB-IIIB	62	50/5	89.1	_	toripalimab + chemo	48	pCR, MPR, TRAE, R0 resection rate
Fang (2023) (48)	_	_	Retro	211	IB–IIIB	64	196/15	85.8	17	ICI + chemo	211	pCR, MPR, ORR, TRAE, R0 resection rate, surgical complications
Cascone (2023) (49)	NEOSTAR (II, open-label)	NCT03158129	Pro	22	IB–IIIA	69.5	10/12	77.3	39.2	nivolumab + chemo	22	pCR, MPR, ORR, TRAE, R0 resection rate
Chen (2023) (50)	_	_	Retro	61	_	_	_	_	_	pembrolizumab + chemo	_	pCR, MPR
Zhao (2023) (51)	_	_	Retro	25	IIB-IIIB	65	22/3	_	_	pembrolizumab + carboplatin or cisplatin+ pemetrexed or nab-paclitaxel	21	pCR, MPR
Han (2023) (52)	_	_	Retro	29	III-IV	_	21/8	72.41	_	ICI + chemo	29	pCR, MPR, ORR, R0 resection rate
Hu (2023) (53)	_	_	Retro	101	IIB-IIIC	58	93/8	64.4	12	ICI + chemo	101	pCR, MPR, ORR, OS, R0 resection rate
Zhuang (2023) (54)	_	_	Retro	129	IIA-IIIB	63	117/12	72.1	_	ICI + chemo	129	pCR, MPR, ORR
Wu (2023) (55)	(Ib/III, double-blind)	NCT04316364	Pro	37	I-III	_	_	_	_	adebrelimab (SHR-1316) + nab-paclitaxel + carboplatin	34	pCR, MPR, ORR, TRAE, surgical complications
Wang (2022) (56)	(II, open-label)	NCT04865705	Pro	33	IIIA-IIIB	_	_	_	_	ICI + chemo	18	pCR, MPR, DFS, OS, R0 resection rate
Zhang (2022) (57)	(II, open-label)	ChiCTR2100044645	Pro	26	IIB-IIIB	_	_	_	_	camrelizumab + albumin paclitaxel + carboplatin or cisplatin	17	pCR, MPR, TRAE, surgical complications
Xu (2022) (58)	_	_	Retro	14	IIIA-IIIB	68	14/0	85.71	_	ICI + chemo	11	pCR, MPR, ORR, TRAE, R0 resection rate, surgical complications

(Continued)

10.3389/fimmu.2023.1273220

TABLE 2 Continued

Author (Year)	Study (Phase, Design)	Registered ID	Study type	Sample size	Stage	Median age (Years)	Gender (M/F)	Smoking history (%)	Median follow-up (month)	Neoadjuvant therapy of intervention Arm	Surgery	Outcomes
Lin (2022) (59)	(II, open-label)	NCT05244837	Pro	37	IIB-III	63	31/6	_	_	tislelizumab + carboplatin + pemetrexed or nab-paclitaxel	27	pCR, MPR, TRAE, R0 resection rate
Dong (2022) (60)	(II, open-label)	NCT04897386	Pro	14	III	64.5	_	_	9.5	durvalumab + chemo	10	pCR, MPR, TRAE, OS, R0 resection rate
Ma (2022) (61)	_	_	Retro	59	IIA-IIIB	61.34	50/9	72.9	_	ICI + chemo	59	pCR, R0 resection rate
Dai (2022) (62)	_	ChiCTR1900023758, NCT04379739, and off-trial	Retro	23	IIB, IIIA-B	63.2	22/1	60.9	15	ICI + chemo	23	pCR, MPR, ORR, TRAE, R0 resection rate, surgical complications
Faehling (2022) (63)	KOMPASSneoOP	_	Retro	59	IIB-IVB (44%)	63.6	30/29	95	24.3	ICI + chemo	59	pCR, MPR, ORR, PFS, OS
Sun (2022) (64)	(II, open-label)	NCT04326153	Pro	20	IIIA-B	59.5	18/2	90	_	sintilimab + nab-paclitaxel + carboplatin	16	pCR, MPR, ORR, DFS, OS, TRAE, R0 resection rate
Gao (2022) (65)	(open-label)	ChiCTR2200057840	Pro	44	IIIA-B	61.5	33/11	33 (75.0)	_	ICI + chemo	44	pCR, MPR, TRAE, R0 resection rate, surgical complications
Qiu (2022) (66)	neoSCORE (II, open-label)	NCT04459611	Pro	60	IB-IIIA	_	_	_	_	sintilimab + carboplatin + nab-paclitaxel or pemetrexed	29	pCR, MPR, ORR, TRAE, DFS, OS
Wu (2022) (67)	_	_	Pro	76	IB-IIIB	62	72/4	67	12.2	pembrolizumab or nivolumab + chemo	76	pCR, MPR, ORR, TRAE, R0 resection rate
Zhai (2022) (68)	_	_	Retro	46	IIIA-IIIB	63	26/20	93.5	15.5	nivolumab + paclitaxel + carboplatin	45	pCR, MPR, TRAE, DFS, OS, R0 resection rate, surgical complications
Zhang (2022) (69)	(II)	ChiCTR1900023758	Pro	50	IIIA	64.84	44/6	76	13.6	sintilimab + carboplatin, gemcitabine or pemetrexed	30	pCR, MPR, ORR, TRAE, DFS, OS, R0 resection rate, surgical complications
Yan (2021) (70)	Renaissance Study (II, open-label)	NCT04606303	Pro	21	IIB-IIIB	62	19/2	85.7	_	toripalimab + cisplatin-based chemo	19	pCR, MPR, TRAE, R0 resection rate, surgical complications

(Continued)

10.3389/fimmu.2023.1273220

TABLE 2 Continued

Author (Year)	Study (Phase, Design)	Registered ID	Study type	Sample size	Stage	Median age (Years)	Gender (M/F)	Smoking history (%)	Median follow-up (month)	Neoadjuvant therapy of intervention Arm	Surgery	Outcomes
Rothschild (2021) (21)	SAKK 16/14 (II, open-label)	NCT02572843	Pro	67	IIIA (N2)	61	35/32	95.5	28.6	cisplatin + docetaxel + durvalumab	55	pCR, MPR, ORR, TRAE, EFS, OS, R0 resection rate
Chen (2021) (71)	_	_	Retro	12	IIIA-IIIB	61	9/3	75	18.17	pembrolizumab or nivolumab + carboplatin + paclitaxel	12	pCR, MPR, TRAE, surgical complications
Chen (2021) (72)	_	_	Retro	35	IIIA-IIIB	_	29/6	77.1	13.29	pembrolizumab + cisplatin + paclitaxel or pemetrexed + paclitaxel	35	pCR, MPR, TRAE, PFS, OS, R0 resection rate
Duan (2021) (73)	(open-label)	_	Pro	23	IIA-IIIB	61.83	22/1	95.7	_	ICI + chemo	20	pCR, MPR, ORR, TRAE, PFS, R0 resection rate, surgical complications
Hong (2021) (74)	_	_	Retro	25	II–III	_	23/2	68	_	pembrolizumab or sintilimab or camrelizumab + taxol + cisplatin or carboplatin	25	pCR, MPR, ORR, R0 resection rate, surgical complications
Hu (2021) (75)	_	_	Pro	20	IB-IIIB	56	18/2	85	_	sintilimab or pembrolizumab or toripalimab + chemo	20	pCR, MPR, ORR, TRAE, R0 resection rate, surgical complications
Shi (2021) (76)	_	_	Retro	27	IIA-IIIB	_	_	_	_	camrelizumab or toripalimab or tislelizumab or sintilimab or pembrolizumab + chemo	27	pCR, MPR, TRAE
Zhang (2021) (77)	(II)	NCT04144608	Pro	18	IIIA-IIIB	57	13/2	_	6	toripalimab + nab-paclitaxel or pemetrexed + carboplatin or cisplatin	15	pCR, MPR, TRAE, R0 resection rate, surgical complications
Zhao (2021) (19, 78)	NeoTPD01 (II)	NCT04304248	Pro	33	IIIA-IIIB	61	27/6	_	4.13	toripalimab + carboplatin + pemetrexed or nab-paclitaxel	30	pCR, MPR, TRAE, EFS, R0 resection rate, surgical complications
Zhou (2021) (79)	_	_	Retro	20	IB-IIIB	_	17/3	85	_	pembrolizumab or toripalimab or sintilimab or camrelizumab + chemo	17	pCR, MPR, ORR, TRAE, R0 resection rate, surgical complications
Shen (2021) (80)	_	_	Pro	37	IIB-IIIB	62.8	35/2	83.8	7	pembrolizumab + ab-Pac + carboplatin	37	pCR, MPR, ORR, TRAE, R0 resection rate, surgical complications

(Continued)

10.3389/fimmu.2023.1273220

TABLE 2 Continued

Author (Year)	Study (Phase, Design)	Registered ID	Study type	Sample size	Stage	Median age (Years)	Gender (M/F)	Smoking history (%)	Median follow-up (month)	Neoadjuvant therapy of intervention Arm	Surgery	Outcomes
Zhang (2021) (81)	_	NCT04324151	Retro	56	IIIA-IIIB	58	54/2	_	11	toripalimab or pembrolizumab + platinum-doublet chemo	45	pCR, MPR, TRAE, R0 resection rate, surgical complications
Provencio (2020) (18)	NADIM (II, open-label)	NCT03081689	Pro	46	IIIA	63	34/12	100	24	paclitaxel + carboplatin + nivolumab	41	pCR, MPR, ORR, TRAE, PFS, OS, R0 resection rate, surgical complications
Shu (2020) (20)	(II, open-label)	NCT02716038	Pro	30	IB-IIIA	67	15/15	100	12.9	atezolizumab + nab-paclitaxel + carboplatin	29	pCR, MPR, ORR, TRAE, DFS, OS, R0 resection rate, surgical complications
Tfayli (2020) (82)	_	NCT03480230	Pro	15	IB-III	65	7/8	73	10	chemo + avelumab	11	pCR, MPR, ORR, TRAE, surgical complications
Zinner (2020) (83)	_	_	Pro	13	IB-IIIA	69	8/5	_	10	nivolumab + cisplatin + pemetrexed or gemcitabine	13	pCR, MPR, TRAE
Liu (2020) (84)	_	_	Pro	13	II-III	63.4	11/2	84.6	3.1	pembrolizumab or toripalimab + platinum-doublet chemo	5	pCR, MPR, ORR, TRAE, R0 resection rate, surgical complications
Hilbe (2015) (85)	INN06 (II, open-label)	Eudract-Nr: 2006-004639-31	Pro	41	IB-IIIB	57.5	24/15	_	44.2	cisplatin + docetaxel + cetuximab	37	pCR, ORR, TRAE, PFS, OS

Retro, retrospective study; PD-1, programmed death 1; pCR, pathologic complete response; MPR, major pathologic response; ORR, objective response rate; TRAE, treatment related adverse events; chemo, chemotherapy; PFS, progression free survival; OS, overall survival; Pro, prospective study; DFS, disease free survival; EFS, event free survival; ab-Pac, albumin-bound paclitaxel.

10.3389/fimmu.2023.1273220

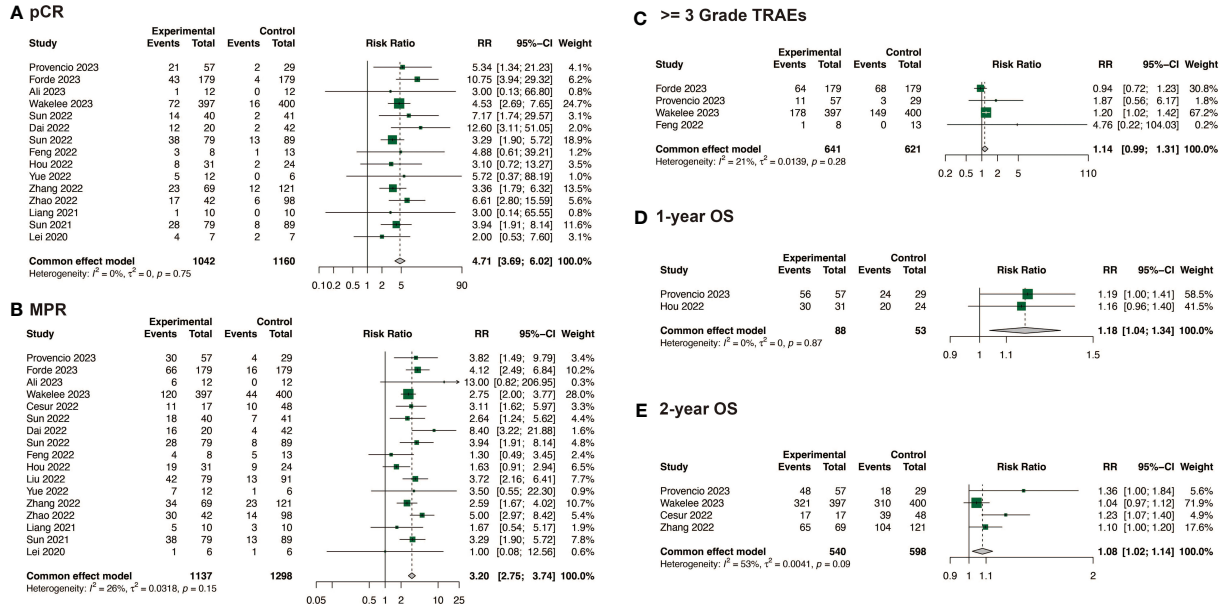

FIGURE 2
Comparison of efficacy, safety and survival between neoadjuvant immunochemotherapy with neoadjuvant chemotherapy alone. **(A)** Comparison of pCR; **(B)** Comparison of MPR; **(C)** Comparison of >= 3 Grade TRAEs; **(D)** Comparison of 1-year OS; **(E)** Comparison of 2-year OS.

higher pCR (0.35, 95% CI: 0.30-0.41) and ORR (0.62, 95% CI: 0.56-0.67) rates. In contrast, avelumab-based neoadjuvant immunochemotherapy demonstrated relatively lower pCR (0.09, 95% CI: 0.00-0.41), MPR (0.27, 95% CI: 0.06-0.61), and ORR (0.27, 95% CI: 0.08-0.55) rates. Pembrolizumab- (0.06, 95% CI: 0.00-0.13) and toripalimab-based (0.02, 95% CI: 0.00-0.08) neoadjuvant immunochemotherapy had significantly lower incidence of 3 or higher grade TRAEs than other ICIs ($p < 0.01$).

4 Discussion

ICIs plus chemotherapy have emerged in the neoadjuvant therapy of NSCLC. This approach has demonstrated good therapeutic effects and safety, offering new hope for the prolonged survival of patients with NSCLC (86). It represents the current direction of NSCLC neoadjuvant therapy. However, there is still a need to further evaluate the efficacy, safety, and survival of this treatment for operable NSCLC. To address this, we conducted this

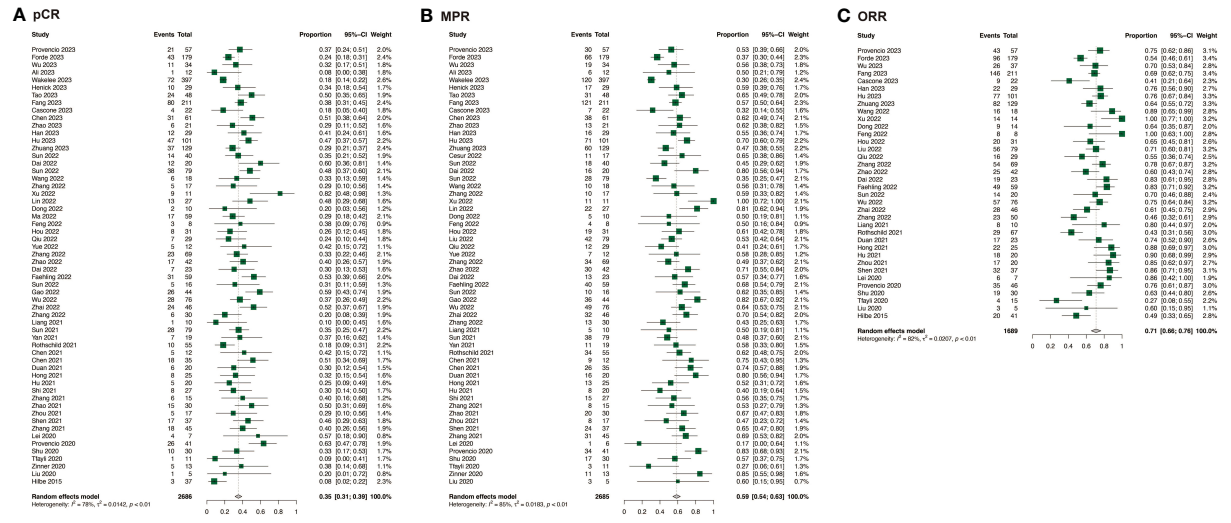

FIGURE 3
Efficacy of neoadjuvant immunochemotherapy in resectable non-small cell lung cancer. **(A)** pCR of neoadjuvant immunochemotherapy in resectable non-small cell lung cancer; **(B)** MPR of neoadjuvant immunochemotherapy in resectable non-small cell lung cancer; **(C)** ORR of neoadjuvant immunochemotherapy in resectable non-small cell lung cancer.

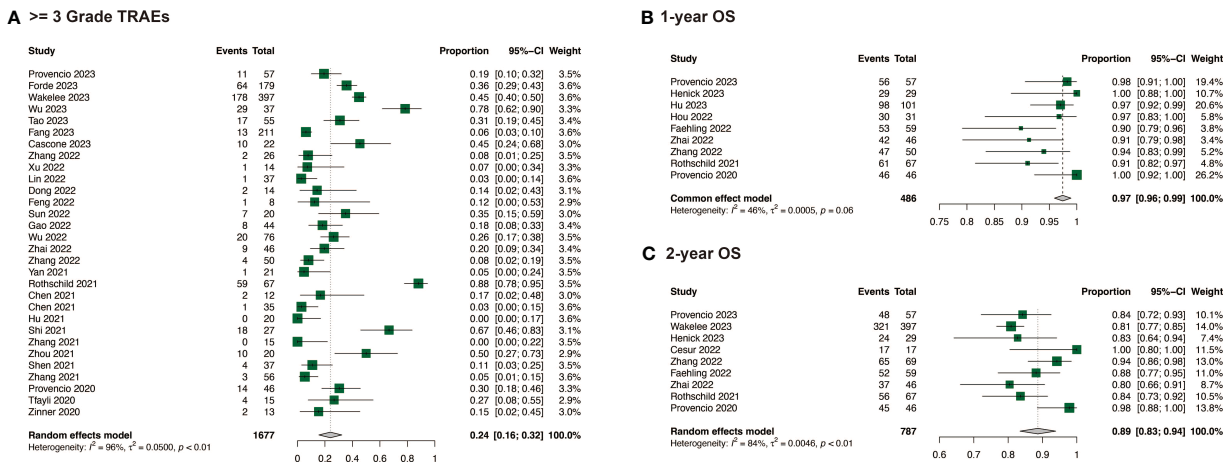

FIGURE 4
Safety and survival of neoadjuvant immunochemotherapy in resectable non-small cell lung cancer. **(A)** >= 3 Grade TRAEs of neoadjuvant immunochemotherapy in resectable non-small cell lung cancer; **(B)** 1-year OS of neoadjuvant immunochemotherapy in resectable non-small cell lung cancer; **(C)** 2-year OS of neoadjuvant immunochemotherapy in resectable non-small cell lung cancer.

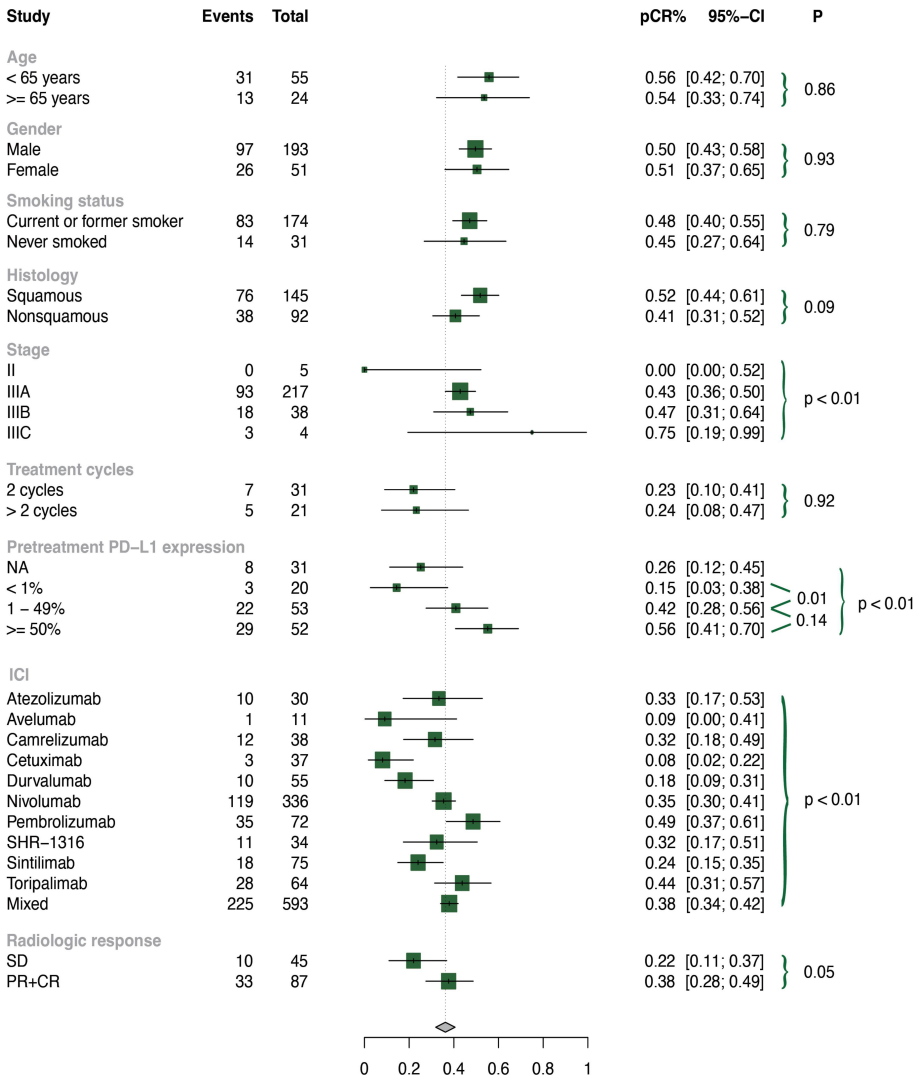

FIGURE 5
Subgroup analysis of pCR by clinical characteristics.

meta-analysis. Our analysis, which included 60 studies and 3,632 patients, found that neoadjuvant immunochemotherapy was superior to neoadjuvant chemotherapy in terms of achieving higher rates of pCR, MPR, and ORR. Additionally, neoadjuvant immunochemotherapy was related to a lower incidence of surgical complications and longer 1-year and 2-year OS, without affecting TRAEs and R0 resection rates. These findings provide valuable reference for the clinical treatment of NSCLC.

Our study investigated the efficacy of neoadjuvant immunochemotherapy for NSCLC, and the results showed that the pooled pCR was 0.35 (95% CI: 0.31, 0.39), MPR was 0.59 (95% CI: 0.54, 0.64), and ORR was 0.71 (95% CI: 0.66, 0.76). These rates were significantly higher than those for neoadjuvant chemotherapy (pooled pCR of 0.04) and neoadjuvant immunotherapy (pCR of no more than 0.10) reported in previous studies (7, 15, 16). Combination therapy can achieve optimal treatment effects by stimulating tumor cell mutations, releasing new tumor antigens, and restructuring the immune microenvironment (87). Our study found that neoadjuvant immunochemotherapy performed better for patients with squamous cell carcinoma, or stage III ($p < 0.01$). Previous studies have also shown that neoadjuvant systemic therapy brings greater clinical benefits to patients with stage III, but caution is needed when assessing pathologic response due to bias introduced by non-operative patients (22). It is possible that patients with squamous cell carcinoma, or stage III are associated with a high level of tumor mutational burden (TMB), inflammation, and PD-L1 expression, which may make them more responsive to immunotherapy (88). However, it is crucial to remember that these factors are not absolute for individual patients.

In neoadjuvant immunochemotherapy for NSCLC, the pooled 1-year OS was 0.97 (95%CI: 0.96, 0.99), and 2-year OS was 0.89 (95%CI: 0.83, 0.94). The benefit of neoadjuvant chemotherapy of OS, compared to operation, is only 5%-6%. The CheckMate 816 trial showed that preoperative nivolumab in combination with chemotherapy resulted in a 37% lower risk of disease recurrence, progression, or death than chemotherapy (22). The SAKK 16/14 trial revealed an encouraging 1-year event-free survival (EFS) of 73% and 2-year EFS of 68% in the neoadjuvant durvalumab plus chemotherapy group (21). EFS measures the time from treatment initiation to the occurrence of any disease-related event and can provide an early assessment of treatment efficacy. However, we did not evaluate EFS in our study because the endpoint of survival is non-uniform, including EFS, OS, progression-free survival (PFS), and disease-free survival, making the survival outcomes difficult to analyze.

Our study suggested that neoadjuvant immunochemotherapy did not increase TRAEs compared with neoadjuvant chemotherapy and may lead to fewer surgical complications, fully confirming its safety. The pooled rate of all grade TRAEs was 0.60 (95% CI: 0.60, 0.81), and that of grade 3 or higher TRAEs was 0.24 (95% CI: 0.16, 0.32). In NSCLC, immune-related adverse events, including pneumonitis, thyroid dysfunction, and skin rash, are the most common types of TRAEs associated with ICIs used in neoadjuvant immunochemotherapy. The pooled rate of surgical complications of neoadjuvant immunochemotherapy was 0.13 (95% CI: 0.07, 0.18), and the pooled R0 resection rate of neoadjuvant immunochemotherapy was 0.98 (95% CI: 0.96, 0.99). Although these adverse events could be serious and potentially life-threatening, they are relatively rare and can usually be managed effectively if detected and treated early. Close monitoring and prompt reporting of any symptoms to the healthcare provider are essential for ensuring the safety of neoadjuvant immunochemotherapy in patients with NSCLC.

Accurately identifying the population for neoadjuvant immunotherapy is critical. Our data show that higher PD-L1 expression (TPS >= 50% or TPS = 1-49%) performed better in neoadjuvant immunochemotherapy ($p < 0.01$). In the published NADIM trial, pCR patients had a higher proportion of PD-L1 positive tumors, but PD-L1 expression was not related to patient survival (18). The results of the CheckMate 816 study revealed that patients with pretherapy PD-L1 above 1% had longer EFS than those with PD-L1 below 1%, supporting PD-L1 as a predictor of neoadjuvant immunotherapy (22). However, in the phase II study of atezolizumab plus chemotherapy, no significant difference was found in MPR and pretreatment PD-L1 (20). TMB is a measure of the number of mutations in a tumor's DNA and has been suggested as a potential predictive biomarker for response to neoadjuvant immunochemotherapy (22). Additionally, the preoperative ctDNA clearance rate may be related to a high predictive effect on postoperative recurrence (22, 40). However, the mechanism and predictive value of ctDNA clearance still need further exploration in basic research. Although our data suggest that these biomarkers can be used as predictors, more marker guidance is needed for patient selection and precise treatment due to the heterogeneity of the data.

Moreover, no significant differences were observed in pCR ($p = 0.92$), MPR ($p = 0.80$), and ORR ($p = 0.61$) between 2 or more treatment cycles, suggesting that increasing cycles of therapy may not increase efficacy. Patients who were PR or CR were related to a higher MPR rate than those in SD ($p < 0.01$). We also found that pembrolizumab- or toripalimab-based neoadjuvant immunochemotherapy performed better in efficacy without affecting >= 3 grade TRAEs. In most included studies, neoadjuvant immunotherapy combined with chemotherapy was used for 2-4 cycles, and operation was performed 4–6 weeks after neoadjuvant immunotherapy (14).

Our study has some limitations. Firstly, the follow-up time of some trials was not long enough to adequately report on long-term survival. Additionally, existing studies are still limited regarding the selection of effective predictors such as ctDNA and the timing of neoadjuvant immunotherapy or adjuvant therapy, making it difficult to obtain more novel results. Thirdly, the study outcomes were non-uniform, making it difficult to pool the survival results of EFS. Therefore, more innovative long-term RCTs are needed to overcome the above obstacles, and the internal mechanism of neoadjuvant immunochemotherapy needs to be further explored. Despite these limitations, this meta-analysis provides objective information on the efficacy, safety, and survival of neoadjuvant immunochemotherapy in operable NSCLC.

5 Conclusion

Our study demonstrates the reliable efficacy, safety, and survival of neoadjuvant immunochemotherapy for operable NSCLC, making it a promising direction for neoadjuvant treatment in the future.

Data availability statement

The original contributions presented in the study are included in the article/Supplementary Material. Further inquiries can be directed to the corresponding author.

Author contributions

YZ: Conceptualization, Data curation, Formal analysis, Methodology, Software, Writing – original draft, Writing – review & editing. BF: Formal analysis, Methodology, Writing – original draft. JC: Formal analysis, Project administration, Writing – review & editing, Funding acquisition. LY: Conceptualization, Funding acquisition, Supervision, Investigation, Resources, Writing – review & editing.

Funding

The author(s) declare financial support was received for the research, authorship, and/or publication of this article. This study was supported by Department of Science and Technology of Sichuan Province (2022YFS0205), the Project of Sichuan Province Key Laboratory Open Funding (grant No.SZKF202210), Natural Science Foundation of Sichuan Province of China (2023NSFSC1883) and the 2024 College Students' Innovative Entrepreneurial Training Plan Program (Project No. C2024130171).

Conflict of interest

The authors declare that the research was conducted in the absence of any commercial or financial relationships that could be construed as a potential conflict of interest.

Publisher's note

Supplementary material

The Supplementary Material for this article can be found online at: https://www.frontiersin.org/articles/10.3389/fimmu.2023.1273220/full#supplementary-material

References

1. Siegel RL, Miller KD, Fuchs HE, Jemal A. Cancer statistics, 2022. *CA: A Cancer J Clin* (2022) 72:7–33. doi: 10.3322/caac.21708

2. Uramoto H, Tanaka F. Recurrence after surgery in patients with NSCLC. *Transl Lung Cancer Res* (2014) 3:242–9. doi: 10.3978/j.issn.2218-6751.2013.12.05

3. Taylor MD, Nagji AS, Bhamidipati CM, Theodosakis N, Kozower BD, Lau CL, et al. Tumor recurrence after complete resection for non-small cell lung cancer. *Ann Thorac Surg* (2012) 93:1813–20. doi: 10.1016/j.athoracsur.2012.03.031

4. Saw SPL, Ong BH, Chua KLM, Takano A, Tan DSW. Revisiting neoadjuvant therapy in non-small-cell lung cancer. *Lancet Oncol* (2021) 22:e501–e16. doi: 10.1016/s1470-2045(21)00383-1

5. Broglio KR, Quintana M, Foster M, Olinger M, McGlothlin A, Berry SM, et al. Association of pathologic complete response to neoadjuvant therapy in HER2-positive breast cancer with long-term outcomes: A meta-analysis. *JAMA Oncol* (2016) 2:751–60. doi: 10.1001/jamaoncol.2015.6113

6. Ettinger DS, Wood DE, Aisner DL, Akerley W, Bauman JR, Bharat A, et al. Non-small cell lung cancer, version 3.2022, NCCN clinical practice guidelines in oncology. *J Natl Compr Canc Netw* (2022) 20:497–530. doi: 10.6004/jnccn.2022.0025

7. Group NM-aC. Preoperative chemotherapy for non-small-cell lung cancer: a systematic review and meta-analysis of individual participant data. *Lancet* (2014) 383:1561–71. doi: 10.1016/s0140-6736(13)62159-5

8. Gandhi L, Rodríguez-Abreu D, Gadgeel S, Esteban E, Felip E, De Angelis F, et al. Pembrolizumab plus chemotherapy in metastatic non-small-cell lung cancer. *N Engl J Med* (2018) 378:2078–92. doi: 10.1056/NEJMoa1801005

9. Borghaei H, Paz-Ares L, Horn L, Spigel DR, Steins M, Ready NE, et al. Nivolumab versus docetaxel in advanced nonsquamous non-small-cell lung cancer. *N Engl J Med* (2015) 373:1627–39. doi: 10.1056/NEJMoa1507643

10. Brahmer J, Reckamp KL, Baas P, Crinò L, Eberhardt WE, Poddubskaya E, et al. Nivolumab versus docetaxel in advanced squamous-cell non-small-cell lung cancer. *N Engl J Med* (2015) 373:123–35. doi: 10.1056/NEJMoa1504627

11. Reck M, Rodríguez-Abreu D, Robinson AG, Hui R, Csőszi T, Fülöp A, et al. Updated analysis of KEYNOTE-024: pembrolizumab versus platinum-based chemotherapy for advanced non-small-cell lung cancer with PD-L1 tumor proportion score of 50% or greater. *J Clin Oncol* (2019) 37:537–46. doi: 10.1200/jco.18.00149

12. Desai AP, Adashek JJ, Reuss JE, West HJ, Mansfield AS. Perioperative immune checkpoint inhibition in early-stage non-small cell lung cancer: A review. *JAMA Oncol* (2023) 9:135–42. doi: 10.1001/jamaoncol.2022.5389

13. Kang J, Zhang C, Zhong WZ. Neoadjuvant immunotherapy for non-small cell lung cancer: State of the art. *Cancer Commun (Lond).* (2021) 41:287–302. doi: 10.1002/cac2.12153

14. Liang W, Cai K, Chen C, Chen H, Chen Q, Fu J, et al. Expert consensus on neoadjuvant immunotherapy for non-small cell lung cancer. *Transl Lung Cancer Res* (2020) 9:2696–715. doi: 10.21037/tlcr-2020-63

15. Forde PM, Chaft JE, Pardoll DM. Neoadjuvant PD-1 blockade in resectable lung cancer. *New Engl J Med* (2018) 379:e14. doi: 10.1056/NEJMc1808251

16. Carbone D, Lee J, Kris M, Wistuba I, Kwiatkowski D, Owen D, et al. OA06.06 clinical/biomarker data for neoadjuvant atezolizumab in resectable stage IB-IIIB NSCLC: primary analysis in the LCMC3 study. *J Thorac Oncol* (2021) 16:S115–S6. doi: 10.1016/j.jtho.2021.01.294

17. Provencio M, Nadal E, Insa A, García Campelo R, Huidobro G, Domine M, et al. Phase II study of neo-adjuvant chemo/immunotherapy for resectable stages IIIA non-small cell lung cancer- nadim study-SLCG. *J Thorac Oncol* (2018) 13:S320. doi: 10.1016/j.jtho.2018.08.236

18. Provencio M, Nadal E, Insa A, García-Campelo MR, Casal-Rubio J, Dómine M, et al. Neoadjuvant chemotherapy and nivolumab in resectable non-small-cell lung cancer (NADIM): an open-label, multicentre, single-arm, phase 2 trial. *Lancet Oncol* (2020) 21:1413–22. doi: 10.1016/s1470-2045(20)30453-8

19. Zhao Z, Chen S, Qi H, Yang CP, Lin YB, Jin JT, et al. Phase II trial of toripalimab plus chemotherapy as neoadjuvant treatment in resectable stage III non-small cell lung cancer (NeoTPD01 Study). *J Clin Oncol* (2021) 39:8541. doi: 10.1200/JCO.2021.39.15-suppl.8541

20. Shu CA, Gainor JF, Awad MM, Chiuzan C, Grigg CM, Pabani A, et al. Neoadjuvant atezolizumab and chemotherapy in patients with resectable non-small-cell lung cancer: an open-label, multicentre, single-arm, phase 2 trial. *Lancet Oncol* (2020) 21:786–95. doi: 10.1016/s1470-2045(20)30140-6

21. Rothschild SI, Zippelius A, Eboulet EI, Prince SS, Betticher D, Bettini A, et al. SAKK 16/14: durvalumab in addition to neoadjuvant chemotherapy in patients with stage IIIA(N2) non-small-cell lung cancer-A multicenter single-arm phase II trial. *J Clin Oncol* (2021) 39:2872–80. doi: 10.1200/jco.21.00276

22. Forde PM, Spicer J, Lu S, Provencio M, Mitsudomi T, Awad MM, et al. Neoadjuvant nivolumab plus chemotherapy in resectable lung cancer. *N Engl J Med* (2022) 386:1973–85. doi: 10.1056/NEJMoa2202170

23. Forde PM, Spicer J, Girard N, Provencio M, Lu S, Wang C, et al. 84O Neoadjuvant nivolumab (N) + platinum-doublet chemotherapy (C) for resectable NSCLC: 3-y update from CheckMate 816. *J Thorac Oncol* (2023) 18:S89–90. doi: 10.1016/S1556-0864(23)00338-6

24. Provencio-Pulla M, Nadal E, Larriba JLG, Martinez-Marti A, Bernabé R, Bosch-Barrera J, et al. Nivolumab + chemotherapy versus chemotherapy as neoadjuvant treatment for resectable stage IIIA NSCLC: Primary endpoint results of pathological complete response (pCR) from phase II NADIM II trial. *J Clin Oncol* (2022) 40:8501. doi: 10.1200/JCO.2022.40.16_suppl.8501

25. Provencio M, Nadal E, González-Larriba JL, Martínez-Martí A, Bernabé R, Bosch-Barrera J, et al. Perioperative nivolumab and chemotherapy in stage III non-small-cell lung cancer. *N Engl J Med* (2023) 389:504–13. doi: 10.1056/NEJMoa2215530

26. Higgins JPT, Green SE. *Cochrane Handbook for Systematic Reviews of Interventions*. Cochrane Collaboration website United Kingdom (2022). Available at: https://training.cochrane.org/handbook/current.

27. Page MJ, McKenzie JE, Bossuyt PM, Boutron I, Hoffmann TC, Mulrow CD, et al. The PRISMA 2020 statement: an updated guideline for reporting systematic reviews. *BMJ* (2021) 372:n71. doi: 10.1136/bmj.n71

28. Higgins JP, Altman DG, Gøtzsche PC, Jüni P, Moher D, Oxman AD, et al. The Cochrane Collaboration's tool for assessing risk of bias in randomised trials. *Bmj* (2011) 343:d5928. doi: 10.1136/bmj.d5928

29. Stang A. Critical evaluation of the Newcastle-Ottawa scale for the assessment of the quality of nonrandomized studies in meta-analyses. *Eur J Epidemiol.* (2010) 25:603–5. doi: 10.1007/s10654-010-9491-z

30. Slim K, Nini E, Forestier D, Kwiatkowski F, Panis Y, Chipponi J. Methodological index for non-randomized studies (minors): development and validation of a new instrument. *ANZ J Surg* (2003) 73:712–6. doi: 10.1046/j.1445-2197.2003.02748.x

31. Wakelee H, Liberman M, Kato T, Tsuboi M, Lee SH, Gao S, et al. Perioperative pembrolizumab for early-stage non-small-cell lung cancer. *N Engl J Med* (2023) 389:491–503. doi: 10.1056/NEJMoa2302983

32. Alì G, Poma AM, Di Stefano I, Zirafa CC, Lenzini A, Martinelli G, et al. Different pathological response and histological features following neoadjuvant chemotherapy or chemo-immunotherapy in resected non-small cell lung cancer. *Front Oncol* (2023) 13:1115156. doi: 10.3389/fonc.2023.1115156

33. Cesur E, Ozer KB, Erus S, Bulutay P, Selcukbiricik F, Tanju S, et al. EP05.02-005 is immunotherapy safer than radiotherapy in combination with chemotherapy in neoadjuvant therapy? *J Thorac Oncol* (2022) 17:S284. doi: 10.1016/j.jtho.2022.07.487

34. Sun X, Liu W, Sun L, Mo H, Feng Y, Wu X, et al. Maturation and abundance of tertiary lymphoid structures are associated with the efficacy of neoadjuvant chemoimmunotherapy in resectable non-small cell lung cancer. *J ImmunoTher Cancer.* (2022) 10:e005531. doi: 10.1136/jitc-2022-005531

35. Dai F, Wu X, Wang X, Li K, Wang Y, Shen C, et al. Neoadjuvant immunotherapy combined with chemotherapy significantly improved patients' overall survival when compared with neoadjuvant chemotherapy in non-small cell lung cancer: A cohort study. *Front Oncol* (2022) 12:1022123. doi: 10.3389/fonc.2022.1022123

36. Sun X, Feng Y, Zhang B, Huang W, Zhao X, Zhang H, et al. The role of neutrophil-to-lymphocyte ratio in predicting pathological response for resectable non-small cell lung cancer treated with neoadjuvant chemotherapy combined with PD-1 checkpoint inhibitors. *Cancer Res Treat* (2022) 54:1017–29. doi: 10.4143/crt.2021.1007

37. Feng Y, Sun W, Zhang J, Wang Y, Chen J, Liu X, et al. Neoadjuvant PD-1 inhibitor combines with chemotherapy versus neoadjuvant chemotherapy in resectable squamous cell carcinoma of the lung. *Thorac Cancer.* (2022) 13:442–52. doi: 10.1111/1759-7714.14280

38. Hou X, Shi X, Luo J. Efficacy and safety of camrelizumab (a PD-1 inhibitor) combined with chemotherapy as a neoadjuvant regimen in patients with locally advanced non-small cell lung cancer. *Oncol Lett* (2022) 24:215. doi: 10.3892/ol.2022.13336

39. Liu Z, Gao Z, Zhang M, Wang X, Gong J, Jiang S, et al. Real-world effectiveness and prognostic factors analysis of stages I-III non-small cell lung cancer following neoadjuvant chemo-immunotherapy or neoadjuvant chemotherapy. *Ann Thorac Cardiovasc Surg* (2022) 28:111–20. doi: 10.5761/atcs.oa.21-00143

40. Yue D, Liu W, Chen C, Zhang T, Ma Y, Cui L, et al. Circulating tumor DNA predicts neoadjuvant immunotherapy efficacy and recurrence-free survival in surgical non-small cell lung cancer patients. *Transl Lung Cancer Res* (2022) 11:263–76. doi: 10.21037/tlcr-22-106

41. Zhang B, Xiao H, Pu X, Zhou C, Yang D, Li X, et al. A real-world comparison between neoadjuvant chemoimmunotherapy and chemotherapy alone for resectable non-small cell lung cancer. *Cancer Med* (2023) 12:274–86. doi: 10.1002/cam4.4889

42. Zhao D, Xu L, Wu J, She Y, Su H, Hou L, et al. Comparison of perioperative outcomes among non-small cell lung cancer patients with neoadjuvant immune checkpoint inhibitor plus chemotherapy, EGFR-TKI, and chemotherapy alone: a real-world evidence study. *Transl Lung Cancer Res* (2022) 11:1468–78. doi: 10.21037/tlcr-22-476

43. Liang H, Yang C, Gonzalez-Rivas D, Zhong Y, He P, Deng H, et al. Sleeve lobectomy after neoadjuvant chemoimmunotherapy/ chemotherapy for local advanced non-small cell lung cancer. *Trans Lung Cancer Res* (2021) 10:143–55. doi: 10.21037/tlcr-20-778

44. Sun X, Feng Y, Zhang B, Huang W, Zhao X, Zhang H, et al. The role of neutrophil-to-lymphocyte ratio in predicting pathological response for resectable NSCLC treated with neoadjuvant chemotherapy combined with PD-1 checkpoint inhibitors. *Cancer Res Treat* (2022) 54:1017–29. doi: 10.4143/crt.2021.1007

45. Lei J, Yan X, Zhao J, Tian F, Lu Q, Jiang T. 62MO A randomised, controlled, multicenter phase II trial of camrelizumab combined with albumin-bound paclitaxel and cisplatin as neoadjuvant treatment in locally advanced NSCLC. *Ann Oncol* (2020) 31:S1441–S2. doi: 10.1016/j.annonc.2020.10.550

46. Henick BS, Gainor JF, Awad MM, Chiuzan C, Izard S, Georgis Y, et al. 3-year update of neoadjuvant atezolizumab + chemotherapy in patients with resectable non-small cell lung cancer. *Cancer Res* (2023) 83:CT217. doi: 10.1158/1538-7445.AM2023-CT217

47. Tao Y, Li X, Liu B, Wang J, Lv C, Li S, et al. Association of early immune-related adverse events with treatment efficacy of neoadjuvant Toripalimab in resectable advanced non-small cell lung cancer. *Front Oncol* (2023) 13:1135140. doi: 10.3389/fonc.2023.1135140

48. Fang M, Hang Q, Jiang H, Cai L, Hu J, Ying H, et al. Efficacy and safety evaluation of neoadjuvant immunotherapy plus chemotherapy for resectable non–small cell lung cancer in real world. *Front Oncol* (2023) 12:1055610. doi: 10.3389/fonc.2022.1055610

49. Cascone T, Leung CH, Weissferdt A, Pataer A, Carter BW, Godoy MCB, et al. Neoadjuvant chemotherapy plus nivolumab with or without ipilimumab in operable non-small cell lung cancer: the phase 2 platform NEOSTAR trial. *Nat Med* (2023) 29:593–604. doi: 10.1038/s41591-022-02189-0

50. Chen Y, Yan B, You J. Neoadjuvant immunochemotherapy of pembrolizumab plus chemotherapy in resectable non-small cell lung cancer. *J Thorac Oncol* (2023) 18:S108–S9. doi: 10.1016/S1556-0864(23)00375-1

51. Zhao G, Zhang H, Xu F, Lu C, Zhu Q, Grossi F, et al. Neoadjuvant pembrolizumab and chemotherapy in resectable clinical stage III non-small-cell lung cancer: a retrospective cohort study. *Transl Lung Cancer Res* (2023) 12:141–9. doi: 10.21037/tlcr-22-871

52. Han R, Zhang Y, Wang T, Xiao H, Luo Z, Shen C, et al. Tumor immune microenvironment predicts the pathologic response of neoadjuvant chemoimmunotherapy in non–small-cell lung cancer. *Cancer Science.* (2023) 114:2569–83. doi: 10.1111/cas.15778

53. Hu X, Hu C, Liu X, Ma F, Xie J, Zhong P, et al. Tumor regression rate, PD-L1 expression, pembrolizumab/nab-paclitaxel–based regimens, squamous cell carcinoma, and comorbidities were independently associated with efficacy of neoadjuvant chemoimmunotherapy in non-small cell lung cancer. *Front Oncol* (2023) 12:1057646. doi: 10.3389/fonc.2022.1057646

54. Zhuang F, Haoran E, Huang J, Wu J, Xu L, Zhang L, et al. Utility of 18F-FDG PET/CT uptake values in predicting response to neoadjuvant chemoimmunotherapy in resectable non-small cell lung cancer. *Lung Cancer.* (2023) 178:20–7. doi: 10.1016/j.lungcan.2023.02.001

55. Yan W, Zhong WZ, Liu YH, Chen Q, Xing W, Zhang Q, et al. Adebrelimab (SHR-1316) in combination with chemotherapy as perioperative treatment in patients with resectable stage II to III NSCLCs: an open-label, multicenter, phase 1b trial. *J Thorac Oncol* (2023) 18:194–203. doi: 10.1016/j.jtho.2022.09.222

56. Wang T, Li L, Huang L, Liu J, Zhu DD, Qin C, et al. 82P Preliminary analysis of tislelizumab (TIS) and chemotherapy as neoadjuvant therapy for potentially resectable stage IIIA/IIIB non-small cell lung cancer (NSCLC). *Immuno-Oncol Technol* (2022) 16:100186. doi: 10.1016/j.iotech.2022.100186

57. Zhang Y, Liu S, Yang L, Liu Y, Wang C, Han Y, et al. Camrelizumab combined with albumin paclitaxel and platinum in perioperative treatment of resectable squamous cell lung cancer: A single-arm, open-label, phase II clinical trial. *Ann Oncol* (2022) 33:S978. doi: 10.1016/j.annonc.2022.07.1067

58. Xu H, Wang W, Yin J, Song C, Li L, Sun Z. Efficacy and safety of the PD-1 inhibitor combined with albumin-bound paclitaxel and nedaplatin in preoperative neoadjuvant therapy of unresectable stage III lung squamous cell carcinoma. *Drug Des Devel Ther* (2022) 16:4269–77. doi: 10.2147/dddt.S388777

59. Lin YB, Long H, Chen YH, Zhai WY, Wang YZ, Rao BY. EP05.02-011 phase II trial of neoadjuvant tislelizumab with chemotherapy for resectable stage IIB-III non-small cell lung cancer. *J Thorac Oncol* (2022) 17:S287. doi: 10.1016/j.jtho.2022.07.493

60. Dong X, Tong F, Zhang R, Liang B, Zhai W, Wang S, et al. Neoadjuvant durvalumab plus chemotherapy in stage III non-small cell lung cancer: A phase II single-center exploratory study. *Immuno-Oncol Technol* (2022) 16:100240. doi: 10.1016/j.iotech.2022.100240

61. Ma T, Wen T, Cheng X, Wang Y, Wei P, Yang B, et al. Pathological complete response to neoadjuvant chemoimmunotherapy correlates with peripheral blood immune cell subsets and metastatic status of mediastinal lymph nodes (N2 lymph nodes) in non-small cell lung cancer. *Lung Cancer.* (2022) 172:43–52. doi: 10.1016/j.lungcan.2022.08.002

62. Dai J, Zhu X, Li D, Huang Y, Liu X, He W, et al. Sleeve resection after neoadjuvant chemoimmunotherapy in the treatment of locally advanced non-small cell lung cancer. *Trans Lung Cancer Res* (2022) 11:188–200. doi: 10.21037/tlcr-22-56

63. Faehling M, Witte H, Sebastian M, Ulmer M, Saetzler R, Steinestel K, et al. Real-world multicentre analysis of neoadjuvant immunotherapy and chemotherapy in localized or oligometastatic non-small cell lung cancer (KOMPASSneoOP). *Ther Adv Med Oncol* (2022) 14:17588359221085333. doi: 10.1177/17588359221085333

64. Sun C, Liu Y, Zhang P, Wang X, Xu Y, Lin X, et al. Interim analysis of the efficiency and safety of neoadjuvant PD-1 inhibitor (sintilimab) combined with chemotherapy (nab-paclitaxel and carboplatin) in potentially resectable stage IIIA/IIIB non-small cell lung cancer: a single-arm, phase 2 trial. *J Cancer Res Clin Oncol* (2023) 149:819–31. doi: 10.1007/s00432-021-03896-w

65. Gao Y, Jiang J, Xiao D, Zhou Y, Chen Y, Yang H, et al. Robotic-assisted thoracic surgery following neoadjuvant chemoimmunotherapy in patients with stage III non-small cell lung cancer: A real-world prospective cohort study. *Front Oncol* (2022) 12:969545. doi: 10.3389/fonc.2022.969545

66. Qiu F, Fan J, Shao M, Yao J, Zhao L, Zhu L, et al. Two cycles versus three cycles of neoadjuvant sintilimab plus platinum-doublet chemotherapy in patients with resectable non-small-cell lung cancer (neoSCORE): A randomized, single center, two-arm phase II trial. *J Clin Oncol* (2022) 40:8500. doi: 10.1200/JCO.2022.40.16_suppl.8500

67. Wu J, Hou L EH, Zhao Y, Yu X, Xu L, Ning Y, et al. Real-world clinical outcomes of neoadjuvant immunotherapy combined with chemotherapy in resectable non-small cell lung cancer. *Lung Cancer.* (2022) 165:115–23. doi: 10.1016/j.lungcan.2022.01.019

68. Zhai H, Li W, Jiang K, Zhi Y, Yang Z. Neoadjuvant nivolumab and chemotherapy in patients with locally advanced non-small cell lung cancer: A retrospective study. *Cancer Manag Res* (2022) 14:515–24. doi: 10.2147/cmar.S344343

69. Zhang P, Dai J, Sun F, Xia H, He W, Duan L, et al. Neoadjuvant sintilimab and chemotherapy for resectable stage IIIA non-small cell lung cancer. *Ann Thorac Surg* (2022) 114:949–58. doi: 10.1016/j.athoracsur.2022.01.039

70. Yan S, Chen J, Wang J, Lv C, Bi J, Yang X, et al. 64P Neoadjuvant toripalimab plus chemotherapy in patients with potentially resectable non-small cell lung cancer: A prospective, single-arm, phase II trial (Renaissance Study). *Ann Oncol* (2021) 32:S1400. doi: 10.1016/j.annonc.2021.10.082

71. Chen T, Ning J, Campisi A, Dell'Amore A, Ciarrocchi AP, Li Z, et al. Neoadjuvant PD-1 inhibitors and chemotherapy for locally advanced NSCLC: A retrospective study. *Ann Thorac Surg* (2021) 113:993–9. doi: 10.1016/j.athoracsur.2021.03.041

72. Chen Y, Yan B, Xu F, Hui Z, Zhao G, Liu J, et al. Neoadjuvant chemoimmunotherapy in resectable stage IIIA/IIIB non-small cell lung cancer. *Transl Lung Cancer Res* (2021) 10:2193–204. doi: 10.21037/tlcr-21-329

73. Duan H, Wang T, Luo Z, Tong L, Dong X, Zhang Y, et al. Neoadjuvant programmed cell death protein 1 inhibitors combined with chemotherapy in resectable non-small cell lung cancer: an open-label, multicenter, single-arm study. *Transl Lung Cancer Res* (2021) 10:1020–8. doi: 10.21037/tlcr-21-130

74. Hong T, Sun T, Zhang M, Liu X, Yuan Y, Dolo PR, et al. Surgical perspective in neoadjuvant chemoimmunotherapy for stage II–III non-small cell lung cancer. *Thorac Cancer.* (2021) 12:2796–802. doi: 10.1111/1759-7714.14127

75. Hu Y, Ren S-Y, Wang R-Y, Zeng C, Li J-N, Xiao P, et al. Surgical outcomes after neoadjuvant chemoimmunotherapy for resectable non-small cell lung cancer. *Front Oncol* (2021) 11:684070. doi: 10.3389/fonc.2021.684070

76. Shi L, Liu Z, Meng Q, Tong L, Li H. Pathologic response to neoadjuvant PD-1 inhibitors and chemotherapy in squamous non-small-cell lung cancer. *J Thorac Oncol* (2021) 16:S979. doi: 10.1016/j.jtho.2021.08.269

77. Zhang Y, Zeng L, Zhang X, Zhou Y, Zhang B, Jiang W, et al. P15.02 toripalimab and platinum-doublet chemotherapy as neoadjuvant therapy for potentially resectable non-small cell lung cancer. *J Thorac Oncol* (2021) 16:S1014–S5. doi: 10.1016/j.jtho.2021.08.339

78. Zhao ZR, Long H. Updated event-free survival of neoadjuvant toripalimab with chemotherapy for resectable stage III NSCLC (NeoTAP01 study). *Ann Oncol* (2022) 33: S984. doi: 10.1016/j.annonc.2022.07.1081

79. Zhou S, Hao X, Yu D, Liu S, Cao X, Su C, et al. Preliminary efficacy evaluation of neoadjuvant immunotherapy combined with chemotherapy in resectable non-small cell lung cancer. *Chin J Lung Cancer.* (2021) 24:420–5. doi: 10.3779/j.issn.1009-3419.2021.102.13

80. Shen D, Wang J, Wu J, Chen S, Li J, Liu J, et al. Neoadjuvant pembrolizumab with chemotherapy for the treatment of stage IIB-IIIB resectable lung squamous cell carcinoma. *J Thorac Dis* (2021) 13:1760–8. doi: 10.21037/jtd-21-103

81. Zhang Y, Zeng L, Zhang X, Zhou Y, Zhang B, Guo L, et al. 1160P Efficacy and biomarker identification of neoadjuvant chemo-immunotherapy in potentially resectable non-small cell lung cancer. *Ann Oncol* (2021) 32:S934. doi: 10.1016/j.annonc.2021.08.1763

82. Tfayli A, Al Assaad M, Fakhri G, Akel R, Atwi H, Ghanem H, et al. Neoadjuvant chemotherapy and Avelumab in early stage resectable nonsmall cell lung cancer. *Cancer Med* (2020) 9:8406–11. doi: 10.1002/cam4.3456

83. Zinner R, Axelrod R, Solomides CC, Cowan S, Leiby B, Bhatia AK, et al. Neoadjuvant nivolumab (N) plus cisplatin (C)/pemetrexed (P) or cisplatin /gemcitabine (G) in resectable NSCLC. *J Clin Oncol* (2020) 38:9051. doi: 10.1200/JCO.2020.38.15-suppl.9051

84. Liu YT, Gao YS, Mao YS, Jiang J, Yang L, Yang JL, et al. [The outcome and safety of neoadjuvant PD-1 blockade plus chemotherapy in stage II~III non-small cell lung cancer]. *Zhonghua Zhong Liu Za Zhi.* (2020) 42:480–5. doi: 10.3760/cma.j.cn112152-20200213-00087

85. Hilbe W, Pall G, Kocher F, Pircher A, Zabernigg A, Schmid T, et al. Multicenter phase II study evaluating two cycles of docetaxel, cisplatin and cetuximab as induction regimen prior to surgery in Chemotherapy-Naive patients with NSCLC stage IB-IIIA (INN06-Study). *PloS One* (2015) 10:e0125364. doi: 10.1371/journal.pone.0125364

86. Zhang B, Zhong H, Han B. Neoadjuvant immunotherapy for patients with non-small cell lung cancer-is a new era coming? *JAMA Oncol* (2023) 9:301–2. doi: 10.1001/jamaoncol.2022.6898

87. Pfirschke C, Engblom C, Rickelt S, Cortez-Retamozo V, Garris C, Pucci F, et al. Immunogenic chemotherapy sensitizes tumors to checkpoint blockade therapy. *Immunity* (2016) 44:343–54. doi: 10.1016/j.immuni.2015.11.024

88. Haddad RI, Seiwert TY, Chow LQM, Gupta S, Weiss J, Gluck I, et al. Influence of tumor mutational burden, inflammatory gene expression profile, and PD-L1 expression on response to pembrolizumab in head and neck squamous cell carcinoma. *J Immunother Cancer.* (2022) 10:e003026. doi: 10.1136/jitc-2021-003026

frontiers | Frontiers in Oncology

TYPE Case Report
PUBLISHED 04 March 2024
DOI 10.3389/fonc.2024.1273043

OPEN ACCESS

EDITED BY
Marco Bregni,
San Raffaele Hospital (IRCCS), Italy

REVIEWED BY
Maha Mohamed Saber-Ayad,
University of Sharjah, United Arab Emirates
Aloukick Kumar Singh,
University of Texas MD Anderson Cancer Center, United States

*CORRESPONDENCE
Woo Kyun Bae
drwookyun@jnu.ac.kr

RECEIVED 05 August 2023
ACCEPTED 08 February 2024
PUBLISHED 04 March 2024

CITATION
Lee SH, Kim HJ, Bang HJ, Park SJ, Yu JE, Jeong SW and Bae WK (2024) Case report: Pembrolizumab as an alternative to atezolizumab following a severe infusion reaction.
Front. Oncol. 14:1273043.
doi: 10.3389/fonc.2024.1273043

Case report: Pembrolizumab as an alternative to atezolizumab following a severe infusion reaction

Seung Hyuk Lee[1], Hyeon Jong Kim[1], Hyun Jin Bang[1], Su Ji Park[2], Ji Eun Yu[3], Seung Woo Jeong[4] and Woo Kyun Bae[1*]

[1]Division of Hematology-Oncology, Department of Internal Medicine, Chonnam National University Medical School and Hwasun Hospital, Hwasun, Republic of Korea, [2]Department of Pharmacy, Chonnam National University Bitgoeul Hospital, Gwangju, Republic of Korea, [3]Division of Allergy and Clinical Immunology, Department of Internal Medicine, Chonnam National University Hospital, Gwangju, Republic of Korea, [4]Chonnam National University College of Medicine, Hwasun, Republic of Korea

The emergence of immune-checkpoint inhibitors (ICIs) has revolutionized the field of oncology, providing promising results in various malignancies. However, ICIs can sometimes lead to severe injection reactions, requiring alternative treatment options. In this case report, we introduce a case of a severe infusion reaction induced by atezolizumab. After atezolizumab infusion, the patient experienced symptoms that were suggestive of anaphylactic shock, including chest tightness, low blood pressure, and loss of consciousness, all of which were restored by immediate administration of steroid, antihistamine, and epinephrine. When selecting a new ICI, we were concerned about cross-reactivity with atezolizumab. As such, we conducted a skin test to establish the underlying mechanism of the previous reaction to atezolizumab infusion, the results of which were highly suggestive of Ig-E-mediated hypersensitivity. The skin test for pembrolizumab, another ICI, was negative. Therefore, we replaced atezolizumab with pembrolizumab, and the infusion proceeded safely. To date, the patient has undergone 13 cycles of pembrolizumab, and the disease has remained stable. This case demonstrates that patients who exhibit severe injection reactions to ICIs can continue treatment safely, without cross-reactions, with alternative ICIs. This case will help provide patients who have experienced drug-related hypersensitivity reactions with a choice to use alternative ICIs, thus expanding their options for chemotherapy.

KEYWORDS

immune-checkpoint inhibitors (ICIs), atezolizumab, pembrolizumab, infusion reaction, hypersensitivity, immune-related adverse drug reactions (ADRs)

Introduction

Immunotherapy has revolutionized the treatment landscape for various malignancies, with immune-checkpoint inhibitors (ICIs) emerging as a promising class of therapeutics (1). ICIs function by blocking immune checkpoints, thereby enhancing the immune system's ability to target cancer cells (1). Although each ICI has a unique molecular target, they share a common mechanism of action and may exhibit overlapping adverse effects (1).

Atezolizumab, a monoclonal antibody targeting programmed death-ligand 1 (PD-L1), has emerged as a promising immunotherapeutic agent for the treatment of various malignancies (2–4). Although atezolizumab has demonstrated significant efficacy in boosting the immune system's ability to combat cancer, its use is occasionally associated with infusion reactions, posing challenges with clinical administration (5).

In the context of cancer immunotherapy, the immune-related adverse drug reactions (ADRs) are an important consideration. The pathophysiology of ICI-related ADRs is complex and involves T-cell activation against self-antigens, leading to inflammatory responses in the affected tissues. However, Infusion reactions related to ICIs are typically non-IgE-mediated hypersensitivity reactions that can occur during or shortly after the administration of these agents. So it is imperative to discern between infusion reactions specific to ICIs and drug hypersensitivity reactions, as the clinical management and potential implications for ongoing cancer treatment significantly differ between the two (1, 2).

Treatment for metastatic urothelial cancer typically includes chemotherapy as a first-line treatment, often with a combination of drugs such as cisplatin and gemcitabine. In recent years, immunotherapy involves drugs like pembrolizumab or atezolizumab has become a vital part of the treatment for metastatic urothelial cancer, especially for patients who don't respond well to chemotherapy (3).

In this case report, we present the clinical course of a patient with metastatic ureter cancer who received atezolizumab as a primary treatment. The patient had a serious and unexpected infusion reaction similar to anaphylaxis during the first injection of atezolizumab. Despite concerns surrounding cross-reactions to other ICIs, pembrolizumab was selected as an alternative and was infused with no adverse effects.

This case report aims to provide a comprehensive review of infusion reactions linked to atezolizumab, including their clinical manifestations, underlying mechanisms, management strategies, and implications for patient care. This unprecedented scenario provides an opportunity to explore the safety, effectiveness, and potential implications of using pembrolizumab as an alternative to atezolizumab, which avoids the drug reaction that occurred during the first infusion. Furthermore, by reporting this case, we aim to contribute to the growing body of literature surrounding immune-related adverse events associated with ICIs.

Case description

A 74-year old man with a past medical history of hypertension underwent nephrectomy and ureterectomy for a right ureter tumor on May 23, 2017. Adjuvant chemotherapy was recommended, but the patient refused and requested regular follow-up only. After 4 years, the patient developed abdominal lymph node metastases and received systemic chemotherapy. The patient was administered a chemotherapy regimen consisting of gemcitabine, dosed at 1000mg/m^2, and cisplatin, dosed at 35mg/m^2. This regimen was scheduled over a three-week cycle, with the patient receiving treatment during the first two weeks and having the third week as a rest period. After seven cycles of chemotherapy, the recurred lesion progressed, and the chemo-agent was changed to atezolizumab, a PD-L1 inhibitor. Ten minutes after the first infusion of atezolizumab, the patient complained of dyspnea and itching, and displayed hypotension with systolic blood pressure decreasing to 40 mmHg. Subsequently, his oxygen saturation decreased to 80% and he lost consciousness. The level of consciousness was assessed as Glasgow coma scale 5. The patient was immediately administered antihistamine, steroid, epinephrine, and fluid to treat the hypersensitivity reaction. Afterwards, blood pressure and consciousness recovered within minutes. As a result, consciousness was restored, and vital signs stabilized. Causality assessments suggested that the event met the WHO-UMC causality assessment as terms of "probable" (4)., with a Naranjo's score of 7 (5).

Given the severity of the reaction to atezolizumab, it was decided to cease further administration; instead, salvage radiation therapy was performed on the recurred lymph node lesions. During the period 22/3/10-3/31, salvage radiation therapy was applied 25 times to the ureter and surrounding lymph nodes, for a total of 3200cGy. Initially, radiation therapy provided a stable response, but the metastatic lymph node lesions worsened again 5 months after the end of radiation treatment. We discussed with the patient whether to re-administer systemic chemotherapy or try another ICI, pembrolizumab, and the patient expressed that they wished to try pembrolizumab. Given the possibility that the severe infusion reaction that occurred after the administration of atezolizumab was type 1 hypersensitivity, and the possibility that a new ICI would cross-react with atezolizumab, we decided to conduct a skin test on both ICIs.

Diagnostic assessment and details of the therapeutic intervention, follow-up, and outcomes

The drug dose used in the skin test was determined by referring to a previous study (6, 7). A positive reaction in the skin test was defined according to the criteria recommended by the American Allergy Society (8): Positive skin test, development of a wheal that is at least 3 mm greater than that observed with the negative control for prick/puncture; or intradermal test (IDT) accompanied by a flare > 5 mm. The skin prick test with atezolizumab at a concentration of 60 mg/mL was negative, and the intradermal test was positive at 0.06 mg/mL and 0.6 mg/mL (IDT, 0.06 mg/mL; wheal, 3.8 × 3.5; flare, 7 × 7 and 0.6 mg/mL; wheal, 5.3 × 4.9; flare, 12 × 8) (Figure 1). The skin prick test (25 mg/ml) and intradermal (0.25 mg/ml) test were performed with pembrolizumab, and both were negative (Figure 1). Therefore, we decided to carefully infuse pembrolizumab, without steroid or antihistamine injection, and the

first injection was completed safely, without any hypersensitivity-related symptoms. We introduced Keytruda at 3-week intervals and conducted restaging CT scans every 3 months. After the 11th chemotherapy session, a partial response was still maintained (Figure 2). After the 20th infusion, CT scan showed disease progression, leading to the discontinuation of Keytruda.

Discussion

As various types of ICIs continue to develop, interest in incidence, mechanisms, preventions of immune-related ADRs are also being actively growing. Previous autoimmune disease, genetic predisposition, combination therapy, using ICIs in combination with other therapies can increase the risk of ADRs. Some evidence suggests that the type and stage of cancer may affect the likelihood of experiencing immune-related ADRs. For instance, melanoma patients treated with CTLA-4 inhibitors may experience different ADRs compared to those with lung cancer treated with PD-1/PD-L1 inhibitors. Research has indicated that there may be sex-based differences in the incidence and severity of immune-related ADRs. However, the data is not entirely conclusive, and more research is needed to understand these differences fully. Elderly patients may have a different risk profile for ADRs due to age-related changes in the immune system and a higher likelihood of comorbidities (9).

Most anticancer agents, including ICIs, carry a risk of adverse drug reactions, especially infusion reactions, with several reports of infusion reactions after using ICIs (10, 11). Infusion reactions can be classified as type 1 hypersensitivity reactions (immune-mediated adverse reaction) and non-allergic reactions, such as cytokine-release syndrome (CRS) (1, 12). Regardless of whether the reaction is allergic or non-allergic, the clinical manifestations are the same and require accurate assessment and acute management (1).

Currently, there is no unified consensus on whether the mechanism of infusion reactions caused by monoclonal antibodies, including ICIs, is immune-mediated or a symptom of CRS (1, 12). However, it is generally accepted that the culprit drug should be discontinued if a serious infusion reaction is observed. Clinically, anaphylaxis is diagnosed by measuring the serum tryptase level, conducting skin tests, and measuring the serum allergen-specific IgE levels to identify the allergen (13). Blood samples for the measurement of tryptase should be obtained 15 min to 3 h after symptom onset. In this case, the tryptase level was measured 4 h after the onset of symptoms and showed a value of 17.4, which is above the normal range (1–11.4 ng/mL).

Severe infusion reactions with atezolizumab are rare, but a few related cases have been reported (6, 14). Although successful desensitization with atezolizumab has been reported (6), re-administration after severe infusion reactions should be carefully considered. There has been no specific evidence reported that suggests anti-PD-L1 ICIs are more likely to cause anaphylactic or immune-related adverse drug reactions (ADRs) compared to other ICIs. The safety profiles of ICIs can vary due to their different molecular structures and mechanisms of action. Anti-PD1 and anti-PD-L1 antibodies differ in their target interactions; for instance, anti-PD1 antibodies block the binding of PD-1 to both of its ligands, PD-L1 and PD-L2, while anti-PD-L1 antibodies specifically block the interaction between PD-1 and PD-L1. These differences could theoretically influence the immunogenicity of the drugs and result in different safety profiles. However, the clinical significance of these differences in terms of ADRs, including anaphylactic reactions, is still being studied and is not fully understood (15).

In this case, we determined whether the infusion reaction that occurred after the use of atezolizumab was IgE-mediated hypersensitivity or CRS. The results of the skin prick test and serum tryptase levels were highly indicative of type 1 hypersensitivity. Typically, type 1 hypersensitivity requires sensitization to a specific antigen, but in this case, the patient had not been previously exposed to atezolizumab. As an example of cross-reactivity, it is possible that this patient was sensitized to a drug or food with a similar epitope to atezolizumab. In the context of alpha-gal syndrome, anaphylaxis can be

FIGURE 1
Skin prick test: negative for atezolizumab and pembrolizumab. Intra-dermal test: positive at 0.06 mg/mL and 0.6 mg/mL of atezolizumab (IDT; 0.06 mg/mL; wheal, 3.8 × 3.5; flare, 7 × 7 and 0.6 mg/mL; wheal, 5.3 × 4.9; flare, 12 × 8), and negative for pembrolizumab.

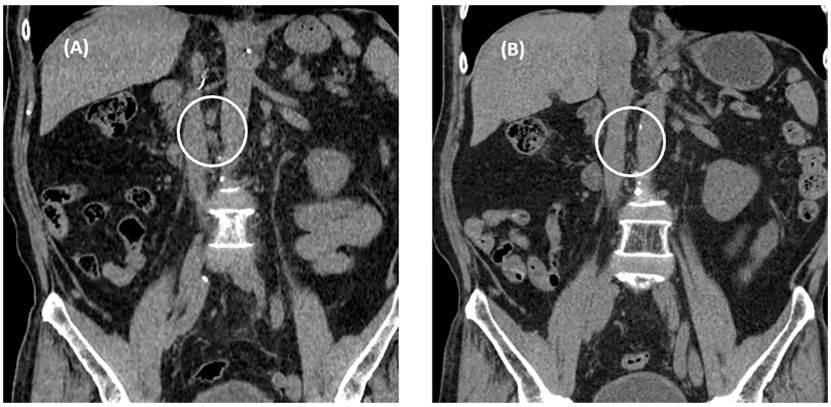

FIGURE 2
Abdominal non-contrast computed tomography after three cycles of pembrolizumab. **(A)** Enlarged metastatic lymphadenopathies in aorto-caval, and para-aortic on CT conducted August 22, 2022. **(B)** A partial response was observed on restaging CT conducted October 18, 2022. White circle means "metastatic LNs".

triggered when an individual who has been sensitized to a sugar molecule called alpha-gal, found in red meat, receives their first dose of the drug cetuximab. Cetuximab contains the alpha-gal molecule, and exposure to it can prompt an allergic reaction in those who have developed sensitivity. The sensitization to alpha-gal can lead to an immune response upon subsequent exposure to it through certain medications, resulting in anaphylaxis (16). However, it is difficult to exclude the possibility that the skin prick test or elevated serum tryptase directly activated mast cells or was a false positive result.

Although the burden of side effects related to cytotoxic drugs has been alleviated with the introduction of ICIs, cases of severe infusion reactions due to ICIs are still reported occasionally (14, 17, 18). Understanding the mechanisms underlying these infusion reactions is critical to effectively manage and mitigate associated risks, but elucidating the hidden pathways of immune responses remains a considerable challenge for physicians. Therefore, as an appropriate alternative, the introduction of another ICI should be carefully considered. This will require individualized treatment decisions based on patient characteristics, including tumor type, previous therapy, and potential for cross-reactivity between ICIs. Strategies for monitoring and managing infusion reactions and other adverse events associated with ICIs are considered worthy of discussion.

Data availability statement

The raw data supporting the conclusions of this article will be made available by the authors, without undue reservation.

Ethics statement

Ethical approval was not required for the studies on humans in accordance with the local legislation and institutional requirements because only commercially available established cell lines were used. Written informed consent was obtained from the individual(s) for the publication of any potentially identifiable images or data included in this article.

Author contributions

SL: Writing – original draft, Writing – review & editing, Conceptualization. HK: Writing – original draft. HB: Writing – original draft. SP: Data curation, Writing – original draft. JY: Conceptualization, Data curation, Writing – original draft. SJ: Investigation, Writing – original draft. WB: Conceptualization, Supervision, Writing – review & editing.

Funding

The author(s) declare financial support was received for the research, authorship, and/or publication of this article. This study was supported by a grant (HCRI15003-1) of the Chonnam National University Hwasun Hospital Institute for Biomedical Science.

Conflict of interest

The authors declare that the research was conducted in the absence of any commercial or financial relationships that could be construed as a potential conflict of interest.

Publisher's note

References

1. Vogel WH. Infusion reactions: diagnosis, assessment, and management. *Clin J Oncol Nurs*. (2010) 14:E10–21. doi: 10.1188/10.CJON.E10-E21

2. Postow MA, Sidlow R, Hellmann MD. Immune-related adverse events associated with immune checkpoint blockade. *N Engl J Med*. (2018) 378:158–68. doi: 10.1056/NEJMra1703481

3. Cathomas R, Lorch A, Bruins HM, Compérat EM, Cowan NC, Efstathiou JA, et al. The 2021 updated european association of urology guidelines on metastatic urothelial carcinoma. *Eur Urol*. (2022) 81:95–103. doi: 10.1016/j.eururo.2021.09.026

4. Behera SK, Das S, Xavier AS, Velupula S, Sandhiya S. Comparison of different methods for causality assessment of adverse drug reactions. *Int J Clin Pharm*. (2018) 40 (4):903–10. doi: 10.1007/s11096-018-0694-9

5. Naranjo CA, Busto U, Sellers EM, Sandor P, Ruiz I, Roberts EA, et al. A method for estimating the probability of adverse drug reactions. *Clin Pharmacol Ther*. (1981) 30:239–45. doi: 10.1038/clpt.1981.154

6. Gonzalez-Diaz SN, Villarreal-Gonzalez RV, De Lira-Quezada CE, Rocha-Silva GK, Oyervides-Juarez VM, Vidal-Gutierrez O. Protocol for desensitization to atezolizumab and bevacizumab after severe anaphylaxis in the treatment of lung adenocarcinoma. *J Investig Allergol Clin Immunol*. (2021) 31:265–7. doi: 10.18176/jiaci

7. Torrado I, Peña MI, Tsopana A, Mendoza I, Beitia JM, Mateo B, et al. Allergy igE-mediated to pembrolizumab and successful desensitization. *J Investig Allergol Clin Immunol*. (2022) p:0. doi: 10.18176/jiaci.0858

8. Khan DA, Banerji A, Blumenthal KG, Phillips EJ, Solensky R, White AA, et al. Drug allergy: A 2022 practice parameter update. *J Allergy Clin Immunol*. (2022) 150:1333–93. doi: 10.1016/j.jaci

9. Poto R, Troiani T, Criscuolo G, Marone G, Ciardiello F, Tocchetti CG, et al. Holistic approach to immune checkpoint inhibitor-related adverse events. *Front Immunol*. (2022) 13:804597. doi: 10.3389/fimmu.2022.804597

10. Roselló S, Blasco I, García Fabregat L, Cervantes A, Jordan K. Management of infusion reactions to systemic anticancer therapy: ESMO Clinical Practice Guidelines. *Ann Oncol*. (2017) 28:iv100–18. doi: 10.1093/annonc/mdx216

11. Chung CH. Managing premedications and the risk for reactions to infusional monoclonal antibody therapy. *Oncologist*. (2008) 13:725–32. doi: 10.1634/theoncologist.2008-0012

12. Lenz HJ. Management and preparedness for infusion and hypersensitivity reactions. *Oncologist*. (2007) 12:601–9. doi: 10.1634/theoncologist.12-5-601

13. Simons FE, Ardusso LR, Bilò MB, El-Gamal YM, Ledford DK, Ring J, et al. World allergy organization guidelines for the assessment and management of anaphylaxis. *World Allergy Organ J*. (2011) 4:13–37. doi: 10.1097/WOX.0b013e318211496c

14. Bian LF, Zheng C, Shi XL. Atezolizumab-induced anaphylactic shock in a patient with hepatocellular carcinoma undergoing immunotherapy: A case report. *World J Clin cases*. (2021) 9:4110–5. doi: 10.12998/wjcc.v9.i16.4110

15. Kwok G, Yau TC, Chiu JW, Tse E, Kwong YL. Pembrolizumab (Keytruda). *Hum Vaccin Immunother*. (2016) 12:2777–89. doi: 10.1080/21645515.2016.1199310

16. Chung CH, Mirakhur B, Chan E, Le QT, Berlin J, Morse M, et al. Cetuximab-induced anaphylaxis and IgE specific for galactose-alpha-1,3-galactose. *N Engl J Med*. (2008) 358:1109–17. doi: 10.1056/NEJMoa074943

17. Kumari S, Yun J, Soares JR, Ding PN. Severe infusion reaction due to nivolumab: A case report. *Cancer Rep (Hoboken)*. (2020) 3:e1246. doi: 10.1002/cnr2.1246

18. Pîrlog CF, Slavu CO, Olaru M, Popa AM, Iaciu C, et al. Nivolumab hypersensitivity reactions a myth or reality in solid tumors-A systematic review of the literature. *Curr Oncol*. (2022) 29:9428–36. doi: 10.3390/curroncol29120741

Frontiers in Immunology

Explores novel approaches and diagnoses to treat immune disorders.

The official journal of the International Union of Immunological Societies (IUIS) and the most cited in its field, leading the way for research across basic, translational and clinical immunology.

Discover the latest Research Topics

See more →

Frontiers

Avenue du Tribunal-Fédéral 34
1005 Lausanne, Switzerland
frontiersin.org

Contact us

+41 (0)21 510 17 00
frontiersin.org/about/contact